PHENOMENOLOGY OF QUANTUM CHROMODYNAMICS

XIII th Rencontre de Moriond - Session I, Les Arcs
(Savoie) France - March 12 - 18, 1978

PHENOMENOLOGY OF QUANTUM CHROMODYNAMICS

ISBN 2-86332-002-5

1978 Editions Frontieres 7 avenue Kennedy
28100 DREUX - France

Printed in Korea

Proceedings of the

THIRTEENTH RENCONTRE DE MORIOND . 13 . 1978.

Les Arcs - Savoie (France), March 12 - March 24, 1978

VOL. I

PHENOMENOLOGY OF QUANTUM CHROMODYNAMICS

edited by

J. TRAN THANH VAN

SPONSORED BY

- INSTITUT NATIONAL DE PHYSIQUE NUCLEAIRE ET DE PHYSIQUE DES PARTICULES
- COMMISSARIAT A L'ENERGIE ATOMIQUE

The First Session of the Thirteenth Rencontre de Moriond on Phenomenology of Quantum Chromodynamics

was organized by

J. TRAN THANH VAN

with the active collaboration of

CHAN Hong Mo
G. KANE
TAN Chung I

Permanent secrétariat:

Rencontre de Moriond

Laboratoire de Physique Théorique et Particules Elémentaires
Bâtiment 211 - Université de Paris-Sud
91405 ORSAY (France)
Tel. 941.73.66

FOREWORD

The XIII th Rencontre de Moriond was held at Les Arcs - Savoie (France) from March 12 to March 24, 1978.

The first such meeting was at Moriond in the French Alps in 1966. There, experimental as well as theoretical physicists, not only shared their scientific preoccupations but also the household chores. The participants at the first meeting were mainly French physicists interested in electromagnetic interactions. In subsequent years, a session on high energy strong interactions was also added.

The main purpose of these meetings is to discuss recent developments in contemporary physics and to promote effective collaboration between experimentalists and theorists in the field of elementary particle physics. By bringing together a relatively small number of participants, the meeting helps to developp better human relations as well as a more thorough and detailed discussion of the contributions.

This concern for research and experimentation of new channels of communication and dialogue which from the start animated the Moriond Meetings, inspired us, starting eight years ago, to organize a simultaneous meeting of biologists on Cellular Differentiation. Common seminars are organized to study to what extent analytical methods used in physics could be applied to biological problems. This year, an introductory talk and a beautiful film "The Genetic Code" was presented by Professor J. TAVLITZKI (Institute of Molecular Biology, Paris), Professor DEDONDER (University of Paris) gave a comprehensive talk on "Genetic Engineering", and Dr D. FOURME (L.U.R.E., Orsay) described the Orsay storage ring facilities for biology experiments. These conferences and lively discussions make us hope that biological problems, at present so complex, may give birth in the future to new analytical methods or new mathematical languages.

The first session of the XIII th Rencontre de Moriond (March 12 - March 18, 1978) was devoted to high energy hadronic interactions. Special emphasis was put on the phenomenology of quantum chromodynamics especially on lepton pair production, gluon physics and multiquark states.

The second session (March 18 - March 24, 1978) was devoted to high energy leptonic interactions. Particular attention was given to e^+e^- physics and recent discoveries in neutrino interactions.

I thank CHAN HONG-MO, G. KANE, TAN CHUNG-I for the first session, M. DAVIER, F. HAYOT, F.M. RENARD and R. TURLAY for the second session and the conference secretaries L. NORRY and N. CORNIQUEL who have devoted much of their time and energy to the success of this Rencontre.

I am also grateful to Mr TOURAILLE, the hotel Director, Mr MONTEGU and Ms FERRANDON, who contributed through their hospitality and active cooperation to the well-being of the participants enabling them to work in a relaxed atmosphere.

P A R T I C I P A N T S

First Session

ABOLINS Maris	Physics Dept, Michigan State University, East Lansing, MI, 48823 (U.S.A.)
AGUILAR-BENITEZ Manuel	Junta de Energia Nuclear, Avda Complutense 22, Madrid-3 (Spain)
BADIER Jean	L.P.N.H.E. Ecole Polytechnique, 91120-Palaiseau (France)
BADIER Simone	L.P.T. U.E.R. Sciences Exactes et Naturelles, 33, rue Saint Leu, 80039-Amiens Cedex (France)
BARATE Robert	DPhPE C.E.N. Saclay, B.P. 2 91190-Gif-sur-Yvette (France)
BAREYRE Michel	DPhPE C.E.N. Saclay, B.P.2 91190-Gif-sur-Yvette (France)
BAUBILLIER Michel	L.P.N.H.E. T.12, Université Pierre et Marie Curie, 4, Place Jussieu, 75230-Paris Cedex 05 (France)
BELLETTINI Giorgio	I.N.F.N. Via Livornese S. Piero a Grado, 56100-Pisa (Italy)
	I.N.F.N. c.p. 13 00044-Frascati (Italy)
BRADAMANTE Franco	Istituto di Fisica, Università di Trieste, e I.N.F.N. Sezione di Trieste, Via A. Valerio 2, Trieste 34100 (Italy)
CAPELLA Alfons	L.P.T.P.E. Université Paris-Sud, Bât. 211, 91405-Orsay (France)
CARTER Antony	Physics Dept. Queen Mary College, Mile End Rd, London EI 4NS (United Kingdom)

CHAN Hong Mo	Theory Division, Rutherford Laboratory, Chilton, Didcot, Oxon OX11 0QX (United Kingdom)
CHEW	Dept of Physics, Nayang University, Jurong Rd, Singapore 22
CHARPENTIER Philippe	DPhPE C.E.N. Saclay B.P. 2 91190-Gif-sur-Yvette (France)
COBB Jhon H.	Lancaster University Lancaster LA14YB (United Kingdom)
	Division E.P. C.E.R.N. 1211-Geneva 23 (Switzerland)
COMBRIDGE Brian	Division TH, C.E.R.N. 1211-Geneva 23 (Switzerland)
CONTOGOURIS Andreas P.	Mc Gill University Rutherford Physics Bldg, Montreal, Quebec H3X3S4 (Canada)
COOL Rodney L.	Rockefeller University, New York N.Y. 10031 (U.S.A.)
COQUEREAUX Robert	Centre de Physique Théorique, C.N.R.S. 31, Chemin J. Aiguier 13274 - Marseille (France)
DAR Arnon	Physics Dpt., Technion Institute of Technology Haifa (Israel)
DASH Jan	Centre de Physique Théorique, C.N.R.S. 31, Chemin J. Aiguier 13274-Marseille (France)
DONOHUE Jack	Laboratoire de Physique Théorique, Université de Bordeaux Domaine du Haut-Vigneau 33170-Gradignan (France)
DUONG Van Minh	University of California Los Alamos Scientific Laboratory, Los Alamos N.M. 87544 (U.S.A.)
ELLIS Stephen P.	Physics Dept. FM-15 University of Washington Seattle Wa. 98195 (U.S.A.)
ENGELS Jürgen	Universität Bielefeld, Fak. F. Physik D-4800 Bielefeld (Fed. Rep. of Germany)
FAVIER Jean	L.A.P.P. B.P. 909 74019 - Annecy Le Vieux (France)

FERRAZ de CAMARGO Filho A.	L.P.T.H.E. Université Paris VII Tour 33, 2 Place Jussieu, 75230-Paris Cedex 05 (France)
FINJORD	Division TH, C.E.R.N. 1211-Geneva 23 (Switzerland)
FRAUTSCHI Steven	L.P.T.H.E. Université Paris-Sud, Bât. 211, 91405-Orsay (France) (On leave from CALTECH)
FREDRIKSSON Sverker	Division TH, C.E.R.N. 1211-Geneva 23 (Switzerland)
FRENCH Bernard C.	Division EP, C.E.R.N. 1211-Geneva (Switzerland)
FRY John	Dpt of Physics, University of Liverpool, P.O.B. 147, Liverpool L69 3BX (United Kingdom)
FUKUGITA Masataka	Rutherford Laboratory, Bldg. R1, Chilton, Didcot, Oxon OX11 0QX (United Kingdom)
GARVEY John	Physics Dpt, University of Birmingham, Birmingham B15 2TT (United Kingdom)
GOUANERE Michel	L.A.P.P. B.P. 909 74019-Annecy-le-Vieux (France)
GOULIANOS Dino	Rockefeller University, New-York N.Y. 10021 (U.S.A.)
GRASSBERGER Peter	Fachhereich Physik, Gesamthochschule Wuppertal, D-56 Wuppertal 1 (Fed. Rep. of Germany)
GRUNBERG Georges	Laboratoire de Physique Mathématique Université des Sciences et Techniques du Languedoc, Place Eugène Bataillon, 34060-Montpellier Cedex (France)
HALLIDAY Ian	Imperial College London, and C.E.R.N. 1211-Geneva 23 (Switzerland)
HANSON Gail	S.L.A.C. Bin 61, P.O.Box 4349 Stanford Ca. 94305 (U.S.A.)

HEUSCH Clemens A.	University of California, Santa Cruz Ca. 95064 (U.S.A.)
HOGAASEN Hallstein	University of Oslo and C.E.R.N. 1211-Geneva (Switzerland)
HONG TUAN Richard	L.P.T.H.E. Université Paris-Sud, Bât. 211, 91405-Orsay (France)
HWA Rudolph C.	Rutherford Laboratory, Chilton, Didcot, Oxon, OX11 0QX (United Kingdom)
JAFFE Robert	Center for Theoretical Physics Massachusetts Inst. Tech. Cambridge Ma. 0 2139 (U.S.A.)
JOHNSON Denis	Inter-University Institute for High Energies, 2 av. de la Plaine, B-1050 Brussels (Belgium)
JOHNSON Robert C.	Mathematics Dpt, Durham University, South Road, Durham DH1 3LE (United Kingdom)
KANE Gordon	Physics Dept. University of Michigan, Ann Arbor Mi. 48109 (U.S.A.)
KIENZLE Maria-Novella	Dept. de Physique Nucléaire et Corpusculaire Université de Genève 1211-Geneva 4 (Switzerland)
KIM Jae Kwan	Korea Advanced Institute of Science P.O.Box 150 Chong yangni, Seoul (Korea)
KOBAYASHI Reido	L.P.T.H.E., Université Paris-Sud, Bât. 211 91405-Orsay (France)
KROLL Peter	University of Wuppertal and C.E.R.N. 1211-Geneva 23 (Switzerland)
KUBAR-ANDRE Joanna	Dept. Physique Théorique, Université de Nice, Parc Valrose, 06034-Nice (France)
LACAZE Robert	DPhT, C.E.N. Saclay,B.P.2, 91190-Gif-sur-Yvette (France)
LAURENS Georges	DPhPE C.E.N. Saclay, B.P. 2, 91190-Gif-sur-Yvette (France)

LEDERMAN Leon	Physics Dept, Columbia University, P.O.Box 133, New York N.Y. 10027 (U.S.A.)
LEGUYADER Jacques	L.P.N.H.E., Tour 32, Université Pierre et Marie Curie, 4, Place Jussieu, 75230-Paris Cedex 06 (France)
MARTIN André	Division TH, C.E.R.N., 1211-Geneva 23 (Switzerland)
MARTIN Alan	Dept. of Physics, University of Durham, South Road, Durham 13 LE (United Kingdom)
MASAIKE Akira	National Laboratory for High Energy Physics, Oho, Tsukuba, Ibaraki-Ken (Japan)
MATSUDA Satoshi	Division TH, C.E.R.N., 1211-Geneva 23 (Switzerland)
MENESSIER Gérard	Dept. Physique Mathématique U.S.T.L. 34060-Montpellier (France)
MICHAEL Christopher	Dept. of Applied Mathematics and Theoretical Physics, University of Liverpool, P.O.Box 147, Liverpool L69 3BX (United Kingdom)
MIETTINEN Hannu Ilmari	Fermi National Accelarator Lab., P.O.Box 500, Batavia Il. 60510 (U.S.A.)
MORGAN David	Rutherford Laboratory, Theory Division, Chilton, Didcot, Oxon, OX11 0QX (United Kingdom)
MORIARTY Kevin J.M.	Royal Holloway College, Dept. of Mathematics University of London, Egham Hill, Egham, Surrey T.W.0EX (United Kingdom)
NAVELET Henri	DPhT C.E.N. Saclay, B.P.2 91190-Gif-sur-Yvette (France)
NICOLESCU Basarab	Division de Physique Théorique, Institut de Physique Nucléaire, Université Paris-Sud, B.P.1, 91406-Orsay (France)

PAULI Eugène	DPhPE, C.E.N. Saclay, B.P.2, 91190-Gif-sur-Yvette (France)
PETRONZIO Roberto	Division TH, C.E.R.N. 1211-Geneva 23 (Switzerland)
PILCHER J.E.	Fermi National Accelerator Lab. P.O.Box 500, Batavia Il. 60510 (U.S.A.)
PORDES Stephen	C.E.R.N. 1211-Geneva 23 (Switzerland)
QUERROU Michel	Laboratoire de Physique Corpusculaire de Clermond-Ferrand, B.P. 45, 63170-Aubière (France)
REHAK Pavel	Brookhaven National Laboratory, Upton N.Y. 11973 (U.S.A.)
RICHARD Jean-Marc	Division de Physique Théorique, Institut de Physique Nucléaire, Université Paris-Sud, B.P.1 91406-Orsay (France)
RINGLAND Gordon	Rutherford Laboratory, Chilton, Didcot, Oxon, OX11 0QX (United Kingdom)
ROBERTS Richard G.	Rutherford Laboratory, Chilton, Didcot, Oxon, OX11 0QX (United Kingdom)
ROBSON David	Dept. of Physics, Manchester University, Manchester M.13 9PL (United Kingdom)
ROIESNEL Claude	Centre de Physique Théorique, Ecole Polytechnique, 91128-Palaiseau (Orsay)
ROMANA Albert	L.P.N.H.E. Ecole Polytechnique, 91120-Palaiseau (France)
SACHRAJDA Chris	Division TH, C.E.R.N. 1211-Geneva (Switzerland)
SCHIFF Dominique	L.P.T.H.E. Université Paris-Sud, Bât. 211, 91405-Orsay (France)
SCHILDKNECHT Dieter	Fak. für Physik, Universität Bielefeld, Postfach 8640, 4800-Bielefeld (Fed. Rep. of Germany)

SIX Jules	Laboratoire de l'Accélérateur Linéaire, Bât. 200, Université Paris-Sud, 91405-Orsay (France)
TAN CHUNG I	Brown University, Providence R.I. (U.S.A.) and L.P.T.P.E. Bât. 211, 91405-Orsay (France)
TEIGER Jacques	DPhPE/SEE C.E.N. Saclay B.P.2 91190-Gif-sur-Yvette (France)
TOUNSI Ahmed	L.P.T.H.E. Université Paris VI, Tour 32, 4, Place Jussieu, 75230-Paris Cedex 05 (France)
TOW Don	Center for Particle Theory, University of Texas, Austin Tx (U.S.A.) and L.P.T.P.E. Université Pierre et Marie Curie, Tour 16, 4, Place Jussieu, 75230-Paris Cedex 05 (France)
TRAN THANH VAN Jean	L.P.T.P.E. Bât. 211, 91405-Orsay (France)
VANNUCCI François	Division EP, C.E.R.N. 1211-Geneva 23 (Switzerland)
VINH MAU Robert	Division de Physique Théorique, I.P.N. Université Pierre et Marie Curie, 4, Place Jussieu, 75230-Paris Cedex 05 (France)
WALKER James K.	Fermi National Accelarator Laboratory, P.O.Box 500, Batavia Il. 60510 (U.S.A.)
WEISZ Sylvain	L.P.N.H.E. Ecole Polytechnique, 91120-Palaiseau (France)
WERNHARD Karl L.	Division EP, C.E.R.N. 1211-Geneva 23 (Switzerland)
WIDGOFF Mildred	Physics Dept. Box 1843, Brown University, Providence R.I. 02912 (U.S.A.)

CONTENTS

I - Q. C. D. AND LEPTON PAIR PRODUCTION

II - Q. C. D. AND MULTIQUARK STATES

PARTON MODEL IDEAS AND QUANTUM CHROMODYNAMICS

C. T. Sachrajda
CERN, 1211 Genève 23
Switzerland

A B S T R A C T

We study several hard scattering processes in quantum chromodynamics for which there is no light cone expansion (e.g., massive lepton pair production, the inclusive production of particles with large transverse momenta, etc.). The results suggest a very simple ansatz for calculating hard scattering cross-sections in quantum chromodynamics.

R E S U M E

Dans le cadre de la chromodynamique quantique, nous examinons des processus de collision violente pour lesquels il n'existe pas de développement sur le cône de la lumière tels que la production de paires de leptons à grande masse invariante et la production inclusive de particules à grande impulsion transverse. Les résultats suggèrent la validité d'une règle simple pour le calcul des sections efficaces de ces processus.

1. - INTRODUCTION

During the last few years there have been many experiments concerning hard scattering processes, processes in which there are large energy and momentum transfers. The data from these experiments are usually interpreted within the parton picture, in which hadrons are assumed to consist of constituents, and it is these constituents which participate in the hard scattering [1)-4)]. To my mind the philosophy of the parton picture is that the strong interactions are described by a quantum field theory, and that the parton model provides an approximation to this field theory for the hard scattering processes. At present, the leading candidate for the theory of strong interactions is quantum chromodynamics. Its property of asymptotic freedom provides an elegant explanation of approximate Bjorken scaling [5),6)] in deep inelastic lepton-hadron scattering, moreover the scaling violations can be calculated and are found to agree with the data [see 7)-9) and references therein]. It is therefore important to see whether our parton model views concerning other processes, e.g., massive lepton pair production, the inclusive productions of particles with large transverse momenta, etc., are also valid in QCD. Until recently one had no means of calculating QCD predictions for these processes, however, during the last few months there has been considerable progress in understanding this problem. It is this progress which I shall review in this talk.

Unfortunately the rigorous predictions of QCD are restricted to deep inelastic lepton-hadron scattering and e^+e^- annihilation. For these processes, to arrive at the predictions one uses the powerful theoretical tools of the operator product expansion and the renormalization group. Unfortunately for the other hard scattering processes, in particular for those with two hadrons in the initial state, no light cone techniques have been developed and one has to make model assumptions. The approach which we shall take here, is that hadrons can be described by soft wave functions, which cannot be calculated using perturbation theory and which strongly damp the invariant masses and transverse momenta (in the infinite momentum frame, for example) of quarks, gluons and antiquarks. We assume further that hard scattering cross-sections are given by the convolution of these soft hadronic wave functions together with the cross-sections for hard scattering subprocesses involving only quarks, antiquarks and gluons. This assumption a priori does not provide a useful prescription, since in principle we need to

calculate the cross-section for the subprocess to all orders of perturbation theory, in spite of the presence of a "running coupling constant" $[\bar{g}(Q^2)$ where Q represents a typical large momentum transfer$]$. This is so, because, although $\bar{g}^2(Q^2) \sim (1/\log Q^2)$ and therefore in appropriate kinematic regions will be small, the integral over the loop momentum often gives a factor of $\log Q^2$ (this will be explained in detail in subsequent sections). Thus we end up with a power series in $\bar{g}^2(Q^2) \log Q^2$, in which every term is of the same order of magnitude. In order to make QCD predictions we must either be able to sum the series (as in deep inelastic scattering), or to define quantities in which the loop momenta do not give the factor of $\log Q^2$.

An example of a process in which the loop momenta do not give a factor of $\log Q^2$ is the production of jets in e^+e^- annihilation [10]. In this case since we are not looking at an exclusive process, but rather at a suitably defined inclusive one, there are no infra-red divergences. In addition if we define each jet as all the particles of an event whose momenta lie in some cone of non-zero half angle (δ, say) and allow for a fraction of the energy up to some maximum (ϵ, say) to be carried by particles outside of the jets, then the limit in which the masses of the quarks are set equal to zero is non-singular. In the limit where these masses are much smaller than Q^2 this will leave us with two mass scales Q^2 and μ^2, where μ is the renormalization point. Any $\log Q^2$ terms must therefore be of the form $\log Q^2/\mu^2$, so that by choosing μ^2 to be equal to Q^2 we end up with a series in $\bar{g}^2(Q^2)$ with no $\log Q^2$ terms. There still remain $\log \delta$ and $\log \epsilon$ terms, so that if the first few terms of this series are to represent accurately the jet cross-section δ and ϵ should not be chosen too small. Explicit examples are given in Ref. 10).

In this talk I shall concentrate on processes in which the $\log Q^2$ factors coming from the loop momenta are present *). One of the most interesting of these processes is the inclusive production of a massive lepton pair in hadronic collisions. The usual explanation of this process is due to Drell and Yan [11] and is that a quark from one of the initial hadrons annihilates an antiquark from the other, the resulting massive photon then decays into the observed lepton pair (Fig. 1a). This is represented by the formula

---

*) In these processes the limit in which the quark masses are set equal to zero is singular. These masses provide the scale for the logarithms.

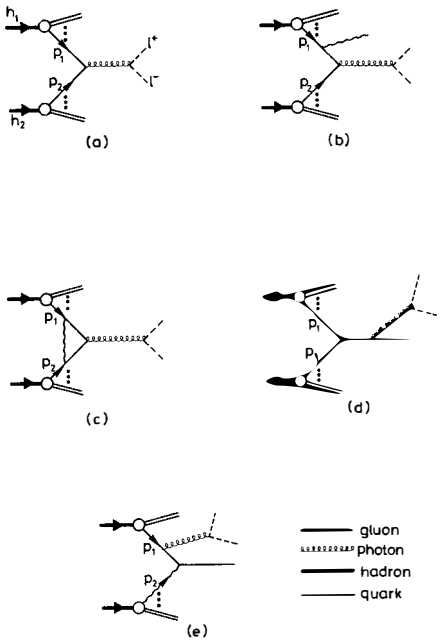

Fig. 1 Sample diagrams which contribute to massive lepton pair production.

$$\frac{d\sigma}{d\,Q^2} = \frac{4\,\pi\,\alpha^2}{3n\,Q^4} \sum_{\substack{\text{quark}\\ \text{flavours a}}} Q_a^2 \int_0^1 dx_1\,dx_2\,x_1\,x_2\,\delta(x_1\,x_2 - \tau) \left[G_{q^a/h_1}(x_1)\; G_{\bar{q}^a/h_2}(x_2) + G_{\bar{q}^a/h_1}(x_1)\; G_{q^a/h_2}(x_2) \right] \tag{1}$$

where h is the number of colours and $G_{q/h}(x)$ is the probability of finding a quark q in a hadron h with a fraction x of its longitudinal momentum. In QCD, however, in addition to the simple diagram of Fig. 1a there exist diagrams such as those of Figs. 1b, 1c, and naïvely it would seem that these diagrams would spoil the simple probabilistic picture of Eq. (1). These diagrams are of higher order in the coupling constant but each factor of g^2 is accompanied by a factor of $\log Q^2$ and so they cannot be neglected. We can also ask what is so special about quark-antiquark annihilation. For example the subprocesses $qg \to \ell^+\ell^- x$ *) (Figs. 1d and 1e) and $q\bar{q} \to \ell^+\ell^- x$ give equally important contributions ($g^2 \log Q^2$ and $g^4 \log^2 Q^2$, respectively). Moreover, for the subprocess $q\bar{q} \to \ell^+\ell^- x$ we can use only valence quarks and therefore this subprocess may be expected to be important. In fact this was the first mechanism suggested for massive lepton pair production [12]. In this talk (Section 3) we will discover why the Drell-Yan model [Eq. (1)] is so special, and why the diagrams of Figs. 1b-1e, or other subprocesses do not invalidate it.

Another interesting process is the production of particles or jets with large transverse momenta in hadronic collisions. The usual parton model philosophy [3] concerning these processes is that an elastic large angle scattering takes place between two "constituents" of the initial hadrons, one of the resulting constituents then fragments forming the trigger particle. This is represented by Fig. 2 and by

$$E_c \frac{d\sigma}{d^3p_c}(A + B \to CX) = \sum_{a,b,c,d} \int_0 dx_a\, dx_b \frac{dx_c}{x_c^2}\, G_{a/A}(x_a)\, G_{b/B}(x_b)\, \tilde{G}_{c/c}(x_c)\, \delta(s' + t' + u') \frac{s'}{\pi} \frac{d\sigma}{dt'}(ab \to cd)$$

$$\left| \begin{array}{l} s' = x_a x_b s \\ t' = \frac{x_a}{x_c} t \\ u' = \frac{x_b}{x_c} u \end{array} \right.$$

(2)

*) Throughout this talk q ($\bar{q}$) signifies a quark (antiquark), g signifies a gluon and ℓ a lepton.

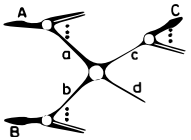

Fig. 2 Parton model description of the inclusive production of particle with large transverse momenta.

where $\tilde{G}_{C/c}(x_c)$ is the probability of constituent c to fragment into particle C, C carrying a fraction x_c of the longitudinal momentum of c. Dimensional counting rules have been derived from which the asymptotic behaviour of the cross-section corresponding to each subprocess (i.e., choice of a,b,c,d) can be calculated. We will see (in Section 4) that within the context of QCD we can predict both the normalization and asymptotic behaviour of the cross-section.

From our studies of the processes mentioned above, and from some other processes (such as the production of massive lepton pairs with large transverse momentum, or the production of jets in deep inelastic scattering, which will be discussed in Section 5), we conclude that there is a surprisingly simple ansatz with which one can adapt the predictions of the parton model to those of QCD. This ansatz is presented in Section 6. We start, however, by considering a well-understood process, deep inelastic lepton hadron scattering, and reproduce the prediction for the violations of Bjorken scaling using a technique which can also be used for other hard scattering processes.

2. - DEEP INELASTIC LEPTON-HADRON SCATTERING

In the case of deep inelastic lepton-hadron scattering, the use of the operator product expansion (OPE) and the renormalization group enable us to predict the violations of Bjorken scaling [5),6)]. In this section we will demonstrate that the same predictions can be obtained from the simple approach outlined in the Introduction and by keeping the leading logarithmic terms in each order of perturbation theory for the hard scattering subprocess.

As an example, let us consider the difference of νW_2 for an up (u) quark and a down (d) quark. This quantity is particularly simple to study within the OPE scheme since each moment with respect to x is asymptotically governed by a single operator *). In terms of diagrams, only those diagrams in which the electromagnetic current couplès directly to the valence quark (e.g., those of Fig. 3a,b,c) do not cancel, since the electromagnetic charges of the up and down quarks are different. Diagrams in which the electromagnetic current couples to the sea quarks (e.g., Fig. 3d,e) in a way which does not depend on the charge of the valence quark cancel.

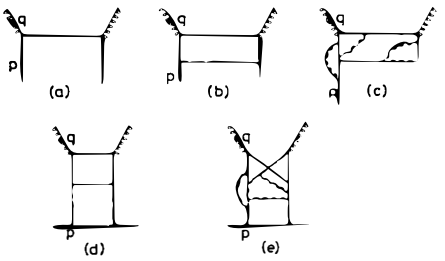

Fig. 3 A sample set of diagrams which contribute to the deep inelastic structure functions of a quark.

From the OPE and the renormalization group [5),6)] we have

$$M^n(q^2) \equiv \int_0^1 \left(\nu W_2^{eu}(x,q^2) - \nu W_2^{ed}(x,q^2)\right) x^{n-2}dx$$

$$q^2 \to -\infty \quad C^h(\bar{g}(q^2),\mu^2)\langle p|O^{(n)}|p\rangle \left[\frac{\bar{g}^2(q^2)}{\bar{g}^2(\mu^2)}\right]^{dn} \tag{3}$$

C^n is a calculable power series in $\bar{g}(Q^2)$, O^n is the relevant operator (in this case $O^n = \frac{1}{2}i^{n-1} S \bar{\psi} \gamma_{\mu_1} D_{\mu_2} \cdots D_{\mu_n} \tau^a \psi$ where S is the symmetrization of the Lorentz indices, τ^a are the flavour group generators and D_μ is the covariant derivative) and μ is the renormalization point. d_n is a calculable constant and is related to the anomalous dimension γ^n of O^n by

---

*) The structure functions themselves involve the mixing of quark and gluon operators ; this mixing slightly complicates the technical details but does not alter the essential features of the present discussion. For simplicity we study here an example without such mixing.

$$d_n = \frac{\gamma_o^n}{2\beta_o} \tag{4}$$

where

$$\gamma^n = \gamma_o^n \frac{g^2}{16\pi^2} + O(g^4) \tag{5}$$

and

$$\beta = -\beta_o \frac{g^3}{16\pi^2} + O(g^5) \tag{6}$$

where β is the usual beta funnction. $< p|$ is a quark state with momentum p.

From Eq. (3) we can recover the leading logarithms of the perturbation series in $g^2(\mu^2)$. Keeping only leading logarithms [i.e., neglecting $g^2(\mu^2)$ with respect to $g^2(\mu^2)\log q^2/\mu^2$] we have from the solution of the equation for the running coupling constant [5),6)]

$$\left[\frac{\bar{g}^2(q^2)}{\bar{g}^2(\mu^2)}\right]^{dn} \simeq \left[\frac{1}{1+\beta_o g^2(\mu^2)\log q^2/\mu^2}\right]^{dn} \tag{7}$$

C^n is a power series in $\bar{g}^2(Q^2)$ with no logarithms, and therefore in our leading logaritbm approximation we keep only the first term which is a constant. The requirement that M^n be independent of the renormalization point μ implies that in the leading logarithm approximation *)

$$\langle p|o^{(n)}|p\rangle = \langle p|o^{(n)}|p\rangle \text{ Bare}\left[1+\beta_o g^2(\mu^2)\log p^2/\mu^2\right]^{dn} \tag{8}$$

Thus if we calculate $M^n(q^2)$, by using ordinary perturbation theory in $g^2(\mu^2)$, and keeping the leading logarithms in $\log q^2/\mu^2$ and $\log p^2/\mu^2$ to each order we would obtain for the sum to all orders

$$M^n(q^2) \alpha \left[\frac{1+\beta_o g^2(\mu^2)\log p^2/\mu^2}{1+\beta_o g^2(\mu^2)\log p^2/\mu^2}\right]^{dn} \tag{9}$$

---

*) $< p|O^n|p >$ in the leading logarithm approximation can also be evaluated directly.

Convoluting (9) with the soft hadronic wave function gives

$$\frac{\int_0^1 dx\, x^{n-2}\left[\nu\omega_2{}^{ep}(x,q^2)-\nu\omega_2{}^{en}(x,q^2)\right]}{\int_0^1 dx\, x^{n-2}\left[\nu\omega_2{}^{ep}(x,q_0^2)-\nu\omega_2{}^{en}(x,q_0^2)\right]} = \left[\frac{\bar{g}^2(q^2)}{\bar{g}^2(q_0^2)}\right]^{dn} \qquad (10)$$

(where p, n signify proton and neutron, respectively) which is the rigorous result. We notice that we have obtained the correct result for the violations of Bjorken scaling in spite of neglecting interactions involving "spectator quarks". Thus we find that the first term in the "renormalization group improved" perturbation series in $\bar{g}^2(Q^2)$ is equivalent to summing the leading logarithms in the perturbation series in $g^2(\mu^2)$. The leading logarithms come from the region of integration in which all gluons carry a transverse momentum which is much smaller than Q^2.

Of course, it is only because we have a light cone expansion that we can have complete confidence in the result of summing leading logarithms. Nevertheless even in the absence of a rigorous technique the leading logarithms may still yield the correct asymptotic result. Indeed in the case of massive QED, the correct asymptotic behaviour of the structure functions was first derived using leading logarithm techniques by Gribov and Lipatov [13], and only later rederived using the light cone expansion by Christ, Hasslacher and Mueller [14]. Equation (9) has recently been derived by purely diagrammatical techniques in QCD [15] [see also Ref. 16].

In this Section we have seen that in the one case which we can study rigorously, the result can also be obtained by summing the series of leading logarithms. In the remaining sections we will study processes for which there is no clean analysis, by calculating diagrams and keeping the leading logarithms.

3. - MASSIVE LEPTON PAIR PRODUCTION

We now consider the inclusive production of a pair of leptons with large invariant mass in hadronic collisions, the Drell-Yan process [11]. Sample diagrams which contribute to this process are shown in Fig. 1.

Let us denote the lowest order contribution to cross-section for the subprocess $q\bar{q} \to \ell^+\ell^- x$ (that corresponding to Fig. 1a) by σ_o. Then when all the radiative corrections of order g^2 are calculated (including those of Fig. 1b and Fig. 1c) in the leading logarithm approximation one finds [17),18)] that these corrections are equal to

$$a(\tau)g^2\left[\log Q^2/p_1^2 + \log Q^2/p_2^2\right] \tag{11}$$

where $\tau \equiv Q^2/s$. It turns out that $a(\tau)$ is a very significant function, it is exactly the same function which appears in the order g^2 corrections to deep inelastic scattering on a quark. The structure function of a quark is proportional to

$$\delta(x-1) + a(x)g^2\log q^2/p^2 + O(g^4\log^2 q^2/p^2) \tag{12}$$

Thus, to this order at least, it seems that the deviations from the naïve Drell-Yan picture are intimately related to the violations of Bjorken scaling in deep inelastic scattering. In other words, the diagrams which spoil the simple Drell-Yan picture (such as those of Figs. 1b and 1c) are related to those which are responsible for the violation of Bjorken scaling (such as those of Figs. 3b, 3c). In particular to this order we can write a modified Drell-Yan formula

$$\frac{d\sigma}{dQ^2} = \frac{4\pi\alpha^2}{3nQ^4} \sum_{\substack{\text{quark} \\ \text{flavours } a}} Q_a^2 \int_0^1 dx_1\, dx_2\, x_1\, x_2\, \delta(x_1\, x_2 - \tau)$$

$$\left[G_q{}^a/h_1(x_1,Q^2)\; G_{\bar{q}}{}^a/h_2(x_2,Q^2) + G_{\bar{q}}{}^a/h_1(x_1,Q^2)\; G_q{}^a/h_2(x_2,Q^2)\right] \tag{13}$$

where the G distribution functions are the appropriate linear combinations of experimentally determined deep inelastic structure functions.

We now turn our attention to other subprocesses which contribute to massive lepton pair production. As an example let us consider qg scattering for which some lowest order diagrams are shown in Figs. 1d, 1e. When one calculates the contribution to the cross-section for the subprocess from the diagrams of Figs. 1d and 1e one finds [19] that the result is proportional to

$$g^2\left(1-2\tau(1-\tau)\right)\log Q^2/p_2^2\ \sigma_o \qquad (14)$$

Again the coefficient of $g^2\sigma_o$ is highly significant. It is the probability of finding an antiquark in a gluon with a fraction τ of its longitudinal momentum *). When the distribution functions are measured in deep inelastic scattering, they include the effects of gluons through diagrams such as those of Fig. 3d,e. Equation (14) implies that the contribution to the distribution functions from these diagrams is related to the contribution to the cross-section for lepton pair production from diagrams such as those of Figs. 1d and 1e. Thus even these diagrams are included in the right-hand side of Eq. (13). In other words the dominant contribution from the subprocess $qg \to \ell^+\ell^- x$ can be expressed as the probability of finding an antiquark in the gluon times the cross-section for this antiquark to annihilate the incident quark.

A similar feature has been found in all other subprocesses which have been studied (e.g., $qq \to \ell^+\ell^- x$, $gg \to \ell^+\ell^- x$ [19]). In each case the leading logarithmic terms can be absorbed into the distribution functions of the incident hadrons, so that the asymptotic behaviour of the cross-section is given by (13), where the G's are extracted from linear combinations of experimentally measured deep inelastic structure functions. Thus the dominant contribution can be represented by Fig. 4 where the shaded blocks represent these non-scaling distribution functions.

---

*) The moments of $1 - 2\tau(1-\tau)$ with respect to τ are thus proportional to one of the off diagonal elements in the anomalous dimension matrix of the lowest twist quark and gluon operators.

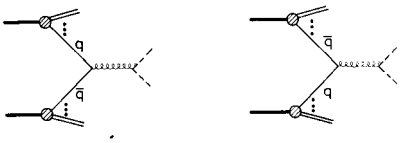

Fig. 4 The dominant contribution to massive lepton pair production in QCD. The shaded blobs represent, experimentally determined, non-scaling distribution functions.

Although this factorization of the leading logarithms has not been proved to all orders, no counter examples have been found so far, and the similarity between the diagrams in deep inelastic scattering and massive lepton pair production strongly suggest that it may indeed be true. An explicit calculation of higher order contributions is being performed by Fishbane and Yan [20].

We can now understand what is so special about the Drell-Yan formula. In its modified form [Eq. (13)] it includes not only the contributions from $q\bar{q}$ annihilation but also the dominant contributions from the other subprocesses. Since the scaling violations in the distribution functions are only logarithmic, the use of the original Drell-Yan formula [Eq. (1)] over a limited Q^2 range should be a good approximation.

I would like to conclude this section by briefly mentioning the corrections to (13). Equation (13) is true only for the leading logarithmic terms [i.e., for the leading term in $\bar{g}^2(Q^2)$], and so there will be logarithmic corrections to it. Whether or not these corrections are important at presently accessible values of s and Q^2 is an open question. It is not yet clear whether these corrections can also be calculated in a similar way to the leading terms *) ; in order for this to be so there would have to be a very remarkable factorization of the non-leading logarithms. This factorization has not been tested so far.

---

*) See, however, the model of Cabibbo and Petronzio [21].

4. - INCLUSIVE PRODUCTION OF PARTICLES AND JETS WITH LARGE TRANSVERSE MOMENTA

Deep inelastic scattering and massive lepton pair production both involve an off-shell photon, in this section we study a purely strong interaction process, the production of particles and jets with large transverse momenta in hadronic collisions. The mechanism usually believed to be responsible for this process has been described in the introduction, and can be summarized by Eq. (2) and Fig. 2. To see what, if anything, QCD can teach us about this process, let us study a concrete example quark (A) + quark (B) → → quark (C) + anything, up to order g^6 in the cross-section and as before in the leading logarithm approximation [22]. For simplicity we start with the case $x < 1$, where $x = (2E_c/\sqrt{s})$, in which case only the inelastic diagrams of Fig. 5 contribute. We notice that even in this order there are diagrams with a three-gluon vertex.

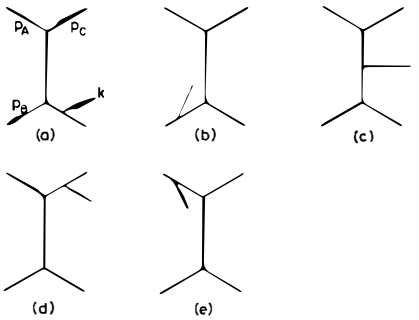

Fig. 5 Lowest order inelastic diagrams which contribute to the process $qq \to qX$.

There are a number of kinematic regions which contribute to the leading logarithmic behaviour. All these contributions can be interpreted in an elegant way. From the region where k is parallel to p_A (p_B) we obtain a contribution to $E_c(d\sigma/d^3p_c)$ of the form $\log s/p_A^2$, ($\log s/p_B^2$) which can be interpreted as being the convolution of the probability of finding a quark in quark A (B), and the Born term for quark-quark elastic fixed angle scattering (Fig.6a,b). In other words the coefficient of these logarithms is just the function "a" of Eqs. (11) and (12) (in spite of the presence of the three-gluon vertex). From the region where k is parallel to p_C,

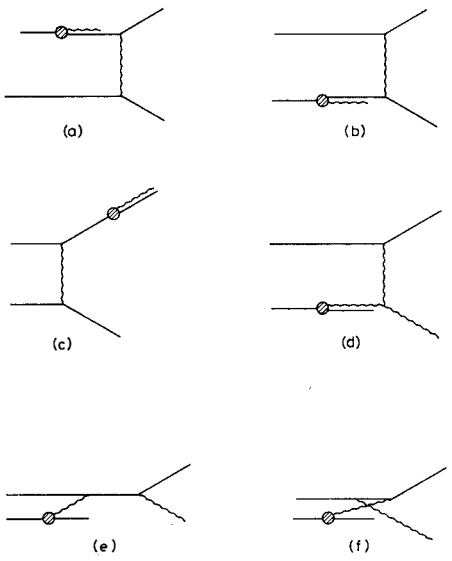

Fig. 6 Symbolic representation of the dominant contribution from the diagrams up to order g^6 for the process $qq \to qX$. The shaded blobs represent the non-scaling distribution and fragmentation functions.

we obtain a contribution which can be interpreted as the convolution of the Born term for q-q elastic fixed angle scattering, and the probability for one of the resulting quarks to fragment into the observed one + anything (Fig. 6c). The fragmentation function is just that which would be calculated from $e^+e^- \to qX$ and is related to the distribution function (in this order at least) by the Gribov-Lipatov reciprocity relations [23]. The final dominant contribution comes from the region in which k balances the transverse momentum of p_G, and this can be interpreted as the probability of finding a gluon in quark B with a fraction of the longitudinal momentum of B *) convoluted with the Born term for gq elastic fixed angle scattering (Figs. 6d, 6e, 6f).

---

*) The moments of this probability are, of course, proportional to an off-diagonal element in the anomalous dimension matrix for the lowest twist quark and gluon operators.

At $x = 1$ in addition to the contributions from the diagrams of Fig. 5, one must also include the diagrams which contribute to the elastic qq scattering amplitude. The leading $\log s/p^2$ contributions can also be absorbed into the initial distribution and final fragmentation functions. In addition to these $\log s/p^2$ terms, after renormalization there will also be $g^6(\mu^2) \log s/\mu^2$ terms. These terms are exactly those which, when combined with the $g^4(\mu^2)$ contribution from the Born term give the first two terms in the expansion of $g^4(s)$, the running coupling constant.

Thus we conclude that the cross-section for $qq \to qX$ to order g^6 in the cross-section and in the leading logarithmic approximation can be written in the form (Fig. 6)

$$E_c \frac{d\sigma}{d^3p_c} (A + B \to CX)$$

$$= \sum_{a,b:c,d} \int_0^1 dx_a \, dx_b \, \frac{dx_c}{x_c^2} \, G_{a/A}(x_a, Q^2) \, G_{b/B}(x_b, Q^2) \, \hat{G}_{c/C}(x_c, Q^2)$$

$$\delta(s' + t' + u') \frac{s'}{\pi} \frac{d\sigma^{(B)}}{dt'} (a + b \to c \, d)$$

$$\left| \begin{array}{l} s' = x_a x_b s \\ t' = \dfrac{x_a}{x_c} t \\ u' = \dfrac{x_b}{x_c} u \end{array} \right. \qquad (15)$$

where $d\sigma^{(B)}/dt'$ is the Born term contribution to the elastic cross-section for qg or qq scattering, calculated using the running coupling constant, and Q^2 represents a typical large invariant mass squared (we assume $s \sim t \sim u \sim Q^2$). In the leading logarithm approximation we cannot distinguish between log s, log t and log u.

Again we have not proved that this simple factorization will hold to all orders and for all subprocesses, nevertheless we feel that the result is significant and very suggestive of an ansatz for calculating cross-sections for inclusive production at large transverse momenta. The ansatz is that the cross-section is given by (15) where now we sum over all combinations of quarks and gluons. This is represented in Fig. 7 where the dotted line represents a quark or a gluon and the shaded blobs represent non-scaling distribution or fragmentation functions. The "B" implies we should take

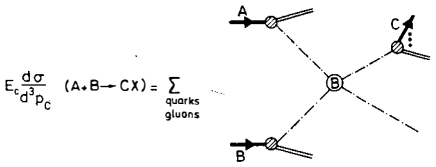

Fig. 7 Dominant contribution to $E_c(d\sigma/d^3p_c)$. The —·—·—·— line represents quarks and gluons, the shaded blobs represent non-scaling distribution and fragmentation functions and the "B" implies we take the Born term contribution calculated using the running coupling constant.

the Born term, calculated using the running coupling constant. Similar prescriptions have already been used by many authors [e.g., Refs. 24)-28)]. Thus if we believe we know the distribution and fragmentation functions (including those for gluons !) we are able to predict not only the behaviour but also the normalization of large $p_\perp$ distributions.

The above results also suggest that the cross-sections for "jet" production at large transverse momenta can be reliably calculated within the present framework ; (up to order g^6 in qq scattering this is a simple consequence of the calculation presented above). All the $\log p_A^2$ and $\log p_B^2$ terms can be absorbed into the initial distribution functions as above, leaving us with a series in $\bar{g}^2(Q^2)$ whose coefficients are calculable and depend on the kinematic parameters of the jet.

5. - SOME MULTIJET PROCESSES

In the previous sections we have seen several examples of processes in which parton model ideas proved to be approximately valid also in QCD. Although, unlike in the parton model, transverse momenta are not bounded in QCD, the leading logarithms in these processes come from a region of integration in which all the quarks and gluons have a transverse momentum relative to the initial particles or trigger particle which is much smaller than Q^2, a typical large invariant of the process. The only dynamical damping in the transverse momentum is due to the propagators, which tend to behave

like $1/k_\perp^2$, but even this gentle damping is sufficient to reproduce the parton-like results. In this section I would like to present some examples where the most naïve parton model expectations are not fulfilled, but nevertheless where definite QCD predictions can still be made.

We start by considering σ_L, the longitudinal cross-section in deep inelastic scattering. It is proportional to the $p^\mu p^\nu$ projection of $W^{\mu\nu}$, where $W^{\mu\nu}$ is the usual tensor of deep inelastic scattering [2]. As an example consider the scattering on a quark of momentum p, the diagram of lowest order which contributes to σ_L (in the limit where we neglect p^2/q^2 terms) is shown in Fig. 8. The numerator of this diagram in the Feynman gauge is proportional to (we average over the quark spins)

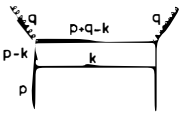

Fig. 8 Lowest order diagram which contributes to the longitudinal cross-section of a quark.

$$\mathrm{Tr}\left[\not{p}\gamma^\lambda\ (\not{p}-\not{k})\ \not{p}\ (\not{p}+\not{q}-\not{k})\ \not{p}\ (\not{p}-\not{k})\gamma\lambda\right]$$
$$\sim\left[(p-k)^2\right]^2 p.(q-k) \qquad (16)$$

Thus we see that both the factors of $1/(p-k)^2$ from the propagators are cancelled and there is no damping of the transverse momentum. The usual parton model derivation [1] of the relation between σ_L and the average transverse momentum squared of a quark

$$\frac{\sigma_L}{\sigma_T} = \frac{4\langle k^2\rangle}{(-q^2)} \qquad (17)$$

relies, among other things, on the assumption that the transverse momentum is damped. It is therefore no surprise that (17) is not valid in QCD. Even in lowest order of perturbation theory it is not valid, since in lowest order

$$F_L \propto g^2 X \tag{18}$$

whereas

$$\frac{\langle k_\perp^2 \rangle F_T}{(-q^2)} \propto g^2(7-2X+4X^2) \tag{19}$$

Nevertheless, the invalidity of (17) does not prevent us from being able to make predictions for σ_L or $\langle k_\perp^2 \rangle$. σ_L in fact can be calculated using renormalization group techniques [7),9)], here we shall consider the transverse momentum distribution of a quark jet (which cannot be studied by such techniques). Some sample lowest order diagrams which contribute to the production of a quark jet with large transverse momentum are shown in Figs. 9a and 9b. From similar considerations to those of the previous sections it seems that the dominant contributions from higher order diagrams (e.g., from Figs. 9c and 9d) will again be absorbed into the non-scaling quark and gluon distribution functions [29)]. Thus we have for the transverse momentum distribution of a quark jet

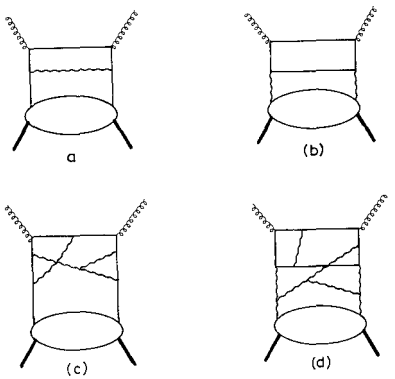

Fig. 9 Sample diagrams which contribute to the production of a quark jet with large transverse momentum.

$$\frac{d\sigma_T}{dk_\perp^2}(x, k_\perp, q^2) = \int_x^1 \frac{dy}{y}\left[G_{q/p}(y, q^2)\frac{d\sigma_T^{(o)}}{dk_\perp^2}\left(\frac{x}{y}, k_\perp, q^2\right) + G_{g/p}(y, q^2)\frac{d\bar{\sigma}_T^{(o)}}{dk_\perp^2}\left(\frac{x}{y}, k_\perp, q^2\right)\right] \quad (20)$$

where $d\sigma^{(o)}/dk_\perp^2$ and $d\bar{\sigma}^{(o)}/dk_\perp^2$ are the contributions from the lowest order diagrams to the cross-section for $q\gamma^* \to qX$ and $g\gamma^* \to qX$, calculated using the running coupling constant. Equation (20) is represented pictorially in Fig. 10. The production of jets with large transverse momentum in deep inelastic scattering has been studied using Eq. (20) by Altarelli and Martinelli [30].

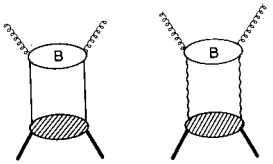

Fig. 10 The dominant contribution to the production of a quark jet with large transverse momentum. The shaded blobs represent non-scaling distribution functions and the "B" implies we take the lowest non-zero contribution for the subprocess, calculated using the running coupling constant.

Another interesting process is the inclusive production of massive lepton pairs with large transverse momenta. The lowest order diagrams for this process are shown in Fig. 11. Again the indications are that the higher order corrections can be absorbed into the quark, antiquark or gluon distribution functions, so that we have

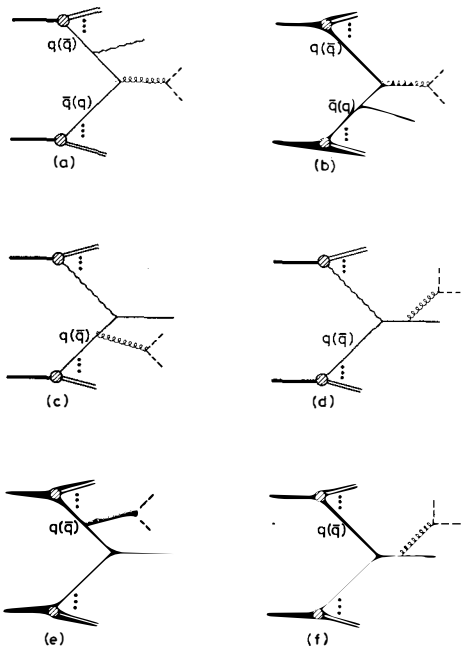

Fig. 11 Dominant contribution to the production of a massive lepton pair with large transverse momentum. The shaded blobs represent non-scaling distribution functions.

$$\frac{d\sigma}{dk_\perp^2 dQ^2} = \int y_1 dy_1 y_2 dy_2 \left\{ \left[G_{q/h_1}(y_1,Q^2)\ G_{\bar{q}/h_2}(y_2,Q^2) + G_{\bar{q}/h_1}(y_1,Q^2)\ G_{q/h_2}(y_2,Q^2) \right] \frac{d\sigma^{(B)}}{dk_\perp^2 dQ^2}(q\bar{q} \to l^+l^- X) + \left[Gg/h_1(y_1,Q^2)\ Gq/h_2(y_2,Q^2) + G_{q/h_1}(y_1,Q^2)\ Gg/h_2(y_2,Q^2) \right] \frac{d\sigma^{(B)}}{dk_\perp^2 dQ^2}(qg \to l^+l^- X) + \left[Gg/h_1(y_1,Q^2)\ G_{\bar{q}/h_2}(y_2,Q^2) + G_{\bar{q}/h_1}(y_1,Q^2)\ Gg/h_2(y_2,Q^2) \right] \frac{d\sigma^{(B)}}{dk_\perp^2 dQ^2}(\bar{q}g \to l^+l^- X) \right\} \tag{21}$$

All the cross-sections are calculated using the running coupling constant. Equation (21) justifies using the shaded blobs in Fig. 11). An approach similar to Eq. (21) has been used by many authors [31)-33)]. Thus, for example, the dominant contribution for the process $qq \to \ell^+\ell^- X$, where the lepton pair has a large transverse momentum, is given by the probability of finding a gluon with small transverse momentum in one of the initial quarks convoluted with the cross-section for this gluon to scatter on the other quark.

There is, however, no simple relationship between the transverse momentum of the lepton pair and the transverse momentum of the quarks in deep inelastic scattering. For example in $q\bar{q} \to \ell^+\ell^- X$ one finds [31)]

$$\langle k_\perp^2 \rangle_{\mu^+\mu^-} \; Q^4 \frac{d\sigma}{dQ^2} \sim Q^2 \; (1-\tau^3) \qquad (22)$$

which should be compared to (18), (19). This is clearly to be expected since when the transverse momenta are of the order of q^2, even in the parton picture the Bjorken x is no longer equal to the fraction of the longitudinal momentum carried by the quark.

The above discussion applies to transverse momenta whose distribution can be calculated perturbatively and which increase with Q^2. In addition there may be a primordial transverse momentum in the hadronic wave function, but this should not increase with Q^2, and we have no way of calculating it. From phenomenological studies it is estimated to be about two to three times the "usual" hadronic transverse momentum cut-off of 300 MeV [31)], and is phenomenologically relevant at present values of Q^2.

6. - CONCLUSIONS

The results presented in this talk suggest that in QCD the correct way to calculate the asymptotic behaviour of hard scattering cross-sections as $Q^2 \to \infty$ (where Q^2 is a typical large invariant of the process) is given by the following simple ansatz :

1) take the parton model hard scattering formula ;

2) replace the scaling distribution and fragmentation functions by the appropriate non-scaling ones ; in the case of quarks and antiquarks these are measured in deep inelastic scattering, whereas, for the gluon distribution, model assumptions have to be made ;

3) keep only the contribution of lowest order in the coupling constant (which is non-zero) for the hard scattering subprocess, calculated using the running coupling constant, $\bar{g}(Q^2)$.

Whether with this ansatz we can understand the present data on hard scattering processes will be discussed in detail during this meeting. It is, however, very satisfying that at last we can make QCD predictions for these processes with some confidence, and that the beautiful probabilistic picture is more general than the parton model.

REFERENCES

1) R.P. Feynman, "Photon-Hadron Interactions" (Published by W.A. Benjamin, Reading, Massachusetts ; 1972).

2) J. Ellis, "Deep Hadronic Structure" (Lectures presented at the Les Houches Summer School ; July 1976). To be published in the Proceedings.

3) D. Sivers, S.J. Brodsky and R. Blankenbecler, Physics Reports 23C, 1 (1976).

4) P.V. Landshoff and J.C. Polkinghorne, Physics Reports 5C, 1 (1972).

5) D. Gross and F. Wilczek, Phys.Rev. D8, 3633 (1973) ; Phys.Rev. D9, 980 (1974).

6) H.D. Politzer, Physics Reports 14C, 129 (1974).

7) A. De Rujula, H. Georgi and H.D. Politzer, Ann.Phys. 103, 315 (1977).

8) A.J. Buras and K.J.F. Gaemers, Nuclear Phys. B132, 249 (1978) ; Phys.Letters 71B, 106 (1977) and references therein.

9) A.J. Buras, E.G. Floratos, D.A. Ross and C.T. Sachrajda, Nuclear Phys. B131, 308 (1977).

10) G. Sterman and S. Weinberg, Phys.Rev.Letters 39, 1436 (1977).

11) S.D. Drell and T.M. Yan, Phys.Rev.Letters 25, 316 (1970) ; Ann.Phys. 66, 578 (1971).

12) S. Berman, D. Levy and T. Neff, Phys.Rev.Letters 23, 1363 (1972).

13) V.N. Gribov and L.N. Lipatov, Soviet J.Nucl.Phys. 15, 438 (1972).

14) N. Christ, B. Hasslacher and A.H. Mueller, Phys.Rev. D6, 3543 (1972).

15) A. Carter and C.H. Llewellyn Smith, Oxford University Preprint (in preparation).

16) D. Amati, R. Petronzio and G. Veneziano, CERN Preprint TH. 2470 (1978).

17) H.D. Politzer, Nuclear Phys. B129, 301 (1977).

18) H.D. Politzer, CALTECH Preprint CALT-68-628 (1977).

19) C.T. Sachrajda, Phys.Letters 73B, 185 (1978).

20) P. Fishbane and T.M. Yan, CERN Preprint (in preparation).

21) N. Cabibbo and R. Petronzio, CERN Preprint TH. 2440 (1978).

22) C.T. Sachrajda, CERN Preprint TH. 2459 (1978), to be published in Phys.Letters B.

23) V.N. Gribov and L.N. Lipatov, Soviet J.Nucl.Phys. 15, 675 (1972).

24) R.F. Cahalan, K.A. Geer, J. Kogut and L. Susskind, Phys.Rev. D11, 1199 (1975).

25) R. Cutler and D. Sivers, Phys.Rev. D16, 679 (1977) ; Argonne Preprint ANL-HEP-PR-77-40 (1977).

26) B.L. Combridge, J. Kripfganz and J. Ranft, Phys.Letters 70B, 234 (1977).

27) R. Raitio and R. Sosnowski, Helsinki Preprint HU-TFT-77-22 (1977).

28) A. Contogouris, These proceedings.

29) K.H. Craig and C.H. Llewellyn Smith, Phys.Letters 72B, 349 (1978).

30) G. Altarelli and G. Martinelli, University of Rome Preprint (1978).

31) G. Altarelli, G. Parisi and R. Petronzio, CERN Preprints TH. 2413 (1977) and 2450 (1978) ;
R. Petronzio, These proceedings.

32) K. Kajantie and R. Raitio, Helsinki Preprint HU-TFT-77-21 (1977).

33) C. Michael, These proceedings.

DILEPTONS AT MORIOND

Leon M. Lederman
Columbia University

Introduction

This lecture will be divided, like Gaul, into 3 parts:

1. Status of Upsilon Data
2. Scaling and X_F(or y) behavior
3. Dilepton Transverse Montenta

We repeat here for convenience, views of the Fermilab E-288 apparatus (Fig.1) and a list of the Columbia-Fermilab-Stony Brook team (Table I). The most relevant features of the apparatus are (1) the resolution (Fig. 2), the mass acceptance (Fig.3) and the fact that same sign pairs are measured in situ as a measure of the background.

We have published data on Υ and continuum [1,2,3] based on about 800 hours (3 calendar months) of data taking - this yielded 26,000 events above 5 GeV and about 1000 Υ events. We have since multiplied the data by about 6-7 - this from Nov 10 to April 10. The 5 calendar months is equivalent to 1500 hours of data taking (factor 2) and a higher luminosity (factor 3-4) deriving from a thicker target, and a careful study of the rate effects in various detectors which resulted in raising the incident beam to 8x10" ppp.
(The new sample of data has only been looked at in a preliminary way.) We have also run at 200 and 300 GeV to study scaling properties and, since 10 April, in a new arrangement designed to improve the resolution from $\sigma\sim 2\ \% \rightarrow \sigma\sim 1\text{-}1\frac{1}{2}\ \%$

II Upsilon Physics

The status of the data is given in table II
Stimulated by a request from the PLUTO group at DESY we have made a careful check of the systematics of the absolute energy scale. In late March, we communicated the results: $m(\Upsilon)=9.45\pm.07$ where the error includes 60% of the probability. We estimated that there is only a 10% chance of the mass being outside of $9.45\pm .10$ GeV. (See para.5) We summarize the upsilon regime by the following points:

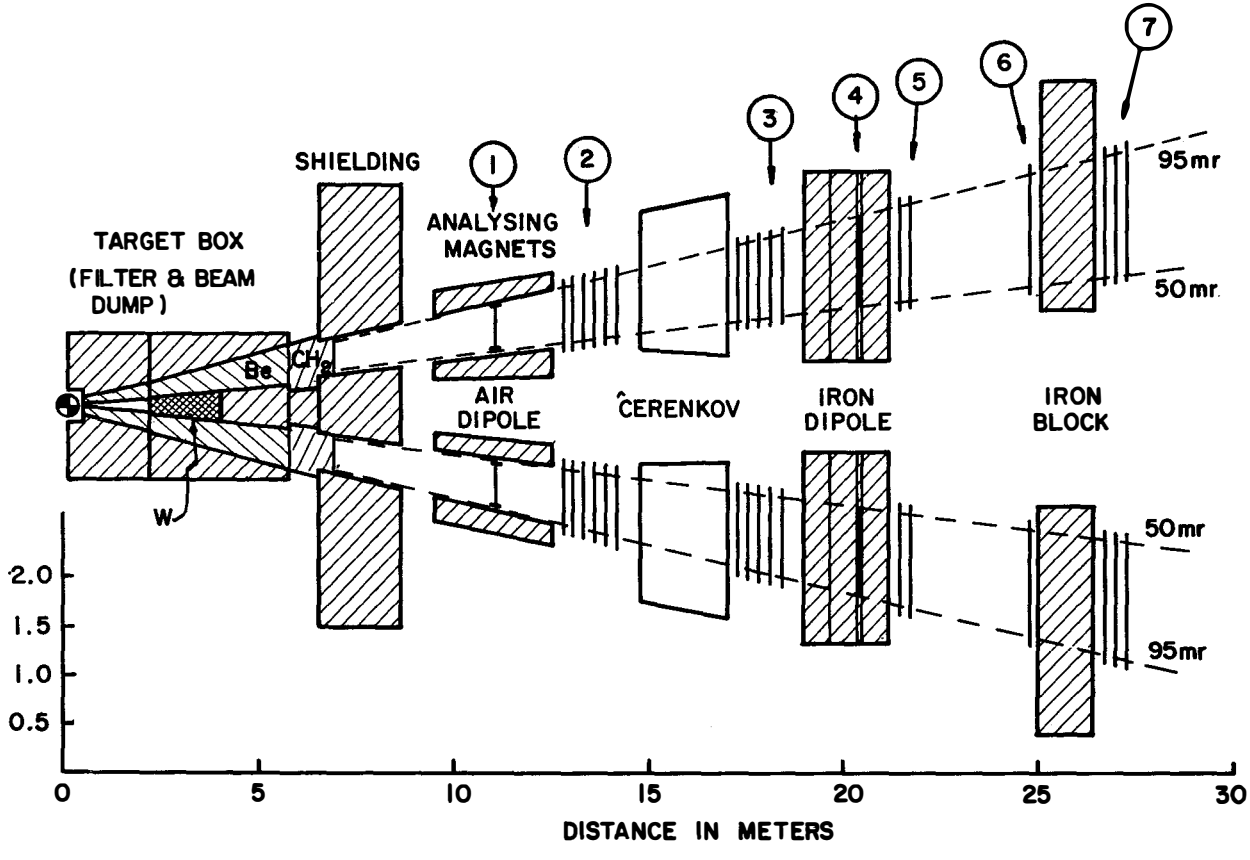

FIG. 1

μμ II apparatus.

TABLE I

Fermilab
E-288

Columbia *	Fermilab +	Stony Brook *
S.W. Herb	W.R. Innes	D.M. Kaplan
D.C. Hom	J.A. Appel	A.S. Ito
L.M. Lederman	B.C. Brown	H. Jostlein
J.C. Sens	C.N. Brown	R.D. Kephart
H.D. Snyder	K. Ueno	
J.K. Yoh	T. Yamanuchi	

* N.S.F.

\+ D.O.E.

TABLE II

Mass Fit Parameters [a],[b],[c]

P_{beam}	200	300	400
$< y >_{acceptance}$	0.40	0.21	0.03
A nb/GeV	10.4±.11±2.2	2.47±0.03±0.5	2.70±.02±0.5
b GeV $^{-1}$	1.39±.02±0.02	1.04±0.01±0.02	0.97±0.01±0.02
x^2/DF	42/34	35/54	78/74
m(Υ) GeV	9.46 (fixed)	9.45±0.02±0.10	9.46±0.012±0.10
B do/dy pb	0.002±0.002	0.094±0.012	0.29±0.012
m(Υ'-Υ) GeV	0.6 (fixed)	0.69±0.05±0.05	0.60±0.03±0.05
B do/dy Υ'/Υ	0.67±0.94	0.46±0.09±0.10	0.38±0.04±0.10
m(Υ''-Υ)	1.0 (fixed)	1.0 (fixed)	0.97±0.10
B do/dy Υ''/Υ	0.10±0.55	0.00±0.06	0.08±0.04±0.04
x^2/DF	12.6/19	12.1/16	14.7/16
Υ/cont. GeV	0.1±.0	0.67±0.10	0.97±0.05
Υ'/cont. GeV	-	0.58±0.14	0.66±0.08
Υ''/cont. GeV	-	0.00±0.13	0.19±0.12

[a] Continuum form: $do/dmdy = A\ e^{-bm}$. Cross sections are evaluated at $y = < y >_{acceptance}$.

[b] The first error is statistical and the second is systematic.

[c] See Ref. 3.

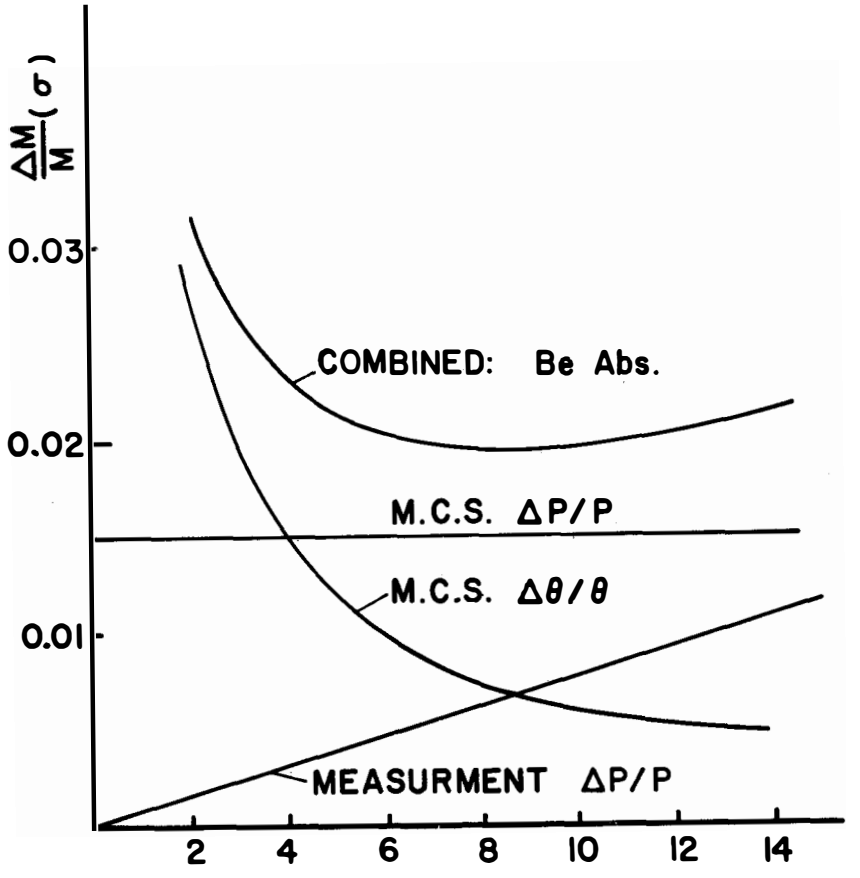

FIG. 2

Mass resolution with all Be absorber

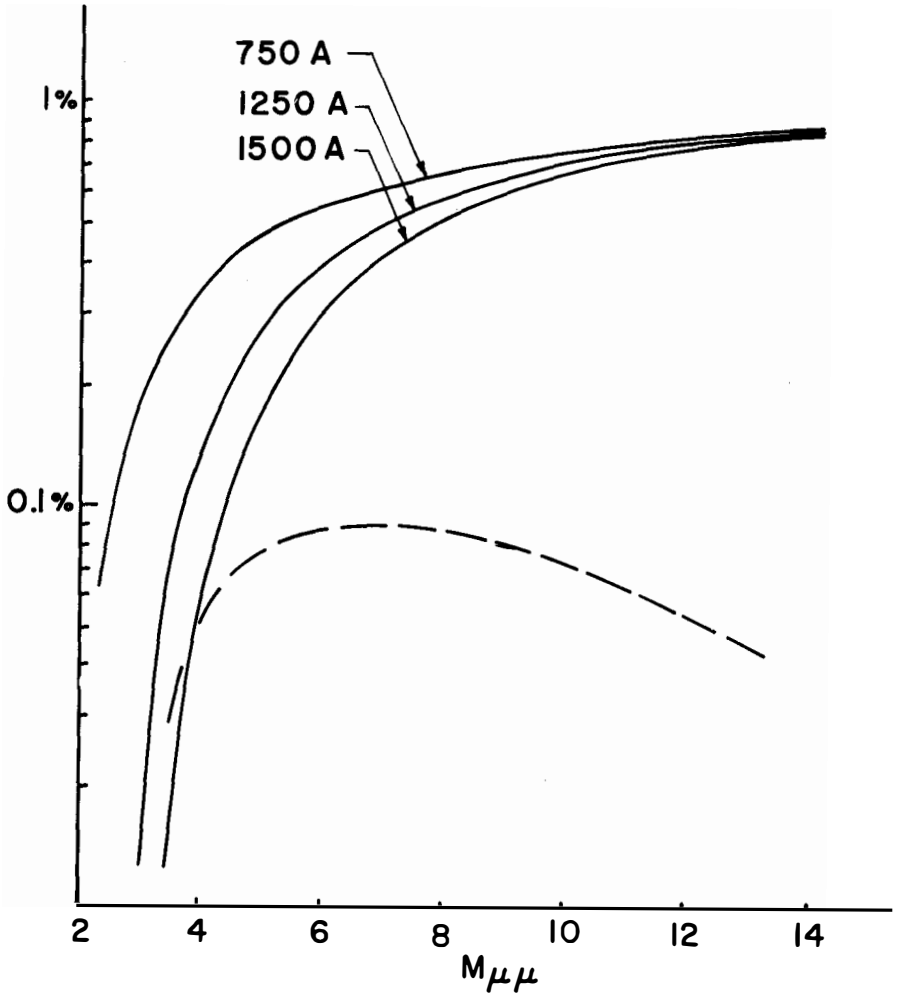

FIG. 3

Mass acceptance for various magnet currents. The dashed curve is the μμ I acceptance. This acceptance is calculated with isotropic decay. There are ~ 30% effects due to other distributions.

1) $\Upsilon''(10.4)$ appears to be well established by a combination of our new data. The bulk of this was taken at high intensity and therefore had slightly worse resolution than our data of last summer. The existence of Υ'' here is very sensitive to the spacing of the first two peaks. Thus we appeal to our most recent running which is designed to improve the resolution. So far the statistical accuracy at the third peak is very small but these data establish the Υ-Υ' splitting as 621 ± 40 MeV (preliminary!). With this fixed the high intensity data finds that a peak at 10.4 GeV is required by 5-6 standard deviations.

2) The ratio of σB for $\Upsilon:\Upsilon':\Upsilon''$ is observed to be $1: .38 \pm .04: .12 \pm .04$, remarkably close to the predicted[4] result 1: .3: .15 based upon a $q\bar{q}$ model with $e_q = 1/3$. One deduction from the ratio of Υ and Υ' is that $\Upsilon' \to \Upsilon + 2\pi$ must be strongly suppressed. (See Gottfried at Hamburg) Absolute yields, $Bd\sigma/dy$ also favors 1/3 charge.

3) The splitting between Υ and Υ' is not given by the linear and coulomb potential which is adjusted to charmonium levels. However it appears that a large class of potentials, including $V_0 \sim \ell nr/r_0$ can be made consistent with both ψ and Υ data. Thus we interpret our splitting result as giving strong evidence that the quark forces are remarkably similar - consistent with the flavor independence which is so crucial to QCD.

4) We can learn something about the hadroproduction process by comparing the P_T and the rapidity, y, behavior of Υ and the continuum of nearby masses. Since these distributions in the Drell-Yan case are characteristic of the annihilating quark motions, it would seem obvious that if Υ were also produced by such a process, its P_T and y behavior should be similar. The data appear to contradict this mechanism although we are still studying this question.

5) Recent (May '78) results from Desy [5] confirm the reaction: $e^+ + e^- \rightarrow \Upsilon$ (9.46). The integrated cross section yields $\Gamma_{ee} = 1.2 \pm .4$ KeV and this shows some preference for Q=1/3. The observation is completely consistent with the $Q\bar{Q} = b\bar{b}$ interpretation of Υ. (The Desy search started at 9.35 and stopped at 9.48.)

6) Finally, we see no bumps above the upsilon and the data contains ~ 30 events above 15 GeV. If we accept the $e_b = 1/3$ interpretation, i.e. Q=b, then we can set a limit on the mass of a hypothetical t ($e_t = 2/3$) quark. Assuming that the hadroproduction of the object $t\bar{t}$ is at least $4 \times \sigma_{\beta}$ for the upsilon, preliminary analysis indicates that $m_t > 7\text{-}7.5$ GeV.

III Scaling

Before launching into a discussion of the dimuon continuum, we show in Fig. 4 the behavior of the cross-section with A i.e. $\sigma \sim A^{\alpha}$. We note that as the mass increases, $\alpha \rightarrow 1$ indicating that for $m \geq 4$ GeV, we are dealing with hard collisions. This is a necessary although far from sufficient condition for the validity of the Drell-Yan process. We will see that there are a variety of tests of the model - the model never fails or fails only in its most "naive" form. This was seen in Prof. Pilcher's data on pion induced dimuon production and in our scaling test. However, a complete and rigouous test eludes us and will probably continue to do so until the data on lepton-nucleon scattering gets much better.

We have taken data at 200 and 300 GeV to compare with the 400 GeV running. In a fixed laboratory arrangement, a decrease of incident energy implies an acceptance which shifts forward. The acceptance in rapidity at 400 GeV is roughly gaussion shaped and extends from y=-0.3 to y=+0.3. At $\sqrt{s}$ =23.7GeV, the mean rapidity shifts to y=+.20 and for 19.4 GeV $\langle y \rangle$=0.40.

Scaling of the inclusive dilepton continuum has an intuitive dimensional appeal. It signals the absence of dimensional parameters (conventionally energy) comparable to $\sqrt{s}$, m.

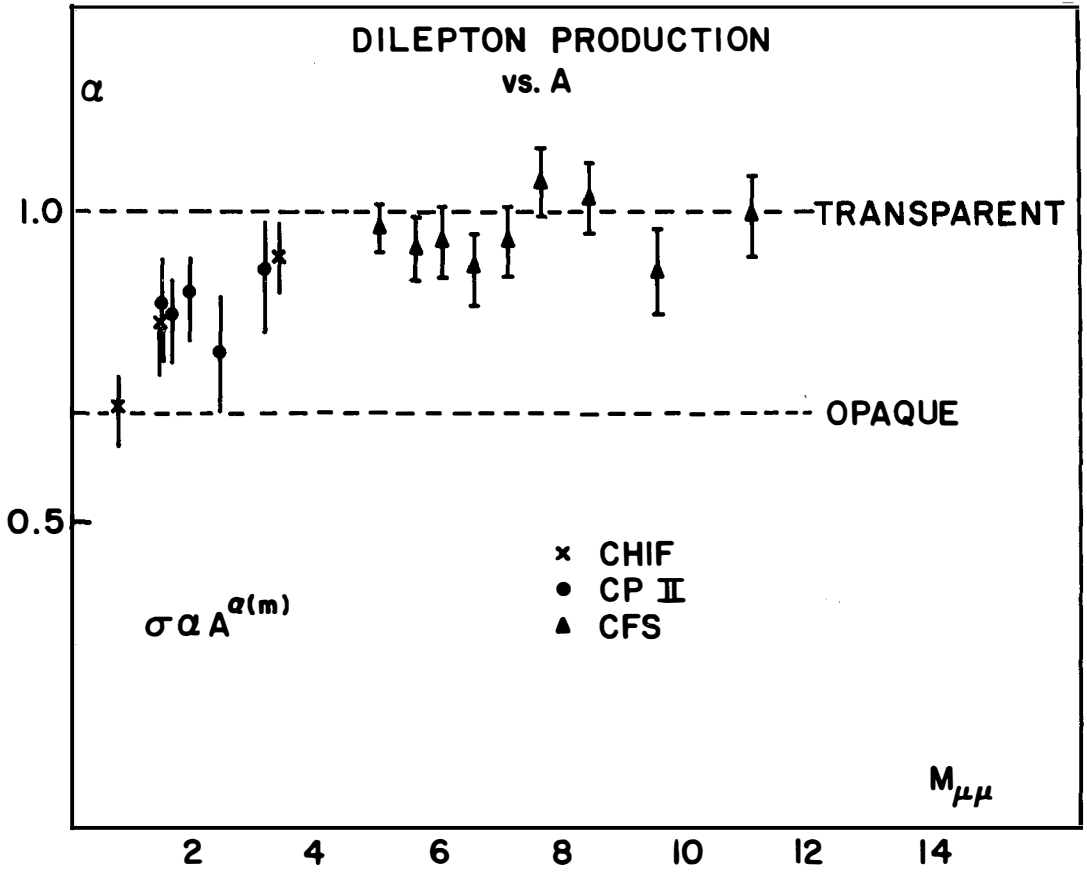

FIG. 4 Behavior of power of A with mass

It has practical applications for future accelerators since it permits prediction of the production rates of higher masses coupled to photons, W's and hadrons created by the same quark-antiquark annihilation process. More recently an extensive literature (and many of the talks presented here) are concerned with issues of scale breaking, asymptotic freedom and QCD. These serve to modify the qualitatively successful annihilation model.

Conventionally scaling is expressed by

$$M^3 \frac{d\sigma}{dM} = F(M^2/s) \qquad (1)$$

In our experiment, we must study the y-behavior first and therefore express the scaling condition as:

$$s \frac{d^2\sigma}{d\sqrt{\tau}\, dy} = G(\tau, y) \qquad (2)$$

Here $\tau = m^2/s$. We plot the data in bins of $\sqrt{\tau}$, as a function of y. Fig 5 illustrates the data. We note firstly that there is reasonably good agreement where the y-intervals overlap. We have fit the y-behavior in each $\sqrt{\tau}$ bin with a quadratic polynomial and obtained the value of G at y=0.2. This is plotted vs $\sqrt{\tau}$ in Fig 6 to illustrate scaling. The raw data is given in Fig.7 and a comparison of these two indicates the validity of the scaling hypothesis.

One may ask whether violations of scaling should in fact be seen if the Drell-Yan model is correct and therefore if $G(\tau, y)$ has a linear dependence on νW_2 -which is known to violate scaling i.e. $\nu W_2 \neq f(x)$. It is easy to see than in the interval of x where we have data, the scaling violations are less than our experimentsl errors.

A global fit to the scaling data is given by:

$$G(\tau, 0.2) = 44 \pm 0.7\ \mu b\ GeV^2\ e^{-(25.5 \pm 2)\sqrt{\tau}}$$

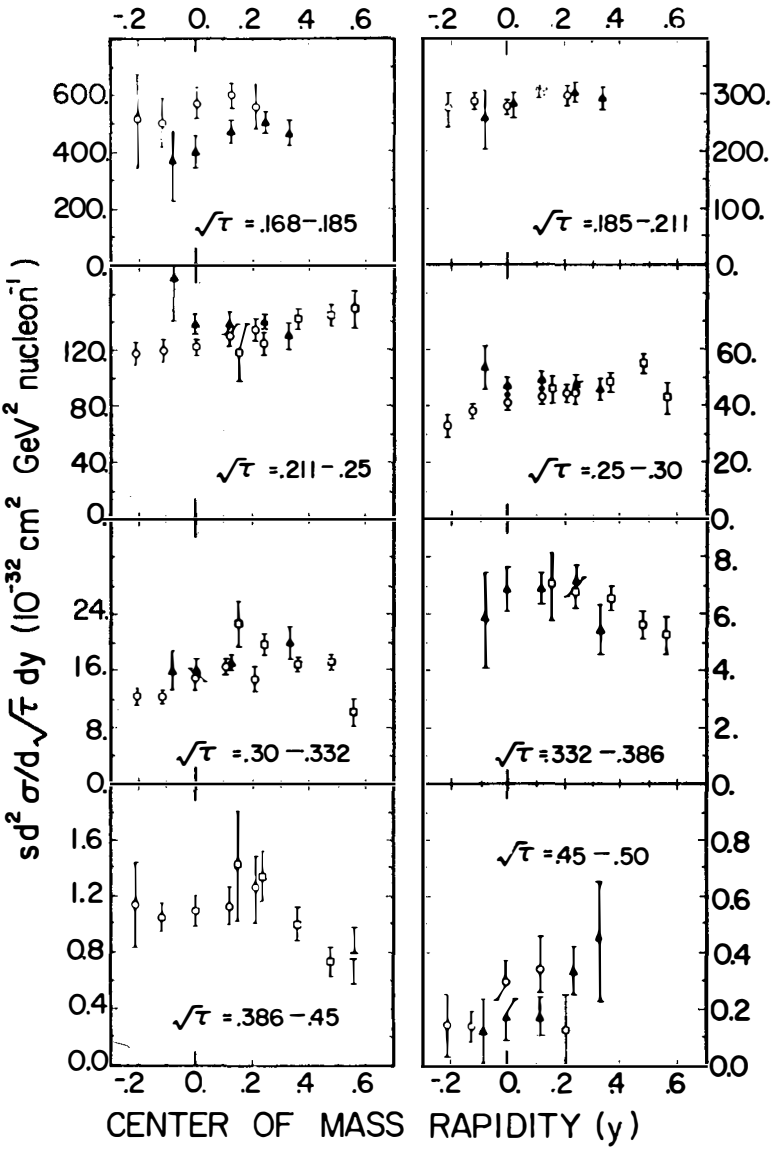

FIG. 5

Cross-section vs. y for various τbins. Circles are 400 GeV, triangles are 300 GeV and squares are 200 GeV.

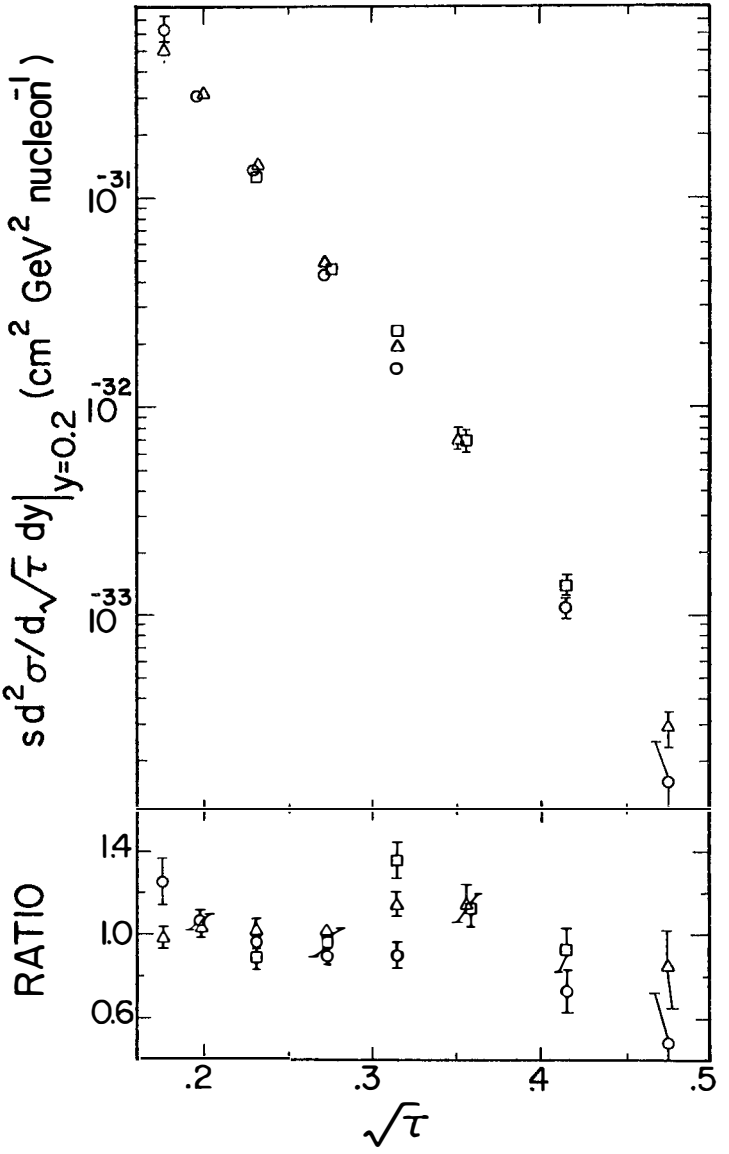

FIG. 6

Scaling data vs τ. Lower graph gives ratio of each energy to the fit.

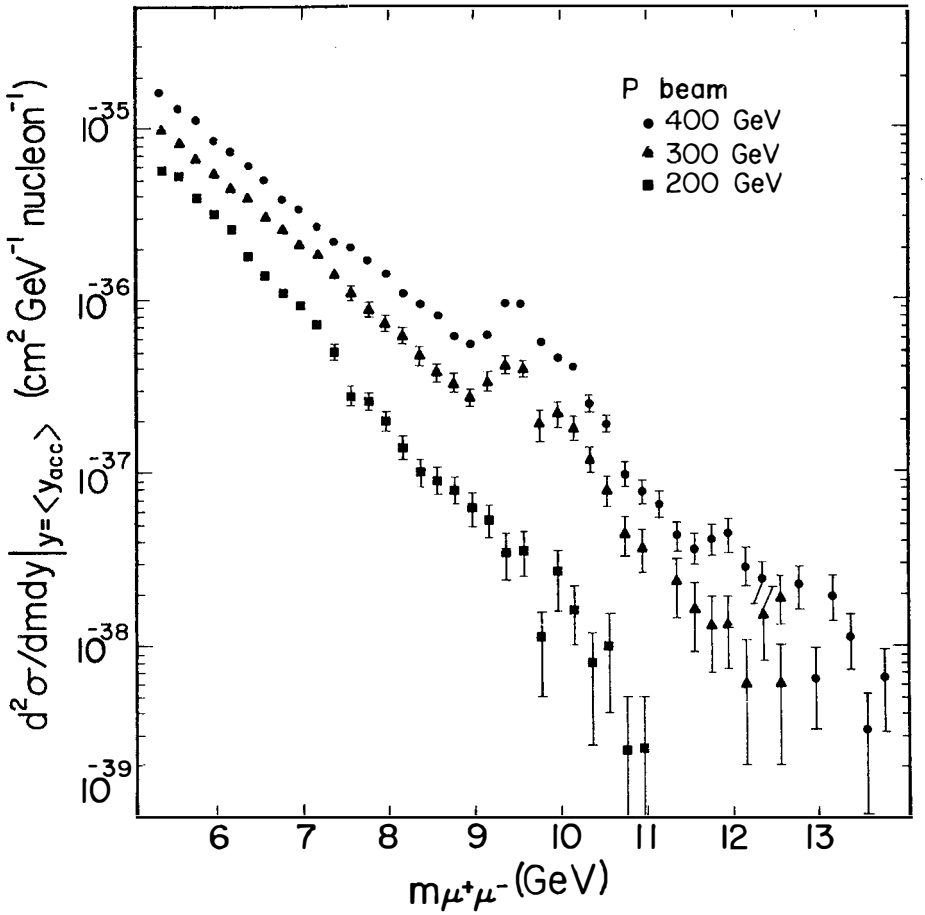

FIG. 7

Dimuon spectra at 200, 300 and 400 GeV.

There is a 25% systematic normalization error superposed here. This may be used to predict the results of ISR studies provided we correct for the fact that ISR observes only pp collisions. Having established the validity of scaling at least over the limited range of $\sqrt{s}$ from 19 to 27 GeV, we can now combine the y slices as observed by the three energies in order to study the behavior of $d\sigma/dmdy$ with y. We first note that there is no symmetry around y=0, the distributions tending to peak near $y \cong 0.3$. This corresponds to the fact that we have pn collisions (as well as the symmetric pp collisions). Events are peaked forward when the incident proton supplies the valence quarks, backward when the target nucleon does so.

In the Drell-Yan model we have

$$s \frac{d^2\sigma}{d\sqrt{\tau}\, dy} = \frac{8\pi\alpha^2}{q} \tau^{-3/2} G'(x_1, x_2) \qquad (3)$$

where

$$M^2 = x_1 x_2 S \qquad (4)$$

$$y = \frac{1}{2} \ell n\, x_1/x_2 \qquad (5)$$

$$G' = \frac{N_p}{A} G^{pp} + \frac{N_n}{A} G^{pn}$$

$$= 0.4\, G^{pp} + 0.6\, G^{pn}$$

for protons on copper

$$G^{pp} = \frac{4}{9}\left[u(x_1)\, S(x_2) + u(x_2)\, S(x_1)\right] + \frac{1}{9}\left[d(x_1)\, S(x_2) + d(x_2)\, S(x_1)\right]$$

$$G^{pn} = \frac{4}{9}\left[u(x_1)\, S(x_2) + d(x_2)\, S(x_1)\right] + \frac{1}{9}\left[d(x_1)\, S(x_2) + u(x_2)\, S(x_1)\right]$$

where we have used the relation $u^p = d^n$ so that all quark structure functions refer to the proton. We have also neglected terms quadratic in S(x) and have taken

$$\bar{u}(x) = \bar{d}(x) = \bar{s}(x) = S(x) \qquad (6)$$

We can study the asymmetry around y=0 by defining a normalized slope of $d\sigma/dy$ near y=0:

$$R \equiv \frac{G'(\Delta y) - G'(-\Delta y)}{2\,\Delta y\, G(0)}$$

$$= \frac{d}{dy} \ln G(y) \Big|_{y=0}$$

Experimentally we take $\Delta y \cong 0.2$

$$R = \frac{3}{2\,\Delta y} \left\{ \left[u(x_1) - d(x_1) \right] S(x_2) - \left[d(x_2) - u(x_2) \right] S(x_1) \right\} \times \left[6.2\, u(x) + 3.8\, d(x) \right]^{-1}$$

where $x = \sqrt{\tau}$ From (5)

$x_1 = \sqrt{\tau}\, e^{\Delta y}$ and $x_2 = \sqrt{\tau}\, e^{-\Delta y}$

, and for a steeply falling sea e.g. $S(x) \sim (1-X)^9$

$$S(x_2) >> S(x_1)$$

and the slope is positive since $u(x) > d(x)$.

The normalized slope is plotted vs $\sqrt{\tau}$ in Fig.8 using a fit to 400 GeV data at y=0 for $S(x) \cong (1-x)^9$ and using simplified functions for u(x) and d(x) taken from νW_2 fits:

$$u(x) = 12.8\, x\, (1 - x)^4$$

$$d(x) = 6.29\, x\, (1 - x)^5$$

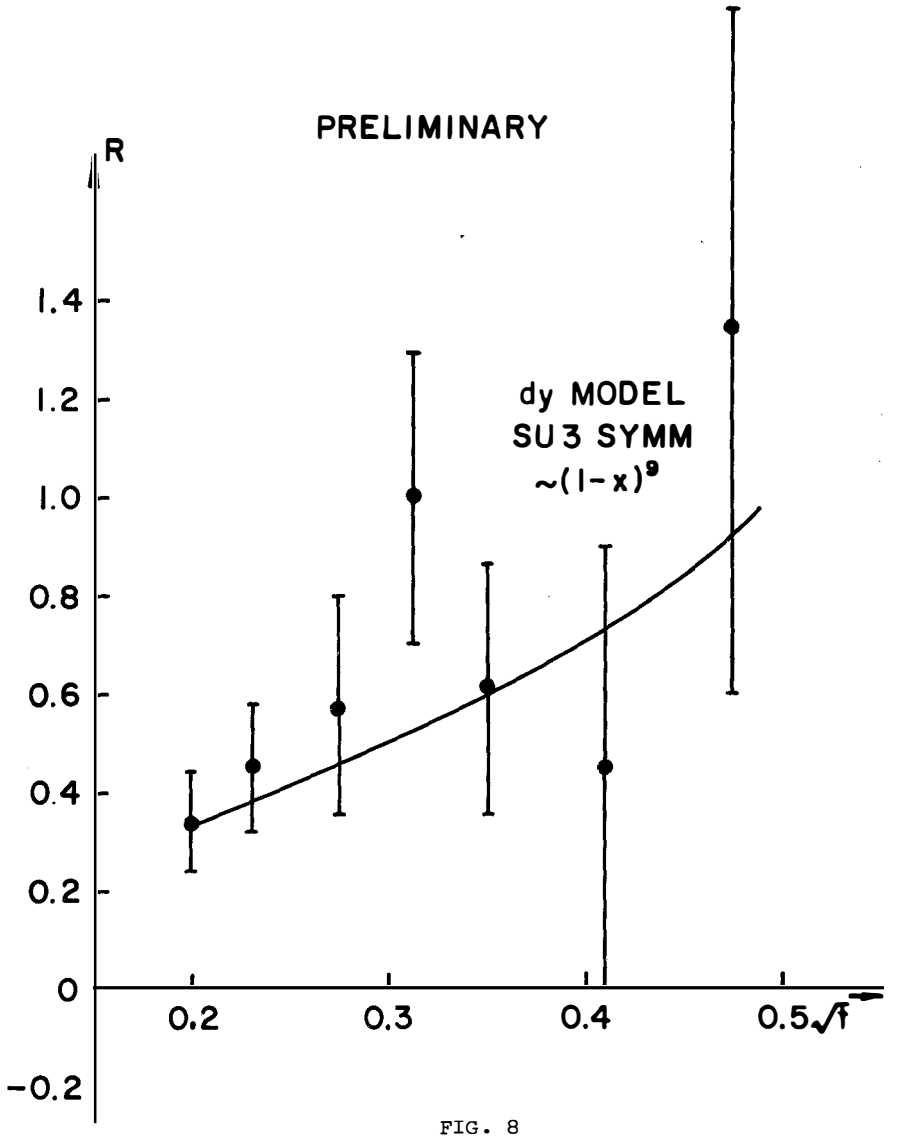

FIG. 8
Slope of y-dependence vs. $\sqrt{\tau}$

We also present preliminary data. There are two comments: (1) The fact that the absolute slopes and the increase of slope with $\sqrt{\tau}$ qualitatively reproduce the data is a new check of the Drell-Yan model over the domain of variables studied.

(2) If the absolute value of the slope were indeed found to be larger than the model predictions, (as Fig. 9 suggests but does not establish) the only fix within the confines of the Drell-Yan model is to modify equation (6) by setting $\bar{u} > \bar{d}$ This step was actually taken for intuitive reasons by Feynman and Field.[5]

IV Transverse Momentum of Dileptons

Probably the area of greatest interest is so far as QCD calculations are concerned is in the P_T behavior of dileptons. The CFS data established a form for the P_T behavior which was invented for our 400 GeV data but provides a very good fit to 300 and 200 GeV:

$$E\frac{d^3\sigma}{dp^3} = C(1 + (P_T/P_o)^2)^{-6} \qquad (7)$$

We present the data on C and P_o in table III. This fit works out to the limit of the data in that if we calculate the moments: $\langle p_T \rangle$, $\langle p_T^2 \rangle$ etc, we find good agreement whether we use equation (7) or if we evaluate the averages directly from the data. This works well up to the 3rd moment. Our results for 400 GeV established (as can be read from the table) the flatness of $\langle p_T \rangle$ with mass. Now this was at first a shock to the QCD'ers because simple considerations predicted that:

$$\langle P_T^2 \rangle \sim M^2$$

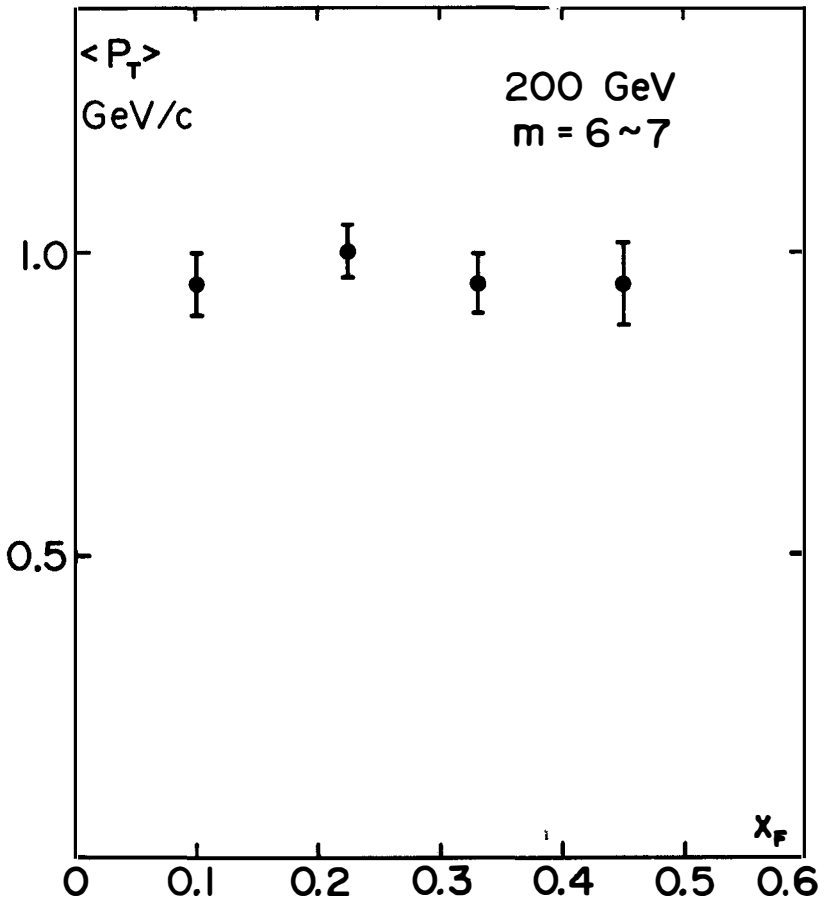

FIG. 9

Variation of average P_T with X_F.

TABLE III

p_T Fit Parameters [a], [b]

$\sqrt{s}$ (GeV)	19.4	
M	C (fb.GeV^{-2})	P_o (GeV)
4.5	7169±208	2.07±.049
5.5	1592± 59	2.34±.055
6.5	470± 21	2.34±.061
7.5	121±9.9	2.19±.099
8.5	26.3 ±4.4	2.01±.186
9.5	7.22±2.07	2.29±.393

	23.7	
	C	P_o
4.5	9006±250	2.25±.055
5.5	2648± 79	2.41±.044
6.5	842± 30	2.60±.055
7.5	326± 16	2.59±.068
8.5	104±8.0	2.53±.097
9.5	70.5±5.5	2.65±.111
10.5	19.3±3.0	2.65±.247

	27.3	
	C	P_o
4.5	10310±419	2.62±.095
5.5	2887± 55	2.70±.035
6.5	1058± 25	2.74±.036
7.5	386± 13	2.86±.050
8.5	163±6.4	2.78±.058
9.5	130±5.6	3.10±.075
10.5	41.8±3.1	2.83±.112
11.5	10.2±1.9	2.21±.202

[a] $E \cdot \frac{d^3\sigma}{dp^3} = C(1 + (\frac{P_t}{P_o})^2)^{-6}$

[b] Significant data extend to about 3 GeV/c in p_T. See Kaplan et al. (Ref. 1).

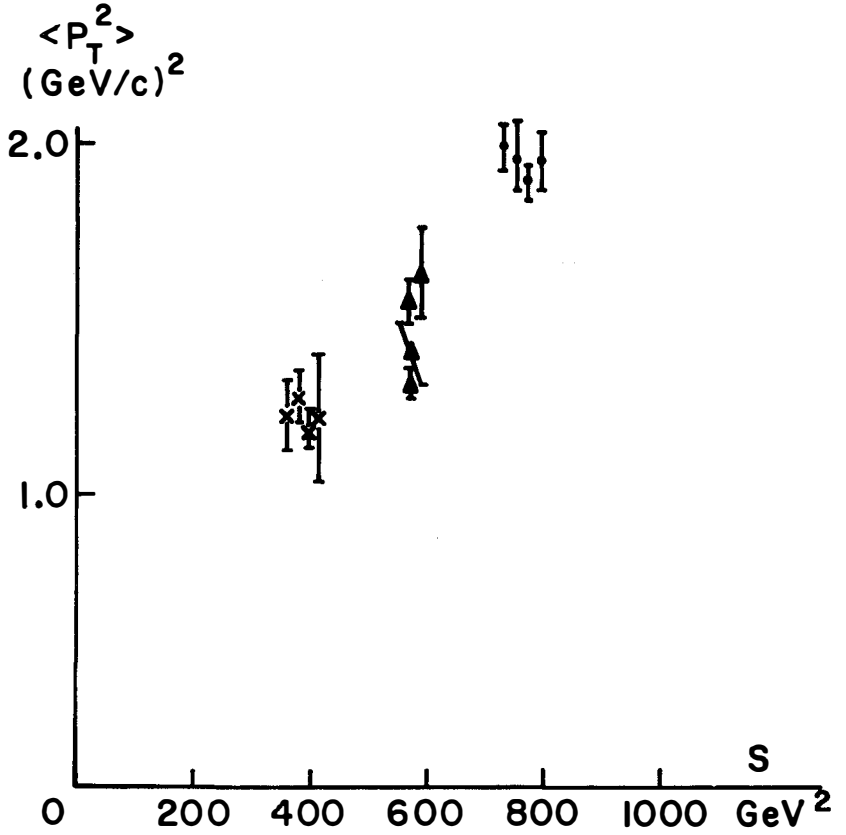

FIG. 10

Energy variation of $\langle P_T^2 \rangle$. The crosses are various mass bins at 200 GeV, the triangles are various mass bins at 300 GeV, the circles are 400 GeV.

TABLE IV

Average P_T Square With Cuts

$\sqrt{\tau}$bin	No Cut	>1GeV/c	>1.4GeV/c
		400 GeV	
.18-.21	2.13±.28	3.57±.48	5.12±.74
.21-.25	1.83±.05	2.97±.08	4.12±.12
.25-.30	1.98±.07	3.24±.11	4.45±.15
.30-.33	2.08±.12	3.27±.17	4.39±.24
.33-.38 †	2.40±.11	3.69±.15	4.93±.21
.38-.45	2.13±.37	3.57±.61	5.00±.91
		300 GeV	
.18-.21	1.20±.12	2.25±.23	3.09±.37
.21-.25	1.35±.05	2.40±.09	3.38±.13
.25-.30	1.68±.07	2.96±.12	4.13±.18
.30-.33	1.76±.18	3.15±.33	4.56±.52
.33-.38	1.52±.10	2.54±.15	3.51±.23 *
.38-.45 †	1.76±.15	2.94±.23	4.16±.33
		200 GeV	
.21-.25	1.11±.14	2.29±.30	3.40±.54
.25-.30	1.25±.08	2.38±.15	3.32±.24
.30-.33	1.41±.11	2.74±.21	3.90±.33
.33-.38	1.19±.07	2.27±.13	3.38±.21
.38-.34	1.27±.16	2.42±.29	3.87±.50

(Since the theory is well covered by the experts in these lectures I will not dwell here). We have now established that the QCD rise is not dampened by some kind of phase space since we see the same flattening at 200 and 300 GeV. The lower energy data gives us an opportunity to study the behavior of $\langle P_T \rangle$ with X_F, or, in our variable of choice, y. Here again QCD predictions were strongly stated: $\langle P_T \rangle$ must drop as y increases.[6] We do not see this drop and our 200 GeV data goes to y~0.6. See Fig.9. We have learned that QCD has troubles for $P_T > 1$GeV and so we have cut our data in order to study the behavior of an artificial $\langle P_T^2 \rangle$ where we ignore all the data below 1 and 1.4 GeV/c. The statistics get poor but we see no tendency to follow the QCD prediction i.e. $\langle P_T > 1\text{GeV} \rangle$ remains flat with y and with mass. This is seen in Table IV. Thus the effects are not dominated by low P_T events. There is one variable that does influence $\langle P_T \rangle$ and this provides the first evidence in dilepton production of scaling violation. See Fig.10. We find that $\langle P_T^2 \rangle$ increases with energy, s. The range of s is small but we find a fit:

$$\langle P_T^2 \rangle = a + bS \qquad (8)$$

This applies for masses $\geq$ 5GeV. We find

$$a = 0.70 \text{ GeV}^2$$

and $$b = .0018$$

Scale violation is implied by the new dimensional constant a. The interpretation seems clear: a represents the "primordial" quark motion presumably induced by the confining potential. It implies a quark momentum of 600-700 Mev/c which is consistent with other observation. To confirm the form of equation 8, we need data at ISR but with masses corresponding to comparable values of the variable $\sqrt{\tau} \geq 0.15$. This means, for ISR, $m \geq$ 9GeV. Considering that the $\underline{\Upsilon}$ now interferes, it becomes crucial to find ~50 events above the $\underline{\Upsilon}$ to provide

the test. One of the "practical" necessities for this information is the search for W which is related to Drell-Yan production. If we extrapolate to the accelerator that will have ~5 times the W-energy i.e. $\sqrt{s} \sim 500$, we predict

$$< P_T >_W \cong 20 \text{ GeV/c}$$

We close by stressing that the form of equation 8 is tested only between $\sqrt{s}$ 19 and 27 GeV.

References

1. S.W. Herb et al, Phys. Rev. Lett. 39 252 (1977)
2. W.R. Innes et al, Phys. Rev. Lett. 39 1240 (1977)
3. D.M. Kaplan et al, Phys. Rev. Lett. 40 435 (1978)
4. S. Ellis et al, CERN TH-2346 (1977)
5. R. Feinman and R. Field, Phys. Rev. D15 2590 (1977)
6. F. Halzen and D.M. Scott, U. of Wisconsin preprint C000-811-21 (1978)

FERMILAB RESULTS ON LEPTON PAIR PRODUCTION*

J. E. Pilcher
Enrico Fermi Institute, The University of Chicago
Chicago, Illinois 60637 U.S.A.

ABSTRACT

Recent results are presented for pion induced μ-pairs with masses above 4 GeV. The data show many of the general features predicted by the Drell-Yan quark-antiquark annihilation model. The P_T dependence of the data is discussed and compared with that for proton induced pairs at a similar incident energy. The Feynman-x dependence of $\bar{p}$ induced J/ψ's is presented and found to be similar to p-induced events.

I will not try to summarize the work of other Fermilab experiments in this field, because Professor Lederman is here to describe the work of his own group. I will concentrate on new results of the Chicago-Princeton collaboration which just finished a data-taking run in January. Previous studies by this group have dealt with μ-pair production by protons and pions for masses up to about 4 GeV.[1] All studies have used the Chicago Cyclotron Spectrometer located in Fermilab's Muon Laboratory. This device offers rather broad acceptance in the Feynman-x (X_F) P_T and mass of the pair. The sensitivity of the measurements is limited primarily by the available beam flux which was ~10^6/pulse in earlier studies.

In our most recent experiment we have substantially improved the sensitivity of the measurements. A beam flux of over 10^7 π^-/pulse was available and several steps were taken to enhance the acceptance and reduce deadtime losses. The final sensitivity of this run is about thirty times our previously published work at the same incident energy of 225 GeV.

Figure 1 shows a plan view of the detector. Four threshold Cerenkov detectors were used in the beam to identify the incident particle type. Targets of carbon, copper, and tungsten were used for various parts of the experiment as I will indicate later. An important improvement for this run was in the multiwire proportional chambers located just upstream of the magnet. The transverse size of the chambers was doubled, compared to earlier work to enhance the efficiency at small values of Feynman-x. We were fortunate to be able to borrow the MWPC's which the CERN-Heidelberg group used for their K-decay studies at CERN. These were added to the detector and performed flawlessly. In total there were three X measurements, three Y measurements and a U and V measurement (45°) on each track upstream of the magnet.

The spectrometer magnet was operated to give a transverse momentum kick of about 1 GeV/c. This figure is well below the maximum attainable and was chosen to retain good acceptance for low momentum muons which arise from either low X_F pairs or very asymmetric decays of the μ-pair system.

Downstream of the magnet twelve spark chamber planes measured the trajectories.

The trigger required exactly one particle in the beam, unaccompanied by any halo particle. Hodoscopes planes J and F were used to constrain the mass of the pair and hodoscope P was used to confirm the presence of at least two muons in the final state. A specially built digital logic system used the counter information from the J and F planes, together with the assumption that the pair originated in the target, to estimate the effective mass of the pair. This calculation was done in ~150 ns. and an arbitrary minimum mass requirement could be imposed on the data without adding to the memory time of the spark chambers. The pair-mass, estimated in this way, was recorded with every event to permit off-line checking of the hardware for proper operation. In addition, once every few hours, the data acquisition computer would test the mass-logic hardware by successively setting all possible hodoscope combinations and reading back the result. This novel, but potentially dangerous, mass-logic hardware performed without incident.

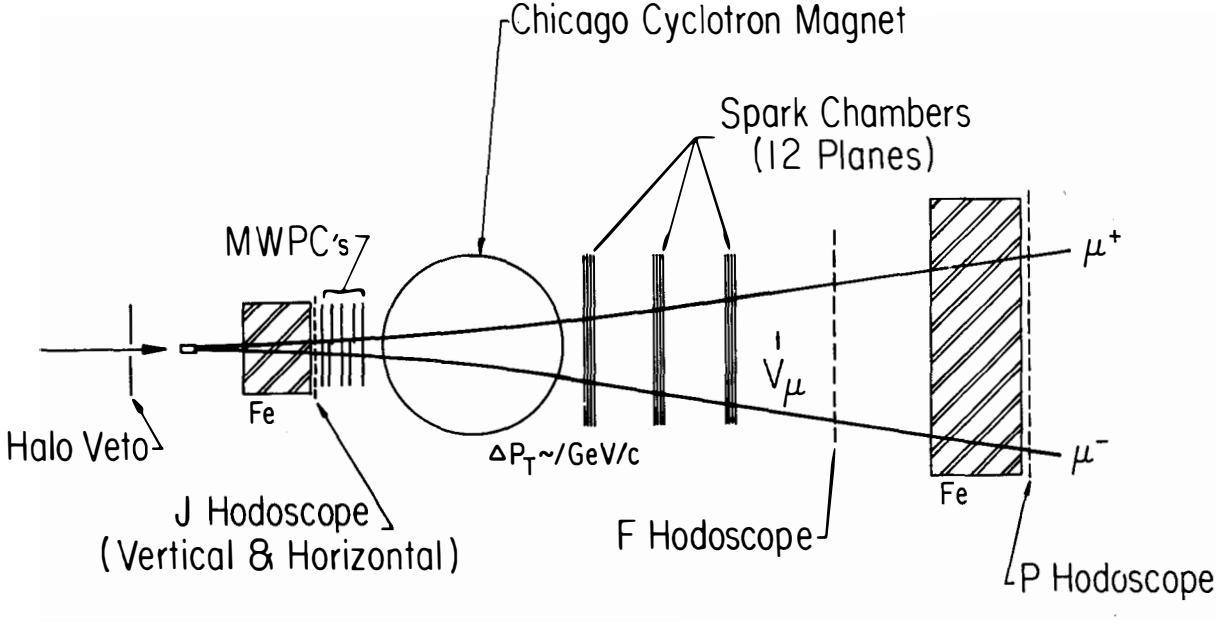

Figure 1. Plan view of the detector.

The acceptance of the detector is a function of M, X_F, P_T and the decay angles of the pair. Figure 2 shows three projections of the acceptance function calculated by Monte Carlo methods. The calculation assumes an isotropic decay angular distribution for the μ-pair system in its own rest frame. The absolute acceptance is large and fairly smooth as is required to study production and decay characteristics of the pairs.

Figure 3 shows the mass spectrum of events produced by a π^- beam on a variety of targets. In this plot the data are uncorrected for acceptance to permit a look at the raw data. The signal from like-sign pairs is also shown. It remains small even after one corrects for the difference in detection efficiencies for like-sign compared to opposite-sign pairs. We conclude that π and K decay produce a negligible background in the data. One should note that these data cover just the same range of M^2/s as the Columbia, Fermilab, Stony Brook data with incident 400 GeV protons.[2] In the latter case $\sqrt{s}$ = 27.4 GeV while in our case $\sqrt{s}$ = 20.6. It is remarkable to see hadron induced events where half the available CM energy is consumed in the creation of a μ-pair. The mass spectrum shows no conclusive evidence for an enhancement at 9.5 GeV as has been seen in the CFS experiment. We would probably not be sensitive to an enhancement if the resonance to continuum levels were as small as the 1 to 1 of the CFS measurement with incident protons.

Figure 4 gives the efficiency corrected mass spectrum. It is interesting to compare the pion induced continuum cross section with the proton induced cross section of the CFS group.[2] For $10 < M_{\mu\mu} < 11$ GeV we find $(d\sigma/dM)_\pi/(d\sigma/dM)_p \sim 330$. To make this comparison we have scaled the CFS data from 400 GeV to 225 GeV using the hypothesis that $d\sigma/dM = M^{-3}f(M^2/s)$. In addition the data are integrated over all $X_F > 0$ using for the proton data the Feynman-x distribution we measure at M=4 GeV. Our own proton induced data do not extend to these high masses simply because the cross section is so low.

A very large ratio for the pion induced cross section compared with proton induced is expected in production models in which the μ-pair is produced through the annihilation of a quark and antiquark from the interacting hadrons (Drell-Yan mechanism).

Detector Acceptance

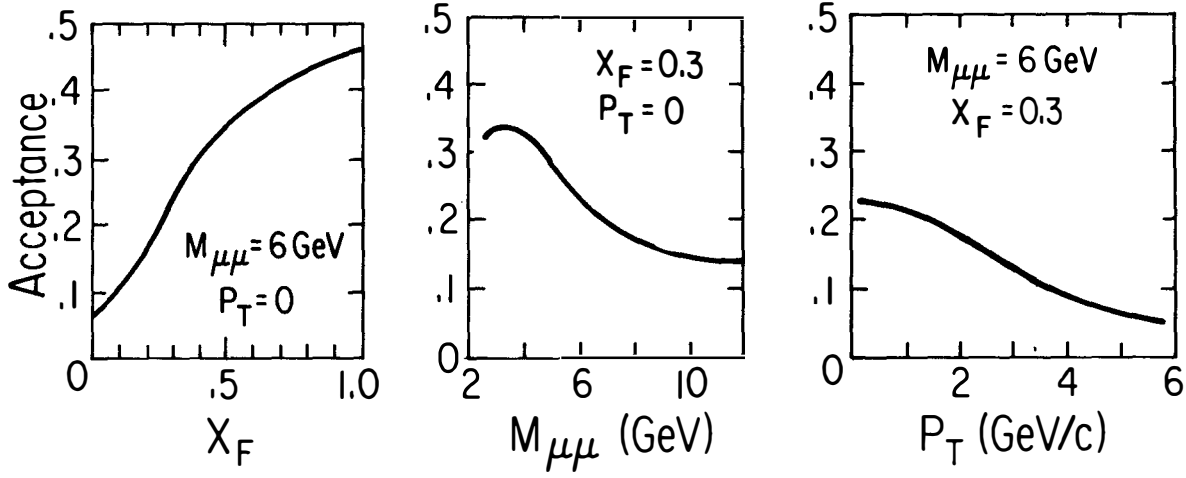

Figure 2. Three projections of the detection efficiency function.

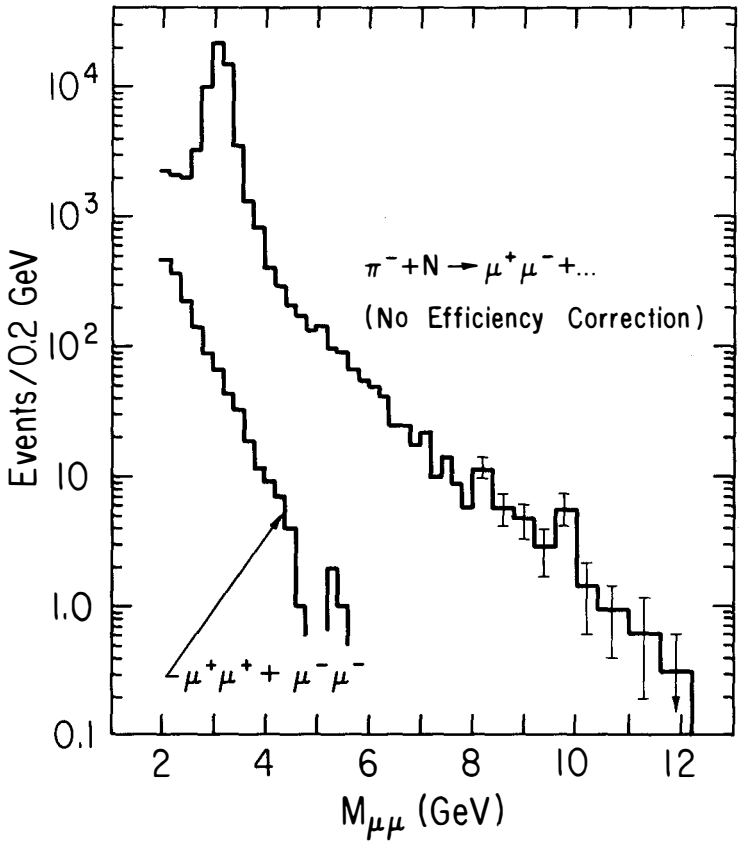

Figure 3. Mass spectrum of π^- induced μ-pairs from nuclear targets. The data correspond to all events with $X_F>0$. Events have not been weighted to correct for acceptance.

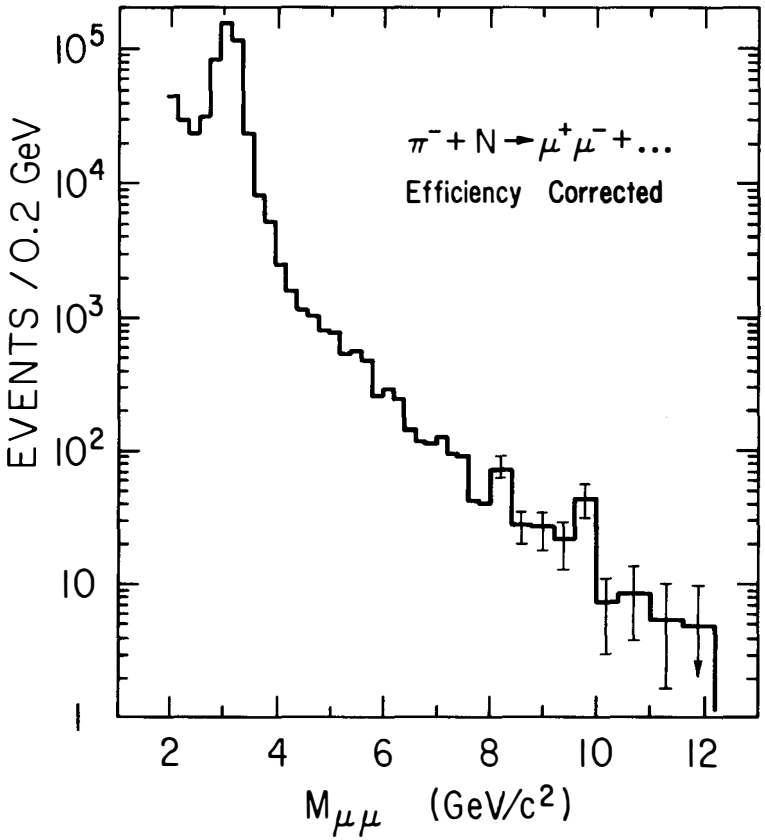

Figure 4. Mass spectrum of π^- induced μ-pairs from nuclear targets for $X_F>0$. Each event has been weighted to correct for acceptance.

The shape of the continuum mass spectrum is well represented by $d\sigma/dM \propto e^{-0.97M}$. This agrees well with the Goliath experiment at the SPS which obtains an exponent of 0.88±0.15 at an incident pion energy of 150 GeV.[3] If the CFS proton induced spectrum is scaled to 225 GeV incident energy, the exponent is found to be 1.3.

Consider next the X_F and P_T dependence of the π^- induced pairs. Figure 5 shows the X_F dependence of the data for different mass intervals. The lowest interval is for J/ψ production and the higher intervals correspond to continuum production. The data show the striking effect that as the μ-pair mass becomes large the X_F spectrum becomes progressively flatter. It should be pointed out that the definition of X_F used for Fig. 5 takes into account the reduction of P^*_{max} due to the creation of a massive pair in the final state. For example, at $M_{\mu\mu}$ = 8.5 GeV, $P^*_{max} = 0.83\sqrt{s}/2$.

Figure 6 shows the mean transverse momentum of the pairs versus the pair mass. Some of our old data at lower masses are shown for comparison. The mean P_T is seen to rise with mass until it reaches a plateau value of about 1.2 GeV/c for masses above 4 GeV/c. The data are integrated over all $X_F>0$. Also shown for comparison in Fig. 6 are $\langle P_T \rangle$ values for proton induced pairs at an incident beam energy of 200 GeV.[4] These data also show the plateau effect for masses above 4 GeV but the level of the plateau is about 200 MeV lower than seen for pion induced pairs. These proton induced data are for X_F=0.

To see if the different plateau heights could be associated with an X_F dependence of $\langle P_T \rangle$ we show in Fig. 7 $\langle P_T \rangle$ for various ranges of X_F and $M_{\mu\mu}$. With a sensitivity of about 100 MeV/c, no variation of $\langle P_T \rangle$ is seen as a function of mass or X_F. The errors shown in many $\langle P_T \rangle$ plots are determined by systematic considerations rather than statistical ones. As our data analysis advances we expect that the error bars can be reduced.

The data taken with a negative beam has given us a sample of $\bar{p}$ induced J/ψ's. Figure 8 shows the mass distribution of $\bar{p}$ induced events with $M_{\mu\mu}$>2 GeV. There are about 100 J/ψ's in this sample. The X_F dependence of these J/ψ events (2.5 < $M_{\mu\mu}$ < 3.5 GeV) is shown in Fig. 9. The curves show the X_F dependence of π^- and p induced J/ψ's for comparison.

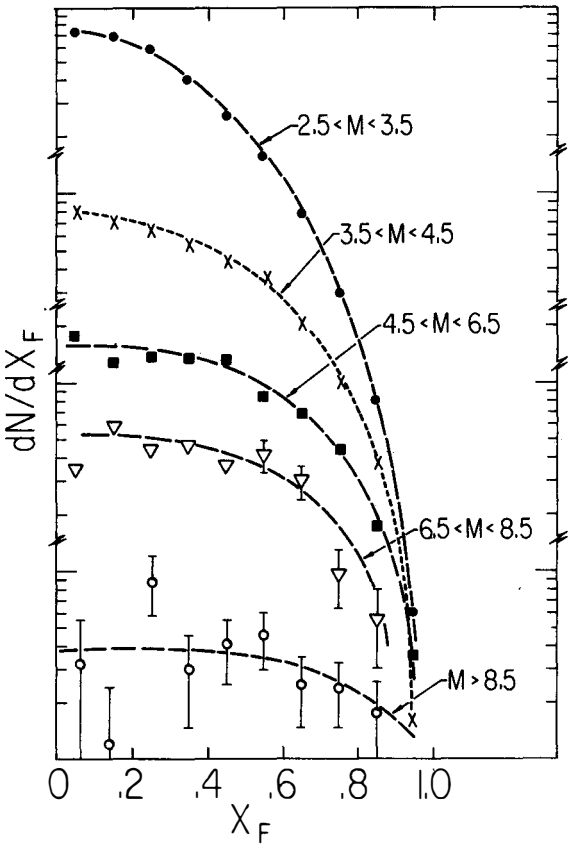

Figure 5. Feynman-x distributions for different μ-pair mass intervals. The relative normalization of data from different mass intervals is arbitrary in this plot.

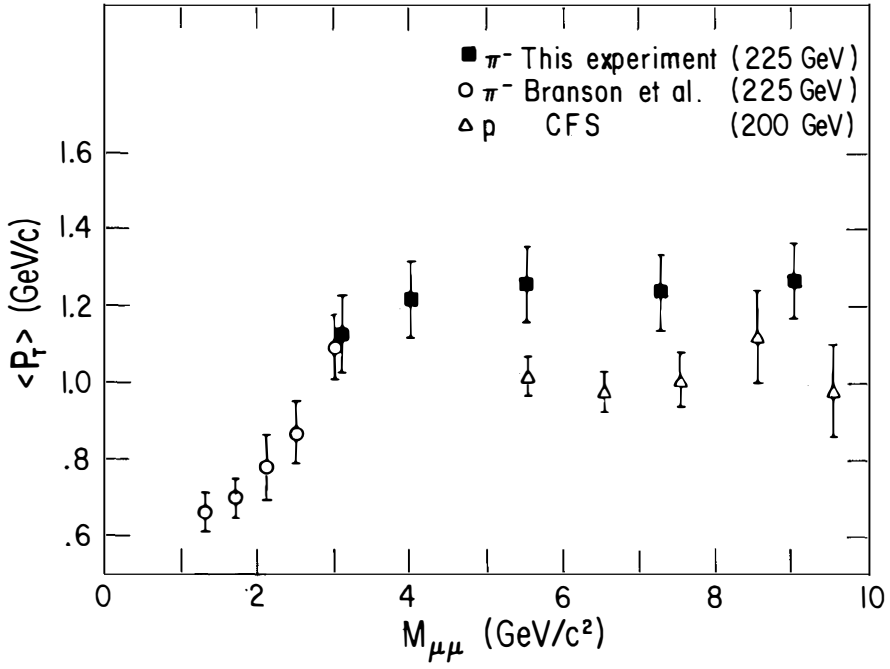

Figure 6. Mean P_T of the pairs versus mass.

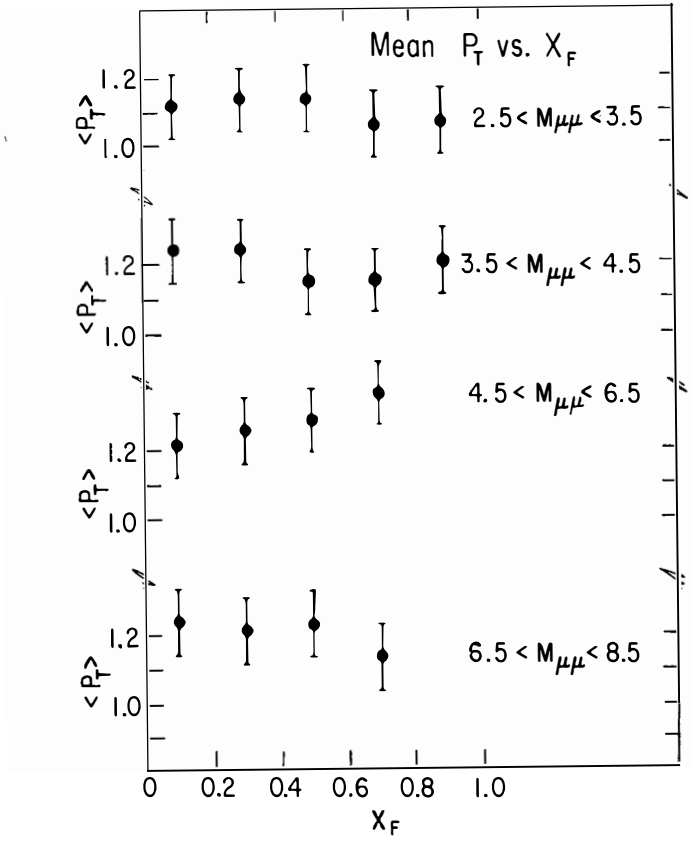

Figure 7. Mean P_T of the pairs for various Feynman-x intervals and mass intervals.

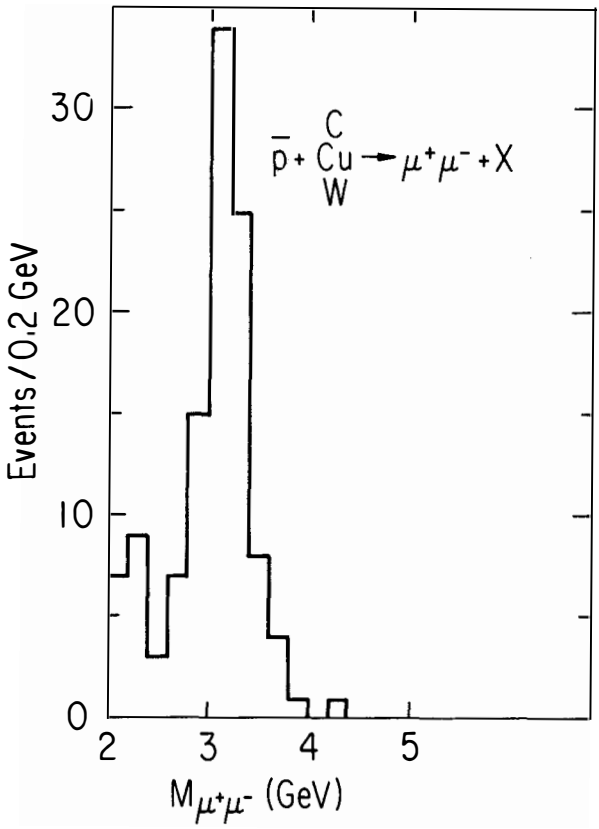

Figure 8. The mass spectrum for $\bar{p}$ induced μ-pairs.

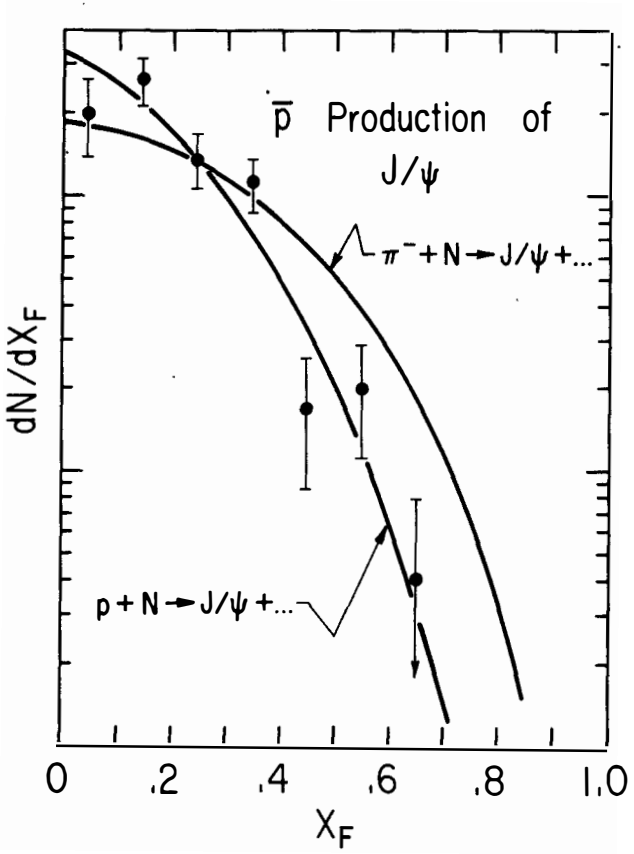

Figure 9. Feynman-x distribution for $\bar{p}$ induced J/ψ's. The observed shapes for π induced and p induced are shown for comparison.

The observed distribution from $\bar{p}$'s more closely resembles the proton induced shape.

An important goal of our experiment has been the comparison of π^+ and π^- production of μ-pairs from an isoscalar target. The issue is whether the pairs are produced through a strong or electromagnetic process. Using a carbon target we compare the cross section $\sigma(\pi^+ + C \to \mu^+\mu^- + \ldots)$ with $\sigma(\pi^- + C \to \mu^+\mu^- + \ldots)$. Since the reactions are charge symmetric the cross sections should be identical if the pairs have a strong interaction origin. On the other hand, an electromagnetic origin could lead to a violation of charge symmetry and unequal cross sections. One specific electromagnetic model is the Drell-Yan model or variations thereof. In this picture a quark from one of the interacting hadrons annihilates with an antiquark of the same flavor and color in the second. The differential cross section is given as,

$$\frac{d\sigma}{dX_F dM_{\mu\mu}} = \frac{8\pi\alpha^2}{3M^3} \sum_i \frac{e_i^2}{(X_T + X_P)} \left[X_T f_i^T(X_T) X_P f_{\bar{i}}^P(X_P) + X_T f_{\bar{i}}^T(X_T) X_P f_i^P(X_P) \right]$$

where the sum is over quark flavors, the f's are the quark distribution functions in the target (T) or projectile (P) hadron, and

$$X_T = \frac{1}{2}\left[-X_F + \sqrt{X_F^2 + 4M_{\mu\mu}^2/s}\right] \quad \text{and} \quad X_P = \frac{1}{2}\left[X_F + \sqrt{X_F^2 + 4M_{\mu\mu}^2/s}\right]$$

are the Feynman-x's for the annihilating quarks in the target and projectile. In writing this expression, transverse momenta have been neglected. Their inclusion would blur the relationship between X_T, X_P and X_F, $M_{\mu\mu}$ in certain kinematic regions.

Both the projectile pion and target nucleon contain antiquarks in the $q\bar{q}$ sea at low X. For X_T and X_P large however valence quarks and antiquarks dominate the lepton pair production. In this case the only antiquark is that of the incident pion; namely, a $\bar{u}$ in the case of a π^- or a $\bar{d}$ in the case of the π^+. Since the target is carbon it contains equal numbers of u and d quarks. Since u(X) for the proton is equal to d(X) for the neutron the target is exactly symmetric in both number and momentum distributions for u and d quarks. Hence, changing from a π^+ to a π^- beam the only change in the production cross section written above is charge of the annihilating quark. Since the charge of $\bar{u}$ is (-2/3) and the charge of $\bar{d}$

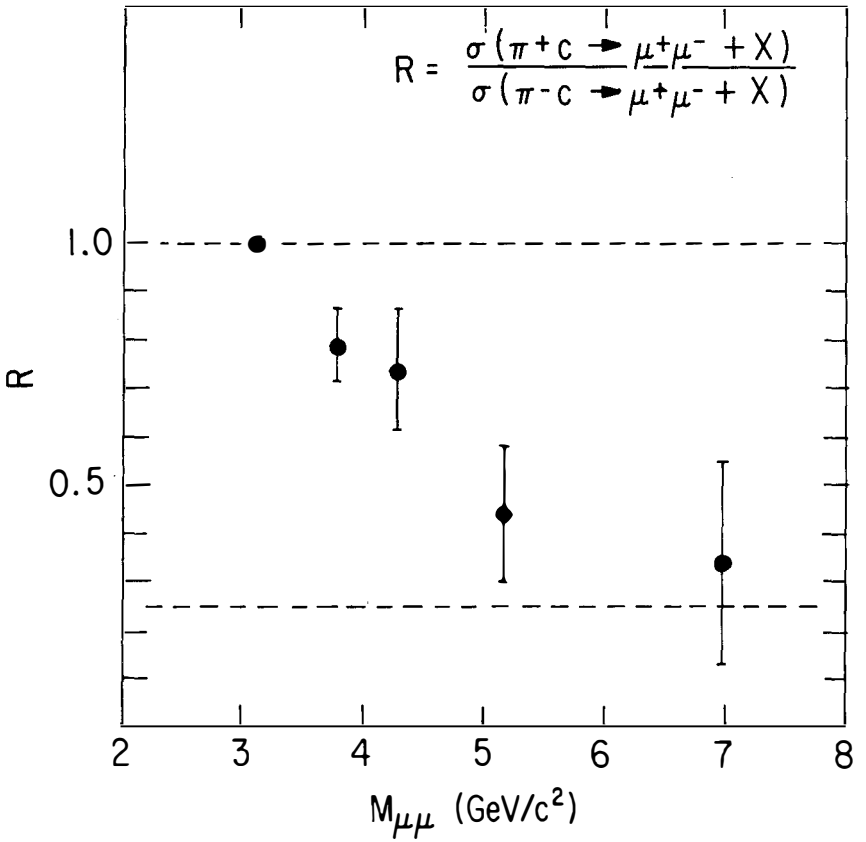

Figure 10. Cross section ratio for π^+ and π^- production of μ-pairs from a carbon target.

is 1/3 the ratio $\sigma(\pi^+ + C \to \mu^+\mu^- + \ldots)/\sigma(\pi^- + C \to \mu^+\mu^- + \ldots)$ should be $(1/3)^2/(-2/3)^2 = 1/4$. If, however, the kinematic region allows the sea quarks to contribute to the production the ratio will be closer to 1. Since for $X_F=0$, $X_T=X_p=M_{\mu\mu}/\sqrt{s}$ we expect that at large values of $M_{\mu\mu}$ the cross section ratio should approach 1/4.

Figure 10 shows the observed cross section ratio as a function of mass. At M=3.1 GeV the cross section is dominated by J/ψ production. Our previous measurements have shown the cross section ratio for J/ψ production is close to unity indicating a strong interaction mechanism for J/ψ production. The data of Fig. 10 are normalized to unity at $M_{\mu\mu}$= 3.1 GeV to avoid normalization uncertainties at this early stage of analysis. The resulting ratio departs from unity for $M_{\mu\mu}$>3.1 GeV and appears to approach 1/4 as predicted by the quark-antiquark annihilation model. The exact approach to 1/4 depends on the quark distribution functions for the pion and nucleon.

In conclusion, we have seen that many features of the data are consistent with quark-antiquark annihilation as the source of μ-pairs with $M_{\mu\mu}$>4 GeV. The large ratio for $\sigma(\pi^- + N \to \mu^+\mu^- + \ldots)/\sigma(p+N \to \mu^+\mu^- + \ldots)$ at high mass, and the ratio $\sigma(\pi^+ + C \to \mu^+\mu^- + \ldots)/\sigma(\pi^- + C \to \mu^+\mu^- + \ldots)$ approaching 1/4 are two striking general features of the data which are predicted by the model. Another important test is the helicity angular distribution for one of the muons in the μ-pair rest frame. This should be $1+\cos\theta^2$ if the pair arises from the annihilation of two spin-1/2 fermions. Our detector is very well suited for this test and analysis is now underway.

Once the quark-antiquark annihilation mechanism is accepted as the dominant source of high mass lepton-pairs the data can be used to extract the pion's quark distribution function which so far, has been only guessed at. Again, our present data are well suited to deduce this function.

We hope to report on these additional measurements in the next few months.

REFERENCES

* Work performed by: K.J. Anderson, R.N. Coleman, K.P. Karhi, C.B. Newman, J.E. Pilcher, E.I. Rosenberg of the University of Chicago, and G. Hogan, K.T. McDonald, G.H. Sanders, A.J.S. Smith and J.J. Thaler of Princeton University. This work was supported in part by the National Science Foundation and the Energy Research and Development Administration and was performed at the Fermi National Accelerator Laboratory.

1] J. G. Branson et al., Phys. Rev. Letters 38, 1334 (1977), and references contained therein.

2] D. M. Kaplan et al., Phys. Rev. Letters 40, 435 (1978).

3] See their report at this Conference.

4] Results presented at the Vanderbilt Conference, March, 1978.

LEPTON PAIR PRODUCTION AND INCLUSIVE π° PRODUCTION AT LARGE TRANSVERSE MOMENTA EXPERIMENTAL RESULTS

J. TEIGER
DPhPE, Centre d'Etudes Nucléaires de Saclay,
BP 2, 91190 Gif-sur-Yvette, France.

SUMMARY

Results on the process $pp \rightarrow e^+e^- + \text{anything}$ are presented at two different ISR energies $\sqrt{s} = 53$ GeV and $\sqrt{s} = 63$ GeV for masses above 1.4 GeV/c^2. The electron pairs are detected at large angle with respect to the initial proton direction in the center of mass of the reaction. We give also results on a measurement of inclusive π° production, $\theta \sim 90°$ from pp collisions at the CERN-ISR.

RESUME

Les résultats de la réaction $pp \rightarrow e^+e^- + X$ sont donnés aux deux énergies des ISR $\sqrt{s} = 53$ GeV et $\sqrt{s} = 63$ GeV pour des masses supérieures à 1,4 GeV/c^2. Les paires d'électrons sont détectées à grand angle par rapport à la direction des protons incidents dans le centre de masse de la réaction. On donne aussi des résultats de la production inclusive des π°, $\theta \sim 90°$ dans les collisions pp aux anneaux de stockage du CERN.

1 - Introduction

a) We report first on measurement of inclusive π^o production at C.M. energies of 53 and 63 GeV, $\theta \sim 90°$ from p-p collisions at the CERN - ISR. The data are given in the range $0.2 < X_T < 0.45$, or in the range $5.25 < P_T(GeV/c) < 16.39$.

b) Results on the process $pp \rightarrow e^+e^-$ + anything are presented also at two different ISR energies $\sqrt{s}$ = 53 and 63 GeV. The electron pairs are detected at large angle with respect to the initial proton direction in the center of mass of the reaction. The experimental problem is to reject the very large background due to pion production and to provide an arrangement selecting electron pairs at the data taking level with good acceptance for low invariant masses. The hadron rejection to a level of 10^6 to 10^8 is obtained by a combination of an air filled Cerenkov counter and lead glass detectors. Converted gamma rays and Dalitz pairs are eliminated by pulse height measurement.

2 - Apparatus

The detector, shown in fig. 1, is a bi-spectrometer located on each side of the ISR interaction region I_7 ; the design is optimized for highly selective electron identification. Each arm spectrometer covers a solid angle of the order of 0.6 Sr around $\theta = 90°$. It is composed of :

- A magnet for momentum measurement of charged particles
- A lead glass Cerenkov array which is used to detect electrons and to measure their energies with $\Delta E/E \sim 12$ % *).
- A twelve cell Cerenkov counter filled with air at atmospheric pressure is embedded in the gap of the analyzing magnet (Threshold for pions is 5.6 GeV/c).
- Six planes of drift chambers on each side of the magnet (precision $\sim$0.2mm).
- Three Sets of scintillators hodoscopes A.E.F.

3 - Results on inclusive π^o production [1)]

The invariant cross sections are averaged over a rapidity interval of $\pm$0.6 unit. By combining the effects of various uncertainties

*The heavy particles detected are in rest in the CM, therefore the mean momentum is of the order of $\frac{M}{2} \sim 1.5$ GeV/c.

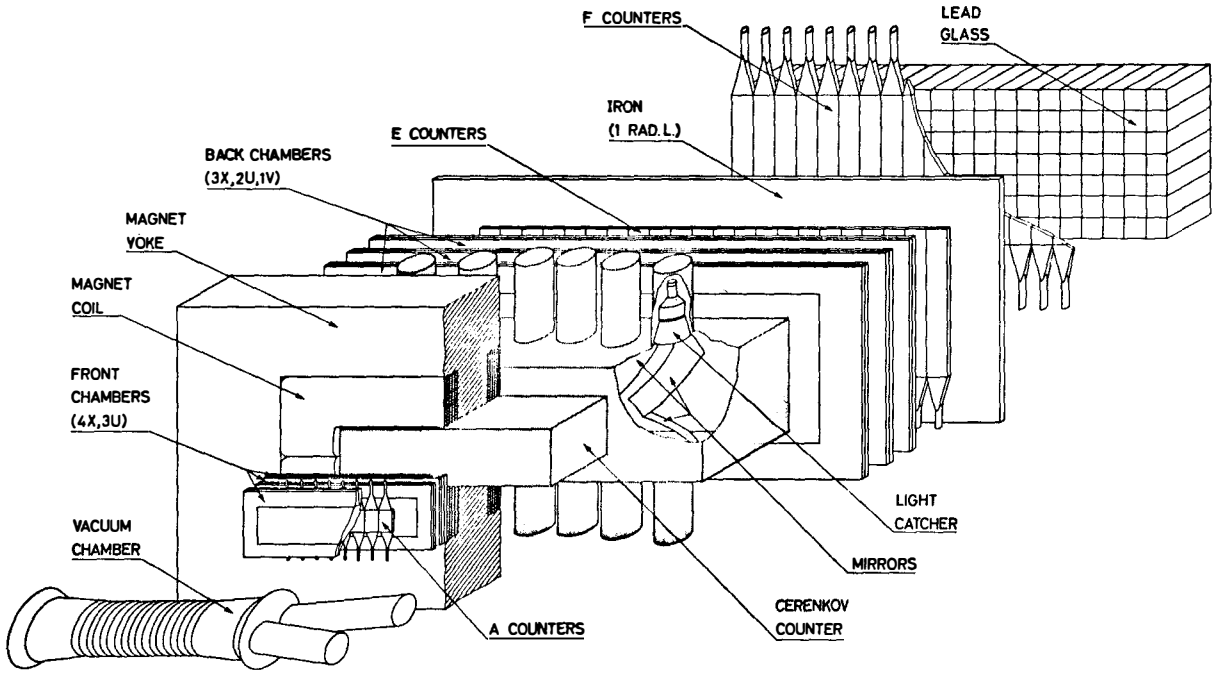
F COUNTERS
LEAD
GLASS
IRON
(1 RAD.L.)
E COUNTERS
BACK CHAMBERS
(3X,2U,1V)
MAGNET
YOKE
MAGNET
COIL
FRONT
CHAMBERS
(4X,3U)
VACUUM
CHAMBER
LIGHT
CATCHER
MIRRORS
CERENKOV
COUNTER
A COUNTERS

Figure 1

(luminosities, trigger corrections, etc...), we evaluate a global uncertainty of ± 17 % on the absolute normalization. Invariant cross sections are displayed in fig. 2 versus $X_T = 2P_T/\sqrt{s}$. In this representation they are expected to exhibit the same dependence upon X_T at different values of $\sqrt{s}$ the relation :

$$E \frac{d^3\sigma}{dp^3} \propto P_T^{-n} f(X_T, \Theta)$$

is valid, and their relative normalization provides a direct measure of n. In the range $5 < P_T < 15$ GeV (in contrast to previous measurements at ISR where P_T inferior)

we find $$E \frac{d^3\sigma}{dp^3} = (55 \pm 15) 10^{-29} P_T^{-(6.6 \pm 0.8)} (1 - X_T)^{9.6 \pm 1.0}$$

with χ^2 of 17 for 17 degrees of freedom. While A and m are strongly correlated parameters, n is defined without ambiguity from the ratio of the cross sections measured at both values of $\sqrt{s}$ *).

4 - Electron pairs production [2]

a) Hadron rejection

- The air Cerenkov counter gives a rejection factor of 10^3

- Simultaneous measurement of the charged particle momentum in the magnet and charged particle energy in the lead glass, the rejection factor is 10^2 by comparing P and E

- Another rejection factor with the pulse height in the F counter hodoscope : 85 % of the electrons shower in the 2 cm of iron in front of this counter.

b) Gamma rays rejection

- Before the magnet, the two electrons of a converted gamma ray are very close together. Hence, the pulse height in the A counters is equivalent to more than 1.5 minimum ionising particle.

- No other hit in the front drift chambers is in less than ± 1 cm of the reconstructed electron track.

*When compared to the Fermilab data [3] on charged pion in the same range of X_T ($n \simeq 8.2$ to 8.5, $m \simeq 9.0$ to 9.9), this result indicates a decrease of n, the X_T dependence not being significantly affected. A similar observation had abready been made in a lower X_T region at the highest ISR energies. In the interval $0.2 < X_T < 0.4$ the ratio between the average 400 GeV charged pion cross sections and the present data corresponds to $n = 7.3 \pm 0.6$.

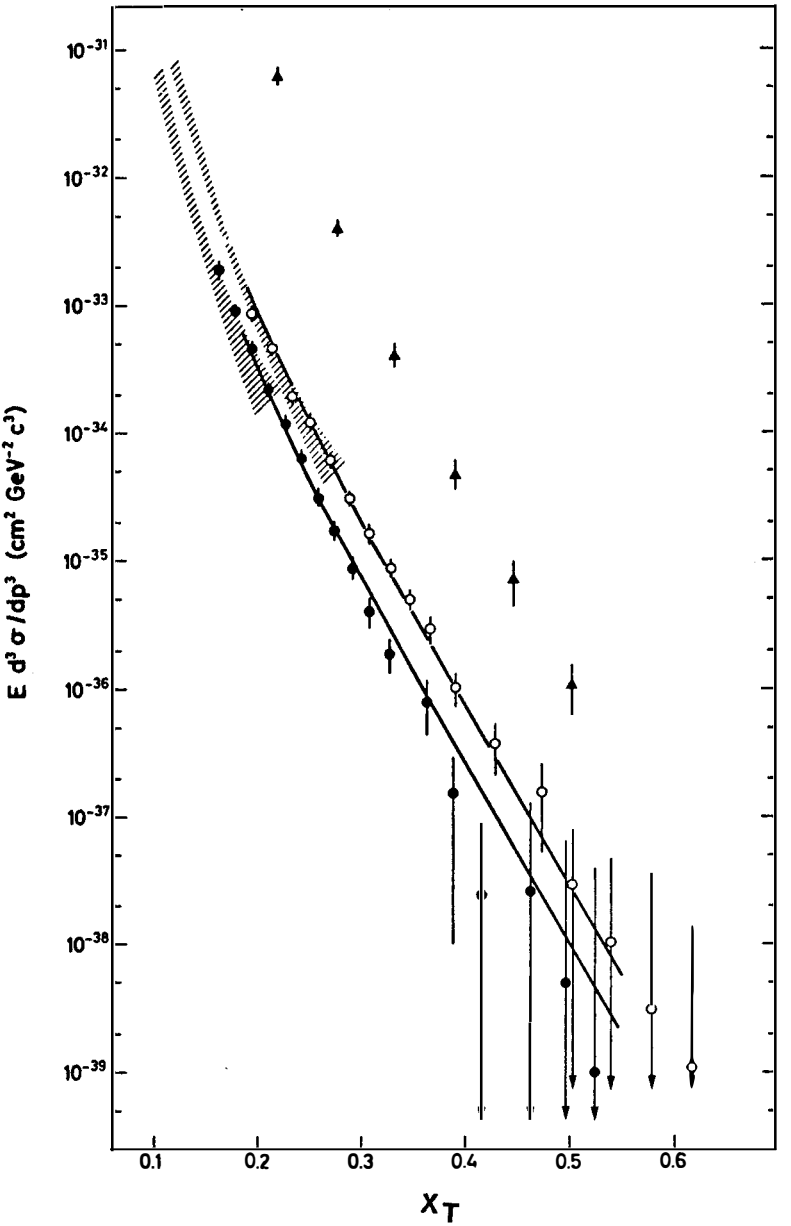
10^{-31}
10^{-32}
10^{-33}
10^{-34}
10^{-35}
10^{-36}
10^{-37}
10^{-38}
10^{-39}
E d³σ/dp³ (cm² GeV⁻² c³)
0.1
0.2
0.3
0.4
0.5
0.6
x_T

Figure 2

5 - Data reduction

An electron is defined as a fully reconstructed track with an associated hit in a Cerenkov cell. The electron energy is defined as the energy deposited in the block hit plus all the adjacent ones. With these minimal requirements an electron pair spectrum using the momentum or the energy in the lead glass shows a clear J/ψ signal. (Fig. 3a,b)

The two electrons are taken in opposite arm of the spectrometer. Fig. 3 represents opposite e^+e^- pairs as well as $(e^+e^+ + e^-e^-)$ pairs of same sign, this is the background of the data. In fig. 4, we represent the same data but with stronger cuts, we require :

- The pulse height in the A counters is equivalent to less than 1.5 minimum ionising particle to avoid Dalitz pairs and γ ray conversions.

- No other hit in the front drift chambers is in less than $\pm$ 1 cm of the reconstructed electron track (same purpose than above)

- No other track than the electron is in the same Cerenkov cell.

- We require that the quantity $-2 < \frac{P-E}{P+E} < 2$

- The F counter pulse height is imposed to be above 1.4 of a minimum ionising particle (a shower has started)

- In conclusion, we get a clean sample of e^+e^- pairs with less than 10 % background.

6 - Cross Section

Events in the mass range 2.5 - 3.4 GeV are considered as J/ψ's. To obtain the cross section as a function of P_T, the acceptance $\Delta y \, \Delta\phi$ of our apparatus (y rapidity, ϕ azimuthal angle) is calculated by Monte Carlo technics.

The invariant cross sections shown in fig. 5 are fitted to the set of formulae [Table 1] :

$$E \frac{d^3\sigma}{dp^3} = Ae^{-bm_T}, \; Ae^{-bp_T}, \; Ae^{-bp_T^2}$$

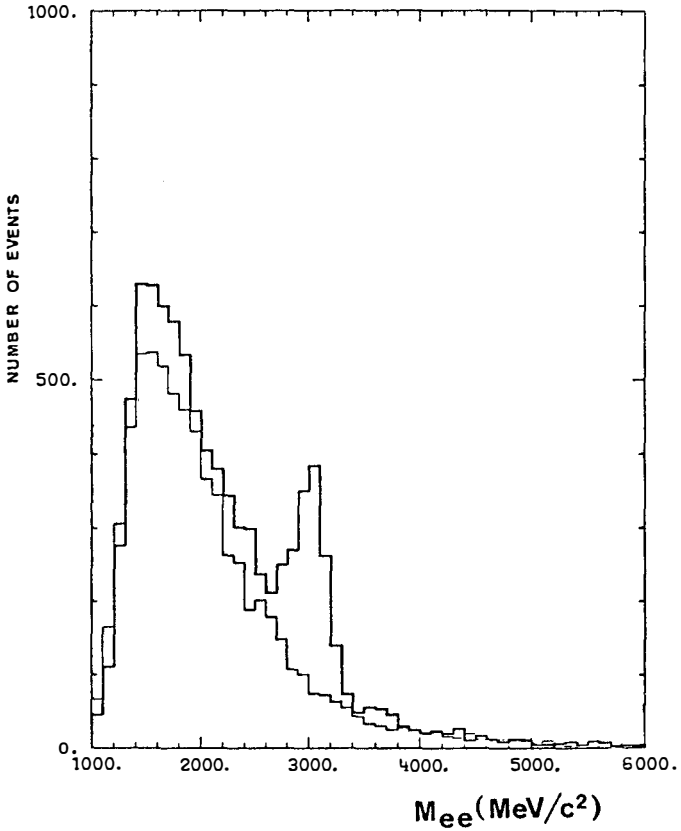

Figure 3a
Electron pair mass spectrum (mass-computed with momentum)
—— like sign
▬▬ unlike sign

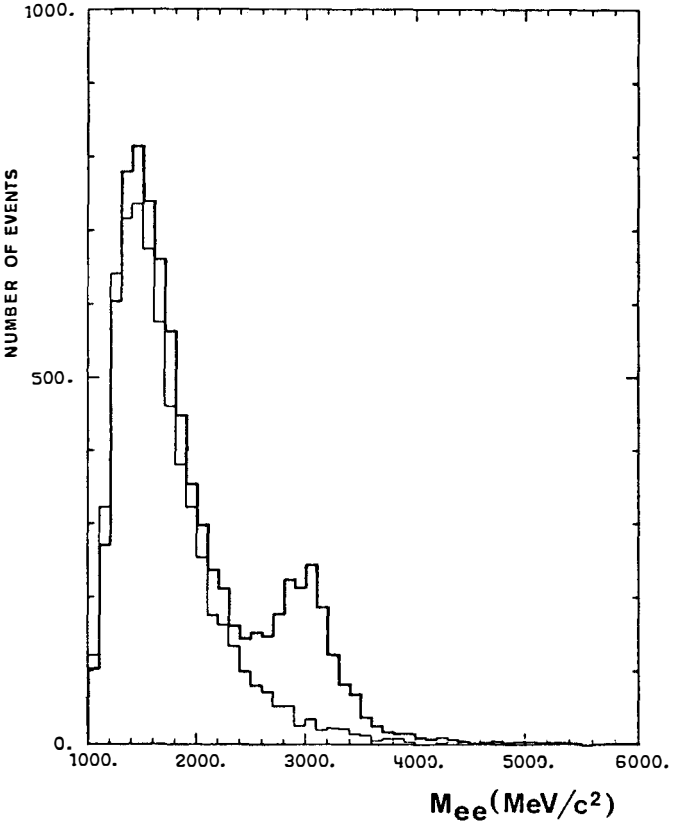

Figure 3b
Electron pair mass spectrum (mass computed with energy)
—— like sign pairs
━━ unlike sign pairs

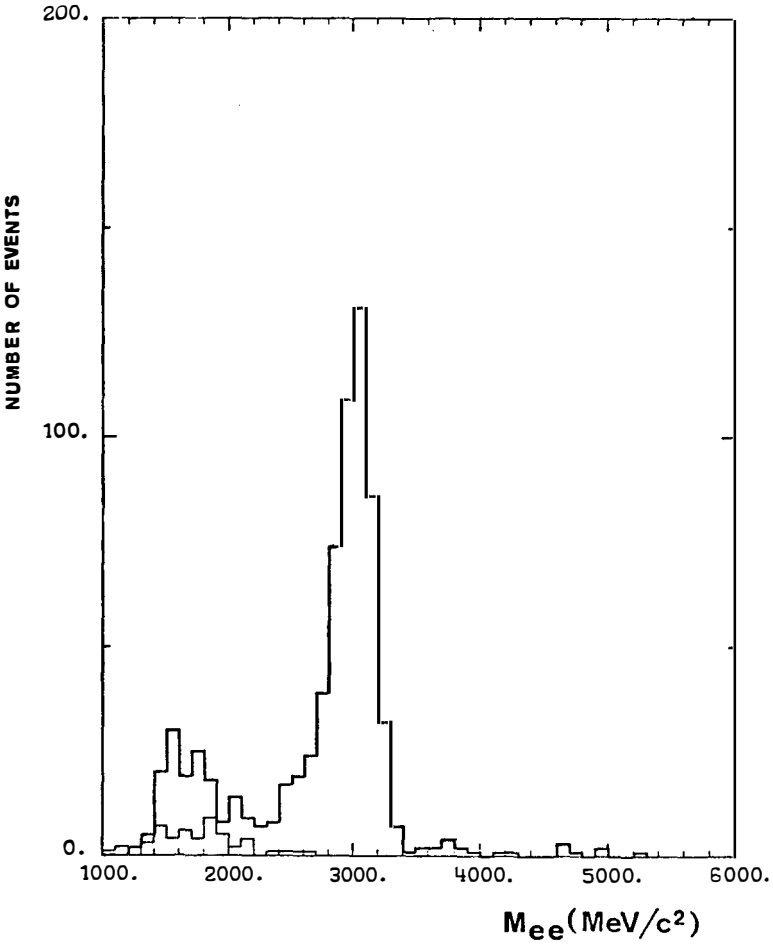

Figure 4
Electron pair mass spectrum with severe cuts
—— like sign
—— unlike sign

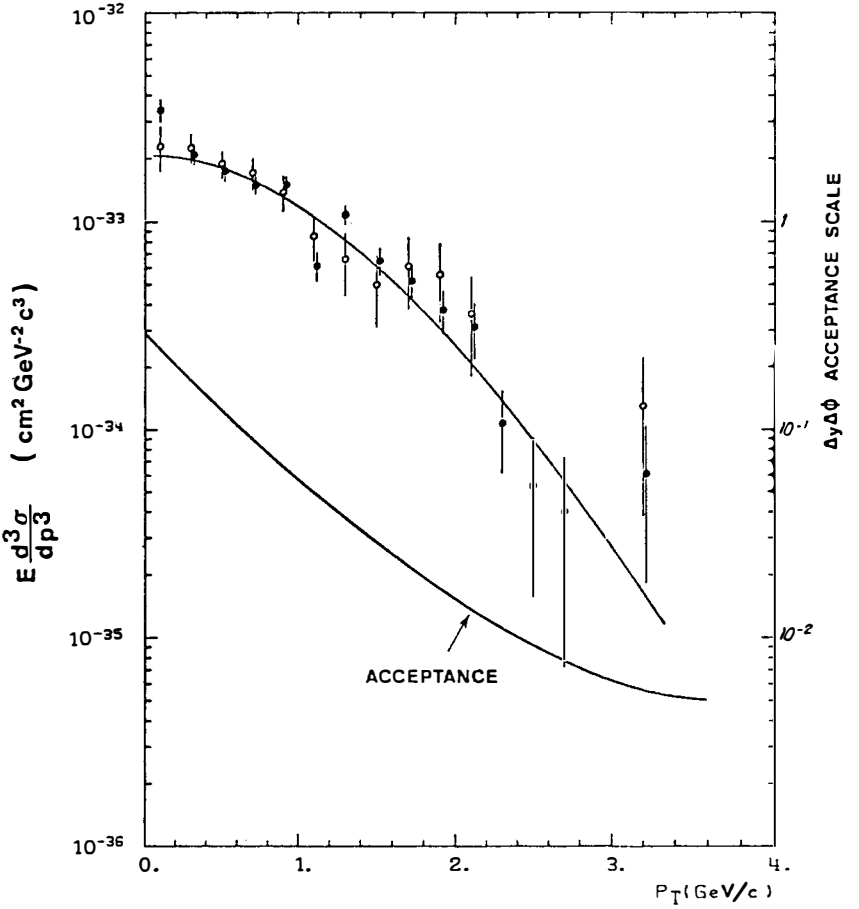

Figure 5

$B\,E\,\frac{d^3\sigma}{dp^3}$ ($pp \to \psi + X$) as a function of P_T

● $\sqrt{s}$ = 52 GeV
o $\sqrt{s}$ = 63 GeV

$\sqrt{s}$	30.6 GeV	52.7 GeV			0.62.4 GeV		
$d\sigma/dy\|_{y=0}$	$(6.58\pm1.76)10^{-33}$	$(1.096\pm0.041)10^{-32}$			$(1.02\pm0.07)10^{-32}$		
		A	B	χ^2	A	B	χ^2
Ae^{-Bp_T}		$(3.53\pm0.23)10^{-33}$	1.27 ± 0.06	42/12	$(3.49\pm0.35)10^{-33}$	1.32 ± 0.1	13/11
$Ae^{-Bp_T^2}$		$(1.99\pm0.11)10^{-33}$	0.52 ± 0.04	46/12	$(2.16\pm0.20)10^{-33}$	0.58 ± 0.8	8/11
$Ae^{-B(m_T-m_\psi)}$		$(2.06\pm0.11)10^{-33}$	3.57 ± 0.25	44/12	$(2.22\pm0.20)10^{-33}$	3.94 ± 0.50	9/11

Table I

In fig. 6 we represent the cross section $B \left.\frac{d\sigma}{dy}\right|_{y=0}$ for the J/ψ at three C.M. energies $\sqrt{s}$ = 30.6, 52.7, 62.4 GeV. These results together with other results [4] are plotted on the excitation curve ; at ISR energies, a plateau has been reached.

7 - Continuum cross section

For masses below 2.5 GeV it is necessary to apply the tight selection criteria. For masses above 2.5 GeV, it was already pointed out that it was not necessary. fig. 7 represents the cross section $\left.\frac{d^2\sigma}{dM\ dy}\right|_{y=0}$ for two ISR averaged energies (53, 63 GeV) as a function of the e^+e^- mass.

The ψ and ψ' decay and the continuum contribute to the cross section. To extract the latter, the ψ and ψ' shape is calculated by taking into account the chamber resolution, the multiple scattering and the bremstrahlung of the electron in the ISR vacuum pipe and in the A counters. The electron pair spectrum is written as :

$$\left.\frac{d^2\sigma}{dM\ dy}\right|_{y=0} = \frac{A}{M^N} + C\,\psi(M) + D\,\psi'(M)$$

where $\psi(M)$, $\psi'(M)$ is the $\psi(\psi')$ shape normalized to one,

$$\int \psi(M)\ dM = 1 \ , \int \psi'(M)\ dM = 1$$

C and D are in fact $B \left.\frac{d\sigma}{dy}\right|_{y=0}$ cross section for ψ and ψ'

The fit is shown in fig. 7

$$A = (10 \pm 3.6) \times 10^{-32}\ cm^2$$

$$N = (5.2 \pm 0.54)$$

$$C = (1.1 \pm 0.04) \times 10^{-32}\ cm^2$$

$$D = (0.021 \pm 0.006) \times 10^{-32}\ cm^2$$

From these values, the ratio of ψ' to ψ production times their branching ratio is $(1.9 \pm 0.6) \times 10^{-2}$.

8 - Comparison with other experiments

We have plotted $M^3 \frac{d\sigma}{dM}$ versus the scaling variable S/M^2 (fig.8). The solid line is the Drell Yan model calculation using the quark

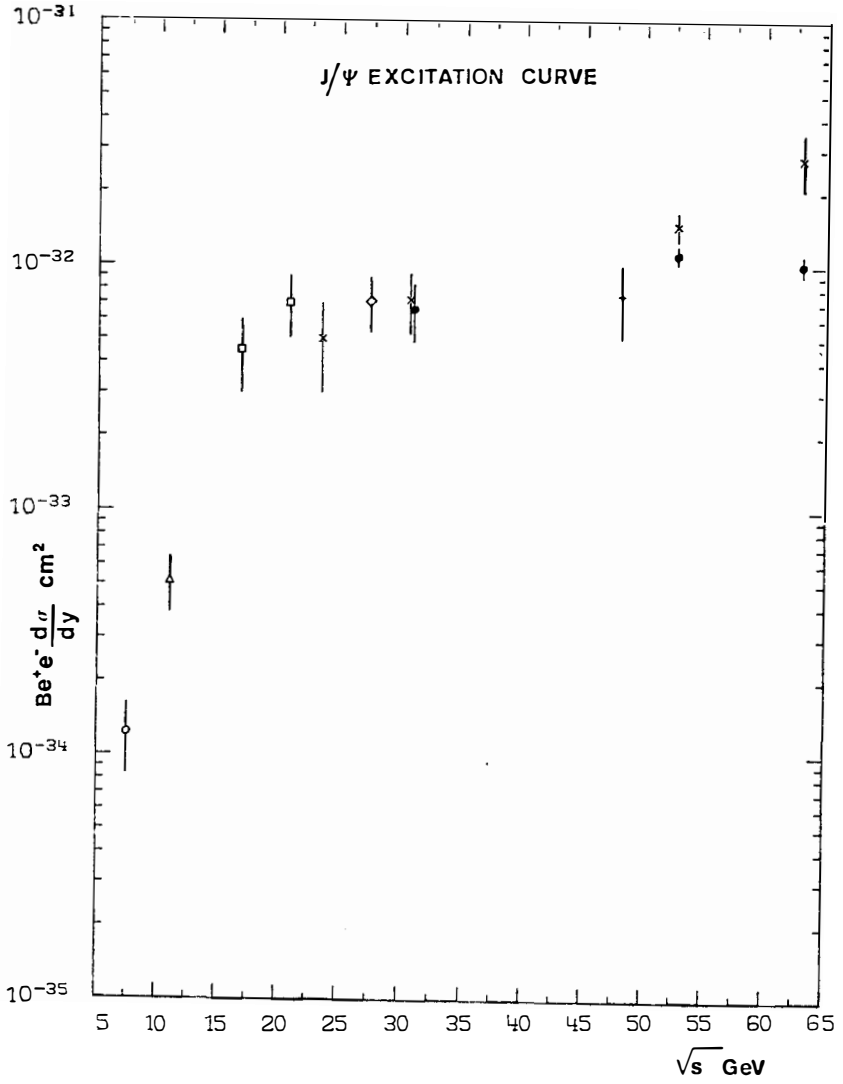
J/ψ EXCITATION CURVE
10^{-31}
10^{-32}
10^{-33}
10^{-34}
10^{-35}
$Be^+e^- \frac{d\sigma}{dy}$ cm²
5 10 15 20 25 30 35 40 45 50 55 60 65
$\sqrt{s}$ GeV

Figure 6

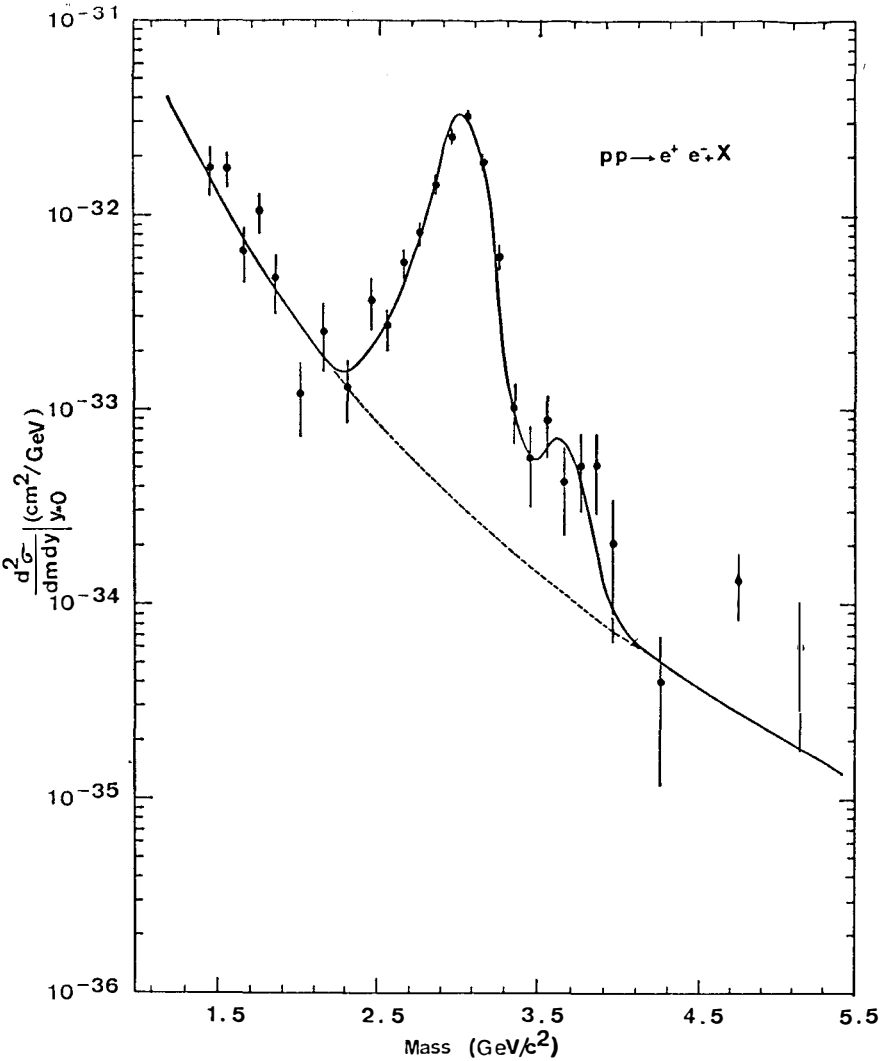
10^{-31}
10^{-32}
10^{-33}
10^{-34}
10^{-35}
10^{-36}
$\frac{d^2\sigma}{dm\,dy}\Big|_{y=0}$ (cm²/GeV)
pp → e⁺ e⁻ X
1.5
2.5
3.5
4.5
5.5
Mass (GeV/c²)

Figure 7

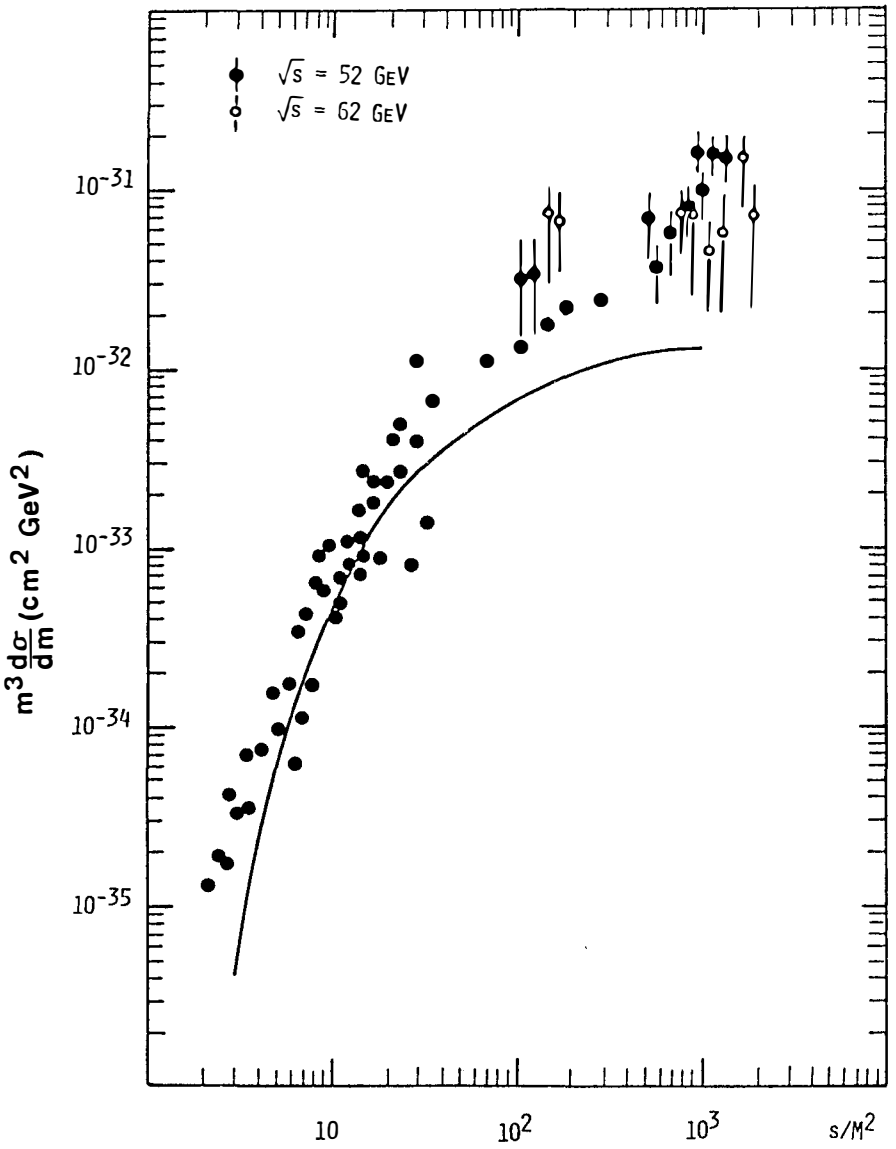
√s = 52 GeV
√s = 62 GeV
10^{-31}
10^{-32}
10^{-33}
10^{-34}
10^{-35}
$m^3 \frac{d\sigma}{dm}$ (cm^2 GeV^2)
10
10^2
10^3
s/M^2

Figure 8

structure function $0.15\ (1-x)^{7\ 5)}$. Our data are one order of magnitude above the curve of the Drell Yan calculation. Let us stress that the experimental points follow a general smooth trend which nevertheless differs from the above Drell Yan computation which was matched to the lower energy points.

9 - Upper limit on the T cross section

In this experiment, no event with electron pair mass above 6 GeV has been observed. The total integrated luminosity is $1.5 \times 10^{37} cm^2$ and with the acceptance of the apparatus it follows that to 90 % confidence level, the cross section :

$$\frac{d\sigma}{dy}\Big|_{y=0} (9.4) < 20 \times 10^{-36} cm^2$$

The increase of cross section between FNAL energy $\sqrt{s}$ = 27 GeV and ISR energy $\sqrt{s}$ = 53 GeV is less than 110.

References

1) A.C. CLARK et al., Physics Letters 74B (1978) 267.

2) A.G. CLARK et al., to be published in Nuclear Physics.

3) D. ANDREASYAN et al., Physical Review Letters 38 (1977) 112.

4) For a recent compilation, see : B.C. BROWN et al., FNAL preprint FERMILAB-77/54-EXP (1977).

5) R.F. PEIERLS et al., BNL-22628 (1977).

PRODUCTION OF MUON PAIRS IN THE CONTINUUM REGION BY 39.5 GeV $\pi^{\pm}$, $K^{\pm}$, p and $\bar{p}$ BEAMS INCIDENT ON A COPPER TARGET

(M.J. Corden, J.D. Dowell, D. Eastwood, J. Garvey, R.J. Homer, M. Jobes, I.R. Kenyon, T.J. McMahon, R.J. Vallance, P.M. Watkins and J.A. Wilson)[1]
(J. Gago, M. Jung, P. Sonderegger, D. Treille and P.L. Woodworth)[2]
(V. Eckardt, J. Fent, K. Pretzl, P. Seyboth and J. Seyerlein)[3] D. Perrin[4]
(B. Chaurand, G. de Rosny, L. Fluri, A. Romana, R. Salmeron and A. Wijangco)[5]
(K.C.T.O. Sumorok)[6]

1) Birmingham University, Birmingham, U.K. ; 2) CERN, European Organization for Nuclear Research, Geneva, Switzerland ; 3) Max Planck Institut für Physik und Astrophysik, München, Germany ; 4) University of Neuchâtel, Switzerland. 5) Ecole Polytechnique, Palaiseau, France ; 6) Rutherford Laboratory, Oxfordshire U.K.

Presented by A. ROMANA

ABSTRACT

We report results on an experiment designed to measure muon pair production by 39.5 GeV/c $\pi^{\pm}$, $K^{\pm}$, p and $\bar{p}$ beam particles incident on a copper target using the CERN Omega spectrometer.

For incident π^-, the data extend up to $M = 5.7$ GeV/c^2 (i.e. $M^2/s \sim 0.4$) The resulting scaling cross section $M^3\, d\sigma/dM$ is much flatter than for p-N reactions and exceeds the latter by two or three orders of magnitude at $M^2/s \approx 0.3$. The $\bar{p}/\pi^-$ cross section ratio is around unity. The π^+/π^- ratio tends to 1/4 at high values of M^2/s.

RESUME

Nous présentons ici les résultats de l'étude de la production de paires de muons par interaction de $\pi^{\pm}$, $K^{\pm}$, p et $\bar{p}$ de 39.5 GeV/c avec une cible de cuivre. Cette expérience a été réalisée au CERN avec le spectromètre Oméga. Les données s'étendent jusqu'à une masse $M = 5.7$ GeV/c^2 ($M^2/s \sim 0.4$) pour les π^- incidents. La section efficace de "scaling" $M^3\, d\sigma/dM$ varie beaucoup moins rapidement que celle des interactions p-N et dépasse celle-ci de deux à trois ordres de grandeur pour $M^2/s \approx 0.3$. Le rapport des sections efficaces $\bar{p}/\pi^-$ est de l'ordre de l'unité; celui de π^+/π^- tend vers une valeur 1/4 pour les grandes valeurs de M^2/s.

PRODUCTION OF MUON PAIRS IN THE CONTINUUM REGION BY 39.5 GeV/c $\pi^{\pm}$, $K^{\pm}$, p and $\bar{p}$ BEAMS INCIDENT ON A COPPER TARGET.

INTRODUCTION.

The aim of the experiment was to study the J/ψ and the dimuon continuum production by the six different beam particles.

Results on the J/ψ production have already been published [1]. We have seen no extra muon in association with the J/ψ. Here we report on the production of dimuons in the continuum mass region.

EXPERIMENTAL FEATURES.

Negative and positive unseparated beams with 39.5 GeV/c momentum from the CERN SPS were incident on a copper target located in the Omega spectrometer. The beam composition was :

negative beam : π^- (93.9%) K^-(3.4%) $\bar{p}$ (2.7%)
positive beam : π^+ (72.2%) K^+(3.7%) p(24.1%).

The layout (Fig.1) has already been described in ref.1; it was designed to detect muon pairs with high efficiency for Feynman x_F- values above 0.0 . Only muon pairs with mass M greater than 1.5 GeV/c^2 were considered in this study; the data extend up to M = 5.7 GeV/c^2 (i.e. $M^2/s \lesssim 0.4$) for incident π^- .

FIG. 1

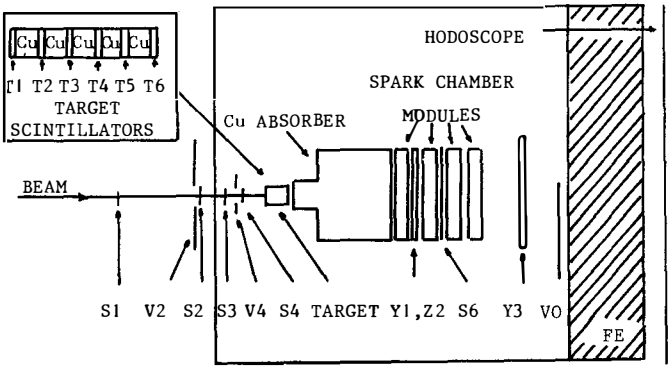

The criteria for event selection are described in ref.1, but for the study of the continuum, we added a further requirement : the demand that both muons were in time with the triggering beam particle. This cut does not decrease the ψ-signal but reduces the amount of like sign muon pairs to a small fraction of $\mu^+\mu^-$ pairs, namely 3% around M = 1.7 GeV/c^2 and less than 1% above 2.7 GeV/c^2.

The effect of secondary interactions is more serious and has been studied by a Monte-Carlo program : this effect averages 15% below the ψ-region and is negligible above ; it is assigned a 50% relative error and is subtracted in the following results.

The good knowledge of longitudinal position of the interaction point ($\pm$ 2 cm) leads to a mass resolution of about 15% (FWHM of the ψ $\sim$ 450 MeV/c^2) in spite of the large multiple scattering in the copper absorber.

The number of dimuon events is given in table 1, corresponding to a number of incident particles on the target of 4.0 x 10^{10} and 1.7 x 10^{10} for negative and positive beam respectively.

TABLE 1 : Number of dimuons for various mass intervals ($x_F > 0$): unweighted $\mu^+\mu^-$, (weighted $\mu^+\mu^-$ number) , [unweighted like sign $\mu\mu$ number] .

Incident particle	π^-	π^+	K^-	K^+	$\bar{p}$	p
1.5 < M $\leq$ 2.7	877 (3795) [33]	191 (784) [8]	33 (90) [0]	8 (40) [0]	27 (90) [0]	28 (102) [2]
M > 3.5	70 (171) [1]	8 (16) [0]	2 (4) [0]	0	2 (5) [0]	0
2.7 < M $\leq$ 3.5 (ψ)	770 (1920) [2]	179 (450) [0]	22 (55) [0]	6 (22) [0]	19 (52) [0]	8 (25) [0]

Positive/Negative Beam $\approx$ .35

RESULTS

Fig.2 shows the differential cross-section per copper nucleus $d\sigma/dM$ as a function of the dimuon mass, for each type of beam particle and for $x_F \geq 0$ (a 20% normalization error is not included in the error). The principal features are that within our errors the cross-sections are similar for π^+ and π^-, and for K^+ and K^- but are different for p and $\bar{p}$. The differential cross-section for π^- falls approximately as exp $(-13\ M/\sqrt{s})$.

FIG. 2

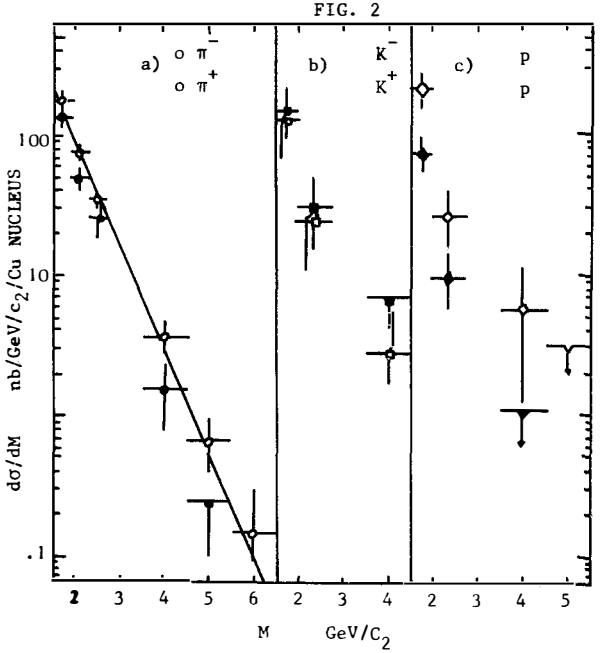

Fig.3 shows several cross-sections relative to the π^- - induced cross section. The decrease of the π^+/π^- ratio from ~ 0.8 at small mass ($M < 2.\ GeV/c^2$ to ~ 0.25 at high mass has already been noticed [2] and follows the trend expected from the Drell-Yan mechanism; the $\bar{p}/\pi^-$ ratio has large errors but is nevertheless compatible with one, which implies that the numerical inferiority of antiquarks in π^- with respect to the $\bar{p}$ is com-

pensated by their flatter x-distribution ; the p/π^- ratio is very low and seems to decrease as the mass increases (in p-N interactions, the antiquarks have to come from the sea and have low x).

FIG. 3

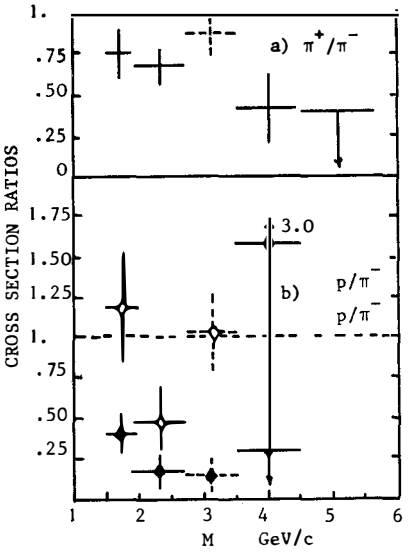

FIG. 4

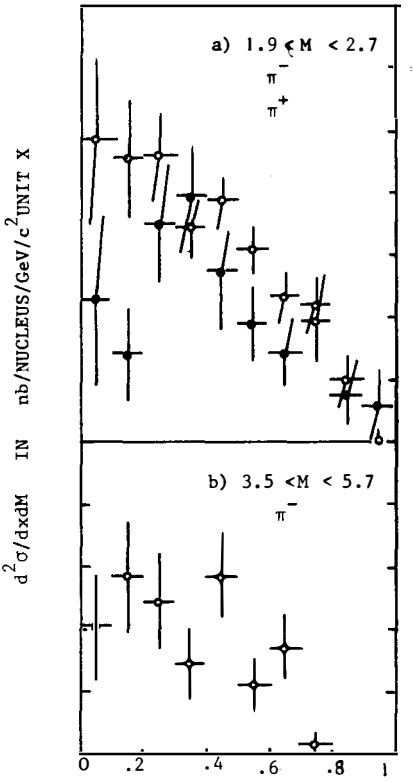

The x_F-distribution is given for π^+ and π^- in the mass interval $1.9 \leq M < 2.7$ GeV/c^2 and for π^- only above 3.5 GeV/c^2 , in Fig.4 . Error bars are large but we can observe that the main differences occur for $x_F \lesssim 0.3$.

In figure 5 our results for π^- and proton are plotted in terms of the scaling variable $M^3 \frac{d\sigma}{dM}$ versus M^2/s. Also shown are previous π^- results which extend only up to $M^2/s \approx 0.04$, and proton data obtained at BNL [3] and FNAL [4].

The ratio π^-/p increases with M^2/s and becomes about 100 at $M^2/s = 0.3$ if π^- are compared to the reanalysed BNL data ($\sqrt{s} \approx 7$ GeV) and about 1 000 if compared to the FNAL data ($\sqrt{s} \approx 28$ GeV).

FIG. 5

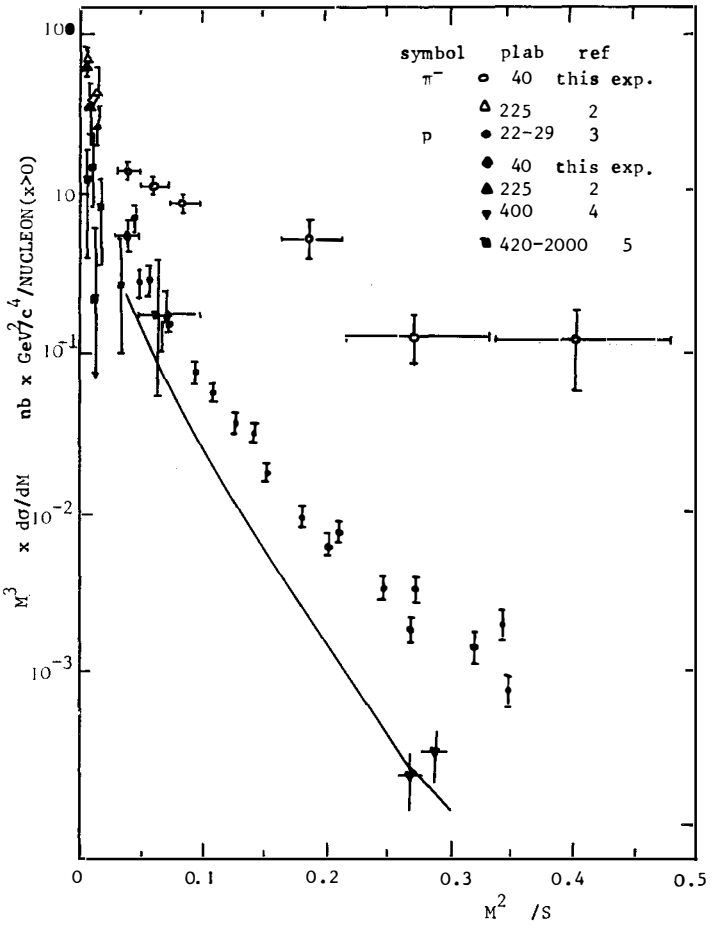

CONCLUSIONS

We can summarise our results as follows :

- the ratio of the π^- - to the p - induced cross section changes from about unity at small M^2/s to 10^2 - 10^3 at $M^2/s \approx .3$
- secondly the ratio of the $\bar{p}$ to π^- induced cross sections is around unity.
- thirdly, the π^+/π^- ratio tends at high M^2/s towards the value 1/4.

These three observations are in agreement with the expectations of the Drell-Yan mechanism.

This experiment will be repeated with improved statistics in Summer 78.

REFERENCES

1) M.J. Corden et al., Physics Letters 68B, 96 (1977)
2) J.G. Branson et al., Phys. Rev. Letters 38, 1334 (1977)
3) J.H. Christenson et al., Phys. Rev. D8, 2016 (1973); data reanalysed by L.M. Lederman and B.G. Pope, Physics Letters 66B, 486 (1977)
4) D.M. Kaplan et al., Phys. Rev. Letters 40, 435 (1978)
5) J.H. Cobb et al., Physics Letters 72B, 273 (1977).

MEASUREMENT OF VECTOR MESON AND DIRECT PHOTON PRODUCTION AT LARGE TRANSVERSE MOMENTUM AT THE CERN ISR

Presented by Pavel Rehak
for
J.H. Cobb, S. Iwata[1], R.B. Palmer, D. Rahm, P. Rehak and I. Stumer
Brookhaven National Laboratory[2], Upton, New York 11973, USA
C.W. Fabjan, E.D. Fowler[3], I. Mannelli[4], P. Mouzourakis,
K. Nakamura[5], A. Nappi[4], W. Struczinski[6] and W. J. Willis
CERN, Geneva, Switzerland
M. Goldberg, N. Horwitz and G.C. Moneti
Syracuse University[7], Syracuse, New York 13210, USA
C. Kourkoumelis and L.K. Resvanis
University of Athens, Athens, Greece
T.A. Filippas
National Technical University, Athens, Greece
and
A.J. Lankford
Yale University, New Haven, Connecticut 06520, USA

ABSTRACT

The production at large transverse momentum of low mass electron pairs was investigated at the CERN Intersecting Storage Rings using lithium/xenon transition radiation detectors and liquid argon calorimeters. Production of the vector mesons ρ^0, ω^0, and ϕ was observed with cross-sections consistent with the assumptions that ρ^0, ω^0, and π^0 production are nearly equal at large p_t and that ϕ production is suppressed by about an order of magnitude relative to ρ^0 and ω^0 production. The observed low mass virtual photon continuum between masses of 200 and 500 MeV was consistent with estimates of Dalitz decays plus predictions of the vector dominance model. The measured cross-section for virtual photon production enabled a limit of (0.5±1.0)% to be placed on the ratio of direct real photon production to π^0 production.

[1]Permanent address: Nagoya University, Nagoya, Japan
[2]Research under the auspices of U.S. Department of Energy
[3]Permanent address: Purdue University, Lafayette, Indiana 47907, USA
[4]On leave of absence from the University of Pisa and INFN Sezione di Pisa, Italy
[5]Permanent address: University of Tokyo, Tokyo, Japan
[6]Now at: Physics Institute, T.H. Aachen, Aachen, Germany
[7]Work supported by the National Science Foundation

MESURES DE LA PRODUCTION DE MESONS VECTORIELS ET DE PHOTONS DIRECTS POUR DE GRANDS MOMENTS TRANSVERSES AU CERN ISR

ABSTRACT

La production de paires d'électrons de faible masse pour de grands moments transverses a été étudiée au CERN Intersecting Storage Rings à l' aide de détecteurs de radiation a transition de lithium et de xénon et à l' aide de calorimètres à argon liquide. La production des mésons vectoriels ρ^o, ω^o, et ϕ à été observée avec une diffusion en accord avec l'hypothèse que les productions de ρ^o, ω^o et π^o, sont à peu près égales pour de larges valeurs de p_t et que la production de ϕ est réduite d'à peu pres un ordre de grandeur par rapport aux productions de ρ^o et ω^o. Le continuum de faible masse de photons virtuels entre les masses de 200 et 300 GeV était en accord avec les estimations des désintegrations de Dalitz et avec les prédictions du modèle du vecteur dominant. La diffusion mesurée pour la production de photons virtuels à permis d' attribuer la limite de (0.5±1.0)% au rapport de la production directe de photons réels et de la production de π^o.

INTRODUCTION

The central purpose of experiment R806 at the CERN ISR is an investigation of inclusive production of electron-positron pairs. After a brief review of the new technique associated with the apparatus, the lower part of e^+e^- invarient mass spectrum is explored.

1. Production of vector meson ρ^0, ω and ϕ is reported. The observed cross section for ρ^0 and ω are nearly equal to π^0 cross section at large p_t and ϕ production is suppressed by about an order of magnitude.
2. The expected relation between low mass electron pairs and real photons is used to determine the direct hadronic production of photons. The observed spectrum is consistent with expectations from the decay of known meson. This leads to a limit of (.5±1.)% on the ratio of direct real photon production to π^0 production at $\langle\sqrt{s}\rangle$ = 55 GeV.

APPARATUS

The apparatus, composed of four subassemblies known as octants, is shown schematically in Fig. 1a,b. Each octant covers 45^o in azimuth and the polar angle interval 45^o - 135^o. An electron emerging from intersecting region and passing through an octant encounters (i) Two low mass PWC's utilizing charge division readout. These chamber's primary function is to provide tracking to the production vertex; (ii) Two sets of scintillators. These are used in tracking and provide an important minimum ionization selection for electrons; (iii) Two lithium foil transition radiators each followed by a Xe filled PWC with charge division readout. Also used for position measurement, the PWC pulse height contributes to hadron rejection when minimum ionizing electrons are selected; (iv) The liquid argon calorimeter. This device provides position information ($\sigma \approx 5$ mm), electromagnetic shower energy measurement ($\sigma/E \approx 12\%/\sqrt{E}$) and additional hadron rejection, in addition to its utilization as a basic component of the various triggers. The two triggers important to the data under discussion require either

a) local energy deposit (> 1 GeV) characteristic of showers in calorimeters of 2 octants (Double High Trigger), or

b) crude track segment correlations formed by the calorimeter hit, scintillation counters, and PWC's, with reduced calorimeter thresholds (Double Correlation Trigger).

All aspects of octant performance were determined by exposure to electron and hadron beams at the CERN P.S.

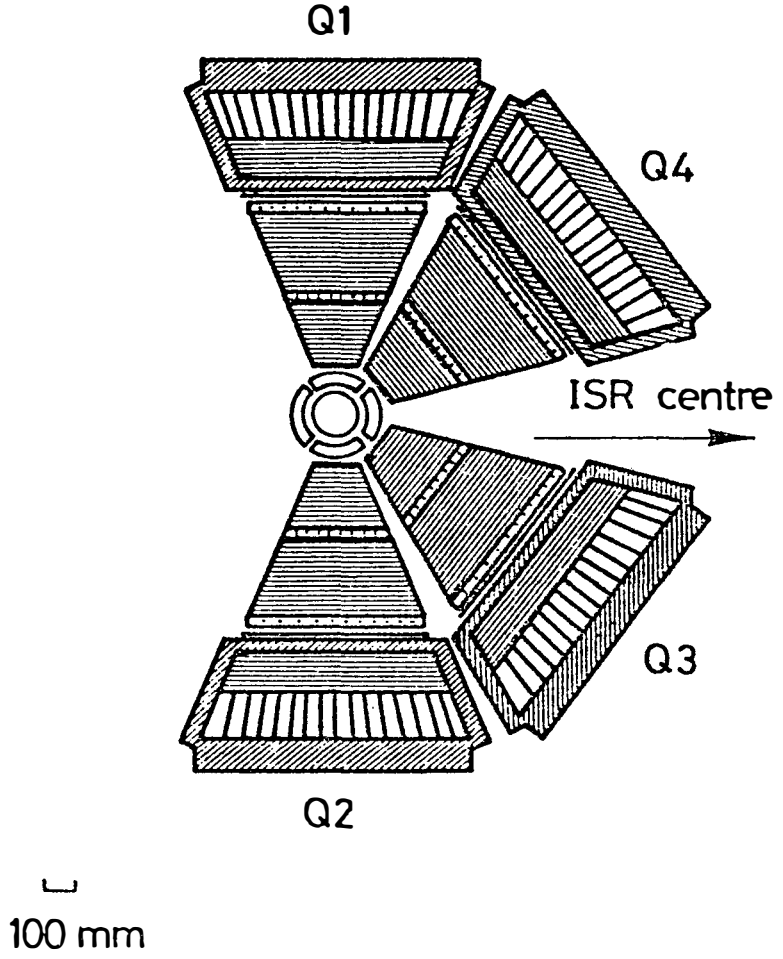

Fig. 1a) Arrangements of four octants around the intersection region.

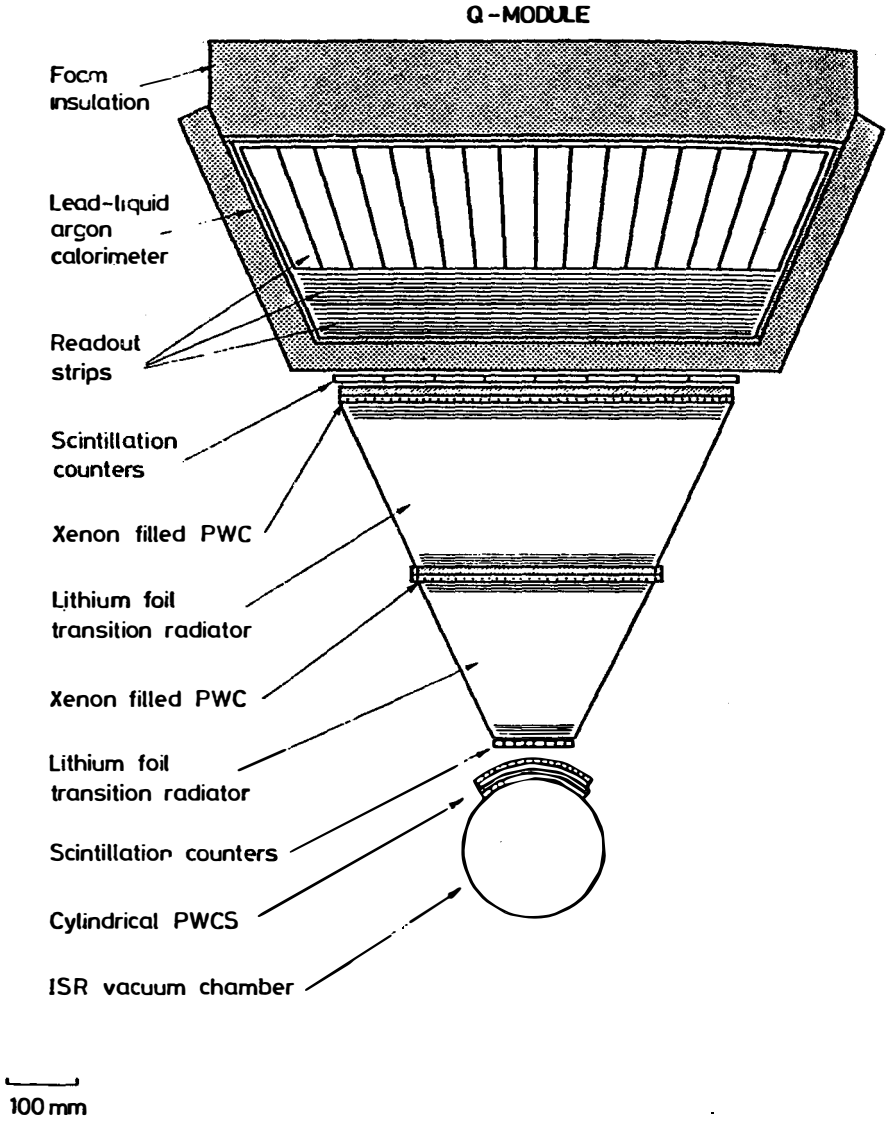

Fig. 1b) Layout of the detectors in an octant.

Further details regarding the experimental apparatus as well as other results not reported here may be found in Reference 1.

THE OLD VECTOR MESONS ρ^o, ω^o, AND ϕ

The cross sections for the production of the old vector mesons ρ^o, ω^o, and ϕ were determined from event triggers from adjacent octants. The acceptance for this sample was higher than for other octant combinations, and the geometrical and trigger efficiency was much less sensitive to uncertainties in the trigger thresholds. The integrated luminosity for this sample was 9.93×10^{36} cm^{-2}, consisting of 9% running at $\sqrt{s}$ = 30 GeV, 59% at $\sqrt{s}$ = 52 GeV, and 32% at $\sqrt{s}$ = 62 GeV.

Backgrounds from charged hadrons were suppressed at the trigger level by demanding longitudinal and radial shower development characteristic of electrons. Residual charged hadrons were eliminated by a requirement on the transition radiation signal. Decay photons could cause background by converting to electron pairs, or by spatially overlapping with a charged track in the detector. These backgrounds were eliminated by strict requirements on pulse height in the scintillator hodoscopes and on geometrical χ^2 of the track and track-shower fits and by searching the detector for another photon which, when combined with an electron candidate, gave the π^o mass. These requirements were made in such a way as to allow the stringency of all cuts to be simultaneously varied, in order to allow study of the background contributions to various mass regions. The off-line requirements chosen for final electron pair identification gave an efficiency of 22% for two true electrons.

Figure 2a shows the electron pair mass distribution after all the requirements were applied. The peaks in the mass spectrum at 775 MeV, 1025 MeV, and 2.95 GeV were associated with the $\rho^o + \omega^o \to$ ee, $\phi \to$ ee, and $J/\psi \to$ ee reactions, respectively. The resonance masses and widths were consistent with the known values combined with experimental resolution. Note that, since opening angles for these pairs are typically about 60°, the p_t of the observed pairs is approximately equal to their mass; thus, the J/ψ peak corresponds to J/ψ produced with $p_t \sim 3$ GeV. The efficiency of the identification requirements was determined from their effect on pairs in a sample of J/ψ events.

The mass distribution of the background remaining after electron-pair identification was assumed to have the same shape as the mass spectrum with no identification (not shown), which was more than 98% background.

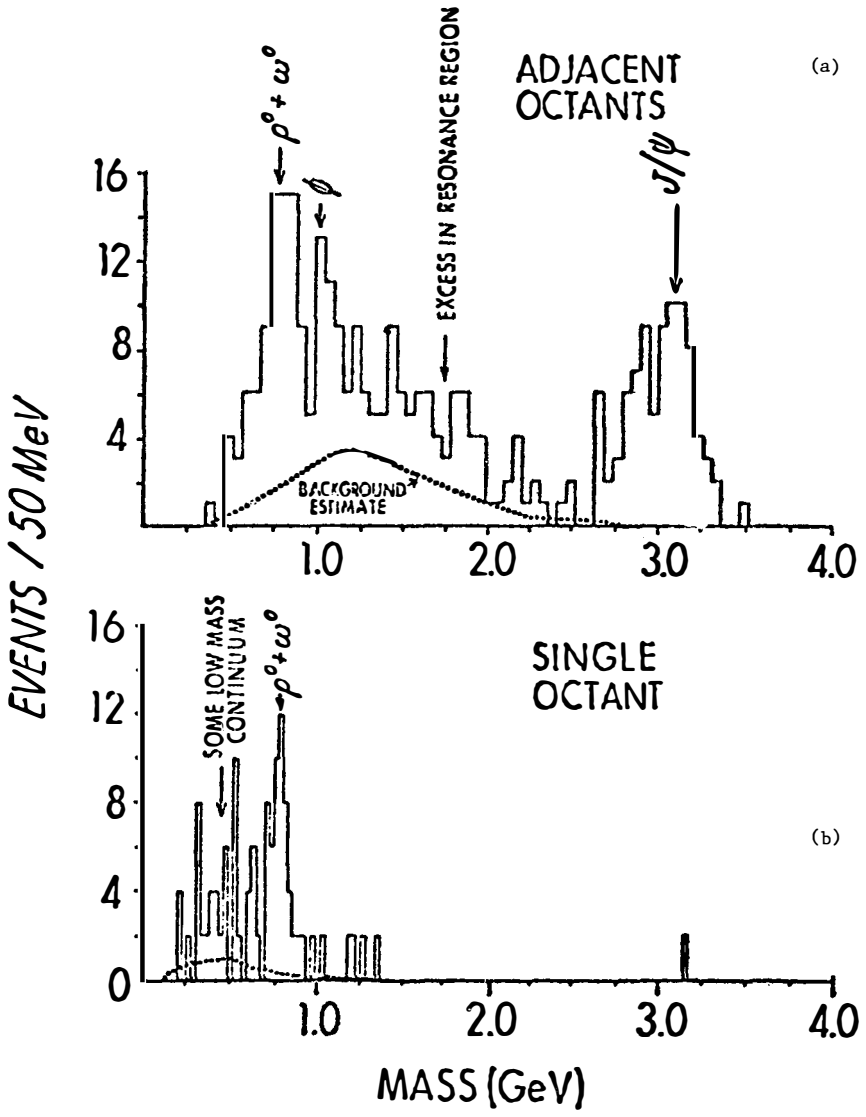

Fig. 2. The experimental mass spectrum for the electron pairs
a) from adjacent octant trigger
b) from the same octant trigger.

This shape incorporated the effects of the geometrical and trigger acceptance for background and any mild correlations in the background. The magnitude of the residual background was determined using two techniques. The first method was to leave the magnitude of the background as a free parameter when the mass distributions were fit for signal and background. The second technique was to first combine an electron candidate from one pair with an electron candidate from another pair to create a "fake" pair candidate. This recombination was performed for all electron candidates in the sample with no identification; however, fake pairs were always formed such that the two candidates of the fake pair were in the same octants as the candidates of the real pair. In this way, the normalization for each octant combination was conserved, in order to maintain some of the possible correlations of the real sample. After the pairs were shuffled in this way, the electron-pair identification requirements were applied. The number of fake pairs which passed the pair-identification requirements was corrected for the presence of real electrons in the sample in order to obtain the likelihood of a background pair passing the requirements. This likelihood was then used to determine the magnitude of the residual background for that particular level of identification requirements. The magnitude of the background determined using this second method was approximately 30% lower than that determined by the fit, that is, the two methods were consistent within the uncertainties of the fitting procedure.

The mass distribution of Fig. 2a was fit in the region $400 < m_{ee} < 1150$ MeV by two Gaussian peaks of variable magnitude and width, one centered at the mean mass (770 MeV) of the ρ^o and ω^o and the other centered at the mass of the ϕ (1020 MeV), plus a background with the shape of the sample before identification and with magnitude initially given by the procedure described above and then made variable.

The geometrical and trigger efficiencies for ρ^o , ω^o , and ϕ produced with $p_t > 1$ GeV were determined by the Monte Carlo acceptance program. An E_T^{-8} ($E_T^2 = m^2 + p_t^2$) distribution was assumed to give the p_t dependence for production of each particle. The program also computed the efficiency of the TR requirement, since that requirement was not applied in an energy-independent way. The trigger acceptance in adjacent octants was maximum at approximately 1.1 GeV. Thus, the ϕ mass was near the peak of the acceptance; whereas the ρ^o and ω^o masses were on the fairly steep threshold for acceptance, with acceptance approximately half that of the ϕ.

The measured cross-sections for $\rho^o + \omega^o \rightarrow$ ee and $\phi \rightarrow$ ee, computed from the weighted average of the two fits (with and without background level fixed) were

$$B_{\rho\rightarrow ee}\left[\frac{d\sigma}{dy}\right]_{\rho^o} + B_{\omega\rightarrow ee}\left[\frac{d\sigma}{dy}\right]_{\omega^o} = (1.19 \pm 0.58) \times 10^{32}\ cm^2$$

$$B_{\phi\rightarrow ee}\left[\frac{d\sigma}{dy}\right]_{\phi} = (2.57 \pm 1.26) \times 10^{-33}\ cm^2.$$

Based on the branching ratios for ρ^o, ω^o, and ϕ determined in e^+e^- storage rings and assuming equal ρ^o and ω^o production cross-sections, the cross-sections determined for production of ρ^o, ω^o, and ϕ were

$$\left[\frac{d\sigma}{dy}\right]_{\rho^o} = \left[\frac{d\sigma}{dy}\right]_{\omega^o} = (1.00 \pm 0.51) \times 10^{-28}\ cm^2$$

$$\left[\frac{d\sigma}{dy}\right]_{\phi} = (8.03 \pm 3.97) \times 10^{-30}\ cm^2.$$

These cross-sections give the ratio, in which most of the systematic uncertainties of the absolute cross-section determination are eliminated, of ρ^o production to ϕ production as

$$\left[\frac{d\sigma}{dy}\right]_{\rho} \Big/ \left[\frac{d\sigma}{dy}\right]_{\phi} = 12.4 \pm 2.9.$$

DIRECT PHOTON PRODUCTION

Copious production of real photons at high transverse momentum by direct, hadronic processes has been suggested by theoretical models[2] and some experimental results.[3] For example, direct photon production at the level of (20 ± 6)% of π^o production has been reported for $2.8 < p_T < 3.8$ GeV and $\sqrt{s}$ = 45 GeV and 53 GeV at the CERN ISR. The accuracy of such measurements of photon production is limited by large subtractions of photons from π^o and other meson decays, anti-neutron and K_L^o backgrounds of poorly known magnitude, and sensitivity to the nonlinearity of the energy response of the detector.[4] If real photons are produced hadronically, there should be a corresponding production of virtual photons which appear as electron pairs. For low electron pair masses, probably measured by the scale of m_p, the relationship between real and virtual photons (Eq. 1 below) should be accurate, allowing an estimate of photon production while avoiding the

above limitations. The measurements are made relative to the production of electron pairs from ρ^o and ω^o decays. Detector acceptance, backgrounds, and energy response are similar for $\gamma_{virtual} \to e^+e^-$ and $\rho^o + \omega^o \to e^+e^-$ samples. Moreover, direct virtual photons are distinguishable from virtual photons from meson decays (i.e. Dalitz pairs) by the mass spectrum of the electron pairs. In an appropriate mass region subtractions of Dalitz contributions from the virtual photon spectrum are small.

For this analysis, electron pairs with invariant masses between 200 and 500 MeV are used. Below 200 MeV the electron pair spectrum is dominated by Dalitz pairs from meson decays, especially from π^o decays at masses below the π^o mass. The $\rho^o + \omega^o \to e^+e^-$ signal observed with the same trigger and electron pair identification verifies the effectiveness of the detection and identification procedure and provides a normalization for the data. The above mentioned trigger b selected events with two showers each having the energy greater than approximately 1 GeV. Two correlated tracks were required within the same detector module but separated in azimuth by at least $8\frac{1}{2}^o$. For these events, analog signals from all planes of the detector modules were recorded for off-line reconstruction of tracks and showers and identification of electron pairs. The resolution of the detector allowed showers to be separated down to a minimum separation of about 3^o. The invariant mass distribution of the observed direct electron pairs from the same octant is shown in Fig. 2b for pairs with $p_T > 2.0$ GeV. The spectrum peaks at the mass of the ρ^o and ω^o, and the width of the peak is consistent with Monte Carlo estimates of the ρ^o mass width combined with the experimental resolution. The mass distribution of Fig. 2b also shows an electron pair signal at masses below the ρ^o and ω^o. This low mass signal, however, is smaller than the ρ^o and ω^o signal and lies in a mass region with 50% more acceptance than at the ρ^o and ω^o mass. There is no significant continuum signal at masses larger than the ρ^o and ω^o.

Studies showed that the level of background suppression in the final sample of electron pairs was similar in the low mass region ($200 < m_{ee} < 500$ MeV) and the ρ^o and ω^o mass region ($575 < m_{ee} < 950$ MeV). Background contributed at most 10% of the ρ^o and ω^o peak and at most 20% of the low mass pairs.

For $1.0 < p_T < 3.0$ GeV the observed yield of low mass electron pairs is shown in Fig. 3a relative to the number observed in the ρ^o and ω^o region. Dalitz pairs from $\eta^o \to \gamma e^+e^-$, $\omega^o \to \pi^o e^+e^-$, and $\eta'(958) \to \gamma e^+e^-$ decays contribute significantly to the observed yield of low mass electron pairs.

Assuming that at large p_T (i) η^o production is 55% of π^o production[15], (ii) η' production is equal to η^o production, (iii) ω^o production is equal to ρ^o production, and (iv) all particle production follows an E_T^{-8} ($E_T^2 = m^2 + p_T^2$) distribution[6], the overall Dalitz contribution to the low mass spectrum is shown by the continuous line in Fig. 3a. The $\eta^o \to \gamma e^+e^-$ contribution is the most significant; however, $\omega^o \to \pi^o e^+e^-$ decays are also important at all masses. At masses near 500 MeV η^o, η', and ω^o Dalitz contributions are approximately equal.

Additional corrections were made for the observed electron pair yields: (i) $\eta' \to \gamma e^+e^-$ contributions in the $\rho^o + \omega^o$ region, (ii) electron pairs from the low mass tail of the ρ^o which were observed with $m_{ee} < 500$ MeV due to finite mass resolution of the detectors, and (iii) continuum contributions to the ρ^o and ω^o region based on the continuum signal in the low mass region. Figure 2b shows the yield of low mass electron pairs in terms of $\rho^o + \omega^o \to e^+e^-$ after these corrections.

The production of electron pairs from virtual photons expected for a given level of photon production is

$$(q^2 + m^2)\ \frac{d\sigma\ (\gamma \to ee)}{d^3q\ dm^2} = \frac{\alpha}{2\pi m^2} \left(\frac{\gamma}{\pi^o}\right) \quad E\ \frac{d\sigma(\pi^o)}{d^3p} \qquad (1)$$

where we have assumed m_T scaling and the invariant π^o cross section for given q and m^2 by the relations

$$P_L = q_L \text{ and } p_T^2 = q_T^2 + m^2.$$

The ratio of direct photon production to π^o production (γ/π^o) and has a p_T dependence which is between p_T^o and p_T^2 in most models. The p_T dependence is not significant for a small p_T interval such as $2.0 < p_T < 3.0$ GeV. The line in Fig. 3b shows the spectrum, including detector acceptance, expected for $\gamma/\pi^o = 10\%$ in this p_T interval. The curve is seen to lie consistently higher than the observed spectrum. For the entire mass region $200 < m_{ee} < 500$ MeV, the expected $\gamma \to e^+e^-/\rho^o + \omega^o \to e^+e^-$ ratio is 2.41 if $\gamma/\pi^o = 10\%$; whereas, the observed ratio is 0.13 ± 0.22, where the error includes systematic uncertainties. The expected spectrum is also significantly higher than the observed spectrum even before Dalitz subtractions.

Interpreting the observed $\gamma \to e^+e^-/\rho^o + \omega^o \to e^+e^-$ ratio in terms of direct photon production gives $\gamma/\pi^o < (0.55 \pm 0.92)\%$ for $2.0 < p_T < 3.0$ GeV. Similar analysis for all $p_T > 2.0$ GeV results in slightly smaller γ/π^o limits. If direct photon production falls more slowly with increasing p_T than the π^o production, the estimate of γ/π^o would be reduced. The

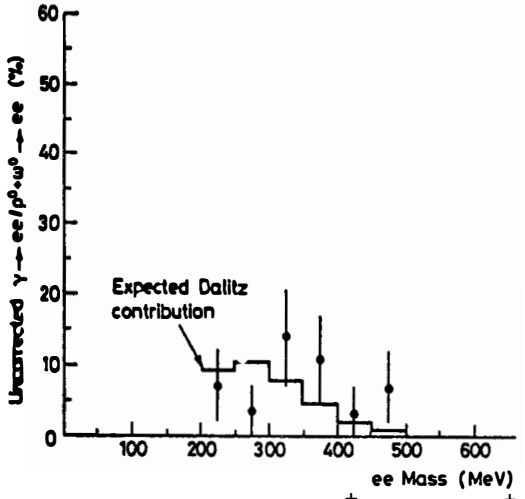

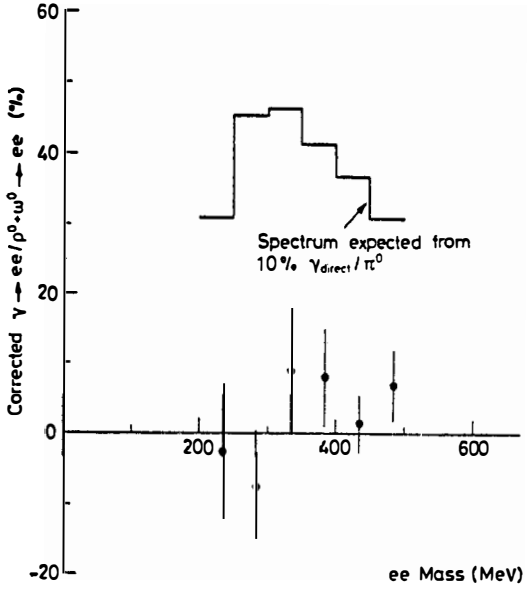

Fig. 3. $\gamma \rightarrow e^+e^-/(\rho + \omega) \rightarrow e^+e^-$ ratio as a function of electron pair effective mass
a) Uncorrected. Estimated Dalitz contribution shown.
b) Corrected. Expected ratio for direct photon production at the level of 10% of the π^0 production shown.
Errors include both statistical and systematic uncertainties.

extrapolated γ/π^0 ratio, based on the observed virtual photon rate after subtraction of Dalitz contributions, is $O(\alpha)$, contrary to the predictions of models suggesting copious production of single photons.

REFERENCES

1. J. Cobb et al., Nuclear Instrum. Methods 140, 1977 (1976).
   J. Fischer et al., Nuclear Instrum. Methods 136, 19 (1976).
   J.H. Cobb et al., Phys. Lett. 68B, 101 (1977); Phys. Lett 72B, 273 (1977); Phys. Lett. 72B, 497 (1978).
   C. Kourkomelis, CERN 77-061 (1977).
   A.J. Lankford, Measurement of Vector Meson Production in Proton-Proton Collisions, CERN/EP Report 78/3.
   J. Cobb, et al., A Large Liquid Argon Shower Detector for an ISR Experiment, sub. to Nuclear Instrum. Methods; W. Willis and V. Radeka, Nuclear Instrum. Methods 120, 221 (1974).
2. G.R. Farrar and S.C. Frautschi, Phys. Rev. Lett. 36, 1017 (1976).
   C.O. Escobar, Nuclear Phys. B98, 174 (1975); University of Cambridge preprint 76/6 (1976).
   E.L. Feinberg, CERN Preprint TH-2156 (1976).
   F. Halgen and D. Scott, Univ. of Wisconsin preprint COO-881-16, Jan. 1978.
   G.R. Farrar, Phys. Lett. 67B, 337 (1977).
3. P. Darriulat et al., Nuclear Phys. B107, 429 (1976).
   R. Walker, presented at the Chicago Meeting of the American Physical Society, 1976.
   J. Cronin, presented at the 1977 International Symposium on Lepton and Proton Interactions at High Energies, Hamburg, 1977.
4. Our result obtained by this direct way is $(\gamma/\pi^0) < 6\%$ at 90% confidence level.
5. M. Della Negra, Proc. VIIth International Colloquium on Multi-particle Reactions, Tutzing, West Germany, 1976 (Max-Planck Institute, Munich, 1976), p. 189.
6. F. Busser et al., Nuclear Phys. B106, 1 (1976).

PRELIMINARY RESULTS ON ψ PRODUCTION AND ASSOCIATED HADRONS BY HADRON COLLISIONS

R. Barate
CERN, Geneva, Switzerland
CEN Saclay, Gif-sur-Yvette, France

P. Bareyre, P. Bonamy, P. Borgeaud, M. David,
J. Ernwein, F.X. Gentit, G. Laurens, Y. Lemoigne, J. Pascual,
J. Poinsignon, A. Roussarie, G. Villet and S. Zaninotti
CEN Saclay, Gif-sur-Yvette, France

M. Abolins*), B. Brabson, R. Crittenden, R. Heinz,
J. Krider and T. Marshall
Indiana University, Bloomington, Indiana, USA

(Presented by R. Barate)

Preliminary results are presented on the ψ and ψ' production in a 140 GeV/c pion beam at the CERN SPS, using the Goliath magnetic spectrometer. Some mass combinations for hadrons associated with ψ are shown.

Nous présentons les résultats préliminaires obtenus sur la production des ψ et ψ' par un faisceau de pions de 140 GeV/c au SPS du CERN dans l'aimant Goliath, et sur quelques combinaisons de masses obtenues avec les hadrons associés au ψ.

*) On leave from Michigan State University, East Lansing, Michigan, USA.

1. INTRODUCTION

The aim of the experiment is to look at the hadronic states associated with the ψ production in the reaction $\pi^- N \rightarrow \psi X$ at 140 GeV/c. The basis of the trigger is to ask for the two-muon decay of the ψ.

2. THE SET-UP (Fig. 1)

The beam hits three beryllium targets in front of the Goliath magnet. The outgoing particles are detected in 11 proportional chambers immersed in a magnetic field of 1.5 Tm (F1, F2, PC1 to 9). PC1 to 9 have 4 planes of sense wires with 2 mm spacing and 1.8 × 0.74 m useful area[1]. The particle identification is achieved by a 28-cell, 2 m long Čerenkov counter filled with CO_2 at atmospheric pressure. It is located outside the magnetic field, before the iron filter. Its thresholds are 5 GeV/c for π, 17 GeV/c for K, and 33 GeV/c for p.

The forward lever arm, also used for the trigger, is composed of

- 2 big proportional chambers (LC1 and LC2, 3.2 × 2.2 m, 4 planes, 3 mm spacing),
- a calorimeter and a chamber (LC3) for e and γ detection,
- horizontal and vertical hodoscopes (H1H, H3H, H3V) defining 4 quadrants and an iron filter for μ identification.

3. TRIGGER PRINCIPLE

To be able to measure the particles associated with the ψ, we need a big length (8.2 m) between the target and the iron shield. This implies a lot of background due to $\pi \rightarrow \mu$ decay. To get partially rid of it at the trigger level, we use the fact that the ψ mass is big with respect to the "background mass".

The ψ mass is roughly given by $M^2 \approx p_{\mu_1} p_{\mu_2} \theta^2_{\mu_1\mu_2}$. To reinforce the ψ signal, the following conditions are required:

- big μ angles - vertical gap of 40 cm centred on the medium horizontal plane;
- big μ momenta - low momenta (< 5 GeV/c) swept out by Goliath or dying in the iron;
- opposite charged μ's - trigger on diagonally opposite quadrants;
- μ halo elimination - veto counter before the magnet;
  - hits in a small interaction counter just behind the targets;
  - a correlation between horizontal slabs of H1H and H3H requires the μ to point towards the target in the vertical plane.

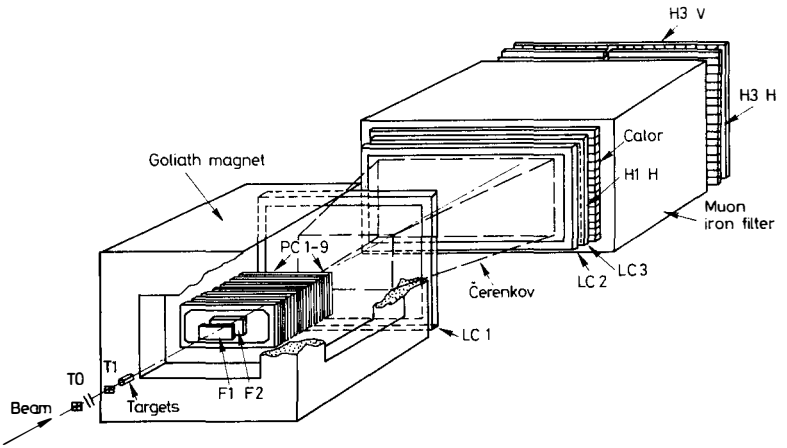

Fig. 1 Experimental set-up

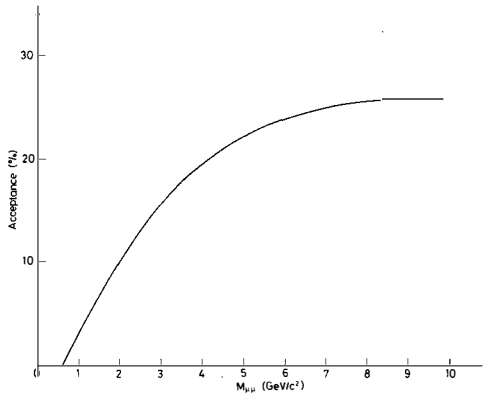

Fig. 2 Mass acceptance

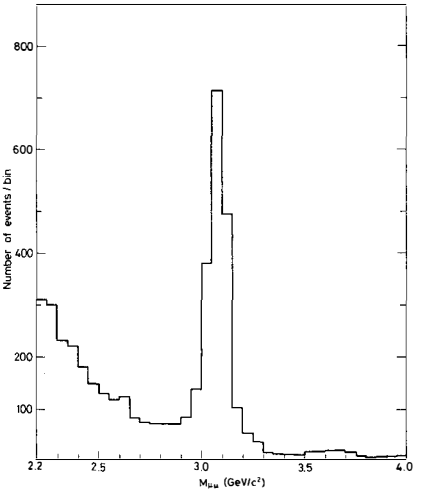

Fig. 3 Raw μμ mass spectrum

4. THE ANALYSIS

The events were taken between March and December 1977 and correspond to almost all the present statistics. We show preliminary results with the $\mu^+\mu^-$ trigger only. A calorimeter for electron and photon identification, constructed by Imperial College, has recently been added to this set-up. The e^+e^- trigger and the identification of e and γ is under way.

For the $\mu\mu$ trigger, the trigger rate was 6×10^{-6} and the ψ production rate about 0.35×10^{-8}. The complete analysis was done only for events with $M_{\mu\mu} > 2$ GeV/c^2. The $\mu^+\mu^-$ acceptance is rather good (Fig. 2) and about 15% at the ψ mass.

The raw $\mu^+\mu^-$ mass spectrum (Fig. 3) contains 1650 ψ with low background in spite of π decays. This is due to the strong constraint of the μ's having to join with the main vertex. The precision obtained on the mass is $\sigma_\psi = \pm 49$ MeV/c (cf. 45 MeV/c expected by Monte Carlo).

In the same log scale plot (Fig. 4) we see the $\mu^+\mu^-$ decay of the ψ'. The subtraction of background, taken as the sum of two exponentials, and the correction for mass acceptance, give:

$$\frac{B_{\mu\mu}\,\sigma_{\psi'}}{B_{\mu\mu}\,\sigma_{\psi}} = (2 \pm 0.5)\% \quad \text{hence} \quad \frac{\sigma_{\psi'}}{\sigma_{\psi}} = (15 \pm 4.25)\%$$

taking into account the present $\mu\mu$ branching ratio[2]. For comparison with other experiments, our cross-sections $d\sigma/dy|_{y=0}$ are given as dots in Fig. 5. They are given in nb/nucleon assuming a linear A dependence. The dashed line is a hand-drawn fit of the cross-sections induced by protons.

For the ψ production, we obtain an x Feynman distribution (corrected for acceptance) centred at $x \sim 0.18$ and not at zero (Fig. 6).

The raw mass spectrum above 4 GeV/c^2 (Fig. 7) is almost free from $\pi\pi \to \mu\mu$ background; after correction for acceptance, it can be fitted by an exponential $e^{-\alpha M}$ with a slope $\alpha = 0.88 \pm 0.15$. The comparison of our data for $M^3(d\sigma/dM)$ as a function of $\sqrt{s}/M$ with other experiments in π and p beams is shown in Fig. 8. The simple quark annihilation picture implies a scaling of this quantity.

The pattern reconstruction program reconstructs the associated hadron tracks coming from the main vertex or from V^0 (Fig. 9) and we use the Čerenkov counter to identify the charged ones. The mean charged multiplicity at the main vertex is 7.5.

The first mass combination done was $\psi\pi^+\pi^-$ to look for the decay of ψ'. It is shown in Fig. 10 with partial statistics corresponding to 980 ψ. To remove background we made the cut[3] $0.4 < M_{\pi\pi} < 0.6$ GeV/c^2 and, to improve the signal, we

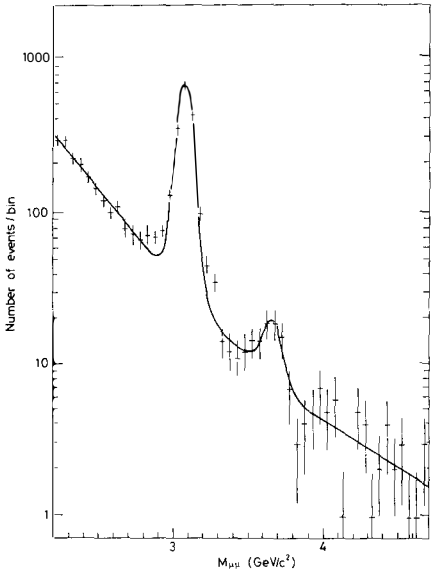

Fig. 4 Raw μμ mass spectrum (log scale)

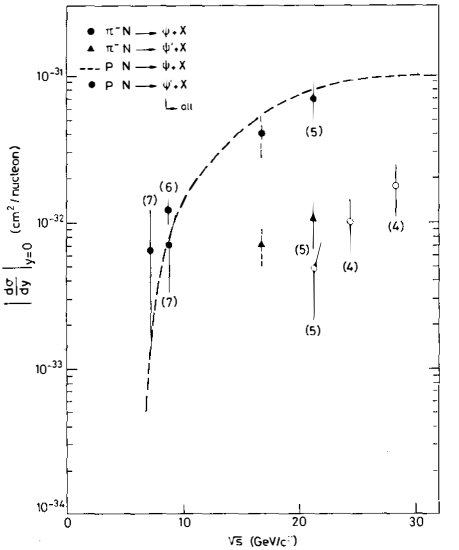

Fig. 5 ψ and ψ′ inclusive cross-sections

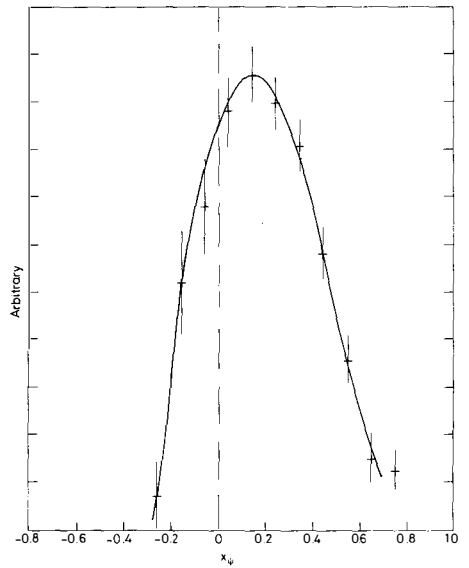

Fig. 6 x Feynmann distribution for ψ

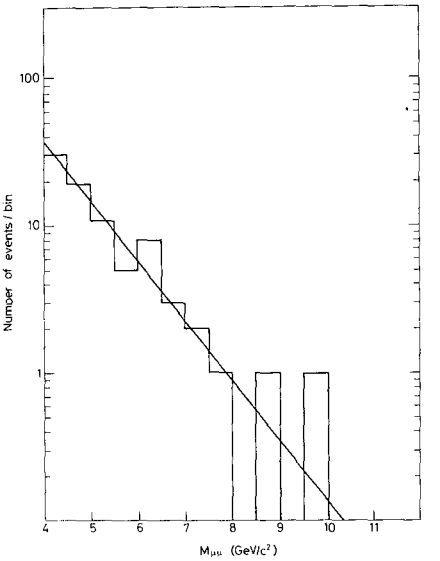

Fig. 7 Raw μμ mass spectrum

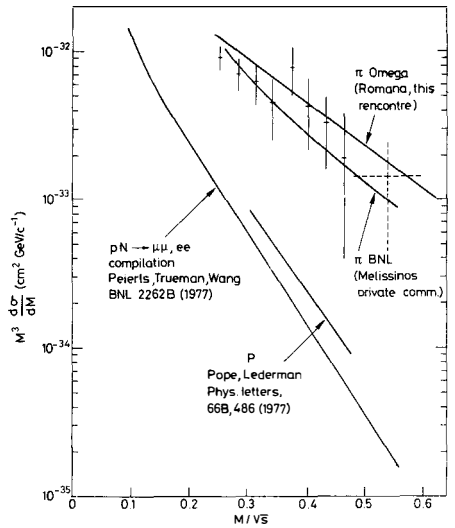

Fig. 8 $pN \to \mu^+\mu^- + X$ and $\pi N \to \mu^+\mu^- + X$ cross-sections

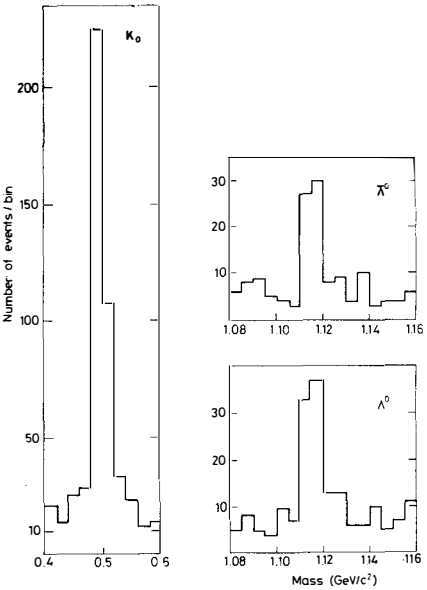

Fig. 9 V^0 mass spectrum (all $\mu\mu$ events with $M_{\mu\mu} > 2$ GeV/c^2)

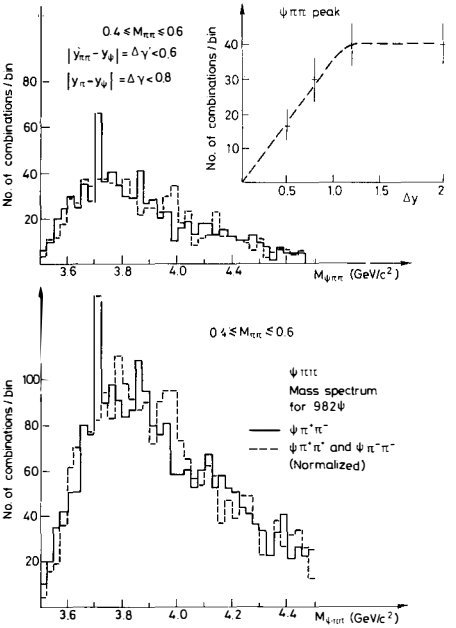

Fig. 10 $\psi\pi\pi$ mass combinations

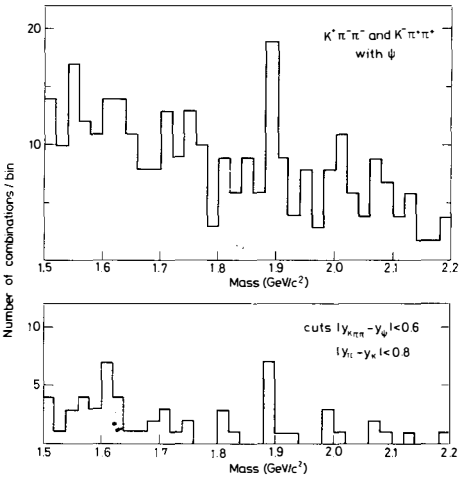

Fig. 11 Exotic $K\pi\pi$ mass combinations associated with ψ

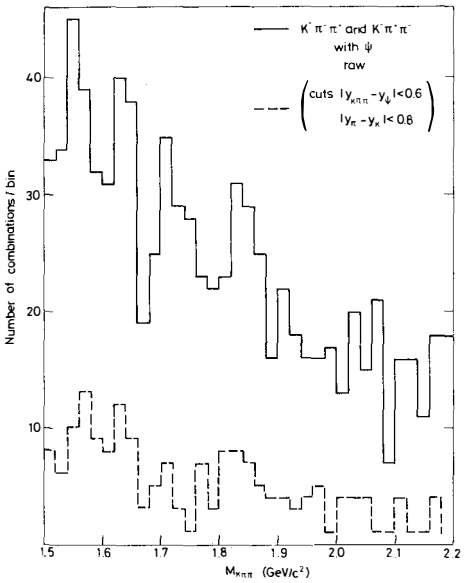

Fig. 12 Non-exotic $K\pi\pi$ mass combinations associated with ψ

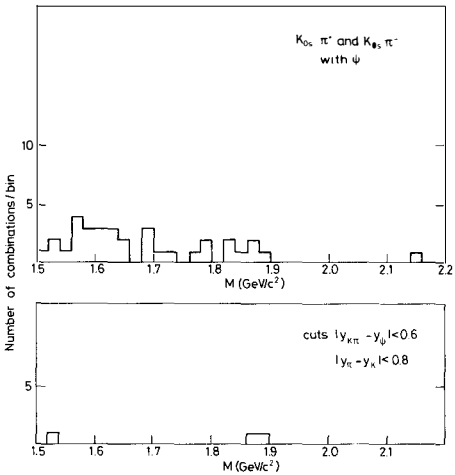

Fig. 13 $K^0_S\pi$ mass combinations associated with ψ

added rapidity cuts between the $\pi\pi$ system and the ψ and between each π and the ψ (the variation of the number of ψ' with this cut is shown in Fig. 10). The number of ψ' obtained in $\psi\pi^+\pi^-$ is in good agreement with the number of ψ' in $\mu^+\mu^-$, taking into account the respective branching ratios and the geometrical efficiencies.

We also tried to see particular mass combinations associated with the ψ: an interesting one is $K^+\pi^-\pi^-$ (expected decay mode of the D^-) or $K^-\pi^+\pi^+$ (from D^+) which are exotic for hadrons composed of u, d and s quarks only. The spectrum is shown in Fig. 11. With rapidity cuts between each π and the K and between the ψ and the $K\pi\pi$ system, we obtain 4 $K^+\pi^-\pi^-$ and 3 $K^-\pi^+\pi^+$ at the D mass. They are all produced near $x_F = 0$.

For comparison we give in Fig. 12 the non-exotic spectrum $K^+\pi^-\pi^+$ and $K^-\pi^+\pi^-$. The background is much higher owing to combinatory effects between pions. With the same rapidity cuts (lower curve Fig. 12), we see no particular enhancement at the D mass.

Another possible decay mode is $D^+ \to \bar{K}^0\pi^+$ or $D^- \to K^0\pi^-$; the raw $K^0_S\pi^+$ and $K^0_S\pi^-$ spectra (Fig. 13) contain very few events; but, with the same rapidity cuts as before, there remain nevertheless 1 $K^0_S\pi^+$ and 1 $K^0_S\pi^-$ events at the D mass over a null background.

All these $K\pi$ and $K\pi\pi$ spectra are statistically weak. Further data will be taken in May 1978.

REFERENCES

1) J. Poinsignon, Description and performance of a large spectrometer equipped with proportional chambers, Communication to the Wire Chamber Conference, Vienna, February 1978, to be published in Nuclear Instrum. Methods.

2) G.S. Abrams, Proc. Internat. Symposium on Lepton and Photon Interactions at High Energies, Stanford, 1975 (Stanford University, 1975), p. 36.
J.A. Kadyk et al., Proc. 10th Rencontre de Moriond, Méribel-les-Allues, France, March 1975, p. 63.

3) G.J. Feldman and M.L. Perl, Phys. Reports 33, 285 (1977).

4) B.C. Brown et al., Fermilab 1977/54-EXP (7100.288).

5) J.G. Branson et al., Phys. Rev. Letters 38, 1331 (1977).

6) M.J. Corden et al., Phys. Letters 68B, 96 (1977).

7) Yu.B. Bushnin et al., Phys. Letters 72B, 269 (1978).

ASYMPTOTIC QCD PERTURBATION THEORY AND TRANSVERSE MOMENTUM DISTRIBUTIONS IN DRELL-YAN PROCESSES

R. Petronzio
CERN
1211 Geneva 12
Switzerland

ABSTRACT

We shortly review to which extent the QCD asymptotic perturbative expansion can be applied to processes which are not light-cone dominated. The transverse momentum distribution of large mass muon pairs produced in hadron-hadron collisions is a very good test of these ideas. At present energies, however, non-perturbative effects like the presence of an intrinsic $p_\perp$ of partons are still relevant.

RESUME

Nous donnons une rapide revue des limites d'application du développement asymptotique en perturbation de QCD pour des processus qui ne sont pas dominés par le light-cone. La distribution en moment transverse des paires de muons de grande masse produits dans des collisions hadron-hadron est un très bon test de cette approche. Toutefois, aux énergies actuelles, des effets non perturbatifs, par exemple la présence d'un $p_\perp$ intrinsèque des partons, jouent encore un rôle significatif.

INTRODUCTION

Prompt lepton pair production in hadron-hadron collisions has a very simple description, in the framework of the parton model ; according to the Drell-Yan picture [1] it is based on the annihilation of a parton-antiparton pair into a massive photon. However, the simple scaling laws predicted by the naïve parton model are experimentally slightly violated : this is a manifestation of interactions among partons. The scaling behaviour of the structure functions of deep inelastic lepton-hadron scattering (DIS) can be in fact related, through the operator product expansion technique, to an underlying field theory of strong interactions in the deep Euclidean region where the mass of the incoming virtual photon q^2 becomes large and negative. The best candidates for reproducing the observed approximate scaling behaviour of structure functions are the asymptotically free gauge theories (AFGT) [2]. They predict logarithmic corrections to exact scaling which are computable perturbatively in the effective strong coupling constant $\alpha_s(Q^2)$.

The predictions obtained by the operator product expansion (OPE) are, however, restricted to those processes which are light-cone dominated ; this is not the case for the Drell-Yan process. The hope is then to reproduce all the results of the OPE in an alternative language, based directly on the parton model, which still remain valid outside the light cone. This can be implemented through the identification of partons with quarks and gluons which interact according to an SU(3) non-Abelian, asymptotically free, gauge theory of strong interactions.

Within this new language, we discuss in Section 1 the corrections to the lowest order predictions of the naïve parton model. Section 2 is devoted to the analysis of the large transverse momentum distributions of muon pairs produced in hadron-hadron collisions which is an application of the general ideas discussed in the first section.

LEADING CORRECTIONS TO NAIVE PARTON MODEL

The aim of this section is to analyze the corrections, for hard processes, to the naïve parton model, under the assumption (which will be briefly discussed at the end) that unknown confinement forces which bind partons inside hadrons will not spoil the basic results of this analysis.

The corrections are calculated in a specific renormalizable field theory ; then, for a given parton cross-section σ depending for simplicity on one external momentum Q, the invariance with respect to different choices of a renormalization mass μ^2 gives :

$$\sum \equiv Q^2\sigma\left[\alpha_s(\mu^2),\ Q^2/\mu^2,\ Q^2/M^2\right] = Q^2\sigma\left[\alpha_s(Q^2),1,\ Q^2/M^2(Q^2)\right] \qquad (1)$$

where m is a parton mass and α_s is the running coupling constant. If Σ has a smooth limit when the parton mass goes to zero, asymptotically it will depend on Q^2 only through the effective coupling constant $\alpha_s(Q^2)$. If, as in an asymptotically free theory, α_s decreases when Q^2 grows, one can make a perturbative expansion in powers of $\alpha_s(Q^2)$.

In general, however, the zero-mass limit is not regular because of the presence of logarithms of parton masses. They arise from kinematical configurations where hard gluons, real or virtual, are emitted parallel to external, both initial and final, quark or gluon legs. These singularities are called mass singularities : they are different from the usual infra-red (IR) singularities generated by massless soft gluons exchanged in radiative corrections [3),4)]. The latter cancel in QED between real and virtual emissions : I assume the same mechanism of cancellation of IR singularities in QCD, even if it has not been proved in general, but only in several particular cases [5)].

In QED the cancellation of IR singularities occurs for a suitable inclusive final state, with an energy uncertainty equal to the resolution of the detector. The definition of a more inclusive final state with an energy and an angular uncertainty, the QCD jet, allows to eliminate also the mass singularities associated with external final legs. Therefore, for a cross-section without partons in the initial state, one can make a perturbative expansion in $\alpha_s(Q^2)$ provided the final state is expressed in terms of jets. This is the case for e^+e^- annihilation in two or more QCD jets as it has been shown recently by Sterman and Weinberg [6)].

For other processes where the parton model can be applied, like deep inelastic lepton-hadron scattering, Drell-Yan processes or large $p_\perp$ hadron scattering, which have partons in the initial state, one cannot avoid the presence of mass singularities. These could spoil the usefulness of a

small $\alpha_s(Q^2)$ and would make the final result dependent on effective parton masses which are presumably determined by the unknown large distance behaviour of the theory.

Physical processes, however, involve hadrons and, for the final predictions, parton cross-sections must be convoluted with appropriate distribution functions. If it is possible to reabsorb mass singularities into the definition of parton densities, the final cross-section expressed in terms of these "renormalized" distributions will have a smooth zero mass limit. In this case, one can compute the asymptotic behaviour with the Born cross-section calculated with the running coupling constant $\alpha_s(Q^2)$. The evolution with Q^2 of parton distributions which enter into the convolution of the elementary cross-section will be governed by "anomalous dimensions" which reflect the presence of mass singularities before the redefinition of parton densities.

The above possibility has been demonstrated to be true to the lowest order of radiative corrections for different hard processes [7)-9)] : recently it has been proved for every hard parton process [10)]. The argument runs in two steps.

The first one results in the universality of leading corrections. Indeed, the corrections of first order in α_s to a given process described by a cross-section $\sigma(\{p_i\},\{q_i\})$, with incoming quarks of momenta p_i and jets in the final state, take the form :

$$\sigma^{(1)}(\{p_i\},\{q_i\}) = \int\left[\prod_j d\, x_j\, q(x_j,Q^2/M^2)\right] \sigma_o\,(\{x_j\, p_i\},\{q_i\}) \qquad (2)$$

where σ_o is the Born cross-section with rescaled incoming momenta and q is a universal function of x_j and Q^2, which contains all the leading mass singularities : it represents the quark structure function. For a free valence quark, it is :

$$q(x,Q^2/M^2) = \delta(1-x) + \frac{\alpha_s}{2\pi} \ln Q^2/M^2 \int_o^1 dy \left[\frac{4}{3}\frac{1+y^2}{1-y}\right]\left[\delta(y-x) - \delta(1-x)\right] \qquad (3)$$

The above form is the first order solution of the Altarelli-Parisi equation [11] for the valence quark density which is known to reproduce the results of OPE in deep inelastic scattering. The sea quarks and gluons have different structure functions corresponding to the order α_s solution of the respective evolution equations. One can analyze the cross-section directly as a function of the fraction of momenta x_i carried by the partons, by fixing appropriate external kinematical variables : in the case of total DIS this can be done by fixing the well-known Bjorken variable $x_B = (Q^2/2p\cdot q)$ or, if more jets are observed in the final state, a generalized variable $(Q^2 + M^2)/2p\cdot q$, where M^2 is the invariant mass produced by the photon-parton system in the current fragmentation region.

As the function $q(x,Q^2/M^2)$ is proportional to the total DIS cross-section, it satisfies by itself a renormalization group equation : as a consequence, the same will be true for $\sigma_o(\{x_j p_i\},\{q_i\})$. Hence, σ_o will depend on Q^2 only through $\alpha_s(Q^2)$ and $q(x,Q^2/M)$ through $\alpha_s(Q^2)$ and $\ell n\, Q^2/M^2$.

Equation (2) allows to form ratios of cross-sections, at the same Q^2 and $\{x_i\}$, with the same initial state, but with different number of jets in the final state, where the universal function $q(x_i,Q^2)$ drops out. These ratios are free from mass singularities and can be expanded in power of $\alpha_s(Q^2)$.

To relate the same cross-section at different values of Q^2, i.e., to calculate the scaling violations, a second step is needed. The structure function of the initial parton must be factorized into a function of Q^2/μ^2 and a function of M^2/μ^2, μ^2 being a suitable normalization mass. Then the latter function can be re-absorbed, independently of Q^2, in a redefinition of the corresponding parton distribution inside the hadron : predictions made by the redefined distributions will be free from mass singularities and computable perturbatively. This requirement is trivially satisfied at the lowest order because of a well-known property of the logarithm : the moments of the function $q(x,Q^2/M^2)$ have the general form

$$\int_0^1 dx\, x^{n-2}\, q(x,Q^2/M^2) = M_n^{(1)} = (1 + C_n\, \alpha_s\, \ell n\, Q^2/M^2)\, M_n^{(o)} \qquad (4)$$

and, up to higher order terms in α_s, can be rewritten as :

$$M_n^{(1)} = (1 + C_n \alpha_s \ln Q^2/\mu^2)(1 + C_n \alpha_s \ln \mu^2/M^2) M_n^{(o)} \qquad (5)$$

To higher order, the factorization holds true, provided the property of universality of corrections in the form expressed in Eq. (2) is preserved. In fact, in the case of total DIS - in all cases, if the corrections are universal - the factorization of the function $q(x,Q^2)$ is guaranteed by the OPE applied to the partons. The light-cone expansion is a statement about a factorization of the Q^2 dependence - contained in the coefficients - with respect to the M dependence - contained in the matrix elements of the local operators. The values of parton distribution measured at a definite Q_o^2 include all the infra-red stuff. At a different Q^2 they will be determined by the anomalous dimensions which are reminiscent of the exorcization of mass singularities and enter into the renormalization group equation.

The discussion developed in this section provides a recipe for the computation of a parton cross-section to the leading log approximation with an arbitrary number of jets in the final state. First, calculate the Born cross-section with the effective coupling constant $\alpha_s(Q^2)$; second, do the convolution with parton densities which have the same Q^2 evolution of the distributions measured in DIS. The experimental test of the predictions which are accessible by QCD perturbative calculation depends heavily on the possibility of detecting QCD jets. I want to stress that they are quite different from usual hadron jets : while the latter have a typical cut-off of transverse momenta, the QCD jets keep the opening angle fixed when the energy increases, without any cut-off on transverse momenta. The reconstruction of the kinematical properties of a QCD jet is a hard experimental task : the large transverse momentum of prompt muon pairs produced in hadron-hadron collisions, which will be discussed in the next section, is a direct measure of the transverse momentum of a QCD jet. In the parton model (see Fig. 1), it represents the kinematical balance of the transverse momentum of a recoiling parton which will originate a QCD jet.

TRANSVERSE MOMENTUM OF MUON PAIRS IN DRELL-YAN PROCESSES

In the first section, we have analyzed the theoretical bases for a perturbative analysis of large transverse momentum muon pairs produced in

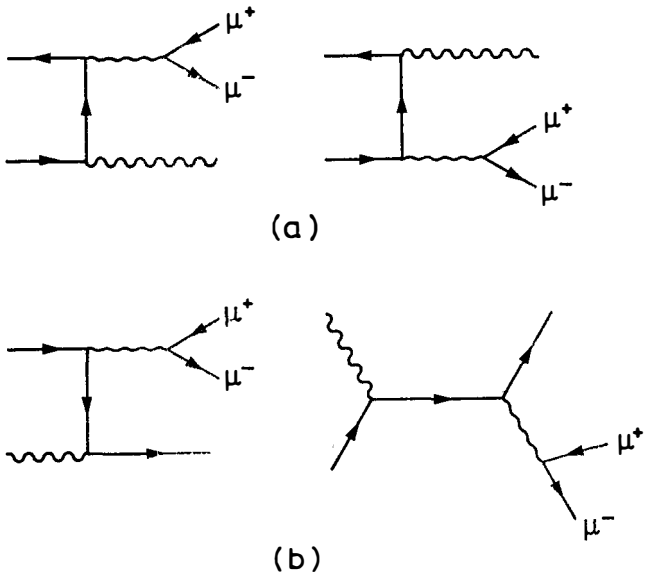

Fig. 1 Lowest order diagrams for :
a) quark + antiquark → gluon + $\mu^+\mu^-$, and
b) gluon + quark (antiquark) → quark (antiquark) + $\mu^+\mu^-$.

hadron-hadron collisions. The basic ingredients are the cross-sections for the elementary reactions $q\bar{q} \to g\mu^+\mu^-$ and $q(\bar{q}) + g \to q(\bar{q}) + \mu\mu^-$. The corresponding diagrams are depicted in Fig. 1 and the cross-sections are :

$$\text{(a)} \quad \frac{d\sigma\, q\bar{q}}{dQ^2\, d\cos\theta} = \frac{8\alpha^2\,\alpha_s}{27\,Q^2}\, e^2 \frac{S - Q^2}{S^2 \sin^2\theta} \left\{ 1 + \cos^2\theta + 4\,\frac{Q^2 S}{(S - Q^2)^2} \right\}$$

$$\text{(b)} \quad \frac{d\sigma\, qg}{dQ^2\, d\cos\theta} = \frac{\alpha^2\,\alpha_s}{18\,Q^2}\, e^2 \frac{S - Q^2}{S^2(1-\cos\theta)}$$

$$\left\{ \frac{2S}{S - Q^2} + \frac{S - Q^2}{2S} (1-\cos\theta)^2 - \frac{2Q^2}{S} (1 + \cos\theta) \right\} \qquad (6)$$

where θ is the centre-of-mass scattering angle between the initial quark (gluon) and the final gluon (quark), Q^2 is the invariant mass squared of the muon pair and S is the total squared energy of the partons. The $k_\perp^2$ of the muon pair is given by :

$$k_\perp^2 = \frac{(S - Q^2)^2}{4\,S} \sin^2\theta \qquad (7)$$

The above cross-sections develop a singularity in the forward direction : it is, however, related to the very low $k_\perp$ region where the perturbative results fail. One expects that the unknown presumably non-perturbative phenomena at small $k_\perp$ will regularize the singularity leaving with smooth distributions.

If one is interested to compute the $< k_\perp^2 >$ [12], the result of the perturbative calculation will not be divergent, even if the absolute value of the final answer will be wrong due to the incorrect treatment of the low $k_\perp$ region. According to the general discussion developed in Section 1, the expression for the $< k_\perp^2 >$ is given, to the leading log approximation, by a convolution of "improved" parton densities (which have the same Q^2 evolution of those which enter in the description of DIS) with the Born cross-section evaluated with the running coupling constant $\alpha_s(Q^2)$:

$$< K_\perp^2 >_P \left(\frac{Q^2 d\sigma}{dQ^2}\right)_{DY} = \frac{\alpha\,\alpha_s\,(Q^2)}{27} \int_\tau^1 dx_1 \int_{\tau/X_1}^1 dx_2\,(1 - \tau/x_1x_2)^3$$

$$\left\{\left[\sum_{\text{flavours}} e_i^2\; q_i^{h_1}(x_1,Q^2)\; \bar{q}_i^{h_2}(x_2,Q^2) + (1\leftrightarrow 2)\right]\left[\frac{16}{3} + \frac{16\,\tau/x_1x_2}{(1 - \tau/x_1x_2)^2}\right] + \right. \tag{8}$$

$$+ \left[\sum_{\text{flavours}} e_i^2\; (q_i^{h_1}(x_1,Q^2) + \bar{q}_i^{h_1}(x_1,Q^2))\; G^{h_2}(x_2,Q^2) + (1\leftrightarrow 2)\right] \cdot$$

$$\left.\left[\frac{3}{2(1-\tau/x_1x_2)} + \frac{1 - \tau/x_1x_2}{4} - 2\tau/x_1x_2\right]\right\}$$

where the label P means "perturbative contribution" and $(Q^2(d\sigma/dQ^2))_{DY}$ is the Drell-Yan total cross-section and is given by

$$\left(Q^2 \frac{d\sigma}{dQ^2}\right)_{DY} = \frac{4\pi\alpha^2}{9S} \int_0^1 dx_1 \int_0^1 dx_2\; \delta(x_1x_2 - \tau)$$

$$\left[\sum_{\text{flavours}} e_i^2\; q_i^{h_1}(x_1,Q^2)\; \bar{q}_i^{h_2}(x_2,Q^2) + (1\leftrightarrow 2)\right] \tag{9}$$

with S the total energy squared of the flavour hadron-hadron system and $\tau = Q^2/S$. Equation (8) has the following structure

$$< K_\perp^2 >_p = \alpha_s(Q^2)\; S.f(\tau,\alpha_s(Q^2)) \tag{10}$$

where $f(\tau,\alpha_s(Q^2))$ is a positive function of τ that vanishes at $\tau = 1$ [at least as $(1-\tau)^2$ as implied by Eq. (7)] and at $\tau = 0$ [as $\tau\,\ell n\,\tau$ if, at $x \to 0$, $xq_i(x)$, $xG(x) \to$ constant]. As a consequence $< k_\perp^2 >_p$ will grow almost linearly with S (or Q^2) only at fixed τ : if the experiments are not done holding τ fixed, the variation of $< k_\perp^2 >_p$ with Q^2 or S will depend in general on the actual form of the function $f(\tau,\alpha_s(Q^2))$. For the explicit evaluation of this function we have used the scaling parton distributions of Ref. 13) for the valence ; the gluon distribution has the form

$$xG(x) = A_n(1 - x)^n \tag{11}$$

where A_n is fixed by momentum conservation and $n = 5$. For the sea distribution we introduced the Q^2 dependence of leading scaling violation, to the first order :

$$S(x,Q^2) = S(x) + \frac{\alpha_s}{2\pi} \ln Q^2/\mu^2 \int_x^1 \frac{dy}{y} \cdot \frac{1}{2}\left[(1 - \frac{x}{y})^2 + (\frac{x}{y})^2\right] G(y) \qquad (12)$$

where $\mu^2 = 100\ GeV^2$ and $xS(x) = 0.54x(1-x)^{10}$ have been found to fit the continuum cross-section [14]. The correction due to the gluon density to the scaling distribution of the sea is needed in the region of large τ (large x for the sea density) where it becomes more important than the scaling contribution. This prevents the function $f(\tau,\alpha_s(Q^2))$ to take unreasonable values in the large τ region where the diagram b of Fig. 1, which depends on the gluon distribution, dominates. In Fig. 2, the function $f(\tau,\alpha_s(Q^2))$ is presented for both proton-antiproton and proton-proton cases. The proton-proton prediction depends crucially on the exponent n of the gluon distribution, while that for proton-antiproton is almost insensitive to changes in that exponent. For τ sufficiently small, up to 0.15, the values of $f_{p\bar{p}}$ and f_{pp} are comparable, while for large τ, of order 0.5, f_{pp} overcomes $f_{p\bar{p}}$.

The $< k_\perp^2 >_p$ for proton-proton collisions is compared in Fig. 3 to the mean experimental value. As expected, its value does not agree with that observed because of the incorrect treatment of the low $k_\perp$ region. The gap of order 1 GeV^2 between the perturbative calculation and the experimental result can be attributed to the presence of a non-perturbative component of partons $k_\perp$: the "intrinsic" $k_\perp$. This is related to the Fermi motion of parton inside the proton. I will assume the following characteristics for this component : i) it is independent of Q^2 ; ii) it depends on a typical hadron scale which is related to the cut-off of transverse momenta of particles produced in hadronic collisions.

The soft, non-perturbative, component of $k_\perp$ produces a smearing of the distributions calculated perturbatively and can be used to regularize them at low $k_\perp$. The form of regularization proposed is the following [15] :

$$\sigma^{reg}(Q^2,\tau,p_\perp^2) = \sigma_{DY}(Q^2,\tau).f(p_\perp^2) + \frac{1}{\pi}\int d^2 K_\perp \sigma_P(Q^2,\tau,\frac{2K_\perp}{\sqrt{s}}) \times$$

$$\left[f\left((p_\perp - K_\perp)^2\right) - f(p_\perp^2)\right] \qquad (13)$$

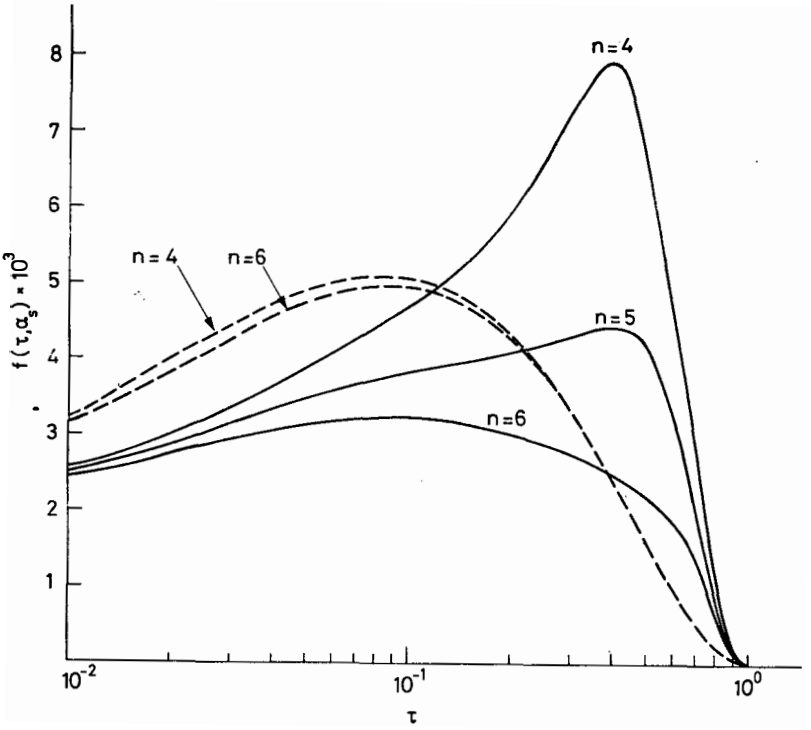

Fig. 2 The functions $f(\tau,\alpha_S)$, defined in Eq. (8), are plotted for both $p\bar{p}$ (dashed lines) and pN (full lines). In each case the dependence of the power n of the gluon distribution is shown for n = 4,6 ($p\bar{p}$) and n = 4,5,6 (pN).

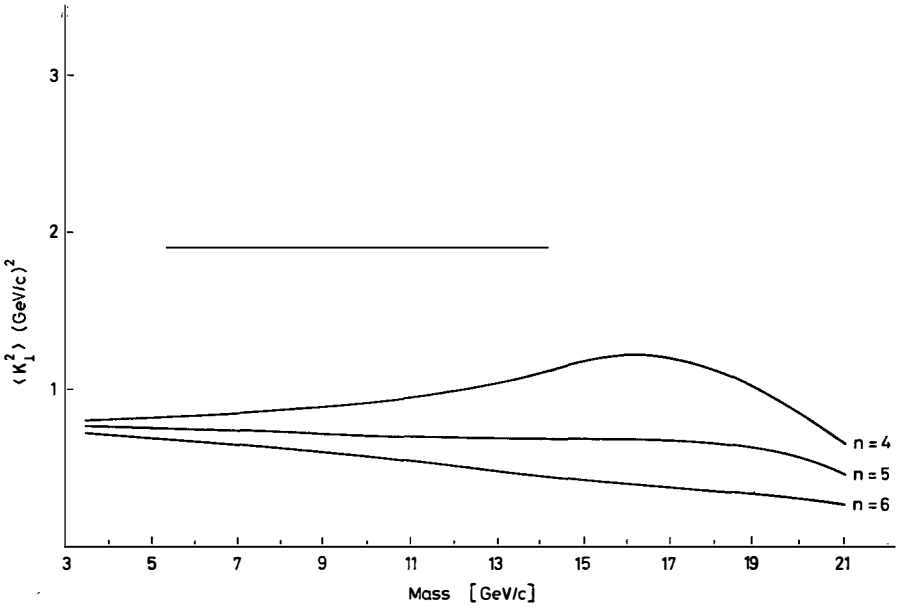

Fig. 3 The hard component of the $\langle k_1^2 \rangle$ of the muon pair as a function of their invariant mass is compared with the mean experimental value taken from Ref. 14) for three different powers n = 4,5,6 of the gluon distribution.

The function

$$\sigma_p\left(Q^2,\ \tau,\ \frac{2K_\perp}{\sqrt{s}}\right) \equiv \frac{d\sigma^p}{dQ\ dp_\perp^2\ dy}$$

is the perturbative cross-section ; even if it diverges, as we will see below, as $1/k_\perp^2$ when $k_\perp$ goes to zero, the singularity is removed by the convolution with the function $f(p_\perp^2)$ which is meant to represent the intrinsic $p_\perp$ distribution of partons inside hadrons and is normalized according to $\int_0^\infty d\ p_\perp^2 f(p_\perp^2) = 1$. The above regularization has the following properties :

i)

$$\int d\ p_\perp^2\ \sigma^{reg}\ (Q^2,\tau,p_\perp^2) = \sigma_{DY}(Q^2,\tau) \equiv \frac{d\sigma}{dQ\ dy} \qquad (14)$$

ii)

$$\frac{\int dp_\perp^2\ p_\perp^2\ \sigma^{reg}\ (Q^2,\tau,p_\perp^2)}{\int dp_\perp^2\ \sigma^{reg}(Q^2,\tau,p_\perp^2)} \equiv < p_\perp^2 >_{reg} = < p_\perp^2>_f + < p_\perp^2>_p \qquad (15)$$

where

$$<p_\perp^2>_f \equiv \frac{\int dp_\perp^2\ p_\perp^2\ f(p_\perp^2)}{\int dp_\perp^2\ f(p_\perp^2)}$$

and $< p_\perp^2 >_p$ is the perturbative contribution already discussed.

iii) At intermadiate values of S the difference betwenn σ^{reg} and σ as function of $x_\perp = (2p_\perp/\sqrt{S})$ is given by :

$$\sigma^{reg}\ (x_\perp) \simeq \sigma_p(x_\perp) + \left[\frac{\sigma'_p\ (x_\perp)}{x_\perp} + \sigma''_p(x_\perp)\right] \frac{<p_\perp^2>_f}{S} + \sigma\left(\frac{<p_\perp^4>_f}{S^2}\right) \qquad (16)$$

The sharpness of the function $\sigma_p(x_\perp)$ makes the corrections, which depend on its derivative, rather large and important in the present experimental range of $p_\perp^2$ and S.

The explicit form of $d\sigma^p/dQ^2 dp_\perp^2 dy\Big|_{y=0}$ is

$$\frac{d\sigma}{dQ\, dp_\perp^2\, dy}\Big|_{y=0} = \frac{8\alpha^2}{27 S^2 Q}\, \alpha_s(Q^2) \cdot \int dx_1 dx_2\, \delta\left[x_1 x_2 - \frac{(x_1 + x_2)}{2}\sqrt{x_\perp^2 + 4\tau} + \tau\right] \times$$

$$\times \sum_{\text{flavours}} \left[e_i^2\, q_i^{h_1}(x_1,Q^2)\, \bar{q}_i^{h_2}(x_2,Q^2) + (1 \leftrightarrow 2)\right] \times F_{q\bar{q}}(x_1 x_2,\, \tau,\, x_\perp) +$$

$$+ \sum_{\text{flavours}} \left[e_i^2\, (q_i^{h_1}(x_1,Q^2) + \bar{q}_i^{h_1}(x_1,Q^2)\; G^{h_2}(x_2,Q^2) + (1 \leftrightarrow 2)\right] F_{qG}^{S}(x_1 x_2, \tau, x_\perp) +$$

$$+ \sum_{\text{flavours}} \left[e_i^2\, (q_i^{h_1}(x_1,Q^2) + \bar{q}_i^{h_1}(x_1,Q^2)\; G^{h_2}(x_2,Q^2) - (1 \leftrightarrow 2)\right] F_{qG}^{a}(x_1, x_2, \tau, x_\perp)$$

(17)

where

$$F_{q\bar{q}}(x_1 x_2, \tau, x_\perp) = \frac{8}{x_\perp^2}\left(1 + \frac{\tau^2}{x_1^2 x_2^2} - \frac{x_\perp^2}{2\, x_1 x_2}\right)$$

$$F_{qG}^{S}(x_1 x_2, \tau, x_\perp) = \frac{3}{8\, x_\perp^2 (x_1 x_2)^3}\left\{x_\perp^2\, x_1 x_2\, (3\tau + x_1 x_2) + \right.$$

$$\left. + (x_1 x_2 - \tau)\left[4(x_1 x_2)^2 - 8\tau\,(x_1 x_2 - \tau)\right]\right\}$$

$$F_{qG}^{a}(x_1, x_2, \tau, x_\perp) = \epsilon(x_1 - x_2)\sqrt{1 - \frac{x_\perp^2\, x_1 x_2}{(x_1 x_2 - \tau)^2}}\,(x_1 x_2 - \tau) \times$$

$$\times \left[x_\perp^2\, x_1 x_2 + 8\tau\, x_1 x_2 - 8\tau^2 - 4(x_1 x_2)^2\right] \times \frac{3}{8\, x_\perp^2 (x_1 x_2)^3} \qquad (18)$$

The function $f(p_\perp^2)$ used is : $f < p_\perp^2 > = A \exp^{-A p_\perp^2}$ which implies $< p_\perp^2 >_f = 1/A$. It is independent of Q^2 and it contains a scale A which has to be fitted from the experiment : a possible dependence on τ has been neglected for simplicity. The theoretical fit to experimental data taken from Ref. 14) is given in Fig. 4. It corresponds to $A = 1\ \text{GeV}^{-2}$ and confirms the value of about 1GeV^2 for the intrinsic $< p_\perp^2 >$ estimated before. In Fig. 5, the way different terms of Eq. (16) contribute to σ^{reg} is displayed. Raising the exponent of gluon distribution in Eq. (11) from 5 to 7, the curve becomes steeper : at $p_\perp = 4$ GeV the effect is to reduce the cross-section by about a factor three.

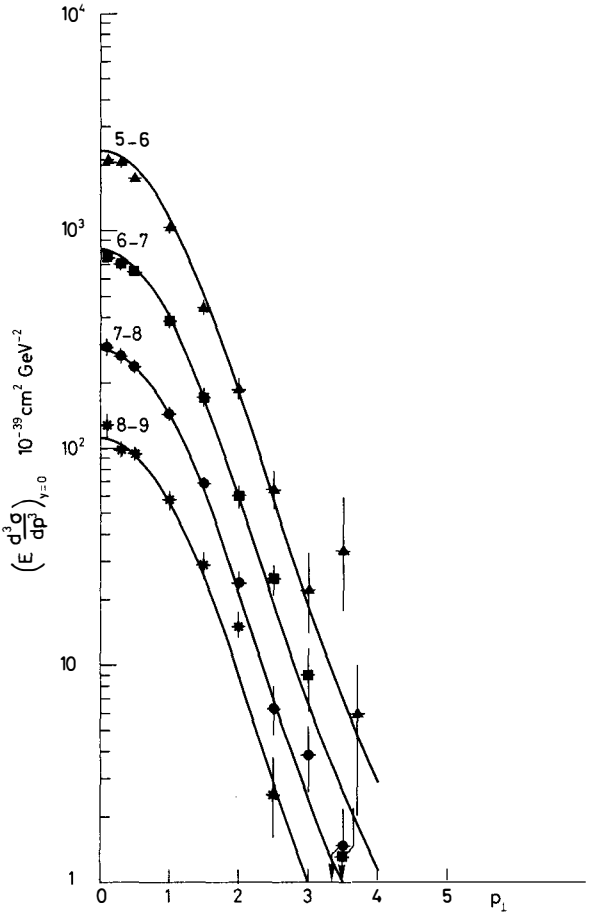

Fig. 4 The theoretical prediction is compared to the experimental data of Ref. 14) for P nucleus collisions.

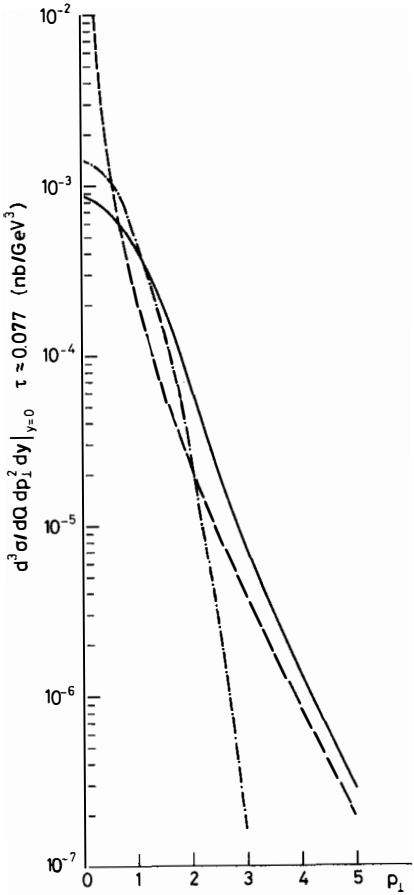

Fig. 5 The cross-section $\sigma^{reg}(Q^2,\tau,p_\perp^2)$ (full line) is compared to $\sigma_H(Q^2,\tau,x_T)$ (dashed line) and to $\sigma_{DY}(Q^2,\tau)\cdot f(p_\perp^2)$ (dotted line) at $\sqrt{S} = 27$ GeV.

While $S^{\frac{5}{2}}(d\sigma^P/dQdp_\perp^2dy)$ would be independent of S at fixed τ and $x_\perp$, neglecting logarithmic scaling violations, the regularized cross-section will have scale breaking effects of order $1/AS$ because of the scale introduced by the intrinsic transverse momentum. These effects, as displayed in Fig. 6, extend up to rather large values of S.

A crucial test of the picture presented above is the variation of transverse momentum of muon pairs with energy. The discussion will be based on preliminary experimental results [16] which give the following fits to the $p_\perp$ distributions at different energies

$$E\frac{d^3\sigma}{dp^3} = A(m) \cdot \left[1 + (a\, p_\perp)^2\right]^{-6}$$

For $E_p = 400$, 300 and 200 GeV, $a = 0.36$, 0.38, 0.43 + 0.44, respectively, at mean values of rapidity 0, 0.17, 0.36.

The corresponding $< p_\perp^2 >$ are : 1.93, 1.73 and 1.35. I shall consider these values to be true for the three different energies at a fixed $\tau \simeq 0.1$: this assumption is supported by the rather flat spectrum observed. Subtracting the same intrinsic $< p_\perp^2 >$ of 1 GeV^2 from the experimental values, one finds the size of the perturbative contributions : 0.93, 0.73, 0.35 GeV^2. Equation (10) states that the ratios of pertubative $< p_\perp^2 >$, at fixed τ, are in the ratios of total energies squared, neglecting logarithmic corrections and differences due to different mean rapidities. The "experimental" values of these ratios are

$$\frac{< p_\perp^2 >_p^{E_p=300\ \text{GeV}}}{< p_\perp^2 >_p^{E_p=400\ \text{GeV}}} = .78 \qquad \frac{< p_\perp^2 >_p^{E_p=200\ \text{GeV}}}{< p_\perp^2 >_p^{E_p=400\ \text{GeV}}} = .38$$

and the ratios of energies 0.75 and 0.5, respectively.

One can proceed with the analysis by looking at the shape of $p_\perp$ distributions at $E_p = 300$ and 200 GeV. This is done by comparing the following quantity

$$R(P_\perp) \equiv \frac{E\frac{d^3\sigma}{dp^3}\Big|_{p_\perp = P_\perp}}{E\frac{d^3\sigma}{dp^3}\Big|_{p_\perp = 0}} \Bigg|_{\text{fixed Q and Y}}$$

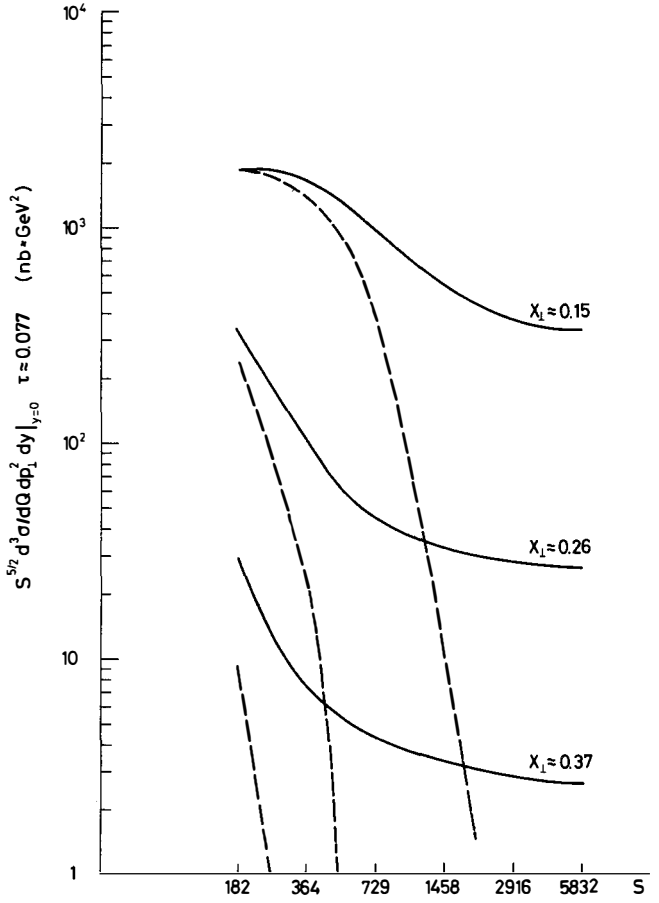

Fig. 6 The dimensionless cross-sections $s^5_2\sigma^{reg}(Q^2,\tau,p_\perp^2)$ (full li. and $s^5_2\sigma_{DY}(Q^2,\tau)\cdot f(p_\perp^2)$ (dashed line) are plotted as functio. of S for different values of x_T.

The Table refers to $Q = 6.5$ GeV and the appropriate rapidities.

	Exp	Th	Exp	Th
R(1)	0.44	0.47	0.35	0.43
R(2)	0.065	0.062	0.034	0.043
R(3)	0.007	0.0053	0.0026	0.0023
R(4)	0.00076	0.00075	0.00023	0.00018
	Ep = 300 GeV, $y \tilde{=} 0.17$		Ep = 200 GeV, $y \simeq 0.36$	

The comparison being performed at fixed M, the release of the assumption of an independence on τ of the intrinsic $p_\perp$ could affect the lowest energy results for low values of $p_\perp$.

CONCLUSIVE REMARKS

The above analysis is a test of QCD predictions representing a comparison of cross-sections with a different number of jets in the final state : in fact the parton distributions, suitably normalized to fit to the continuum totally inclusive cross-section, have been used to predict the $p_\perp$ distribution of the semi-inclusive one-jet cross-section.

The comparison among different processes depends on the possibility of using the same parton structure functions in different reactions. For a world made of partons only, this has been demonstrated to the leading log approximation : the next-to-leading terms, however, modify by corrections of order α_s the leading distributions of valence, gluons and sea. In the latter case, they might play a crucial rôle : the distribution $S(x,Q^2)$ obtained by the leading log approximation will presumably change into $S(x,Q^2) + C(x)\ \alpha_s(Q^2) \times G(x,Q^2) + \ldots$ where $G(x,Q^2)$ is the gluon density to the leading log approximation and dots stand for less relevant corrections. Because of the difference between gluon and sea densities, the next-to-leading correction might be, in this case, as big as the leading one. In addition the coefficient $C(x)$ is no longer process-independent, the latter being a property restricted to dominant (leading log) corrections.

As a consequence, the distribution of the effective sea measured experimentally, for example in the DIS of neutrinos off hadrons, can be very different from the one measured in lepton pair production. This fact represents a problem for the comparison of data referring to very massive lepton pairs to data extracted from DIS experiments at relatively low Q^2 which are boosted to high Q^2 through the evolution equations which embody only the leading log approximation [17]. Under this respect, a part of next-to-leading corrections are automatically included in the parton distributions obtained by fitting the total Drell-Yan cross-section and used to evaluate the $p_\perp$ distributions in the same range of Q^2.

The main source of uncertainty in the identification of parton densities of different processes comes from interactions inside the hadrons with spectator quarks which do not participate in the elementary hard scattering process. They should not affect the Q^2 evolution of parton densities, but could modify the absolute normalization : an analysis of mass singularities of interactions with spectators might give an indication on the universality of the absolute normalization. A definite answer to this problem is strictly connected to the unsolved problem of the large distance structure of the theory. The comparison of experimental data with the perturbative $< p_\perp^2 >_p$ indicates the presence of a non-perturbative component. The analysis of $p_\perp$ distributions requires some phenomenological ansatz on this component ; the predictions are consistent with the pattern of experimental results, but show that, at present energies, perturbative contributions are still masked by non-perturbative effects. The presence of an intrinsic $p_\perp$ is one of them : it gives rise to sizeable scale breaking effects which, in Drell-Yan processes or large $p_\perp$ hadron scattering [18], could change drastically, up to rather large energies, the approximate scaling behaviour of QCD.

ACKNOWLEDGEMENTS

I thank Professor L.M. Lederman for making available some of his data prior to publication.

REFERENCES

1) S.D. Drell and T.M. Yan - Phys.Rev.Letters 25, 316 (1970).

2) For a review, see : H.D. Politzer - Physics Reports 14, 129 (1974).

3) T. Kinoshita - J.Math.Phys. 3, 650 (1962) ;
T.D. Lee and M. Nauenberg - Phys.Rev. 133, 1549 (1964).

4) N. Nakanishi - Progr.Theor.Phys.(Kyoto) 19, 159 (1968).

5) For a review, see : W. Marciano and H. Pagels - Physics Reports 36, 137 (1978) and references therein.

6) G. Sterman and S. Weinberg - Phys.Rev.Letters 39, 1436 (1977) ;
G. Sterman - Stony Brook Preprints ITP-SB-77-69 and ITP-SB-77-72.

7) H.D. Politzer - Nuclear Phys. B129, 301 (1977) ;
C.T. Sachrajda - CERN Preprint TH. 2416 (1977).

8) C.T. Sachrajda - CERN Preprint TH. 2459 (1978).

9) K.H. Craig and C.H. Llewellyn Smith - Phys.Letters 72B, 349 (1978).

10) D. Amati, R. Petronzio and G. Veneziano - CERN Preprint TH. 2470 (1978).

11) G. Parisi - Proc. 11th Rencontre de Moriond (1976), Ed. J. Tran Thanh Van ;
G. Altarelli and G. Parisi - Nuclear Phys. B126, 298 (1977).

12) G. Altarelli, G. Parisi and R. Petronzio - CERN Preprint TH. 2413 (1977), to be published in Phys.Letters B. For a review, see, for example, the talk of R.C. Hwa at the same meeting and references therein.

13) L.L. Wang - BNL Preprint 22661 (April 1977).

14) S.W. Herb et al. - Phys.Rev.Letters 40, 435 (1978).

15) G. Altarelli, G. Parisi and R. Petronzio - CERN Preprint TH. 2450 (1978).

16) L.M. Lederman - Private communication.

17) For a comparison of DIS data to massive muon pair production to the leading log approximation, see : N. Cabibbo and R. Petronzio - CERN Preprint 2440 (1978), to be published in Nuclear Phys. B.

18) A.P. Contogouris, R. Gaskell and S. Papadopoulos - McGill University Preprint, Montreal (1977) ;
R.D. Field - Cal-Tech Preprint 68-633 (1977).

HADRON JETS PRODUCED AWAY FROM A LARGE Q_T MASSIVE LEPTON PAIR TRIGGER

D.Schiff
Laboratoire de Physique Théorique et Hautes Energies
Université de Paris-Sud, 91405 Orsay, France.

ABSTRACT

It has been proposed to explain the large Q_T tail of massive lepton pair distribution via a $2 \to 2$ hard scattering subprocess winning over the Drell-Yan mechanism. We show that the observation of a hadron jet away from the large Q_T pair is a clear test of this hypothesis and the jet quantum number is a specific signature of the subprocess, especially of perturbative QCD.

RESUME

Il a été proposé d'expliquer la partie à grand Q_T de la distribution des paires de leptons massives en termes d'un sous-processus dur $2 \to 2$ qui l'emporte sur le mécanisme de Drell-Yan. Nous montrons qu'un test clair de cette hypothèse réside dans l'observation d'un jet de hadrons opposé à la paire de leptons à grand Q_T et que le contenu en nombres quantiques du jet est une signature spécifique du sous-processus, spécialement de QCD perturbatif.

The mean transverse momentum of massive $\mu^+ \mu^-$ pairs produced in hadronic collisions has recently been measured[1] and found to be large: $< Q_T > \simeq 1.2$ GeV/c in proton-nucleus collisions. In the framework of the Drell-Yan model, this implies parton transverse momenta much larger than the usual limited momentum assumed in the parton model. Thus, the idea has emerged that apart from the Drell-Yan process, with parton Fermi motion taken into account, a new mechanism sets in at large Q_T. It is indeed more economical that the virtual photon large transverse momentum be balanced by a single parton, as the result of a $2 \rightarrow 2$ hard scattering (Fig.1b), in contradistinction with the Drell-Yan mechanism where the recoil is taken coherently by all the spectators (Fig.1a).

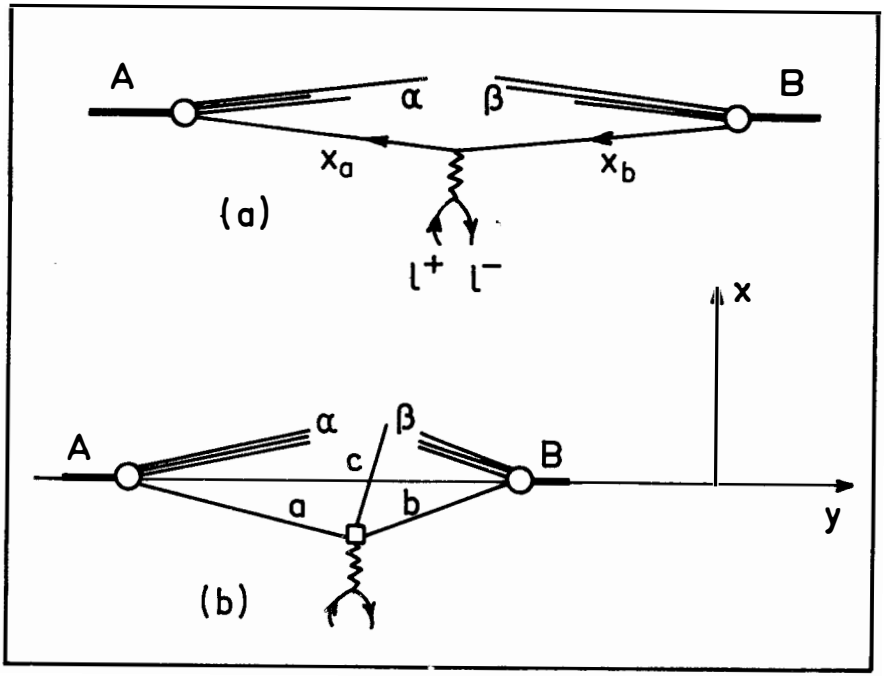

Fig.1

In the QCD approach[2,3] the partons entering in the hard scattering subprocess are either quarks or gluons: $q + \bar{q} \to \gamma^* + g$ and $q + g \to \to \gamma^* + g$ subprocesses have been considered. On the other hand, the following CIM subprocesses have also been considered[4]: $q + M \to q + \gamma^*$ $(qq) + \bar{q} \to q + \gamma^*$. Both pictures lead to satisfactory fits of $d\sigma/dQ_T$. There are, however, ambiguities connected in particular with the relative weight of the soft (Drell-Yan) and hard (QCD or CIM) components and possibility of double counting between them[3]. In this contribution[5], we want to show that the observation of hadrons in correlation with a large Q_T lepton pair allows to clearly determine whether mechanism (b) in Fig.1 is really at work. More precisely one expects, within this picture, to see a jet of hadrons recoiling against the lepton pair and thus to observe a striking increase of the large p_T hadron multiplicity in the central region (as observed in hadronic large p_T phenomena). The analysis of the quantum number content of the jet is moreover a way to distinguish QCD from CIM. In the case of mechanism (a),on the contrary, the pair transverse momentum is balanced by the spectators: they travel coherently in the forward and backward directions with a transverse momentum of the order $Q_T/2$, which leads to observation of large p_T hadrons mainly in the large x_F region.

For clarity, we shall present detailed results of the QCD approach and summarize the conclusions for the CIM, emphasizing striking differences in particular for particle ratios.

Let us turn to a quantitative study of mechanism (b). We shall give predictions for the multiplicity dN/dYdz of hadrons with rapidity Y, momentum $\vec{p}$ observed in correlation with a massive lepton pair with mass $\sqrt{Q^2}$, transverse momentum $\vec{Q}_T$, rapidity y; z is the fraction of the jet momentum Q_T taken away: $z=p_x/Q_x$ (*). dN/dYdz is defined as:

$$\frac{dN}{dYdz} = \frac{d\sigma^{(2)}}{dQ^2 d\vec{Q}_T\, dydYdz} \Big/ \frac{d\sigma^{(1)}}{dQ^2 d\vec{Q}_T dy} \qquad (1)$$

(*) The xOz plane is the scattering plane defined by the beam axis along Oz and the virtual γ^* momentum.

The double inclusive cross-section is straightforwardly written under the form:

$$\frac{d\sigma^{(2)}}{dQ^2 d\vec{Q}_T\, dy\, dY\, dz} = \frac{4}{3}\left(\frac{\alpha}{2\pi}\right)^2 \frac{1}{s^2}\frac{1}{Q^2}(-T^{\mu}{}_{\mu})\,\frac{G_{a/A}(x_a)G_{b/B}(x_b)}{x_a x_b}\,D_c^h(z) \qquad (2)$$

where $G_{a/A}(x_a)$ is the probability to find a parton a in hadron A with longitudinal momentum fraction x_a. $D_c^h(z)$ is the probability that parton fragments into hadron h which takes away a fraction z of the jet momentum. $T^{\mu}{}_{\mu} = \sum_{\mu} \mathcal{M}^{\mu}\mathcal{M}^{*}{}_{\mu}$ with $\mathcal{M}^{\mu}$ being the matrix element of the subprocess $a + b \to \gamma^{*\mu} + c$. p_y (hadron momentum component $\perp$ to the production plane) has been integrated upon and

$$x_{\substack{a\\b}} = \frac{Q^{(\pm)} + Q_T e^{\pm Y}}{\sqrt{s}} \quad \text{with} \quad s = (p_A + p_B)^2,\ Q^{(\pm)} = Q_0 \pm Q_{//} = (Q^2 + Q_T^2)\,e^{\pm y}$$

The single inclusive cross-section is simply given by

$$\frac{d\sigma^{(1)}}{dQ^2 d\vec{Q}_T dy} = \int dY\, \frac{4}{3}\left(\frac{\alpha}{2\pi}\right)^2 \frac{1}{s^2}\frac{1}{Q^2}(-T^{\mu}{}_{\mu})\,\frac{G_{a/A}(x_a)G_{b/B}(x_b)}{x_a x_b}$$

and thus dN/dYdz is clearly normalized to $\int \frac{dN}{dYdz} dY = D_c^h(z)$.

Typical values for kinematics are $\sqrt{s}$=20 GeV, y=0, Q^2=16GeV^2, Q_T= 2 GeV/c for which we may expect a large enough counting rate. We expect that for this value of Q_T, processus (b) already dominates (a). This is true in the calculation by Altarelli et al.,[3] with intrinsic parton momenta assumed to be of the order of 600MeV/c.

We shall mainly discuss the results for π^- beams (p and $\bar{p}$ are discussed elsewhere [5,6]).

i) $q + \bar{q} \to \gamma^* + g$

The virtual photon inclusive distribution has already been calculated by many authors. We use the following expressions for the various structure and fragmentation functions which enter in (2).

gluon structure function.

$$G_{g/h}(x) = \frac{k+1}{2}\,(1-x)^k \qquad (3)$$

assuming that gluons carry half the hadron momentum and dimensional

counting which predicts k to be 3-5 and 5-7 for h=pion and proton respectively. We take k=3(6) for the pion(proton).

Quark structure function.

For $G_{q/p}(x)$ we use a fit due to Gunion[7] and $G_{q/\pi}(x)$ is taken under the expression :

$$G_{q/\pi}(x) = 2x(1-x) + .72(1-x)^3/x + .15(1-x)^5/x \qquad (4)$$

already used in calculations of large p_T reactions with pion beams[8]

Quark fragmentation into charged hadrons

$$D_q^{ch}(z) = \frac{1-z}{z} \qquad (5)$$

assuming dimensional counting and that the momentum taken away by charged hadrons is half the jet momentum.

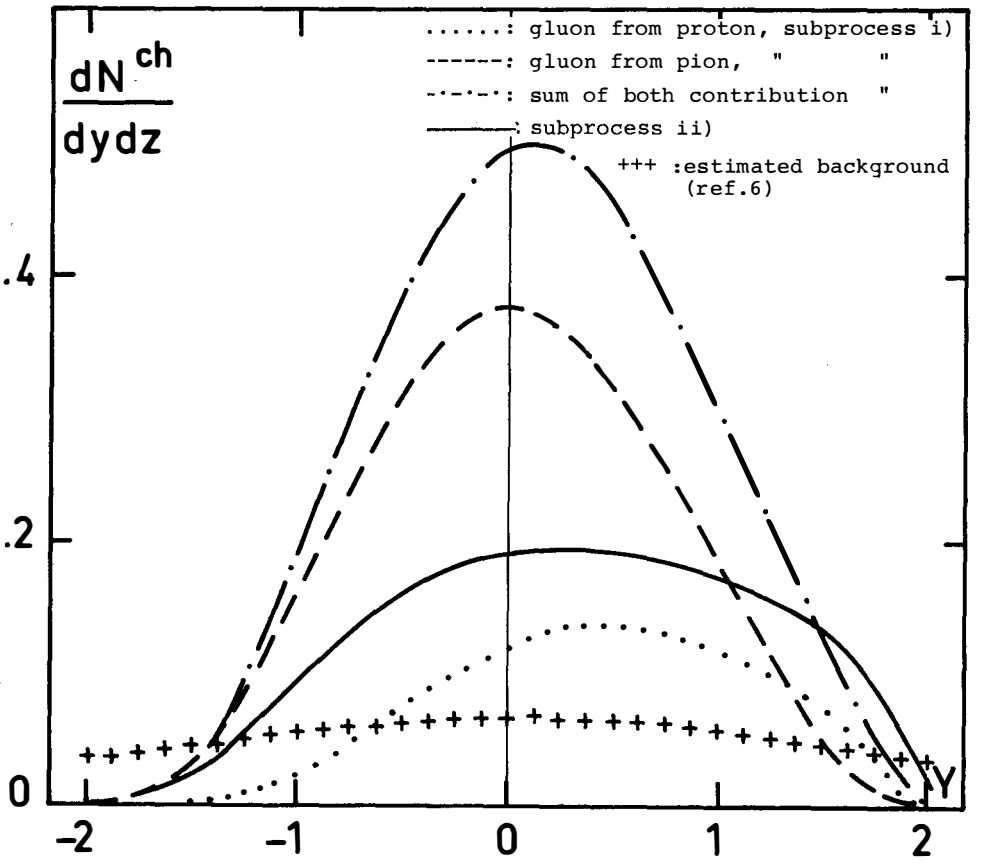

Fig. 2

The resulting charged multiplicity (z=1/2) is shown in Fig.2 where separate contributions for the two possibilities where the gluon comes either from the π^- or from the proton are shown. The asymmetry of the rapidity distribution in the latter case reflects the fast decrease of the gluon structure function in the proton when $x \to 1$ compared with the quark in the pion.

ii) $q + \bar{q} \to \gamma^* + g$

The gluon fragmentation into charged hadrons has to be specified:

$$D_g^{ch}(z) = \frac{2(1-z)^3}{z} \qquad (6)$$

assuming that gluon jets are similar[9] to quark jets and follow dimensional counting and that charged hadrons take half the gluon momentum. The results (z=1/2) are shown in Fig.2. QCD predicts the relative normalization of subprocess (i) and (ii) but in a model-dependent way in particular with regards to choices of gluon structure and fragmentation functions which are essentially unknown. With (3) and (6) we find that $\frac{d\sigma^{(2)}}{dQ^2 d\vec{Q}_T dy\, dY\, dz}$ are equal within 30% for z=1/2 and Y=0 for i) and ii).

As we shall see in the following, experimental data on the quantum number content of the away jet will determine which of i) and ii) dominates, if any.

The quantum number content of the away jet may be described in terms of the ratio of the multiplicities at given Y and z of hadrons h_1 and h_2. In case i)

$$\frac{h_1}{h_2} = \frac{dN^{h_1}/dYdz}{dN^{h_2}/dYdz} = \frac{\sigma^{(2)}_{g/\pi}(Y)\left(\frac{8}{9} D_u^{h_1}(z) + \frac{1}{9} D_d^{h_1}(z)\right) + \sigma^{(2)}_{g/p}\left(\frac{4}{9} D_{\bar{u}}^{h_1}(z) + \frac{1}{9} D_d^{h_1}(z)\right)}{id\ (h_1 \to h_2)} \qquad (7)$$

where $\sigma^{(2)}$ is straightforwardly taken from (2) with $D_c^h(z)$ and the charge factor divided out. For example in fig.3 we show the ratio $K^+/K^-(Y,z)$ using Feynman Field[10] quark fragmentation functions in (7). The Y dependence of K^+/K^- comes from differences in the Y variations of $\sigma^{(2)}_{g/\pi}$ and $\sigma^{(2)}_{g/p}$. In the case ii) h_1/h_2 is independent of Y and z and equal to 1 so that in each case i) and ii), h_1/h_2 is a clear signature of the subprocess. Summing both subprocesses

(assuming $D_g^{K^\pm} = \frac{1}{2} D_g^{\pi^\pm} = \frac{1}{3} \frac{(1-z)^3}{z}$) leads to the result shown in fig.3 for K^+/K^- which is closer to 1 than with i) only.

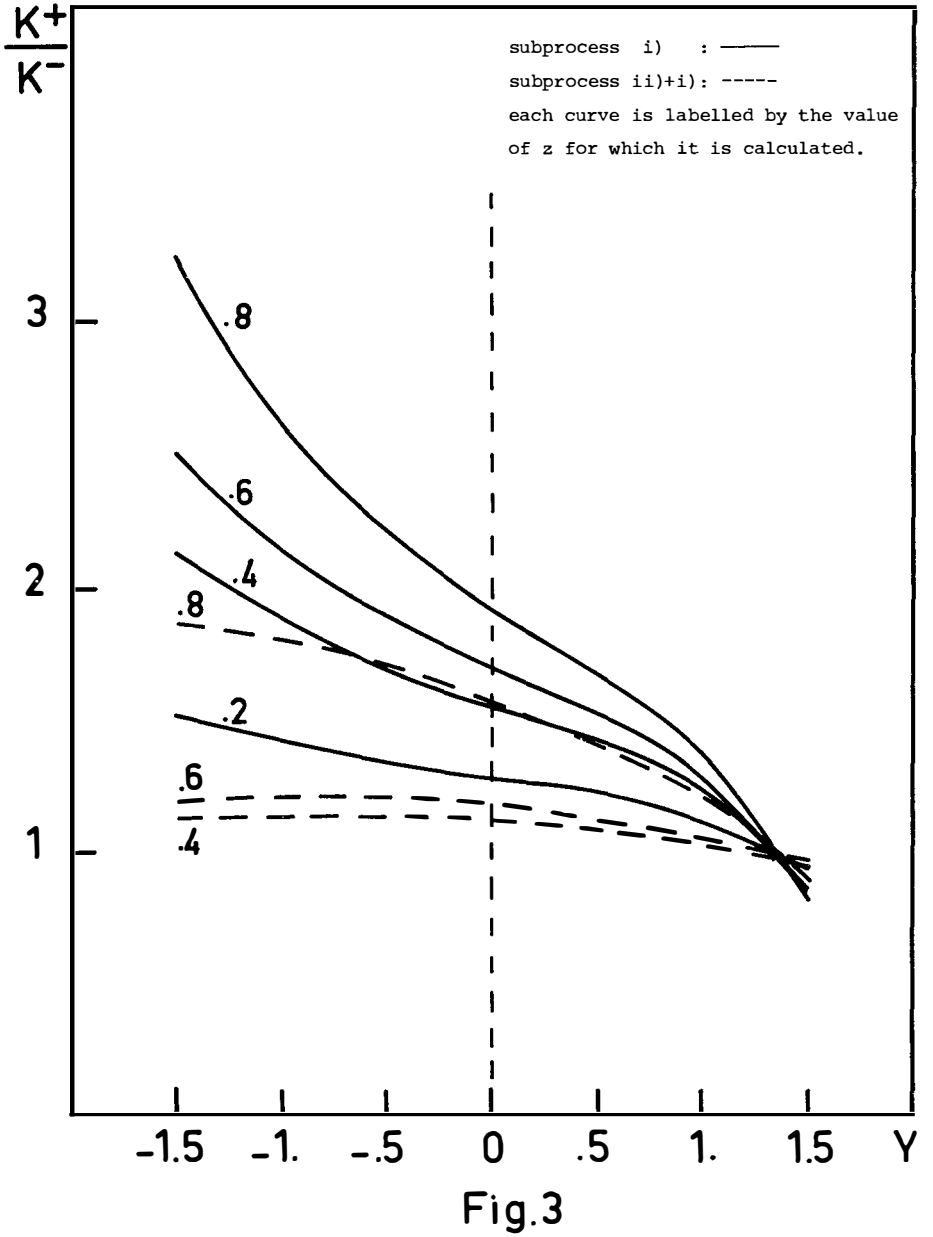

Fig.3

Let us contrast this situation with the results of the CIM approach which we shall sum up. (A detailed description may be found in (5)).

α) $M + q \rightarrow \gamma^* + q$

where M is essentially the initial π^-. The valence d quark of the π^- takes the recoil and since it has a large longitudinal momentum the multiplicity distribution of its fragments is strongly peaked at large Y and negligible around Y =0.

β) $(qq) + \bar{q} \rightarrow \gamma^* + q$

(qq) comes from the proton. The multiplicity distribution is roughly symmetric. The recoiling jet is a u or a d quark and the ratio h_1/h_2 should depend only slightly on Y. Moreover, the ratio K^+/K^- should be very large at large enough z since it is difficult to produce a K^- from a u or a d quark.

These features are very distinctive from the above listed for QCD. To summarize, from correlation data, one will learn whether mechanism (b) and especially perturbative QCD is at work.

REFERENCES

1) D.M.Kaplan et al., Phys.Rev.Lett. 40(1978)435.
2) J.Kogut, Phys.Lett. 65B(1977)377;
D.Soper, Phys.Rev.Lett. 38(1977)461
I.Hinchliffe and C.H.Llewellyn-Smith, Phys.Lett.66B(1977)281
A.V.Radyushkin, Phys.Lett.69B(1977)245;
C.S.Lam et T.M.Yan, Phys.Lett.71B(1977)173;
H.Fritzsch and Minkowski, Phys.Lett.73B(1978) 80
H.D.Politzer, Nucl.Phys.B129(1977)301
K.Kajantie, J.Lindfors and R.Raitio, Helsinski preprint HU/TFT/78-5.
3) G.Altarelli, G.Parisi, R.Petronzio CERN preprints TH-2413 and TH-2450.
4) G.Chu and J.F.Gunion, Phys.Rev.D10(1974)3672
M.Fontannaz, Phys.Rev D14(1976) 3127
K.Kinoshita, Y.Kinoshita, J.Cleymans and B.Petersson, Phys.Lett. 68B(1977)355.
Duong Van M. and R.Blankenbecler preprint SLAC-PUB 2017.
5) J.M.Brucker and J.Husser, Thesis (University of Strasbourg,1978).
6) J.M.Brucker and J.Husser, D.M.Fontannaz, B.Pire, D.Schiff (in preparation).
7) J.F.Gunion Phys.Rev. D10(1974)242.
8) M.Fontannaz and D.Schiff Phys.Lett 64B(1976)314.
9) G.Kane, contribution to this meeting.
10) R.P.Feynman and R.D.Field Phys.Rev.D15(1977)245.

DECAY DISTRIBUTIONS FOR LEPTON PAIRS AND QUARK TRANSVERSE MOMENTUM

J.T. DONOHUE

Laboratoire de Physique Théorique
Université de Bordeaux I

The decay angular distribution for hadron produced lepton pairs is computed in a Drell-Yan model generalized to include transverse momentum for the quark-partons. An exceedingly simple behavior is found if the Collins-Soper choice of axes is made.

La distribution angulaire de décomposition pour des paires de leptons produites dans les réactions hadroniques est calculée pour un modèle du type Drell-Yan, mais généralisé pour tenir compte du moment transverse des quarks-partons. Un comportement très simple est trouvé pourvu que l'on emploie le système d'axes proposé par Collins et Soper.

The Drell-Yan model for massive lepton pair production in the reaction $a + b \rightarrow e^+e^- + X$ relates the differential cross-section for producing a pair of mass M and c.m. rapidity y to the probability of finding quarks and anti-quarks in the hadrons a and b. The standard formula may be written

$$M^3 \frac{d^2\sigma}{dMdy} = \frac{8\pi\alpha^2}{9} x_a x_b \sum_i e_i^2 \{q_i(x_a)\bar{q}_i(x_b) + \bar{q}_i(x_a)q_i(x_b)\} \qquad (1)$$

where $x_a = (M/\sqrt{s})\, e^y$,

$x_b = (M/\sqrt{s})\, e^{-y}$,

and $q_i(x_a)$ represents the probability of finding a quark of flavor i having a fraction x_a of the momentum of hadron a. The same quark and anti-quark distribution may be measured in deep-inelastic lepton scattering, although in practice the anti-quark (or equivalently the sea-quark) distributions are not well-determined. As is discussed elsewhere in these Proceedings, the predictions of the Drell-Yan model are in general agreement with the data. One aspect of lepton pair production, which is somewhat unexpected, is that the transverse momentum of the pair is substantial, with $\langle P_\perp \rangle \simeq 1$ GeV. An important question is the origin of this transverse momentum, and, as is discussed elsewhere in these Proceedings, attempts have been made to calculate the $P_\perp$ dependence using Q.C.D.. Here we shall take a different approach, and generalize the form of eq.(1) to include intrinsic quark transverse momentum k_T. Now since the introduction of a transverse momentum distribution will necessarily increase the number of parameters available, it becomes interesting to consider the decay angular distribution of the lepton pairs.

The general angular distribution for a massive photon decaying into leptons is

$$W(\theta,\varphi) = \frac{1}{4\pi}\{1 + K\frac{\sqrt{10}}{2}\sum_{N=-2}^{+2} t_2^N D_{NO}^2(\varphi,\theta,0)\} \qquad (2)$$

where $K = (M^2-4\mu^2)/(M^2+2\mu^2)$,

μ is the lepton mass, D_{NO}^2 are the usual Wigner rotation functions, and the t_2^N are the multipole parameters describing the virtual photon polarization. If the initial hadrons are unpolarized, and parity is conserved in the production process, then the t_2^N are real and satisfy $t_2^N = (-1)^N t_2^{-N}$, provided the quantization axis lies in the production plane. Observation of the pair decay distribution thus provides, in addition to $d\sigma$, three new quantities, $d\sigma\, t_2^N$, with N = 0, 1 and 2.

In experiments having a large angular acceptance, it is possible to measure directly the $d\sigma\, t_2^N$ as functions of s, M, y, $P_\perp$ etc.. In experiments

having a more restricted acceptance, a direct measurement is not feasible, and one is obliged to postulate a form for the t_2^N in order to obtain the "true" cross-section from the "observed" cross-section. In both cases it is of interest to have an estimate of the possible effects of an intrinsic quark transverse momentum.

In ref.[1] a specific generalization of the Drell-Yan model to include $\vec{k}_T$ was proposed, namely, for $p + p \to \mu^+\mu^- + X$

$$\frac{d\sigma}{d^4P}\{1,t_2^N\} = \sum_i \int dx_1 dx_2 d^2k_{T_1} d^2k_{T_2}\, \delta^4(P-k_1-k_2)$$

$$\{G_{i/p}(x_1,k_{T_1})G_{\bar{i}/p}(x_2,k_{T_2})\sigma(q_i+\bar{q}_i \to \mu^+\mu^-)\}\{1,D^2_{NO}(R)/\sqrt{10}\} \quad (3)$$

where R denotes a rotation from the $q\bar{q}$ line-of-flight to the quantization axis, and the quark distributions were of the form

$$G(x,k_T) = \begin{cases} x_R^{-1}\, x\, G(x)\, f(k_T) & x > 0 \quad (4a) \\ 0 & x < 0 \quad (4b) \end{cases}$$

where x_R denotes $(x^2+4k_T^2/s)$. In explicit calculations the Field and Feynmann[2] choice for G(x) was used. As for the k_T cut-off, f was normalized to

$$\int f(k_T)\, d^2k_T = 1 \quad (5)$$

and various trial forms (gaussian, exponential, power-behaved) were studied. It should be remarked that the smearing in k_T destroys the one-to-one relationship between (M,y) and (x_1,x_2).

In order to compute quantities of experimental interest, one must choose quantization axes in the pair rest-frame. Popular choices are the t-channel or Gottfried-Jackson axes, (where z lies along the beam direction), and the s-channel or helicity axes. In ref.[1] it was found that the s-channel axes were ill-suited, since the t_2^N displayed a rather strong variation as functions of the kinematic variables. Recently Collins and Soper[3] have studied the same question, and they have proposed a set of axes which treats the beam and target directions symmetrically. With this choice of axes, the beam and target momenta have the form (in the pair rest-frame)

$$\vec{p}_a = |\vec{p}_a|(-\sin\Psi\,\hat{e}_x + \cos\Psi\,\hat{e}_z) \quad (6a)$$

$$\vec{p}_b = |\vec{p}_b|(-\sin\Psi\,\hat{e}_x - \cos\Psi\,\hat{e}_z) \quad (6b)$$

as depicted in Fig. 1. The angle Ψ between the Collins-Soper z-axes and the beam direction is given by, (neglecting beam and target masses)

$$\tan\Psi/2 = P_\perp/M \quad (7)$$

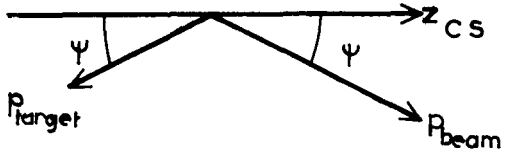

Fig. 1 Orientation of beam and target momenta in the lepton pair rest-frame, using the Collins-Soper choice for the z-axis. The t-channel or Gottfried-Jackson axis points along the beam direction (y axis rising out of page).

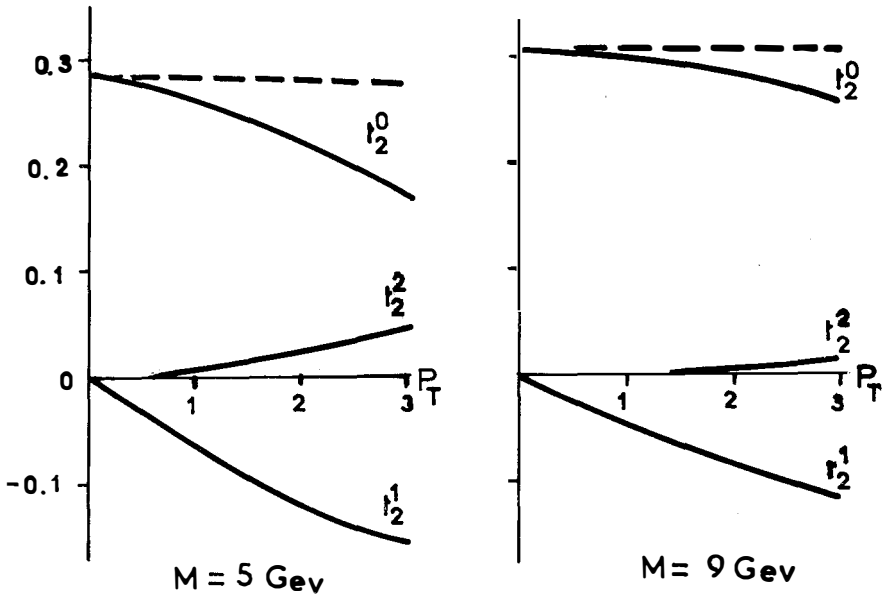

Fig. 2 The multipole moments t_2^M as functions of $P_\perp$ (in GeV/c) for pair masses of 5 and 9 GeV, in p p $\to \ell^+\ell^-$ + X, at 400 GeV/c and y $\simeq$ 0, calculated using a gaussian cut-off in k_T. The solid curves refer to t-channel axes, the dashed curves to the Collins-Soper choice, for which t_1^1 and t_2^2 are negligible and not drawn. For comparison the standard Drell-Yan prediction for $k_T = 0$ is $t_2^0 = 1/\sqrt{10}$, $t_2^1 = t_2^2 = 0$.

Our explicit calculations for the t_2^N using both the t-channel and Collins-Soper axes are shown in Fig. 2, as a function of $P_\perp$, for two values of the pair-mass. The k_T cut-off was gaussian, and the calculation was done for $y \simeq 0$. We observe that for the Collins-Soper choice the t_2^N are independent of $P_\perp$, with $t_2^1 \simeq t_2^2 \simeq 0$, whereas there is still some significant $P_\perp$ behaviour in the G-J axes. Although there is some slight dependence on the explicit form of the k_T cut-off, such a behavior is a general prediction of our approach. Hence it would be of great interest to experimentally confirm or disprove this prediction.

REFERENCES

1) E.L. Berger, J.T. Donohue and S. Wolfram, Phys.Rev. D17 (1978) 858.
2) R.D. Field and R.P. Feynmann, Phys.Rev. D15 (1977) 2590.
3) J.C. Collins and D.E. Soper, Phys.Rev. D16 (1977) 2219.

LEPTON PAIR PRODUCTION IN HADRON REACTIONS- PHENOMENOLOGICAL ASPECTS

D. Schildknecht
Department of Theoretical Physics
University of Bielefeld
Germany

Abstract

A recently proposed model for lepton pair production based on hadronlike production characteristics is reviewed.

I. Introduction

Most theorists, and sometimes also experimentalists, start their talk on lepton pair production in hadron reactions by showing the by now well known diagram first suggested by Drell and Yan[1], and more recently supplemented by QCD gluon contributions. My talk will be quite different.

I will start from the hypothesis that lepton pair production in hadron reactions is not much different from ordinary inclusive hadron production. Thus I will use hadronic concepts, functions and parameters throughout. While such an approach may be most controversial for lepton pair masses of 5 GeV or more (at present energies), it seems certainly appropriate at lower lepton pair masses, where resonances (e.g. ρ,ρ',ρ'' ...) play an important role and where the DY approach is known to yield a cross section which is too low by about an order of magnitude.

The work I am going to talk about has been done[2,3,4] in collaboration with H. de Groot, K. Kinoshita, M. Kuroda and H. Satz. Section II will contain the model description and its test in the low mass region ($M_{\mu^+\mu^-} \lesssim 4$ GeV), essentially discussing the $p_\perp$, $p_\parallel$, s and $M_{\mu^+\mu^-}$ - dependence. In section III the model will be confronted with the data in the high mass region, $M_{\mu^+\mu^-} \gtrsim 4$ GeV. Some concluding remarks will be contained in section IV.

II. Low Mass Region

As mentioned, we will start from the regularities observed in inclusive hadron production and extend them to inclusive lepton pair production by essentially replacing the hadron mass by the lepton pair mass. Such a procedure may be motivated within a picture in which hadronic clusters of spin 1 are formed, which with a certain probability decay into lepton pairs via an intermediate massive timelike virtual photon.

II.1 $p_\perp$-Dependence

We start by looking at the transverse momentum ($p_\perp$) dependence. It has been well known for a long time that various hadron inclusive spectra may be described in a universal way, if the transverse kinetic energy $E_\perp$ is introduced instead of $p_\perp$,

$$\frac{d\sigma}{dp_\perp^2} \Big/ \left(\frac{d\sigma}{dp_\perp^2}\right)_{p_\perp=0} = f(E_\perp), \qquad (1)$$

$$f(0) = 1$$

with

$$E_\perp = \sqrt{p_\perp^2 + m_h^2} - m_h \qquad (2)$$

As seen in Fig. 1, inclusive spectra for pp → (π,K,p)+X are fitted well in the low $p_\perp$ region by $f(E_\perp) = \exp(-E_\perp)$ with $\lambda = 6\ GeV^{-1}$ (corresponding to an average $p_\perp$ for pions of 333 MeV).

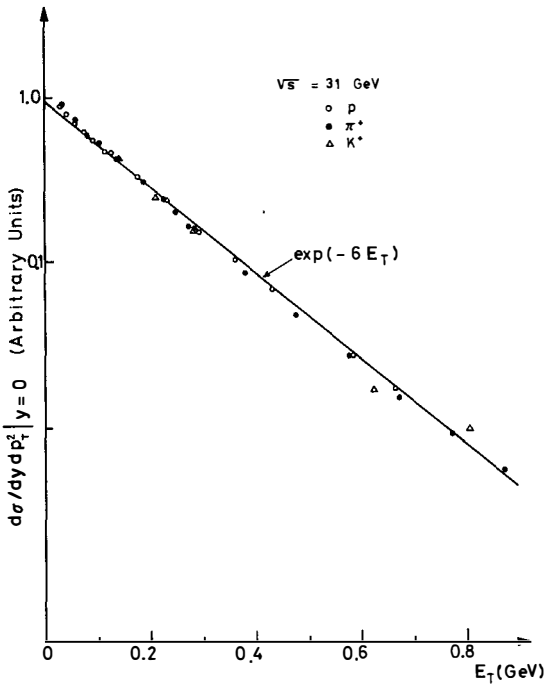

Fig. 1: Data (ref.5) on pp→(p,π^+,K^+)+X at 90° compared with $\exp(-6E_\perp)$

Assuming that hadrons at high energies are produced in a statistically independent emission process ("uncorrelated jet model" [6], "independent emission model") in which the production is essentially determined by phase space with a transverse kinetic energy cut-off, eqs. (1) and (2) must actually be replaced by (ref. 3,7,8,9)

$$\frac{d\sigma}{dp_\perp^2} \Big/ \left(\frac{d\sigma}{dp_\perp^2}\right)_{p_\perp=0} = \exp\left(-\lambda E_\perp - \frac{1}{\langle n\rangle \langle p_\perp^2\rangle_\infty} p_\perp^2\right) \qquad (3)$$

The additional factor appearing in (3) is a kinematic correction term due to transverse momentum balance in the hadronic final state. It is equal to the probability that the hadronic system X, consisting on the average of $\langle n\rangle(s)$ pions,

has the same absolute value of the transverse momentum as the observed hadron h. ($\langle p_\perp^2 \rangle_\infty$ is the average transverse momentum at infinite energy of the produced hadrons). As seen in Fig. 2 [3],

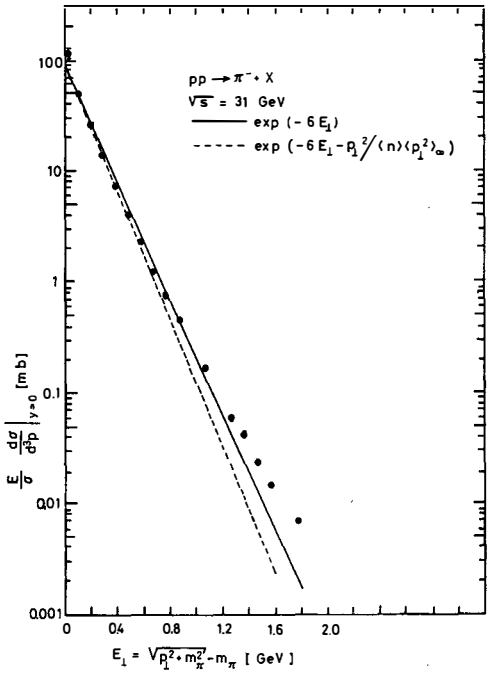

Fig. 2: The $p_\perp$ distribution of pions (ref. 10), showing the relatively small effect of the Gaussian transverse momentum balance factor in (3) and the well known deviations from "low $p_\perp$ physics" for $p_\perp \gtrsim 1$ GeV.

the additional factor has but a minor effect for production of low mass hadrons (π,p), where $\exp(-6E_\perp)$ is dominating. The additional factor in (3) is important, however, for very high masses of the produced secondary, as will be discussed in section III.

Generalizing eqs. (1), (2) to the case of lepton pairs, we expect (with $m_h \to m(\mu^+\mu^-)$)

$$\frac{d\sigma}{dq_\perp^2} \Big/ \left(\frac{d\sigma}{dq_\perp^2}\right)_{q_\perp=0} = \exp\left[-6\left(\sqrt{q_\perp^2 + m(\mu^+\mu^-)^2} - m(\mu^+\mu^-)\right)\right] \qquad (4)$$

In fact, as seen in Fig. 3, for various resonant and non resonant mass bins including the J/ψ, we obtain [2] one universal curve, which moreover agrees with the hadronic one. (The correction factor from eq. (3) is still fairly unimportant in this mass range and yields a correction, which is within the experimental error bars.

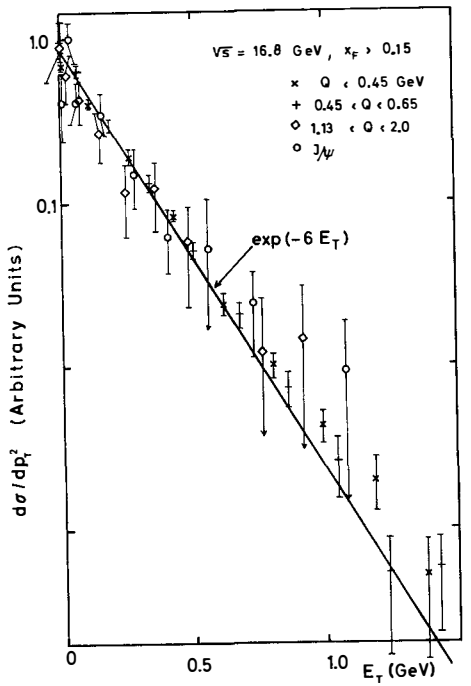

Fig. 3: Data (ref.11) on $pp \to \mu^+\mu^- + X$ for various mass bins $Q \equiv m(\mu^+\mu^-)$ compared with $\exp(-6E_\perp)$

II.2 The $p_{\parallel}$ and energy dependence

The well known scaling behaviour in $X_F \equiv \frac{2p_\parallel}{\sqrt{s}}$ or $X_o \equiv \frac{2p_o}{\sqrt{s}}$ of inclusive hadron spectra may most simply be obtained from phase space with transverse energy cut-off. In the uncorrelated jet model one has

$$\frac{X_o}{\sigma_{tot}} \frac{d\sigma}{dX_F} \sim f(E_\perp) \frac{\Omega_{LPS}\left((P-p)^2\right)}{\Omega_{LPS}(P^2)} , \tag{5}$$

where p is the four momentum of the observed secondary, and P is the total four momentum, $P^2 \equiv s$. As longitudinal phase space grows powerlike, one obtains from (5)

$$\frac{X_o}{\sigma_{tot}} \frac{d\sigma}{dX_F} \sim f(E_\perp) \left(\frac{M^2_{X,long.}}{s}\right)^\alpha \simeq f(E_\perp) \begin{cases} (1-x_o)^\alpha & \text{for } \frac{m^2}{s} \to o \\ (1-\frac{m}{\sqrt{s}})^{2\alpha} & \text{for } p_\parallel^2 << m^2 \end{cases} \tag{6}$$

with

$$X_o = \frac{2\sqrt{p_\perp^2+p_\parallel^2+m^2}}{\sqrt{s}} \tag{7}$$

With this formula we have an immediate connection between the scaling behaviour in $X_o \tilde{=} X_F$ as observed in the $p_{||}$ dependence of low mass inclusive hadron production (power α) and the energy dependence of the production of high mass hadronic states of mass m_h at small $p_{||}$ (power 2α). In $pp \to \pi^o + X$, the power α is found[12] to be $\alpha \tilde{=} 3.5$. Assuming hadronlike behaviour for lepton pair production and replacing the hadron mass m_h by the lepton pair mass $M(\mu^+\mu^-)$, we obtain two predictions:

1) the $p_{||}$ distributions of lepton pairs in pp scattering should lie on a universal curve, when plotted against X_o rather than X_F. The universal curve should agree with $(1-X_o)^{3.5}$.

2) The energy dependence for large mass lepton pairs should follow the behaviour $\left(1-\frac{m}{\sqrt{s}}\right)^7$. Both predictions are in agreement with the data, as seen in Figs. 4 and 5. (A universal behaviour for the $p_{||}$ dependence does not hold, if X_F is used instead of X_o (ref. 11)).

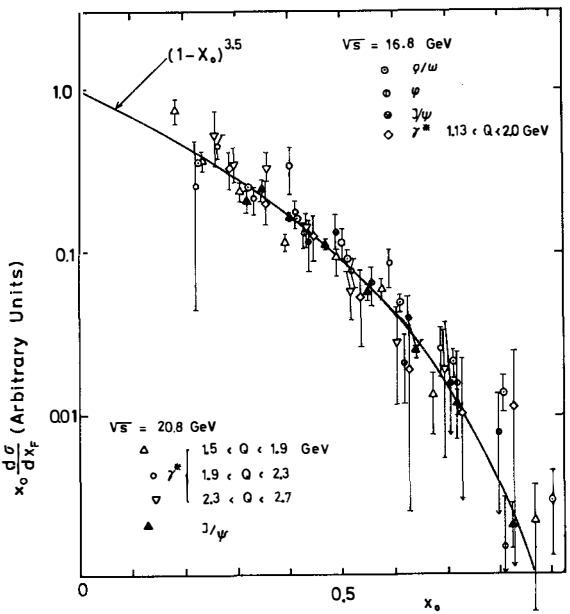

Fig. 4:
Data (ref. 11) on the distribution in $X_o \equiv 2p_o/\sqrt{s}$ for $pp \to \mu^+\mu^- + X$ at s=16.8 GeV and 20.8 GeV for various lepton pair masses compared with the hadronlike prediction $(1-X_o)^{3.5}$

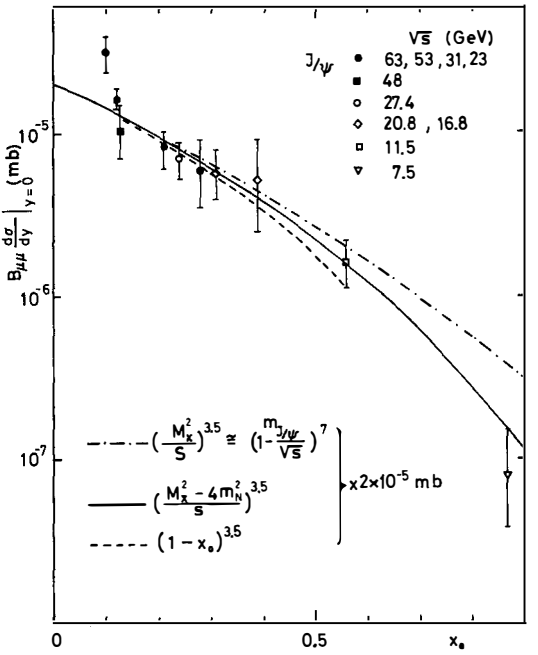

Fig. 5: J/ψ production data (ref. 13) at various energies compared with the theoretical prediction from (5).

Let me finally add the remark that the power α is beam dependent and significantly lower[4] for $\pi p \to (\mu^+\mu^-)+X$, where $\alpha \simeq 1.2$ to 1.5. This has important consequences[4] for the $\pi p/pp$ ratio.

II.3 The mass dependence

As the $p_{\parallel}$, $p_{\perp}$ and s dependence for lepton pair production has thus been obtained by using hadronic functions and the parameters λ and α determined in hadron physics, the only remaining freedom is a purely mass dependent function. Integrating the lepton pair distribution over transverse momentum and specializing to y=o, we have

$$\left.\frac{d\sigma}{dmdy}\right|_{y=o} = g(m)\left(1 - \frac{m}{\sqrt{s}}\right)^{2\alpha} \qquad (8)$$

i.e. a generalized scaling law[14] in the sense of a factorizing mass and $m/\sqrt{s}$ dependence. To specify g(m), duality considerations between continuum and vector meson production should be appropriate, the absolute normalization of the cross-section then being fixed by the production of the low lying vector mesons

(ρ^o,ω,Φ). For simplicity we have fitted g(m) by a power law ansatz and found that

$$g(m) = \frac{const}{m^\beta} , \qquad (9)$$

with β=5 yields an adequate representation of the data for lepton pair masses $M(\mu^+\mu^-) \lesssim 4$ GeV. For the comparison with experiment I refer to the original publication[2]. Let me remind you, however, that we heard from Teiger this morning that the CERN-CEN-SACLAY-ZÜRICH collaboration at the ISR has found β=5.2±0,54 for $M(\mu^+\mu^-) \lesssim 5.5$ GeV in agreement with our result obtained by fitting data at lower energies.

III. The High Mass Region ($M(\mu^+\mu^-) \gtrsim 5$ GeV).

The hadronlike model for lepton pair production developed in the last section will now be compared with the experimental data for large lepton pair masses $M(\mu^+\mu^-) \gtrsim 5$ GeV. As data in the high mass region have so far been taken at energies up to $\sqrt{s} \cong 27$ GeV only, the kinematical situation is such that $\tau = M/\sqrt{s}$ becomes fairly large for large $M(\mu^+\mu^-)$. If one considers the hadronlike model as a consequence of uncorrelated production of heavy clusters subsequently decaying into lepton pairs, one is clearly testing the model under fairly extreme conditions, as soon as τ becomes large and an appreciable fraction of the primary energy is converted into a lepton pair. Nevertheless, it is important to know, which of the hadronlike production features survive under these extreme conditions of large τ, e.g. $\tau \gtrsim 0.1$.

III.1 The transverse momentum dependence

For large masses $M(\mu^+\mu^-) >> 3$ GeV, we may expand the exponent in (3) to yield a Gaussian dependence on $q_\perp$ [3]

$$\left(\frac{d\sigma}{dq_\perp^2 dy}\right)_{y=o} \Big/ \left(\frac{d\sigma}{dq_\perp^2 dy}\right)_{y=o,\ q_\perp=o} = \exp\left(-(\lambda/2M_{\mu^+\mu^-}+1/\langle n\rangle\langle p^2\rangle_\infty)q_\perp^2\right) = \exp\left(-a(M,\sqrt{s})q_\perp^2\right). \qquad (10)$$

In this expression, λ=6GeV^{-1} from hadron physics. The energy available for the hadronic system X produced in conjunction with the lepton pair of mass $M_{\mu^+\mu^-}$ at rapidity $y\cong o$ is approximately given by $\sqrt{s}-M_{\mu^+\mu^-}$. The average particle multiplicity $\langle n\rangle$ in (10) is thus to be taken as the multiplicity of a hadronic system of energy $\sqrt{s}-M_{\mu^+\mu^-}$. The value λ=6GeV^{-1} implies $\langle p_\perp^2\rangle_\infty$=0.19 GeV^2 for pions and $\langle p_\perp^2\rangle_\infty$=0.43 GeV^2 for nucleons. Both these values enter the evaluation of (10), as the expression $\langle n\rangle\langle p_\perp^2\rangle_\infty$ has to be understood as $\sum_i \langle n_i\rangle\langle p_{\perp i}^2\rangle_\infty$, where the sum runs over all different particle types.

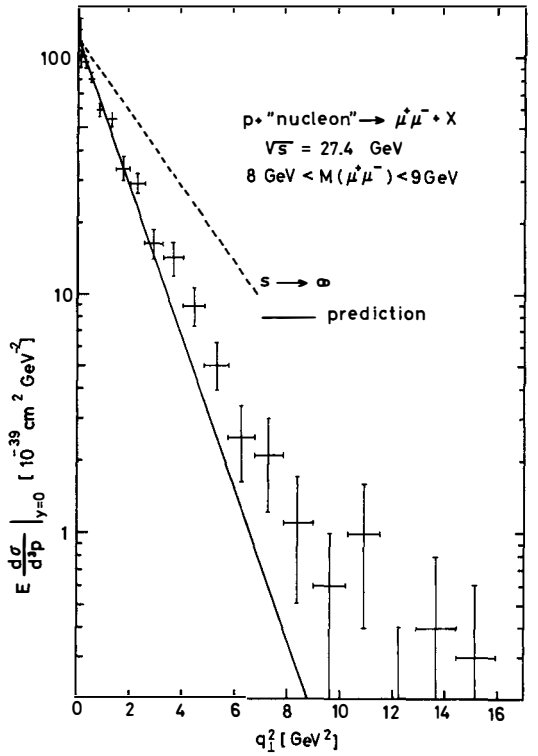

Fig. 6: The transverse momentum distribution of lepton pairs (ref. 16) compared with the uncorrelated jet model prediction from (10). The distribution for $s \to \infty$ is also indicated.

The parameter free prediction (10) for the $q_\perp$ distribution is compared with recent CFS data in Figures 6[3] and 7[3]. Both Figures show good agreement of the Gaussian prediction (10) with experiment as long as $q_\perp$ is not too large. Just as in inclusive hadron production at large $q_\perp$ the cross section (for lepton pair production) is larger than the one predicted from a universal transverse energy law. Thus, if one discriminates "low $p_\perp$" and "large $p_\perp$" physics in inclusive hadron production, one should also do so in massive lepton pair production.

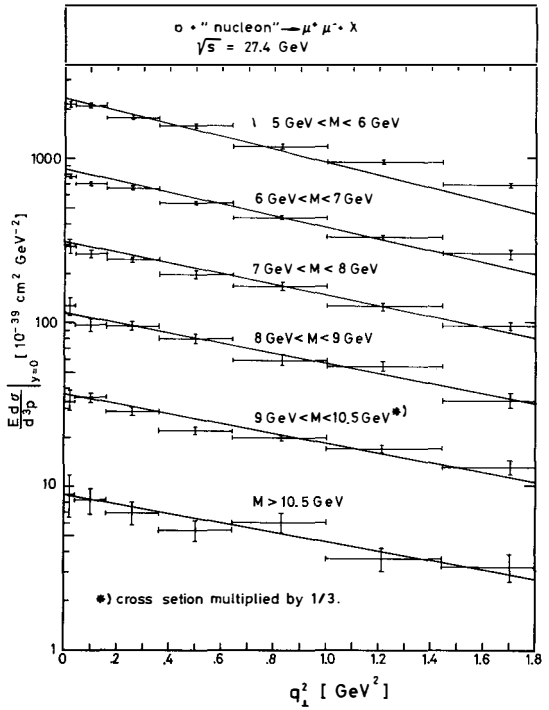

Fig. 7: The low transverse momentum distribution for different mass intervals as measured by the CFS collaboration (ref.16) compared with the uncorrelated jet model prediction (10).

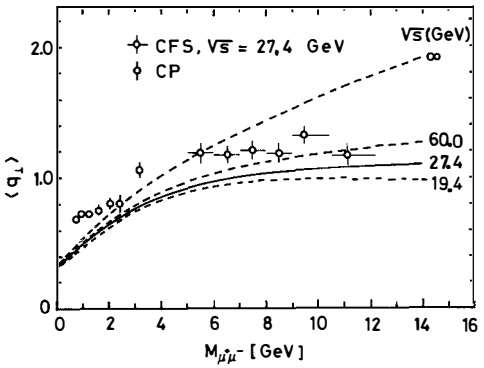

Fig. 8: The average transverse momentum of lepton pairs (ref. 16) as a function of the lepton pair mass compared with the predictions from (10) and (11).

Fig. 8[3] shows the data for the average transverse momentum $\langle q_\perp \rangle$ compared with the prediction from (10)

$$\langle q_\perp \rangle = \frac{\sqrt{\pi}}{2} \frac{1}{\sqrt{a(M, \sqrt{s})}} . \qquad (11)$$

The flattening of $\langle q_\perp \rangle$ as a function of $M_{\mu^+\mu^-}$ for sufficiently large $M_{\mu^+\mu^-}$ at any finite energy $\sqrt{s}$ is a consequence of the transversely limited phase space of the other produced particles. At any finite $\sqrt{s}$, for sufficiently large $M_{\mu^+\mu^-}$, the limited number of secondaries $\langle n \rangle$ (which number even decreases substantially as M increases) produced in conjunction with the lepton pair can provide the necessary momentum balance only at the cost of a considerable damping of the cross section. Conversely, from the flat behaviour of $\langle q_\perp \rangle$ with mass, we expect that the hadrons produced in conjunction with a lepton pair of transverse momentum $q_\perp \lesssim 1.5$ GeV show the transverse momentum behaviour usually observed in hadron physics.

III.2 Mass and energy dependence

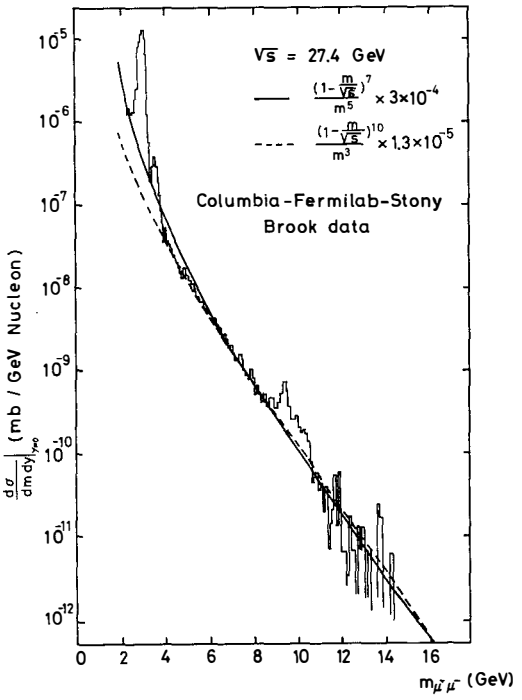

Fig. 9: Data[17] on lepton pair production for $M(\mu^+\mu^-) \geq 3$ GeV compared with the prediction (8) and (9).

Fig. 9[2] shows that the mass dependence as measured by CFS[17] at 400 GeV laboratory energy is consistent with the prediction from (8) and (9) with $2\alpha=7$ as obtained from hadron physics. For comparison a prediction based on the Drell Yan mechanism is also indicated. While (8) and (9) agree with data in the whole mass range from $M_{\mu^+\mu^-} = m\rho$ to $M_{\mu^+\mu^-} = 15$ GeV the Drell Yan prediction is too low by an order of magnitude in the region of very low masses

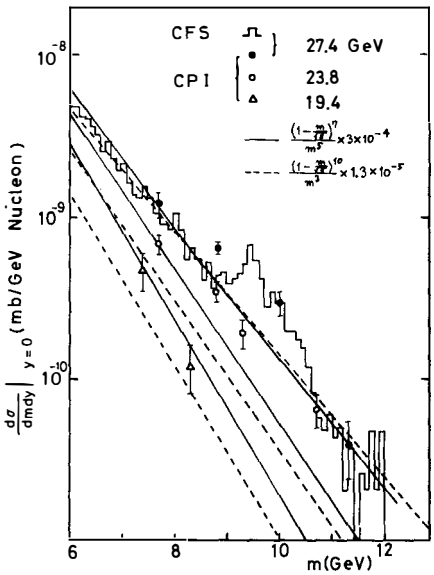

Fig. 10: Data[17,18] on lepton pair production for different energies compared with prediction (8), (9).

Fig. 10 shows that the data at different energies, which have been published so far, do not allow a discrimination of the two forms, i.e. scaling of $m^5 d\sigma/dmdy$ is not ruled out versus scaling of $m^3 d\sigma/dmdy$, which latter form is suggested by teh D.Y. formula and naive dimensional analysis. The CFS data at 200 and 300 GeV shown by Ledermann[19] at this meeting, however, seem to favor scaling of $m^3 d\sigma/dmdy$ in the high mass region. The power β in $m^\beta d\sigma/dmdy$ should actually be treated as a fit parameter, just as the power of $1/p_\perp$ in large $p_\perp$ physics. Provided $m^3 d\sigma/dmdy$ at present energies $\sqrt{s} \approx 20$ and $M_{\mu^+\mu^-} \gtrsim 5$ GeV shows approximate scaling as a function of $\tau = m/\sqrt{s}$, it will be an important question to be answered at ISR energies, which variable actually determines the scaling region, i.e. is it $M_{\mu^+\mu^-} \gtrsim M_o \cong 5$ GeV or is it $\tau \gtrsim \tau_o$ (with e.g. $\tau_o \approx 0.1$) which defines the scaling region?

Let me add a remark at this point on the beam ratio $\pi p/pp$. As mentioned,

whereas for pp the power of $(1-M/\sqrt{s})$ is $2\tilde{\alpha}=7$, for πp this power is significantly lower, $2\tilde{\alpha}=2.5$. This difference yields a beam ratio, which is strongly increasing with increasing lepton pair masses[4], $\pi p/pp >> 1$.

IV. Concluding Remarks

I have discussed a hadronlike model[2,3] for lepton pair production in hadron collisions based on

$$\frac{X_o d\sigma}{dX_p dq_\perp^2 dm} = \frac{c}{m^{\tilde{\beta}}} \left(\frac{M_X^2}{s}\right)^{\alpha} b \exp(-\lambda E_\perp - q_\perp^2/\langle n\rangle\langle p_\perp^2\rangle_\infty). \qquad (12)$$

This ansatz has been motivated by the independent emission model for inclusive hadron production. (In (12), b is chosen such that b·exp is normalized to 1 upon integration over $q_\perp^2$). The values of α ($\tilde{\alpha}=3.5$ for pp, $\tilde{\alpha}=1.5$ for πp) and $\lambda=6$ GeV^{-1} have been taken from hadron physics, while c is essentially determined by normalizing to low mass vector meson (ρ^o,ω,Φ) production. The power $\tilde{\beta}=5$ has been fitted in the low mass region ($M_{\mu^+\mu^-} \lesssim 4$ GeV).

We have found that the $q_\perp$ dependence (for $q_\perp \lesssim 1.5$ GeV) is described by (12) in the whole mass range, which has so far been explored, $M_{\mu^+\mu^-} \lesssim 15$ GeV ($\sqrt{s}\lesssim 27$ GeV). The $q_{||}$ and s-dependence in the low mass region ($M_{\mu^+\mu^-}\lesssim 4$ GeV) is well represented by (12). As yet unpublished data of the CFS collaboration indicate that the mass and energy dependence in the high mass region (or the high $\tau=M_{\mu^+\mu^-}/\sqrt{s}$ region ?) may be different from (12) with $\alpha=3.5$ and $\beta=5$. As for beam ratios, due to the fact that for πp scattering $\tilde{\beta}=5$, but $\tilde{\alpha}=1.2$, we expect[4] a strong increase of $\pi p/pp$ with increasing lepton pair mass, $\pi p/pp >> 1$.

References

1) S.D. Drell and T.M. Yan, Phys. Rev. Lett. 25 (1970), 316 and Ann. Phys. (N.Y.) 66 (1971), 578

2) K. Kinoshita, H. Satz and D. Schildknecht, Phys. Rev. D17 (1978), 1834

3) E.H. de Groot, H. Satz and D. Schildknecht, Phys. Lett. to be published

4) M. Kuroda and D. Schildknecht, to be published

5) B. Alper et al., Nucl. Phys. B87 (1975), 19

6) A. Krzywicki, Nuovo Cim. 32, (1964), 1067
L. v. Hove, Rev. Mod. Phys. 36, (1964), 655

7) R. Baier et al., Nuovo Cim. 28A, (1975), 455
E.H. de Groot, Nucl. Phys. B40, (1972), 295

8) C. Michael, L. Vanryckeghem, Liverpool preprint, LTH 31

9) H. Satz, Phys. Rev. D17, (1978), 914

10) B. Alper et al., Nucl. Phys. B100, (1975), 237

11) K.J. Anderson et al., Phys. Rev. Lett. 37 (1976), 4 for $\sqrt{s}$ = 16.8 GeV;
J.G. Branson et al., 38 (1977), 1331, 1334, and
K.J. Anderson et al., Contribution to the Tbilisi Conference (1976) for

$\sqrt{s}$ = 20.8 GeV.

12) F.E. Taylor et al., Phys. Rev. D14 (1976), 1217

13) J.H. Cobb et al., Phys. Lett. 68B (1977), 96, and data compiled therein.

14) J.J. Sakurai, Nucl. Phys. B76 (1972), 445

15) J. Teiger, these proceedings, and
A.G. Clark et al., Preprint May 1978

16) D.M. Kaplan et al., Phys. Rev. Lett. 40, (1978), 435

17) S.W. Herb et al., Phys. Rev. Lett. 39 (1977), 252

18) D. Antreasyan et al., Preprint CP 77-6 (1977)

19) L. Ledermann, these proceedings.

DILEPTON PRODUCTION AT LARGE TRANSVERSE MOMENTUM

C. Michael and T. Weiler
Department of Applied Mathematics and Theoretical Physics
University of Liverpool
Liverpool L69 3BX, U.K.

(presented by C. Michael)

Abstract: Data on the hadronic production of a massive lepton pair at large transverse momentum are compared directly with a QCD perturbation theory estimate.

Résumé: Les données expérimentales concernant la production hadronique des dileptons massives á grand transfert sont comparées directement á une évaluation de la théorie de perturbation de QCD.

INTRODUCTION

The production of massive dileptons is well studied experimentally and provides a testing ground for the ideas of quantum chromodynamics (QCD). The expectation [1] in a QCD framework is that the dominant contribution comes from quark antiquark fusion to form a massive photon. We wish to study in detail the distribution of the transverse momentum (k_T) of the produced dilepton. The sum over all k_T will be reproduced by the Drell-Yan mechanism of $q\bar{q}\to\mu^+\mu^-$ as mentioned above. At large k_T, however, particular subprocesses may dominate and we consider

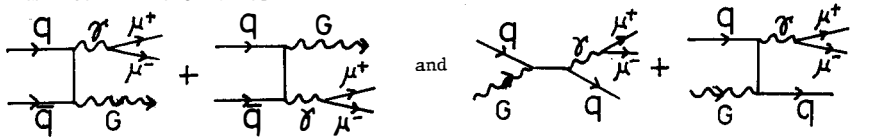

where G refers to a gluon. Here the final state G or q can balance the large k_T carried by the $\mu^+\mu^-$ pair. Such processes will dominate provided a QCD perturbation theory approach is valid and the effective coupling constant is small enough. At large enough k_T, this should be the case. It has been shown that a QCD perturbation theory treatment can be justified [1] provided scale breaking structure functions are used and the "running" coupling constant α_s is used. We shall evalute the subprocesses $q\bar{q}\to\mu^+\mu^-G$ and $qG\to\mu^+\mu^-q$ and compare with data [2] on hadronic $\mu^+\mu^-$ production at large k_T. The formulae are given in the Appendix. See refs. (3) and (4) for other evaluations. We avoid the divergence of these expressions at $k_T=0$ by concentrating attention on data for large k_T.

EVALUATIONS

The "running" coupling constant is taken from the fit [5] to scale breaking in deep inelastic scattering data which yields $\Lambda=0.5$ GeV. For the valence quark distributions in proton and neutron (the data is for proton-nucleus collisions) we take a conventional form for small Q^2 values [6] together with a parametrization [7] of the observed scale breaking effects at large Q^2 as $(Q^2/Q_0^2)^{-.25-x}$. $Q_0^2=2+12x^2$ provides a good description of the data fit in ref. 6. The sea or antiquark distribution is required for $x>0.2$ and is taken from a $q\bar{q}\to\mu^+\mu^-$ subprocess applied to the data integrated over k_T. This yields [2] $G_{\bar{u}N}(x)=G_{\bar{d}N}(x)=0.5(1-x)^9/x$ when the scale breaking of the valence distribution is taken into account. The remaining uncertainty is the gluon distribution. Unfortunately the $qG\to\mu^+\mu^-q$ mechanism gives a larger contribution than the $q\bar{q}\to\mu^+\mu^-G$ so that a knowledge of the gluon distribution is essential. The main constraint on the gluon distribution is that approxi-

mately 50% of the momentum of a proton is carried by glue. Using a dependence like $(1-x)^n$ then gives a distribution $G_{GN}(x)=0.5(1-x)^n(1+n)/x$ and n=5 is a conventional choice. The evaluation is sensitive to the gluon distribution for x>0.2. A larger value in this region can be obtained by using a less simple x-dependence.

One such expression is $(13.50 + 1.07/x)(1-x)$ which results from normalizing a typical glue distribution of ref. 5 to 50% of the nucleon momentum. This broad distribution and the conventional glue distribution are shown in fig. 1.

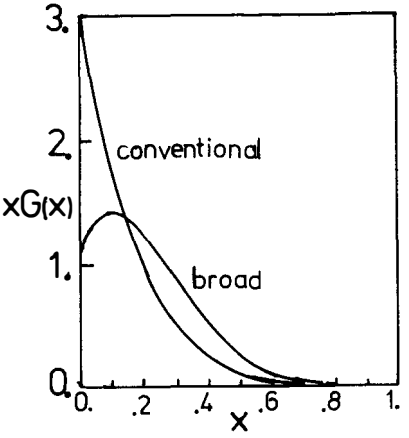

Fig. 1 Gluon distribution

Comparison with data is shown in fig. 2. With the conventional glue and nonscaling quark distributions, the QCD perturbation theory result lies below the data even at $k_T \sim 4$ GeV and Q=8.5 GeV. The result is insensitive to the sea distribution since the $qG \to \mu^+\mu^- q$ mechanism dominates. However, the broader gluon distribution does give a reasonable representation of the data for $k_T \gtrsim 2.5$ GeV. Since the scale breaking parametrization we use was obtained from a fit [7] to 1 GeV$^2 \lesssim |q^2| \lesssim 40$ GeV^2 leptoproduction data, the extrapolation to Q=8.5 requires some faith. To display the sensitivity of our results to scale breaking, an optimized solution of broad glue and no scale breaking is also shown for the Q=8.5 data. Clearly the uncertainty in the shape of the glue and in the exact nature of scale breaking allows model fits to the large k_T data.

DISCUSSION

This is a situation very reminiscent of that in large p_T hadron production where the QCD perturbation theory result is smaller than data and has a flatter p_T dependence. There agreement is possible for values of $p_T \gtrsim 6$ GeV, however.[8] The inclusion of "primordial" parton k_T makes a substantial improvement at smaller values of p_T. A similar approach has been tried in large k_T dilepton production [2] and introducing an ad-hoc "primordial" parton k_T distribution gives better agreement at small k_T. One possible

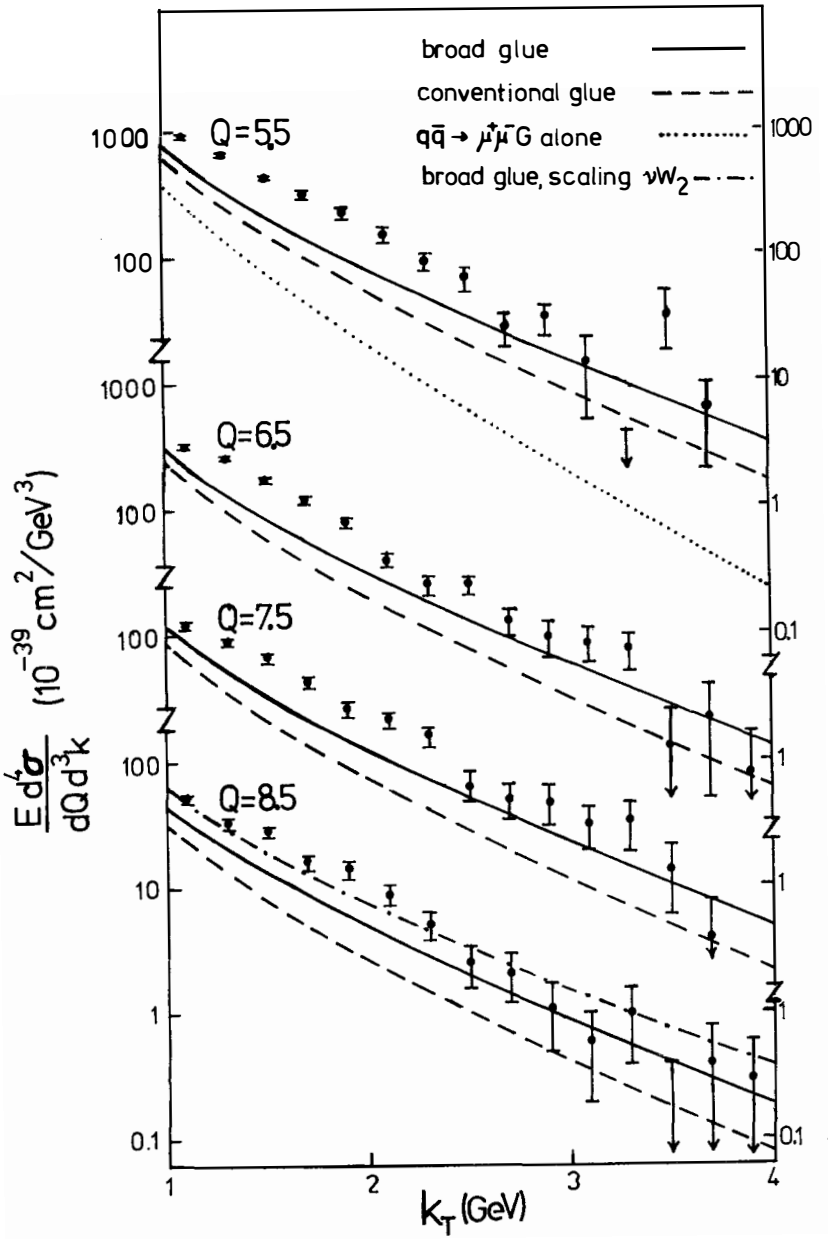

Fig. 2. Comparison of QCD predictions with data

worry is that anomalous nuclear rescattering effects are present for large p_T hadronic production and similar effects should be investigated experimentally in large k_T dilepton production of nuclei. Higher order QCD diagrams can also be important since α_s is 0.25-0.30 for the evaluations shown in the figure. One may conclude that detailed predictions of QCD perturbation theory must await a determination of the gluon distribution from other experiments. Qualitatively the theory gives a reasonable estimate of the large k_T tail but is not adequate to describe the complete k_T dependence of present data. Comparison with data on the fraction of events $\eta(2)$ with $k_T>2$ GeV rather than with $\langle k_T \rangle$ or $\langle k_T^2 \rangle$ would be preferable when statistics are too low to give the full distribution.

Let us discuss how this fraction $\eta(2)$ might be expected to depend on other variables such as incoming energy $\sqrt{s}$, incoming beam, rapidity y of the $\mu^+\mu^-$ pair, etc. The tail at large k_T will get progressively flatter with increasing $\sqrt{s}$ and thus $\eta(2)$ will increase with $\sqrt{s}$. The details of the increase depend on structure functions, etc. Data do show that $\langle k_T^2 \rangle$ increases as $\sqrt{s}$ varies from 19 to 27 GeV.

Comparison of data from differing incident beams provides a potentially clean test of the QCD mechanisms. In pN scattering, the lowest order Drell-Yan mechanism is suppressed due to the sea nature of the antiquarks. Thus the large k_T tail is relatively enhanced and $\eta(2)$ should reflect the $qG \to \mu^+\mu^- q$ subprocess. However, with π or $\bar{p}$ beams, valence antiquarks enhance lowest order Drell-Yan and give $q\bar{q} \to \mu^+\mu^- G$ as the dominant large k_T subprocess. Since the large k_T tail from π or $\bar{p}$ scattering is insensitive to the gluon component, and since the continuum data fixes the q and $\bar{q}$ distributions, πN or $\bar{p}N$ data will allow a clean test of QCD. Preliminary data [2] suggest that $\langle k_T \rangle$ is greater for πN than for pN at the same s and Q values. However, the "primordial" low k_T distributions of the constituents of the pion may differ from those of the proton, so that $\eta(2)$ rather than $\langle k_T \rangle$ is the relevant observable for a QCD test.

Further, the y dependence of $\eta(2)$ is completely predictive in the QCD context. Preliminary evidence [2] favors a $\langle k_T \rangle$ roughly independent of rapidity, which contradicts a theoretical estimate [4] obtained by folding the QCD k_T tail with a primordial k_T distribution. Since the calculation requires a rather arbitrary regularization of infinities at small k_T we emphasize again the importance of $\eta(2)$ as the observable directly applicable to QCD.

APPENDIX

The contributions of the subprocesses $a+b\to\mu^+\mu^-+d$ to the inclusive dilepton invariant cross section $A+B\to\mu^+\mu^-+X$ is given by

$$\frac{d^4\sigma}{dQ\ dy\ d^2k_T} = \sum_{ab}\int_{\xi_L}^{\xi_U} d\xi\ \frac{2\xi}{\pi s(\xi-\tau)^2|\cos\hat{\theta}|}\ G_{aA}(x_a)G_{bB}(x_b)\ \frac{d^2\hat{\sigma}}{dQd\cos\hat{\theta}}(ab\to\mu^+\mu^-d)\Big|_{\hat{s}=\xi s}$$

where the a b centre of mass scattering angle of the dilepton with respect to the incoming constituent a is given by

$$\cos\hat{\theta} = \pm\{(\xi-\tau)^2 - 4\xi K\}^{\frac{1}{2}}/(\xi-\tau)$$

where $\tau = Q^2/s$, $K = k_T^2/s$ and $\xi = x_a x_b$. One has

$$x_{\substack{a\\b}} = (\xi + x_R^2)^{\frac{1}{2}} \pm x_R$$

with $x_R = \sqrt{\xi}\ \sinh\left[y-\sinh^{-1}\left(\frac{(\xi-\tau)\cos\hat{\theta}}{2\sqrt{\xi}\ \sqrt{\tau+K}}\right)\right]$.

The limits are $\xi_L = \tau+2K + 2\sqrt{(\tau+K)K}$ and the upper limit on ξ is given by $x_a<1$ and $x_b<1$. For $y = 0$, $\xi_U = (\sqrt{\tau+K}-\tau)/(1-\sqrt{\tau+K})$.

For $q\bar{q}\to\mu^+\mu^-+G$: $\frac{d^2\hat{\sigma}}{dQd\cos\hat{\theta}} = \frac{16\ \alpha^2\alpha_s e_q^2(\xi-\tau)}{27\ s^{\frac{3}{2}}\sqrt{\tau}\xi^2\sin^2\hat{\theta}}\ \{1+\cos^2\hat{\theta} + \frac{4\tau\xi}{(\xi-\tau)^2}\}$

For $qG\to\mu^+\mu^-+q$: $\frac{d^2\hat{\sigma}}{dQd\cos\hat{\theta}} = \frac{\alpha^2\alpha_s e_q^2(\xi-\tau)}{9\ s^{\frac{3}{2}}\sqrt{\tau}\xi^2(1-\cos\hat{\theta})}\ \{\frac{2\xi}{\xi-\tau} + \frac{\xi-\tau}{2\xi}\ (1-\cos\hat{\theta})^2 - \frac{2\tau}{\xi}\ (1+\cos\hat{\theta})\}$.

REFERENCES

1) C. Sachrajda, Proc. XIIIth Rencontre de Moriond, ed. Tran Thanh Van, Orsay (1978).

2) D.M. Kaplan et al., Phys. Rev. Letters 40, 435 (1978).
L. Lederman, Proc. XIIIth Rencontre de Moriond, ed. Tran Thanh Van, Orsay (1978).
J.E. Pilcher, Proc. XIIIth Rencontre de Moriond, ed. Tran Thanh Van, Orsay (1978).

3) G. Altarelli, G. Parisi and R. Petronzio, CERN preprint TH2413 (1977).

H. Fritzsch and P. Minkowski, CERN preprint TH2400 (1977).
K. Kajantie and R. Raitio, Helsinki preprint HU-TFT-77-21 (1977).
K. Kajantie, J. Lindfors and R. Raitio, Helsinki preprint HU-TFT-78-5 (1978).
G. Altarelli, G. Parisi and R. Petronzio, CERN preprint TH2450 (1978).
4) F. Halzen and D.M. Scott, Madison Wisconsin preprints COO-881-16, 21 (1978).
5) G.C. Fox, Nucl. Phys. B131, 107 (1978).
6) V. Barger and R.J.N. Phillips, Nucl. Phys. B73, 269 (1974).
7) D. Perkins et al., Phys. Letters 67B, 347 (1977).
8) A. Contogouris, Proc. XIIIth Rencontre de Moriond, ed. Tran Thanh Van, Orsay (1978).
S. Ellis, Proc. XIIIth Rencontre de Moriond, ed. Tran Thanh Van, Orsay (1978).

QUANTUM CHROMODYNAMICS AND LARGE p_T HADRON PRODUCTION(+)

A.P. Contogouris
Department of Physics, McGill University, Montreal, Quebec, Canada

Abstract: With quark and gluon distributions determined from exact requirements of Quantum Chromodynamics (QCD) and partons carrying transverse momentum, inclusive meson production at large p_T is studied. It is concluded that within present theoretical and experimental uncertainties this approach offers a fair account for the data. Also, it offers an application of very recently advanced QCD ideas.

Résumé: On étudie la production inclusive des mésons à grand p_T à partir des distributions des quarks et des gluons determinées par des conditions exactes de Chromodynamique Quantique et des partons avec moment transverse. Etant donné les incertitudes théoriques et expérimentales actuelles, on conclut que cette méthode donne une description des expériences assez satisfaisante. Elle fournit aussi une application des idées de CDQ développées très récemment.

(+) Supported by the National Research Council of Canada and the Québec Department of Education.

We consider inclusive production of a hadron C (e.g. pion) at large transverse momentum p_T in the collision of the hadrons A,B. We assume that it takes place via the mechanism of Fig. 1a[1]. Then the inclusive cross-section for AB→C+X is of the form ($\theta_{cm}=90°$):

$$(1) \qquad E\frac{d\sigma}{d^3p}(p_T,s) \sim \sum_{a,b,c} \int\int dx_a dx_b \frac{F_{a/A}(x_a)}{x_a} \frac{F_{b/B}(x_b)}{x_b} \frac{d\hat{\sigma}}{d\hat{t}} \frac{G_{C/c}(z)}{z^2}$$

The probability function $F_{a/A}$ is determined from the distribution of the parton a inside the hadron A (similarly $F_{b/B}$) and $G_{C/c}$ is the fragmentation function for the parton c to produce C.

Suppose that the cross-section $d\hat{\sigma}/d\hat{t}$ is given by quark-quark scattering (qq) via single gluon exchange[1] (subprocess of Fig. 1b). Then $d\hat{\sigma}/d\hat{t} \sim \hat{s}^{-2} \sim p_T^{-4}$ and if $F_{a/A}$, $F_{b/B}$ and $G_{C/c}$ scale exactly we obtain

$$(2) \qquad E\frac{d\sigma}{d^3p} \sim \frac{1}{p_T^4} f(x_T) \qquad x_T = 2p_T/\sqrt{s}$$

Experimental situation: Parametrize $pp\to\pi^0+X$ (or $\frac{\pi^++\pi^-}{2}+X$) as follows:

$$(3) \qquad E\frac{d\sigma}{d^3p} \sim \frac{1}{p_T^n}(1-x_T)^m$$

Data of ISR and FNAL in the range $2 \lesssim p_T \lesssim 7$ GeV give:

$$n \simeq 8.35 \qquad m \simeq 8.5$$

However, very recent ISR data for $5.25 \le p_T \le 16.4$ give[2]

$$(4) \qquad n = 6.6 \pm .8 \qquad m = 9.6 \pm 1.0$$

It can be said that the highest p_T data favor $n<8$; but, anyway, $n>4$.

There is a number of effects, however, related in one way or another with Quantum Chromodynamics (QCD):

(A). Nonscaling distributions.

Present data on $ep\to e+X$, $\mu p\to\mu+X$ and $\nu p\to\mu+X$ indicate clear scale violations and, in fact, with the pattern predicted by QCD[3]. This implies that in (1) we must replace

$$(5) \qquad F(x) \to F(x,Q^2)$$

where Q the 4-momentum of the exchanged gluon (Fig. 1b). It can be seen[4] that, roughly, most of the contribution to the integral in (1) comes from integrating near

$$(6) \qquad x_a \sim x_b \sim x_T \ ;$$

then the kinematics of Fig. 1 implies[4] $Q^2 \sim 2p_T^2$. For most of x_a, x_b

of interest, QCD predicts that $F_{a/A}(x_a,Q^2)$, $F_{b/B}(x_b,Q^2)$ decrease with Q^2. Thus in Eq. (2) QCD scale violation increases the effective exponent of $1/p_T$ beyond the value n=4.[4][5]

Field theoretic arguments suggest that the fragmentation function should also be replaced: $G_{C/c}(z) \to G_{C/c}(z,Q^2)$; this was also done in Refs. 4 and 6. However, with respect to this point, the experimental situation (analyses of data on $eN \to eh+X$ and $\nu N \to \mu h+X$) is less clear.

(B). QCD running coupling constant.

The asymptotically free nature of QCD is manifest in the use for quark-gluon coupling:

$$\frac{\alpha_s^2}{4\pi} \equiv \alpha_s(Q^2) = \frac{12\pi}{25\ \log(Q^2/\Lambda^2)} \qquad \Lambda = .3 \sim .5\ \text{GeV} \tag{7}$$

This further increases the effective exponent of $1/p_T$.

Since long ago[5][4][6] the effects (A) and (B) have been exploited to stress the fundamental importance of scaling violations in understanding large p_T hadron production while preserving the essential ingredients of the BBK mechanism[1], and in particular without having to resort to arbitrary forms like[7] $d\sigma/d\hat{t} \sim 1/\hat{s}\hat{t}^3$. Specifically, a model[4] satisfying a number of QCD requirements and leading to logarithmic decrease of the moments of the structure functions has been shown to account for all the essential data on $pp \to h+X$ with $h=\pi^{\pm}$, π^0, $K^{\pm}$[4], as well as on large p_T correlations[6] (same-side and opposite-side momentum correlations, opposite-side rapidity distributions and transverse momentum sharing x_e distributions).[8]

It must be stressed that very recent work in perturbative QCD[9]-[11] is now providing important theoretical justification for the replacements of Eq. (5) used in Refs. 4-6 and here.

(C). Gluon effects.

In QCD gluon and quark distributions are generally inseparable. More recently such distributions satisfying exact QCD requirements became available in tractable and transparent form[12]. Then a straightforward extension of the BBK mechanism requires the inclusion of quark-gluon (qg) and gluon-gluon (gg) scattering subprocesses (e.g. Figs. 1c, 1d). These are also of order $\alpha_s(Q^2)$ and contribute significantly to the inclusive cross-section, in particular at moderate p_T.[13]

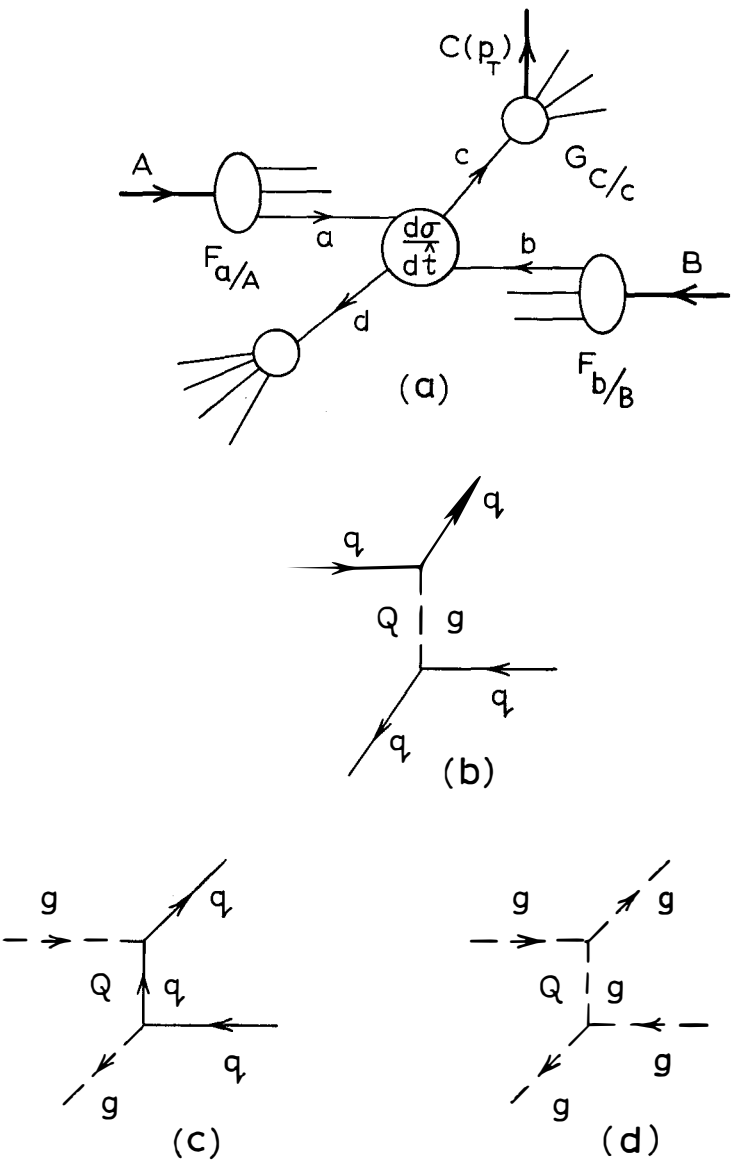

Fig. 1

(D). Quark and gluon transverse momentum.

It is now clear that the transverse momentum k_T of the initial quarks or gluons with respect to the hadrons should not be neglected. This further requires replacing

$$F \to F(x,Q^2;k_T)$$

Usual phenomenology proceeds with a factorable form $F \to F(x,Q^2)D(k_T)$. We present calculations with an exponential $D(k_T) \sim \exp(-bk_T)$ corresponding to $\langle k_T \rangle = 2/b = \text{const.}$[14] Use of a gaussian $D(k_T)$ does not significantly alter the results. Also we replace $G_{C/c} \to G_{C/c}(z,Q^2)D(k_T')$.

We determine $F(x,Q^2)$ in terms of the quark and gluon distributions of Ref. 12. As stated, these have been determined via exact QCD requirements, as well as via detailed fits to old and new data on nucleon structure functions. The fragmentation functions $G_{C/c}$ are also determined in terms of data on electro- and neutrino-production of hadrons as well as sum-rule requirements.[14] The gluon distribution is of the form

$$(8) \qquad g(x,Q^2) \sim (1-x)^{\gamma+\beta(\bar{s})} \qquad \bar{s} = \log \frac{\log(Q^2/\Lambda^2)}{\log(Q_o^2/\Lambda^2)}$$

QCD completely specifies the function $\beta(\bar{s})$ but not the constant γ. From Ref. 12: $\Lambda=.3$ and $Q_o^2 = 1.8\ \text{GeV}^2$. Thus in our calculation there are only two free parameters: γ and $\langle k_T \rangle$.[15] We choose the "standard" value $\gamma=5$, but present results for other γ as well.[14] Finally, we take

$$\langle k_T \rangle = 0.5\ \text{GeV} ;$$

in this choice we are guided by the second of Ref. 7 and by other similar calculations.[16]

Notice that the absolute magnitude of $Ed\sigma/d^3p$ is fully specified from $\alpha_s(Q^2)$. This has been stressed repeatedly[4]-[6] and stands in clear contrast to the $d\sigma/dt \sim 1/\hat{s}^3$ approach, in which not only the p_T-dependence but also the magnitude of the inclusive cross-section is introduced by hand.[7]

Our conclusions concerning gluon effects are summarized in Fig. 2. Clearly the qg and gg subprocesses dominate at $p_T=2\sim4$ GeV. As p_T increases, however, they drop faster than qq. Arguing on the basis of Eq. (6), this is due to the relatively large $\gamma=5$; but also to the fact that, at least in Ref. 12, the exponent $\beta(\bar{s})$ increases with Q^2 faster than the corresponding QCD exponents of the quark valence.

Concerning parton k_T-effects (Figs. 2,3) we conclude: (a) They are very important at $p_T \simeq 2 \sim 4$.[7][16] (b) At fixed p_T, with decreasing s the k_T effects significantly increase;[16][7] this is due to the steeper $Ed\sigma/d^3p$ at lower s. (c) They are very important for qg and gg due to the steep $g(x,Q^2)$.

Fig. 3 shows the comparison with experiments for $pp \to \pi^0 + X$ and $\to \frac{\pi^+ + \pi^-}{2} + X$. ISR data are well accounted for. When our calculations were performed[14] only data up to $p_T \simeq 12$ GeV were available. Thus beyond this value the curves of Fig. 3 constitute predictions of QCD.[14] Here we have added the very recent highest p_T data;[2] as far as we can say (large errors), they are in agreement.

With $\langle k_T \rangle = .5$ FNAL data ($\sqrt{s} = 19.4$) are less well accounted for. However it is evident (point (b) above) that increasing $\langle k_T \rangle$ affects more the predictions at low $\sqrt{s}$ and improves agreement with FNAL.[17] The prediction is also somewhat sensitive to the exact value of γ; lower γ ($=3$) improves the agreement (Fig. 3).

Very recently R.D. Field, implicitly denouncing previous work[7] has produced similar calculations.[18] He uses the relation

$$\langle k_T \rangle = \frac{1}{\sqrt{2}} \langle q_T \rangle_{\mu^+\mu^-} \tag{9}$$

where $\langle q_T \rangle_{\mu^+\mu^-}$ the mean transverse momentum of muon pairs in $pp \to \mu^+\mu^- + X$. With $\langle q_T \rangle_{\mu^+\mu^-} = 1.2$ he obtains[20]

$$\langle k_T \rangle = .848 \text{ GeV}$$

Further, he uses the parton distributions of Ref. 19, in which, apparently, the gluons contribute generally stronger than in Ref. 12. He also uses fragmentation functions nonzero at z=1,[7] which violate the Brodsky-Farrar counting rules and the Drell-Yan-West relation (via the Gribov-Lipatov reciprocity), but appear necessary if one wishes to obtain $\langle z \rangle = p_\pi / \langle p_{jet} \rangle \sim .85$[21]. In this way he shows for both ISR and FNAL data a perfect fit.

Returning to our work,[14] we may interpolate the results of our calculations by the parametrization of Eq. (3) for the same range of p_T and $\sqrt{s}$ of Ref. 2 (i.e. $5.25 \leq p_T \leq 16.4$ and $53 \leq \sqrt{s} \leq 63$). We obtain the effective values:

$$n = 6.34 \qquad m = 9.45 \tag{10}$$

to be compared with Eq. (4).

The model appears to have no particular difficulty to account for the correlation data (calculations under way). The same-side

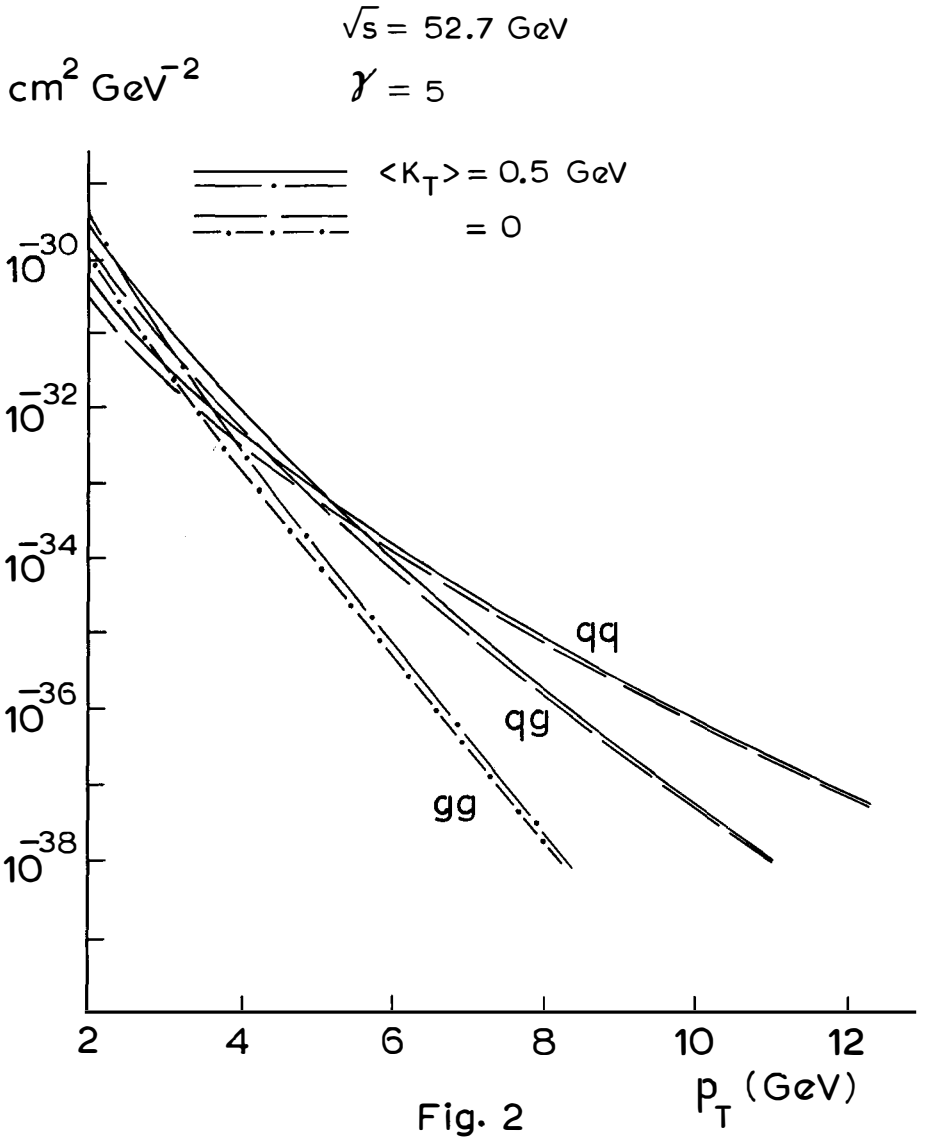
√s = 52.7 GeV
cm² GeV⁻²
γ = 5
<K_T> = 0.5 GeV
= 0
10⁻³⁰
10⁻³²
10⁻³⁴
10⁻³⁶
10⁻³⁸
qq
qg
gg
2
4
6
8
10
12
p_T (GeV)

Fig. 2

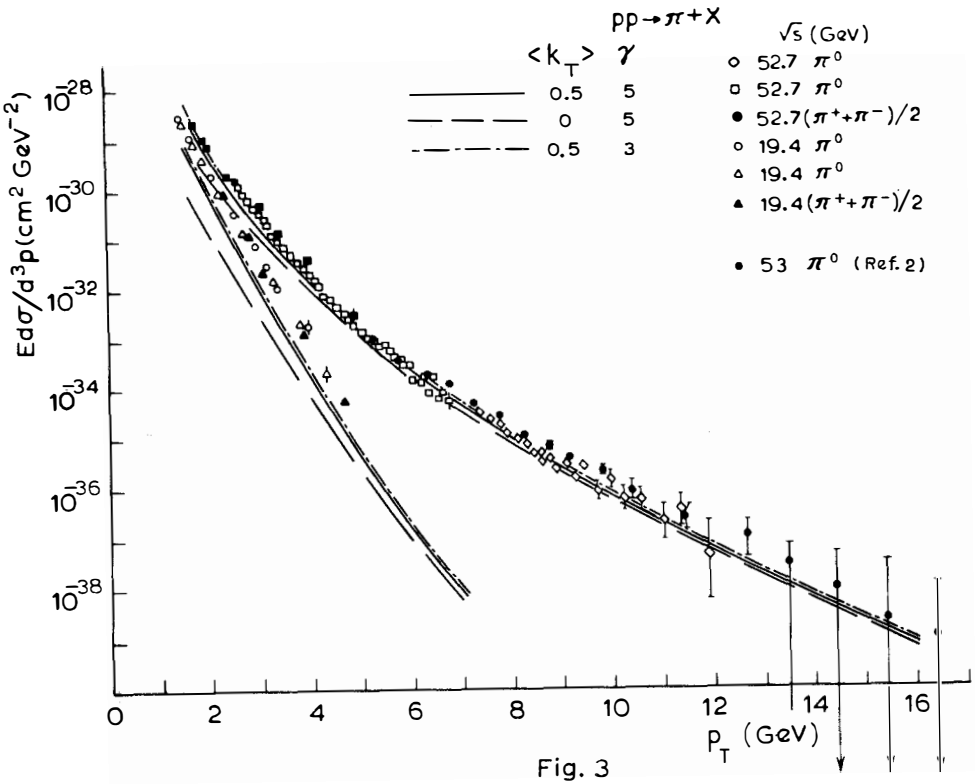
pp→π+X
√s (GeV)
<k_T> γ
0.5 5
0 5
0.5 3
52.7 π⁰
52.7 π⁰
52.7(π⁺+π⁻)/2
19.4 π⁰
19.4 π⁰
19.4(π⁺+π⁻)/2
53 π⁰ (Ref. 2)
Edσ/d³p(cm² GeV⁻²)
10⁻²⁸
10⁻³⁰
10⁻³²
10⁻³⁴
10⁻³⁶
10⁻³⁸
0
2
4
6
8
10
12
14
16
p_T (GeV)

Fig. 3

and opposite-side momentum correlations and the opposite-side rapidity distributions much resemble those of Ref. 6; and the x_e-distributions are reasonable, if the spectator partons are taken into account.[21][6]

In conclusion, it can be said that, within present theoretical and experimental uncertainties, QCD accounts for large p_T meson production reasonably well, certainly at ISR energies. Our overall effort can, probably, be considered as a useful application of very recently advanced ideas based on perturbative QCD.[10][9][22]

REFERENCES AND FOOTNOTES

1. S. Berman, J.Bjorken, and J.Kogut, Phys.Rev.D4, 3388 (1971)(BBK).
2. A.Clark, P.Darriulat et al, CERN preprint, reported to this Conference.
3. H.D.Politzer, Phys.Reports 14, 129(1974); A.de Rujula, H.Georgi and H.D. Politzer, Annals of Phys. (N.Y.) 103, 315 (1977).
4. A.P.Contogouris, R.Gaskell and A.Nicolaidis, Phys.Rev.D17, 839(1978) (McGill preprint February 1977); Progr.Theor.Phys.58, 1238(1977).
5. R.C.Hwa, A.Spiessbach, and M.Teper, Phys.Rev.Lett.36, 1418 (1976); R.Cahalan, K.Geer, J.Kogut and L.Susskind, Phys.Rev.D11, 1199 (1975).
6. A.P.Contogouris, R.Gaskell and A.Nicolaidis, Phys.Rev.D1 (in press) (Orsay preprint LPTPE/77/24, May 1977); A.P.Contogouris, Proc.of VIII Intern. Symposium on Multiparticle Dynamics, Kaysersberg (June 1977), p.B-225.
7. R.D.Field and R.P.Feynman, Phys.Rev.D15, 2590 (1977); R.P.Feynman, R.D.Field and G.C.Fox, Nucl.Phys.B128, 1(1977) and several papers.
8. In Refs.4 and 6 the moments $M_n(Q^2)$ of the structure function $\nu W_2(x,Q^2)$ behave as $M_n \sim (\log Q^2)^{-n}$ QCD predicts $M_n \sim (\log Q^2)^{-\gamma_n}$ with $\gamma_o=0$ but $\gamma_n \sim \log n$ for $n \gg 1$. Thus the scale violation is somewhat stronger than QCD, in particular near x=1. In the first of Ref.5 M_n behave as inverse powers of Q^2.
9. C.T.Sachrajda, CERN preprint TH.2459 (February 1978); Phys.Lett.B73, 185(1978); report to this Conference.
10. H.D. Politzer, Nucl. Phys. B129, 301 (1977).
11. D.Amati, R.Petronzio and G.Veneziano, reported by R.Petronzio.
12. A.J.Buras and K.Gaemers, Nucl.Phys. B132, 249 (1978).
13. B.Combridge, J.Kripfganz and J.Ranft, Phys.Lett.B70, 234 (1977); J. Owens, E.Reya, and M.Gluck, FSU preprint HEP77-09-07 and Erratum; R. Cutler and D.Sivers, Phys.Rev.D17, 196(1978).

14.A.P.Contogouris, R.Gaskell and S.Papadopoulos, Phys.Rev.D1(in press)
15.In the presence of k_T effects, to avoid divergence of $d\sigma/d\hat{t}$, the rule is to replace $\hat{s} \to \hat{s}+M_s^2$, $\hat{t} \to \hat{t}-M_t^2$. (7)(16)(14) We use the standard hadronic mass $M_s^2=M_t^2=1$ GeV^2. (16) We have now tested the sensitivity of our predictions by varying M_s, M_t in the range $0.09 \leq M_s^2=M_t^2 \leq 1$. With $\langle k_T \rangle = .5$ for $p_T \gtrsim 3$ the results are not sensitive; for $p_T=2$ the predicted $Ed\sigma/d^3p$ are enhanced by factors $\lesssim 2$ at ISR and by factors $\lesssim 4.5$ at FNAL energies. Also notice Figs.2,3 correspond to $G_{C/c}$ independent of Q^2. For Q^2-dependent $G_{C/c}$ see Ref. 14.
16.M. Fontannaz and D. Schift, Nucl.Phys. B132, 457 (1978).
17.Very large values of $\langle k_T \rangle$ (and of $\langle k_T' \rangle_{c\to\bar{c}}$) are excluded by data on dN/dp_{out} and $\langle p_{out} \rangle$ (acoplanarity).
18.R.D. Field, preprint CALT-68-633.
19.G.C. Fox, Nucl Phys. B131,107 (1977) and CALT-68-619. This work analyzes in detail various subtle points, but shows nowhere the resulting quark, antiquark and gluon distributions as functions of Q^2.
20.Eq. (9) is now being contested, see C.T. Sachrajda and other reports to this Conference. It is important to distinguish between "soft" and "hard" component of $\langle q_T \rangle_{\mu^+\mu^-}$.
21.J.C. Polkinghorne, Rapporteur report, Budapest Intern. Conference (July 1977); P.V. Landshoff Proc. of Workshop on Large-p_T, Bielefeld (Sept. 1977) p. 280; S.D. Ellis, Review Talk,Annual Meeting of DPF/APS, Argonne (October 1977).
22.S.C. Frautschi, Conclusions of this Conference (to be edited by J. Tran Thanh Van).

A REVIEW OF THE THEORY AND PHENOMENOLOGY OF LEPTON PAIR PRODUCTION

Rudolph C. Hwa*
Rutherford Laboratory,
Chilton, Didcot, Oxon, OX11 0QX, England

ABSTRACT: Recent experimental data and theoretical developments on the production of lepton pairs in hadron collisions are reviewed. With emphasis on the interplay between theory and experiment, the relevance of theoretical calculations to the data available at present energies is critically examined. The Dreĭl-Yan mechanism is found to be phenomenologically dominant provided that the parton distribution functions contain effects of gluon radiation in a narrow cone. Explicit QCD perturbative calculations of the non-Drell-Yan type yield results that are apparently important at large transverse momenta, but are contradicted by subsequent data at 400 GeV and below. A consistent picture in the parton model is sketched. Further experiments to probe the basic mechanism are suggested.

*On leave of absence from the Physics Department, University of Oregon, Eugene, Oregon 97403, U.S.A.

PREAMBLE

The contents of this review are influenced strongly by the experimental papers presented during the lepton-pair session and by the recent theoretical development in the framework of QCD. No effort toward completeness has been attempted. On the whole this review covers the development of the subject since summer 1977. For earlier work and for basic kinematics, reference to, for example, the review articles [1] of Shochet (experimental) and Craigie (theoretical) is suggested. Details of important recent data and theoretical investigations relevant to our arguments in this paper are to be found in the articles by Pilcher, Lederman, and Sachrajda, contained in these proceedings.

I. INTRODUCTION

Lepton pair production in hadronic collisions has recently been the subject of intensive investigation both experimentally and theoretically. While many reasons can be given for the high level of interest in the subject, one single underlying theme seems to be that through the detection of dileptons in hadronic collisions one is given a direct access to a picture of the constituent structure of the hadrons. Deep inelastic leptoproduction has been the standard approach for nearly a decade, but it is limited to the nucleons and is hard to reach high-momentum-transfers. Semi-inclusive leptoproduction can provide some more information about the constituents but at the price of involving the quark fragmentation functions. Similar drawback is present in large-p_T inclusive reactions, while in small-p_T processes there are other complications that are not well understood. In lepton pair production many kinematical variables are readily accessible to experimental control, which can therefore be tuned to map out the parton distribution functions. Theoretically, it is also a fertile ground for testing the predictions of quantum chromodynamics (QCD). Indeed, it is the possibility of a high degree of interplay between theory and experiment that has perhaps stimulated the recent activities in this subject.

An inclusive reaction in hadron-hadron collisions in which only a pair of leptons is detected depends in total seven independent variables. They are (1) the initial c.m. energy squared s; (2) the invariant mass of the lepton pair M; (3) the rapidity y or Feynman variable x_F of the lepton pair; (4) the transverse momentum q_T of the lepton pair; (5) the angle θ of the

leptons in the lepton rest frame in either the Gottfried-Jackson or helicity coordinate system; (6) nature of the beam particle; and (7) nature of the target. A complete description of the inclusive cross section would require the use of a multidimensional space. However, most of the essential features of the lepton-pair production (LPP) process can be conveyed by the description of how $d\sigma/dMdy$ and $\langle q_T \rangle$ separately depend on M, s, and y. This is a 2 x 3 matrix of data presentation which we shall go through systematically in this review. We shall separately discuss the beam and target dependences first. Angular distribution in θ as well as other topics will be considered at the very end.

Contrasting $d\sigma/dMdy$ against $\langle q_T \rangle$, it should be remarked that the former is an inclusive cross section integrated over q_T and therefore represents the bulk of the cross section. On the other hand, $\langle q_T \rangle$, or more explicitly, $d\sigma/dMdyd q_T$, contains information pertaining to the rarer events at large q_T. As is common in hadronic reactions, certain dynamical features that are manifest in rare events are washed out in the integrated results so that the mechanism responsible for the dominant features may be quite different from the physics governing the reactions in some fringe regions of phase space. For that reason we shall separate the discussion of the bulk cross sections from that of the q_T dependence. As it turns out, the former is far less controversial; consequently, we shall be brief. It is the latter that will occupy most of our attention.

Theoretical understanding of the LPP process is not on firm ground because many of the well-tested techniques useful in deep inelastic scattering, such as short-distance expansion and light-cone dominance, [2] are not applicable to LPP. The quark-antiquark annihilation mechanism of Drell and Yan [3] has been amazingly successful even though the reason for its success has been unclear, at least not until very recently. The Drell-Yan mechanism is constructed in the framework of the naive quark-parton model, [4] which in its own right is in need of modification to account for such effects as scaling violation. Some progress has been made in the past few months to elucidate the dominance of the Drell-Yan mechanism in the context of QCD, which is the only candidate theory of strong interaction at the constituent level. While many QCD diagrams are found in perturbative calculations to fall into the general category of Drell-Yan type annihilation process, there are kinematical regions in which they remain distinctly as non-Drell-Yan type diagrams. Since QCD itself, having no intrinsic scale, cannot specify those regions a priori,

only phenomenology can determine where certain QCD diagrams are important. It is one of the aims of this review to make that phenomenological analysis and assess to what extent QCD has been tested in LPP.

There are, of course, a number of other models which claim to fit the LPP data. One of them is based on the constituent interchange model [5] (CIM), whose results agree remarkably well with all the data considered, when parameters determined in large-p_T reactions are used. Whether the agreement is maintained in view of the recent changes of the data both in LPP [6] and in large-p_T processes [7] remains to be seen. Although the success of CIM in LPP processes should not be overlooked, it will not be pursued further in this review. Interested readers are referred to Ref. 5). Another model discussed at this meeting [8] is thermodynamic in character and emphasizes the relationship between the production of hadrons and dileptons. Because it de-emphasizes the role played by the virtual photon, one expects it to have difficulty explaining the charge-dependent data, such as the π^+ to π^- beam ratio at high mass LPP. Again, we shall not return to this model in the remainder of this review.

Except for the next section where we shall discuss the theoretical basis for the Drell-Yan mechanism, attempts will be made in all subsequent sections to maximize the interplay between theory and experiment. Not all data will be discussed, obviously. We shall selectively present only the data that are relevant to some theoretical issues. On the whole we shall follow an outline which goes through the 2 x 3 matrix of data presentation mentioned earlier.

II. THE DRELL-YAN MECHANISM

How much can we believe in the Drell-Yan mechanism [3] as the dominant process in LPP? If this is a theoretical question, it can be answered only within the framework of some theory, and QCD is the only one available, which is what will be discussed below. If it is a phenomenological question, then the answer resides in checking whether the parton momentum distributions in LPP assuming the Drell-Yan mechanism are consistent with those in DIS (deep inelastic scattering). This aspect of the quark parton model will be considered in Section VII, after the theoretical and other phenomenological questions about LPP are settled.

Present technology in QCD is inadequate to answer fully the question of Drell-Yan dominance. One outstanding difficulty is the question of interaction among the spectator partons of the two hadrons. There must be such interactions at some level if the final state hadrons are all colour singlets. The initial and final state interactions can ruin Drell-Yan's factorizable form for direct quark-antiquark annihilation. The problem is difficult to handle in QCD because the hadronic wave functions are involved which cannot be treated precisely so far. In Regge theory some statement can be made: [9] all the Pomeron exchange terms cancel. Its relevance to the parton picture is, however, not at all clear. In the literature on partons and QCD all complications related to the spectator interactions have been ignored, as they were in the original work of Drell and Yan. [3]

What one can do in QCD is to calculate perturbatively the gluon corrections to the Drell-Yan process. Some of the low-order diagrams are shown in Fig. 2.1.

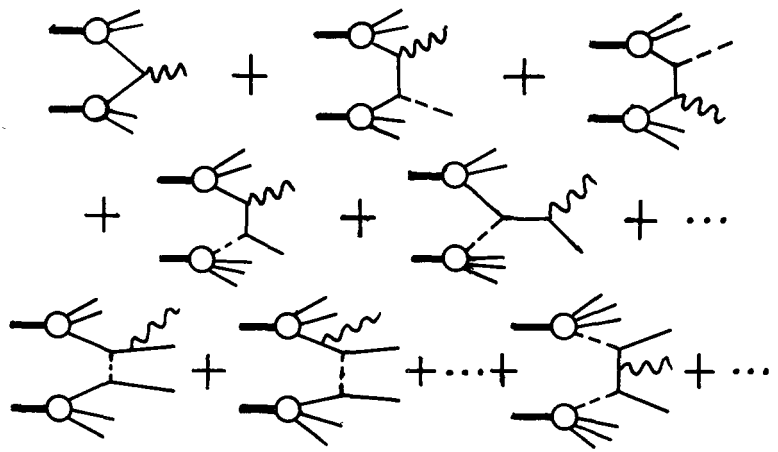

FIG. 2.1

In these diagrams the heavy, light, dashed, and wavy lines represent hadrons, quarks (q) [or antiquarks ($\bar{q}$)], gluons (g), and virtual photons, respectively. The bubbles represent the intrinsic parton distributions in the hadrons, containing all the low Q^2 confinement effects (such as the Fermi motion of the partons) that are not calculable in perturbation theory in QCD. It was shown by Politzer [10] (for the initial partons being $q\bar{q}$) and by Sachrajda [11] (for the partons being qg, qq, and gg) in the leading log Q^2 calculations

that two important phenomena occur at high Q^2. One is that the contribution of all the diagrams in Fig. 2.1 to LPP can be put in a factorizable form so that the Q^2 dependence can be absorbed into the hadronic structure function as shown in Fig. 2.2. Thus in the leading log approximation the Drell-Yan

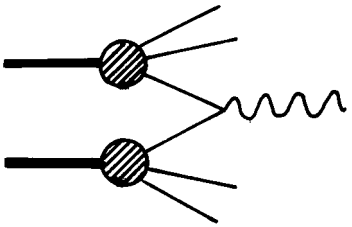

FIG. 2.2

form is recovered.[12] Moreover, the log Q^2 dependence of the structure functions in Fig. 2.2 (indicated by the cross-hatched bubbles) is exactly the same as that for electroproduction (in leading log) with $Q^2 = |q^2|$ in both cases. These features of QCD contribute partially to an explanation of why the Drell-Yan mechanism seems to work better than one would naively expect, as we shall see in the following sections.

The calculations referred to above are done by studying low order diagrams in perturbation theory. One could with good reasons ask about the importance of the higher-order gluon-correction terms. Such contributions are hard to calculate even in leading log approximation, since it involves power series in $\bar{g}^2(Q^2)$ log Q^2 where $\bar{g}^2(Q^2)$ is the square of the running coupling constant [13][14] that varies inversely as log Q^2; thus each order in perturbation theory gives a comparable contribution to the correction terms. Amati, Petronzio and Veneziano [15] have developed a method for studying the problem, which promises to be able to generalize the Politzer-Sachrajda result to higher orders.

There is then also the question of non-leading log terms. It should be recognized that a power of log Q^2 is developed each time an internal line of a tree diagram (with vertex and propagator insertions) is nearly on mass shell. [16] It means that for hard gluon radiation the quark and emitted gluon must be nearly collinear. Thus in the leading log approximation all quarks and hard gluons must be restricted to a forward cone with a small half-angle δ.* In other words, the transverse momenta k_T of the partons are

*We shall refer to this in the following as the "narrow" gluon correction.

limited:

$$k_T^2 < \varepsilon Q^2 \qquad (2.1)$$

where ε is a fixed small number. This inequality arises becasue in an integration of dk_T^2/k_T^2 from p^2 to Q^2 it is the lower portion from p^2 to εQ^2 that gives rise to log Q^2/p^2. Indeed, for a related reason, the jet structure in e^+e^- annihilation is also described in terms of cones. [17] Now, if a parton (quark or gluon) in a certain QCD diagram is forced to have a large k_T, such as in a process in which a large q_T dilepton is detected, then one of the internal lines must be far off shell, and one loses a power of log Q^2. Such terms are not included in the leading log computation, and one must calculate separately and explicitly hard-scattering diagrams. There can, of course, still be further gluon corrections to the basic hard-scattering subprocess. Again, in leading log approximation (i.e. collinear gluon emission) of low-order diagrams Sachrajda shows in a separate paper [18] that the effects of narrow gluon corrections to a hard-scattering process are also factorizable and can be absorbed into the distribution (or fragmentation) functions for the initial (or final) partons undergoing the hard collision. The implication for LPP is then that when a detected lepton-pair has a large q_T^2, say, of order Q^2, one should calculate explicitly the Born diagrams, i.e. second to fifth, in Fig. 2.1 with the bubbles cross-hatched as in Fig. 2.2 so that the Q^2 and small k_T dependences due to the narrow gluon corrections can be taken into account. The last three diagrams of Fig. 2.1 are thereby automatically taken into account if the gluons are near mass shell.

In the investigation of the factorization question in perturbation theory [10)11)15)18] it is the integrated cross section (integrated over k_T of all narrow gluon corrections) that is studied. The resulting Q^2 dependence of the structure function is then found to be the same (in leading log) as for νW_2. It has not been possible to determine what the k_T dependence is of the distribution function $G(x, k_T, Q^2)$ before the integration over k_T. That dependence is, of course, of crucial importance to the calculation of $\langle q_T \rangle$ especially for the direct $q\bar{q}$ annihilation process of Drell-Yan. In the absence of any definitive prediction in QCD and in anticipation of the phenomenology to follow, let me identify two components of parton k_T in $G(x, k_T, Q^2)$, the meaningfulness of which is only a conjecture at this point. One is the intrinsic component $\langle k_T \rangle_o$ usually taken to the roughly 300 MeV/c. It is due to the Fermi motion or binding effects in the hadron, probably independent of Q^2 but may depend on x. [19)20] The other component,

$\langle k_T \rangle_{narrow}$, is due to hard gluon bremsstrahlung in a narrow cone; it can be Q^2 dependent but at most to the extent of (2.1). How small ε is or how narrow the cone is cannot be answered within QCD. An estimate of 10^o to 15^o by Sterman and Weinberg [17] for jets in e^+e^- annihilation is not unreasonable here. The two components collectively form the hadronic $\langle k_T \rangle_{had}$ which is an estimate of the total transverse spread of the momenta of the partons in a hadron with gluon interactions as probed by deep inelastic scattering. The corresponding distribution function $G(x, k_T, Q^2)$ is to be used in any parton-model calculation that needs a description of the supply of partons in a hadron.

For LPP with "small" values of q_T, i.e. not much greater than $\langle k_T \rangle_{had}$, Drell-Yan picture applies, provided that the above $G(x, k_T, Q^2)$ is used. For significantly "larger" q_T the Drell-Yan mechanism cannot be trusted, so explicit non-Drell-Yan type diagrams must be calculated. Indeed, to test some clean predictions of QCD it is necessary to go outside the hadronic ("small") region. Since QCD in itself does not provide the range of $\langle k_T^2 \rangle_{had}$, only phenomenology can determine where "small" q_T ends and where "large" q_T begins. A significant portion of our discussion later on will be addressed to this problem.

For now we need some theoretical framework in which to begin discussing the data. Since the q_T distribution of the dilepton cross section falls off rapidly with increasing q_T, the bulk of the cross section at present energies is in the region where the hadronic k_T is mainly responsible for the q_T. (Some aspect of the phenomenological conclusion to be reached later on has been used in making the last statement.) Thus we shall adopt as our working hypothesis that for the integrated (over q_T) cross section, $d\sigma/dMdy$, the Drell-Yan mechanism dominates. For $\langle q_T \rangle$, on the other hand, or more particularly for $d\sigma/dMdydq_T^2$, we leave it as an open question to be examined in detail.

For later use let us collect here some equations expressing the Drell-Yan process in various ways. We include the color factor 1/3, and use $G_h^{f,\bar{f}}(p,k,q)$ to denote the distribution function for a quark (or antiquark) of flavor f (or $\bar{f}$) in a hadron h. It depends on the invariants built out of the momenta of the hadron p, parton k, and photon q. [21] The inclusive cross section in the Drell-Yan approximation is

$$\frac{q_o}{d^3q}\frac{d\sigma}{dM^2} = \frac{2\pi\alpha^2}{9M^2}\sum_f e_f^2 \int\left[G^f_{h_1}(p_1,k_1,q)G^{\bar{f}}_{h_2}(p_2,k_2,q) + (f\leftrightarrow\bar{f})\right]$$

$$\cdot\ \delta^4(k_1 + k_2 - q)\ \frac{d^3k_1}{k_1^0}\ \frac{d^3k_2}{k_2^0} \tag{2.2}$$

where e_f is the charge of the quark of flavor f in unit of e. If k_T is ignored and $\vec{q}$ integrated, then (2.2) yields

$$\frac{d\sigma}{dM^2} = \frac{4\pi\alpha^2}{9M^4}\int_0^1 dx_1 \int_0^1 dx_2\ \delta(x_1x_2 - \tau)\ \sum_f e_f^2\left[F^f_{h_1}(x_1,M^2)F^{\bar{f}}_{h_2}(x_2,M^2)+(f\leftrightarrow\bar{f})\right] \tag{2.3}$$

where

$$\tau = M^2/s \tag{2.4}$$

$$x_i = q^2/2p_i\cdot q \tag{2.5}$$

$$F^{f,\bar{f}}_h(x,M^2) = \int G^{f,\bar{f}}_h(q^2=M^2)\,d^2k_T \tag{2.6}$$

Finally, if the lepton pair is detected at y = 0, we have

$$\left.\frac{d\sigma}{dMdy}\right|_{y=0} = \frac{4\pi\alpha^2}{9M^3}\sum_f e_f^2\left[F^f_{h_1}(x,M^2)F^{\bar{f}}_{h_2}(x,M^2) + (f\leftrightarrow\bar{f})\right] \tag{2.7}$$

where $x = \sqrt{\tau}$.

III. TARGET AND BEAM DEPENDENCES

Most experiments on LPP are done using nuclear targets. The dependence of the cross section on the atomic number of the target may be parametrized as

$$\frac{d\sigma}{dM} \propto A^{\alpha(M)} \tag{3.1}$$

The variation of $\alpha(M)$ with M is shown in Fig. 3.1 with data from various experiments [22)-27)] using both proton and pion beams. It is evident that for $M \gtrsim 3$ GeV the dependence on A is nearly linear, signifying incoherence of scatterings from individual nucleons. Under such circumstances one can admit the possibility of the Drell-Yan mechanism to work since impulse

approximation cannot be ruled out. But for $M \lesssim 3$ GeV, α deviates significantly from one, so the nuclear coherence and rescattering effects are not negligible. The impulse approximation needed for the parton model is then not justified. Thus the Drell-Yan mechanism should not be applied to LPP with $M \lesssim 3$ GeV; failure of the Drell-Yan formula to account for $d\sigma/dM$ in that region is therefore not unexpected. [28),29)] In the following we shall not attempt to interpret the data for $M \lesssim 3$ GeV when nuclear targets are used. We await with great interest the results from ISR [30)] in that mass region, especially when the statistics can be improved.

The dependence on the beam type is as dramatic as it is effective in illustrating the utility of the simple quark-parton model and the general validity of the Drell-Yan mechanism. Consider the cross sections for antiproton vs. proton beams. An antiproton has much more antiquarks at large x than does a proton, so the $\bar{q}q$ annihilation process at large τ (thus involving large x partons) is much more enhanced for the $\bar{p}$ as compared to the p beams. One therefore expects $\sigma(\bar{p})/\sigma(p)$ to increase significantly with τ. The beam dump experiment at CERN SPS with Ω spectrometer verifies this increase despite their poor statistics. [31)] Similar situation is true for $\sigma(\pi)$ when compared to $\sigma(p)$, as shown in Fig. 3.2; [31)32)] a ratio of 330 was reported by Pilcher [26)] for $M = 10.5$ GeV at $p_{beam} = 225$ GeV/c.

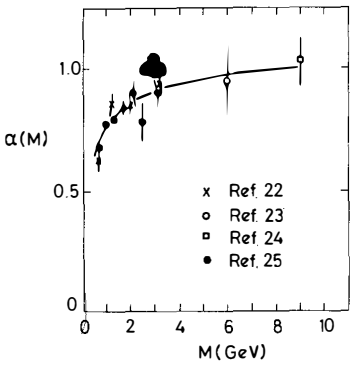

FIG. 3.1

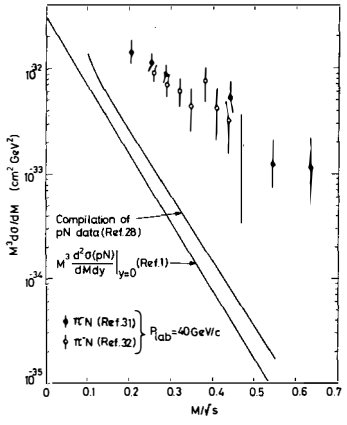

FIG. 3.2

Another aspect of the quark-parton model (QPM) concerning the charges of the constituents is also tested in LPP if one examines the $\sigma(\pi^+)/\sigma(\pi^-)$ ratio for isoscalar targets. The valence quarks of π^+ are $u\bar{d}$, while those of π^- are $d\bar{u}$. The annihilation of the antiquarks with the corresponding quarks in a nucleon at large x should lead to a ratio of the squares of the charges e_d^2/e_u^2. Thus one expects $\sigma(\pi^+)/\sigma(\pi^-)$ to approach 1/4 as $\tau \to 1$. This is verified by the recent data [25),26),31)] as shown in Fig. 3.3.

One must conclude here that the Drell-Yan mechanism is operative for the major part of the integrated cross sections.

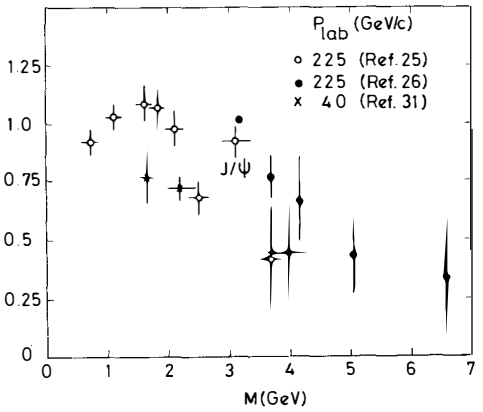

FIG. 3.3

IV. THE INCLUSIVE CROSS SECTION $d\sigma/dMdy$

We now consider the bulk of the cross section $d\sigma/dMdy$ (integrated over q_T) and discuss its dependences on M, s and y in that order. As we have argued in Section II, for the integrated cross section we shall think in the framework of the Drell-Yan process whenever necessary. We shall see that the data offer no critical test of the model and can be readily accommodated by it.

At fixed y, particularly at y = 0, the dependence of the cross section on M has been well measured up to M ≃ 14 GeV both for proton [6),27)] and pion beams. [26)] Because of the unknowns contained in (2.7), the data by themselves cannot provide a precise check on the validity of the Drell-Yan

process. In fact, the CFS data [6] have been used in conjunction with νW_2 to determine the antiquark distribution; depending on what is used, a number of fits are possible. [6),33),34] Based on the q and $\bar{q}$ distributions of the proton so determined, one could then use the CP data [26] to map out the parton distributions of the pion, a result that will surely be forthcoming before long.

The dependence on the beam energy has also been studied by both the CP and CFS groups. [24),27] Fig. 4.1 shows the result for proton beam at y = 0. [27] To exhibit scaling the data at y = 0.2 have been plotted in terms of the dimensionless quantity $M^2 d\sigma/d\sqrt{\tau}dy$ versus $\sqrt{\tau}$, as in Fig. 4.2. One sees that the data satisfy scaling amazingly well - in fact, almost too well for comfort. According to (2.7) and disregarding the small value of y, the quantity plotted should be a function only of $\sqrt{\tau}$, or x, except for the scaling violating M^2 dependences (hence s dependences for fixed τ) of the parton distribution functions, which are not negligible for the range of s explored. However,

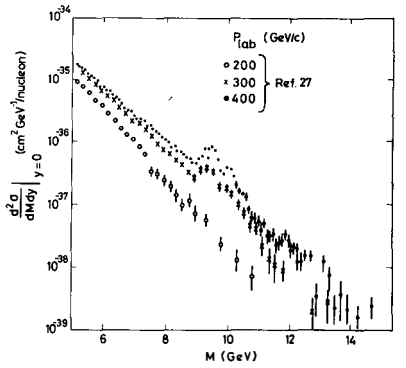

FIG. 4.1

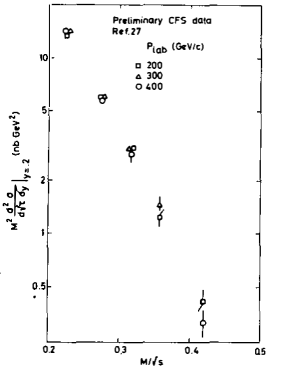

FIG. 4.2

we know from νW_2 probed in deep inelastic leptoproduction [35] that the scaling violation of the structure function has a pivotal point at $x \approx 0.2$ and that for $x > 0.2$ it decreases with increasing Q^2. Qualitatively, this feature is preserved in the data shown in Fig. 4.2 if one identifies $x = \sqrt{\tau}$, although an exact parallel is not expected since the quark and antiquark distributions (having different behaviours of scaling violation at large x) appear multiplicatively in LPP but additively in DIS (deep inelastic scattering).

There are also some data from ISR [36] at $\sqrt{s}$ from 28 to 62 GeV. Although the error bars are large, their values for $M^3 d\sigma/dMdy$ at y = 0 for $\sqrt{\tau}$

from 0.08 to 0.25 are in general agreement with the CFS data. Thus on the whole one can say that scaling seems to work rather well in LPP.

The y or x_F dependence of the cross section for various bins of M values greater than 3 GeV is now also known from the CP and CFS experiments. [26),27)] Because of the extra $\bar{q}$ content in the pion, the x_F dependences are expected to be quite different for the π and p induced cross sections. The new CP data ought to be able to put enough constraints on the Drell-Yan formula (2.2) to determine the parton distribution functions for the pion.

In using the large x_F data one must be careful about kinematical limitations since the annihilating quarks and antiquarks may not originate from separate hadrons as in the usual Drell-Yan picture, but from the same hadron. [37)] In that case the $q\bar{q}$ annihilation process is then closely related to the $q\bar{q}$ recombination process [38)] responsible for the production of mesons at large x_F. [39)-42)] The ratio of lepton-pair to π^o or ρ^o production at large x_F with nucleon target should then provide a direct clue to the recombination function.

The CFS data also show the y distribution for both positive and negative values of y. The asymmetry shown in Fig. 4.3 for $\sqrt{\tau}$ between 0.2 and 0.25 is at first sight larger than is anticipated from the use of nuclear targets.

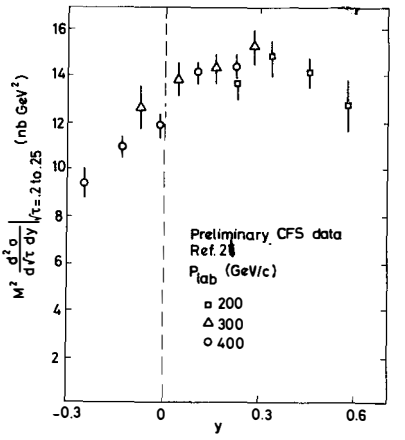

FIG. 4.3

However, a quick estimate can be made if, for extreme simplicity, we assume that all quark distributions are alike in protons as well as in neutrons, and similarly for all antiquark distributions. Since no asymmetry can arise when the beam proton strikes a proton in the target, we need only consider the pn collision. Counting the squares of the charges only, on the proton side uud leads to (4+4+1)/9, while on the neutron side udd leads to (4+1+1)/9. Assuming equal proportions of p and n in the target nucleus, we see that the excess on the beam side is 3 out of 18, which is not negligible. This estimate is extremely crude but is sufficient to infer that the observed asymmetry presents no puzzle. A quantitative calculation in the Drell-Yan picture is straightforward.

V. TRANSVERSE MOMENTUM OF THE LEPTON PAIR

There are two aspects about the average transverse momentum $\langle q_T \rangle$ of the dileptons that are noteworthy. The CFS data [6] at 400 GeV shown in Fig. 5.1 serve to illustrate the situation. First, the value of $\langle q_T \rangle$ is about 1.2 GeV/c for $M \gtrsim 4$ GeV, a value much higher than is naively expected. Secondly, over the same range in M it is remarkably flat except for the T point, a phenomenon that needs explanation. The data have stimulated a great deal of theoretical activities because model calculations can be made on the subject with predictions that can be compared with data. There have also been hopes that QCD can be tested. Since there are a number of methods of treating the

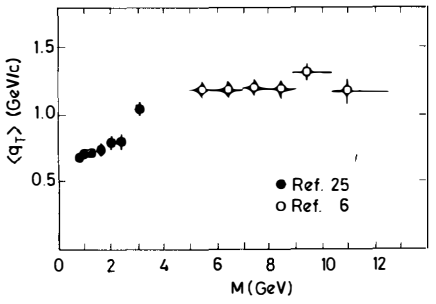

FIG. 5.1

problem even within the context of QCD, I shall organize the discussion by first identifying two distinct approaches, commenting on the difficulties in

each, and then making a conclusion based on phenomenological fact. In order to be relevant to the data available now or forthcoming, it is important to bear in mind what is calculable and what is not, and to distinguish the two at present energies.

A. BACKDOOR APPROACH

This is the approach along the avenue of space-like q^2. Calculate the average parton transverse momentum $\langle k_T \rangle$ and then infer the dilepton's $\langle q_T \rangle$. Ref. 43)-46) are examples of considerations along this line. Schematically, the steps followed are:

$$\text{QCD} \xrightarrow{\text{(a)}} \text{DIS} \xrightarrow{\text{(b)}} \text{R} \xrightarrow{\text{(c)}} \langle k_T^2 \rangle \xrightarrow{\text{(d)}} \langle q_T^2 \rangle$$

It is in the last step that the Drell-Yan mechanism is assumed and the backdoor crossed. In Ref. 46) steps (b) and (c) are short-circuited. We remark now on each of the steps.

(a) QCD $\longrightarrow$ DIS

QCD, being an asymptotically free gauge theory, [13),14)] has been successfully applied to DIS where operator product expansion and light-cone ideas are useful. [2)] Scaling violations of the moments of the structure fucntion can be calculated using renormalization group method and they are not inconsistent with the present data, [47)] although one cannot claim on that basis that QCD has been successfully tested.

(b) DIS $\longrightarrow$ R

Here R is

$$R = \frac{\sigma_L}{\sigma_T} = (1 + \frac{\nu^2}{Q^2})\frac{W_2}{W_1} - 1 \equiv \frac{F_L}{F_T} \tag{5.1}$$

This ratio is zero in the lowest order and requires a calculation of the one-loop corrections to the Wilson coefficients. [48)-50)] Because the latter are related to the moments of the structure functions, an inversion to F_L and F_T themselves results in an integral relation, [51)] which in the lowest order for F_T is

$$F_L(\omega,Q^2) = 4C_2(R)\frac{g^2}{16\pi^2}\frac{1}{\omega^2}\int_1^\omega d\omega'\ \omega'\ F_T(\omega',Q^2) \tag{5.2}$$

where $\omega = 1/x$, and $C_2(R)$ is the quadratic Casimir operator evaluated in the representation R for the quarks. Eq. (5.2) is given here mainly to show that the relationship between F_L and F_T is not simple. In the limit $\omega \to 1$, the integral is approximated by a linear dependence on $\omega - 1$, and one obtains

$$R \sim C \frac{1 - x}{\log Q^2/\Lambda^2} \quad , \quad x \to 1 \tag{5.3}$$

where the log factor appears because of the running coupling constant g^{-2}. Among other things the constant C depends on the rate at which F_T vanishes as $\omega' \to 1$. For lack of a more reliable but simple formula, (5.3) has been used as a QCD description of R for the entire range of x from 0 to 1. The value of C is therefore devoid of precise meaning. Depending upon the user of (5.3) or other considerations, various values have been assigned to it: C = 16/25 in Ref. 43), 1/2 in Ref. 45) and later 1/"4" in Ref. 52). The prediction of QCD as expressed in (5.3) is thus unreliable in both normalization and x dependence.

More careful numerical calculations of R have been carried out [50),53)] in the framework of QCD and renormalization group techniques. The results are consistently and significantly lower than the old data [54),55)] particularly at high x. The new data [56)] give an even higher value of R (0.25 ± 0.10 when averaged with the R value using the old data), so that the discrepancy is even worse. To account for the difference Nachtmann[47)] found that a fit of the old data would require the addition of a component attributable to the intrinsic transverse momenta of the partons, which he took to be

$$\langle k_T^2 \rangle_o = 0.5x \ (\text{GeV/c})^2 \tag{5.4}$$

Note the x dependence. The new data on R would require an even larger $\langle k_T^2 \rangle_o$ which should not vanish at x=0. *)

(c) $R \longrightarrow \langle k_T^2 \rangle$

The discussion immediately above refers to a relationship between R and the parton $\langle k_T^2 \rangle$, which in the naive quark-parton model (QPM) is [4)]

$$R = \frac{4\langle k_T^2 \rangle}{Q^2} \tag{5.5}$$

*) According to Quirk (private communication) the CHIO group has measured in deep inelastic muoproduction a value of $R = 0.5 \pm 0.2$ at x=0.025 for Q^2 in the range 1-4 $(\text{GeV/c})^2$.

where the quark confinement effects are included in $\langle k_T^2 \rangle$. Combining with (5.3) one has [52]

$$\langle k_T^2 \rangle = \frac{C}{4} \frac{(1-x)}{\log Q^2/\Lambda^2} Q^2 + \langle k_T^2 \rangle_0 \tag{5.6}$$

The validity of this expression depends not only on how good (5.3) is as an approximation for R, but also on (5.5) which is good only if $\langle k_T^2 \rangle$ is very small, as is usually assumed in QPM. Indeed, on the basis of (5.5) one ordinarily expects R to vanish at high Q^2. However, if R shows no decisive dependence on Q^2, as is apparent in the data, [56] or depends on Q^2 only very mildly as in (5.3), then $\langle k_T^2 \rangle$ must increase with Q^2, contrary to the assumption in QPM. The validity of (5.5) is then called into question. Indeed, the description of the QPM itself would need serious modification. In QCD the relationship between R and $\langle k_T^2 \rangle$ is not well understood.

(d) $\langle k_T^2 \rangle \longrightarrow \langle q_T^2 \rangle$

In this last step Drell-Yan mechanism is the key link between the parton k_T and the dilepton's q_T. According to the results of Politzer [10] and Sachrajda [11] discussed in Section II, the Drell-Yan formula is made more acceptable if the parton distributions contain the Q^2 dependences due to gluon corrections, same as in DIS. How much k_T is allowed in the same parton distributions as a result is not clear, except that in the leading log calculations only "small" k_T in the narrow cone satisfying (2.1) is included. To apply the parton $\langle k_T^2 \rangle$, as calculated in step (c) above, to the Drell-Yan formalism and then to infer the dilepton's $\langle q_T^2 \rangle$ is a procedure based on the assumption that the calculated $\langle k_T^2 \rangle$ is indeed "small". Diagrams in which some parton propagators are far off shell do not contribute to the leading log terms; their effects on LPP are not factorizable and thus not re-expressible in the Drell-Yan form. If one examines the calculations leading to (5.2) and therefore to the determination of R, [16), 48)-51)] one finds that it is precisely the non-leading log terms that are responsible for the answer, i.e. the parton k_T is not restricted to the narrow cone. Hence, it is in principle inconsistent to apply the Drell-Yan picture to the component $\langle k_T^2 \rangle_R$ [the first term on the r.h.s. of (5.6)] obtained from R. However, in practice, it may be loosely regarded as an approximate way of estimating $\langle q_T^2 \rangle$ from renormalization-group-improved perturbative calculation of R.

Overlooking the above reservation we proceed to a discussion of what has been obtained for $\langle q_T^2 \rangle$. The Drell-Yan formula, given in (2.2), involves in general, a rather complicated convolution of the transverse momenta of the annihilating partons over the surface of an ellipsoid. If k_T is infinitesimal (which is not the case at hand), the convolution integral can be simplified and the following approximate relation obtains

$$\langle q_T^2 \rangle = \langle k_{1T}^2 \rangle + \langle k_{2T}^2 \rangle \tag{5.7}$$

where the two terms on the r.h.s. refer to the $\langle k_T^2 \rangle$ for the two hadrons at the appropriate x values. For the lepton pair at $x_F=0$, and for identical hadrons, it reduces to

$$\langle q_T^2 \rangle = 2\langle k_T^2 \rangle \tag{5.8}$$

We stress that this formula is valid only for infinitesimal $\langle k_T \rangle$, and that significant departure from it actually prevails [33] for the kinematical range of available data.

Comparisons with data have been made on the basis of (5.6) and (5.8). In Fig. 5.2 are shown two theoretical curves assuming $\langle q_T \rangle = \langle q_T^2 \rangle^{\frac{1}{2}}$: the dashed line [43] is for C = 16/25 and $\langle k_{T_2}^2 \rangle_o = 0$, while the solid line [52] is for C = 1/4 and $\langle k_T^2 \rangle_0 = (0.3)^2$ (GeV/c)^2. The agreement is not outstanding.

FIG. 5.2

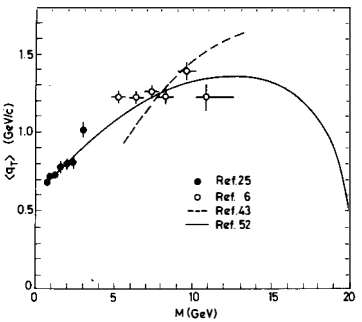

As we have seen above, the predictive power of QCD in this approach is weakened by various uncertainties, not the least of which are: (i) the value of C, (ii) the x dependence of R, (iii) the size of $\langle k_T^2 \rangle_o$, (iv) the x dependence of $\langle k_T^2 \rangle_o$, (v) the validity of (5.5), and (vi) the departure from (5.8). If we take seriously Nachtmann's attempt [47] to make up for the difference between the calculated R in Ref. 50) and the data, but do it for the new value, [56] then we would conclude that the part calculable in QCD is

overwhelmed by the part due to the hadronic component $\langle k_T^2 \rangle_{had}$ that is not calculable. In that case one might as well fit the data out right. This is not to say that QCD is at fault. It merely means that at present energies the kinematical variables do not extend to the region where the part calculable dominates over that which is not.

Lam and Yan [46] circumvent the issue of R by generalizing the evolution equation of Altarelli and Parisi [57] and studying the generation of the parton k_T in the same way that scaling violation is generated by the renormalization group method. This ought to be the proper way of investigating the problem in QCD if the Drell-Yan mechanism is assumed. There are questions of uniqueness of the generalized master equation (particularly about the kernel) that requires further investigation. Assuming a simple form for the kernel and using an intrinsic $\langle k_T \rangle_o$ of 300 MeV/c, [58] a reasonable fit of the data can be obtained upon applying (5.8) to infer $\langle q_T \rangle$.

It should be mentioned that Soper [59] also followed the backdoor approach but in a very different way. Working in a renormalizable field theory that is not exactly asymptotically free, he studied the large k_T behaviour of the parton distribution function using light-cone techniques in operator-product analysis. Terms falling off as k_T^{-2} and k_T^{-4} are found, whereupon q_T^{-2} and q_T^{-4} behaviour are inferred for the lepton pair. Whether these behaviours attributed to the Drell-Yan mechanism are distinct from the non-Drell-Yan processes at large q_T is not clear.

B. FRONTDOOR APPROACH

Having reviewed the backdoor approach, it should come as no surprise that one could also approach the subject of $\langle q_T \rangle$ directly, keeping q^2 time-like throughout. By studying some low-order perturbation diagrams, one can, in fact, calculate $d\sigma/dMdyd\vec{q}_T^2$. Comparison with the data on q_T distributions would be a far more stringent test of QCD than that with $\langle q_T \rangle$. Besides, the Born term calculations are clean and not too difficult to do. Although one should bear in mind that cleanliness is no guarantee for relevance, they certainly should be done. The idea did not occur to just one or two, but has led to a multitude of papers, Ref. 60) to 64) being only a few examples of the collection.

The diagrams to be considered are those shown in Fig. 2.1, although in actuality only the calculations to the lowest nontrivial order in $\bar{g}$ have

been done, i.e. the second to fifth diagrams of Fig. 2.1. We recall that all the diagrams in that figure can be put in the Drell-Yan form, Fig. 2.2, in the leading log Q^2 approximation, [10),11)] which means "small" k_T and q_T. To put Q^2 dependent distribution functions in the diagrams of Fig. 2.1 would be double counting for small q_T. However, if one is only interested in large q_T, then the distribution functions should include Q^2 and "small" k_T dependences. Calculating in that way for large q_T it is hoped that the second to fifth diagrams of Fig. 2.1 give clean predictions of QCD that can be compared with experiment.

Clearly, the two approaches are distinctively different. The backdoor approach depends on the Drell-Yan mechanism, while the frontdoor approach is mainly interested in the non-Drell-Yan processes. The two are actually complementary. On the other hand, if $\langle k_T^2 \rangle_R$ is recognized as basically non-Drell-Yan in origin as we have discussed, then that part of the contribution in the backdoor approach is not unrelated to the calculation in the present approach.

We now examine more closely the issues involved in the perturbative calculations of the non-Drell-Yan processes. What has thus far been done is to assume no k_T for the initial partons of the subprocesses ($q\bar{q}$ annihilation and qg "Compton scattering"), and then to convolute the computed cross sections of the subprocesses with the appropriate parton distribution functions, whose x dependences are partly inferred from DIS and partly guessed. All calculations suffer from the trouble at small q_T where, owing to the masslessness of the quarks and gluons, the cross section $d\sigma/dMdydq_T^2$ diverges as $1/q_T^2$, as $q_T \to 0$. It is a reflection of the fact that a massless quark can emit or absorb a massless gluon collinearly without violating energy-momentum conservation. Since in reality the cross section does not diverge, and for reasons already stated regarding Drell-Yan, the result is not to be trusted at small q_T. However, it has been hoped [60)-64)] that the calculation gives a fair description of LPP at large q_T, in both normalization and shape. Fig. 5.3 shows the comparison of the theoretical predictions with data [6)] at $y = 0$; it is taken from Ref. 63), and is typical of results obtained also by others. [60)-62),64)] The agreement is regarded as a significant and favourable test of QCD. However, this may be an over-optimistic view, as I shall present arguments later to the contrary.

Because of the divergence at $q_T = 0$, computation of $\langle q_T \rangle$ is meaningless. To emphasize the high q_T portion of the distribution one should consider at least the second moment $\langle q_T^2 \rangle$, for which the role of the divergence is

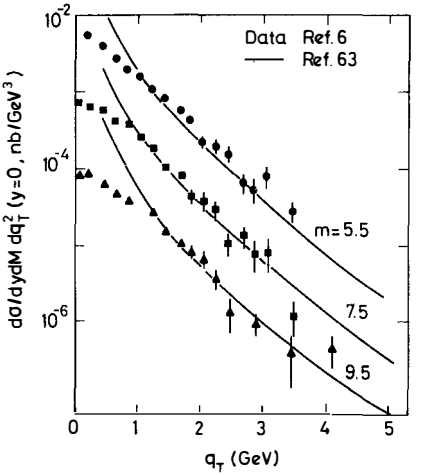

FIG. 5.3

suppressed. The computed result which we denote by $\langle q_T^2 \rangle_{pert}$ turns out to be too small compared to data.[62),63)] To fit the data a hadronic $\langle k_T^2 \rangle_{had}$, discussed in Section II, must be added, i.e.

$$\langle q_T^2 \rangle = 2\langle k_T^2 \rangle_{had} + \langle q_T^2 \rangle_{pert} \tag{5.9}$$

where (5.8) and the idea of Drell-Yan has been used. If $\langle k_T^2 \rangle_{had}$ is allowed to have a dependence on x or Q^2, which is unknown, then perturbative calculation in QCD has no predictive power on $\langle q_T^2 \rangle$. Assuming a constant $\langle k_T^2 \rangle_{had}$ the data in Fig. 5.1 can be fitted using [63)]

$$\langle k_T^2 \rangle_{had} = 0.4\ (\text{GeV/c})^2 \tag{5.10}$$

This is significantly larger than $\langle k_T^2 \rangle_o = (0.3)^2\ (\text{GeV/c})^2$ used by Politzer [52)] in connection with Fig. 5.2 or by Lam and Yan.[58)] It is consistent with the conclusion reached toward the end of the previous subsection. Thus we find here the first indication of a phenomenological support for the conjecture we made in Section II that $\langle k_T^2 \rangle_{had}$ includes not only the intrinsic $\langle k_T^2 \rangle_o$ but also a "narrow" component $\langle k_T^2 \rangle_{narrow}$ associated with the scaling violation of the parton distribution. The component calculated through R in the last subsection is over and above $\langle k_T^2 \rangle_{had}$, just like the contribution of the

perturbative calculation in the present approach.

Because the two terms on the r.h.s. of (5.9) are comparable in magnitudes at present energies, that procedure of determining $\langle q_T^2 \rangle$ is unsatisfactory, except for the merit of rendering a very quick and rough estimate of the two effects. The narrow divergence at $q_T = 0$ cannot be ignored. It does not get cancelled by contributions from other diagrams as in the case of the "soft" divergences. [65),66)] The only work that has given attention to the problem (by giving a regularization procedure) is described in the second paper of Altarelli, Parisi and Petronzio. [62)] Because the implication of the regularization is relevant to our discussion below, we give here the essence of their procedure.

Let $F_{pert}(q_T) = d\sigma/dq_T^2\big|_{pert}$ be the q_T distribution determined in perturbative calculation. It is singular at $q_T = 0$. The integrated cross section, $\sigma_{pert} = \int_0^\infty F_{pert}(q_T)dq_T^2$, is therefore infinite. However, the true (regularized) distribution $F_{reg}(q_T) = d\sigma/dq_T^2\big|_{reg}$ has no singularity at $q_T = 0$, and the corresponding integrated cross section σ_{reg} is finite. If one believes that the only disease with F_{pert} is at small q_T, and that its large q_T behaviour is a faithful statement of reality, then a procedure of subtracting out the diseased small q_T part ought to yield F_{reg}. Suppose that the realistic, but uncalculable, small q_T component, which arises out of the k_T distribution in the hadron, and which is responsible for the first term on the r.h.s. of (5.9), is described by $f(q_T)$, suitably normalized. Then, consider

$$\int dq_T'^2 F_{pert}(q_T')f(q_T' - q_T) - \sigma_{pert} f(q_T) \tag{5.11}$$

The first term is a convolution which installs the proper small q_T behaviour but carries the wrong normalization; the second has the same characteristics by construction. The two are both infinite quantities but the difference is finite. If $f(q_T)$ falls off faster than $F_{pert}(q_T)$, then (5.11) has the same large q_T behaviour as $F_{pert}(q_T)$. These are just the properties that one wants to ascribe to the realistic quantities in the combination

$$F_{reg}(q_T) - \sigma_{reg} f(q_T) \tag{5.12}$$

Hence, the identification of (5.11) with (5.12) defines $F_{reg}(q_T)$. This regularization procedure has been used to fit the data with $f(q_T)$ being an arbitrary function. Assuming $f(q_T)$ to be a Gaussian with a mean $\langle q_T^2 \rangle_{had} = 0.8$ GeV/c, corresponding to [67)]

$$\langle k_T \rangle_{had} = 0.66 \text{ GeV/c} \quad , \tag{5.13}$$

APP II [62] obtained a good fit of the data on q_T distributions. [6] The hadronic "small" k_T component needed is very close to that found in (5.10). The goodness of fit of the data has no great significance since an arbitrary function is at one's disposal, but the M dependence of the data seems to be well described by $F_{reg}(q_T)$ without the necessity of invoking an M dependence of $f(q_T)$.

The regularization procedure leads to the conclusion that the non-Drell-Yan type perturbative calculations in QCD can at present energies account for a portion of the q_T effects in agreement with the rough estimate made earlier. In quantitative terms it apparently accounts for approximately half of $\langle q_T^2 \rangle$ and for the part of $d\sigma/dq_T^2$ with $q_T > 2$ GeV/c. If it is true, then one ought to (1) come to terms with the conclusion made toward the end of the previous subsection regarding the Drell-Yan picture and (2) seek other phenomenological tests that are sensitive to the non-Drell-Yan component. The latter will be considered in the next section with results damaging to the conclusion just made. We shall attempt to show that the resolution of the dilemma will at the same time allow a co-existence between the two approaches considered in this section.

Before leaving this discussion, let us locate the loop hole in the argument that led to the conclusion of the regularization procedure, which incidentally is not unique, but is accepted here for argument's sake. The expression in (5.12) contains all the essential ingredients. The first term is the data, and the second is the hadronic component uncalculable in perturbation theory. The difference, identified with (5.11), is then the contribution from the non-Drell-Yan terms calculated. In APP II [62] $f(q_T)$ was assumed to be a Gaussian with an adjustable width. But it could just as well have been a power-law fall-off with a tail resembling the data. The point is that the more the second term of (5.12) resembles the data over a wider range of "small" q_T, the more the non-Drell-Yan contribution is pushed out to "larger" q_T. With an arbitrary function $f(q_T)$ to adjust, the data can be fitted in an infinite number of ways, especially since the parton distribution needed for the calculation of F_{pert} are mostly still adjustable also. At present there is no way a priori to determine where the "small" q_T range stops and the effects of the perturbative calculations emerge. The demarkation may even change with energy. Only phenomenology can give us

further clues - at present and future energies.

VI. FURTHER PROPERTIES OF $\langle q_T \rangle$

In the preceding section we have dwelt mainly on the theoretical issues related to $\langle q_T \rangle$. They have not been resolved by the confrontation with data on $\langle q_T \rangle$ or $d\sigma/dq_T^2$ as functions of M. We now bring to bear on the problem other phenomenological facts, viz. their dependences on the beam type, x_F , and s. The data are all very new [26),27)] and provide a timely hint toward a more complete picture.

Let me first summarize the findings of the last section. In the back-door approach one identifies

$$\frac{1}{2}\langle q_T^2 \rangle = \langle k_T^2 \rangle = \langle k_T^2 \rangle_{had} + \langle k_T^2 \rangle_R \tag{6.1}$$

where $\langle k_T^2 \rangle_R$ is obtained through the QCD calculation of R, and $\langle k_T^2 \rangle_{had}$ is more than the intrinsic $\langle k_T^2 \rangle_o = (0.3)^2$ (GeV/c)^2. While $\langle k_T^2 \rangle_{had} = \langle k_T^2 \rangle_o$ is assumed in Fig. 5.2, a sizeable difference between them is needed to fit the experimental value of R. In the frontdoor approach one has

$$\langle q_T^2 \rangle = 2\langle k_T^2 \rangle_{had} + \langle q_T^2 \rangle_{pert} \tag{6.2}$$

where $\langle q_T^2 \rangle_{pert}$ is obtained by perturbative calculation of explicit non-Drell-Yan diagrams. It is not clear to what extent $\langle q_T^2 \rangle_{pert}$ can be identified with $2\langle k_T^2 \rangle_R$, but they must in some way be related. Their difference is to be absorbed by the uncalculable $\langle k_T^2 \rangle_{had}$ in the two cases. Phenomenology discussed so far infers that $\langle k_T^2 \rangle_{had}$ is roughly 0.4 (GeV/c)^2 in both cases. According to our discussion in Section II, $\langle k_T^2 \rangle_{had}$ can be further decomposed into two components which we express here in a naive additive form as

$$\langle k_T^2 \rangle_{had} = \langle k_T^2 \rangle_o + \langle k_T^2 \rangle_{narrow} \tag{6.3}$$

While $\langle k_T^2 \rangle_o$ is identified with the static property of the hadron at low Q^2, $\langle k_T^2 \rangle_{narrow}$ is associated with the transverse momentum in the parton distribution confined to a "narrow" cone arising from gluon radiation. It is the parton's transverse spread in a jet, whether it be quarks in a hadron or hadrons in a quark (or gluon) jet. $\langle k_T^2 \rangle_{narrow}$ may depend on Q^2 but should satisfy (2.1).

Since the frontdoor approach is more direct and transparent, our discussion on the QCD results in the following will refer only to that type of perturbative calculations. Although the low-order calculation in perturbation theory is unambiguous, the procedure to eliminate the divergence at $q_T = 0$ is not, resulting in an uncertainty in the estimation of the actual contribution from the non-Drell-Yan process. The situation can best be illustrated by the schematic plots of two possibilities shown in Fig. 6.1 (a) and (b). The open regions under the curves represent the contributions

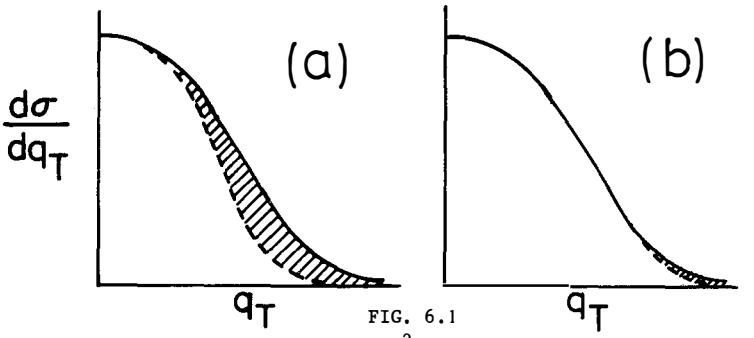

FIG. 6.1

from the hadronic "small component $\langle k_T^2 \rangle_{had}$, the part described by $f(q_T)$. The shaded regions represent the effects of the non-Drell-Yan terms at "large" q_T. Data fitted by the overall (solid) curves admit the possibility of $f(q_T)$ being either (a) a Gaussian with smaller $\langle k_T^2 \rangle_{had}$, or (b) a powerlaw fall-off with a larger $\langle k_T^2 \rangle_{had}$. The conclusions of Ref. 62 to 64 suggest case (a), in which the shaded region contributes a significant fraction (roughly half) of $\langle q_T^2 \rangle$. Case (b) is not ruled out, but we proceed with our discussion assuming (a) to be the case.

Consider now the dependence of $\langle q_T \rangle$ on beam type. Pilcher [26] showed the CP data on π beam at 225 GeV and compared with the CFS data on p beam at 200 GeV. As can be seen from Fig. 6.2, $\langle q_T \rangle^{\pi} \simeq 1.2$ GeV/c while $\langle q_T \rangle^{p} \simeq 1.0$ GeV/c in the flat region. One does not know whether the difference of 0.2 GeV/c should be attributed to the hadronic $\langle k_T \rangle_{had}$ or the perturbative $\langle q_T \rangle_{pert}$ parts of the beam particles, or both. The difference $\langle q_T^2 \rangle^{\pi}_{pert} - \langle q_T^2 \rangle^{p}_{pert}$ can in principle be calculated if the parton distributions in the pion is known, and if $\langle k_T^2 \rangle^{\pi}_{had} = \langle k_T^2 \rangle^{p}_{had}$. It must be positive because the contributions to $\langle q_T^2 \rangle_{pert}$ from the diagrams in Fig. 2.1 are enhanced by the excess antiquark in the pion. Thus the least one can conclude is that $\langle q_T^2 \rangle_{pert}$ ought to be larger than $\langle q_T^2 \rangle^{p}_{pert}$, but probably not as much as the entire difference implied by Fig. 6.2 since

since $\langle k_T \rangle^{\pi}_{had}$ may be larger than $\langle k_T \rangle^{p}_{had}$ too.

We now see, for both $\langle q_T^2 \rangle^{p}$ and $\langle q_T^2 \rangle^{\pi}$, that $\langle q_T^2 \rangle^{p,\pi}_{pert}$ and $2\langle k_T^2 \rangle^{p,\pi}_{had}$ share roughly equal proportions according to the argument above and the conclusion of the perturbative calculations discussed in Section V.-B. We

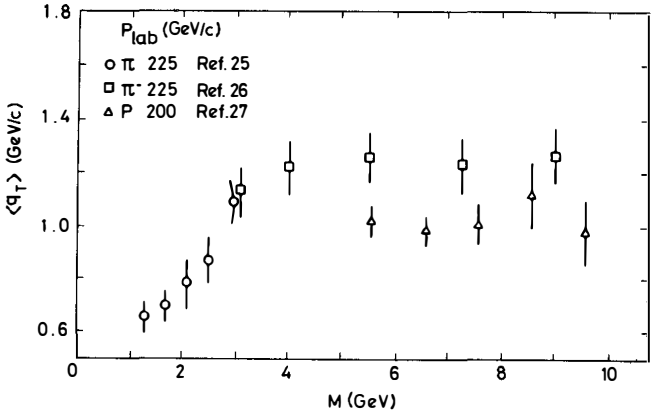

FIG. 6.2

come next to the y or x_F dependence of $\langle q_T \rangle$. Both Lederman [27] and Pilcher [26] showed data on that dependence and indicated that within errors they are essentially constant. (See Fig. 6.3.) This is highly significant, especially for the pion data [26] since they cover a wider range of x_F. The independence of $\langle q_T \rangle$ on x_F contradicts the earlier conclusion that $\langle q_T^2 \rangle_{pert}$ is an important part of $\langle q_T^2 \rangle$ because it has been shown that $\langle q_T^2 \rangle_{pert}$ decreases dramatically with x_F. [63] This is shown in Fig. 6.4. This behaviour may be understood as

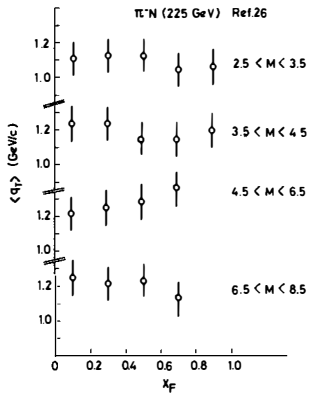

FIG. 6.3

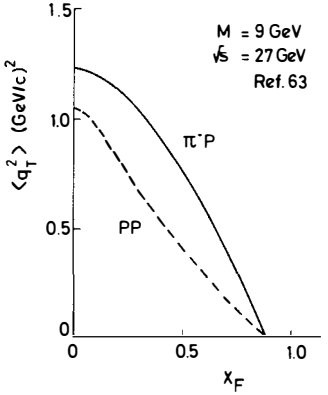

FIG. 6.4

a reflection of the fact that the subprocesses of the lower order non-Drell-Yan diagrams in Fig. 2.1 are all two-body scatterings. The two-body kinematics implies that large-angle scattering (hence large q_T) yields dileptons mainly at small x_F while small-angle scattering (small q_T) leads to dileptons at large x_F. There are complications due to convolution over the parton momenta; however, the dominance of $d\sigma/dMdx_F$ at small x_F makes this physical picture a reasonable interpretation of the numerical result [63] shown in Fig. 6.4.

From the contradiction between Figs. 6.3 and 6.4 one concludes that $\langle q_T^2 \rangle_{pert}$ cannot be a significant part of $\langle q_T^2 \rangle$. This conclusion would be even more inevitable if Fig. 6.3 were a plot of $\langle q_T^2 \rangle$ rather than $\langle q_T \rangle$, although I doubt that the constancy of $\langle q_T \rangle$ does not reflect the same for $\langle q_T^2 \rangle$. In order that $\langle q_T^2 \rangle_{pert}$ be negligible at present energies, thereby negating the earlier conclusion, it is necessary to regard case (a) in Fig. 6.1 as unrealistic. That is, the "small" q_T component described by $f(q_T)$ need not fall off sharply as in a Gaussian. Assuming that it is damped more slowly like in a power law so that the observed q_T distribution follows closely $f(q_T)$ over most of the q_T range explored, as in case (b) in Fig. 6.1, the region where the perturbative calculations are relevant is then pushed out to higher values of q_T not yet measured. One then has

$$\langle q_T^2 \rangle \approx 2\langle k_T^2 \rangle_{had} \tag{6.4}$$

The question is whether this is compatible with the independence on x_F.

The last question cannot be answered in the context of QCD since it is the uncalculable component. However, it arises due to the Drell-Yan mechanism. Recall from Fig. 5.1 that $\langle q_T^2 \rangle$ is independent of τ at $x_F = 0$ where $x_1 = x_2 = \sqrt{\tau}$. Thus $\langle q_T^2 \rangle$ is insensitive to which x regions of the parton distribution functions that contribute to the formation of the lepton pair. As x_F increases different x_1 and x_2 regions are probed. The insensitivity mentioned above then implies the approximate independence of $\langle q_T^2 \rangle$ on x_F.

Comparing (6.4) to (6.1) infers that $\langle k_T^2 \rangle_R$ is negligible also. This is not inconsistent with our discussion in Section V.-A. The calculated values [50),53)] of R are small compared to the old experimental values [54),55)] of R, let alone the new one. [56)]

In light of (6.4) the value of $\langle k_T^2 \rangle_{had}$ must now be revised upward. This brings us to the question of s dependence. The CFS data [27)] shown in Fig. 6.5

exhibit an increase in $\langle q_T \rangle$ as P_{lab} ranges from 200 to 400 GeV/c. For the flat region the following parametrization is given

$$\langle q_T^2 \rangle = 0.7 + 0.0018s \ (\text{GeV/c})^2 \tag{6.5}$$

If $\langle q_T^2 \rangle_{pert}$ were important, one would naturally associate with it the s dependent term above, since it can be shown from perturbative calculation that [61)-63)]

$$\langle q_T^2 \rangle_{pert} = \alpha_s(Q^2) \ s \ h(\tau, \alpha_s) \tag{6.6}$$

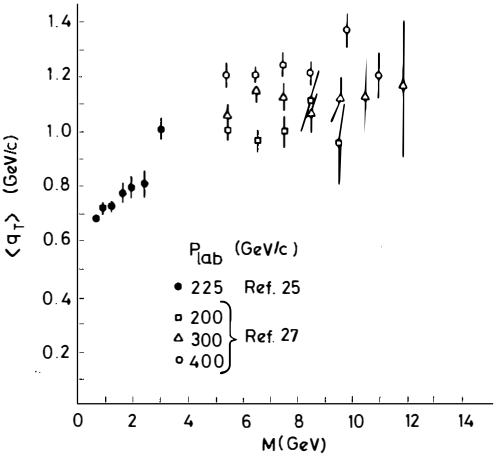

FIG. 6.5

where the scaling function $h(\tau, \alpha_s)$ does not depend on α_s at the lowest non-trivial order. Quantitatively, for the range of values of M currently explored, (6.6) is in the general vicinity of the second term in (6.5). It is unfortunate that this association cannot be made on account of the x_F independence. The burden is then on $\langle k_T^2 \rangle_{had}$ to produce the correct s dependence.

Recalling (6.3) we note that while $\langle k_T^2 \rangle_o$ is some fixed number independent of Q^2, $\langle k_T^2 \rangle_{narrow}$ can depend on Q^2, hence, s for fixed τ. Here we are relying on the conical structure of the jet (partons in a hadron) to allow $\langle k_T^2 \rangle_{narrow}$ to increase with energy, since a conical distribution has no inherent scale. Quantitative results have been obtained in a model study and are in agreement with the data. They will be discussed in the next section.

The conclusion we draw in this section is that the lepton pairs detected so far in hadron-hadron collisions are mainly produced by the direct annihilation of quarks and antiquarks in the parton jets of the incident particles. In consequence, the dileptons have an average $\langle q_T \rangle$ that is independent of x_F. In contrast, the perturbative calculations in QCD essentially study four jet events, two of which are remnants of the incident hadrons, the third is the lepton pair at a large angle, and the last one is the quark or gluon jet recoiling against the dilepton. The $\langle q_T \rangle$ of such processes are naturally sensitive to x_F. The four-jet events will no doubt emerge at high energy and should be looked for to check QCD. However, they constitute an insignificant portion of the events detected now. The situation is analogous to the large-p_T physics for pion production. Distinct QCD features such as p_T^{-4} have not yet appeared. [7] For $p_T < 5$ GeV/c the parton transverse momentum plays an important part in the shape of the inclusive distribution. Similarly, in LPP one must also focus on the tail of the q_T distribution and study correlation between opposite jets to isolate the simple QCD effects studied in perturbative calculations.

VII. QUARK PARTON MODEL WITHOUT NEGLECTING PARTON k_T

Phenomenology of LPP at present energies has forced us to the view that the Drell-Yan mechanism is dominant and is repsonsible for almost the entire range of q_T measured. Thus the q_T of the dilepton owes its origin to the parton k_T in the distribution functions. The component of k_T due to quark binding cannot be reliably calculated; the other component due to gluon corrections in a narrow cone at high Q^2 should, in principle, be calculable in QCD just like the effects of scaling violation. [46] However, at present there are no unambiguous results free from adjustable parameters. In the absence of any definitive description of the k_T dependence of the distribution functions $G(x,k_T,Q^2)$ in QCD, the problem of LPP can only be dealt with in a phenomenological investigation in the framework of QPM suitably generalized to account for non-negligible k_T. This, of course, would not be very meaningful if the Drell-Yan mechanism is found not to be dominant. The object of the investigation would then change from making predictions in QCD to checking consistency among all processes to which QPM is relevant and on which data are available. This has been done in Refs. 33) and 68); we give here some of the results of Ref. 33).

Since $G(x,k_T,Q^2)$ includes only the hadronic k_T components indicated in (6.3), the partons are all nearly on shell. It is only when a gluon is emitted with a large k_T that the associated quark goes off mass shell and a power of $\log Q^2$ is lost in the calculation of the structure function. Thus in the generalization of the QPM we continue to use the usual assumptions that partons are on mass shell and impulse approximation applies. However, we let k_T to be non-negligible, while keeping it within the bound of

$$\langle k_T^2 \rangle_{\text{narrow}} < \varepsilon Q^2 \quad . \tag{7.1}$$

This inequality is, of course, not very precise for our purpose here since ε is undetermined and Q^2 may not be very large. Its origin [cf. discussion following (2.1)] follows from the mathematical properties of divergent integrals as $Q^2 \to \infty$. For finite values of Q^2, ε need not be infinitesimal to keep the parton from going significantly off mass shell. Thus at "low" M^2, say $20(\text{GeV/c})^2$, $\langle k_T^2 \rangle_{\text{had}}$ may well be as large as the observed $1\ (\text{GeV/c})^2$. The generalized QPM has been extended to include that region.

Because k_T is not negligible, a number of new features arise that are absent in the naive QPM. The Bjorken variable x is not necessarily the parton's longitudinal-momentum fraction, which in itself is no longer a Lorentz invariant. A new scaling variable z is needed to describe the transverse degree of freedom. Through z DIS and LPP can be kinematically related and unified by a common parton distribution function. In recognition of the conical structure of the k_T dependence, the distribution function G has been parametrized in terms of a radial scaling variable and an angle. It is found that in terms of a single G function (with appropriate separation of quark and antiquark components) all data on DIS and LPP can be simultaneously fitted; more specifically, they are νW_2, R, $d\sigma/dMdy$ at $y = 0$, and $\langle q_T \rangle$ vs. M.

It is also discovered that significant and interesting departure from (5.8) occurs for a wide range of M where data exist. This is shown in Fig. 7.1. It is a manifestation of the fact that k_T is not negligible and that the convolution in (2.2) over an ellipsoidal surface introduces the discrepancy between $\langle k_T \rangle$ and $\langle q_T \rangle/\sqrt{2}$. Note that where $\langle q_T \rangle$ is flat in accordance to the data, $\langle k_T \rangle$ increases with M, a behaviour reminiscent of Fig. 5.2. Thus in that figure the agreement with data is actually better than meets the eye.

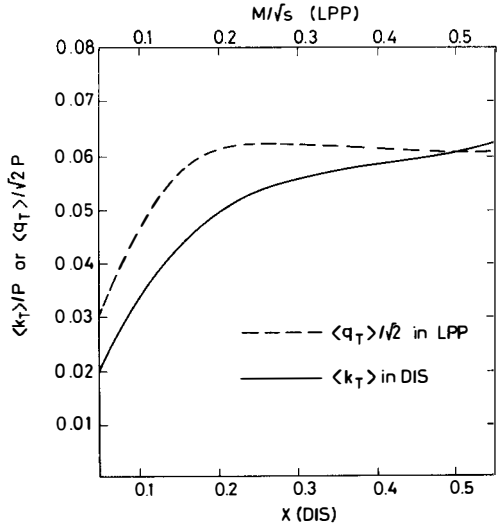

FIG. 7.1

Since the parametrization of G has no scale, the calculated $\langle q_T \rangle$ must increase with $\sqrt{s}$ for fixed τ. It is found that the value in the flat, plateau region behaves as

$$\langle q_T \rangle_{\text{plateau}} = 0.042\ \sqrt{s} \tag{7.2}$$

at large s. This result was obtained before the data [27] on energy dependence became known. It agrees with (6.5) rather well.

The conical structure of the parton distribution in a hadron can best be described in the Breit frame for DIS, which is free of the constraint between x and Q^2 in LPP. In that frame $k_L = Q/2$ and $x = k_L/P$, P being the momentum of the hadron. In a schematic drawing that exaggerates the transverse scale, the parton distributions for various values of P ($P_1 < P_2 < P_3$) may look like:

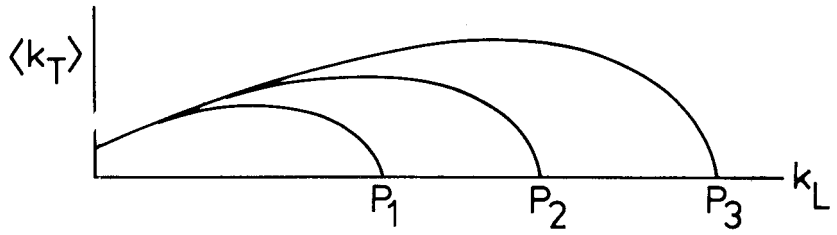

Apart from the kinematical turn-over at high k_L the relationship between $\langle k_T \rangle$ and k_L is basically conical. Plotted against x, $\langle k_T \rangle$ exhibits a "flying" sea-gull effect in that at fixed x it increases with Q. The independence of the dilepton's $\langle q_T \rangle$ on M is to be understood through the difference between $\langle k_T \rangle$ and $\langle q_T \rangle / \sqrt{2}$ as shown in Fig. 7.1. The increase with $\sqrt{s}$ is self-evident. It is anticipated that the same properties are possessed by the jet structure of parton decay into hadrons.

VIII. OTHER TESTS OF THE DRELL-YAN MECHANISM

In previous sections we have discussed how well the Drell-Yan mechanism works in LPP when all available data on the process are collectively taken into account. In this section we mention three possible tests to check the mechanism further. Corresponding experiments to carry out the tests are therefore suggested.

A. SUM RULES

So far in applying the Drell-Yan mechanism some adjustable functions describing the quark and antiquark distributions must be assumed to fit the data. Thus there are always some free parameters in the model. However, if the Drell-Yan formula is strictly correct, exact sum rules can be derived from it that are free from any adjustable parameters.[69] Confrontation with data can then provide a clean test of the dominance of the mechanism.

To be free from the uncertainties related to the distribution functions $G_h^{f,\bar{f}}$ in (2.2), we recall the exact sum rules well-known in leptoproduction

$$\int \frac{d^3k}{k_o} \left[G_p^f - G_p^{\bar{f}} \right] = \begin{cases} 2 \\ 1 \\ 0 \end{cases}, \quad \text{for } f = \begin{cases} u \\ d \\ s \end{cases} \tag{8.1}$$

and other similar ones for different hadrons. In order to make use of them in LPP, we consider the integral (for fixed M^2)

$$I = \int_0^1 \frac{d\tau}{\tau} M^4 \left[\frac{d\sigma}{dM^2}(\bar{h}_1 h_2) - \frac{d\sigma}{dM^2}(h_1 h_2) \right] \tag{8.2}$$

where h_1 and h_2 stand for the beam and target hadrons, and $\bar{h}_1$ is the anti-particle of h_1. Substituting (2.3) into (8.2), one obtains

$$I = C \sum_f e_f^2 (N_{h_1}^f - N_{h_1}^{\bar{f}})(N_{h_2}^f - N_{h_2}^{\bar{f}}) \qquad (8.3)$$

where $C = 4\pi\alpha^2/9$ and $N_h^{f,\bar{f}} = \int G_h^{f,\bar{f}} \, d^3k/k^o$. Now equations such as (8.1) can be used for various h_1 and h_2, yielding the following table for I:

$(\bar{h}_1, h_1)$	$h_2 = p$	$h_2 = n$
$\bar{p}, p$	$\frac{17}{9}C$	$\frac{10}{9}C$
π^-, π^+	$\frac{7}{9}C$	$\frac{2}{9}C$
K^-, K^+	$\frac{8}{9}C$	$\frac{4}{9}C$

These sum rules are independent of the details about the G functions, and of the value of M provided that it is high enough to warrant the Drell-Yan picture.

The integration in (8.2) is over τ for fixed M^2; thus it is effectively over s, which is not easy to do experimentally. If we neglect scaling violation which is not unreasonable in view of Fig. 4.2, (8.2) may be re-expressed in terms of an integral over M^2 for fixed s

$$I = \int_0^s dM^2 \, M^2 \left[\frac{d\sigma}{dM^2}(\bar{h}_1 h_2) - \frac{d\sigma}{dM^2}(h_1 h_2) \right] \qquad (8.4)$$

Here the two terms inside the square bracket must cancel at small M^2 since they diverge individually. If they do not cancel in the limit $M^2 \to 0$, it means that the observed $d\sigma/dM^2$ differs from the prediction of the Drell-Yan formula in a way which is not invariant under charge conjugation of the beam hadron; in that case the identification of (8.4) with (8.2), and consequently with the values in the above table, is invalid, and one is then forced back to the use of (8.2).

Verification of the sum rules provides an unambiguous affirmation of the applicability of the Drell-Yan mechanism.

B. ANGULAR DISTRIBUTION OF THE LEPTONS

One can also learn about the LPP mechanism by studying the angular distribution of the leptons in the rest frame of the lepton pair relative to

some axis.[70)-73)] If that axis is along one of the incident hadrons, then it specifies the Gottfried-Jackson angle θ, which we use here for definiteness. In a Drell-Yan picture if the annihilating quark and antiquark have no transverse momentum relative to the incident hadrons, then the Gottfried-Jackson frame is the same as the c.m. system of the subprocess $q\bar{q} \to \gamma^* \to \mu^+\mu^-$ with the z axis along the initial partons. Hence, one expects

$$\frac{d\sigma}{d\cos\theta} \propto 1 + \cos^2\theta , \qquad (k_T = 0) \tag{8.5}$$

On the other hand, if the parton transverse momenta are nonzero, it can be shown that (8.5) is modified to

$$\frac{d\sigma}{d\cos\theta} \propto 1 + A\cos^2\theta , \qquad (k_T \neq 0) \tag{8.6}$$

where the coefficient A is less than one and depends on other kinematical variables of LPP. It is in the character of A that one hopes to find indications of the nature of the production mechanism.

If in a direct $q\bar{q}$ annihilation of the Drell-Yan type the only transverse momenta of the partons are "intrinsic" and fixed, e.g. $\langle k_T \rangle_o$, then A decreases with increasing M^2 and is therefore nonscaling.[71),72)] On the other hand, if the production mechanism is of the explicitly non-Drell-Yan type that involves hard gluon emission with large k_T, then A scales apart from logarithms[73),74)] i.e. it is a function of x_T and τ. However, there is the intermediate region corresponding to k_T being in the narrow cone, the situation which we have argued to be the predominant one. There is no explicit statement of the behaviour of A in that case. Further work is needed to map out the behaviours of A (in both normalization and shape) as functions of M^2, x_T and τ for all three cases mentioned above. Experiments on the angular distribution remain to be done.

C. HADRON PRODUCTION WITH DILEPTON TRIGGER

Another way to learn about the LPP mechanism is to use LPP as a trigger in studying the production of hadrons at low p_T but large x.[75)] A meaningful prediction about this type of correlation relies on a sensible model for hadron production in the fragmentation region. The parton recombination model[38)] has been successful[39)-42),76)] in giving a quantitative understanding of the meson inclusive distributions at low p_T. In that model a meson at

at large x is produced by a fast valence quark of the incident hadron recombining with an antiquark from the sea of the same hadron. Thus if the same fast valence quark is needed for the dilepton trigger, then the meson distribution will obviously be seriously affected.

In Ref. 75), the Drell-Yan mechanism is assumed for LPP and the ratios of the semi-inclusive cross sections for the production of π^+ and π^- are calculated for various beam particles and for various values of τ of the dilepton trigger. The most dramatic feature predicted is in $\sigma(\pi^+)/\sigma(\pi^-)$ vs. τ for π^+p collision. As $\sqrt{\tau}$ increases from 0 to 0.4, the ratio at x = 0.5 increases by more than a factor 2. This is to be understood as follows. The π^+ beam particle has a $\bar{d}$ valence quark which is highly efficient in depleting the d valence quark of the target proton in forming a high τ lepton pair. The remaining valence quarks of the proton are both u-type which can readily produce π^+ at large x but not π^-.

Ref. 75) does not address itself to the question of testing the difference between Drell-Yan and non-Drell-Yan mechanisms. In the light of our discussion in Section VI it is not difficulty to extend their argument to provide such a test. Since the non-Drell-Yan processes are expected to be important only at large q_T, one should study, for example, the ratio $\sigma(\pi^+)/\sigma(\pi^-)$ in π^+p collisions mentioned above as a function of q_T for some fixed large x and large τ. As q_T increases, if the "Compton" subprocess $\bar{d} + g \to \bar{d} + \gamma^*$ at large angle becomes important, the $\bar{d}$ quark in the proton is not annihilated a good fraction of the time; consequently the ratio should decrease accordingly. The dependence of the ratio on q_T is therefore a good measure of the extent to which the "Compton" subprocess plays an important role. According to perturbative calculations in QCD [62)-64)] it is dominant at high q_T; the proposed experiment would determine how high is "high".

IX. CONCLUSION

We have reviewed the recent data on LPP and used them to examine and interpret the many theoretical papers that have been written on the subject. Our emphasis has been to extract from the theoretical results their physical relevance to the phenomenology of LPP at present energies. On the whole we have found that the Drell-Yan mechanism works extremely well; in fact, we have found no significant conflict with any data. Theoretically, QCD explains why it works better than one should naively expect.

QCD, however, also predicts that there are distinctly non-Drell-Yan processes which should become important at high q_T. Phenomenology has led us to conclude that the kinematical region in which it is dominant has not yet been reached at present energies. Thus we are in the unfortunate situation where what is needed theoretically to describe LPP (i.e. the parton distribution functions) cannot be calculated in QCD by perturbative or other means.

In the absence of meaningful and quantitative QCD predictions about the data available now, one turns to phenomenological analyses of the data in the framework of the QPM. One finds that a consistent picture can be given, in which the partons in a hadron have a jet-like distribution. That is, in addition to an intrinsic k_T component reflecting the binding effects at low Q^2, there is also a "conical" component of k_T the mean value of which grows slowly with the hadron momentum. The latter component is due to hard gluon radiation in a narrow cone, the same mechanism that gives rise to scaling violation. It is also the non-Drell-Yan type effects which can be factorized and absorbed into the distribution functions with the consequence that the Drell-Yan mechanism is thereby restored.

Experiments are suggested to reveal further the basic mechanism for LPP. If they confirm the picture outlined above, then the distribution of partons in a hadron holds the key to most of the properties of LPP, and the urgency for a theoretical understanding of it becomes all the more pressing. But then that is, after all, one of the primary reasons for doing experiments on LPP in the first place.

ACKNOWLEDGEMENT

I wish to thank many who have generously shared with me their insights which are invaluable to this review; they include, in particular, C. T. Sachrajda, T. M. Yan, S. Matsuda, R. G. Roberts, H. I. Miettinen, and R. Petronzio. The warm hospitality of members of the Theory Division at the Rutherford Laboratory, especially that of R. Phillips, is also gratefully acknowledged.

REFERENCES

1. M. J. Shochet, Proceedings of SLAC Summer Institute 1977, SLAC-PUB-204; N. S. Craigie, to be published in Physics Reports C.
2. J. Ellis, Proceedings of Les Houches Summer School, 1976.
3. S. D. Drell and T. M. Yan, Phys. Rev. Lett. 25, 316 (1970); Ann. Phys. (N.Y.) 66, 578 (1971).
4. R. P. Feynman, "Photon-Hadron Interactions", Benjamin, N.Y. (1972).
5. M. Duong-van, K. Vasavada and R. Blankenbecler, Phys. Rev. D16, 1389 (1977). M. Duong-van and R. Blankenbecler, SLAC-PUB-2017 (1977).
6. D. M. Kaplan et al., Phys. Rev. Lett. 40, 435 (1978).
7. A. G. Clark et al., CERN preprint (1978).
8. D. Schildknecht, XIIIth Rencontre de Moriond, 1978.
9. J. L. Cardy and G. A. Winbow, Phys. Lett. 52B, 95 (1974); C. E. de Tar, S. D. Ellis, and P. V. Landshoff, Nucl. Phys. B87, 176 (1975).
10. H. D. Politzer, Nucl. Phys. B129, 301 (1977).
11. C. T. Sachrajda, Phys. Lett. 73B, 185 (1978).
12. This softens the objections of H. Georgi, Harvard preprint HUTP-77/A090 (1977).
13. D. J. Gross and F. Wilczek, Phys. Rev. D8, 3633 (1973); D9, 980 (1974).
14. H. D. Politzer, Phys. Reports C14, 129 (1974); H. Georgi and H. D. Politzer, Phys. Rev. D9, 416 (1974).
15. D. Amati, R. Petronzio and G. Veneziano, CERN preprint Ref.TH.2470 (1978).
16. K. H. Craig and C. H. Llewellyn Smith, Phys. Lett. 72B, 349 (1978).
17. G. Sterman and S. Weinberg, Phys. Rev. Lett. 39, 1436 (1977).
18. C. T. Sachrajda, CERN preprint Ref. TH.2459 (1978).
19. P. V. Landshoff, Phys. Lett. 66B, 452 (1977).
20. R. J. Hughes, J. Phys. G: Nucl. Phys. 3, L255 (1977); A. C. Davis and E. J. Squires, Phys. Lett. 69B, 249 (1977); J. S. Bell and A. J. G. Hey, Phys. Lett. 74B, 77 (1978); J. Kripfganz and G. Ranft, CERN preprint Ref. TH.2398 (1977).
21. R. C. Hwa, S. Matsuda and R. G. Roberts, RL-77-117/A, Phys. Lett. (to be published).
22. M. Brinkley et al., Phys. Rev. Lett. 37, 571 (1976).
23. D. C. Hom et al., Phys. Rev. Lett. 37, 1274 (1976).
24. D. Antreasyan et al., Phys. Rev. Lett. 37, 1451 (1976).
25. J. G. Branson et al., Phys. Rev. Lett. 38, 457, 1334 (1977).
26. J. E. Pilcher, XIIIth Rencontre de Moriond, 1978.
27. L. M. Lederman, XIIIth Rencontre de Moriond, 1978.
28. R. F. Peierls, T. L. Trueman, and L. L. Wang, Phys. Rev. D15, 1397 (1977).
29. F. T. Dao et al., Phys. Rev. Lett. 39, 1388 (1977).
30. J. Teiger, XIIIth Rencontre de Moriond, 1978.
31. A. Romana, XIIIth Rencontre de Moriond, 1978.
32. R. Barate, XIIIth Rencontre de Moriond, 1978.

33. R. C. Hwa, S. Matsuda, and R. G. Roberts, CERN preprint Ref. TH.2456 (1978).

34. N. Cabibbo and R. Petronzio, CERN preprint Ref. TH.2440 (1978).

35. H. L. Anderson et al., Phys. Rev. Lett. 38, 1450 (1977).

36. J. H. Cobb et al., Phys. Lett. 72B, 273 (1977).

37. M. J. Teper, Rutherford Laboratory report RL-78-015/A (1978).

38. K. P. Das and R. C. Hwa, Phys. Lett. 68B, 459 (1977); 73B, 504 (1978); XIIth Rencontre de Moriond, 1977.

39. D. W. Duke and F. E. Taylor, Fermilab-Pub-77/95-THY (1977).

40. F. C. Erne and J. C. Sens, CERN preprint (1978).

41. M. J. Teper, Rutherford Laboratory report RL-78-C22 (1978).

42. R. G. Roberts, R. C. Hwa and S. Matsuda, Rutherford Laboratory report RL-78-040 (1978).

43. J. Kogut and J. Shigemitsu, Nucl. Phys. B129, 461 (1977).

44. I. Hinchliffe and C. H. Llewellyn Smith, Phys. Lett. 66B, 281 (1977).

45. H. D. Politzer, Phys. Lett. 70B, 430 (1977).

46. C. S. Lam and T. M. Yan, Phys. Lett. 71B, 173 (1977).

47. O. Nachtmann, Proceedings of the 1977 International Symposium on Lepton and Photon Interactions at High Energies, Hamburg (1977), p.811.

48. A. De Rujula, H. Georgi, and H. D. Politzer, Ann. Phys. (N.Y.) 103, 315 (1977).

49. M. Calvo, Phys. Rev. D15, 730 (1977).

50. A. J. Buras, E. G. Floratos, D. A. Ross, and C. T. Sachrajda, Nucl. Phys. B131, 308 (1977).

51. A. Zee, F. Wilczek, and S. Treiman, Phys. Rev. D10, 2881 (1974).

52. H. D. Politzer, CALT-68-628 (1977).

53. G. C. Fox, Nucl. Phys. B131, 107 (1977).

54. E. M. Riordan et al., SLAC-PUB-1634 (1975).

55. R. E. Taylor, Proceedings of the 1975 International Symposium on Lepton and Photon Interactions at High Energies, Stanford (1975), p.679.

56. L. Hand, Proceedings of the 1977 International Symposium on Lepton and Photon Interactions at High Energies, Hamburg (1977), p.417.

57. G. Altarelli and G. Parisi, Nucl. Phys. B126, 298 (1977).

58. C. S. Lam, Lecture at the Banff Summer Institute, 1977.

59. D. E. Soper, Phys. Rev. Lett. 38, 461 (1977).

60. K. Kajantie and R. Raitio, Helsinki preprint HU-TFT-72-21 (1977).

61. H. Fritzsch and P. Minkowski, Phys. Lett. 73B, 80 (1978).

62. G. Altarelli, G. Parisi and R. Petronzio, CERN preprints Ref. TH.2413 (1977) and Ref. TH.2450 (1978).

63. F. Halzen and D. M. Scott, Wisconsin preprint COO-881-21 (1978).

64. C. Michael and T. Weiler, XIIIth Rencontre de Moriond, 1978.

65. T. Kinoshita, J. Math. Phys. 3, 650 (1962).

66. T. D. Lee and M. Nauenberg, Phys. Rev. 133, 1549 (1964).

67. R. Petronzio, XIIIth Rencontre de Moriond, 1978.
68. J. Kubar-Andre and F. E. Paige, BNL-23530 (1977).
69. R. C. Hwa, Phys. Rev. Lett. 40, 1218 (1978).
70. K. V. Vasavada, Phys. Rev. D16, 146 (1977).
71. J. C. Collins and D. E. Soper, Phys. Rev. D16, 2219 (1977).
72. E. L. Berger, J. T. Donohue, and S. Wolfram, ANL-HEP-PR-77-63 (1977).
73. K. Kajantie, J. Lindfors, and R. Raitio, Helsinki preprint HU-TFT-78-5 (1978).
74. K. Kajantie (private communication).
75. T. A. DeGrand and H. I. Miettinen, Phys. Rev. Lett. 40, 612 (1978).
76. H. I. Miettinen, XIIIth Rencontre de Moriond, 1978.

BARYONIUMS AND RELATED STATES

Chan Hong-Mo
Rutherford Laboratory,
Chilton, Didcot, Oxon, OX11 0QX, England

ABSTRACT: A brief introduction is given to current theoretical ideas on baryonium states with particular emphasis on their interpretation as 'colour molecules'. It is argued that baryonium spectroscopy provides a valuable test for colour as a new degree of freedom.

BARYONIUMS AND RELATED STATES

I. Preamble

Initially, Tran Thanh Vanh has asked me for a theoretical review, but because of both the present unsettled state of the subject and my own limited acquaintance with it, I have decided to give instead an introduction. This seems to me more appropriate since there are quite a few experts speaking after me at this meeting who can describe to you some aspects of the subject much better than I can. Therefore, I shall make it my job only to help you appreciate their later presentations, and to fill in some gaps which I, as co-ordinator, know that they will not have time to cover.

The name 'baryonium' was suggested first, I believe, by Geoff Chew, for a group of resonance states recently discovered in the $B\bar{B}$ channel. The name carries with it a fair amount of theoretical prejudice, and may not be entirely appropriate. However, as many other labels invented by Chew, this one has also stuck. I shall therefore follow the convention and refer to these states as 'baryoniums', although I shall attempt to free myself from the theoretical prejudices that the name entails.

There are now about a dozen such states reported in the literature with masses ranging from below $N\bar{N}$ threshold to about 3 GeV. The experimental evidence for their existence is fairly convincing in some cases but highly controversial in others. Later on, Lucien Montanet will give you a full, expert's review of the experimental situation. In addition there will be talks by Tony Carter, Bernard French and Jules Six on several states of particular interest.

There are several outstanding properties which make these states interesting:- [1)]

(A) They show a particular reluctance for decaying into meson channels in spite of the favourable phase space available. Most of them have so far been seen only in channels containing a $B\bar{B}$ pair. In those few cases where mesonic decays have been observed, the partial widths are only of the order of a few MeV.

(B) The widths of these resonances vary greatly. In the same mass range, 2 - 3 GeV, some are broad [e.g. T(2.15), U(2.31), V(2.48)] with widths around 100 - 200 MeV which seem normal for hadronic decays in this mass range, while

others are narrow [e.g. 2.020, 2.204, 2.85, 2.95] with widths within the experimental resolution, $\Gamma \lesssim 20$ MeV. All the narrow ones except S(1.936) near threshold, have been seen so far only in production experiments. At least one of them, 2.204, has been looked for in formation and not found. This indicates perhaps that there are two types of baryonium states with widely different couplings to baryon-antibaryon.

(C) The quantum members of these are in most cases unknown. All known cases have moderately high spins [$T(J^P = 3^-)$, $U(J^P = 4^+)$, $V(J^P = 5^-)$].

Because of their unusual affinity to the baryon-antibaryon system, it is generally believed that they are not ordinary $q\bar{q}$ mesons. The two possible alternatives suggested are:-

(i) Baryon-antibaryon resonances held together by nuclear forces. [2)3)] The physical mechanism here is very similar to the binding of a proton with a neutron to form a deuteron, except that the forces here are known to be more attractive and therefore capable of binding more states. We shall refer to them in future as 'nuclear molecules'.

(ii) Diquark-antidiquark hadron states held together by colour confining forces, in much the same (unknown) way as a $q\bar{q}$ pair is bound to form the ordinary mesons. We shall call these 'colour molecules' for distinction.

On the surface, at least, these two possibilities represent two distinct sets of states. There seems no reason to me why they cannot exist together.

A feature common to the two alternatives is that they both require baryonium states to have high spins. The reason for this is the following. Naively, without introducing a new, ad hoc, and therefore unsatisfactory, selection rule (such as 'junction conservation' proposed by some authors [4)5)]) one does not see in general why the quarks in either (i) or (ii) cannot rearrange or annihilate as in Fig. 1 leading to purely mesonic final states with large widths, in contradiction to experimental observation (A). However, all the processes in Fig. 1, require the transfer of quarks between the two portions of the molecule. So long as the two portions are separated by a high angular momentum L, then such processes will be inhibited by the angular momentum barrier. This is a solution subscribed to by most authors either explicitly or implicitly in models of both types. Now, as noted already in (C), J is indeed quite high for those experimental states for which J^P is known at present. If it turns out, however, that some baryoniums are later shown to have low spins, then most existent models in both categories could be in trouble.

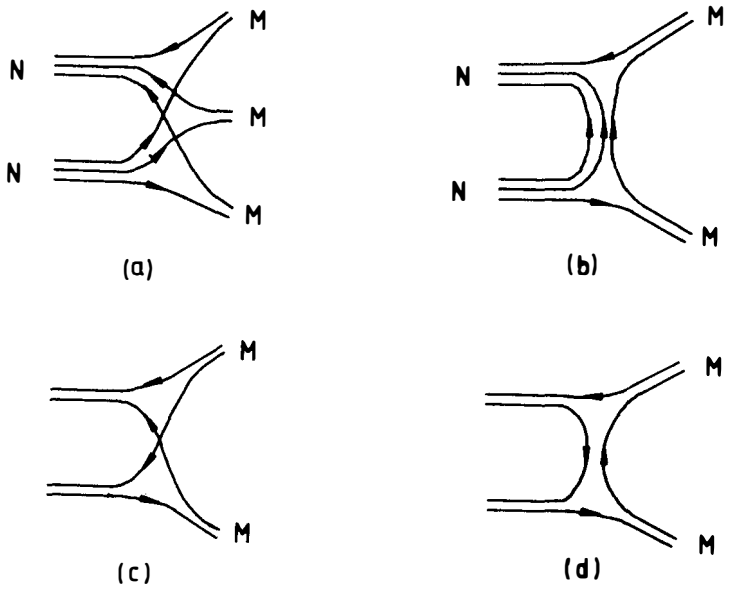

FIGURE 1: Mesonic decays of baryoniums

The main qualitative difference between the alternatives (i) and (ii) is that the nuclear forces responsible for binding the molecules in (i) are short-ranged so that one does not expect stable states with high angular momentum to exist high above the $N\bar{N}$ threshold. On the other hand, the colour confining forces in (ii) are believed to increase in strength with increasing distance. It should therefore be possible to have metastable states even at very high mass and angular momentum. Thus if the narrow states reported around 3 GeV were established and shown to have high spin J, they are more likely 'colour molecules' than 'nuclear molecules'. Of course, in order to make a clear identification in either case, one would need to perform detailed calculations so as to predict both the spectrum and the properties of the resonances.

Since Vinh Mau is here to show you how this is done for the nuclear bound states in (i), I shall concentrate here on the 'colour molecules'.

II. "Diquoniums"

The colour molecules formed from a diquark qq and an antidiquark $\bar{q}\bar{q}$ is similar to a charmonium state formed from a c and a $\bar{c}$. We shall therefore call these states, by analogy, 'diquoniums'. For reasons already stated, we shall restrict ourselves only to diquonium states in which the diquark is separated from the antidiquark by an orbital angular momentum $L > 0$. Those states with $L = 0$ [6] are themselves also very interesting and will be discussed later in the session by Bob Jaffe and Alan Martin.

A special interest in diquonium spectroscopy is that it may prove to be a valuable testing ground for the concept of colour. [7] As you all know, it is nowadays popularly believed (and indeed, amply documented in this meeting) that colour is the source of all strong interactions, and if so it is as fundamental to nature at least as electric charge. In spite of its general appeal however, its main success has so far only been in rationalising existing models which were already found to be successful. Apart from the much quoted examples of the ratio $R = \sigma(e^+e^- \to x)/\sigma(e^+e^- \to \mu^+\mu^-)$ in e^+e^- annihilation and the decay rate of $\pi^0 \to \gamma\gamma$, colour has given us as yet hardly any new predictions which can be tested directly against experiment. Instead, if colour were as basic as it claims to be one has the right to expect a whole new class of phenomena quite distinct from those of a colourless world.

Now one obvious place to look for manifestations of colour is in hadron spectroscopy, where because of the new degree of freedom so introduced one expects an additional richness of states to occur. However, it is not entirely straightforward, since hadrons are all supposed to be colour singlets so that to distinguish colours, one has to go to subhadronic levels. Also, it is not enough to study just the ordinary $q\bar{q}$ mesons and qqq baryons since in order to obtain a colour singlet qqq state, the diquark qq in a baryon must be in a $\bar{3}$ representation of colour SU(3), same as $\bar{q}$ in a $q\bar{q}$ meson. For more colourful consequences, one must investigate some more complicated systems, and the next simplest is $qq\bar{q}\bar{q}$, i.e. diquonium.

II.1 Their Spectrum [8)9)]

A quark q is a triplet 3 in colour, a doublet 2 in spin and a triplet $\underline{3}$ in flavour, which we denote by $(3,2,\underline{3})$. A diquark qq can then be $3 \times 3 = \bar{3} + 6$ in colour, $2 \times 2 = 1 + 3$ in quark spin, and $\underline{3} \times \underline{3} = \bar{\underline{3}} + \underline{6}$ in flavour. In what follows we shall mostly be interested in a diquark in the ground state which

we assume to be purely s-wave. In that case, because of the Pauli Principle, only the following combinations of colour, spin and flavour for qq are admissible:

$$(\bar{3},1,\underline{3}) \ , \quad (\bar{3},3,\underline{6}) \ , \quad (6,1,\underline{6}) \ , \quad (6,3,\underline{\bar{3}}) \ . \tag{1}$$

Similarly, an antidiquark has the conjugate representations:

$$(3,1,\underline{3}) \ , \quad (3,3,\underline{\bar{6}}) \ , \quad (\bar{6},1,\underline{\bar{6}}) \ , \quad (\bar{6},3,\underline{3}) \ . \tag{2}$$

Combining a diquark with an antidiquark to form a diquonium, one then has the following possibilities:

$$\left.\begin{aligned}
(\bar{3},1,\underline{\bar{3}}) \times (\underline{3},1,\underline{3}) &= (1,1,\underline{9}) \\
(\bar{3},1,\underline{\bar{3}}) \times (3,3,\underline{\bar{6}}) &= (1,3,\underline{\overline{18}}) \\
(\bar{3},3,\underline{6}) \times (3,1,\underline{3}) &= (1,3,\underline{18}) \\
(\bar{3},3,\underline{6}) \times (3,3,\underline{\bar{6}}) &= (1,1,\underline{36}) \\
(\bar{3},3,\underline{6}) \times (3,3,\underline{\bar{6}}) &= (1,3,\underline{36}) \\
(\bar{3},3,\underline{6}) \times (3,3,\underline{\bar{6}}) &= (1,5,\underline{36})
\end{aligned}\right\} \text{"T"}$$

$$\left.\begin{aligned}
(6,1,\underline{6}) \times (\bar{6},1,\underline{\bar{6}}) &= (1,1,\underline{36}) \\
(6,1,\underline{6}) \times (\bar{6},3,\underline{3}) &= (1,3,\underline{18}) \\
(6,3,\underline{\bar{3}}) \times (\bar{6},1,\underline{\bar{6}}) &= (1,3,\underline{18}) \\
(6,3,\underline{\bar{3}}) \times (\bar{6},3,\underline{3}) &= (1,1,\underline{9}) \\
(6,3,\underline{\bar{3}}) \times (\bar{6},3,\underline{3}) &= (1,3,\underline{9}) \\
(6,3,\underline{\bar{3}}) \times (\bar{6},3,\underline{3}) &= (1,5,\underline{9})
\end{aligned}\right\} \text{"M"} \tag{3}$$

One sees indeed a doubling of the number of states due to colour as expected. We denote the two sets of states formed from colour 3 and 6 diquarks by T and M respectively.

Since the colour of a diquark is not necessarily diagonal in the total diquonium Hamiltonian, the two sets of states T and M will in general mix, for example by gluon exchange between the two portions. We claim, however, that the mixing will vanish when the two portions become separated by a high orbital angular momentum, namely for those configurations we wish to associate with baryonium. [9] The basis for this claim is the following. A gluon carries no flavour - it can therefore only mix diquark states with the same flavour. From (1), one sees that one cannot then flip the colour of a diquark without also flipping its spin. Now if the interaction between quarks were indeed due to gluon exchange as stipulated then by analogy with Coulomb forces in QED the spin-dependent part of the interaction is short-ranged and should vanish when the distance between the quarks increases. That this is indeed the case can be demonstrated directly in phenomenology by plotting the mass

differences between the spin-triplet and singlet states along a $q\bar{q}$ meson trajectory as a function of the orbital angular momentum L. This mass difference is due exactly to the spin-dependent part of the interaction between $q\bar{q}$ and should thus vanish for increasing L if our stipulation is correct. In Fig. 2, we show the mass differences ($\rho - \pi$, $A_2 - B$, $g - A_3$) and ($K^* - K$, $K^{**} - Q_B$, $K^{***} - L$) along two meson trajectories and they do decrease rapidly with increasing L as expected. We claim therefore that for sufficiently high L, the two types of diquonium states T and M will become approximate eigenstates of the total Hamiltonian.

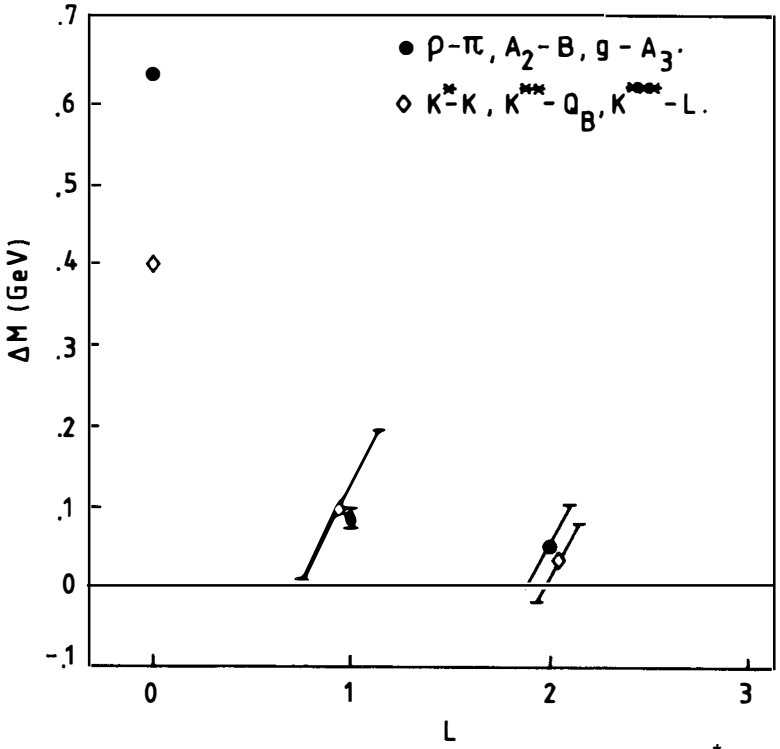

FIGURE 2: Mass differences between resonances on the $\rho - \pi$ and $K^* - K$ trajectories as a function of the orbital angular momentum L between the quark and the antiquark.

For finite L, of course, the states will mix. At each L, one can estimate the mixing between them as follows. From perturbation theory, the mixing angle θ is of the order:

$$\tan\theta \sim \langle T|V|M\rangle/\Delta E \qquad (4)$$

where V is the mixing interaction and ΔE the mass difference between the states. Now the colour magnetic splitting alone between the colour $\bar{3}$ and 6

s-wave diquarks is of the order of $m_\rho - m_\pi$. In addition there is in general further mass splitting due to colour electric forces, both within the diquark and between the two portions of diquonium. On the other hand, the mixing interaction strength V due to colour magnetic forces between the portions of diquonium. On the other hand, the mixing interaction strength V due to colour magnetic forces between the portions is measured by the splitting between spin triplet and singlet states at a given L value, e.g. $m_{A_2} - m_B$ at L = 1 and $m_g - m_{A3}$ at L = 2. Hence, from Fig. 2, we obtain the estimates $\tan\theta \lesssim .2$ and .1 at L = 1 and 2 respectively. We see therefore that except for L = 0, the mixing is quite small and we may regard T and M as belonging to distinct families for most practical purposes.

Next, we proceed to estimate the masses of diquoniums. For the present, let us ignore entirely the spin-dependent interactions between the diquark and the antidiquark in a diquonium. Then, within each family and for each value of L, the masses of the different spin states listed in (3) are split only by the diquark mass differences due to the colour magnetic introduction between the 2 quarks. Since this interaction is short-ranged, we argue by asymptotic freedom that it is sufficient to treat this perturbatively and approximate it by one-gluon exchange. [10] For s-wave diquarks, only the spin-spin term is relevant, which is of the form: [6]

$$V = - C \sum_{a=1,\ldots,8} \lambda^a_{\underline{1}} \sigma_{\underline{1}} \cdot \lambda^a_{\underline{2}} \sigma_{\underline{2}} \qquad (5)$$

where C is proportional to the gluon coupling α_s, and depends on the overlap of the quark wave-function with the potential. We can estimate the value of C by calculating mass differences between N and Δ, or π and ρ, for example, in terms of (5). This gives C a value of about 20 MeV between ordinary quarks n and p, consistently from several different estimations. [9] The mass splittings between diquark spin states are then trivially given by diagonalising (5), explicitly:

$$-8C, \quad \tfrac{8}{3}C, \quad 4C, \quad -\tfrac{4}{3}C \qquad (6)$$

for the diquarks in (2) respectively. Hence, the mass splitting between diquoniums of the same family and the same value of L is entirely calculable.

To estimate the dependence of diquonium masses on the orbital angular momentum L requires a more explicit model for confinement. At present the only model capable of doing so is the MIT bag model. Within that framework, Johnson and Thorn [11] have studied the problem of high L states in general.

They showed that for high L a hadron bag becomes elongated, taking on the shape of a long thin tube. The quarks inside aggregate at either end of the tube and are held together by colour flux lines confined inside the tube, as illustrated in Fig. 3. Asymptotically, the Regge trajectory becomes linear, namely,

$$L = \alpha' M^2 \tag{7}$$

The slope α' is shown to depend only on the total colour charge x of the quark aggregates at either end, explicitly:

$$\alpha'_x \propto 1/\sqrt{\mathcal{C}}_x \tag{8}$$

where $\mathcal{C}_x$ is the value of the quadratic Casimir operator for the colour x. One sees then that for T-diquonium with x = 3, the Regge slope α' is asymptotically the same as that for ordinary meson and baryon trajectories, whereas for M-diquonium, we have

$$\alpha'_6 = \sqrt{\mathcal{C}_s/\mathcal{C}_s}\ \alpha'_3 = \sqrt{\frac{2}{5}}\ \alpha'_3 \tag{9}$$

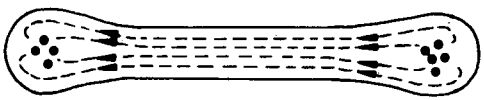

FIGURE 3: Bag model of high spin state

Assuming that the trajectories are linear even for small L values as apparently they are for ordinary meson and baryon trajectories, we have then determined the spectrum of T- and M-diquonium each up to only one parameter, namely the effective intercepts of the trajectories. These last parameters are not easy to estimate theoretically but may be fitted phenomenologically to identified baryonium states. The spectra for diquoniums containing only n,p quarks corresponding to one particular choice of intercepts are shown in Fig. 4.

II.2 Their Decay

The angular momentum barrier argument mentioned above applies to both "T" and "M"-diquoniums and suggests that both families have suppressed decays into meson channels. Their decays into baryon-antibaryon pairs however are governed by very different mechanisms. The decay of "T"-diquonium into $B\bar{B}$ can be effected by cutting a colour 3 bag and creating one $q\bar{q}$ pair to seal

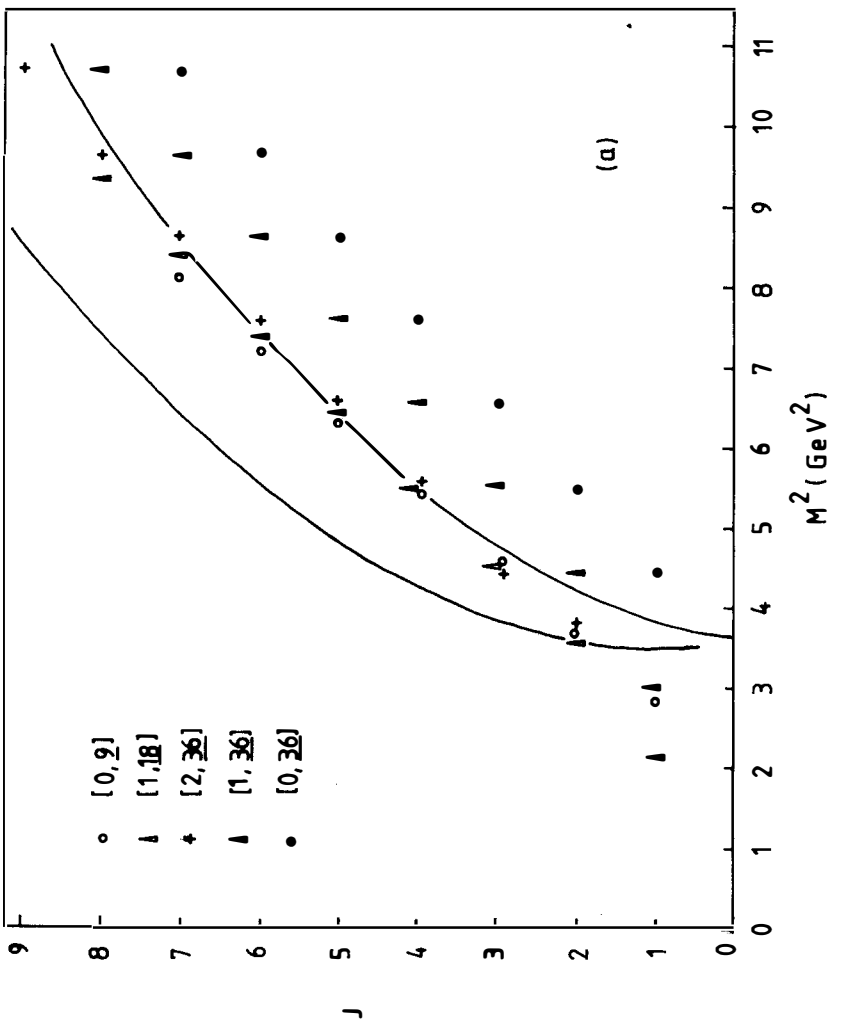

FIGURE 4 (a): T-diquonium spectrum

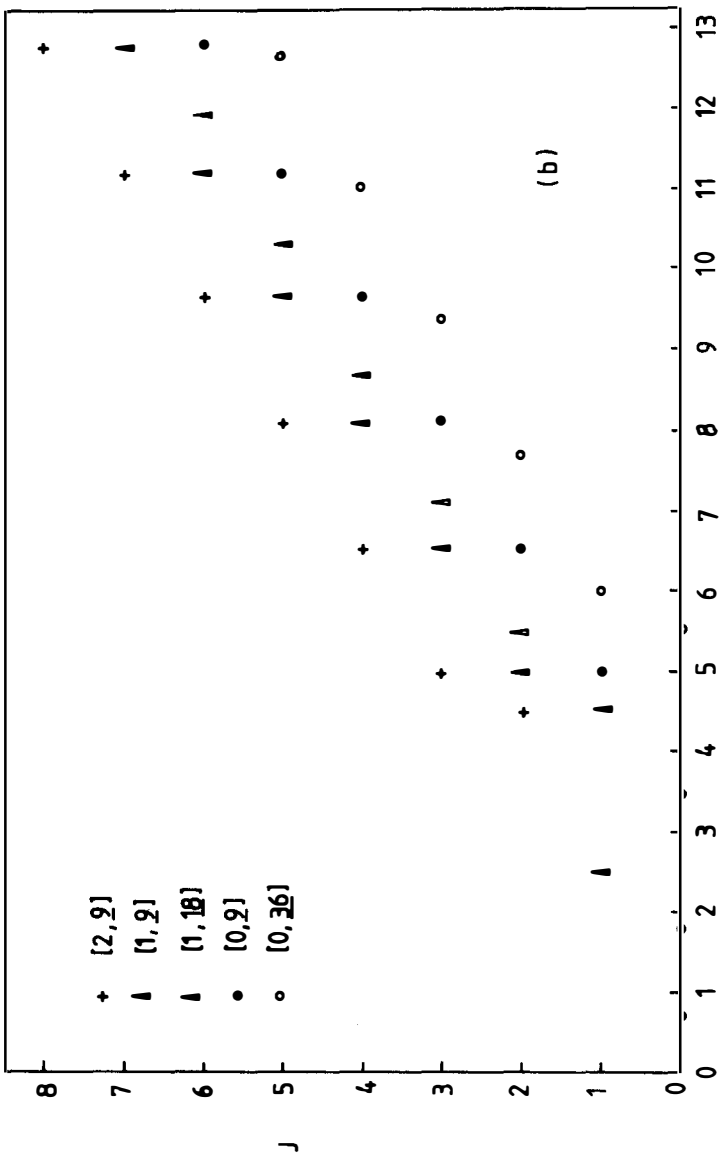

FIGURE 4 (b): M-diquonium spectrum

off the exposed colour lines, as illustrated in Fig. 5(a). This being similar to ordinary hadronic decays such as $N^* \to N$ in Fig. 6 one expects T-diquoniums to have normal widths, say $\Gamma \sim 100$ MeV, for masses around 2 - 3 GeV. On the other hand, the same mechanism is not available to M-diquonium since to neutralise a colour 6 flux, at least two $q\bar{q}$ pairs have to be created. As illustrated in Fig. 5(b), the result is then not a $B\bar{B}$ pair as for T-diquonium, but two new "M"-diquoniums. Besides, since two quark pairs have to be created, such a decay mode is expected to be suppressed in any case at high resonance masses. In order to decay into a $B\bar{B}$ pair, an M-diquonium has to undergo some gymnastics, either by annihilating or exchanging quarks as for mesonic decays, or, more profitably, by first mixing with T-diquonium. Since this mixing is small for $L > 0$, the coupling of M-diquonium to $B\bar{B}$ is suppressed: [7]

$$\Gamma(\text{"M"} \to B\bar{B}) \sim \tan^2\theta \times \Gamma(\text{"T"} \to B\bar{B})$$
$$\lesssim .04 \times 100 \text{ MeV} \sim 4 \text{ MeV!} \qquad (10)$$

One sees therefore that M-diquoniums decay into $B\bar{B}$ essentially only by default of the other modes.

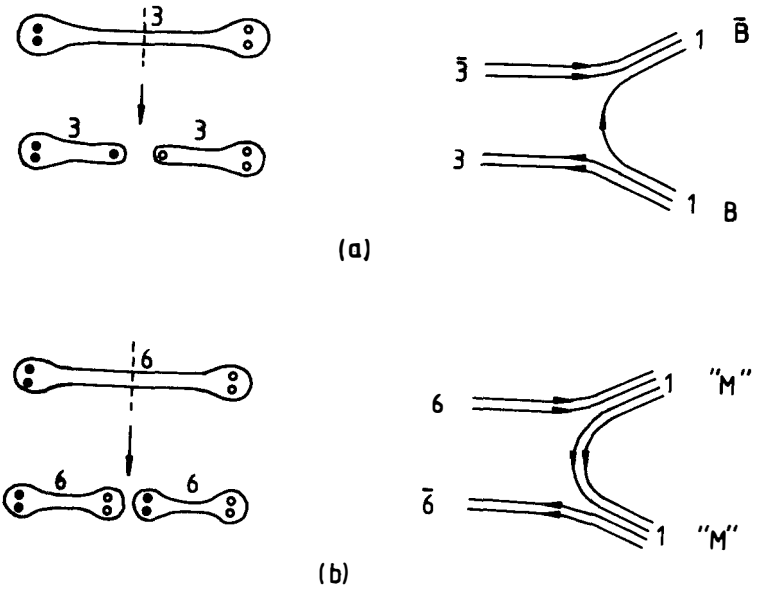

FIGURE 5: Decays of diquoniums by fission

A more likely mode for M-diquonium decay is a cascade via meson emission into a resonance of the same type, [7] as illustrated in Fig. 7. Even this, however, is considerably more difficult than a normal cascade of an ordinary $q\bar{q}$ meson or qqq baryon. [12] These latter decays can be effected simply by lopping off a small section of a colour 3 tube creating one quark pair as illustrated in Fig. 6. The same straightforward cascade is again not available to an

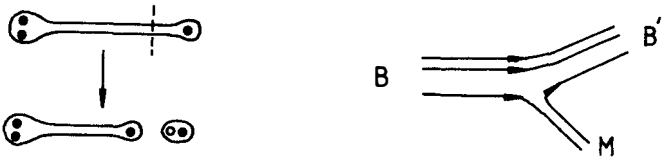

FIGURE 6: Decay of ordinary qqq baryon

M-diquonium. The outcome is that one expects an M-diquonium to be narrow in general, and a T-diquonium to be broad. The situation would be qualitatively very similar to what is seen in experiment as indicated in (B) above.

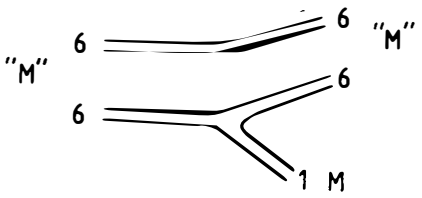

FIGURE 7: Cascade decay of M-diquonium

The cascade patterns of M-diquoniums if known can be a very useful signature for their identification. Now it has long been realised that cascade decays of resonances on leading Regge trajectories are mainly governed by kinematics, [13)14)15)] because of the scarcity of final states available, they are highly constrained by the angular momentum barrier, preferring those channels in which a light particle (π-meson) is emitted leaving a product resonance whose angular momentum J' and mass M' are such that the difference from the decaying states $\Delta J = J - J'$ is small and $\Delta M = M - M'$ is large. One sees therefore that it is much easier for a resonance on a low-lying Regge

trajectory to cascade to a resonance on a high-lying one than the other way round. For example, in Fig. 4, one expects bigger widths for the cascade:

$$(1,3,\underline{18}) \rightarrow (1,5,\underline{9}) + \pi \qquad (11)$$

than for

$$(1,5,\underline{9}) \rightarrow (1,3,\underline{18}) + \pi \qquad (12)$$

Moreover, using the existing(mainly kinematical) models in the literature for cascade decays [14)15)], one can even estimate their relative rates, and hence predict the general decay pattern of various M-diquoniums. Such a study has been done and suggests, for example, that the most prominent final states for resonances on the $(1,5,\underline{9})$ and $(1,3,\underline{18})$ trajectories are: [9)]

$$(1,5,\underline{9}) \rightarrow B\bar{B} \qquad (13)$$

$$(1,3,\underline{18}) \rightarrow B\bar{B}\pi \qquad (14)$$

Predictions like these, though only qualitative, can be very useful for the experimental identification of M-diquonium.

II.3 Production

Since T-diquoniums are strongly coupled to the $B\bar{B}$ channel they are most easily found in formation experiments in $N\bar{N}$ collisions. Indeed, most of the likely candidates existing for T-diquoniums, such as S(1.936), T(2.150), U(2.310) and V(2.48) are so discovered. [1)] Since the resonances are in general broad and the spectrum rich, detailed experiments capable of a full amplitude analysis are usually required for their identification. By a judicial selection of the final state, one can select out certain states in the spectrum for study. A good example is provided in this meeting by Tony Carter's analysis [16)] of the reaction $p\bar{p} \rightarrow K^+K^-$ to be reported later in this session.

M-diquoniums, on the other hand, are supposed to have suppressed couplings to $B\bar{B}$ and will therefore give only weak signals in similar formation experiments. Indeed, sicne their couplings to mesons are suppressed also, it may be questioned how they can even be observed. Notice however that this suppression in couplings is due not to any selection rule but, we believe, only to angular momentum barrier effects. Thus, for example, the colour mixing between T- and M-diquoniums though very small at high L, becomes so large for L = 0 that it no longer makes sense to distinguish the two families. Imagine now that we produce a diquonium state via the exchange of a $qq\bar{q}\bar{q}$ trajectory, as illustrated in Fig. 8. The exchanged reggeon at $t < 0$ has a component with L = 0 between the diquarks for whcih colour is interchangeable. It appears

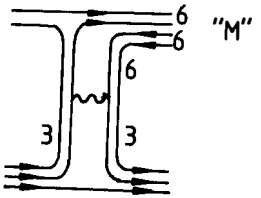

FIGURE 8: Production of M-diquonium

therefore that M-diquoniums would be as easily produced in this case as are T-diquoniums. [7)9)] The situation here is quite similar to the more familiar case of J/ψ , which decays into hadrons with a width of only $\sim$ keV, yet couples sufficiently strongly in scattering to normal hadrons to yield a $\sigma_T(J/\psi\ p)$ of $\sim$ mb. This phenomenon was readily explained in dual unitarisation by the mass dependence of the mixing angle between the $c\bar{c}$ and $q\bar{q}$ systems, which, though sizeable in the scattering region for $t = m^2 < 0$, becomes very small on the resonance mass-shell when $t = m^2_{J/\psi} > 0$. [17)]

This interpretation, if correct, gives yet another valuable signature for identifying M-diquoniums - they can be easily produced but not so easily formed. It may be significant, therefore, that all the narrow baryoniums reported experimentally (except S near threshold) have been found only in production. Among these, the states at 2.020 and 2.204 are known to have formation cross sections in elastic scattering of $<$ .3 mb as compared with 4-7 mb for T-diquonium candidates such as S(1.936), T(2.15) and U(2.31). [1)]

Of course, the production of diquonium states need not always proceed via $qq\bar{q}\bar{q}$ exchange as indicated in Fig. 8, otherwise the cross section would be very small at high energy. They can be produced as well by baryon exchange, and in some cases even diffractivley through the mixing between the Pomeron and the $qq\bar{q}\bar{q}$ trajectories. Also, diquoniums need not always be produced directly in the 'ground' state where the two quarks in a diquark and in a relative s-wave. If an excited level is produced where the two quarks are in a p-wave, say, it will quickly de-excite, emitting a pion, for example, and drop down to one of the 'ground' states we have been considering. The inclusive cross section for producing M-diquonium could thus be in the range of $\sim$ 1 μb, and be readily observable in the present generation of track chamber experiments. [9)]

The phenomenology of diquonium resonances based on these premises is already quite developed [8)9)18)] and its comparison with experiment reasonably encouraging. Some of the results will be discussed later, I hope, by Holstein Høgaasen and Bob Jaffe.

The weakest link in the whole theoretical structure is probably its reliance at certain points on the MIT bag model. Previously, some attempts have been made by Rossi and Veneziano [5)] to understand the confinement of multiquark states in terms of a topological expansion of QCD, somewhat analogous to 't Hooft's $1/N_c$ expansion. The result is closely related to a naive string picture in which the strings themselves do not interact. There is then no possibility of obtaining a stable configuration corresponding to M-diquoniums. [12)] These considerations are extended again recently by Konishi and Hansson [19)] to include such configurations. Unfortuantely all these QCD models are amenable to calculations at present only in 2-dimensions and are therefore unlikely to yield concrete phenomenological results in the near future.

III. Discussion

We have considered two interpretations of baryonium states as respectively 'nuclear' and 'colour' molecules. Off-hand, there seems no reason why the two types cannot exist side by side. As matters stand at present, there is room enough for both in the experimental spectrum. It is then up to the theoreticians to refine their predictions so as to identify their favourite states if and when they are finally observed.

Though perhaps equally uncertain, the two interpretations carry with them different bonuses. The discovery of a nuclear molecule would be moderately interesting. It would confirm our belief that we know something about nucleon-nucleon forces at long and medium range and teach us something about annihilation at short distances. We may then proceed to analyse similar systems such as the possible $D^{*-}\bar{D}^{*}$ nuclear molecule corresponding to the peak in R at 4.028 seen in e^+e^- annihilation. [20)]

The discovery of T^- and M-diquoniums, on the other hand, would have implications of a different magnitude. It would establish colour as a new degree of freedom, enhance our hope for quantum chromodynamics, and open up a whole new dimension in hadron spectroscopy.

Indeed, if the picture I described in the last section is correct, it is obvious that diquoniums are but special cases of a large class of metastable colour molecules. The following are some immediate generalisations: $(q\bar{q})\overset{8}{\text{---}}(q\bar{q})$, $(q\bar{q})\overset{8}{\text{---}}(qqq)$, $(qq)\overset{3,6}{\text{---}}(qq\bar{q})$, $(qqq)\overset{8,10}{\text{---}}(qqq)$, etc, some of which will be considered later by Halstein Høgaasen and Masataka Fukugita. They share the common property of having two quark aggregates of non-zero charge (i.e. non-colour-singlets) linked together by tubes of colour flux which neutralise their colours. They are therefore vaguely similar to an electrical-chemical system such as $Na^{+}\text{---}Cl^{-}$ in which two charged ions are linked by an electrovalent band, and may conveniently be described by borrowing some of the chemists' concepts and terminology. By analogy then, let us call our coloured quark aggregates 'ions', and the colour flux tubes linking them 'chromovalent' bonds. Because of the different group structure, however, 'chromovalent' bonds can be of several types and have very different properties from their electrical counterparts. For example, they cannot break except by the creation of quark-antiquark pairs and are expected to increase in stability for increasing length. Neutral atoms do not form 'chromovalent' bonds with one another but they may still be bonded by e.g. 'Van der Waals' forces, to form molecules. This then is the interpretation in our present language of the deuteron and of Vinh Mau's baryoniums, if they exist.

Now, in ordinary chemistry, one has the experience that much would be known about a molecule once one knows the properties of its component bonds and ions. A great simplification of concept is thereby attained by reducing the study of a multitude of molecules to that of a much smaller number of ions and of bonds. It seems likely that in colour chemistry also a similar simplification is possible. At present, we have only a very crude knowledge of chromovalent bonds and of coloured ions, but one can well imagine that, as in ordinary chemistry, one may design experiments and theoretical calculations specifically to measure their properties. By compiling then a list [21] of bonds and ions, we should be able to construct molecules to our own specifications and to predict their general properties from those of their components. One need not be restricted only to the 'diatomic' molecules so far considered. One may attempt, for example, to construct analogues for the long linear chain or something similar to the benzene ring as indicated in Fig. 9. Many of these molecules will have very bizarre properties. Apart from serving as sensitive probes for testing colour dynamics, it is amusing to imagine that one day in the far distant future they might even serve some practical purpose.

FIGURE 9: Examples of complex colour molecules

I am deeply grateful to Tran Thanh Vanh for inviting me to this meeting which has been both instructive and enjoyable.

REFERENCES

1. For a comprehensive review on the experimental situation see L. Montanet, paper presented at this meeting. See also L. Montanet, CERN preprint EP/Phys 77-22 (1977).
2. M. Vinh Mau, paper presented at this meeting.
3. F. Myhrer, CERN preprint TH.2348 (1977).
4. M. Imachi, S. Otsuki and F. Toyoda, Prog. Theoret. Phys. 57 (1977) 517.
5. G. C. Rossi and G. Veneziano, Nucl. Phys. B123 (1977) 507.
6. R. L. Jaffe, MIT preprint CTP. No. 657 (1977).
7. Chan Hong-Mo and H. Høgaasen, Phys. Letters 72B (1977) 121.
8. R. L. Jaffe, MIT preprint CTP. No. 657 (1977).
9. Chan Hong-Mo and H. Høgaasen, Rutherford Lab. preprint RL-77-144/A (1977), to be published in Nucl. Phys. B.
10. A. De Rujula, H. Georgi and S. L. Glashow, Phys. Rev. D12 (1975) 147.
11. K. Johnson and C. Thorn, Phys. Rev. D13 (1976) 1934.
12. Chan Hong-Mo and H. Høgaasen, Phys. Letters 72B (1978) 400.
13. H. Goldberg, Phys. Rev. Letters 21 (1968) 21.
14. Chan Hong-Mo and Tsou Sheung Tsun, Phys. Rev. D4 (1971) 156.
15. Frank von Hippel and C. Quigg, Phys. Rev. D5 (1972) 624.
16. A. A. Carter, paper presented at this meeting and Rutherford Lab. preprint RL-78-032 (1978).
17. See e.g. Chan Hong-Mo and Tsou Sheung Tsun, Rutherford Lab. preprint RL-76-080 (1976), to appear in Proceedings of the Bielefeld Summer Institute (1976) NATO Advanced Institute Series.
18. Tsou Sheung Tsun, Oxford Mathematical Institute preprint, February (1978) to be published in Nucl. Phys. B.
19. T. H. Hansson and K. Konishi, Rutherford Lab. preprint RL-78-021 (1978).
20. A. De Rujula, H. Georgi and S. L. Glashow, Phys. Rev. Letters.
21. Chan Hong-Mo, M. Fukugita, T. H. Hansson, H. J. Hoffman, K. Konishi, H. Høgaasen and Tsou Sheung Tsun, Rutherford Lab. preprint RL-78-027 (1978).

THE NEW SPECTROSCOPY IN THE BAG MODEL

R. L. Jaffe*
Center for Theoretical Physics
Laboratory for Nuclear Science and Department of Physics
Massachusetts Institute of Technology
Cambridge, Massachusetts USA 02139

ABSTRACT

Unconventional hadrons are reviewed. The two quark-two antiquark states which are expected to be prominent in the low energy meson-meson S-wave and in baryon antibaryon annihilation are discussed in detail.

RÉSUMÉ

On revoit les hadrons non-conventionels. On discute en détail les états à deux quarks et deux antiquarks qui devraient être importants dans les ondes S méson-méson à basse énergie et dans l'annihilation baryon antibaryon.

*A.P. Sloan Foundation Fellow

We are all familiar with the success of the quark model in the realm of meson and baryon spectroscopy.[1] Quark and antiquark make a meson. Three quarks make a baryon. This simple scheme has received striking confirmation with the discovery of the charmonium system, charmed mesons and perhaps charmed baryons.[2] The next few years promise to bring an extension of this spectroscopy to the T and its brethren reported by the Columbia-Stony Brook-Fermilab group.[3]

I am going to refer to all of this as "Q spectroscopy". We have a fair idea of what to expect from $Q\bar{Q}$ and Q^3 systems, based on phenomenological adaptations of QCD such as potential models[4] and the bag.[5]

However QCD seems to promise a much richer spectrum than has yet been observed. There are at least three major spectroscopic families beyond mesons and baryons to be expected in simple models.[6] First are multiquark states: color singlet hadrons made of more than three quarks or antiquarks. Some of these have exotic quantum numbers, but others (crypto-exotics) may masquerade as ordinary $Q\bar{Q}$ mesons or Q^3 baryons. Second are hadrons containing gluons either exclusively ("glueballs") or in conjunction with quarks. Third are so-called Type II exotics: mesons with J^{PC} not accessible to non-relativistic $Q\bar{Q}$ systems (0^{--} and 0^{+-}, 1^{-+}, 2^{+-}, etc.) or baryons with certain peculiar SU(6) quantum numbers. Type II exotics may be found among the hadrons of the first two families or may have an independent origin. A fourth family — liberated quarks and gluons — with an extraordinarily rich spectrum — will be present if confinement is not perfect.

Among the states of this new spectroscopy the ones most accessible to experiment appear to be the multiquark states. Glueballs and gluon-quark combinations do not have distinctive signatures.[7] Type II exotic mesons, if they exist, have the nasty habit of decaying only into rather complicated multi-meson final states.[8] Multiquark states have the twin virtues of clear signature: some possess exotic quantum numbers, other have conventional quantum numbers but peculiar decay patterns; and prominence: they appear to be very important in S-wave meson-meson scattering and may generate strong and/or narrow resonances in the baryon-antibaryon system. In light of this I will spend the remainder of my talk discussing multiquark hadrons and in particular the mesons constructed of two-quarks and two-antiquarks.

The aim of these studies is to look for tests of QCD. To appreciate the possibilities notice that $Q^2\bar{Q}^2$ is the least complicated system with any freedom in its internal color wavefunction. There is only one color singlet $Q\bar{Q}$-wavefunction. Likewise there is only one color singlet baryon (Q^3) wavefunction. Although two quarks could be either symmetric or antisymmetric in color:

$$\underline{3} \otimes \underline{3} = \bar{\underline{3}} \oplus \underline{6} \tag{1}$$

(the $\bar{\underline{3}}$ is antisymmetric; the $\underline{6}$ symmetric) only the antisymmetric state can combine with the third quark to give a color singlet[12]

$$\underline{6} \otimes \underline{3} = \underline{8} \oplus \underline{10} \tag{2}$$

$$\bar{\underline{3}} \otimes \underline{3} = \underline{1} \oplus \underline{8} \tag{3}$$

$Q^2\bar{Q}^2$ is richer. According to Eq. (1) the two quarks may be coupled either to a $\bar{\underline{3}}$ or $\underline{6}$. Likewise the two antiquarks may be coupled to either a $\underline{3}$ or $\bar{\underline{6}}$. From these, two singlets may be constructed: one from the $\bar{\underline{3}}$ and $\underline{3}$ according to Eq. (2); the other from the $\underline{6}$ and $\bar{\underline{6}}$ according to the Clebsch-Gordon series:

$$\underline{6} \otimes \bar{\underline{6}} = \underline{1} \oplus \underline{8} \oplus \underline{27} \tag{4}$$

Many of the distinctive signatures expected of the $Q^2\bar{Q}^2$ system can be traced to the existence of two types of color singlets. Finding these would argue strongly for color and QCD.

Historically $Q^2\bar{Q}^2$ mesons have been an embarrassment for quark models and dual models alike. The first modern discussion (*ie* cognizant of color) of multiquark states was given by Nambu in 1966.[13] He pointed out that Coulomb-like color forces, proportional to $\underset{\sim}{\lambda}_i \cdot \underset{\sim}{\lambda}_j$ (λ_i are the 8 color-SU(3) matrices of the ith quark), saturate with the formation of singlets. So color-singlet mesons and baryons do not attract each other with strong confining forces. [We shall shortly see that this is only half the story.] In 1968 Rosner[14] realized $Q^2\bar{Q}^2$-resonances posed a problem for duality. According to

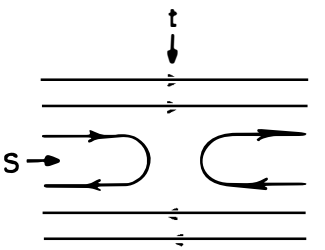

$Q^2\bar{Q}^2$ resonances in S-channel, dual to $Q\bar{Q}$ exchange in the t-channel.

the duality diagram on the last page, $Q^2\bar{Q}^2$ configurations should produce the prominent resonances in $B\bar{B}$ elastic scattering, dual to ordinary meson exchange. This led to the expectation of exotics at relatively low mass.[14,15] Experimentalists were unable to find any and the situation remained confused for many years.

Times have changed. We now have a theory of interquark forces: QCD; and several models for the way color-interactions bind quarks to form hadrons. We also have more reasons to believe in quarks and perhaps more courage to face up to former embarrassments. In the bag model the $Q^2\bar{Q}^2$ system is not qualitatively different from $Q\bar{Q}$ and Q^3 hadrons. Approximations developed to study the $Q\bar{Q}$ and Q^3 sectors can be applied to the $Q^2\bar{Q}^2$ sector with few if any additional parameters. There are two limits in which the bag model is known to simplify: at low angular momentum, where hadrons are roughly spherical; and at high angular momentum for deformed hadrons on the leading Regge trajectory. I propose to discuss the $Q^2\bar{Q}^2$ system in these limits.

I. Spherical $Q^2\bar{Q}^2$ States: Color-magnetism and the Meson-Meson S-wave

A. The Spectrum

The generators of color SU(3) annihilate the singlet:

$$\Lambda^a|\underline{1}\rangle \equiv (\sum_j \lambda_j^a - \sum_k \lambda_k^{*a})|\underline{1}\rangle = 0 \qquad (5)$$

($\lambda_j^a(-\lambda_k^{a*})$ are the 8 color matrices of the quarks (antiquarks)). This is the origin of Nambu's remark that color singlets do not attract with confining forces. However, to lowest order in QCD two color singlet mesons can exchange a transverse gluon becoming color octets, which may then bind strongly. The overall color state remains, of course, a singlet. The coupling is proportional to the product of each quark's spin and color matrices which, in general, does not annihilate a color singlet. This is the van der Waals force of QCD. It is expected to be short range. In fact, in the bag model it operates only when the quarks are all in the same bag. In the non-relativistic limit this would be a magnetic force be-

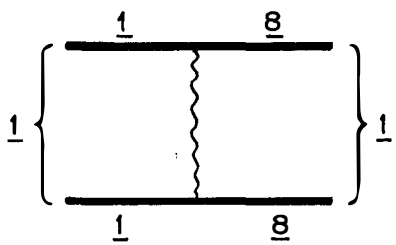

tween quarks hence "color magnetism".

Color magnetism accounts for the major SU(6) violations among ordinary S-wave[16] mesons and baryons.[4,5] It splits the ρ from the π, the Δ from the nucleon and the Σ from the Λ, all in the right direction and by roughly the right amount. What does color magnetism do in the $Q^2\bar{Q}^2$ sector? Remarkably, it elevates the masses of states with exotic quantum numbers and lowers the masses of some cryptoexotics,[17,18] which may in part explain the experimental absence of low mass exotics. This result is more general than the bag model in which it was discovered. It follows from the color and spin tensor structure of the lowest order color magnetic interaction between quarks. Since the derivation has been given several times in the literature,[19] I won't repeat it here.

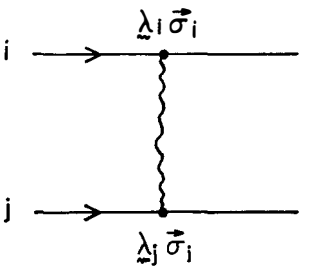

Color Magnetic Interaction between Quarks i and j

The ground state of $Q^2\bar{Q}^2$ turns out[6] to be a flavor-SU(3) nonet with $J^{PC}=0^{++}$. The quark content of the nonet is shown in Figure 1. The masses and decay couplings in the limit of no OZI-violation are illustrated schematically in Figure 2. Notice the unusual patterns. In the $Q\bar{Q}$ sector we expect a degenerate isovector and isoscalar (eg., ρ and ω or f and A_2), degenerate because they contain only ordinary (u and d) quarks. An $s\bar{s}$ isosinglet lies at a heavier mass (eg. ϕ or f') and betrays its quark content by its anomalous coupling to $K\bar{K}$. In contrast the $Q^2\bar{Q}^2$ nonet has a lighter, isolated isosinglet ($u\bar{u}d\bar{d}$) which does not couple to $K\bar{K}$. The degenerate isosinglet and isovector contain a hidden $s\bar{s}$ pair. Consequently the second isosinglet couples anomalously to $K\bar{K}$.

The 0^{++} mesons have always been a problem for the quark model. In 1974 Morgan made a heroic attempt to gather the ε, S*, δ and κ into a nonet.[20] The fit was awkward. It requires large and OZI violating singlet-octet mixing, accidental degeneracies and ignores threshold enhancements in $(\pi\pi)^{I=0}$ and $(\pi K)^{I=\frac{1}{2}}$ S-waves. I believe a case can be made for classifying the light 0^{++} mesons as (predominantly) a $Q^2\bar{Q}^2$ nonet. Since the case for this may be found in the

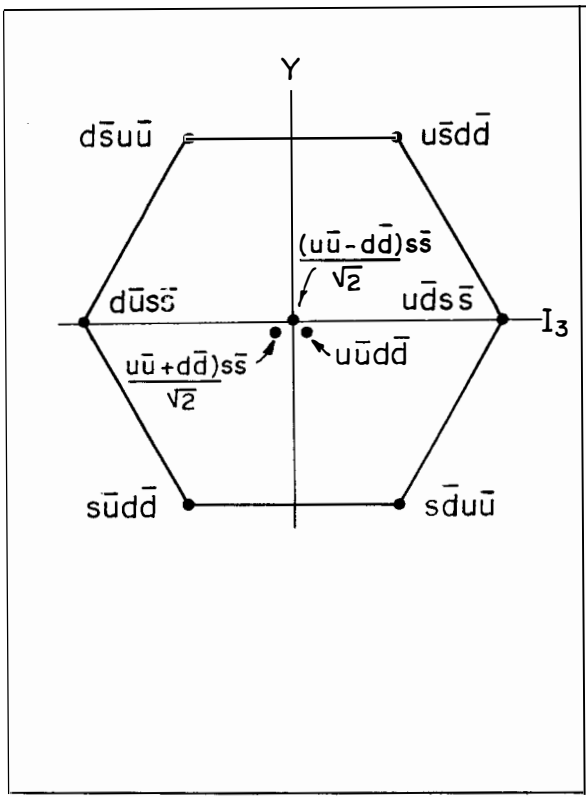

Figure 1: SU(3)-flavor weight diagram and quark content for $Q^2\bar{Q}^2$ nonet.

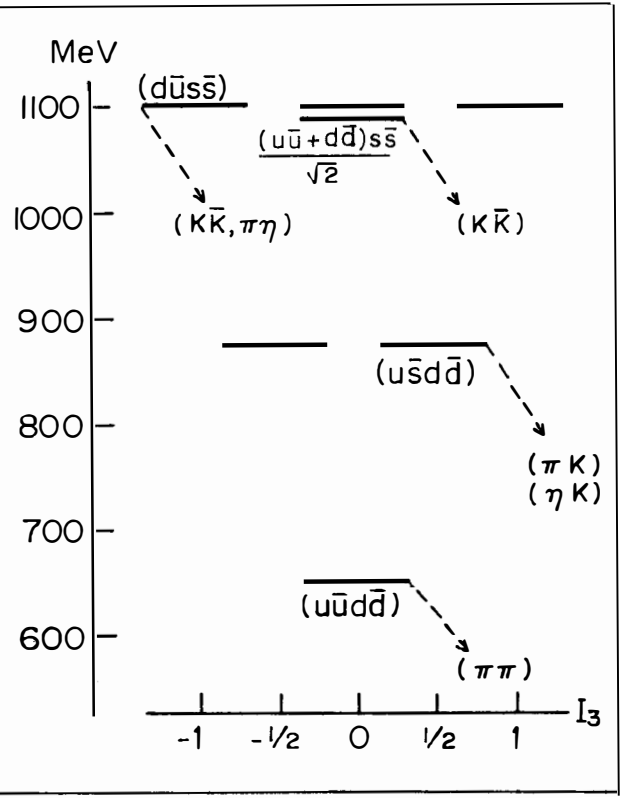

Figure 2: Masses and OZI allowed decays of 0^{++} $Q^2\bar{Q}^2$ meson nonet in the bag model.

literature[17] I won't repeat it here.

If the light 0^{++} mesons are $Q^2\bar{Q}^2$ states, where are the $[Q\bar{Q}]^{0^{++}}_{L=1}$ states? Presumably heavier. A fundamental prediction of this scheme is the presence of more 0^{++} mesons: At least one other nonet — for the $[Q\bar{Q}]^{0^{++}}_{L=1}$ states — and perhaps more $Q^2\bar{Q}^2$ multiplets (to say nothing of $Q\bar{Q}G$ and so forth). The other known L=1 $Q\bar{Q}$ states (eg. the 2^{++} mesons) have masses ranging upward from about 1200 MeV. At these energies we must expect additional 0^{++} states. These are likely to mix with the lowest $Q^2\bar{Q}^2$ states, breaking degeneracies and foiling selection rules. However the basic observation remains: there should be (at least) two of everything.

Alan Martin discusses the possibility of two nonets of 0^{++} mesons in detail in his contribution to these proceedings,[21] so I will be brief. The most exciting new development is the recent evidence for a second isovector 0^{++} state at about 1270 MeV. The "first" isovector, the $\delta(980)$, is one of the best substantiated scalar mesons. For several years there has been evidence for some resonant S-wave behavior near 1300 MeV in $K^o_s K^o_s$ and K^+K^-.[22,23] The isospin has been controversial. Recent University of Geneva data[24] on $\pi^- p \to K^- K^o_s p$ at 10 GeV/c shows an S-wave enhancement at 1270 MeV[25] in $K^- K^o_s$ (which is uniquely isovector). Perhaps one of these two isovectors is the first of the long sought $Q^2\bar{Q}^2$ mesons. A speculative identification of both scalar nonets is given in the Table below.

Isospin	Name (Mass)	Two 0^{++} Nonets? Couplings—Comments*	Predominant Quark Content
0	$\varepsilon(700)$	broad; $\pi\pi >> K\bar{K}$, $\delta<90°$	$u\bar{d}d\bar{u}$
0	$S^*(993)^+$	narrow; $K\bar{K} >> \pi\pi$	$1/\sqrt{2}\ s\bar{s}(u\bar{u}+d\bar{d})$
1	$\delta(980)^+$	medium; $K\bar{K}, \pi\eta$; nearly degenerate with S^*	$u\bar{d}s\bar{s}$
½	$\kappa(800\text{-}1100)$	broad; πK, $\delta<60°$	$u\bar{s}d\bar{d}$
0	$\varepsilon'(1300)^+$	medium; $\pi\pi$	$1/\sqrt{2}\ (u\bar{u}+d\bar{d})$
0	$S'^*(?)$	?	$s\bar{s}$
1	$\delta'(1270)^+$	medium; $K\bar{K}$	$u\bar{d}$
½	$\kappa'(1400)^+$	medium; $K\pi$	$u\bar{s}$

\+ Rather well established
* Including channels in which it's seen

Notice that I have associated $Q^2\bar{Q}^2$ states with broad, non-resonant enhancements in the $\pi\pi$ and πK S-waves. Otherwise there would be insufficient structure (in say the $\pi\pi$ S-wave) to accommodate 3 reso-

nances: the $\varepsilon(700)$, $S^*(993)$ and $\varepsilon'(1300)$.

It has always been thought that quark states should show up as conventional resonances in partial wave analyses. This is not at all clear for multiquark states. In the limit that quark pair creation is "turned off" $Q\bar{Q}$ and Q^3 resonances like the ρ, A_2 and Δ become stable (poles on the real axis). They then move continuously off into the complex plane as pair creation is turned on.

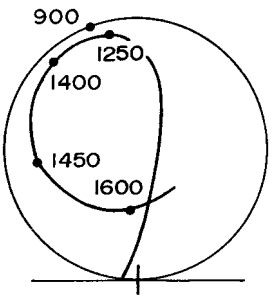

I=0 S-wave $\pi\pi$-Amplitude

There is no similar limit for $Q^2\bar{Q}^2$ resonances. They must be considered intrinsically as phenomena in the open $Q\bar{Q}$–$Q\bar{Q}$ channels to which they couple. Recently Francis Low and I have undertaken to study $Q^2\bar{Q}^2$ bag "states"in this manner. We find that $Q^2\bar{Q}^2$ (and other multiquark) bag configurations need not be manifest as conventional resonances in meson-meson phase shifts.[26] I will give a brief account of this work.

B. Dynamics

We[26] consider bag states as approximate eigenstates of a quark colored-gluon Hamiltonian subject to boundary conditions. In the spherical cavity approximation[27] the boundary condition amounts to the requirement that the density of hadronic matter vanish outside of a sphere of radius R.[28] Consider $Q\bar{Q}$ and Q^3 states and suppress pair creation. Because confinement prevents quarks from separating the spectrum calculated with a boundary condition approximates the physical spectrum. In contrast try the same approach to the non-relativistic dynamics of a point proton and neutron whose interactions are finite range. Eigenstates subject to the boundary condition that the wavefunction vanish outside some separation b are not directly related to the actual spectrum of bound and continuum states of the p-n system.

In the $Q^2\bar{Q}^2$ system two types of $Q\bar{Q}$–$Q\bar{Q}$ channels are present: color $\underline{8}$–$\underline{8}$ in which the forces are long-range and confining, and color $\underline{1}$–$\underline{1}$ in which the forces are short-range and do not confine. The bag calculation imposes the same boundary condition in all chan-

nels. This is a poor approximation to the actual wavefunction in the unconfined channels. However this approach has the advantage that treating all channels similarly, the internal (QCD) dynamics can be separated from the external meson-meson scattering states.

The situation is reminiscent of Wigner's R-matrix approach to S-wave resonances of the compound nucleus.[29,30] Wigner idealized particle-nucleus scattering by taking the compound nucleus to be a region of radius b outside which no interaction takes place. He observed that at resonance the slope of the external wavefunction vanishes at r=b:[31]

$$\frac{d}{dr}\,(r\psi(r))\Big|_{r=b} = 0 \tag{6}$$

and parameterized the exterior scattering wavefunction as follows:

$$\psi_{ij}(r,E) \propto -\frac{\delta_{ij}}{r}\,\sin k_j(r-b) + \frac{R_{ij}(E)}{k_j r}\,\cos k_j(r-b) \tag{7}$$

Here i and j label external channels ($k_j \equiv \sqrt{2\mu_j E}$, μ_j being the reduced mass in channel j). Then Eq. (6) will be satisfied when $R_{ij}(E)$ has a pole. From R(E) it is possible to obtain the S-matrix:

$$S = e^{-ikb}\,\frac{1+i\sqrt{k}R\sqrt{k}}{1-i\sqrt{k}R\sqrt{k}}\,e^{-ikb} \tag{8}$$

The advantage of this approach is that R depends only on the dynamics <u>inside</u> r=b. For example, poles in R occur at energies $\{E_n\}$ which are solutions to the interior Hamiltonian problem

$$H\psi_n = E_n\psi_n \qquad r<b$$

$$d/dr[r\Psi_n(r)] = 0 \qquad r=b \tag{9}$$

H describes the dynamics inside r=b. This finesses the difficult dynamical question of how the projectile and nucleus couple to the compound nuclear states.

The bag provides a different set of information. Inside the bag, quarks and gluons are the dynamical variables. The amplitude associated with the $Q\bar{Q}$–$Q\bar{Q}$ relative separation vanishes outside some radius b which is related to the bag radius R. We interpret the eigenenergies of the spherical bag calculation as the energies $\{E_n\}$ for which the meson-meson wavefunction vanishes at some radius, b. Imitating Wigner we parameterize the exterior scattering wave in the

meson-meson center of mass by

$$r\,\psi_{ij}(r,E) \propto k_j \delta_{ij} \cos k_j(r-b) + P_{ij}(E) \sin k_j(r-b) \qquad (10)$$

Therefore the bag calculations yield the energies of poles in the real symmetric matrix $P_{ij}(E)$. It is also possible to extract information about the pole residues from the bag model calculation.[26] From $P_{ij}(E)$ we construct the S-matrix:

$$S = -e^{-ikb} \frac{1 - i\frac{1}{\sqrt{k}} P \frac{1}{\sqrt{k}}}{1 + i\frac{1}{\sqrt{k}} P \frac{1}{\sqrt{k}}} e^{-ikb} \qquad (11)$$

Low and I have studied some of the formal properties of the P-matrix and have attempted to fit the S-wave (pseudoscalar) meson-meson phase shifts in this manner.[26] We find that broad non-resonant enhancements are expected of this dynamics when $Q^2\bar{Q}^2$ bag states are near but above dominant decay thresholds (as is the case in $(\pi\pi)^{I=0}$ and $(\pi K)^{I=\frac{1}{2}}$). We find narrow resonances when $Q^2\bar{Q}^2$ bag states are at or below dominant decay thresholds (as is the case in $(KK)^{I=0,1}$). And finally we find slowly falling negative phase shifts followed by enhancements in channels where the lowest $Q^2\bar{Q}^2$ states are far above dominant thresholds. Remembering that exotic $Q^2\bar{Q}^2$ configurations are made heavier by color-magnetic interactions it is apparent that they fall into this last category. This work is still in progress and will be more fully reported elsewhere.[26]

II. High Angular Momentum $Q^2\bar{Q}^2$ States: Color and Baryonium

The Harari Rosner diagram for baryon-antibaryon — reproduced here with some color indices added — serves to emphasize the special role of $Q^2\bar{Q}^2$ resonances in the baryon-antibaryon system. For many years the failure to find exotic mesons discouraged attempts to use the quark model to classify $B\bar{B}$ resonances. Meanwhile potential models[32] and dual models[33] of the $B\bar{B}$ system were developed. The bag model and color magnetic forces now provide some understanding of the absence of low

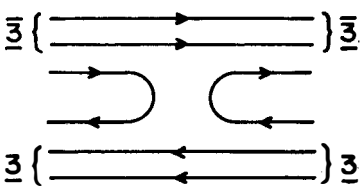

mass exotics. Also Johnson and Thorn[34] have developed a semi-quantitative model of high angular momentum states of arbitrary (color singlet) collections of colored quanta. It is now possible to begin enumerating the $Q^2\bar{Q}^2$ states (their quantum numbers, masses and partial widths) expected to couple to baryon antibaryon channels. First steps in this program were taken last summer by myself[35] and by Chan and Høgaason.[36] I will spend the remainder of my time describing the qualitative features of this work.

The lightest $Q^2\bar{Q}^2$ states are at about 1 GeV. By $B\bar{B}$ threshold we are already dealing with a complex system with lots of internal excitation energy. An arbitrary $Q^2\bar{Q}^2$ state bears no particular relation to the $B\bar{B}$ system. If, however, the diquark (Q^2) and antidiquark ($\bar{Q}^2$) are separated by an angular momentum barrier then this barrier inhibits decay into purely mesonic states. Such a configuration may decay into baryon-antibaryon or by meson cascade to a similar state.

Johnson and Thorn[34] showed that the bag states shown at right lie on linear Regge trajectories whose slope may be calculated in terms of the color representation of the quanta at either end:

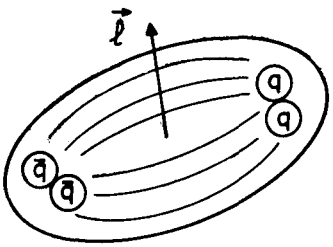

$Q^2\bar{Q}^2$ state on Leading Regge Trajectory

$$\frac{1}{2\pi\alpha'} = \sqrt{8\pi\alpha_c B C^2} \qquad (12)$$

Here B is the bag constant ($B^{1/4}$=145 MeV) and α_c is the QCD fine structure constant (α_c=.55). C^2 is the quadratic Casimir operator of the color representation on either end of the elongated bag. For meson ($Q\bar{Q}$) and baryon (Q^3) trajectories the color configuration is always $\bar{3}$–3 (ie. color anti-triplet on one end, color triplet on the other). In this case C^2=16/3 and α'=.9 GeV^{-2}. Two color configuraations occur among the $Q^2\bar{Q}^2$ states which couple to $B\bar{B}$: $\bar{3}$–3 and 6–$\bar{6}$. The former have ordinary Regge slopes (α'=.9 GeV^{-2}), while the latter lie on trajectories with anomalous slope: α' (6–$\bar{6}$)=.56 GeV^{-2}. This was first pointed out by Johnson and Thorn.

Any pair of quarks in a baryon are always in a color $\bar{3}$ (See Eqs. (2) and (3)). It is tempting to argue from this that the $\bar{3}$–3

$Q^2\bar{Q}^2$ states couple strongly to $B\bar{B}$ while the color $\underline{6}$–$\bar{\underline{6}}$ $Q^2\bar{Q}^2$ states do not. This is an important conjecture. Much of the systematic classification of Refs. 35 and 36 rests on it. Assuming this, the $\underline{6}$–$\bar{\underline{6}}$ states would likely be anomously narrow[35,36] since they have only cascade meson emission available.[36] These would be the first examples of a new class of hadrons which are stable because of their internal color structure. To borrow from nuclear physics we might call them "color-isomers". A catalogue of $\underline{6}$–$\bar{\underline{6}}$ $Q^2\bar{Q}^2$ states may be found in Ref. 36. The $\bar{\underline{3}}$–$\underline{3}$ $Q^2\bar{Q}^2$ states are enumerated in Ref. 35.

Why should the $\underline{6}$–$\bar{\underline{6}}$ $Q^2\bar{Q}^2$ states decouple from baryon-antibaryon? The argument rests on the way color forces are thought to fall off with distance. In the bag model only the color-electric monopole ("Coulomb") force remains constant independent of distance. All spin dependent and color-flip[37] forces fall with separation of color sources just like in free space.[38] In the picture of Johnson and Thorn, as a hadron elongates forces which flip color or spin die off. At large J the color and spin of the quarks on either end of the cigar-shaped hadron are good quantum numbers. There is some evidence for this effect in the meson spectrum.[36]

Suppose we accept that at high-J the $\underline{6}$–$\bar{\underline{6}}$ $Q^2\bar{Q}^2$ states have little admixture of $\bar{\underline{3}}$–$\underline{3}$. The selection rule ($\underline{6}$–$\underline{6}$)$\not\to B\bar{B}$ requires in addition that the Q^2 or $\bar{Q}^2$ color is not flipped during the decay. A typical color flip decay which violates the selection rule is shown at right. It is possible that the rapid fall off of color-flip forces with distance suppresses these decays. But I know of no model calculation to support the conjecture and therefore have no estimate of the minimum angular momentum above which these decays are suppressed. So the selection rule $\underline{6}$–$\bar{\underline{6}}\not\to B\bar{B}$ is still on shaky ground.

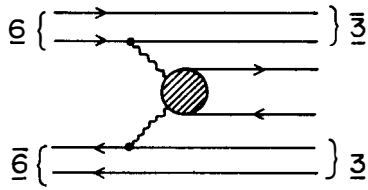

In fact this type of selection rule is already well known in the quark model. Long ago Micu[39] proposed that $Q\bar{Q}$-pairs created or destroyed in a quark-line diagram carry vacuum quantum numbers and have no effect on the pre-existing quarks and anti-quarks. The selection rule we have been discussing is a special case of this. The arguments put forth to justify the special case (e.g. color, spin

and flavor flip forces fall rapidly with distance) would also suffice to derive the more general rule. This rule has been independently rediscovered by several groups[40] and is known in the literature under several names: QPC-model (for quark pair creation), $^3P_0$-model (for the non-relativistic quark configuration required for vacuum (0^{++}) quantum numbers), and so forth. The model has been successful in describing ordinary baryon and meson decays.

I mention the QPC-model because of its implications for the quark model treatment of $B\bar{B}$ systems. It leads to some remarkable selection rules.[35] If these selection rules were violated it would be very hard to understand why $\underline{6}$–$\bar{\underline{6}}$ $Q^2\bar{Q}^2$ should not decay to $B\bar{B}$. This would forbid a specific color flip matrix element while allowing various other color, spin and flavor information to be transferred from the created pair to the pre-existing quarks. The most striking selection rules are $L=\ell\pm1$ and $s-1\leq S\leq s+1$ where $\ell(L)$ and $s(S)$ are the orbital and spin angular momentum of the $Q^2\bar{Q}^2$ ($B\bar{B}$) system.

These selection rules can already help us classify states. Consider, for example, the series of resonances seen by Carter et al.[41] in the reaction $N\bar{N}\to\pi^+\pi^-$. These must be coupled to the $N\bar{N}$ spin triplet with $J=L\pm1$. Carter et al.[41] find $J=L-1$ predominates. These resonances coincide with the familiar elastic $N\bar{N}$ resonances known as the T and U mésons. It is tempting to put them on the "leading" $Q^2\bar{Q}^2$ trajectory, the one with $J=\ell+2$. In fact this was proposed in Ref. 36. However this violates a QPC selection rule since $L=\ell+3$. Instead we must look for a trajectory with $J=\ell$. Not by chance the QPC predicts $J=\ell$ trajectories to be very strongly coupled to the $J=L-1$ channel of $N\bar{N}$. In any event the assignment of Carter et al.'s resonances to a $J=\ell+2$ trajectory is inconsistent with the usual argument[36] used to rule out $\underline{6}$–$\bar{\underline{6}}\to B\bar{B}$.

In addition to selection rules the QPC model also yields quantitative information about which $Q^2\bar{Q}^2$ states couple to which $B\bar{B}$ channels. A casual glance at Refs. 35 and 36 is depressing. There are a myriad of $Q^2\bar{Q}^2$ trajectories. Other things being equal the experimentalist would appear to be lost in a sea of overlapping resonances. According to QPC calculations,[35] however, only a handful of $Q^2\bar{Q}^2$ trajectories are expected to couple strongly to $N\bar{N}$. These may be prominent elastic $N\bar{N}$ resonances. Of the remainder only the potentially narrow $\underline{6}$–$\bar{\underline{6}}$ states seem interesting.

The QPC model is very crude. It allows us to hope that the $\underline{6}$–$\bar{\underline{6}}$ states will be narrow and that the $\bar{\underline{3}}$–$\underline{3}$ states can be sorted out.

What is really needed here is what neither the quark model nor duality has ever provided: a dynamical theory of resonance production (and decay) in terms of quark degrees of freedom.

Acknowledgements

The work described in Section IB of this talk was developed in collaboration with Francis Low. I have also benefitted from conversations with Chan Hong Mo, Carleton DeTar, Hallstein Høgaasen, Alan Martin, David Morgan, Viki Weisskopf. I would also like to thank Tran Thanh Van for making this conference possible.

References

1) See, for example, J.L. Rosner, Physics Reports 11C, 189 (1974).
2) For a review, see lectures by G. Feldman and J.D. Jackson in Proceedings of the Summer Institute on Particle Physics, 1976 SLAC Report, No 198, November 1976, M.C. Zipf editor.
3) S.W. Herb et al., Phys. Rev. Letters 39, 752 (1977); see also the talk by L.D. Lederman in these proceedings.
4) A. DeRujula, H. Georgi and S.L. Glashow, Phys. Rev. D12, 147 (1975).
5) T.A. DeGrand, R.L. Jaffe, K. Johnson and J. Kiskis, Phys. Rev. D12, 2060 (1975).
6) R.L. Jaffe and K. Johnson, Phys. Letters 60B, 201 (1976).
7) For a review see D. Robson, Nucl. Physics B130, 328 (1977).
8) Among mesons the clearest signature I know of is $J^{PC}I^{G}=1^{-+}1^{-}$ decaying into $\pi\eta$ in a P-wave. Next most attractive is $0^{--}1^{+}$ decaying to $\pi\omega$ also in a P-wave. Among baryons, Type-II exotics are a subject of theoretical debate. The non-relativistic quark model predicts that the first negative parity baryons form an SU(6)×O(3) $[70]_{L=1}$. Relativistic models predict a $[56]_{L=1}$ nearby.[9] In non-relativistic models a negative parity [56] occurs only at the third oscillator level. Recently Cutkowski et al.[10] gave argued for the presence of a $\Delta(5/2^{-})$ resonance at 1960 MeV. The $\Delta(5/2^{-})$ is unique in that it occurs in the $[56]_{L=1}$ but not in the $[70]_{L=1}$. This could be taken as evidence for a Type II exotic. However Dalitz, Horgan and Reinders[11] have argued a mass of 1960 MeV is not too low for a state with three oscillator quanta in their model.
9) C. Rebbi, Phys. Rev. D14, 2362 (1976).
10) R. Cutkowski et al. in Proceedings of the Topical Conference on Baryon Resonances, Oxford, 1976 (Rutherford Lab., Didcot, 1976) ed. by R.T. Ross and D.H. Larson.
11) R.H. Dalitz, R.P. Horgan and L.J. Reinders, Journal of Physics G, Nuclear Physics 3, L195 (1977).
12) Color serves merely as a label in which to antisymmetrize the Q^3 wavefunction.
13) Y. Nambu, in Preludes in Theoretical Physics, ed. by A.deShalit, H. Feshbach and L. van Hove (North Holland, Amsterdam, 1966).
14) J.L. Rosner, Phys. Letters 21, 950, 1422 (1968).
15) H.J. Lipkin, Nucl. Phys. B9, 349 (1969); Phys. Letters 32B, 301 (1970).
16) By "S-wave" I mean states in which all quarks occupy the low-

est bag eigenmode with $J^P=\frac{1}{2}^+$. Semiclassically these bag states are spherical. They comprise the 0^- and 1^- meson nonets and the $\frac{1}{2}^+$ octet and $3/2^+$ decuplet of baryons.
17) R.L. Jaffe, Phys. Rev. D15, 267, 281 (1977).
18) Cryptoexotics are defined to be states of more than three quarks and/or antiquarks with non-exotic flavor quantum numbers.
19) See, for example, R.L. Jaffe "Extraordinary Hadrons" in Quark Spectroscopy and Hadron Dynamics, Proceedings of the 1977 SLAC Summer Institute on Particle Physics, M. Zipf ed. (SLAC-REPORT 204, 1977).
20) D. Morgan, Phys. Lett. 51B, 71 (1974).
21) A. Martin, Durham University preprint, April 1978, "Do Multiquark States Exist among the 0^{++} Mesons", published in these proceedings.
22) N.M Cason, et al., Phys. Rev.Letters 36, 1485 (1976).
23) A.J. Pawlicki et al., Phys. Rev. D15, 3196 (1977).
24) R. Baldi, et al. University of Geneva Preprint, to be published in Nuclear Physics B.
25) A.D. Martin et al., CERN preprint "A Study of Isopsin 1 Meson States", January 1978.
26) R.L. Jaffe and F.E. Low, in preparation.
27) A. Chodos, R.L. Jaffe, K. Johnson, C.B. Thorn, Phys. Rev. D10, 2594 (1974).
28) R is determined so that no energy or momentum flows across the surface of the sphere.
29) E.P. Wigner, Proc. Natl. Acad. Sci., 32, 302 (1946); Phys. Rev. 70, 15, 606 (1946); E.P. Wigner and L. Eisenbud , Phys. Rev. 72, 29 (1947).
30) For a review see J.M. Blatt and V.F. Weisskopf, Theoretical Nuclear Physics (J.M. Wiley and Sons, New York, 1952).
31) One is always faced with the question of how to define resonance. When Eq. (6) is satisfied the phase shift at r=b is $\pi/2$ so $\delta=\pi/2-kb$. For compound nuclear excitations $kb<<1$ and δ is about $\pi/2$. The important thing here is that the boundary condition (Eq. (6))separates the interior problem from the exterior.
32) I.S. Shapiro, Sov. Phys. Usp. 16, 173 (1973); L.N. Bogdanova, O.D. Dalkarov and I.S. Shapiro in Proceedings of the 4th International Symposium on NN̄ Interactions, Syracuse 1975; W.N. Cottingham, M. Lacombe, B. Loiseau, J.M. Richard and R. Vinh Mau, Phys. Rev. D8, 800 (1973); Phys. Letters 44B, 1 (1973); M. Lacombe, B. Loiseau, J.M. Richard, R. Vinh Mau, P. Pires and R. de Tourreil, Phys. Rev. D12, 1495 (1975); For a review with further references see C.B. Dover, in Proceedings of the 4th International Symposium on NN̄ Interactions, Syracuse (1975).
33) C. Rosenzweig, Phys. Rev. Letters 36, 697 (1976); for a review of previous work see G. Chew in Proceedings of the 3rd European Symposium on NN̄ Interactions, Stockhom, 1976, ed. by G. Ekspong and S. Nilsson; see also G.C. Rossi and G. Veneziano, Nuclear Physics B123, 507 (1977) and M. Pennington, CERN Preprint Th-2457-CERN (1978).
34) K. Johnson and C.B. Thorn, Phys. Rev. D13, 1934 (1976).
35) R.L. Jaffe, Phys. Rev. D17, 1444 (1978).
36) Chan H.-M. and H. Høgaasen, Phys. Letters 72B, 121 (1977); Rutherford Laboratory preprint RL-77-121/A (October 1977).
37) By color-flip forces in the $Q^2\bar{Q}^2$ sector I mean (for example) those which induce a transition from $\bar{3}$ to the 6 configuration for Q^2.

38) Bag boundary conditions (See Ref. 5) forbid isolated color charges. Higher multipoles, both electric and magnetic are not grossly modified by the bag boundary conditions. The forces between separated localized color (electric or magnetic) dipoles, quadrupoles etc. fall with the same power of distance as in free space.
39) L. Micu, Nuclear Physics B10, 521 (1969).
40) For references and a review see J.L. Rosner, Ref. 1.
41) A.A. Carter et al., Phys. Letters 67B, 117 (1977).

BARYONIUM AS BARYON ANTIBARYON BOUND STATES AND RESONANCES

R. VINH MAU
Division de Physique Théorique[+], Institut de Physique Nucléaire
91406 ORSAY Cedex-France

and

Laboratoire de Physique Théorique des Particules Elémentaires,
Université Pierre et Marie Curie, 75230 Paris Cedex 05

Abstract : A brief review of the general properties of the nucleon-antinucleon interaction and their relationships with better known hadronic processes is given. Difficulties connected with the large annihilation cross section and the existence of narrow resonances are discussed and a possible remedy proposed.

Résumé : Les propriétés générales de l'interaction nucléon-antinucléon et leurs relations avec des systèmes hadroniques mieux connus sont passées en revue. Les difficultés dues à l'existence des états de largeur étroite et à la grande section efficace d'annihilation expérimentalement observée sont discutées et une solution possible proposée.

[+]Laboratoire associé au C.N.R.S.

In this talk, I would like to review some aspects of baryonium related to what is referred to by H.M. Chan as "nuclear molecules". Those aspects can be somehow considered as complementary to the $qq\bar{q}\bar{q}$ aspects described at this meeting by H.M. Chan and R.L. Jaffe. As a matter of fact, if a strict analogy with the well known positronium is to be retained, the name baryonium rather suggests the following definition :

baryonium $\equiv$ baryon-antibaryon ($\bar{N}N$, $\bar{N}\Delta$, $\bar{\Delta}\Delta$ etc...) bound states or resonances

This definition implies the assumption that the subhadronic constituent degrees of freedom are frozen but as a counterpart, one ought to deal with realistic baryon-antibaryon forces and therefore with real nuclear forces.

At present, most of the experimental information refer to the nucleon-antinucleon sector. I shall therefore limit myself to this sector and from what I just said, a careful study of the nucleon-antinucleon interaction and its relationship with real nucleon nucleon forces is to be made

As far as the experimental situation is concerned, we are now getting used to the narrow bound states and resonant states which have been abundantly discussed during the last few months (Cf., for example, L. Montanet talk at this meeting). However, I wish to recall that, besides these bound and resonant states, there exist also more ancient experimental results on the $N\bar{N}$ scattering and annihilation into ordinary mesons, one proeminent result is that $\sigma_{annih.}/\sigma_{elast.} \sim 1.5 - 2$ for a rather wide energy range. This feature has been puzzling in the past, it could be even more puzzling in the light of the newly discovered narrow states and any realistic theoretical model should be able to cope with all those results (i.e. strong annihilation cross section and narrow resonances).

General properties of the NN and $N\bar{N}$ interactions

The unitary condition in the t channel is

$$\mathrm{Im}\langle \bar{n}_1 n_2 | T | p_1 \bar{p}_2 \rangle = \sum_{\alpha} \langle \bar{n}_1 n_2 | T^+ | \alpha \rangle \langle \alpha | T | p_1 \bar{p}_2 \rangle$$

for the NN interaction and

$$\mathrm{Im}\langle n_1 \bar{n}_2 | T | p_1 \bar{p}_2 \rangle = \sum_{\beta} \langle n_1 \bar{n}_2 | T^+ | \beta \rangle \langle \beta | T | p_1 \bar{p}_2 \rangle$$

for the $N\bar{N}$ interaction.

The s channels are defined as $p_1+n_1 \to p_2+n_2$ for the NN case and as $p_1+\bar{n}_1 \to p_2+\bar{n}_2$ in the $N\bar{N}$ case.

These relations can be expressed diagrammatically as :

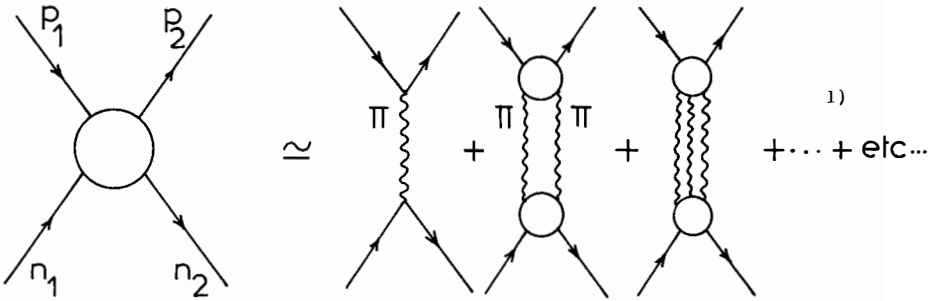

1)

for the NN interaction and

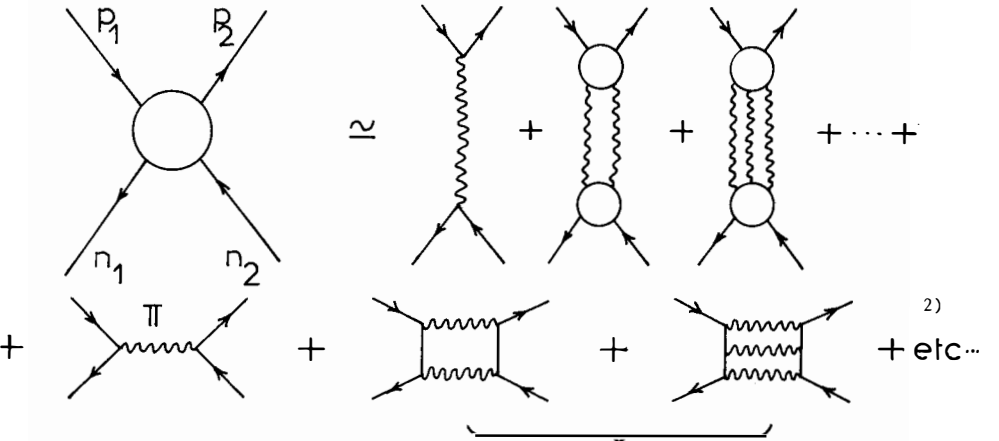

2)

for the $N\bar{N}$ interaction.

These conditions give us the absorptive part of the NN and $N\bar{N}$ interactions from which one gets the interactions themselves via dispersion relations.

Also, from the same unitarity conditions one can see that, in addition to the "scattering graphs" which exist in both NN and $N\bar{N}$ cases, the $N\bar{N}$ case contains "annihilation graphs". Therefore, the $N\bar{N}$ interaction or potential can be expressed as :

$$V_{N\bar{N}} = U_{N\bar{N}} + iW_{N\bar{N}}$$

where $U_{N\bar{N}}$ refers to the scattering part and $W_{N\bar{N}}$ to the annihilation part of a complex potential $V_{N\bar{N}}$. This complex potential is endowed with the following two properties :

1) $U_{N\bar{N}} = G\, U_{NN}$

where G refers to the G parity of the intermediate state occuring in the scattering graphs of relation 2). For example G = - 1 for the π , G = + 1 for two pions, etc.... This G parity rule connects the $N\bar{N}$ scattering part $U_{N\bar{N}}$ to the NN potential U_{NN}.

2) $U_{N\bar{N}}$ has a much longer range ($\frac{1}{m_\pi}$, $\frac{1}{2m_\pi}$, etc...) than $W_{N\bar{N}}$,the range of which is at most $\frac{1}{2m}$ = 0.10 fm.

These two general properties can be proved quite rigorously but are also apparent from the unitarity relation 2). They are very important theoretical guiding principles and should be always kept in mind. The G parity rule connects the $N\bar{N}$ forces to the NN forces, however, it can be applied only to the situation where the NN forces are due to particle exchanges and it is unapplicable to the purely phenomenological NN interactions. We shall accordingly consider only the particle exchange NN potentials which fit well all relevant nuclear data.

Particle exchange NN potentials

1) The One Boson Exchange (OBE) Potentials

The simplest particle exchange model to the NN forces is the one boson exchange model due to the exchange of the π,ρ,ω,σ, etc... mesons considered as stable particles. This model has been studied extensively by various groups and the different versions come from different values for the coupling constants. One defect

of the OBE potentials is that some of the exchange mesons are not physical, the low mass scalar and isoscalar σ meson needed is rather fictitious since the corresponding observed resonance is broad and has a rather high mass. We shall consider the Bryan-Scott version [1] which yields, via the G parity rule, the Bryan-Phillips [2] $N\bar{N}$ potential.

2) Particle Exchange Potentials derived from dispersion relation dynamics

In this approach, the long range forces are due to the one pion exchange which is well known and well established, the next longest range forces are due to the two pion exchange. This two pion exchange contribution has been carefully calculated[3] from the πN scattering amplitude and the $\pi\pi$ interaction via analyticity, unitarity and crossing properties of the S matrix. In this way, effects of the $\pi\pi$ S and P wave resonances (ε and ρ mesons) as well as nucleonic resonances (Δ_{33}, P_{11}, etc...) are automatically and realistically taken into account. Adding to this the ω exchange contribution as part of the three pion exchange one gets the ($\pi + 2\pi + \omega$) exchange potential -the Paris potential- which has been shown to give a good description of the long and medium range (LR and MR) part of the NN forces (internucleon distances $r \gtrsim 0.8$ fm).

One can note that if the following approximations are made, namely, effects of the nucleonic resonances are ignored (their contributions are actually significant), the $\pi\pi$ S and P wave resonances are treated in the zero width approximation, one recovers the OBE models.

In fig.1, we display, for comparison, the central component of the ($\pi + 2\pi + \omega$) exchange Paris $N\bar{N}$ potential denoted by U^P and the One Boson exchange $N\bar{N}$ potential considered by Bryan and Phillips denoted by U^{BP}. As it can be seen, the attraction is weaker in the Paris potential than in the Bryan Phillips potential. The reason is that in the NN case this OBE model needs a strong ω exchange repulsion ($g_\omega^2/4\pi = 23.7$) to partly

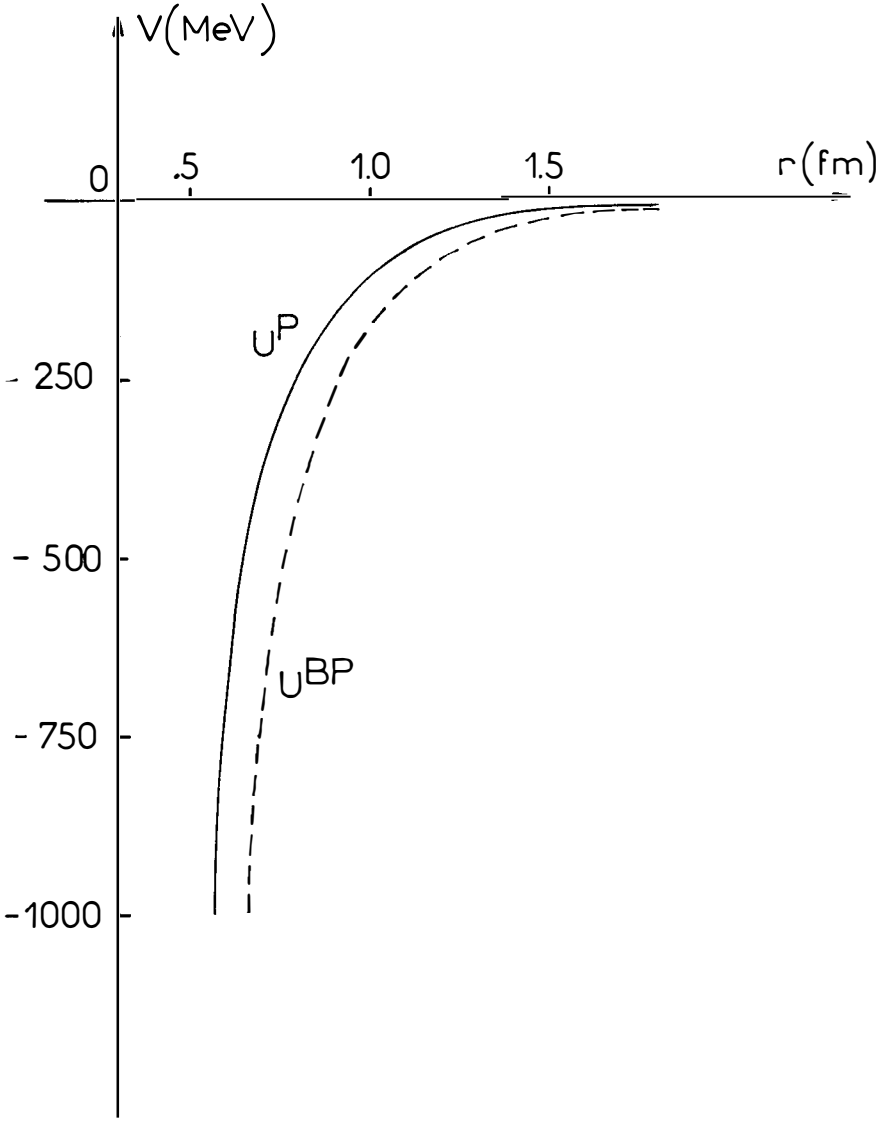

Fig.1 - The I = 1 central component of the $N\bar{N}$ potentials. The solid curve represents the Paris potential U^P and the dashed curve the Bryan-Phillips potential U^{BP}.

compensate for the σ exchange attraction. In the Paris potential, one does not need such a strong ω coupling ($g_\omega^2/4\pi$ is only 9.5).

$N\bar{N}$ Bound States and Resonances

In the early calculations [4], attempts were made to reproduce, from the OBE potentials, the ordinary mesons like π,ρ,ω,σ etc... as levels of the $N\bar{N}$ spectrum. This bootstrap viewpoint has several drawbacks, the main one being that binding energies are very large so that the potential concept might be dubious. We do not consider this viewpoint but instead the one which was introduced first by I.S. Shapiro and collaborators [5]. According to this view, one expects the existence of quasinuclear (deuteron like) $N\bar{N}$ states where the nucleon and antinucleon are separated by distances $\sim$ 1 fm, large compared with the range of the annihilation interaction.

Since the $(\pi + 2\pi + \omega)$ exchange potential U_{NN} provides a good description of the LR + MR nucleon nucleon forces ($r \geq 0.8$ fm) and since the annihilation potential $W_{N\bar{N}}$ is very short ranged, we expects the corresponding $U_{N\bar{N}}$ potential to be a reliable for distances $r \geq 0.8$ fm. This means that our attention should be directed to the bound states and resonances lying near threshold $2m = 1878$ MeV and having high angular momentum values. It is then expected that the masses of the bound states and resonances of this type are mostly due to the LR + MR part of the interaction and remain unaffected by the annihilation component of the interaction.

For illustration, we show in Table I the results obtained with the simple prescription [6] :

$$V_{N\bar{N}}(r) = \begin{cases} U^P(r) & \text{for} \quad r > r_c \\ U^P(r_c) & \text{for} \quad r \leq r_c \end{cases} \qquad \text{with } 0.6 \text{ fm} < r_c < 0.8 \text{ fm}$$

Table I

The C.M.S. energies (with respect to threshold) in MeV for the $N\bar{N}$ bound states and resonances calculated with $r_c = 0.7$ fm. The notation is $(^{2I+1,2S+1}L_J)$.

$^{31}S_0$	- 262	$^{13}P_0$ (n=0)	< - 800
		(n=1)	- 102
$^{31}P_1$	- 55	$^{13}S_1$-$^{13}D_1$(n=0)	< - 800
$^{33}P_1$	- 116	$^{13}S_1$-$^{13}D_1$(n=1)	- 39
$^{33}S_1$-$^{33}D_1$	- 202	$^{13}P_2$-$^{13}F_2$(n=0)	- 788
$^{31}D_2$	165	$^{13}D_3$-$^{13}G_3$	- 457
$^{33}D_2$	85	$^{13}F_4$-$^{13}H_4$	- 89
$^{33}F_3$	> 200	$^{13}G_5$-$^{13}I_5$	307

It is amazing to notice, in passing, that for $r_c = 0.675$ fm one gets the following states

$^{33}D_2$ at m = 1933 MeV

$^{31}D_2$ at m = 1993 MeV

$^{11}P_1$ at m = 1787 MeV

which can be compared with the experimental ones at 1932 MeV, 2000 MeV, 1794 MeV.

The calculations also show that

i) tensor forces are very important, not only because of their diagonal matrix elements but also because of their non diagonal ones especially in the isospin I = 0 states.

ii) the results are quantitatively sensitive to variations of the core parameter r_c, however these variations do not alter the spectroscopic order of the levels.

The annihilation potential

At present, there exists no theoretical model for the annihilation interaction. Long ago, in order to fit the cross sections, Bryan and Phillips chose a phenomenological Woods-Saxon form

$$W_{N\bar{N}} = - G/(1+ e^{r/r_a})$$

Although the range parameter r_a was chosen such that W is short ranged (r_a = 0.17 fm), they need values of G $\sim$(20-65 GeV) to fit the cross sections. This makes the effects of $W_{N\bar{N}}$ important even at large distances (several hundred MeV at 1 fm) and therefore all partial waves are affected. It was found [7] recently, that such an absorption destroys the resonances and bound states produced by the real part of the potential. However, for distances as small as 0.1-0.2 fm, there is no reason to believe that the interaction is local and energy independent. One would rather expect a state dependent (energy and angular momentum dependent) absorptive potential $W_{N\bar{N}}(\ell,E;r)$. It may be then possible to reconcile large annihilation cross sections with narrow resonances by assuming for example, $W(\ell,E;r)$ to be large for $\ell < \ell_{min}$ and small for $\ell > \ell_{min}$ so that it absorbs mainly the low partial waves and only slightly the higher waves leaving still room for narrow bound states and resonances. A first approximation towards such a model is provided by annihilation graphs of the type shown in fig.2 where, remembering that annihilation into 4 pions is dominant, one keeps only as intermediate states the 4 pion states approximated themselves by the ρ-ε, ε-ε, ρ-ρ ones. Clearly, the absorptive potential arising from these diagrams are energy and angular momentum dependent. Work along this

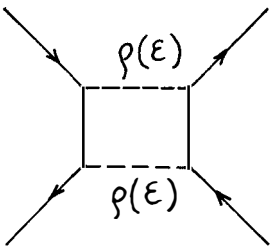

Fig.2

line is currently under progress [8]. Of course, in this model, the bound states and resonances will have high angular momentum values (say $L > 2$). However, it should be pointed out that all existing models of baryonium (bag, dual, QCD or $B\bar{B}$ models) possess this common feature. This is not surprising since the arguments leading to the narrow widths, even though they are formulated very differently in different models, are ultimately related to centrifugal barrier effects.

Exotic states

It is sometimes argued that in contrast with the quasi-nuclear $N\bar{N}$ model the $qq\bar{q}\bar{q}$ model can predict exotic states with high isospin values ($I > 2$), a feature which would provide a definite way to decide between the two approaches. However, at higher energies the $N\bar{N}$ system can be coupled to $\Delta\bar{N}$ and $\Delta\bar{\Delta}$ systems, the thresholds of which being respectively $m + m_\Delta = 2200$ MeV and $2m_\Delta = 2700$ MeV. Of course, such a coupling gives rise to higher spin and higher isospin states.

Concluding remarks

In this talk, I have tried to show the intimate connections between the $N\bar{N}$ system and the NN, πN and $\pi\pi$ systems. Our knowledge on these latter systems is now sufficiently accurate to provide a good understanding for the long and intermediate range $N\bar{N}$ forces. The problem still remains unsolved for the annihilation forces. In any case, an ultimate subhadronic "theory" should meet most of the properties described here.

I wish to express many thanks to M. Lacombe and J.M. Richard with whom most of the work described here has been done.

References

1) R.A. Bryan and B.L. Scott, Phys. Rev. 177 (1968) 1435.

2) R.A. Bryan and R.J.M. Phillips, Nucl. Phys. B5 (1968) 201.

3) W.N. Cottingham, M. Lacombe, B. Loiseau, J.M. Richard and R. Vinh Mau, Phys. Rev. D8 (1973) 800.
For a review, see "the Paris NN potential" by R. Vinh Mau, to appear in "Mesons and Nuclei" edited by D. Wilkinson and M. Rho - North-Holland Editors.

4) See for example J.S. Ball, A. Scotti and D.Y. Wong, Phys. Rev. 142 (1966) 1000.

5) See for example, L.M. Bogdanova, O.D. Dalkarov and I.S. Shapiro, Ann. Phys. 84 (1974) 261.

6) J.M. Richard, M. Lacombe and R. Vinh Mau, Phys. Lett. 64B (1976) 121.

7) F. Myhrer and A. Thomas, Phys. Lett. 64B (1976) 59 ;
F. Myhrer and A. Gersten, Nuovo Cimento 37A (1977) 21 ;
O.D. Dalkarov and F. Myhrer, CERN preprint TH-2280 (1977).

8) B. Moussalam, M. Lacombe, J.M. Richard and R.Vinh Mau, in preparation.

EXPERIMENTAL REVIEW ON BARYOMIUM CANDIDATES

L. Montanet
CERN, Geneva, Switzerland

Abstract: Experimental evidences for baryon-antibaryon bound or resonant states are reviewed.

Résumé: Bref exposé des résultats expérimentaux suggérant l'existence d'états liés ou résonants du système baryon-antibaryon.

1. INTRODUCTION

The discovery of charmonium resonances in November 1974 has stimulated a wealth of experimental searches for baryonium states, i.e. states mainly coupled to the nucleon-antinucleon system. We shall briefly review here the results of these activities, leaving aside the theoretical interpretations[1].

To avoid repetition, we shall assume that the reader is familiar with the review given at the EMS Conference, Boston, April 1977[2], and shall therefore present this review as an up-dating of our knowledges since April 1977.

2. TOTAL ELASTIC AND CHARGE-EXCHANGE CROSS SECTIONS

There are no new experimental results on $\bar{p}p$ total cross section since 1976, the most relevant information for our purpose coming from Abrams et al.[3], Carroll et al.[4] and Chaloupka et al.[5]. The $\bar{p}p$ elastic scattering data of Eisenhandler et al.[6] have now been matched with the differential cross section at 0^o

$$\frac{d\sigma}{d\sigma}(0^o) = \frac{k^2}{\pi^2}\sigma^2_{tot}(1+\rho^2),$$

using the total cross section as measured by Abrams[3] and Carroll[4] and the ratio

$$\rho = \frac{\text{Real } A_{p\bar{p}}}{\text{Im } A_{p\bar{p}}}$$

as recently measured by Jenni et al.[7] and Kaseno et al.[8]. It results from this (Coupland et al.[9]) a better determination of the total elastic cross section which leads to a new determination of the mass, width and height of the two broad bumps observed in the mass range accessible to this experiment (fig. 1).

Altogether, from threshold (M = 1878 MeV) to M $\sim$ 2500 MeV, three bumps have been observed in $\bar{p}p$ total and elastic cross sections. Their characteristics are summarized in table 1. A comparison of $\bar{p}p$ to $\bar{p}d$ total cross section suggests that the S bump[4] is a mixture of I = 0 and I = 1 states, as well as the U bump[3].

The charge exchange cross section $\bar{p}p \to \bar{n}n$ shows no bump in the S mass region[5,10] and much smaller enhancements in the T and U mass region[11] than those observed in elastic scattering (table 1).

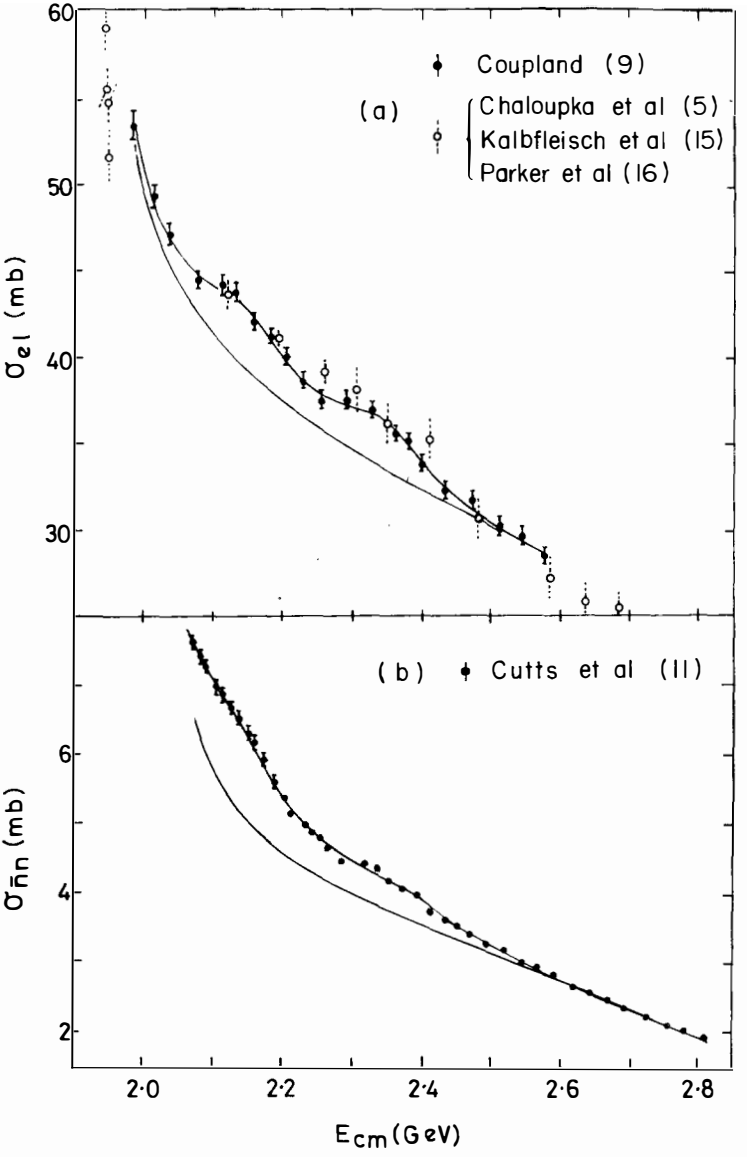

Fig. 1

pp total elastic cross section and charge exchange cross section. The curves show the results of the fits of Coupland et al[9].

TABLE 1

	S	T	U
Mass (MeV)	1936 ± 1	2185 ± 5	2355 ± 5
Width (MeV)	8 - 4	130 ± 30	180 ± 20
σ_t (mb)	10.6 ± 2.4	5.0	3.1
Isospin	1 (0)	1	0 and 1
σ_{el} (mb)	7.0 ± 1.4	2.9	2.8
σ_{CE} (mb)	0.3 ± 0.3	1.2	0.4

Coupland et al.[9] have determined the mass, width, and height of the T and U enhancements observed in total, elastic and charge exchange cross sections, using a uniform parametrization to allow a more reliable comparison of these three cross sections. Their results are given in table 1.

One possible explanation of the differences observed between the elastic scattering and charge exchange cross sections is the presence of strong interference effects with the background[12,13]. Another explanation is the presence of pairs of resonances, with I = 0 and I = 1, in the vicinity of the S, T and U enhancements. As mentioned above, $\bar{p}p$ and $\bar{p}d$ total cross sections show already some support for this last hypothesis for the S and U enhancements. Additional support comes for the S from a detailed study of the annihilation channels[14] (fig. 2). The study of $\bar{p}p$ annihilations near threshold shows an excess in the 5π annihilation channel which can be parametrized by a Breit-Wigner shape with M = 1940 MeV and Γ = 60 MeV ($\Delta\sigma$ = 6 mb for the $2\pi^+2\pi^-\pi^o$ final state). It has been shown that this 5π enhancement can be attributed, to a large extent, to the final state $\rho^o\omega^o$, giving $I^c = 1^+$. Moreover, an analysis of the density matrix elements of this final state leads to the conclusion that $J^P = 2^+$ or 4^+. These results on $\bar{p}p$ annihilations into 5π can be compared to a recent publication[24] where a partial wave analysis of the annihilation channel

$$\bar{p}n \to \pi^-\pi^-\pi^+$$

is performed between 1.9 and 2.07 GeV (cm energy). A large contribution ($\sim$ 15%) is attributed to the $J^P = 2^+$ $I^c = 1^+$ state.

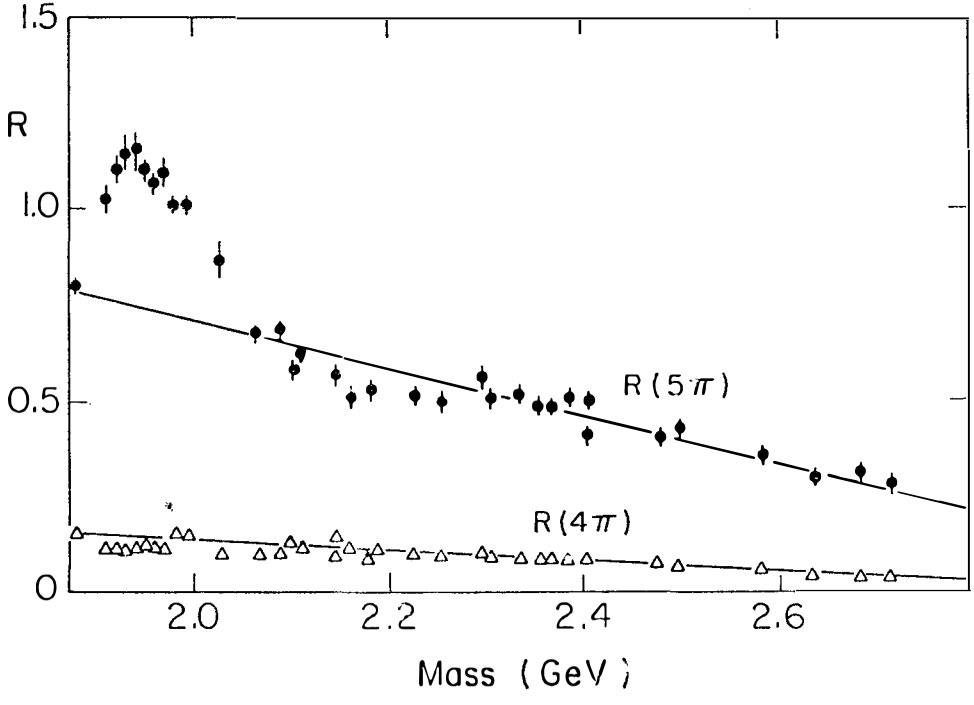

Fig. 2

$\bar{p}p$ annihilation into 5π[14].

An analysis of the $\bar{p}p$ backward elastic scattering[17] also suggests the presence of a $J^{PC} = 2^{++}$ or 4^{++} state of 60 MeV width in the 1.9 to 2.0 GeV mass range. Adding to these observations the conclusions of A. Carter[18] who presented some arguments based on the observation of the zeroes of the $\bar{p}p$ elastic scattering differential cross section, supporting the spin-parity assignment $J^{PC} = 2^{++}$ for S(1936), one is tempted to conclude that the S(1936) enhancement consists of two resonances, with $J^{PC} = 2^{++}$, I = 0 and I = 1, the isovector having a width of 60 MeV, whereas the isoscalar could be 4 to 8 MeV wide. The elasticity of these resonances could be rather large, $x \sim 0.3$ ($x = \Gamma_{\bar{p}p}/\Gamma_{tot}$, i.e. $2x = \Gamma_{\bar{N}N}/\Gamma_{tot}$).

No similar analysis is available for the T and U enhancements. See, however, the results on $\bar{p}p \to \pi^+\pi^-$, $\pi^o\pi^o$ and K^+K^- which will be discussed below.

3. $\bar{p}p \to \pi^+\pi^-$, $\pi^o\pi^o$ and K^+K^-

Carter et al.[19] have made a detailed amplitude analysis of the annihilations $\bar{p}p \to \pi^+\pi^-$ in the 2.0 - 2.6 GeV mass range. Their results provide strong evidence for three resonances with spin 3, 4, 5 (table 2). The evidence for an isoscalar resonance with $J^P = 4^+$ near 2300 MeV is confirmed by another experiment, studying the annihilations $\bar{p}p \to \pi^o\pi^o$ in the same mass range[20], but this $\pi^o\pi^o$ experiment reveals large interference effects between J = 2 and J = 4 below 200 MeV which may affect the overall analysis for these annihilation channels. A complete and simultaneous analysis of the $\pi^+\pi^-$ and $\pi^o\pi^o$ data is therefore necessary before drawing firm conclusions.

A method for understanding the structures in differential cross sections in regions of energy and angle where it is dominated by a single partial wave has been given by Carter[21] and has been applied to the process $\bar{N}N \to \pi\pi$[22]. In contrast to πN scattering, where J^P states can each be described by a single partial wave, there are two initial angular momentum states for triplet $\bar{N}N$ scattering that may couple to a $\pi\pi$ state of spin J: the ratio of helicity amplitudes $|f^J_{++}|/|f^J_{+-}|$ is not known a priori and depends upon the dynamics of the reaction. If one calls α this ratio, one can draw loci in the $\cos\theta^*$ complex plane for the zeroes of the differential cross sections of pure spin states J.

Between $p_{inc} = 0.8$ and 1.2 GeV/c, the experimental $\bar{p}p \to \pi^+\pi^-$ points cluster on the J = 3 locus, the position on this locus corresponding to α small (large spin flip amplitude). Then, as the incident momentum increases, the experimental points tend to cluster on the J = 4 locus with a large value of α, between 1.6 and 2.0 GeV/c. Finally, the experimental points reach the J = 5 locus in the 2.0 -

2.4 GeV/c incident momentum range, α being again small. The observations agree qualitatively well with the results of the amplitude analysis given in table 2.

Table 2

J^{PC} I^{G}	Mass (MeV)	Width (MeV)
3^{--} 1^{+}	2150	200
4^{++} 0^{+}	2310	210
5^{--} 1^{+}	2480	280

At this conference, A. Carter has presented an extension of his method to the analysis of the channel $\bar{p}p \to K^{+}K^{-}$. The $K^{+}K^{-}$ experimental data[19,23] are not as detailed as for $\pi^{+}\pi^{-}$ and the number of states opened to $K^{+}K^{-}$ is twice as much as for $\pi^{+}\pi^{-}$. The conclusions can therefore only be tentative but they indicate very interesting regularities.

The behaviour of the zero loops suggest the dominance of J = 3, 4, 5 in the vicinity of 2.15, 2.30 and 2.50 GeV respectively but with a ratio of spin flip f^{J}_{+-} to non-spin flip amplitude f^{J}_{++} which is small for the entire c.m. energy range. This last observation suggests the dominance of I = 0 states rather than I = 1 as observed for J = 3 and 5 for the $\pi^{+}\pi^{-}$ final state.

Combining the results of this analysis for the $\pi^{+}\pi^{-}$ and $K^{+}K^{-}$ final states, one is led to conclude that there is a strong evidence for J = 3 states with I = 0 and I = 1 at 2.15 GeV. The J = 4 I = 0 already observed in $\pi^{+}\pi^{-}$ and $\pi^{o}\pi^{o}$ is confirmed by the Carter's analysis of the $K^{+}K^{-}$ system. Above 2.40 GeV, J = 5 seems to dominate, both I = 0 and I = 1 being possibly present.

4. EVIDENCE FOR NARROW BOUND STATES RELATED TO THE $\bar{p}p$ SYSTEM

T. Kalogeropoulos[25] has shown how the use of off-mass shell neutrinos in deuterium could give interesting results on $N\bar{N}$ resonances and bound states near threshold. No new results have been reported in this field. The observation of the γ ray spectrum associated to $\bar{p}p$ annihilations at rest allowed P. Pavlopoulos et al.[26] to present some evidence for three $\bar{p}p$ bound states with the properties

given in table 3 and fig. 3. This experiment was performed in a low energy $\bar{p}$ beam at Cern, the antiprotons being stopped in a hydrogen target and the gamma rays being detected in a large Na I spectrometer. The three peaks are not observed when a helium target is used. The energy calibration is controlled with the $\pi^- p$ radiative capture line at 129 MeV which is fitted to be 132 ± 6 MeV.

TABLE 3

Mass (MeV)	Width (MeV)	Yield per annihilation
1693 ± 7	19	$(7.2 \pm 1.7) \times 10^{-3}$
1660 ± 9	21	$(6.0 \pm 1.9) \times 10^{-3}$
1456 ± 34	34	$(8.5 \pm 2.0) \times 10^{-3}$

5. PRODUCTION EXPERIMENTS

Three groups have reported new results in the last twelve months.

J. Six[27] has reported new results on the 2020 and 2200 MeV peaks observed in a baryon exchange experiment performed at CERN with a π^- beam of 9 and 12 GeV/c, using the Omega spectrometer[28]. The analysis has now been extended to $\pi^+ p$ reactions

$$\pi^+ p \rightarrow p_f \pi^+ \bar{p}\bar{p}$$

where p_f means a forward proton with a momentum larger than $p_{inc}/2$.

The ratios of cross sections for π^+ to π^- incident particle are

$$\sigma_+/\sigma_- = 5.2 \pm 2.7 \text{ for the 2020 MeV enhancement,}$$
$$= 5.0 \pm 4.0 \text{ for the 2200 MeV.}$$

We expect 9 for I = 1/2 exchange and 2.25 for I = 3/2.

Other "decay modes" of the $\bar{p}p$ enhancements have been looked for. No signal is reported for $\pi^+\pi^-$, K^+K^-, and $p\bar{p}\pi^o$ final states, given upper limits (at 90% CL) of 15%, 15% and 35% for $\pi^+\pi^-/\bar{p}p$, $K^+K^-/\bar{p}p$, $\bar{p}p\pi^o/\bar{p}p$, respectively.

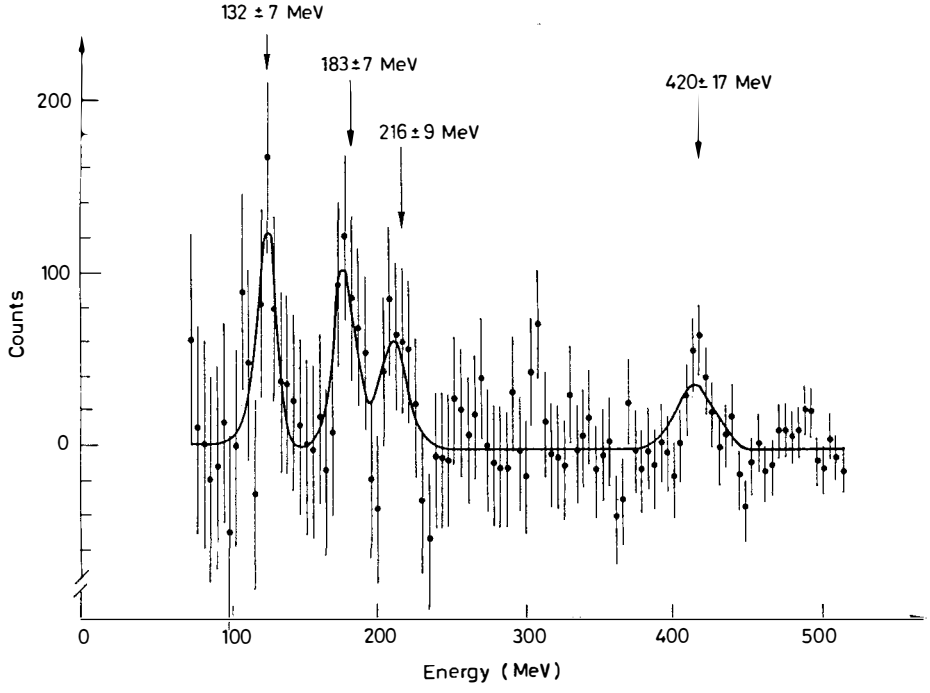

Fig. 3

The gamma ray spectrum associated to $\bar{p}p$ annihilations at rest[26].

Charged enhancements ($p\bar{p}\pi^-$, $\bar{p}n$) have also been looked for, in association or not with Δ^o, N^*, p_f. No significant signal is observed. The absence of a signal in the reaction

$$\pi^- p \to p_f M^-,$$

which is pure I = 3/2 exchange, may indicate that the signals observed in the reaction

$$\pi^- p \to \Delta^o M^o$$

are dominated by I = 1/2 exchanges.

The observation of $\bar{p}p$ enhancements which seem to correspond to "nucleon" exchanges raises the problem of its comparison to on-shell $\bar{p}p$ elastic scattering. A direct comparison of on-shell to off-shell $\bar{p}p$ production had been attempted in[2]. Following a suggestion of S. Flatté[29], we have also estimated this ratio using the ρ meson analogy as sketched in fig. 4. Taking 10 and 20 nb for the production cross section of the 2020 and 2200 MeV $\bar{p}p$ enhancements, respectively, we should observe on-shell $\bar{p}p$ scattering enhancements of 2 to 8 mb. The experimental upper limits are of the order of 0.4 mb[30]. Similarly, an enhancement in the charge exchange cross section should show up with the same magnitude

$$\bar{p}p \to \bar{n}n,$$

if dealing with a pure isotopic spin state and if no important interferences are present. Upper experimental limits of 0.1 mb can be assigned for charge exchange excess at 2020 and 2200 MeV, using the published results of M. Alston-Garnjost[10] and D. Cutts[11], respectively.

Moreover, on-shell $\bar{p}p$ elastic scattering enhancements can be parametrised in terms of the relative $\bar{p}p$ motion wave length λ, the spin J and elasticity x

$$\Delta_{el} = \pi \lambda^2 (2J + 1) x^2,$$

leading to an enhancement in the total $\bar{p}p$ cross section of

$$\Delta_{tot} = \pi \lambda^2 (2J + 1) x.$$

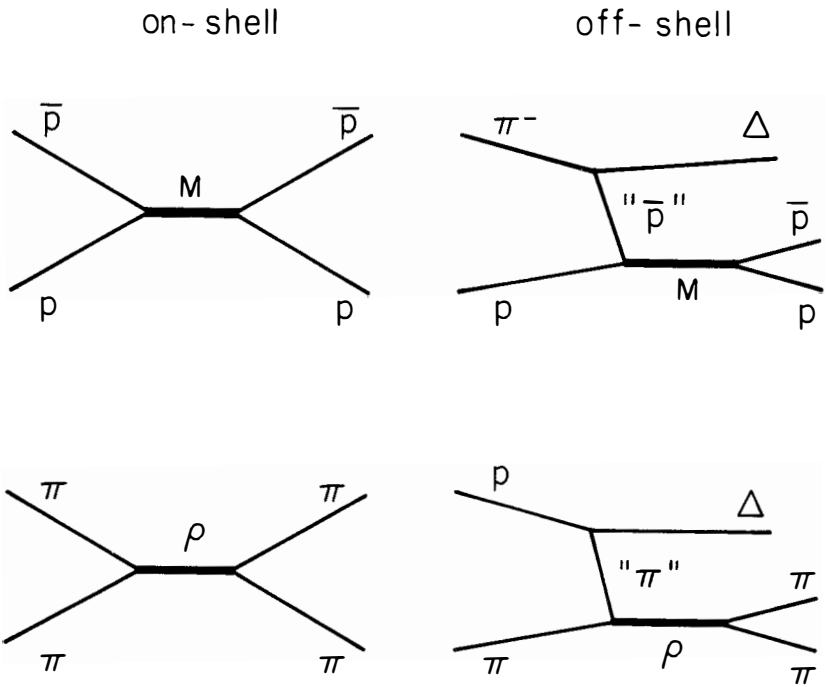

Fig. 4

Diagrams for on-shell formation and off-shell production of $\bar{p}p$ enhancements. Comparison to the formation and production of ρ meson.

If we assume the maximum elasticity x = 0.5 for these $\bar{p}p$ objects, one should observe enhancements of several millibarns in the total $\bar{p}p$ cross section. One experiment[31] has been performed with a mass resolution which is good enough to allow a useful comparison in the 2200 MeV mass region. No narrow enhancement is observed, and, assuming a width of 16 MeV, an upper limit of 0.5 mb can be given at 90% CL.

Finally, Peaslee et al.[32] have measured the G-parity excess in the $\bar{p}p$ annihilations around 2200 MeV. An anomaly at 2200 MeV could be the indication for the presence of an object of well defined G-parity. No sign for such an excess is observed.

Evangelista et al.[33], studying the forward production of the $(\bar{p}p_f \pi^-)$ system in a 16 GeV/c $\pi^- p$ experiment using the Omega spectrometer at CERN, have reported the observation of an enhancement at 2950 MeV (5 to 6 s.d.) with a width of 20 ± 5 MeV, consistent with the mass resolution of the experiment (fig. 5). The total mass spectrum yields an observable cross section (multiplied by the branching ratio) of the order of 1 μb. There is some evidence that this 2950 MeV enhancement decays into substates where the $\bar{p}p$ mass spectrum shows an excess at 2200 MeV, one of the two mass values where Benkheri et al.[28] have observed a $\bar{p}p$ enhancement. The same collaboration is now repeating this experiment with statistics significantly improved.

The narrow $(K^o 3\pi)$ enhancement, observed in $\bar{p}p$ annihilation with M = 2600 MeV and Γ < 18 MeV[34] has not been confirmed by another bubble chamber experiment perform on the same channel with similar statistics[34]. It seems that the difference in mass resolution of these two experiments could not explain the absence of the 2600 MeV enhancement in the second one.

Final results on the 12 GeV/c $K^+ p$ experiment, performed at CERN with the Omega spectrometer, with a trigger on fast outgoing antiprotons[36] are not yet available. The strong $\bar{\Lambda}N$ threshold enhancement observed at the early stage of the experiment[2] is one of the striking results of this experiment.

6. CONCLUSIONS

The S(1936) presents all the features expected for a good baryonium candidate. There are evidences that two resonances, with I = 0 and I = 1, are simultaneously present in this mass region. Further experiments should clarify this point.

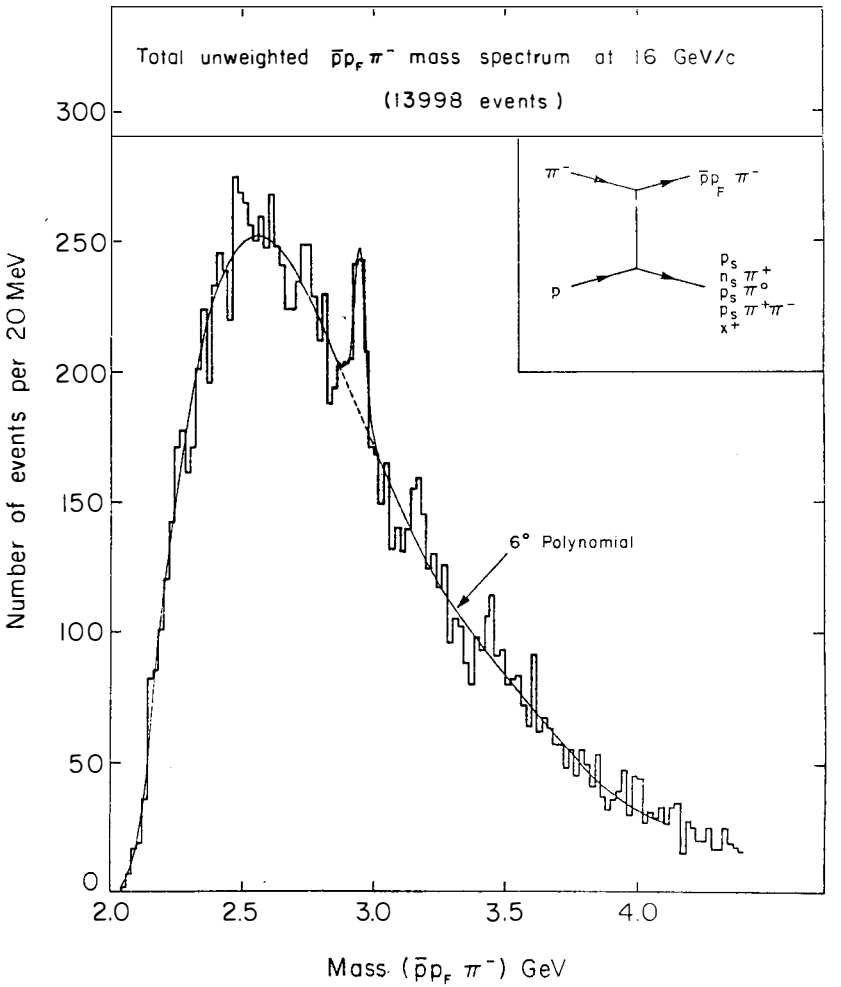

Fig. 5

$M(\bar{p}p\pi^-)$ from π^-p interactions at 16 GeV/c[33].

The analysis of the annihilation channels $\bar{p}p \to \pi^+\pi^-$ and $\bar{p}p \to K^+K^-$ suggests that the broad enhancements observed at 2150 MeV in total and elastic $\bar{p}p$ cross sections could be related to another doublet of isospin, I = 0 and I = 1, with $J^P = 3^-$.

A spin parity 4^+ broad resonance is observed in $\bar{p}p \to \pi^+\pi^-$ and $\bar{p}p \to \pi^o\pi^o$ at 2330 MeV. It may be related to the isospin 0 component of the second broad enhancement observed in $\bar{p}p$ total and elastic cross section.

Above 2400 MeV, J = 5 seems to dominate, both I = 0 and I = 1 being possibly present.

It is not proven, of course, that these J = 3, 4, 5 resonances are genuine baryonium states. In particular, very little is known on a possible 4π decay mode.

For the time being, the two narrow $\bar{p}p$ peaks observed at 2020 and 2200 MeV at two different incident energies, remain the best evidence for production of baryonium states.

REFERENCES

1) See for instance the reports of Chan Hong-Mo, H. Hogasen, Vinh Mau at this conference.

2) L. Montanet, 5th International Conference on experimental meson spectroscopy, Boston, 29-30 April 1977, preprint CERN EP/PHYS 77-22.

3) R.J. Abrams et al., Phys. Rev. D1 (1970) 1917.

4) A.S. Carroll et al., Phys. Rev. Lett. 32 (1974) 247.

5) V. Chaloupka et al., Phys. Lett. 61B (1976) 487.

6) E. Eisenhandler et al., Nucl. Phys. B113 (1976) 1.

7) P. Jenni et al., Nucl. Phys. B94 (1975) 1.

8) H. Kasenc et al., Phys. Lett. 61B (1976) 203 and 68B (1977) 487.

9) M. Coupland et al., RHEL report - RL-77-098/A.

10) M. Alston-Garnjost et al., Phys. Rev. Lett. 35 (1975) 1685.

11) D. Cutts et al., Phys. Rev. D17 (1978) 16.

12) R.L. Kelly and R.J.N. Phillips, RHEL report RL-76-053/T.

REFERENCES (Cont'd)

13) E. Eisenhandler, Proceedings of the 3rd European symposium on antinucleon-nucleon interactions, Pergamon Press, Oxford and N.Y. 1977.

14) Ch. Defoix et al., Collège de France, LPC 75-04 and private communication (Feb. 1978).

15) G. Kalbfleisch et al., Nucl. Phys. B30 (1971) 466.

16) D.L. Parker et al., Nucl. Phys. B32 (1971) 29.

17) Ch. d'Andlau et al., Phys. Lett. 58B (1975) 223.

18) A.A. Carter, Nucl. Phys. B132 (1978) 176.

19) A.A. Carter et al., Phys. Lett. 67B (1977) 117.

20) De Marzo et al., Bari-Brown-MIT Collaboration (work in progress).

21) A.A. Carter, Journal of Physics G, Nucl. Phys. 3 (1977) 1215.

22) A.A. Carter, Phys. Lett. 67B (1977) 122.

23) H. Nicholson et al., Phys. Rev. Lett. 23 (1969) 603.

24) S.N. Tovey et al., The reaction $\bar{p}n \to \pi^-\pi^-\pi^+$ at incident momenta below 1 GeV/c, UM-P-77/43.

25) T. Kalogeropoulos and G. Tzanakos, Search for $\bar{N}N$ resonances and bound states near threshold. Antinuclear-nucleon interactions, Proceedings of the 3rd European symposium, The Wenner-Gren center, Stockholm, 1976 (Pergamon Press).

26) P.G. Pavlopoulos et al., Phys. Lett. 72B (1978) 415.

27) J. Six, CERN, Collège de France - Ecole polytechniques Orsay collaboration, See the communication given by J. Six at this conference.

28) P. Benkheri et al., Phys. Lett. 68B (1977) 483.

29) S. Flatté, Boston 1977, private communication and S.D. Protopopescu et al., Phys. Rev. D7 (1973) 1279.

30) E. Eisenhandler et al., Nucl. Phys. 113 (1976) 1.

31) D.C. Peaslee et al., Phys. Lett. 57B (1975) 189.

32) D.C. Peaslee et al., Phys. Lett. 73B (1978) 385.

33) C. Evangelista et al., Phys. Lett. 72B (1977) 139.

34) A. Apostolakis et al., Phys. Lett. 66B (1977) 185.

35) G.W. van Apeldoorn et al., Phys. Lett. 72B (1978) 487.

36) T. Armstrong et al., University of Glasgow.

RESULTS ON $N\bar{N}$ STATES IN BARYON EXCHANGE REACTIONS FROM EXPERIMENTS IN Ω SPECTROMETER

J. SIX

Laboratoire de l'Accélérateur Linéaire

Université Paris-Sud - Centre d'Orsay

91405 - ORSAY (France)

ABSTRACT :

Results coming from experiments made on baryon exchange reactions in the Omega spectrometer by a CERN-Collège de France-Ecole Polytechnique-Orsay collaboration* are given. Results concerning the narrow $p\bar{p}$ resonances at 2020 and 2204 MeV are reviewed. New results are given, in particular upper limit cross sections for a M^- state at 2020 and 2204 MeV decaying in $\bar{p}n$ state and produced in the reaction $\pi^- p \to p_F \bar{p} n$.

RESUME :

Des résultats sont donnés concernant des expériences d'échanges de baryons faites avec le spectromètre Oméga par une collaboration CERN-Collège de France-Ecole Polytechnique-Orsay*. Les résultats concernant les résonances étroites $p\bar{p}$ à 2020 et 2204 MeV sont rappelés. De nouveaux résultats sont donnés, en particulier des sections efficaces maximum pour la production d'états $M^- \to \bar{p}n$ à 2020 et 2204 MeV dans la réaction $\pi^- p \to p_F \bar{p} n$.

*P. Benkheiri, J. Boucrot, B. Bouquet, P. Briandet, B. d'Almagne, C. Dang Vu, B. Eisenstein, A. Ferrer, P. Fleury, B. Grossetête, G. Irwin, A. Jacholkowski, A. Lahellec, H. Nguyen, P. Petroff, F. Richard, P. Rivet, G. de Rosny, P. Roudeau, A. Rougé, M. Rumpf, J. Six, J.M. Thénard, D. Treille, A. Volte, D. Yaffé, T.P. Yiou, H. Yoshida.

1. Introduction

Since our discovery of two new narrow $p\bar{p}$ resonances at 2020 and 2204 MeV[1], we have investigated in our experiments some reactions which can be compared to the reaction $\pi^- p \to p_F p\bar{p}\pi^-$ where the M°(2020) and M°(2204) appeared. Here is a presentation of these results. Except if it is specified, the results concern all the statistics available.

2. Summary of the experiments

The experimental set up of these experiments is shown in fig. 1. All experimental details can be found in various published papers on these data[2-8]. Here is given only a summary of each experiment with its sensitivity (see table 1). The so-called "fast proton" experiment used a fast forward proton

Experiment		Number of triggers × 10^6	sensitivity for four prong events
"fast proton" experiment	9 GeV/c $\pi^- p \to p_F X$	1.65	∿ 2 evt/nb
	12 GeV/c $\pi^- p \to p_F X$	1.1	∿ 1.3 evt/nb
	9 GeV/c $\pi^+ p \to p_F X$	0.2	∿ 0.1 evt/nb
"exotic" experiment	12 GeV/c $\pi^- D \to p_F - X$	0.75	∿ 0.6 evt/(nb×nucleon)

Table 1 : Summary of the statistics of the experiments

trigger (momentum $p_F > p_{beam/2}$, $\theta_{beam-p_F} < \pm$ 150 mrad). This wide trigger allowed the study of various exchange baryon reactions initiated by $\pi^\pm$ nucleon reactions. The so-called "exotic" experiment used a more restrictive trigger (fast proton + two negative particles) specially conceived for the search of an exotic $p\bar{p}\pi^-\pi^-$ state produced in the reaction $\pi^- n \to p_F p\bar{p}\pi^-\pi^-$. The negative result has been already reported[2].

3. Summary of the published results[1] on M°(2020) and M°(2204) resonances

These new narrow $p\bar{p}$ resonances were seen at 9 and 12 GeV/c in the reaction $\pi^- p \to p_F p\bar{p}\pi^-$ (isolated by a 4C fit) in particular in association with a $\Delta^\circ(1232)$ or a $N^\circ(1520)$ decaying in $p_F\pi^-$. The significance of the peaks are more than 6 s.d. The data suggest strongly a simple two body reaction mediated

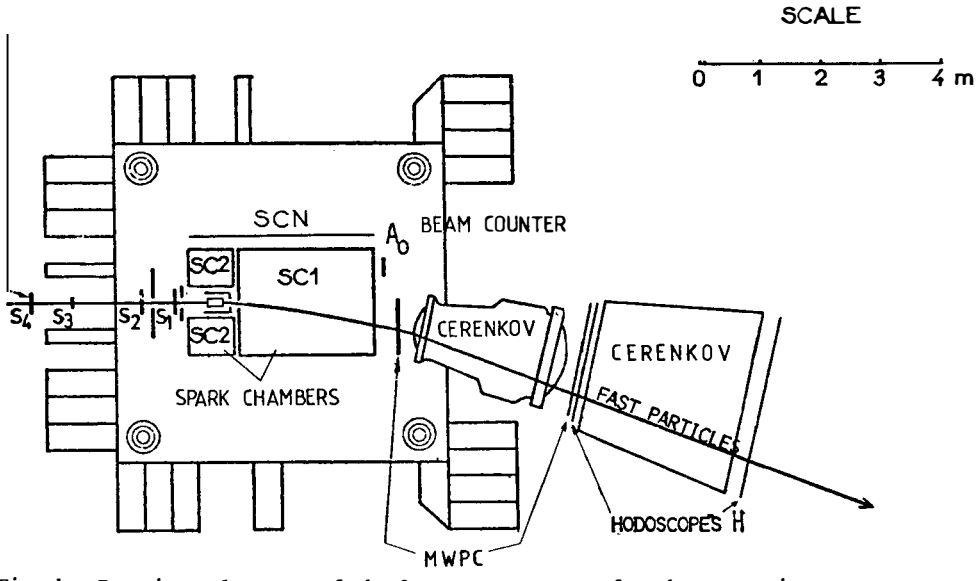

Fig. 1 : Experimental set up of the Omega spectrometer for these experiments (horizontal view).

SC1 : forward set of 80 optical spark chambers
SC2 : lateral sets of 2 × 32 optical spark chambers
A_o : veto counter for the beam
MWPC : multiwire proportional chambers used with a trigger matrix
Cerenkovs : high and low pressure Cerenkov counters
SNC : slow negative **counter** for "exotic" experiment.

by a baryon exchange mechanism.

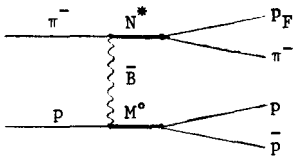

The background accompanying this reaction comes mainly from meson or pomeron exchange mechanism giving a $\bar{p}$ at the upper vertex. This is seen in the strong peaking of the $\bar{p}$ decay angular distribution computed in the $p\bar{p}$ rest system. Cutting one half of the cos θ distribution we obtain a better signal/noise ratio for the $p\bar{p}$ resonances. This is seen in fig. 2 where the first peak may be associated to the well known S(1936) resonance.

Mass (MeV)	Natural width (MeV)	cross section for $\Delta^\circ(1232)$ M° $\hookrightarrow p\pi^-$ $\hookrightarrow p\pi^-$	cross section for $N^\circ(1520)$ M° $\hookrightarrow p\pi^-$ $\hookrightarrow p\bar{p}$
1930 assumed	10 assumed	— 9 ± 5 nb	— 7 ± 5 nb
2020 ± 3	24 ± 12	18 ± 5 nb	30 ± 12 nb
		10 ± 4 nb	26 ± 8 nb
2204 ± 5	16^{+20}_{-16}	17 ± 5 nb	—
		21 ± 5 nb	—

Table 2 : Mass, width of the $p\bar{p}$ resonances and their cross sections found in the reaction $\pi^- p \to \Delta^\circ(1232)$ or $N^\circ(1520)$ + M° (first line at 9 GeV/c, second line at 12 GeV/c).

Table 2 gives the numerical results for mass, width and cross sections obtained for these resonances. No indication of spin, isotopic spin and type of baryon exchange process may be obtained with the data on this reaction $\pi^- p \to p_F p\bar{p}\pi^-$.

4. Study of the reaction $\pi^+ p \to p_F \pi^+ p\bar{p}$

This reaction isolated by a 4C fit shows a production of a $\Delta^{++}(1232)$ in $p\pi^+$ and $p_F\pi^+$ combinations. The $p\bar{p}$ invariant mass distribution associated to the

Fig. 2 : The distribution of the $p\bar{p}$ invariant mass with a Δ^0 selection, $1175 < M(p_F\pi^-) < 1300$ MeV and $\cos\theta < 0$ for the two samples 9 and 12 GeV/c $\pi^- p \to p_F p\bar{p}\pi^-$. θ is the Jackson angle between the target proton and the outgoing p in the $p\bar{p}$ rest frame.

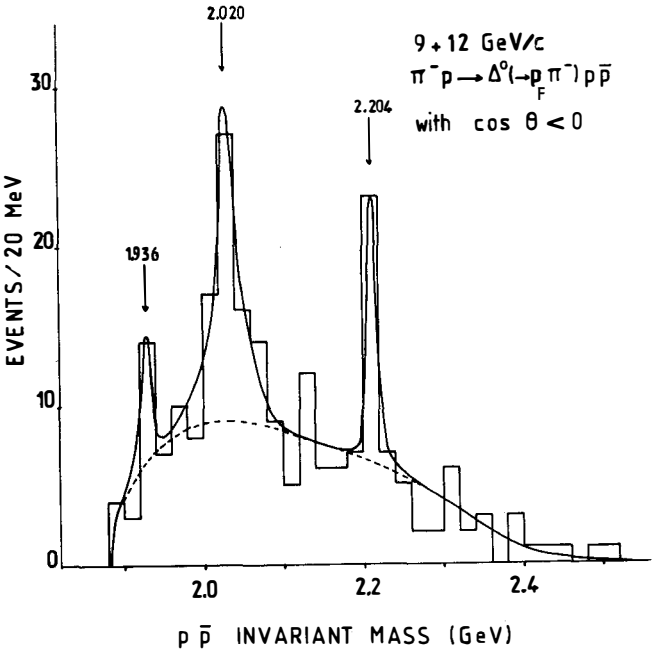

Fig. 3 : The distribution of the $p\bar{p}$ invariant mass with a Δ^{++} selection ($M_{p_F\pi^+} < 1300$ MeV) for the 9 GeV/c $\pi^+ p \to p_F p\bar{p}\pi^+$ reaction.

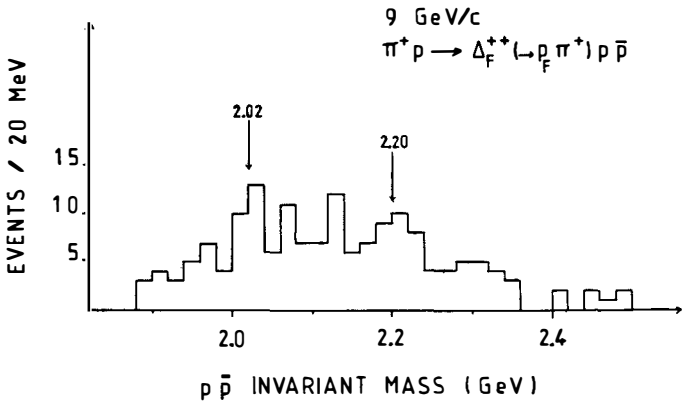

$\Delta^{++}(1232) \to p_F\pi^+$ is shown in fig. 3. Despite the small statistics available (see table 1) the data are compatible with the presence of the M°(2020) and M°(2204) resonances. Comparing the cross sections σ_- for the reaction $\pi^-p \to \Delta^0(\to p\pi^-)M^0$ and σ_+ for the reaction $\pi^+p \to \Delta^{++}(\to p\pi^+)M^0$ we obtain the ratios $\sigma_+/\sigma_- = 5.2 \pm 2.7$ and $\sigma_+/\sigma_- = 5.0 \pm 4.3$ for the M°(2020) and M°(2204) respectively. These results are compatible with a two body reaction mediated by an I = 1/2 ($\sigma_+/\sigma_- = 9$) or an I = 3/2 ($\sigma_+/\sigma_- = 9/4$) baryon exchange mechanisms.

5. Search for decay modes of M° resonances

In the same experiment, the 4C fit reactions $\pi^-p \to p_F\pi^+\pi^-\pi^-$ and $\pi^-p \to p_FK^+K^-\pi^-$ have been studied[6,8]. The 1C fit reaction $\pi^-p \to p_Fp\bar{p}\pi^0\pi^-$ has been also investigated[2]. No enhancement is seen in the M°(2020) or M°(2204) regions. The comparison with the reaction $\pi^-p \to p_Fp\bar{p}\pi^-$ allowed to compute upper limits for branching ratios. These are given in table 3.

	$\frac{M^0 \to p\bar{p}}{M^0 \text{ total}}$	$\frac{M^0 \to \pi^+\pi^-}{M^0 \to p\bar{p}}$	$\frac{M^0 \to K^+K^-}{M^0 \to p\bar{p}}$	$\frac{M^0 \to p\bar{p}\pi^0}{M^0 \to p\bar{p}}$
M°(2020)	> 14 %	< 15 %	< 11 %	——
M°(2204)	> 16 %	< 17 %	< 16 %	< 35 %

Table 3 : Upper limit (90 % C.L.) for the branching ratios of the M° resonances. The given values are given from the total statistics except the $p\bar{p}\pi^0$ mode which is derived from the 12 GeV/c run only.

An inclusive study of the reaction $\pi^-p \to p_F\pi^-X$ has been made. No enhancement is seen in the invariant mass distribution in the $\Delta^0(1232)$ or $N^0(1520)$ but this can be explained by the poor resolution in the calculated invariant missing mass squared ($\sim 0.2\ GeV^2$). These distributions allowed to calculate a lower limit for the ratio $\frac{M^0 \to p\bar{p}}{M^0 \text{ total}}$ given in table 3.

If M° resonances are simple ones, one should have $\frac{M^0 \to n\bar{n}}{M^0 \to p\bar{p}} = 1$ and thus the results given in table 3 are compatible with a large $N\bar{N}$ branching ratio, which is waited in various baryonium models. However it can be noted that in the model of Chan Hong Mo and Høgaasen[9], the narrowness of the states are explained by a "mock" baryonium which can have substantial mesonic decay modes.

6. Search for a state $M^- \to p\bar{p}\pi^-$

The $p\bar{p}\pi^-$ invariant mass has been investigated in the reactions $\pi^- p \to p_F p\bar{p}\pi^-$ and $\pi^- n \to p_F p\bar{p}\pi^-\pi^-$. In particular from this last channel, the reaction $\pi^- n \to \Delta^0(\to p_F\pi^-)p\bar{p}\pi^-$ can be compared to the reaction $\pi^- p \to \Delta^0(\to p_F\pi^-)p\bar{p}$. No enhancement in the $p\bar{p}\pi^-$ invariant mass is seen between 2 and 3 GeV. The $M^0(2020)$ is just at the threshold of the $p\bar{p}\pi^-$ mass and thus in table 4 we give only the cross sections upper limits obtained for a $M^-(2204) \to p\bar{p}\pi^-$. However, the main decay mode of an hypothetical M^- should be probably the $\bar{p}n$ system.

7. Search of a state $M^- \to \bar{p}n$

This state was looked for in the reaction $\pi^- p \to p_F\bar{p}n$. From the two prong events the missing mass spectrum to the $p_F\bar{p}$ hypothesis exhibits a clear peak at the neutron mass and the corresponding reaction was constrained by a 1C fit. For these events, in the Jackson frame, the $\bar{p}$ decay angular distribution of the $\bar{p}n$ system exhibits two peaks as seen in fig. 4. The backward peak is explained by mesonic exchange giving a fast $p_F\bar{p}$ system. The less important forward peak is due to the baryon exchange process which we are interested in. No significant peak exists in the $\bar{p}n$ invariant mass as can be seen in fig. 5 and 6. At 12 GeV/c where more phase space is available we see clearly the shape of the $\bar{p}n$ mass for the two competing processes, baryon exchange (slow $\bar{p}n$ masses) and mesonic exchange (high $\bar{p}n$ masses). Assuming the width of the M^0 resonances as given in table 2 and taking into account the experimental resolution ($\sim \pm 7$ MeV on $\bar{p}n$ mass) and the corrections and normalisation factors, we extracted upper limits cross sections given in table 4.

	$\pi^- p \to p_F M^- \to \bar{p}n$	$\pi^- p \to p_F M^- \to p\bar{p}\pi^-$	$\pi^- N \to \Delta^0 + M^- \to p_F\pi^- \; p\bar{p}\pi^-$
2020	14 nb	—	—
	1 nb	—	—
2204	11 nb	5 nb	—
	30 nb	4 nb	12 nb

Table 4 : Upper limits (90 % C.L.) for the production cross sections of a possible state M^- in $\bar{p}n$ or $p\bar{p}\pi^-$ modes. (first line at 9 GeV/c and second line at 12 GeV/c).

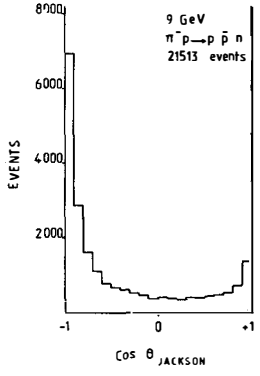

FIG. 4

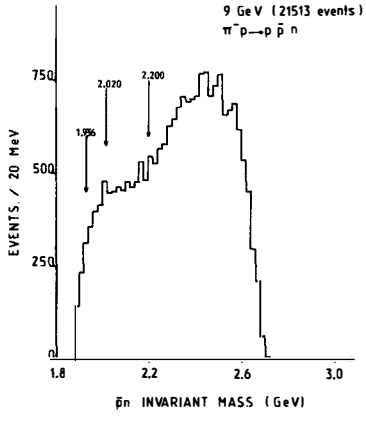

FIG. 5

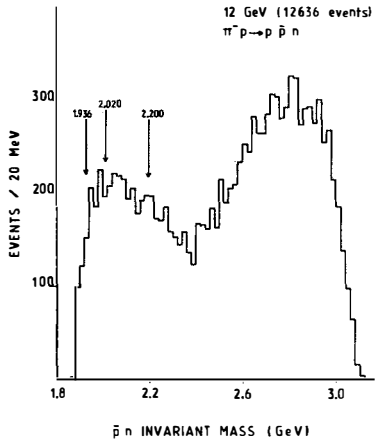

FIG. 6

Fig. 4 : The cos θ distribution for the $\bar{p}$ decay of the $\bar{p}n$ system for the 9 GeV/c $\pi^- p \to p_F \bar{p} n$ reaction. θ is the Jackson angle between the target proton and the outgoing $\bar{p}$ in the $\bar{p}n$ rest frame.

Fig. 5 : The distribution of the $\bar{p}n$ invariant mass for the 9 GeV/c $\pi^- p \to p_F \bar{p} n$ reaction.

Fig. 6 : The distribution of the $\bar{p}n$ invariant mass for the 12 GeV/c $\pi^- p \to p_F \bar{p} n$ reaction.

The upper limits cross sections can be compared to those obtained for the reactions $\pi^- p \to \Delta^\circ(1232)$ or $N^\circ(1520) + M^\circ(\to p\bar{p})$ (see table 2) and also for the reactions $\pi^- p \to \Delta^\circ(1232)$ or $N^\circ(1520) + \rho^\circ$(or π°) and $\pi^- p \to p_F \rho^-$ (or π^-) measured in this experiment[3,4,5,8]. Cross sections productions of M and ρ (or π) can be compared for reactions involving a same upper vertex in a baryon exchange mechanism production. For reactions involving a Δ^{++} exchange, we have the following ratio $\dfrac{\sigma(\pi^- p \to p_F M^-(\to \bar{p}n)}{\sigma(\pi^- p \to p_F \rho^-)} < 0.007$ or < 0.014 for a $M^-(2020)$ or a $M^-(2204)$ respectively. For measured reactions involving a Δ^+ or P exchange, we have $\dfrac{\sigma(\pi^- p \to \Delta^\circ(\text{or } N^\circ)M^\circ)}{\sigma(\pi^- p \to \Delta^\circ(\text{or } N^\circ)\rho^\circ)} \sim 0.06 \pm 0.02$ for the $M^\circ(2020)$ and $M^\circ(2204)$.

It is difficult to derive a definitive statement for the comparison of these very different ratios. However two simple explanations exist :

1 - The M° resonances have isotopic spin 0

2 - The M resonances are strongly coupled to the $N\bar{N}$ system and weakly coupled to the $\Delta\bar{N}$ system. In that case, the reactions $\pi^- p \to \Delta^\circ(\text{or } N^\circ)M^\circ$ are dominated by a nucleon exchange. In the first hypothesis the Δ exchange is impossible.

In the second hypothesis, the M resonances can have isotopic spin 1 but it is perhaps better to search the corresponding M^- state in reactions involving a nucleon exchange.

REFERENCES

1) P. Benkheiri et al, Phys. Lett. 68B (1977) 483.

2) J. Boucrot et al, Nucl. Phys. B121 (1977) 251.

3) A. Rougé et al, Phys. Lett. 69B (1977) 115.

4) J. Jacholkowski et al, Nucl. Phys. B126 (1977) 1.

5) P. Benkheiri et al, Lettere al Nuovo Cimento 20 (1977) 297.

6) T. Hofmokl et al, Nucl. Phys. B129 (1977) 19.

7) A. Ferrer et al, Phys. Lett. 74B (1978) 287.

8) Backward production in $\pi^- p \to p_F \pi^+ \pi^- \pi^-$ reaction at 9 and 12 GeV/c - A. Ferrer et al, subm. to Nucl. Phys. (may 1978).

9) Chan Hong Mo and H. Høgaasen, Phys. Lett. 72B (1977) 121.

A NEW INTERPRETATION OF THE REACTIONS $\bar{p}p \to \pi^-\pi^+$ AND $\bar{p}p \to K^-K^+$ BETWEEN 2.0 AND 2.6 GeV

A.A. Carter,
Department of Physics, Queen Mary College, London.

Abstract: An amplitude analysis of the reaction $\bar{p}p \to \pi^-\pi^+$ between 2.0 and 2.6 GeV has revealed resonances with $J^{PC}I^G = 3^{--}1^+$, $4^{++}0^+$, $5^{--}1^+$, and widths ~150-200MeV. The differential cross section zeros of $\bar{p}p \to K^-K^+$ confirm these results and provide evidence for new states with $J^P = 3^-$, 5^- with I=0, at masses close to those of the I=1 states.

Résumé: Une analyse d'amplitude de la réaction $\bar{p}p \to \pi^-\pi^+$ entre 2.0 et 2.6 GeV a révélé des résonances ayant $J^{PC}I^G = 3^{--}1^+$, $4^{++}0^+$, $5^{--}1^+$, et des largeurs comprises entre 150 et 200MeV. Les zeros des sections efficaces différentielles de la réaction $\bar{p}p \to K^-K^+$ confirment ces résultats et montrent l'existance de nouveaux états ayant $J^P = 3^-$, 5^- avec I=0, et dont la masse est proche de celle des états I=1.

1. Introduction

In an amplitude analysis of the reaction $\bar{p}p \to \pi^-\pi^+$ in the energy range 2.0 to 2.6 GeV[1] we have previously shown evidence for the formation of conventional width mesons, $\Gamma \sim 150$-200 MeV, with $J^{PC}I^G = 3^{--}1^+$, $4^{++}0^+$, $5^{--}1^+$ at masses of 2.15, 2.31 and 2.48 GeV/c^2. The quantitative results confirmed the properties initially indicated by the zeros of the differential cross sections[2]. This reaction allows a complete determination of the quantum numbers of a state once the spin is known, since even and odd J are in I=0, I=1 respectively. However, both isospin values are permitted for all values of J in the $\bar{p}p \to K^-K^+$ channel. Although differential cross section and polarization data[3),4),5)] exist for this reaction, no amplitude analysis has so far been carried out, and indeed one would not be possible unless some simplifying assumptions were made. However, the process should be investigated in order to compare with the proposed properties of the $\pi^-\pi^+$ channel. Its potentially rich spectrum of states could also extend our present understanding of multiquark systems. Here we summarise the results previously obtained from the dipion reaction and compare them with new results from a zeros' analysis of the K^-K^+ channel. These suggest the presence of I=0 mesons with $J^P = 3^-$, 5^- at masses close to those of their I=1 partners.

2. Method of Zeros for Spin $(\frac{1}{2} + \frac{1}{2}) \to$ Spin $(0 + 0)$

This process can be described in terms of two helicity amplitudes, F_{++}, F_{+-} where

$$\frac{d\sigma}{d\Omega} = |F_{++}|^2 + |F_{+-}|^2$$

$$F_{++} = \frac{1}{2p} \sum_J (J + \tfrac{1}{2}) f^J_{++} P_J(z)$$

$$F_{+-} = \frac{1}{2p} \sum_J \frac{(J + \frac{1}{2}) f^J_{+-} P^1_J(z)}{\sqrt{J(J+1)}}$$

with z the cosine of the c.m. scattering angle and p the c.m. momentum of the initial system. The isospin decompositions for the diboson reactions in $\bar{p}p$ scattering are given by :-

(i) $\bar{p}p \to \pi^-\pi^+$, $f^J = \frac{1}{\sqrt{6}} f^J_{I=0}$ for J even

$f^J = \frac{1}{2} f^J_{I=1}$ for J odd

(ii) $\bar{p}p \to K^- K^+$, $f^J = \frac{1}{2} f^J_{I=0} + \frac{1}{2} f^J_{I=1}$

An individual spin state, J, will then have a cross section

$$\left(\frac{d\sigma}{d\Omega}\right)_J = \left[\frac{J+\frac{1}{2}}{2p}\right]^2 \left\{ |f^J_{++}|^2 \left[P_J(z)\right]^2 + \frac{1}{J(J+1)} |f^J_{+-}|^2 \left[P^1_J(z)\right]^2 \right\}$$

which provides its own characteristic pattern of zeros in the complex z-plane. However, the ratio between $|f^J_{++}|$ and $|f^J_{+-}|$ is not known a priori, and is determined by the dynamics of the reaction. It is thus convenient to construct loci of the characteristic zeros of pure spin states as a function of their $|f^J_{++}|^2 : |f^J_{+-}|^2$ ratio[2]. A comparison of the energy dependent zeros' trajectories of experimental data with these loci can then demonstrate the energy regions dominated by a state of well defined spin and constant helicity amplitude ratio.

In the analysis experimental differential cross sections are fitted, at each energy, to a series expansion in Legendre's polynomials; this is then solved for the zeros as a function of complex z. For the reactions we are considering interference effects between adjacent spin states manifest themselves in the data as contributions antisymmetric in sign under the interchange $z \to -z$. To eliminate these terms we present results that correspond to the data having been folded about Re(z)=0.

3. Results for $\bar{p}p \to \pi^- \pi^+$

The trajectories of zeros are shown in fig.1, together with the characteristic loci for pure J=2, 3, 4 and 5 states. We see that below an energy of ∿2.18 GeV. only one zero is present and this remains in the region of the single zero required by a J=3 state with $|f^3_{++}|^2 : |f^3_{+-}|^2 = \sim 0.4 : 1$, from 2.1 to 2.16 GeV. As the energy increases an additional zero enters from Re(z)=1 and at ∿2.33 to 2.36 GeV both zeros cross the appropriate J=4 loci at values corresponding to $|f^4_{+-}|^2 : |f^4_{++}|^2 = \sim 0.1\text{-}0.4 : 1$. When the energy approaches 2.5 GeV both experimental trajectories indicate the presence of the zeros needed for a J=5 state with $|f^5_{++}|^2 : |f^5_{+-}|^2 = \sim 0.4 : 1$. The detailed analysis in reference (1), incorporating polarization results, confirmed the presence of these dominant amplitudes and suggested the existence of resonances with $J^P I = 3^-1$, 4^+0, 5^-1 at masses ∿2.15, 2.31, 2.48 GeV/c^2 with widths ∿150-200MeV.

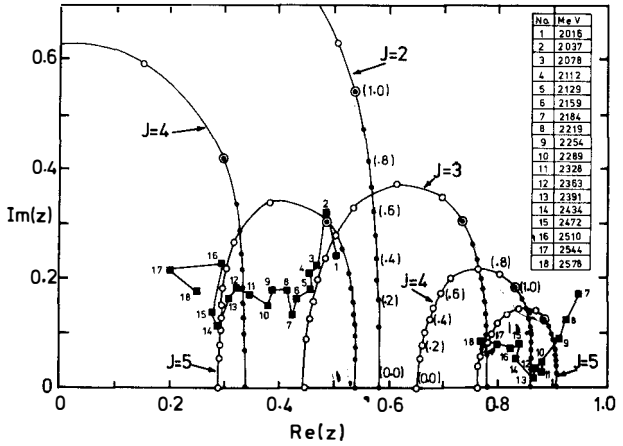

Fig.1. shows the trajectories of experimental zeros in the z-plane for $\bar{p}p \to \pi^- \pi^+$, for 2016 < Ec.m. < 2578 MeV, together with the loci for pure spin states with J=2, 3, 4 and 5. The values of the $|f^J_{++}|^2 : |f^J_{+-}|^2$ ratios are indicated by open circles at 0.1 intervals between 0 and 1. The values of the inverse ratio, also between 0 and 1, are indicated by dots. Their properties on the Re(z)=0 axis are not shown.

4. Results for $\bar{p}p \to K^- K^+$

The zeros' trajectories are given in figs. 2, 3 and 4 and can be interpreted through the following three consecutive energy regions:

(1) 2.0 to 2.25 GeV. Fig 2a shows the trajectories from the data of Eisenhandler et al[3], together with the loci of pure J=2 and 3 states. The corresponding results using the combined data of Fong et al and Nicholson et al[4] are shown in fig 2b. The two sets of results are seen to be in good quantitative agreement.

Below 2.075 GeV the data have only one zero. This moves rapidly through the J=2 locus at an energy near 2.04 GeV and remains near a fixed point on the backward branch of the J=3 locus throughout the energy range 2.08 to 2.16 GeV. In the same range the corresponding zero exists on the Re(z)=0 branch of the J=3 locus, with the same $|f^3_{+-}|^2 : |f^3_{++}|^2$ ratio of approximately 0.8 : 1. The trajectory for the $\bar{p}p \to \pi^- \pi^+$ reaction, shown in fig 1, also indicated a dominant J=3 state which we interpreted as a resonance. In that reaction $|f^3_{+-}|$ is seen to be much larger than $|f^3_{++}|$ whereas in the $K^- K^+$ channel <u>both</u> amplitudes are significant. A straightforward explanation of the identical energy dependence in the two reactions, but with different amplitude ratios, can

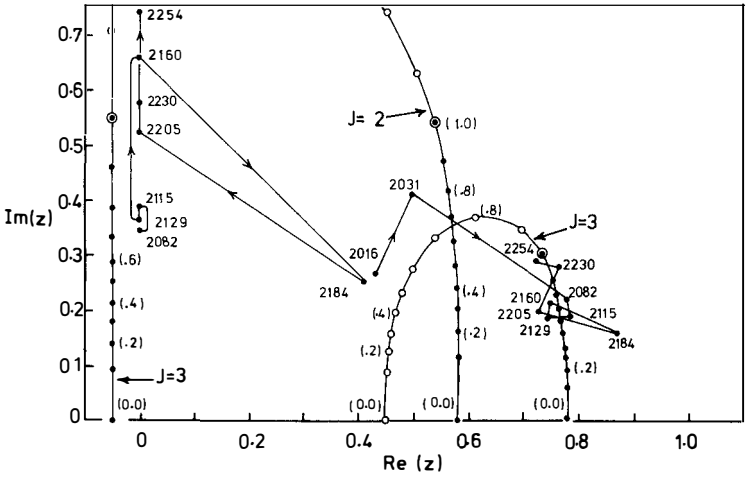

Fig.2a. shows the zeros' trajectories for $\bar{p}p \to K^- K^+$ in the range $2016 < E_{cm} < 2254$ MeV for the data of ref.(3), together with the loci for pure J=2 and 3 states. The notation is the same as given previously.

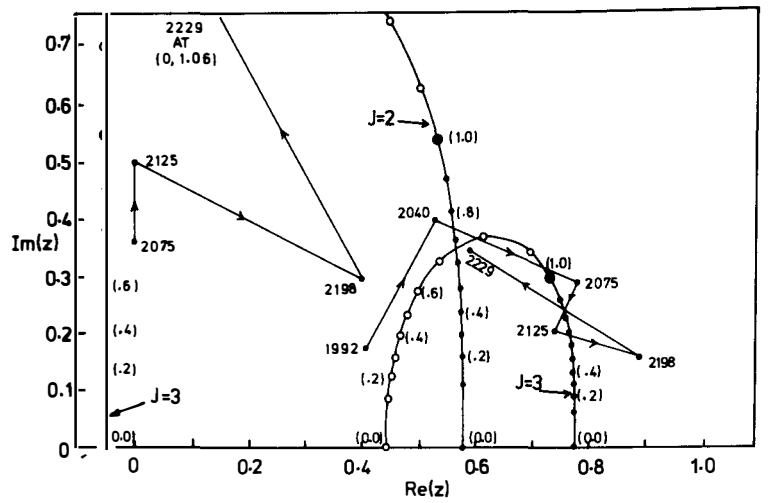

Fig.2b. shows the zeros' trajectories for $\bar{p}p \to K^- K^+$ for the data of ref.(4) in the range $1992 < E_{cm} < 2229$ MeV.

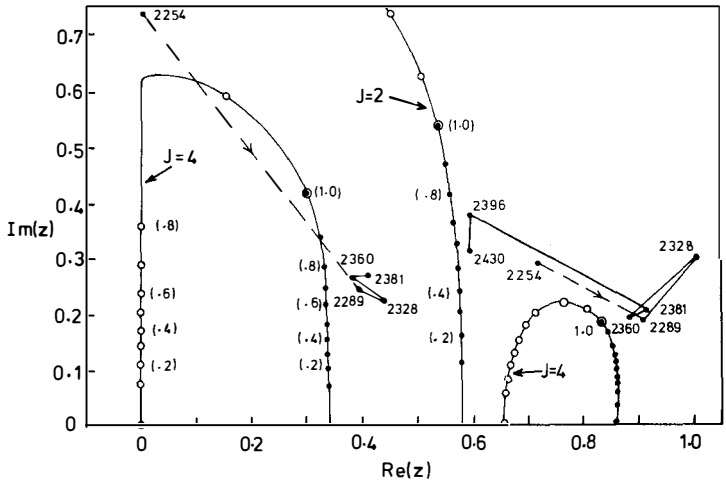

Fig. 3. shows the zeros' trajectories for $\bar{p}p \to K^- K^+$ for the data of ref.(3) for $2254 < E_{cm} < 2430$ MeV.

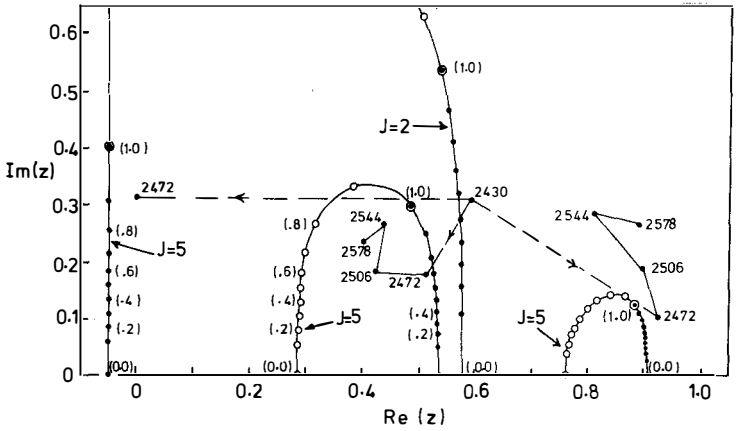

Fig. 4. shows the zeros' trajectories for $\bar{p}p \to K^- K^+$ for the data of ref.(3) for $2430 < E_{cm} < 2578$ MeV.

be given in terms of nearly mass degenerate resonances existing in both the I=1 and I=0 states. Only the former can couple to $\bar{p}p \to \pi^-\pi^+$ whereas both may exist in the K^-K^+ channel. As the helicity amplitudes of the diboson channels correspond explicitly to coupling eigenstates of the tensor force[6] we can see that these results may indicate the importance of the tensor force in the antinucleon-nucleon interaction. Indeed, they suggest that I=0 and 1 states are associated predominantly with f_{++} and f_{+-} amplitudes respectively.

Figs. 2a and 2b both show that the data take a rapid excursion away from the J=3 loci onto those of a spin 4 state between 2.18 and 2.2 GeV, and then return close to the previous J=3 positions. This phenomenon could be explained by the dominant J=3 amplitudes below 2.18 GeV interfering destructively with an additional spin 3 state to reveal the J=4 state that itself resonates at higher energy. It is to be noted that this effect is observed close to the energy of one of the narrow enhancements seen in the $\bar{p}p$ effective mass distribution in the production reaction $\pi^- p \to p_F p\bar{p}\pi^-$ [7].

(2) 2.25 to 2.43 GeV. This region is shown in fig.3, where between 2.3 and 2.38 GeV the trajectories correspond to a dominant J=4 state. This is in agreement with the resonant $J^P=4^+$, I=0 state at 2.31 GeV seen in the $\bar{p}p \to \pi^-\pi^+$ analysis, with a similar $|f^4_{++}| : |f^4_{+-}|$ ratio. However, a comparison of that analysis with the data for $\bar{p}p \to \pi^o\pi^o$ [8], where only even spin states are allowed, indicates that we overestimated the contribution of the broad resonant amplitude and obtained a central mass value that may be ∿30 MeV too low.

(3) 2.43 to 2.58 GeV. The results are given in fig.4, where the initial single zero at Re(z)≈0.6 splits into the three zeros of a dominant J=5 state at 2.47 GeV. This agrees well in mass with the $J^P=5^-$, I=1 resonance seen in $\bar{p}p \to \pi^-\pi^+$ at 2.48 GeV. However, there the f^5_{+-} amplitude dominates, whereas now we have an additional significant contribution from f^5_{++}. Again this contrast in the helicity amplitude couplings between the two channels may be explained by the presence of nearly mass degenerate $J^P= 5^-$ resonances in both I=0 and I=1 states close to 2.5 GeV.

5. The Integrated Cross Sections

Fig. 5. shows data[3)8)] for the integrated cross sections of the three diboson channels, $\bar{p}p \to \pi^-\pi^+$, $\bar{p}p \to K^-K^+$ and $\bar{p}p \to \pi^o\pi^o$. All show structure indicative of the 4 resonance behaviour in the region 2.3 to 2.38 GeV. The 3^-, 5^- states cannot occur in the $\pi^o\pi^o$ channel, but their existence is supported by the enhancements seen in the cross sections in figs. 5a and 5b. In table 1

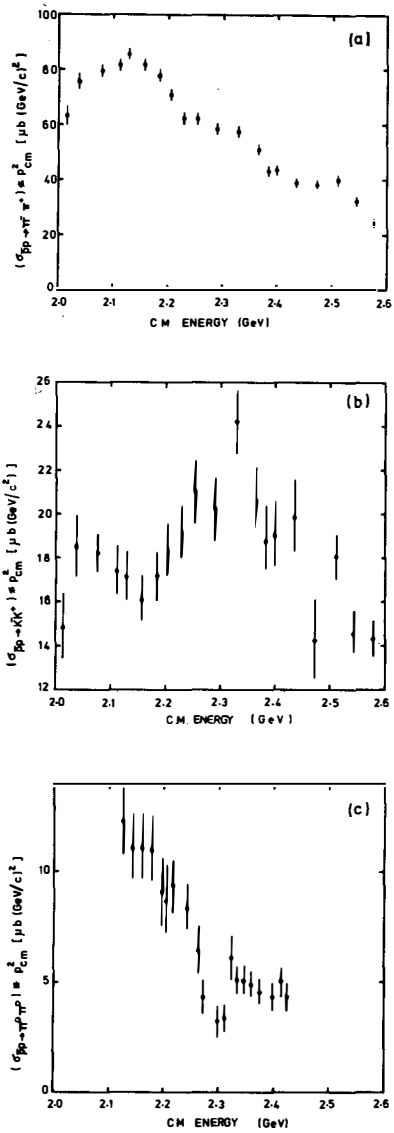

we summarise the properties of the proposed meson resonances of conventional width, $\Gamma \sim 150$ MeV, that result from our analyses of the charged diboson channels.

6. Conclusions

An understanding of the anti-nucleon-nucleon interaction from the properties of multiquark states has recently been proposed by Chan and Høgassen and by Jaffe[9]. Such models provide a unifying picture of the resonances that couple strongly to the elastic channel but also weakly to the diboson final states. The general features of their predicted resonance spectra are certainly compatible with the present experimental data on $\bar{p}p$ formation processes. Our previous zeros' analysis of the elastic channel[10] indicated the presence of high spin states that support the conclusions from the $\pi^-\pi^+$ data. The results presented here for $\bar{p}p \to K^-K^+$ provide evidence for isospin doublet resonances with $J^P = 3^-$, 5^- at masses $\sim$2.14 and $\sim$2.5 GeV/c^2. In addition they indicate a 4^+ state at $\sim$2.34 GeV/c^2 with I=0, which may be the isospin partner of the I=1 enhancement seen in the total cross section[11] at the same energy.

Fig. 5. shows the integrated cross section times the c.m. momentum squared in the $\bar{p}p$ system as a function of the c.m. energy for (a) $\bar{p}p \to \pi^-\pi^+$, (b) $\bar{p}p \to K^-K^+$, both using the data of Eisenhandler et al[3], and (c) $\bar{p}p \to \pi^0\pi^0$ using the data of De Marzo et al[8].

Table 1 gives a summary of the evidence for resonant states seen in the zeros' analyses of the reactions pp → charged dibosons.

J^P	MASS (GeV/c^2)	$\bar{p}p \to \pi^-\pi^+$	$I_{\pi\pi}$	$\bar{p}p \to K^-K^+$	I_{KK}
3^-	2·10→2·18	$f^3_{+-} >> f^3_{++}$	1	$f^3_{+-} < f^3_{++}$	1+0
4^+	2·30→2·38	$f^4_{+-} << f^4_{++}$	0	$f^4_{+-} < f^4_{++}$	0
5^-	2·47→2·51	$f^5_{+-} >> f^5_{++}$	1	$f^5_{+-} < f^5_{++}$	1+0

References

(1) A.A. Carter et al., Phys. Lett. 67B(1977)117.

(2) A.A. Carter, Phys. Lett. 67B(1977)122.

(3) E. Eisenhandler et al., Nucl. Phys. B96(1975)109.

(4) H. Nicholson et al., Phys. Rev. D9(1973)2572.

(5) A.A. Carter et al., Nucl. Phys. B127(1977)202.

(6) C.B. Dover and J.M. Richard, Brookhaven Report BNL22727(1977).

(7) P. Benkheiri et al., Phys. Lett. 68B(1977)483.

(8) C. De Marzo et al; in review by L. Montanet, Proceedings Vth Int. Conf. on Exptl. Meson Spectroscopy, Boston(1977).

(9) H.M. Chan and H. Høgassen, CERN preprint TH2388(1977).
R.L. Jaffe, MIT preprint CTP No.657(1977).

(10) A.A. Carter, Nucl. Phys. B132(1978)176.

(11) R.J. Abrams et al., Phys. Rev. D1(1970)1917.

EXPERIMENTAL REVIEW OF STRANGE DIBARYONS

E. PAULI
DPhPE, Centre d'Etudes Nucléaires de Saclay,
BP 2, 91190 Gif-sur-Yvette, France.

SUMMARY

The long history of the experimental strange dibaryons research is summarized. There are only a few reasonable candidates. The most recent one in the Λp system at M = 2129 MeV/c^2, looks rather convincing.

RESUME

La longue histoire de la recherche expérimentale de dibaryons étranges est brièvement résumée. Il n'y a que quelques candidats raisonablement valables. Le plus récent, qui est observé dans le sytème Λp à une masse de 2129 MeV/c^2, semble très convaincant.

Introduction

This contribution presents a short, selective review of the experimental investigation of the S = -1, -2 dibaryon systems. Nevertheless, the references which are given and the references therein represent a rather complete bibliography of the subject.

The strange dibaryons have mostly been looked for in the Λp system. But a few other channels have been studied. This research started in the early sixties in low statistics bubble chamber experiments. One of their by-products has been the possible existence of these exotic states.

Based on the confinement theory, recent predictions of n > 3 quarks states are made[1], specially dibaryons. They could be one mean to see colour. Therefore, a new excitement has reached this experimental area.

Due to specific problems in each category of reactions, I divided this review into three sections :

- direct Λ-proton scattering
- interactions on hydrogen and deuterium
- interactions on nuclei.

In each section, the experiments are ordered, in principle, by increased sensitivity.

1 - Λ-proton scattering

- G. ALEXANDER et al.[2] have studied 378 Λ-p elastic scattering events in the 81 cm H_2 bubble chamber in a stopping K^- experiment of 200 000 pictures, equivalent to 0.5 event per millibarn. The differential and total cross sections, measured in several momentum intervals between 120-320 MeV/c, are consistent with predominantly S-wave scattering. No significant indication for the existence of a low-energy Λ-p resonance has been found.

- J.M. HAUPTMAN et al.[3] looked for the following reactions :

$$\Lambda + p \rightarrow \Lambda + p \quad \text{(584 events)}$$
$$\Lambda + p \rightarrow \Sigma^{\pm} + p + \pi^{\mp}$$
$$\Lambda + p \rightarrow \Lambda + p + \pi^{+} + \pi^{-}$$
$$\Lambda + p \rightarrow \Sigma^{\circ} + p$$
and various Ξ° p interactions (25 events).

The incident Λ flux was produced by the exposure of a platinum target mounted inside the SLAC 82-inch bubble chamber to a 12 GeV/c K^- beam. The mean momentum of the Λ was 2 GeV/c.

They have no evidence for a cusp-like or a resonant behaviour near the

threshold $\Lambda + p \rightarrow \Sigma^{\circ} + p$.

These two papers are given as examples. Many other authors have studied this subject. No resonance was found.

2 - Interactions on hydrogen and deuterium

a) p + p reactions

The most important reaction in this section is p + p → hyperon + K + nucleon.

- M. FIREBAUGH et al.[4] have done a systematic survey of strange-particle final states produced by 8 GeV/c protons in the BNL 80-in. hydrogen bubble chamber. With a sensitivity of 1 event per microbarn, no strong strange dibaryon resonance was observed.

- E. BIERMAN et al.[5] have carried out a search for dibaryon states in p-p collisions at 5 GeV/c in the 80-in. Brookhaven bubble chamber with 4 events per microbarn. The analysis concludes that the data are consistent with the one-pion-exchange model.

- W. CHINOWSKY et al.[6] have obtained 1746 examples of the reaction p + p → hyperon + K + nucleon in a 20 events per microbarn LRL 72-in. hydrogen bubble chamber experiment at 6 GeV/c. Strong N^* production is observed in all channels. The data are always consistent with a production process dominated by a single-pion exchange mechanism. No evidence is found for a dibaryon state in either the Λ-proton or Σ-nucleon system.

- A.C. MELISSINOS et al.[7] and J.T. REED et al.[8] analyzed the spectrum of K^+ mesons produced in p-p collisions at 2.85 and 2.4 GeV/c. This counter experiment was performed at the Brookhaven Cosmotron and three spectrometer channels were established at 0°, 17°, and 32°. The $d\sigma/d\Omega$ was less than 6μb/ster in the laboratory both at 0° and 17°. The upper end of the K^+ spectrum was perfectly fitted with an effective-range formalism and therefore no evidence for a resonant Λp state is reported.

- V.L. FITCH, T.F. KYCIA et al.[9] very recently studied the reaction

$$p + p \rightarrow K^+ + K^+ + \text{missing mass}$$

between ↓ and 6 GeV/c in a double arm spectrometer at Brookhaven. They obtained a sensitivity of 0.2 event/nanobarn with AGS dedicated time. Until now, no evidence for a double strange dibaryon system is claimed in this experiment. Their preliminary results establish a 90 % c.l. upper limit of ∿ 30 nb for any narrow states produced in this reaction (see figure 1).

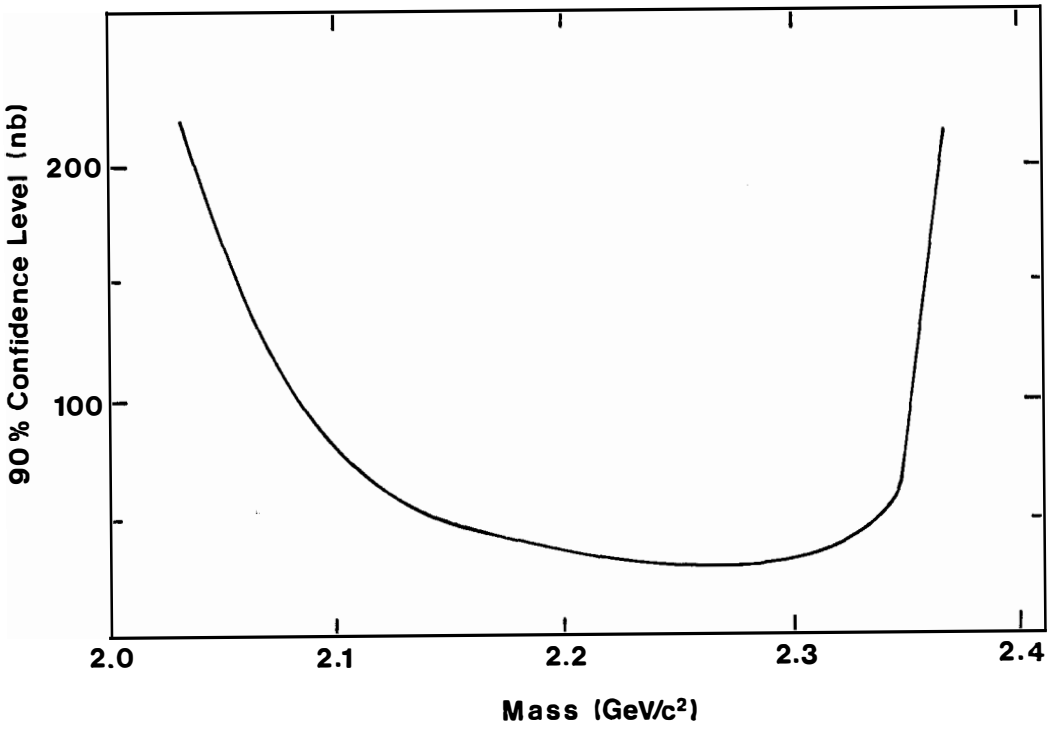

FIG. 1. 90 % c.l. upper limits on narrow state production cross section as a function of missing mass against K^+K^+ in the reaction $p + p \to K^+ + K^+ +$ missing mass between 5 and 6 GeV/c.

b) K^-d reactions

Looking at the results, it seems that these reactions correspond to the most promising initial state.

- TAI HO TAN[10] studied the Λp system in the reaction $K^- + d \rightarrow \pi^- + p + \Lambda$ at rest in the Columbia-Brookhaven 30-in. deuterium bubble chamber with 2 events per microbarn. Two resonances are found to be necessary to describe the Λp mass spectrum (Figure 2)

$$M_1 = 2128.7 \pm 0.2 \text{ MeV/c}^2 \qquad \Gamma_1 = 7.0 \pm 0.6 \text{ MeV/c}^2$$

$$M_2 = 2138.8 \pm 0.7 \text{ MeV/c}^2 \qquad \Gamma_2 = 9.1 \pm 2.4 \text{ MeV/c}^2$$

The closeness of the first peak to the Σ^+n threshold makes it impossible to distinguish between a possible genuine Λp resonant state that may exist a fraction of an MeV below the ΣN threshold from a threshold cusp effect. The observed peak may be a superposition of both.

- The same peak at 2129 MeV/c^2 was observed by D. EASTWOOD et al.[11] in a 81 cm Saclay deuterium bubble chamber experiment at ∿ 1.5 GeV/c with a sensitivity of 3 events per microbarn and by O. BRAUN et al.[12] in the reaction

$$K^- + d \rightarrow \Lambda\, p\, \pi^-$$

at ∿ 750 MeV/c in the same bubble chamber with 7 events per microbarn. By selecting the very forward going π^-, they observe a very nice peak (Figure 3) at a mass of $M = 2129$ MeV/c^2 and a width $\Gamma = 6$ MeV/c^2.
This peak has also been seen at 400 MeV/c by D. CLINE et al.[13] and at 1000 MeV/c by G. ALEXANDER et al.[14].

- The analysis of this peak by H.G. DOSCH and V. HEPP[15] shows that the enhancement of the (Λp) invariant mass at 2129 MeV/c^2 cannot be explained by a cusp due to deuteron dynamics. Their conclusion is that the data indicate the existence of a Λp resonance at this energy and a ΣN bound state decaying into Λp.

3 - Interactions on nuclei

When these interactions are studied in bubble chambers, there are always severe experimental problems of combinations in the mass spectra, identification of the protons in one event, short tracks, etc...

a) Λp mass spectrum.

- P.A. PIROUE[16] studied the K^+ spectrum at 30° in p - Be interactions at 3 GeV/c at the Princeton-Penn Accelerator, in a beam servey experiment. It was found that the K^+ momentum spectrum exhibits a rather large deviation from the expected phase space. One possible explanation given by the author is the existence of a strange dibaryon resonance at 2.36 GeV/c^2. But this peak was not seen in pp interactions by [7] and [8].

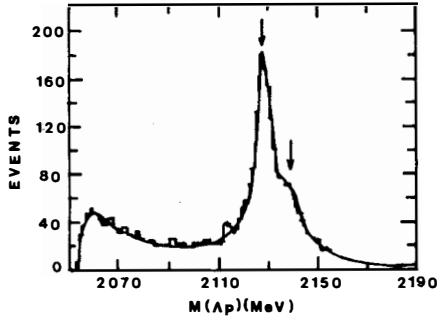

FIG. 2. Λp combined mass ideogram for all events in the reaction $K^- + d \to \pi^- + p + \Lambda$ at rest.

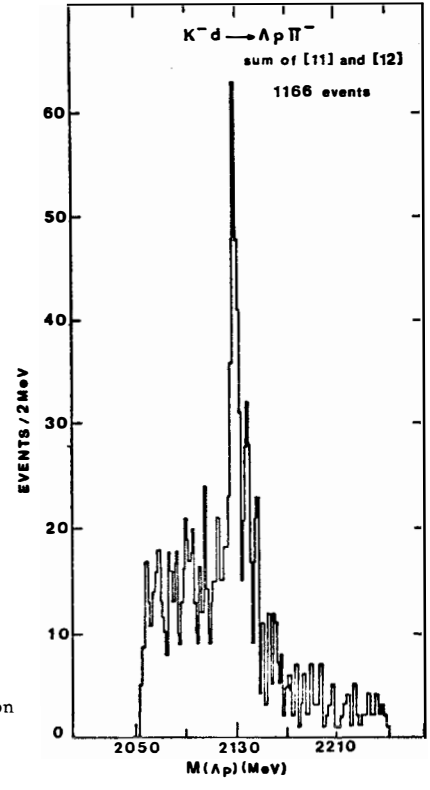

FIG. 3. Λp mass spectrum.
The π^- is selected in the forward direction $\cos(K\pi) > 0.8$ for [11] and > 0.9 for [12].

- T. BURAN[17] plotted all the Λp mass combinations in an experiment of the Ecole Polytechnique heavy liquid bubble chamber filled with CF_3Br using K^- at rest. They observe an enhancement at 2220 MeV/c^2. The width is ∿ 20 MeV/c^2.

- P. BEILLIERE et al.[18] have no evidence for any enhancement in the Λp mass spectrum in a RHEL/UCL heavy liquid (propane + freon) bubble chamber experiment with incident K^- of 2.1 GeV/c. Their conclusion is that such effects already observed in other experiments, are difficult to observe in more complex nuclei.

- B.A. SHAHBAZIAN et al.[19] in the JINR 55 cm propane bubble chamber have taken 150 000 pictures with 7 GeV/c neutrons and 120 000 pictures with 4 GeV/c π^-. They have scanned the pictures for all the interactions containing V° particles and they observed 3 peaks (Figure 4). The two first peaks at 2058 MeV/c^2 and 2127 MeV/c^2 are interpreted as effects of a negative Λp and Σp scattering length, respectively. The third peak is explained by the existence of a Λp resonance with M = 2252 MeV/c^2 and Γ = 21 MeV/c^2.

b) Λn mass spectrum

- H.O. COHN et al.[20] have produced Σ^- at rest in the Northwestern University helium bubble chamber using K^- at rest. Then, they have studied the reaction

$$\Sigma^- + {}^4He \rightarrow \Lambda^\circ + n + {}^3H$$

They observe a peak in the triton momentum spectrum (Figure 5). A best fit is obtained with an admixture of the impulse model and a Breit-Wigner shaped resonance M = 2098 MeV/c^2 and Γ = 20 MeV/c^2.

c) ΛΛ and Ξ^-p mass

- B.A. SHAHBAZIAN et al.[19], in the same experiment described earlier, claim also a resonance in the ΛΛ system at M = 2365 MeV/c^2 and Γ = 47 MeV/c^2. Another enhancement in this ΛΛ mass spectrum is thought to be due to a negative ΛΛ scattering length.

- G.A. WILQUET et al.[21] have rescanned the 2.1 GeV/c K^- experiment in the RL/UCL heavy liquid bubble chamber. No significant ΛΛ structure is observed. They do not confirm the 2.37 GeV/c^2 peak previously reported by the same group and also seen by B.A. SHAHBAZIAN et al.[19].

- Finally, J.G. GUY et al.[22] observe no enhancement in the ΛΛ and Ξ^-p mass combinations produced by 12 GeV/c K^- interactions in a platinum plate in the SLAC/LBL 82 in. hydrogen bubble chamber.

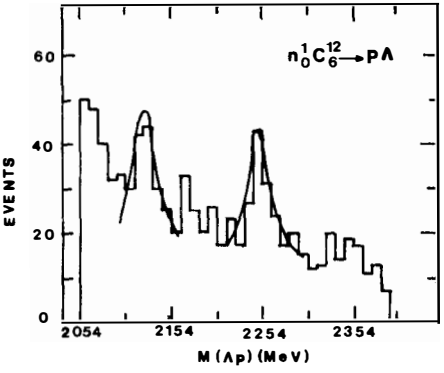

FIG. 4. Λp effective mass spectrum for all one-proton events from a neutron-propane exposure at 7 GeV/c.

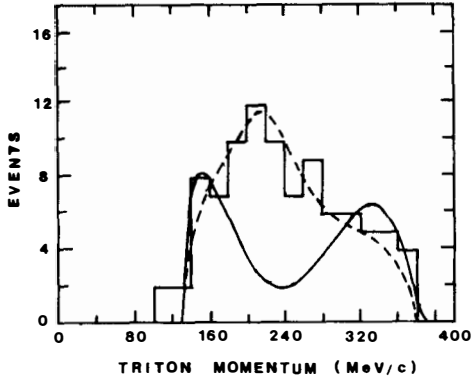

FIG. 5. Triton momentum spectrum in the reaction $\Sigma^- + {}^4He \rightarrow \Lambda^\circ + n + {}^3H$ at rest. The solid curve is the impulse-model prediction normalised to the total number of events. The dashed curve represents impulse model and resonance ($M = 2098$ MeV/c^2, $\Gamma = 20$ MeV/c^2) combined.

Conclusion

Several structures have been observed in the strange dibaryon systems. In the discussion of these experimental results, one has always to decide whether the peak observed corresponds to a bound state, or a resonance, a cusp-effect, a S-wave scattering, or a 6-quarks bag. One state in one channel cannot easily solve the problem. The theoretical background of these systems will be much better understood only when a reasonable spectroscopy of well established states will exist.

Experimentally, scattering experiments seem to be the most direct method for the observation of strange dibaryons. But, there is an absence of low-energy hyperon beams (and naturally also hyperon targets).

Then one has to look for narrow ($\Gamma < 50$ MeV/c^2) resonances.

The nucleon-nucleon interactions between 5 and 8 GeV/c can be useful, but there is an important background, for example in the 2050-2300 MeV Λp mass spectrum. Also, the cross sections, due to baryon exchange, will be very low.

Interactions of K^- of different momenta with light nuclei seem to be more fruitful (problems increase with the target atomic number). One has to analyse carefully the multiple scattering of the primary and secondary particles on the moving nucleons in the target. Kinematical enhancements due to known Y^*, N^* have also to be subtracted. Otherwise, these interactions have certainly given the most interesting results, if not promises.

A summary of the results reported here is given in table 1.

REFERENCES

1) R.L. JAFFE, Phys. Rev. Letters 38, 195 (1977) ; Phys. Rev. Letters 38, 617 (1977)
A.Th.M. AERTS et al., THEF-NYM-77.5 (1977)
V.A. MATVEEV and P. SORBA, Fermilab-Pub 77/56-THY, June 1977 ; ibid, Lettere al Nuovo Cimento 20, 435 (1977)
P. GNADIG et al., Phys. Letters B64, 62 (1976)
N.S. CRAIGIE and G. PREPARATA, Nuclear Phys. B102, 497 (1976).
CHAN HONG-MO and H. HØGAASEN, CERN preprint TH.2388 (1977); ibid, RL-77-144/A

2) G. ALEXANDER et al., Phys. Rev. 173, 1452 (1968).

3) J.M. HAUPTMAN et al., Nuclear Phys. B125, 29 (1977).

4) M. FIREBAUGH et al., Phys. Rev. 172, 1354 (1968).

5) E. BIERMAN et al., Phys. Rev. 147, 922 (1966).

6) W. CHINOWSKY et al., Phys. Rev. 165, 66 (1968).

7) A.C. MELISSINOS et al., Phys. Rev. Letters 14, 604 (1965).

8) J.T. REED et al., Phys. Rev. 168, 1495 (1968).

9) A.G.S. Proposal 703. Preliminary results of this experiment are reported in the A.G.S. Proposal 722 - A.S. CARROLL et al.

10) TAI HO TAN, Phys. Rev. Letters 23, 395 (1969).
11) D. EASTWOOD et al., Phys. Rev. D3, 2603 (1971).
12) O. BRAUN et al., Nuclear Phys. B124, 45 (1977).
13) D. CLINE et al., Phys. Rev. Letters 20, 1452 (1968)
14) G. ALEXANDER et al., Phys. Rev. Letters 22, 483 (1969).
15) H.G. DOSCH and V. HEPP, TH-2310-CERN, April 1977.
16) P.A. PIROUE, Phys. Letters 11, 164 (1964).
17) T. BURAN et al., Phys. Letters 20, 318 (1966).
18) P. BEILLERE et al., Preprint IIHE-76.9, November 1976.
19) B.A. SHAHBAZIAN et al., Nuclear Phys. B53, 19 (1973) ; ibid. Lettere al Nuovo Cimento 6, 63 (1973).
20) H.O. COHN et al., Phys. Rev. Letters 13, 668 (1964).
21) G. WILQUET et al., Phys. Letters 57B, 97 (1975).
22) J.G. GUY et al., RL-77-054/A, May 1977.

Table 1

Interactions	Channel	Mass, width (MeV/c^2)	Reference	Comments
K^-d	Λ p	M = 2129 Γ = 6	[10],[11],[12] [13],[14]	
	Λ p	M = 2139 = 9	[10]	To be confirmed
On Nuclei	Λ p	M = 2252 Γ = 21	[19]	To be confirmed
	Λ P	M = 2360	[16]	Not seen in pp [7],[8]
	Λ n	M = 2098 Γ = 20	[20]	To be confirmed
	Λ Λ	M = 2365 Γ = 47	[19]	Not confirmed by [21]
p p	"Λ Λ"	M $\simeq$ 2200	[9]	< 3 standard deviation effects

DIBARYON RESONANCES: DO THEY EXIST ?

P. KROLL
Department of Physics, University of Wuppertal
Germany

Abstract:
Possible candidates for (non-strange) dibaryon resonances are discussed. It will turn out that at present there are only two good candidates.

Resumé :
On discute des candidats possibles pour des resonances dibaryon (non-etranges). Il se montre que maintenant il n'y a que deux bons candidats.

1. INTRODUCTION

For many years it was believed that every resonance is built up of 3 quarks (baryons) or of $\bar{q}q$ pairs (mesons). Exotic states made of more quarks should not exist. This believe, of course, was born out of the experimental situation in the late Sixties, early Seventies: no convincing experimental evidence for the existence of exotic resonances had been found.

Now, recently the situation has changed both theoretically and experimentally. Jaffe[1], for example, found that in the MIT bag model the same force which produces the spectrum of the ordinary hadrons, generates also exotic states. Experimentally, states have been found which may be considered as candidates for $q^2\bar{q}^2$ mesons.

These results have revived the interest in the old question whether dibaryon resonances exist. During the last twenty years or so several enhancements have been reported which in principle could be due to dibaryons but have been explained by nonresonant mechanisms, mostly only on the qualitative level. More recently however, a few bumps have been found which seem to be rather serious candidates for dibaryons. Still other explanations (e.g.strong inelastic thresholds, cusps or final state interactions) are not completely excluded and the discussion of the various ways out of the resonance interpretation will be the main subject of this contribution.

2. PROTON-PROTON ELASTIC SCATTERING

With the polarized beam and target total cross-section in pure spin states have been measured at Argonne. The cross-sections are related to the s-channel helicity amplitudes by

$$\sigma_{tot} = \frac{1}{2}\left(\sigma(\overrightarrow{\leftarrow})+\sigma(\overrightarrow{\rightarrow})\right) = 2\sqrt{\pi}\ \mathrm{Im}\ (\phi_1+\phi_3)\big|_{t=o} \qquad (1)$$

$$\Delta\sigma_T = \sigma(\uparrow\downarrow) - \sigma(\uparrow\uparrow) = -4\sqrt{\pi}\ \mathrm{Im}\ \phi_2\big|_{t=o} \qquad (2)$$

$$\Delta\sigma_L = \sigma(\overrightarrow{\leftarrow}) - \sigma(\overrightarrow{\rightarrow}) = 4\sqrt{\pi}\ \mathrm{Im}\ (\phi_1 - \phi_3)\big|_{t=o} \qquad (3)$$

Instead of showing the experimental results of these cross-sections separately I present in fig. 1 combinations of them which project out certain groups of partial waves

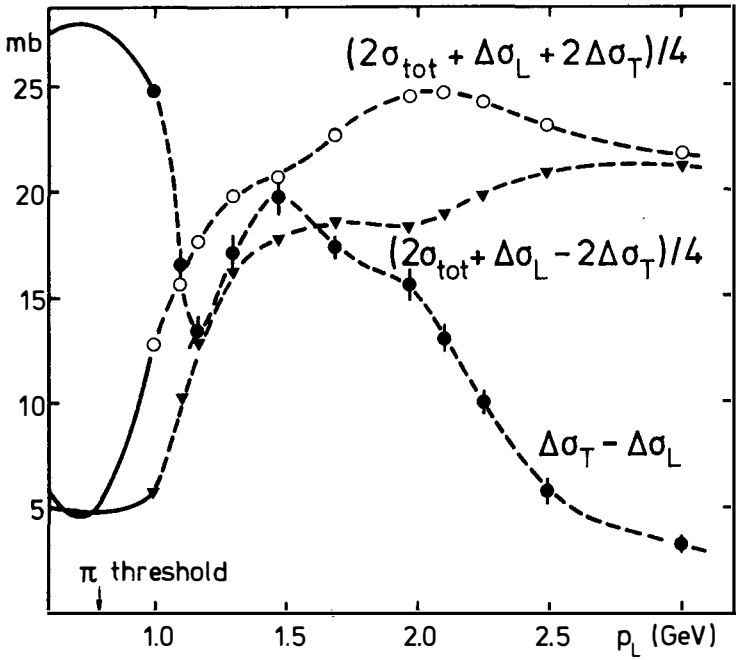

Fig.1: Combinations of total cross-sections. Data taken from ref.3-5). Solid limes are values reconstructed from phase shifts[6], dashed lines are drawn to guide the eyes.

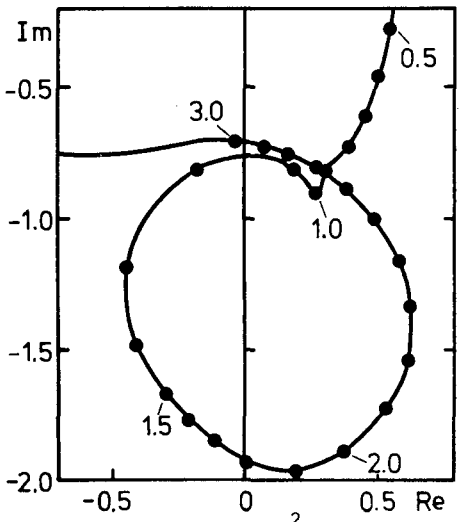

Fig.2:Argand plot of $q^2(\phi_1+\phi_2-\phi_3)/\sqrt{\pi}$ at t=o.p_L values spaced by o.1GeV.

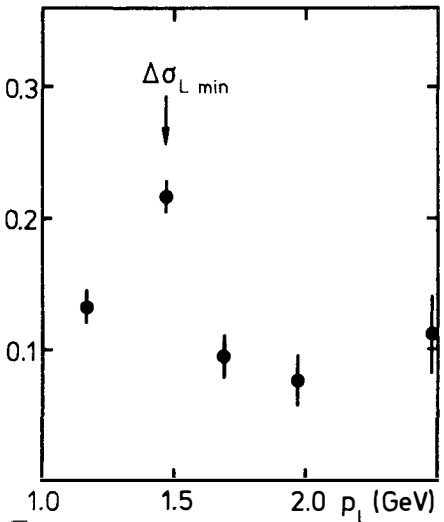

Fig.3: The spin correlation parameter A_{LL} at 9o°. Data taken from ref. 5).

$$\frac{1}{4}(2\sigma_{tot}+\Delta\sigma_L+2\Delta\sigma_T) = \frac{4\pi}{q^2}\sum_{J(even)}(2J+1)\ \mathrm{Im}\ R_J \qquad (4)$$

$$\frac{1}{4}(2\sigma_{tot}+\Delta\sigma_L-2\Delta\sigma_T) = \sum \text{ coupled triplets} \qquad (5)$$

$$\Delta\sigma_T - \Delta\sigma_L = \frac{4}{9}\sum_{J(odd)}(2J+1)R_{JJ} - \sum \text{ coupled triplets} \qquad (6)$$

where q being the cm momentum and R_i the partial waves in the notation of Scotti and Wong.[2)]

All three combinations show strong threshold effects due to π-production but in addition there is a very pronounced bump in $\Delta\sigma_T - \Delta\sigma_L$ at around p_L = 1.5 GeV and - with less evidence - another bump in the spin singlet states R_J at around 2 GeV. It is tempting to identify these bumps with pp resonances in an uncoupled triplet state R_{JJ} (the bump is positive) and in a singlet state.

Another hint at a resonance behaviour comes from a dispersion analysis[7)] of all three forward amplitudes, which is now made feasible by the new Argonne data: the bumps are related to circles of the corresponding amplitudes in an Argand plot (compare fig.2).

Let us assume that both the structures are resonances. Fitting Breit-Wigner formulae to the amplitudes, one obtains

R_J:	m = 2390 MeV	$\Gamma \simeq$	100 MeV
R_{JJ}:	2320 MeV		280 MeV

(7)

Both resonances are strongly inelastic (note the diameter of the circle in fig. 2 is equal to $(2J+1)\Gamma_{el}/\Gamma$).

The possible existence of a R_{JJ} state has first been mentioned by Hidaka et al.[8)]. They studied the energy dependence of the coefficients of a Legendre polynomial expansion of $d\sigma/dt$ and the polarization and came to the conclusion that this resonance is very likely in the $^3F_3$ wave. A recent phase shift analysis performed by Hoshizaki[9)] is not inconsistent with this assignment.

Further support for the resonance interpretation of the structure in the R_{JJ} waves is obtained from measurements[5)] of the spin correlation parameter A_{LL} at large angles. From fig. 3 where the A_{LL} data at 90^o are shown, one sees that A_{LL} develops a bump at about the same position as $\Delta\sigma_L$.

All these arguments in favour of a resonance interpretation, even if they are quite convincing, do not yet rule out the possibility

that these effects are reflections of the (non-resonant) dynamics of the open inelastic channels. In order to discuss this the cross-sections are separated into their elastic and inelastic parts

$$\Delta\sigma_T = \Delta\sigma_T^{el} + \Delta\sigma_T^{in} \quad ; \quad \Delta\sigma_L = \Delta\sigma_L^{el} + \Delta\sigma_L^{in} \tag{8}$$

The inelastic parts have been calculated from unitarity, taking into account only the $NN\pi$ intermediate states and using specific models for single pion production. So, for example, Berger et al.[10] performed a Deck model calculation, others[11] used the fact that π-production goes mainly via $N\Delta$ and constructed an OBE model for this reaction. Also a coupled channel three body calculation was carried out[12]. The basic dynamical input in all these models is one pion exchange and it is therefore no surprise that the results essentially agrees with each other: $\Delta\sigma_T$ is more or less saturated by $\Delta\sigma_T^{in}$ whereas $\Delta\sigma_L^{in}$ comes out positively just above threshold but experimentally $\Delta\sigma_L$ is negative. In some models $\Delta\sigma_L^{in}$ changes sign between p_L = 1.5 and 2 GeV.

From the existing A_{LL} data[5], interpolating smoothly between them and the forward values taken from the dispersion analysis[7], one can estimate the elastic part of $\Delta\sigma_L$

$$\Delta\sigma_L^{el} = -2\int dt\, A_{LL} \frac{d\sigma}{dt}\,(pp \to pp) \tag{9}$$

At p_L = 1.47 GeV one finds for $\Delta\sigma_L^{el}$ a value between - 6 and -8mb. So, $\Delta\sigma_L^{el}$ and $\Delta\sigma_L^{in}$ from pion exchange <u>do not</u> saturate the experimental value of $\Delta\sigma_L$ (= - 17 mb at 1.47 GeV). This result is consistent with the interpretation that the structure being a strongly inelastic resonance, its contribution to pion production is not taken into account in $\Delta\sigma_L^{in}$. Lack of data does not allow a similar estimate of $\Delta\sigma_T^{el}$.

From the above considerations one may conclude that at least the $^3F_3$ bump seems to be a genuine resonance. The R_J enhancement needs confirmation.

3. OTHER DIBARYON RESONANCES

Besides elastic proton-proton scattering several other bumps which could be due to (non-strange) dibaryon resonances have been reported (compare table).

Table: Enhancements in deuteron reactions

m (MeV)	Γ (MeV)	reaction	ref.
2170	35...50	$\sigma_{tot}(\gamma d \to pn)$	13
		m(pp), m(πd),.....	14
		$\frac{d\sigma}{dt}, \sigma_{tot}$ of $pp \to d\pi^+$	15
2900 3600		$\frac{d\sigma}{dt}$ $(pp \to d\pi^+)$	15
2380	100...200	polarization of $\gamma d \to pn$ at 90^o	16

The general belief is that these bumps are not dibaryon resonances but due to particularities of the deuteron dynamics. For example, Yao[17] tried to explain the bumps seen in $pp \to d\pi^+$ by the graph shown. Going through the kinematics one can assure oneself that forward production of the deuteron is controlled by backward πN scattering - the πN resonances should show up in $pp \to d\pi^+$. However, this model fails quantitatively. It is, of course, not clear whether this idea is fundamentally wrong or the failure is only a consequence of the usual technical problems with the deuteron, as for example unknown off-shell corrections, neglect of the D wave deuteron and so on. So, the situation for the enhancements at 2900 and 3600 MeV remains unclear. Only the 2170 MeV bump, the so-called d^*, can be quantitatively explained as a final state interaction with an intermediate Δ. So, at present there is no reason to consider it as a candidate for a dibaryon resonance. On the other hand the enhancement at 2380 MeV seen in the photodisintegration of the deuteron seems to be a proper candidate.

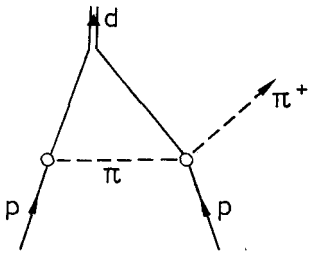

4. CONCLUSIONS

Dibaryon resonances - if they exist at all - seem to be rather rare objects. At present, there are only two structures which are probably non-strange dibaryon resonances. One or two states are known in the strange sector. However, future experiments specifically designed for the search of dibaryons may change the situation. Production and formation experiments with polarized beams and targets (e.g. $\vec{p}\vec{p} \to \pi NN$, $\pi^+ d$) may be particularly helpful.

From the theoretical point of view it should be noted that one has here the same problem as for the new mesons. It is by no means clear that these states are single bag states with 6 quarks in the bag[1], states which may be called colour molecules. But they may be equally well two bag states bound by van der Waals type forces (nuclear potentials), that means they may be states very similar to the deuteron. So, for example, Kamae and Fujita[18], have shown that a standard OBE potential for $\Delta\Delta$ has some deeply bound states (order of 1oo MeV) one of which may be the 238o MeV enhancement.

REFERENCES

1) R.L.Jaffe, Phys.Rev.Lett. 38, 195 (1977) and ref. therein
2) A.Scotti and D.Y. Wong, Phys.Rev. 138, B145 (1965)
3) W.de Boer et al., Phys.Rev.Lett. 34, 558 (1975)
   E.Biegert et al., Phys.Lett. 73B, 235 (1978)
4) I.P.Auer et al., Phys.Lett. 67B, 113 (1977), 7oB, 475 (1977)
5) Reported in H.Spinka, preprint ANL-HEP-CP 77-8o (1977)
6) R.A.Arndt et al., Phys. Rev. C15, 1oo2 (1977)
7) W.Grein and P.Kroll, Nucl.Phys.B,to be published
8) K.Hidaka et al., Phys.Lett. 7oB, 479 (1977)
9) N.Hoshizaki, Prog.Theor.Phys. 58, 716, (1977)
1o) E.L.Berger et al., preprint ANL-HEP-75-72 Argonne (1975)
11) G.N.Epstein and D.O.Riska, preprint, Michigan (1976)
12) W.M. Kloet et al., Phys.Rev.Lett.39, 1643 (1977)
13) J.C.Keck and A.V.Tollestrup, Phys.Rev.1o1, 36o (1956)
14) O.Denegri et al, Nucl.Phys. B28, 13 (1971) and ref. therein
15) H.L.Anderson et al., Phys.Rev.Lett.21, 853 (1968)
16) T.Kamae et al., Phys.Rev.Lett. 38, 468 (1977)
17) T.Yao, Phys.Rev. 134, B454 (1964)
18) T.Kamae and T.Fujita, Phys.Rev.Lett. 38, 471 (1977)

EXOTIC BARYONIUM EXCHANGES

Basarab Nicolescu
Division de Physique Théorique[+]
Institut de Physique Nucléaire
91406 Orsay Cedex-France
and
Laboratoire de Physique Théorique des Particules Elémentaires,
Université Pierre et Marie Curie, Paris

Abstract : We review the prominent effects supposed to be associated with the exchange of exotic baryonium Regge trajectories. The experimental presence of all expected effects leads us to suggest that the baryonium exchange mechanism is a correct phenomenological picture and that mesons with isospin 2 or 3/2 or with strangeness 2, strongly coupled to the baryon-antibaryon channels, must be observed.

Résumé : Nous montrons que tous les effets associés à l'échange du baryonium sont effectivement présents dans les données expérimentales. Notre analyse suggère l'existence de mésons d'isospin 2 ou 3/2 ou d'étrangeté 2, fortement couplés aux voies baryon-antibaryon.

[+]Laboratoire **associé au C.N.R.S.**

I. INTRODUCTION

Let me begin by making a trivial, but important remark. The existence of "true" exotic mesons (i.e. mesons whose quantum numbers cannot be obtained from a $q\bar{q}$ system but only from a multiquark system) is crucial for all existing theoretical schemes of baryonium [1]. Even in the baryonium models (e.g., the bag model [2]) in which the role of colour is very much emphasized compared with the role of flavour, the existence of the "true" exotics is a necessary condition for the validity of these models. Of course, the "true" exotic states are expected, for various reasons, to decouple from the meson-meson channels. However, no analogous argument has been given for their systematic decoupling from the baryon-antibaryon channels, and in fact one expects them to be strongly coupled to these channels [3].

In spite of the present proliferation of the meson states which are good candidates for being members of the baryonium family [4], for the moment only few of them could be "true" exotics. In fact there are only three candidates for the "true" exotics : one I=2 meson strongly coupled to the $N\bar{N}\pi$ channel [5] and two I=3/2 mesons strongly coupled to the $\bar{\Lambda}\Delta^{++}$ or $\bar{Y}^{*++}p$ channels [6]. Their existences are not well established ; the corresponding experimental data are either controversial [5),7] or very preliminary [6].

However, we can already extract some important information concerning these "true" exotic baryonium states from the data involving their exchange as Regge poles [8]. The short review I present here will be devoted to the answering of the following questions : 1) is there some phenomenological evidence for the existence of exotic baryonium as Regge pole exchange ? ; 2) if these exotic baryonium Regge poles are indeed present in the data, what are their main properties ?

II. ARGUMENTS FOR THE EXISTENCE OF EXOTIC BARYONIUM EXCHANGES

Since the " cryptoexotic" baryonium contribution is mixed with the ordinary meson contribution, the separation of the baryonium contribution will be, in general, delicate and ambiguous. Therefore, in order to make crucial tests of the existence of the baryonium exchange, one must look at the special class of reactions involving pure baryonium (i.e., "true" exotic) t-channels.

The reactions involving pure baryonium t-channels studied in this section [9)-13)] are of the following types :

$$B_1\ B_2 \to D_1\ D_2 \qquad (1)$$

$$\bar{B}\ B \to \bar{D}\ D \qquad (2)$$

$$\bar{B}_1\ B_1 \to \bar{B}_2\ B_2 \qquad (3)$$

$$M_1\ B_1 \to M_2\ D_2 \qquad (4)$$

and

$$M_1\ B_1 \to M_2\ B_2 \qquad (5)$$

where M denotes mesons belonging to the 0^- octet, B denotes baryons belonging to the $1/2^+$ octet, and D denotes baryons belonging to the $3/2^+$ decuplet.

In fact, we will focus our discussion on the reactions of the type (1), (2) and (4) involving production of $3/2^+$ decuplet baryons. The reasons for this restriction are both theoretical and practical.

It is well known that empirically there is an important suppression of the reactions (3) and (5) involving production of $1/2^+$ octet baryons when compared with the reactions of the type (1), (2) or (4). For example, at p_L=4.2 GeV/c the forward differential cross section for $K^-p \to \pi^+ Y^{*-}$ is ten times larger then the one for $K^-p \to \pi^+ \Sigma^-$ [10k),13)].

Theoretically, as was shown by Hoyer and Quigg [14)] one can understand this suppression using the triple-Regge expansion at fixed s and different $(\text{mass})^2$ of the produced baryon. The

explicit (mass)^2 dependence of cross sections implies that the larger the mass of the produced resonance - the larger the "forbidden" cross section. For some particular cases the suppression of octet final states is reinforced by SU(6) Clebsch-Gordan coefficients. For example, the coupling of $\bar{p}Y^{*-}$ to baryonium is $4\sqrt{2}$ that of $\bar{p}\Sigma^-$ [15].

On a practical level, the above discussed suppression implies that the detection of the experimental effects in the pure baryonium channels for the reactions (3) and (5) is possible only in high precision experiments, which unfortunately are rare at the present time.

The particular reactions used in our analysis are the following :

i) pure I=2 baryonium channel [9a)-h)] (corresponding, e.g., to a $u\,u\,\bar{d}\,\bar{d}$ exchange)

$$pn \to \Delta^-\Delta^{++} \qquad (6)$$

and

$$\pi^- p \to \pi^+\Delta^- \quad \text{or} \quad \pi^+ n \to \pi^-\Delta^{++} \qquad (7)$$

ii) pure I=3/2 baryonium channel [9c)-d),10a)-k)] (corresponding, e.g., to $s\,d\,\bar{u}\,\bar{u}$ or $s\,u\,\bar{d}\,\bar{d}$ exchanges)

$$\bar{p}p \to \overline{Y^{*+}}\,Y^{*-} \qquad (8)$$

and

$$\pi^- p \to K^+ Y^{*-} \qquad (9)$$

$$K^- p \to \pi^+ Y^{*-} \qquad (10)$$

iii) pure S= 2 baryonium channel [9c)-d),10h),11a)-b)] (corresponding, e.g., to $s\,s\,\bar{u}\,\bar{u}$, $s\,s\,\bar{d}\,\bar{d}$ or $s\,s\,\bar{u}\,\bar{d}$ exchanges)

$$K^- p \to K^+ \Xi^{*-} \qquad (11)$$

(There is no data for the interesting reaction $\bar{p}p \to \overline{\Xi^{*+}}\Xi^{*-}$).

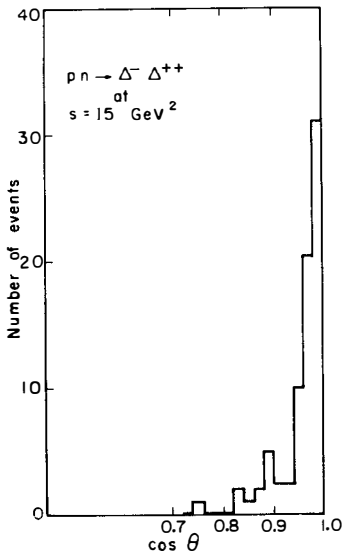

Fig.1a) Forward peak in $pn \to \Delta^{-}\Delta^{++}$ (Ref. 9b)).

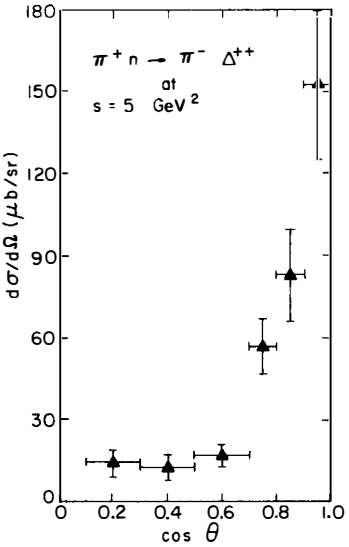

Fig. 1b) Forward peak in $\pi^{+}n \to \pi^{-}\Delta^{++}$ (Ref. 9d)).

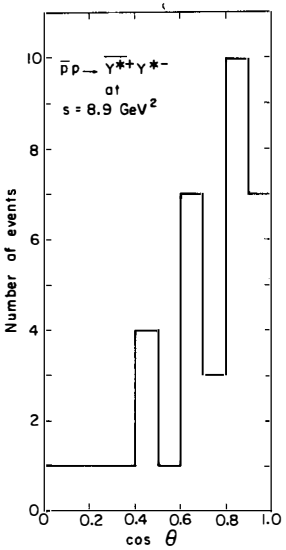

Fig. 1c) Forward peak in $\bar{p}p \to \overline{Y^{*}}^{+}Y^{*-}$ (Ref. 10a)).

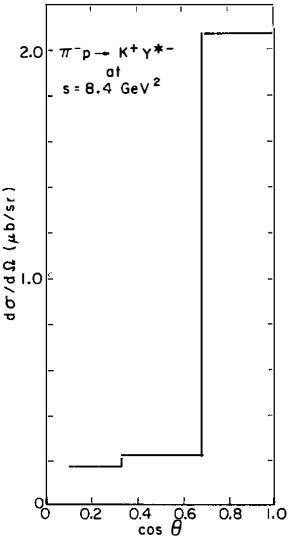

Fig. 1d) Forward peak in $\pi^{-}p \to K^{+}Y^{*-}$ (Ref. 9d)).

Let us notice that the I=3/2 and the S= 2 baryonium channels can also be reached from the corresponding reactions involving the production of $1/2^+$ octet baryons. There is some significant data [12),13)] for reactions like

$$\bar{p}p \to \bar{\Sigma}^+ \Sigma^- \qquad (12)$$

and

$$K^- p \to \pi^+ \Sigma^- \qquad (13)$$

which will also be used in our analysis.

One must note that the quality of the existing data for the reactions (1), (2) and (4) do not allow a very detailed quantative Regge analysis ; however, there is a relatively large number of data points in the medium energy region ($p_L \simeq 2$-10 GeV/c) and their precision is sufficient to test the major qualitative effects expected from the exchange of baryonium trajectories.

One must also remark that much of the existing data in the medium energy region is concentrated at the lower end of this energy range ($p_L \simeq 2$-4 GeV/c) where a Regge expansion is not accurately valid. However, this fact is not essential for the present purpose which is to look for generic and not for detailed quantitative features associated with the exchange of baryonium. Therefore we expect that our basic conclusions will not be altered by a more accurate treatment.

1) The existence of forward peaks in the pure baryonium channels.

This subject received some attention in the early 1970's, after the discovery of "forbidden" peaks in the reactions (6)-(11), where the differential cross section shows a typical decrease of one order of magnitude in the forward hemisphere (see figs. 1a)-f) for some examples). A comprehensive review of the experimental situation at that time was given by Rosner [15)]. The excitement provoked by this discovery was soon dulled by skepticism, due to

the following three fundamental objections :

a) the lack of evidence for forward peaks in octet-production reactions ·

b) the possibility of simulating forward peaks in decuplet- production reactions by "kinematical" reflections, as first suggested by Berger [16] or of producing them by double-reggeon exchange [17] ;

c) the spectroscopic absence of baryonium states.

This skeptical attitude persisted until last year. However, now the experimental situation is rather drastically changed.

First, forward peaks in octet-production reactions are observed. For example, high statistics experimental data showing the definite confirmation of a forward peak in $K^- p \to \pi^+ \Sigma^-$ at p_L=4.2 GeV/c were published last year [13]. Also, there is evidence of a forward peak in $\bar{p}p \to \bar{\Sigma}^+ \Sigma^-$ at p_L=3.6 GeV/c [12]. As we explained above, the fact that it is so difficult to observe the expected effects in the octet-production reactions must not be considered surprising, due to the natural suppression of lower-mass produced baryons in the class of reactions involving pure baryonium channels.

Secondly, the "kinematical" reflections (see fig.2 for an example) which are surely a possible process, cannot account quantitatively for the forward peaks in the reactions (6)-(11), as was discussed extensively in the literature (see e.g. Refs. 9b),9d),10f),10k)). Moreover, the "kinematical" reflections obviously cannot occur in the reactions involving stable particle final states, like $K^- p \to \pi^+ \Sigma^-$, where the forward peaks are nevertheless observed. Therefore the "kinematical" reflections cannot be the general mechanism giving forward peaks in the pure baryonium channels.

The alternative mechanism of double-Regge exchange can, of course, account qualitatively for all the observed"forbidden" forward peaks. However, at the quantitative level, the existing models [17)-20)] show a tendency of giving too low values for the forward cross sections. For example, they predict for $K^- p \to \pi^+ \Sigma^-$,

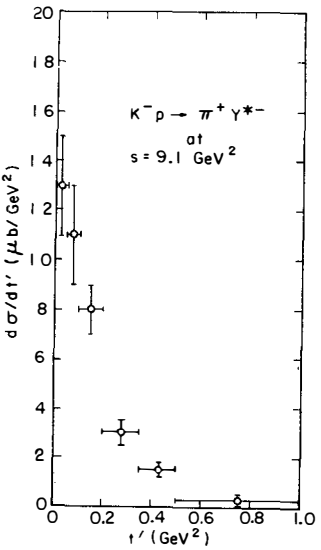

Fig. 1e) Forward peak in $K^- p \to \pi^+ Y^{*-}$ (Ref. 10k)).

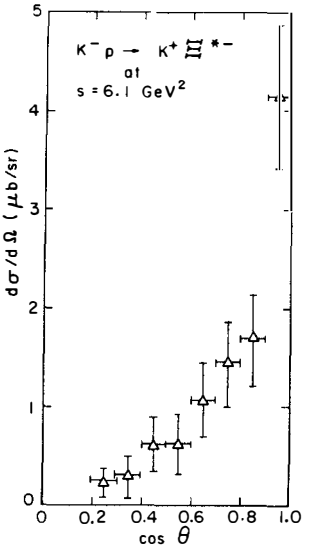

Fig. 1f) Forward peak in $K^- p \to K^+ \Xi^{*-}$ (Ref. 9d)).

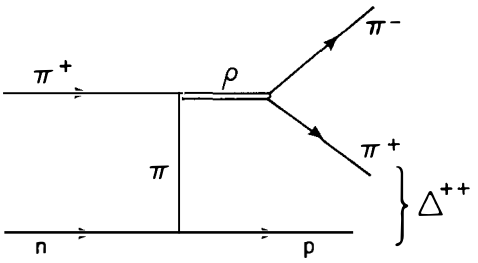

Fig. 2 Possible "kinematical" reflections in $\pi^+ n \to \pi^- \Delta^{++}$.

at $p_L \simeq 4$ GeV/c ,a value of $\sim 0.1 \mu b/GeV^2$ or even smaller, while the experimental value is 10 times larger.

Finally, narrow-width mesons which are good candidates for being baryonium states were recently discovered [4]. It is true that these mesons have the usual quantum numbers (i.e. they can be considered only as "cryptoexotics") but in the baryonium scheme they appear on the same footing as the I=2 or 3/2 or S=2 mesons.

In conclusion, the main objections against the description of the "forbidden" forward peaks as resulting from baryonium exchange seem now to weaken.

2) The change of the energy variation regime from the low energy to the medium energy region.

The fast decrease of the cross sections with the energy ($\simeq s^{-9} - s^{-10}$) below 2 GeV/c is common to many inelastic reactions, involving or not pure baryonium channels. After 2 GeV/c there is known to be a break in the energy dependence, showing the transition to a Regge regime, not only in the reactions involving the usual meson exchanges but also in the octet-production reactions (3) and (5) [17]. Here we will show that the same break, in agreement with the Regge-pole behavior, occurs in the decuplet-production reactions (1), (2) and (4). In order to extract the Regge intercepts corresponding to the baryonium trajectories, we will use the data on the integrated cross section in the forward direction, σ_f, which, in the Regge pole model, has the approximate form :

$$\sigma_f \simeq K. \left(\frac{s}{s_0}\right)^{2\alpha(0) - 2} \Big/ \ln\left(\frac{s}{s_0}\right) \qquad (14)$$

(here K is a constant and s_0 is fixed at the standard value $s_0 = 1$ GeV^2). In fig.3 we present a compilation of the world-data for the reactions (6)-(11). By plotting the quantity $\sigma_f . \ln s$ as a function of s one can directly extract from the data the baryonium intercepts.

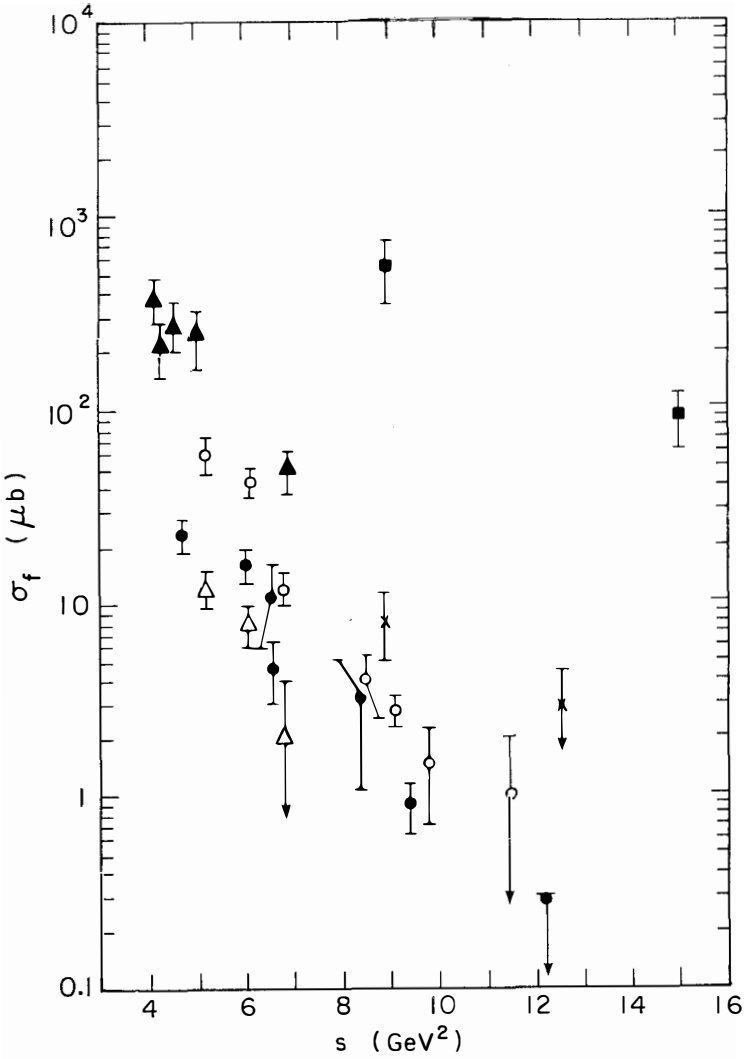

Fig. 3 The integrated cross section in the forward hemisphere σ_f for : $\bar{p}pn \to \Delta^{--}\Delta^{++}$, $\pi^- p \to \pi^+\Delta^{*-}$ (or $\pi^+ n \to \pi^-\Delta^{++}$), $\bar{p}p \to \bar{Y}^{*+}Y^{*-}$, $K^- p \to \pi^+ Y^{*-}$, $\pi^- p \to K^+ Y^{*-}$, and $K^- p \to K^+ \Xi^{*-}$ (Refs. 9a)-h), 10a)-k), 11a)-b)).

i) I=2 (S=0) baryonium

From the data on $\pi^- p \to \pi^+ \Delta^-$ and $\pi^+ n \to \pi^- \Delta^{++}$, one obtains (see fig.4a))

$$\alpha_{\mathcal{B}(I=2)}(0) = -0.75 \pm 0.2 \qquad (15)$$

The data on $pn \to \Delta^- \Delta^{++}$ are in agreement with the corresponding energy variation $\sim s^{-3.5}$ (fig. 4a)).

This value (15) of the isospin 2 baryonium intercept is in agreement with a recent theoretical estimate in the framework of S-Matrix theory. Namely, using a simple planar self-consistent multiperipheral model with a finite-energy sum-rule constraint one generates, without any free parameters, an infinitely-rising baryonium trajectory, dual to vector exchange [21]. This trajectory (see fig .5) satisfies to a high degree of accuracy the isospin I=0, 1, 2 degeneracy property and at t=0 is consistent with the value (15).

Obviously, due to the arbitrary assignment of the different quantum numbers and in particular of the spin, we by no means claim that all the experimental states shown in fig .5 lie on our baryonium trajectory. However, the agreement between, on one side, the predicted and the experimental mass spectrum of baryonium states and, on the other side, the theoretical and the experimental intercept is rather impressive and strongly suggests the existence of isospin 2 baryonium states.

ii) I=3/2 (S=1) baryonium.

From the data on $\pi^- p \to K^+ Y^{*-}$ or $K^- p \to \pi^+ Y^{*-}$, one obtains (see fig. 4b))

$$\alpha_{\mathcal{B}(I=3/2)}(0) \simeq -1.2 \pm 0.2 \qquad (16)$$

The data on $\bar{p}p \to \overline{Y^{*+}}\, Y^{*-}$ are in agreement with the corresponding energy variation $\sim s^{-4.4}$.

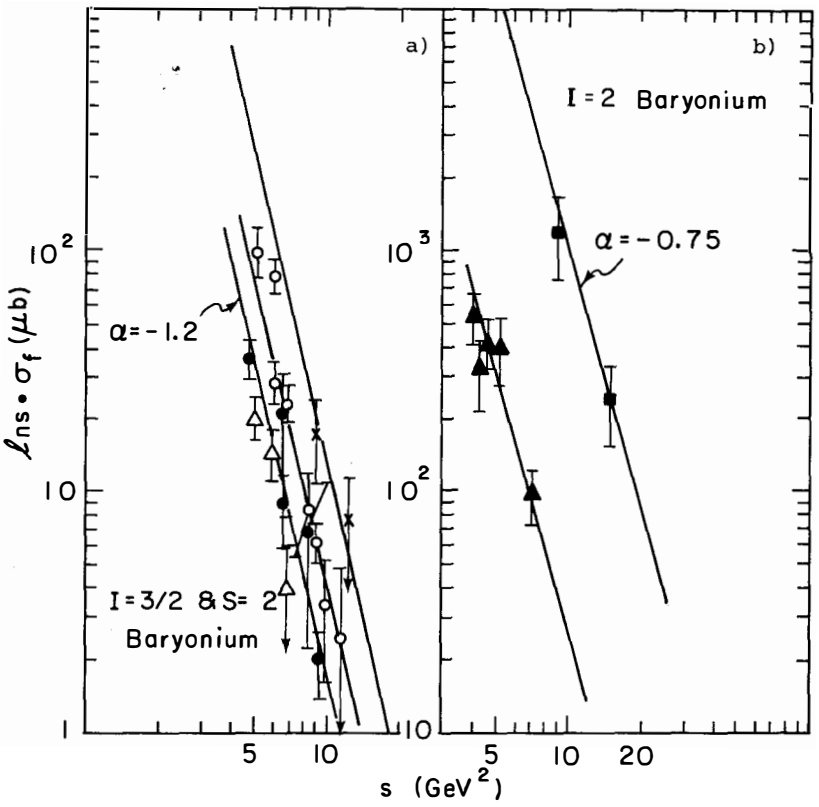

Fig. 4 The Regge behavior of σ_f. Data as in Fig.3.

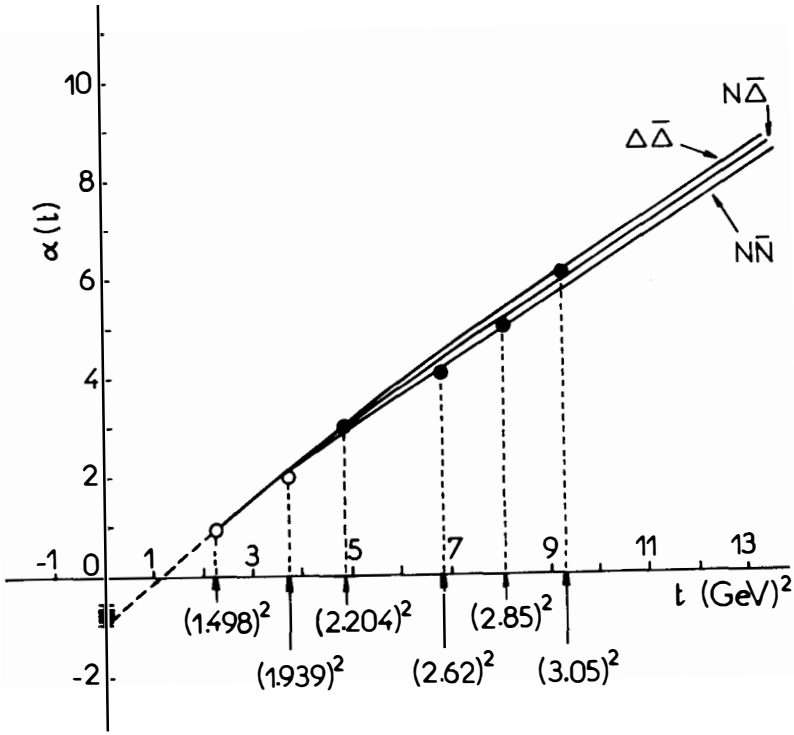

Fig. 5 The non-strange (S=0) baryonium Regge trajectory evaluated without free parameters from the model of Ref.21 for $N\bar{N}$, $N\bar{\Delta}$, and $\Delta\bar{\Delta}$ scattering, respectively (solid curves). The experimental masses of all the recently discovered mesons which can possibly be associated with the Regge recurrences of this trajectory are indicated on the horizontal axis. The open circles correspond to mesons whose spins are well established experimentally. The linear extrapolation from the $\alpha=1$ and $\alpha=2$ states on the $N\bar{N}$ trajectory is indicated by the dashed line. The value (15) of the isospin 2 baryonium intercept is also indicated on this figure.

One notes the relative suppression of the S=1 pure baryonium channels compared with the S=0 ones. For example, $\sigma_f(\pi^- p \to K^+ Y^{*-}) = 4.74 \pm 1.66$ μb at $p_L = 3$ GeV/c [9d], while $\sigma_f(\pi^- p \to \pi^+ \Delta^-) = 50.1 \pm 12.2$ μb at a similar value of p_L (p_L=3.2 GeV/c) [9d]; at $p_L \simeq 3.7$ GeV/c, $\sigma_f(\bar{p}p \to Y^{*+} Y^{*-}) = 8 \pm 3$ μb [10a], while $\sigma_f(pn \to \Delta^- \Delta^{++}) = 550 \pm 200$ μb [9a].

One can also note the difference in magnitude between $K^- p \to \pi^+ Y^{*-}$ and $\pi^- p \to K^+ Y^{*-}$: $\sigma_f(K^- p \to \pi^+ Y^{*-})$ is systematically higher than $\sigma_f(\pi^- p \to K^+ Y^{*-})$. For example, at $p_L \simeq 4$ GeV/c, $\sigma_f(K^- p \to \pi^+ Y^{*-}) = 2.8 \pm 0.5$ μb [10k], while $\sigma_f(\pi^- p \to K^+ Y^{*-}) \simeq 1$ μb [10g]. This difference in magnitude, which results from the line-reversal symmetry breaking, is a similar phenomenon to that observed in the analogous reactions involving usual meson exchanges, for example $K^- p \to \pi^- \Sigma^+$ and $\pi^+ p \to K^+ \Sigma^+$ [22].

Let us finally remark that, assuming the universal slope and the approximate isospin 1/2 and 3/2 degeneracy, one obtains also a rich spectrum of the strange baryonium states. For example, one expects a narrow-width spin 3 particle near the $N\bar{\Sigma}$ threshold, a narrow-width spin 4 particle near the NY^* threshold, and a narrow-width spin 5 particle near m ≃ 2500 MeV. The spin 5 recurrence is not far from the region of mass (m ≃ 2460 MeV) in which a narrow (Γ < 20 MeV) isospin 3/2 meson seems to be observed [6].

iii) S=2 baryonium.

There is not a sufficient number of data on $K^- p \to K^+ \Xi^{*-}$ in order to make a precise evaluation of the corresponding baryonium intercept. However, from fig. 4b) one can deduce that

$$\alpha_{\mathcal{B}(S=2)}(0) \lesssim \alpha_{\mathcal{B}(I=3/2)}(0) \simeq -1.2 \pm 0.2 \qquad (17)$$

One may also observe the relative suppression of the S=2 pure baryonium channels compared with the S=1 ones. For example, at p_L=3 GeV/c, $\sigma_f(K^- p \to K^+ \Xi^{*-}) = 2 \pm 2$ μb, while $\sigma_f(K^- p \to \pi^+ Y^{*-}) = 12 \pm 2$ μb [10h]. Concerning the mass spectrum of the S=2 baryonium states, one expects from (17) and the assumed universal slope, that it will be rather similar to that of S=1 baryonium states.

One must note that the above discussed energy dependence of the "forbidden" peaks is not in obvious contradiction with the double-Regge model, which is very flexible in its predictions. For example, in $\pi^- p \to K^+ Y^{*-}$ a ρ-K^* cut will correspond to $\alpha(0) \simeq -0.3$, while a π-K cut will correspond to $\alpha(0) \simeq -1.25$, the phenomenological value of the intercept being $\alpha(0) \simeq -1.2$.

However, the consistency between the information on the baryonium Regge trajectory, extracted from the negative t region, and the new mesons, which are possibly Regge recurrences corresponding to the same trajectory is indeed an attractive feature of the baryonium scheme. The alternative mechanism, that of Regge cuts, cannot provide, by its very nature, any connection with the observed new mesons.

3) The slopes of the forward "forbidden" peaks.

At fixed s, the t-dependence of the forward peaks corresponding to the exchange of baryonium will be much sharper than the t-dependence corresponding to the Regge-Regge cut. This fact is a direct consequence of the relation between the Regge slopes ($\alpha'_{cut} \simeq 1/2\ \alpha'_{pole}$) and of the hypothesis of approximately constant Regge residues near the forward direction.

As an example, in the table given below, we compare the available experimental slopes of the forward peaks in $\pi^- p \to K^+ Y^{*-}$ and $K^- p \to \pi^+ Y^{*-}$ (corresponding, as usual, to an exponential parametrization) with the slopes due to the baryonium Regge pole exchange (with $\alpha' \simeq 1$ GeV^{-2}).

Table Ia) Slopes of the forward peaks in $\pi^- p \to K^+ Y^{*-}$ (Ref. 9d)).

p_L, GeV/c	2	3	4
Experimental slope, GeV^{-2}	3.2 ± 0.8	4 ± 1	5.4 ± 2
$2\alpha'$ ℓns($\alpha' \simeq 1$ GeV^{-2})	≃ 3.1	≃ 3.8	≃ 4.3

Table Ib) Slopes of the forward peaks in $K^- p \to \pi^{\mp} Y^{*-}$ (Refs. 9d) and 10k)).

p_L , GeV/c	2.1	2.6	4.2
Experimental slope, GeV^{-2}	2.2 ± 0.8	3 ± 1	5.7 ± 0.5
$2\alpha' \ell ns$ ($\alpha' \simeq 1$ GeV^{-2})	≃ 3.3	≃ 3.6	≃ 4.4

One can note the general agreement between the predicted slopes and the experimental slopes. The slopes due to the Regge cut exchange are systematically lower (by ≃50%) than the experimental slopes.

One can conclude that not only the s-dependence, but also the t-dependence of the forward "forbidden" peaks seems to be consistent with the baryonium Regge pole exchange mechanism.

III. SOME PROPERTIES OF THE EXOTIC BARYONIUM COUPLINGS.

1) The coupling of baryonium to the meson-meson channel.

An interesting regularity in the data is the smallness of cross-sections in the reactions (4)-(5) (involving the coupling of baryonium to both baryon-antibaryon and meson-meson channels), as compared with those in the reactions (1)-(3) (involving the coupling of baryonium only to baryon-antibaryon channels).

For example, assuming that, for I=2 baryonium exchange,

$$\sigma_f(pn \to \Delta^- \Delta^{++}) = K_1 \cdot s^{-3.5}/\ell n\ s$$

and

$$\sigma_f(\pi^- p \to \pi^+ \Delta^- \quad \text{or} \quad \pi^+ n \to \pi^- \Delta^{++}) = K_2 . s^{-3.5}/\ell n\ s \qquad (18)$$

one obtains from the existing data on these reactions

$$K_1/K_2 \simeq 25\text{-}50 \qquad (19)$$

(see fig.6, which corresponds to $K_1/K_2 \simeq 38$).

By comparing (in the case of I=3/2 baryonium exchange)

$$\sigma_f(\bar{p}p \to \overline{Y^{*+}}\, Y^{*-}) = K_3.s^{-4.4}/\ell n\ s \qquad (20)$$

and

$$\sigma_f(\pi^- p \to K^+ Y^{*-}) = K_4.s^{-4.4}/\ell n\ s \qquad (21)$$

with the data one obtains also a relatively large ratio

$$K_3/K_4 \simeq 5 - 10 \qquad (22)$$

(see fig.6, which corresponds to $K_3/K_4 \simeq 7.5$).

It is interesting to note that a large value of the ratio of the couplings can also be obtained by comparing the octet-production reactions (3) and (5). For example, $\sigma_f(\bar{p}p \to \bar{\Sigma}^+\Sigma^-) = 5.9 \pm 1.1$ μb at s=8.76 GeV^2 [12], while $\sigma_f(K^-p \to \pi^\pm\Sigma^\mp) = 0.6 \pm 0.1$ μb at s=9.06 GeV^2 [13], and these values correspond to a ratio of the couplings of the order ≃10.

The above mentioned regularity was already interpreted [2a] as due to a spin effect. However, in order to check this interpretation one needs, e.g. in the case of I=2 baryonium exchange, data involving ρ production, data which are not available now.

Another possible interpretation, obviously less attractive on theoretical grounds, is that the selection rule responsible for the small widths of the baryonium states [3),23)], is not too badly violated in going from the positive t to the small negative t region.

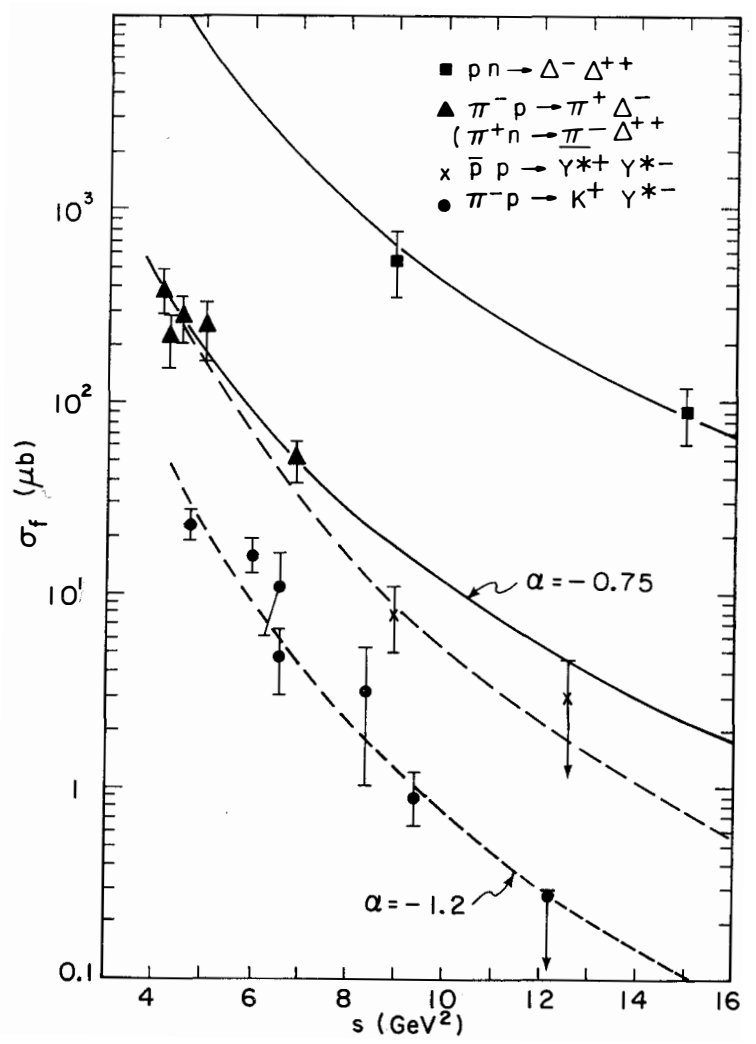

Fig. 6 Illustration of the property discussed in Section III.1).

2) A possible enhancement of the baryonium exchange in the case of baryon decuplet production.

A striking feature of the experimental data is the fact that the pure baryonium channel cross sections ($\sigma_{\mathcal{B}}$) for the decuplet-production is quite comparable with those corresponding to the usual mesonic Regge exchanges (σ_R). From the assumed Regge behavior of the cross sections one has

$$\frac{\sigma_{\mathcal{B}}}{\sigma_R} = \frac{\beta^2_{\mathcal{B}}}{\beta^2_R} \; s^{2[\alpha_{\mathcal{B}}(0) - \alpha_R(0)]} \tag{23}$$

where β denotes the respective Regge residue.

Because of the relatively large gap between the Regge intercepts one expects large suppression factors to occur. For example, if $0 \lesssim \alpha_R(0) \lesssim 1/2$ and if $\beta^2_R/\beta^2_{\mathcal{B}} \simeq 1$, one expects at $s \simeq 10$ GeV^2 a suppression factor $\simeq 1/30 - 1/300$ for the I=2 baryonium cross sections, and a suppression factor $\simeq 1/250 - 1/2500$ for the I=3/2 baryonium cross sections.

The experimental ratios $\sigma_{\mathcal{B}}/\sigma_R$ are in fact much larger than these values expected from the naive Regge arguments. For example $\sigma_f(pn \to \Delta^- \Delta^{++})/\sigma_f(pn \to \Delta^{++}\Delta^-) \simeq 1/2$ at s=8.94 GeV^2 [9a] and $(d\sigma/dt)\,(K^- p \to \pi^+ Y^{*-})/(d\sigma/dt)\,(K^- p \to \pi^- Y^{*+}) \simeq 1/6$ at s=9.06 GeV^2 and near the forward direction [10k]. One is therefore forced to draw the rather surprising conclusion that, for decuplet-production reactions,

$$\beta^2_{\mathcal{B}} \gg \beta^2_R \quad . \tag{24}$$

In particular, the baryonium coupling to the baryon-antibaryon channel is much stronger than the usual meson coupling. (Obviously this conclusion depends critically on the assumption, which we regard as reasonable, that the scale factor $s_0 \simeq 1$ GeV^2). Therefore one has a much weaker suppression of the pure baryonium channels than that expected on the basis of the rather large gap between the reggeon intercepts.

In order to test this effect as being a true dynamical effect and not a spurious one as due to a dip in the forward direction in the usual Regge exchange reactions, one needs much more data on the corresponding pair of reactions.

One must note that, at comparable energies, there is a much stronger suppression of the pure baryonium channels for the baryon octet production. For example, $(d\sigma/dt)\ (K^-p\to\pi^+\Sigma^-)/(d\sigma/dt)\ (K^-p\to\pi^-\Sigma^+) \simeq 1/700$ at $s\simeq 9.06\ GeV^2$ and near the forward direction [13]. This value of the suppression factor is in the range given by the above discussed naive Regge arguments.

IV. CONCLUSIONS

In the present talk we have reviewed the major experimental effects supposed to be associated with the exchange of exotic baryonium trajectories.

The presence of all expected prominent effects, strongly suggests that the baryonium exchange mechanism is a correct phenomenological picture and that mesons with isospin 2 or 3/2 or with strangeness 2, coupled essentially to the baryon-antibaryon channel, must be observed.

Of course, the double-Regge exchange mechanism can explain some of the effects observed in the pure baryonium channels and therefore this alternative scheme cannot be completely ruled out at the present time. We think that the only crucial test in order to choose between the baryonium scheme and Regge-Regge cut scheme is provided by the existence or non-existence of the "true" exotic mesons, strongly coupled to the baryon-antibaryon channel. This test is not yet performed. However, the recent discovery of narrow-width mesons which can be interpreted as baryonium states, the tendency of all existing double-Regge models to give too low cross-sections for $K^-p\to\pi^+\Sigma^-$, as well as the systematic trends in the s and t-dependence of the forward "forbidden" peaks favor, in our opinion, the baryonium exchange mechanism. The non-existence of the "true" exotic baryonium states would therefore be highly surprising.

ACKNOWLEDGMENTS

I thank Prof. J. Tran Thanh Van for the kind invitation to give this talk. I am also very grateful to Profs. L.A.P. Balázs and G.F. Chew and to Drs. P. Hoyer and D.M. Tow for enlightening discussions.

REFERENCES

1) For the bag model and the potential model of baryonium see, e.g., the talks of Chan Hong-Mo, R.L. Jaffe and R. Vinh Mau at this Conference ; for the S-Matrix approach see G.F. Chew and C. Rosenzweig, "Dual Topological Unitarization : an Ordered Approach to Hadron Theory", Physics Reports (to be published) ; for a QCD type of model see G. Veneziano, "The Color and Flavor 1/N Expansions", Proceedings of the XIIth Rencontre de Moriond, Flaine (April 1977), edited by J. Tran Thanh Van.

2) a) Chan Hong-Mo and H. Høgaasen, Phys. Lett. 72B, 121 (1977); Rutherford Laboratory preprint RL-77-144/A T.209 (1977).

b) R.L. Jaffe, Phys. Rev. D17, 1444 (1978).

3) P.G.O. Freund, R. Waltz and J.L. Rosner, Nucl. Phys. B13, 237 (1969).

4) See, e.g., the talk of L. Montanet at this Conference.

5) A. Rogers, report on preliminary results of the Purdue-Indiana-Vanderbilt Collaboration at SLAC, V International Conference on Experimental Meson Spectroscopy, Northeastern University, April 29-30, 1977.

6) R.M. Turnbull, talk at the Workshop on "Unusual Hadron States and Multiquark Spectroscopy", Abingdon, January 21-22, 1978.

7) J. Boucrot et al., Nucl. Phys. B121, 251 (1977).

8) B. Nicolescu, Nucl. Phys. B134, 495 (1978).

9) Data for $pn \to \Delta^{-}\Delta^{++}$:

a) H.O. Cohn et al., Phys. Lett. 26B, 598 (1968) ;

b) G. Yekutieli et al., Phys. Rev. Lett. 25, 184 (1970).

Data for $\pi^{-}p \to \pi^{+}\Delta^{-}$ or $\pi^{+}n \to \pi^{-}\Delta^{++}$:

c) P.M. Dauber et al., Phys. Lett. 29B, 609 (1969) ;

d) P.L. Hoch, Ph. D. Thesis, Parts 1-3, LBL-1051, LBL-1052, and LBL-1053 (1972) ;

e) L.D. Jacobs, Ph. D. Thesis, UCRL-16877 (1966) ;

f) R.J. Manning, Ph. D. Thesis, UCRL-19339 (1969) ;

g) D.M. Chew et al., "π^+p, π^+n, and π^+d Interactions - a Compilation : Part II", LBL-53 (1973) ;

h) J.P. Baton and G. Laurens, Nucl. Phys. B21, 551 (1970).

10) Data for $\bar{p}p \to \bar{Y}^{*+}Y^{*-}$:

a) C. Baltay et al., Phys. Rev. 140, B1027 (1965) ;

b) H.W. Atherton et al., Nucl. Phys. B29, 477 (1971) ;

c) J.E. Enstrom et al., "$\bar{N}N$ and $\bar{N}D$ Interactions - a Compilation", LBL-58 (1972).

Data for $\pi^-p \to K^+Y^{*-}$:

d) D.H. Miller et al., Phys. Rev. 140, B360 (1965) ;

e) T.P. Wangler et al., Phys. Rev. 137, B414 (1965) ;

f) D.J. Crennell et al., Phys. Rev. Lett. 26, 1280 (1971) ;

g) G. Gidal (private communication), LBL group experiment (to be published) ;
see also Refs. 9c) and 9d).

Data for $K^-p \to \pi^+Y^{*-}$:

h) J. Badier et al., Note C.E.A. 532, CEN-Saclay (1965), unpublished ;

i) M. Aguilar-Benitez et al., Phys. Rev. D6, 29 (1972) ;

j) J. Mott et al., Phys. Rev. 177, 1966 (1968) ;

k) S.O. Holmgren et al., Nucl. Phys. B119, 261 (1977) ;
see also Refs. 9c) and 9d).

11) Data for $K^-p \to K^+\Xi^{*-}$:

a) J. Badier et al., Phys. Lett. 16, 172 (1965) ;

b) G.S. Abrams et al., Phys. Rev. D175, 1697 (1968) ;
see also Refs. 9c)-d),10h).

12) H.W. Atherton et al., Phys. Lett. 42B, 522 (1972).

13) G.G.G. Massaro et al., Phys. Lett. 66B, 385 (1977).

14) P. Hoyer and C. Quigg, Nucl. Phys. B80, 127 (1974).

15) J.L. Rosner, "Review of Exotic Mesons", in "Experimental Meson Spectroscopy", Columbia University Press (1970), p.499-533, edited by C. Baltay and A.H. Rosenfeld.

16) E.L. Berger, Phys. Rev. Lett. 23, 1139 (1969) ;
E.L. Berger and R.A. Morrow, Phys. Rev. Lett. 25, 1136 (1970).

17) G.C. Fox and C. Quigg, Ann. Rev. Nucl. Sci. 23, 219 (1973) and Refs. quoted therein.

18) C. Michael, Phys. Lett. 29B, 230 (1969).

19) F.S. Henyey, G.L. Kane, and J.J.G. Scanio, Phys. Rev. Lett. 27, 350 (1971).

20) C. Quigg, Nucl. Phys. B34, 77 (1971).

21) L.A.P. Balázs and B. Nicolescu, Phys. Lett. 72B, 240 (1977).

22) P. Zeczykowski, Jagellonian University TPJU-3/77 preprint (1977).

23) G.C. Rossi and Veneziano, Nucl. Phys. B123, 507 (1977).

DO MULTIQUARK STATES EXIST AMONG THE 0^{++} MESONS?

A. D. Martin
Department of Physics, University of Durham, England.

Abstract:

It has been proposed that, in addition to the conventional P wave $q\bar{q}$ nonet of 0^{++} mesons, there should be a second 0^{++} nonet composed of $qq\bar{q}\bar{q}$ states nearby in mass. This nonet contains the lightest multiquark states and is therefore particularly suitable for experimental investigation. We review the status of 0^{++} mesons in the light of this proposal.

Précis:

Il a été proposé que, par surcroît au P wave $q\bar{q}$ nonet normal des 0^{++} mesons, il y a besoin d'un deuxième 0^{++} nonet composé des $qq\bar{q}\bar{q}$ états proche en masse. Ce nonet contient les états multiquark les plus légers et donc c'est particulièrement convenable pour l'investigation expérimentale. Nous passons en revue l'état des 0^{++} mesons du point de vue de cette proposition.

The $J^{PC} = 0^{++}$ mesons are of unusual importance in meson spectroscopy. However, they continue to be a centre of controversy, both theoretically and phenomenologically. The reasons are clear. On the theoretical side we may expect, in the quark-gluon approach to strong interactions, a rich spectrum of 0^{++} states below about 1.4 GeV. First we have the conventional P wave $q\bar{q}$ nonet of 0^{++} mesons. In addition, there is also the possibility of $qq\bar{q}\bar{q}$ states. The apparent spectroscopic absence of such multiquark hadrons could be because the mass of the hadron increases roughly linearly with the number of quarks. Jaffe[1] has studied the S wave $qq\bar{q}\bar{q}$ states and, with the magnetic gluon interaction for the mass splitting[2], finds the lowest lying multiquark states belong to a 0^{++} nonet. Interestingly, an explicit quark-bag model calculation[1] estimates the mass of such states to be about 1 GeV or less. So if multiquark states exist, we expect two 0^{++} nonets below about 1.4 GeV. A third possibility for 0^{++} mesons are states built entirely from gluons (glueballs). The expectations here are hard to quantify and we will not consider this further. However, it should be borne in mind that an (I=0) 0^{++} two-gluon state could exist as low as 1 GeV[3].

On the phenomenological side the identification of 0^{++} mesons has been far from easy. This is true despite their strong coupling to the readily accessible 0^-0^- channels, such as $\pi\pi$, πK, $K\bar{K}$. The resonances either appear very broad, or near the $K\bar{K}$ threshold, or hidden under the leading peripheral 2^{++} states. In each case they are prone to ambiguity.

To establish notation for the members of a 0^{++} nonet, we denote the isotriplet by δ, the isodoublets by κ and $\bar{\kappa}$, the isosinglets by ε and S. If the nonet satisfies magic mixing we take S to contain an $s\bar{s}$ pair, and ε to be built entirely of non-strange quarks. Suppose that the S and ε mix magically in the conventional $q\bar{q}$ nonet, then ε and δ will be degenerate in mass with the S state at higher mass. On the other hand, if the S and ε states are magically mixed in the $qq\bar{q}\bar{q}$ nonet, then the quark content is as shown in Fig. 1. That is, the S and δ are degenerate in mass and the ε lies at lower mass. The resulting mass spectrum for the two nonets is sketched in Fig. 2. It was the approximate degeneracy of the observed S*(990) and δ(970) which prompted Jaffe to assign these states to the $qq\bar{q}\bar{q}$ nonet, together with broad $\varepsilon(\pi\pi)$ and $\kappa(K\pi)$ states. Indeed, the only obvious problem with this identification is the observed width of the $\delta \to \pi\eta$ decay; since $qq\bar{q}\bar{q} \to q\bar{q} + q\bar{q}$ are "fall apart" decays, it should be

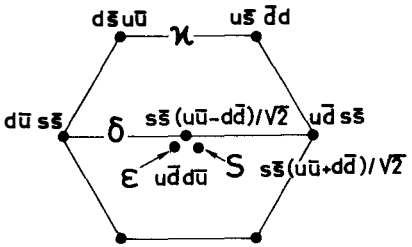

Fig.1

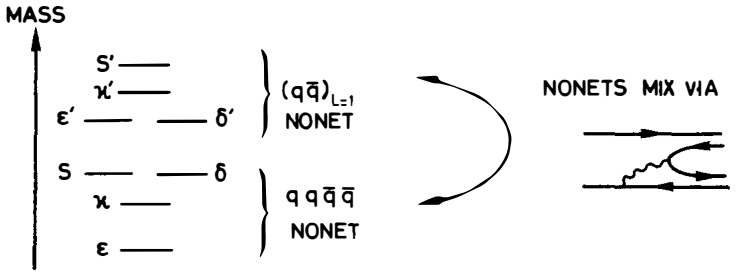

Fig.2

much broader. Of course this approach raises the problem of observing another nearby 0^{++} nonet (ε',δ', κ', S' of Fig. 2).

The spectrum described above represents an idealized situation. There will be complications. First the members of the two nonets can mix by gluon exchange, as shown in Fig. 2. Second we expect some violation of magic mixing. For example, in a $qq\bar{q}\bar{q}$ state one $q\bar{q}$ pair spends a fraction of the time in a colour octet state[1] or in a 0^- state. In either case this will lead to violations of magic mixing.

Now let us review the observed spectrum so that we may compare it with the above expectations. The $\delta(970)$ is clearly established in the $\pi\eta$ channel. The S*(990) is seen both in the $\pi\pi$ and $K\bar{K}$ channels, though with some flexibility in the couplings. The 0^{++} partial waves extracted in $\pi\pi$ and $K\pi$ phase shift analyses

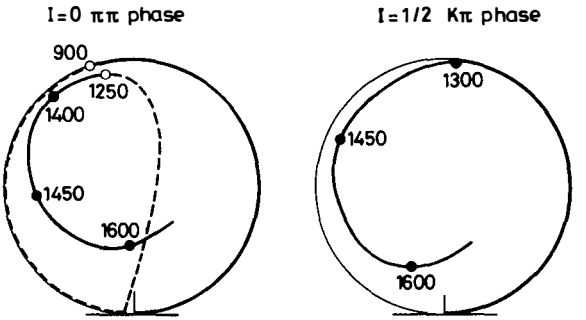

Fig.3

are shown in Fig. 3. These represent the general trend of almost all solutions, though the solutions differ in detail. In both cases the phases rise slowly to 90^o and then rotate rapidly anticlockwise in the region of 1.45 GeV. It is

conceivable that this behaviour can accommodate the broad† ε, κ and the ε', κ' states, though clearly without definitive identification.

So far the situation is much as Morgan[5] studied in 1974. He found the observed decays $\varepsilon, S^* \to \pi\pi, K\bar{K}$; $\delta \to \pi\eta, K\bar{K}$; $\kappa \to K\pi$ could be made compatible with a $q\bar{q}$ non-magically mixed nonet (mixing angle about 70^o), provided the states were taken to be $S^*(980)$, $\delta(970)$, $\kappa(1200)$, $\varepsilon(1300)$. Also the $\varepsilon(1300)$ was an elastic $\pi\pi$ resonance.

Recent developments have occurred in the $K\bar{K}$ channels. The processes studied are of the type $\pi N \to K\bar{K}N$. Here $K\bar{K}$ production in the I=0 S wave state (ε, S) proceeds dominantly via π exchange, whereas I=1 S wave production (δ) proceeds via B or Z exchange. Z is used to denote a possible 2^{--} exchange trajectory which couples to helicity non-flip at the nucleon vertex, whereas both π and B exchange couple to helicity flip.

The S wave $K\bar{K}$ mass spectrum obtained from $K^o_s K^o_s$ and K^+K^- production data[6,7] show a significant bump near 1.3 GeV. This structure was originally attributed[6] to a state in the I=1 $K\bar{K}$ channel, but a more recent analysis[8] favours an I=0 assignment. To help unravel the I=0 and I=1 $K\bar{K}$ effects the ANL group[7,8] studied both $\pi^- p \to K^- K^+ n$ and $\pi^+ n \to K^- K^+ p$. In Fig. 4 we plot the S wave contribution

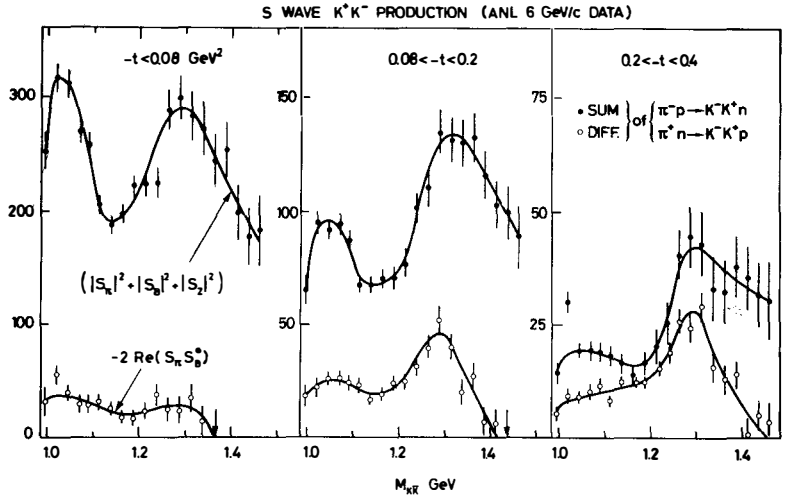

Fig.4

isolated from the sum and from the difference of these data for three different t intervals. For the sum we use the moments $\langle Y^{0,2}_4 \rangle$, $\langle Y^2_2 \rangle$ and $\langle Y^0_0 \rangle$ to isolate

†See ref.4 for a model for the phase behaviour of these states.

$|S|^2 = |S_\pi|^2 + |S_B|^2 + |S_Z|^2$. For the difference we simply plot $-\langle Y_0^0 \rangle$, since the higher moments indicate that this is essentially S wave, namely $-2\mathrm{Re}(S_\pi S_B^*)$; S_Z does not contribute to this I=0,1 interference if we assume A_1 quantum number exchange is negligible compared to π exchange. The effect of the S*(990) is clearly visible in the sum, $|S|^2$, with a t dependence characteristic of π exchange. On the other hand the structure at 1.3 GeV does not have π exchange t dependence which is expected for I=0 $K\bar{K}$ production.

Independent information on S wave $K\bar{K}$ production has recently been obtained from an analysis of University of Geneva 10 GeV/c $\pi^- p \to K^- K^0 p$ data[9]. The relevant results[9a], Fig. 5, show evidence for an S wave structure just below

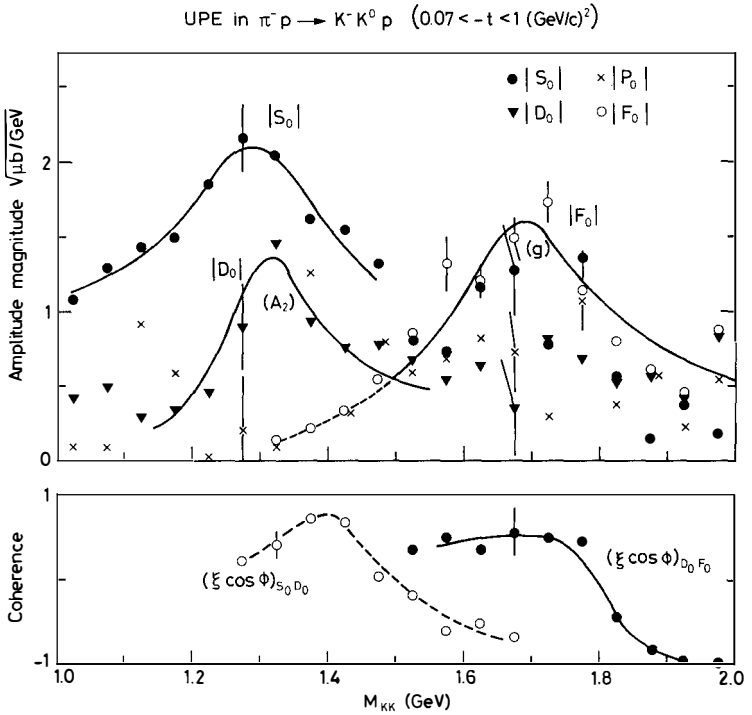

Fig.5

1.3 GeV. Here it must be I=1, that is $|S_0|^2 = |S_B|^2 + |S_Z|^2$. Moreover, the t dependence[9b] of the S wave indicates that Z exchange dominates for $-t \lesssim 0.15$ GeV^2. This correlates nicely with the behaviour of $\mathrm{Re}(S_\pi S_B^*)$ of Fig. 4, which suggests S_B becomes relatively more important at larger $|t|$.

If the resonance identification, $\delta'(1270)$, of this I=1 structure is confirmed, this will be clear evidence for the existence of the two 0^{++} nonets

Moreover, this structure cannot account for the entire S wave bump in the K^+K^- data; there is a residual I=0 S wave effect, perhaps arising from the ϵ'. However, for the moment we must conclude the existence of multiquark states remains an open question. On the other hand, we have seen the low mass 0^{++} states offer a good testing ground. Investigation of $\pi\pi$, $K\bar{K}$ channels in other charge configurations, or of the $\eta\eta$ channel, would be invaluable in this respect. This, together with a quantitative analysis of the observed couplings, should settle the issue.

Acknowledgements

I thank Robert Jaffe, David Morgan, Emin Ozmutlu, Euan Squires and the members of the Geneva collaboration for useful discussions.

References

1. R. L. Jaffe, Phys. Rev. D15, 267 (1977)
2. A. De Rújula, H. Georgi and S. L. Glashow, Phys. Rev. D12, 147 (1975)
3. R. L. Jaffe and K. Johnson, Phys. Lett. 60B, 201 (1975)
   D. Robson, Nucl. Phys. B130, 328 (1977)
4. R. L. Jaffe and F. E. Low; see R. L. Jaffe, these proceedings
5. D. Morgan, Phys. Lett. 51B, 71 (1974)
6. N. M. Cason, V. A. Polychronakos, J. M. Bishop, N. N. Biswas, V. P. Kenny, D. S. Rhines, W. D. Shephard and J. M. Watson, Phys. Rev. Lett 36, 1485 (1976)
7. A. J. Pawlicki, D. S. Ayres, D. Cohen, R. Diebold, S. L. Kramer and A. B. Wicklund, Phys. Rev. D15, 3196 (1977)
8. D. Cohen, Proc. 5th Experimental Meson Spectroscopy Conf., Boston (1977)
9. A. D. Martin, E. N. Ozmutlu, R. Baldi, T. Böhringer, P. A. Dorsaz, V. Hungerbühler, M. N. Kienzle-Focacci, M. Martin, A. Mermoud, C. Nef and P. Siegrist; a) Phys. Letts. (1978); b) Submitted to Nucl. Phys. (1978)

PHENOMENOLOGY WITH MULTIQUARK STATES

H. Høgaasen

CERN -- Geneva

and

University of Oslo

ABSTRACT

We show some simple aspects of spectroscopic consequences and expected exchange mechanisms in the colour isomer multiquark model.

Quelques aspects simples concernant les conséquences spectroscopiques ainsi que les mécanismes d'échange attendus sont étudiés dans les systèmes isomères de couleur à plus de trois quarks.

In this talk I shall describe some of the whys and hows of multiquark spectroscopy in the colour isomer approach.

The why is (for me) obvious: previously in physics, when a new degree of freedom has been established, it has shown itself in spectroscopy through an increase in the number of states. The spatial extension of molecules and nuclei shows up in vibrational and rotational states; the spin of nucleons and leptons is seen in the Zeeman splitting of atomic levels. Extra flavours, such as strangeness and charm of quarks, show up both in hidden (ϕ, ϕ', ψ, ψ') and naked forms (K, Λ, D, F).

Today, we are all excited by the possibility that Quantum Chromodynamics gives a key to the understanding of hadron physics. In this theory, colour plays the same rôle for strong interactions as electric charge for electrodynamics. Therefore, it would be of the greatest importance to find direct spectroscopic evidence for the colour degree of freedom. In $q\bar{q}$ mesons and qqq baryons, this degree of freedom is, however, completely frozen: there is one, and only one, way of combining q and $\bar{q}$ or three quarks to a colour singlet.

The simplest meson systems that can show extra states due to colour are $qq\bar{q}\bar{q}$ states, the simplest baryons with this property must be made of $qqqq\bar{q}\bar{q}$. In the talks given by Chan and Jaffe at this meeting, the theory of such states is well discussed; I shall add something about phenomenology.

Is there any evidence for such multiquark states? Being careful, I would rather say that there is no evidence to the contrary, and we indeed hope that colour isomers have already been found in the $qqq\bar{q}\bar{q}$ system. For the true baryonium states which are bound by a colour triplet bond between qq and $\bar{q}\bar{q}$ (and which should have the property of being much more strongly coupled to $B\bar{B}$ than to mesons) there are many candidates seen in $p\bar{p}$ formation experiments[1),2)]. This is, however, the type of state predicted in dual models[3),4)] and in string models and they were expected to exist long before the colour charge was taken seriously by the majority of physicists.

The other family of $qq\bar{q}\bar{q}$ states, namely the ones where qq ($\bar{q}\bar{q}$) is in a colour 6 ($\bar{6}$) state[5)] should really be the proof of the existence of colour isomers. They should be weakly coupled <u>both</u> to mesons and to baryons and have a tendency to decay in cascade.

In December 1977, Chan, Tsou and myself, were convinced that the colour 6 bound states existed[6)]. However, there are now some clouds in the sky because the six standard-deviation effects at 2.95 GeV in the $p\bar{p}\pi^-$ system has not been reconfirmed. This has been reported by French.

In spite of this, I shall describe what made us so optimistic because it can serve as an example of the predictive power of the model, even if it is still in its infancy.

The slope of the Regge trajectory of the states bound by an elongated tube of colour N field lines is in the MIT bag proportional to the square root of the Casimir operator C_N of the N dimensional representation[7)-10)]. With the normalization $C_3 = 16/3$, one has $C_6 = 40/3$ and $C_8 = 12$. The slope α'_6 of a colour 6 bound state is then

$$\alpha'_6 = \sqrt{\frac{C_6}{C_3}}\,\alpha'_3 = \sqrt{\frac{5}{2}}\,\alpha'_3$$

where

$$\alpha'_3 = 0.9 - 1 \text{ (GeV/c)}^2$$

and the slope α'_8 of a colour 8 bound state is

$$\alpha'_8 = \sqrt{\frac{C_8}{C_3}} = \frac{2}{3}\,\alpha'_3$$

The orbital excitations M_L corresponding to an angular momentum L between two quark clusters, each with colour $N(\bar{N})$ is supposed to be given by

$$L = \alpha_{0,N} + \alpha'_N\,(M_L)^2$$

For a given orbital angular momentum, the maximal spin is $J = L + S_1 + S_2$, where S_1 and S_2 are the spins of the two clusters.

The states with the same L are degenerate in this approximation, this degeneracy is then partly lifted by the colour-magnetic interaction inside each of the two clusters at the ends of the colour-electric tube.

To fix the spins and masses of all the multiplets of such a system, we need then only to know $\alpha_{0,N}$. One established state will give us $\alpha_{0,N}$ and all others are then (approximately) determined.

Let us now show what happens if we [like Chan et al.[5)]] suppose that the 2.95 GeV $p\bar{p}\pi^-$ state of Evangelista et al. is a $J^P = 4^-$ state of $qq\bar{q}\bar{q}$ with a colour sextet bond. Additional states are then predicted (shown by arrows in Fig. 1).

These states are all in the non-strange sector of the $qq\bar{q}\bar{q}$ system. Tsou[11)] wondered where the $I = \frac{1}{2}$, $S = +1$ states on the leading strange trajectory would lie; she calculated this in a completely parameter-free manner and compared the

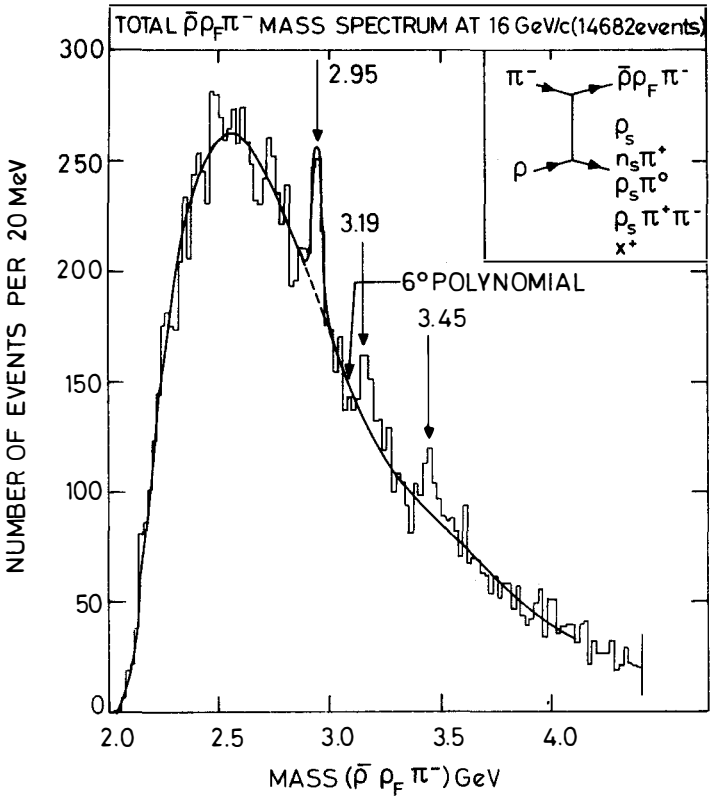

Fig. 1

so predicted states with preliminary data[12] on $K^-p \to \bar{\Lambda}pp$, $\bar{\Lambda}pp\pi^0$ and $\bar{\Lambda}p\pi^+n$ at 12 GeV. The mass of her predicted states is shown by arrows on Fig. 2. I would not say that these figures confirm the existence of colour 6 bound states but clearly they do not contradict them either.

If there is little evidence for narrow high-mass baryonium states there are still less states that could be convincing representatives for narrow $qqqq\bar{q}$ states. The only ones could be the narrow $\Lambda\pi^+\pi^-$ and $\Lambda^+\pi^-\pi^+$ states with masses 2.13 and 2.26 GeV [13]. Their production cross-section is, however, so high that our present understanding[5),14),15] of multiquark production gives us trouble with their interpretation. The masses, however, fall in the region where octet-bound (qqq) $(q\bar{q})$ states would lie[15]. Fukugita will tell more about colour 6 bonds between $qq\bar{q}$ and qq. Here I shall tell some of the results[15] coming

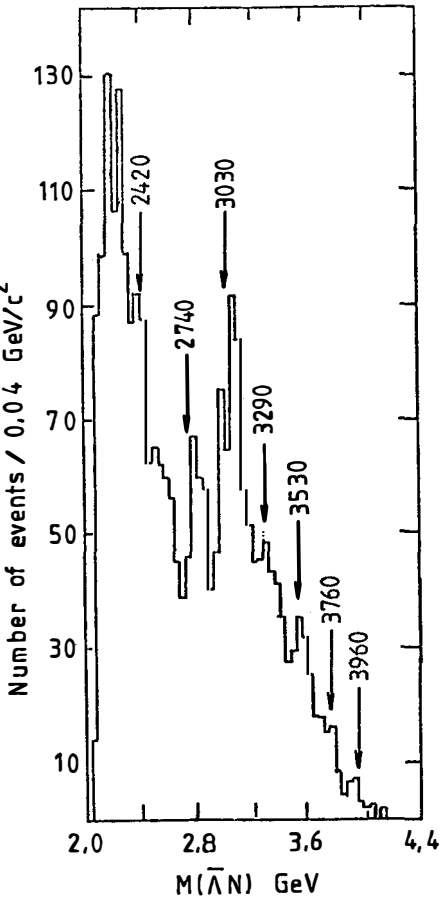

Fig. 2

from work by Paul Sorba and myself which concerns curvature of Regge trajectories. We have solved the problem of calculating the splitting of the s wave states due to the colour-magnetic interaction -- the results would, in the MIT bag model, be inside the bounds found for such states by Jaffe[16]. As in the diquonium case the effect of the s wave binding has quite interesting consequences for the shape of the Regge trajectories. There, the very strong attraction in the s wave of the lowest-lying nonet would suggest a fairly high-lying trajectory with very small slope at $t = 0$. Nicolescu[17] wonders if this could be what is called the effective ρ' trajectory known from pi-nucleon charge exchange.

In the $qqqq\bar{q}$ system the same phenomena happens for an exotic trajectory, namely the one containing the $Y = 2\ Z^*(I = 0)$ state. Any reasonable extrapolation of this trajectory to $M^2 = 0$ will give an intercept above -1. This would

mean that K^-n backward scattering should be almost as slowly varying with energy as processes that involve normal hyperon exchanges. This is shown in Fig. 3. This corresponds to (approximately) the lower limit where the $Z^*(I = 0)$ states, marked with crosses, can be found. Unhappily, there are no data on backward K^-n scattering. For the $Z^*(I = 1)$ the curvature is opposite, the repulsion due to the colour-magnetic interaction is greater in the ground state than for L excited states. We therefore have no problem in understanding why K^-p backward scattering has such fast decrease with energy.

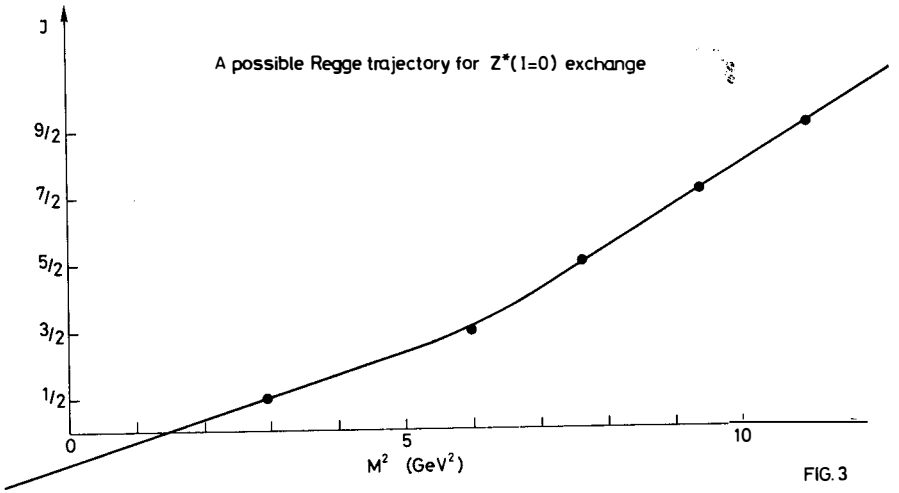

FIG. 3

REFERENCES

1) A.A. Carter, Phys. Letters 67B, 117 and 122 (1977) and talk given at this meeting.

2) L. Montanet, CERN preprint EP/Phys. 77-22 (1977) and talk given at this meeting.

3) J.L. Rosner, Phys. Rev. Letters 21, 950 (1968).

4) G. Veneziano, CERN TH.2425 (1977) and references therein.

5) Chan Hong-Mo and H. Högaasen, Phys. Letters 72B, 121 (1977) and RL-77-144/A (to be published in Nuclear Physics).

6) C. Evangelista et al., Phys. Letters 72B, 139 (1977).

7) K. Johnson and C. Thorn, Phys. Rev. D13, 1934 (1976).

8) Chan Hong-Mo and H. Högaasen, Phys. Letters 72B, 400 (1978).

9) T.H. Hansson and K. Konishi, RL-78-021/A (1978).

10) R.L. Jaffe, MIT preprint CTP No. 657 (1977) and talk given at this meeting.

11) Tsou Sheung Tsun, Oxford University preprint (1978).

12) T. Armstrong et al., quoted by L. Montanet, CERN/EP/PHYS 77-2.

13) W. Lockman et al., Saclay preprint D.Ph.PE 78-01 and UCLA preprint No. 1109 (1978).

14) M. Fukugita, K. Konishi and T.H. Hansson, RL-78-007/A, to be published in Phys. Letters B (1978).

15) H. Högaasen and P. Sorba, CERN preprint to appear.

16) R.L. Jaffe, Oxford Topical Conference on Baryon Spectroscopy, p. 454 (1976).

17) B. Nicolescu, LBL preprint 6701, to be published in Nuclear Phys. See also his talk at this meeting.

RL-78-053
T.222

MULTIQUARK STATES : FURTHER POSSIBILITIES OF OBSERVATION

M. Fukugita
Rutherford Laboratory, Chilton, Didcot, Oxon, England

ABSTRACT

We consider two possible places for observing multiquark states: (i) The $B\bar{B}B\bar{B}$ channel in which bound states of qq with $q\bar{q}q\bar{q}$ might be observed and (ii) e^+e^- annihilation as an additional means of seeing four quark states. Possible spectra and decay systematics are presented.

New families of resonances have been reported in $B\bar{B}$ channels and in channels associated with $B\bar{B}$ [1]. They are naturally regarded as candidates for the so-called baryonium configurations, bound states of a diquark and antidiquark. In this report we shall consider two possible places where multiquark states can be observed other than the channel associated with $B\bar{B}$: (i) one might look for $4q + 1\bar{q}$ states in $BB\bar{B}$ channel - such bound states of qq with $qq\bar{q}$ form an analogue of baryonium but with baryon number B = 1; (ii) secondly, one might look for $2q + 2\bar{q}$ states in e^+e^- annihilation experiment, especially below the $B\bar{B}$ threshold.

Model. We take a model originally proposed by Chan and Høgaasen for the baryonium [2]. The baryonium configurations are bound states of a diquark and an antidiquark confined in a kind of bag and separated by an orbital angular momentum centrifugal barrier, which inhibits the baryonium from dissociating into two $q\bar{q}$ pairs. In other words, baryonium is a string-like

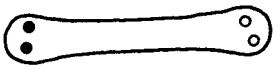

FIG. 1

object with (qq) and $(\bar{q}\bar{q})$ at the two ends (Fig. 1). The diquark (antidiquark) is assumed to stay in an S-wave.

We have two kinds of baryonia, depending on whether the diquark (antidiquark) forms $\underline{3}^*$ ($\underline{3}$) or $\underline{6}(\underline{6}^*)$ representation of colour SU(3). We call them T- and M-baryonia (or T- and M-diquonia). The T-baryonium can be cut at the middle of the string and is expected to have a normal decay width into a baryon-antibaryon pair. Candidates for this kind of baryonia are T(2.18), U(2.31) and V(2.48) [1,3]. The M-baryonium cannot simply be split into a $B\bar{B}$ pair because of a colour $\underline{6}$ flux passing along the tube. The narrow states which have been reported at 2.02, 2.20 [4], 2.95 [5], etc. are obvious candidates for M-type baryonia.† ‡ The decay of baryonium into mesons is also shown to be suppressed from the viewpoint of duality. The extension of the model to more general multiquark states is straightforward [6]. For B = 0, we have $(q\bar{q})_8$ - $(\bar{q}q)_8$, $(qqq)_8$ - $(\bar{q}\bar{q}\bar{q})_8$, $(qqq)_{10}$ - $(\bar{q}\bar{q}\bar{q})_{10^*}$, $(qq)_{3^*}$ - $(q\bar{q}\bar{q}\bar{q})_3$ etc. in addition to the baryonia: $(qq)_{3^*}$ - $(\bar{q}\bar{q})_3$, $(qq)_6$ - $(\bar{q}\bar{q})_{6^*}$.

† It is of prime importance to establish their existence beyond doubt.

‡ A doubt is being thrown on the existence of 2.95 [5].

(1) $qq - qq\bar{q}$ states ("Pseudobaryon") [7]

We have two kinds of five quark configurations for B = 1: a bound state of $q\bar{q}$ (colour $\underline{8}$) with qqq (colour $\underline{8}$), and a compound of qq with $qq\bar{q}$. We call the former "mesobaryon" and the latter "pseudobaryon" (see Fig. 2).

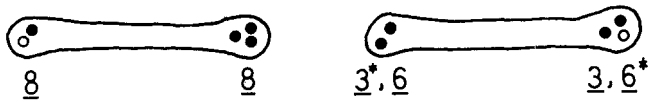

FIG. 2

The pseudobaryon is the B = 1 analogue of baryonium (diquonium) in the sense that it is obtained by replacing an antiquark in the baryonium with a diquark. It is further divided into two classes according to whether the two clusters form colour triplet or sextet representation (T- and M-pseudobaryons). Some of the M-pseudobaryons will have narrow decay widths, while T-pseudobaryon configurations will have normal width into a baryon plus mesons. Hereafter we shall concentrate on the M-pseudobaryon, which is more interesting from the viewpoint of observability.

Spectrum. The M-pseudobaryon is classified into six families according to the spin content of its constituent clusters:

	colour SU(3), spin $qq \times qq\bar{q}$	total quark spin	flavour SU(3) $qq \times qq\bar{q}$
I :	$(\underline{6},\underline{1}) \times (\underline{6}^*,\underline{2})$	1/2	$\underline{6} \times (\underline{3} \oplus \underline{15})$
II :	$(\underline{6},\underline{1}) \times (\underline{6}^*,\underline{4})$	3/2	$\underline{6} \times (\underline{3} \oplus \underline{15})$
III :	$(\underline{6},\underline{1}) \times (\underline{6}^*,\underline{2})'$	1/2	$\underline{6} \times (\underline{3} \oplus \underline{6}^*)$
IV :	$(\underline{6},\underline{3}) \times (\underline{6}^*,\underline{2})$	1/2, 3/2	$\underline{3}^* \times (\underline{3} \oplus 15)$
V :	$(\underline{6},\underline{3}) \times (\underline{6}^*,\underline{4})$	1/2, 3/2, 5/2	$\underline{3}^* \times (\underline{3} \oplus 15)$
VI :	$(\underline{6},\underline{3}) \times (\underline{6}^*,\underline{2})'$	1/2, 3/2	$\underline{6} \times (\underline{3} \oplus \underline{6}^*)$

In order to get a mass spectrum, we assume (i) linear rising trajectories with a Regge slope proportional to the inverse of colour flux in the tube [8]; (ii) a mass for the ground state (extrapolation to L = 0) given by the sum of effective quark masses involved and an interaction energy proportional to the colour SU(3) Casimir operator for the clusters; and (iii) a colour-magnetic hyperfine interaction [9-11] among quarks (and/or antiquarks) in the S-wave, which gives rise to a mass splitting among states in different

colour-spin representations. The spectrum (for L ≥ 1) is shown in Fig. 3. (The orbital angular momentum and parity are shown as L^P).

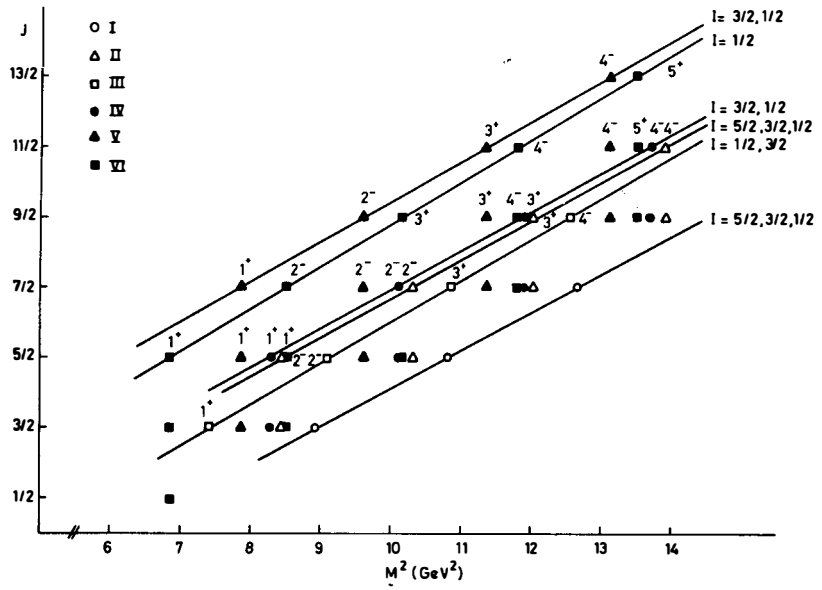

FIG. 3

Decay. As in M-baryonia, M-pseudobaryons (we denote it as $\mathcal{B}$) cannot be split into a baryon and a baryonium($\mathcal{M}$). A dominant decay mode would appear to be by cascade, i.e., by emission of a meson or a baryon from one of the clusters:

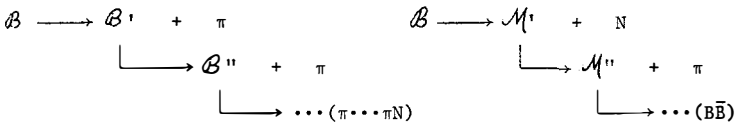

When the final state $\mathcal{B}'$ (or $\mathcal{M}'$) has the same orbital angular momentum L as the initial state $\mathcal{B}$, i.e., $\Delta L = 0$, no suppression mechanism works and the decay has a normal width provided that the phase space is sufficient. On the other hand, cascade decays changing L ($\Delta L \neq 0$) require a quantum fluctuation followed by an emission of π(N) and they may be relatively suppressed. A prime candidate for $\Delta L \neq 0$ cascade decay is given by X(2.95)→X(2.20)+π [5],

where X(2.95) and X(2.20) are assigned to $J^{PC} = 4^{--}$(L=3) and 3^{--}(L=1), respectively [2]. Taking $\Delta \to N\pi$ as an example of $\Delta L = 0$ cascade, we have the suppression factor $\Gamma[X(2.95) \to X'(2.20) + \pi](m_X^2/p^3) / \Gamma[\Delta \to N + \pi](m_\Delta^2/p^3) \approx 1/50$.

In Fig. 4 we show an estimate of the total width and branching ratio to N + baryonium ($L \neq 0$) for the parent pseudobaryons in the typical mass region $11 \lesssim M^2 \lesssim 14$ (GeV)^2 ($L = 3 \sim 5$).

	Γ_{tot}(MeV)	BR (%)	
I	150-300	5-20	J = L + 1/2
II	30-80	<20	J = L + 3/2
IV	200-400	5-30	J = L + 3/2
V	20-60	5-40	J = L + 5/2
III	20-40	<10	J = L + 1/2
VI	5-15	10-30	J = L + 3/2

FIG. 4

The result shows that the states II, III, V, VI listed above should be seen as narrow peaks. Of these the state V ($\Gamma_{tot} \lesssim 20$ MeV) has a substantial branching ratio (10-30%) for the mode $\mathcal{B} \to N + \mathcal{M}$ ($L \gtrsim 1$), where $\mathcal{M} \to B\bar{B}$. The state V has similar properties ($\Gamma_{tot} \lesssim 50$ MeV, BR = 25 $\sim$ 40%). Although the non-strange members of the states IV(V) have non-exotic isospin and may appear as an ordinary baryon (crypto-exotic) [11], a clear signature of the pseudobaryon will be given by a characteristic decay pattern a cascade into $pp\bar{p}$ with $p\bar{p}$ forming one of the narrow baryonium states X(2.0), X(2.2), etc.

Mesobaryon. Some of the mesobaryon states, if they exist, may have narrow total widths. The mesobaryons, however, are distinguished from the pseudobaryon by their decay modes. The former decays into another mesobaryon by emitting π or into mesonium by emitting N and finally it decays into a nucleon + multipions. In the decay of the pseudobaryon an $NN\bar{N}$ mode can be significant.

Production. We expect that the pseudobaryon is produced diffractively in the proton fragmentation region as $pp \to \mathcal{B}$ + anything, where $\mathcal{B} \to (pp\bar{p})_{forward}$. This is quite analogous to the diffractive production of baryonium $\pi^- p \to \mathcal{M}$ + anything, where $\mathcal{M} \to (p\bar{p})_{forward}$.

Both productions go through the mixing between qq and $qq\bar{q}\bar{q}$ states in the Pomeron (see Fig. 5). Ignoring mass effects, we may expect

$$\sigma(pp \to \mathcal{B} + \text{anything}) / \sigma(\pi p \to \mathcal{M} + \text{anything}) \approx \sigma_T(pp) / \sigma_T(\pi p).$$

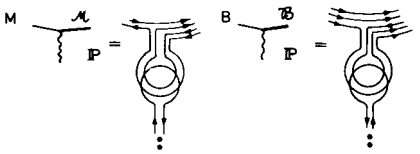

Using an empirical production cross section $\sigma(\pi^- p \to X(2.95) + \text{anything}) \cdot B(2.95 \to pp + \pi) \approx$ ≈ 1 μb [5], we estimate $\sigma(pp \to B + \text{anything}) B(\mathcal{B} \to pp\bar{p}) \approx$ $\approx .1$ μb.

FIG. 5

(2) Multiquark states in e^+e^- reactions [12]

Electron-positron annihilation seems to give us a good place to study multiquark states at low energies due to the restrictive nature of the one photon process. Let us confine ourselves to the low energy region such as $W \leq 2$ GeV. The only baryonia couple to e^+e^- in this mass reigon have $L = 1$. (Note that parity $P = (-)^L$.)

We have to take account of the $\vec{L}\cdot\vec{S}$ force for baryonia with $L = 1$, which has been ignored so far. (The $\vec{L}\cdot\vec{S}$ force gives $\approx$ 300 MeV mass splitting in the $L = 1$ ordinary mesons.) We estimate the $\vec{L}\cdot\vec{S}$ force in baryonia, by assuming a formula suggested from one gluon exchange interaction and setting the scale from the A_2, A_1, δ mass splitting. We fix the overall spectra for T-baryonia by $T(2.15, J^{PC} = 3^{--})$ and for M-baryonia by $X(2.2, J^{PC} = 3^{--})^\dagger$, both of which are assigned as members of $L = 1$ multiplets. We have found that this prescription explains the fine structure of narrow peaks in $p\bar{p}$ system ($\pi^- p \quad p\bar{p} + \ldots$) in the mass region 2-2.22 GeV. [4] We present in Fig. 6 the spectrum of baryonium ($L = 1$) for $M \lesssim 2$ GeV).

Decay. T-baryonia decay into $p\bar{p}$ with a normal width ($\Gamma \lesssim 100$ MeV), if they are above threshold. In M-baryonia and in T-baryonia below the $p\bar{p}$ threshold, the following suppressed decay modes are competing: (i) Cascade decays between T-(M-) baryonia with $\Delta L = 0$ (shown in Fig. 6) (ii) Decays into ππ (or πρ) due to a rearrangement of a $q\bar{q}$ pair or an annihilation

---

† Recent observation in a $\bar{p}p \to K^+K^-$ analysis suggests the assignment $J^{PC} = 3^{--}(I^G = 0)$ for X(2.2) [3].

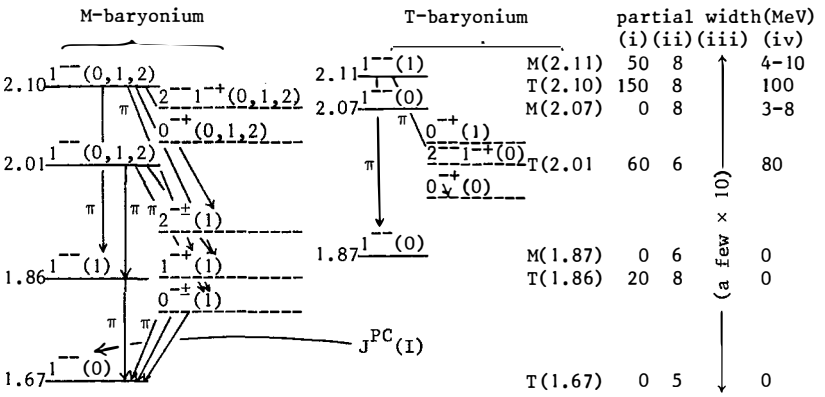

FIG. 6

followed by a creation of a $q\bar{q}$ pair. A suppression of this mechanism is suggested by dual unitarization scheme [2]; A suppression factor $|\delta|^2 \simeq 1/30$ is estimated from $\Gamma(T \to \pi^+\pi^-) / \Gamma(T \to p\bar{p}) \simeq 1/12$ [1]; (iii) Cascade decays into L = 0 baryonia (L = 1). A typical width is estimated to be $\Gamma \simeq$ (a few) x 10 MeV. (iv) M-baryonia may decay into $p\bar{p}$ above threshold due to colour $\underline{3}^* - \underline{6}$ mixing.

An estimate of widths is given in Fig. 6. We predict that some of the baryonium states have narrow widths $\Gamma \lesssim$ several x 100MeV. This value should be compared with the width of ordinary meson $\Gamma \simeq$ several x 10 MeV. The decay (i) and (iv) may give good signals for baryonia.

Production of baryonia. The production includes a vertex which is forbidden by the generalized OZI rule or Freund-Walz—Rosner rule [13] (Fig.7).

FIG. 7

Assuming a suppression factor δ for a forbidden production (annihilation) of a $q\bar{q}$ pair, we have the following suppression:

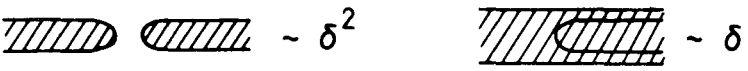

Consideration of various OZI rule forbidden processes suggests that $|\delta|^2 \simeq (0.05)^2$ [14]. From this we obtain $|\delta|^2 \simeq 1/20$ in agreement with the estimate $|\delta|^2 \simeq 1/30$ from $T \to \pi\pi / T \to p\bar{p}$. Thus we predict that the production

cross section of baryonia is 20-30 times smaller than that of ordinary vector mesons.

Other multiquark states. We can also hope to observe "mesonium" configurations $(q\bar{q})_8 - (q\bar{q})_8$ in e^+e^- annihilation. In mesonia an I = 1 state is always degenerate with an I = 0 state, while only I = 0 states appear in the lower levels of the baryonium spectrum. The systematics of decay is essentially the same as for baryonia.

The above considerations extend to configurations with even more quarks and suggest that one might be able to observe narrow multiquark states with more than 6 quarks even at low energies (due to a possible big hyperfine energy in some cluster states [6]). It turns out, however, that such states are generally unstable against dissociation of a $q\bar{q}$ pair from one of the clusters (super-allowed decay). Baryonia and mesonia appear to be the only multiquark states of narrow width which one would expect to observe in e^+e^- annihilation for $W < 2$GeV.

ACKNOWLEDGEMENT

I thank David Morgan and Hans Hansson for reading the manuscript.

REFERENCES

1) For review: L. Montanet, CERN preprint CERN/EP/Phys 77-22 (1977) and a report to this conference.

2) Chan H-M and H. Høgaasen, Phys. Lett. 72B (1977) 121; 400; Rutherford Laboratory preprint RL-77-144/A (1977).

3) A.A. Carter et al., Phys. Lett. 67B (1977) 117; A. A. Carter, Rutherford Laboratory preprint RL-78-032 (1978).

4) P. Benkheiri et al., Phys. Lett. 68B (1977) 483.

5) C. Evangelista et al., Phys. Lett. 72B (1977) 139; B. French, a report to this conference.

6) Chan H-M et al., Rutherford Laboratory preprint RL-78-027 (1978).

7) M. Fukugita, K. Konishi and T. H. Hansson, Phys. Lett. 74B (1978) 261.

8) K. Johnson and C. B. Thorn, Phys. Rev. D13 (1976) 1934.

9) A. de Rújula, H. Georgi and S. L. Glashow, Phys. Rev. D12 (1975) 147.

10) T. de Grand et al., Phys. Rev. D12 (1975) 2060.

11) R. L. Jaffe, Phys. Rev. D15 (1977) 267; 281.

12) M. Fukugita, T. H. Hansson and K. Konishi, in preparation.

13) P. G. O. Freund, R. Walz and J. L. Rosner, Nucl. Phys. B13 (1969) 237.

14) J. Arafune, M. Fukugita and Y. Oyanagi, Phys. Lett. 70B (1977) 221.

WHAT IS GLUE GOOD FOR? or GLUONS COME OUT OF THE CLOSET

S. D. Ellis †
Department of Physics
University of Washington
Seattle, Washington, U.S.A. 98195

Abstract

The possible role of gluons in hadronic processes as suggested by the quark-parton model and QCD is discussed and evaluated. Attention is focused on heavy (e.g., charmed) hadron production, large p_T hadronic physics, and massive lepton pair production at large p_T. A discussion of more rigorous tests of QCD and the role of gluons in e^+e^- annihilation is also given.

†Research supported by the U. S. Department of Energy.

Introduction

The most dramatic and encouraging development in Strong Interaction physics in the past few years has been the emergence of a candidate field theory to describe these interactions. This situation is in sharp contrast to that which obtained ten years ago when, at least at one well known institution of higher learning, it was "taught" that field theory was irrelevant to Strong Interactions[1]. It is important to keep in mind this rapid rate of recent developments when assessing the value of the physics discussed below. In particular, while quarks have now become well established as important (and valid) phenomenological and theoretical entities (albeit after a rather checkered early history), it is only with the recent emergence of a possibly correct theory of interacting quarks and vector gluons, Quantum Chromo-Dynamics (QCD), that a similar role has been thrust upon gluons. Crudely stated, if the gluons are present inside hadrons, then it is important to consider in what fashion the gluons make their presence explicitly felt in the interaction of hadrons. Skepticism about the role of gluons should be considered in the light of earlier skepticism about the role of quarks, a skepticism which has now largely vanished in the face of repeated successes.

This talk is intended as a partial review[2] of recent progress in the study of the role of gluons in hadronic interactions. The general outline is to proceed from highly phenomenological (i.e., conjectural) topics to more rigorous applications of gluon physics which are explicitly related to the basic field theory. In particular, the last section of the talk is devoted to one attempt to define experimental tests of the basic properties of QCD and gluons which can be unambiguously calculated in perturbation theory.

Quarks and Gluons in QCD

Within the context of QCD the gluons (which form an octet under "color" transformations) serve to mediate the interactions between the quarks and among the gluons themselves. These interactions exhibit strong infrared divergences and it is presumed that the long distance interactions are sufficiently strong to insure the "confinement" of all color nonsinglet states. At the

other end of the spectrum the non-Abelian character of the theory (and the gluons) insures that the effective "runnning" coupling is small at short distances and vanishes in the limit of zero separation[3]. This feature of the theory is generally accepted as the explanation of the apparent success (or more precisely, near success) of the naive quark-parton model as applied to processes involving interactions at "short distances". Within the naive model the quarks are treated as free at short distances while the distributions of quarks within a hadron (which involve long distance, confinement physics) are assumed to depend only on the fraction of the total momentum carried by the quark (scaling). A similar assumption is made concerning the distribution of final state hadrons which arise from the evolution of the scattered quark. In this case the scaling is in terms of the fraction of the quark's momentum carried by the hadron and the distribution is referred to as the distribution of hadrons in a jet. In situations where some rigor is possible, e.g., $e^+e^- \to$ hadrons and $ep \to eX$ (see fig. 1a and 1b), the corrections to this naive picture which result

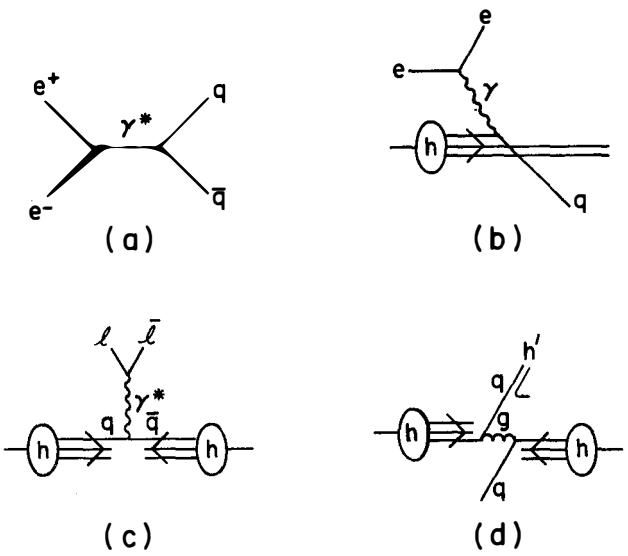

Fig. 1 Simple quark processes: a) $e^+e^- \to$ hadrons;
b) $ep \to eX$;
c) Drell-Yan;
d) large p_T.

from the interactions inherent in QCD are found to be rather small[3]. Cross sections do not scale precisely but rather moments of the cross sections vary as prescribed powers of the logarithm of the relevant large kinematic variable, a behavior in good agreement with the data. The application of the naive quark model to more complex processes involving two initial hadrons, e.g., the Drell-Yan process[4] consisting of quark-antiquark annihilation into a massive virtual photon (see fig. 1c), or large p_T hadronic production[5] involving large angle quark-quark scattering (see fig. 1d), was accomplished by the assumption that these processes can be described by the incoherent convolution of up to three components as suggested in fig. 1. For the large p_T example the three components are: 1) the distributions of quarks in the initial hadrons, taken, for example, from single hadron processes like ep → eX; 2) the quark-quark scattering process in lowest order; 3) the hadron distribution in the produced large p_T jet, taken, for example, from e^+e^- → πX. More explicitly this structure, for the process A + B → C + X, can be expressed as

$$E\frac{d^3\sigma}{d^3p}\Bigg|_{A+B\to C+X} = \int dx_a d^2k_a F_{a/A}(x_a,k_a)\int dx_b d^2k_b F_{b/B}(x_b,k_b)$$

$$\int \frac{dz_C}{z_C^2} d^2k_C D_{C/c}(z_C,k_C)\ \frac{\hat{s}}{\pi}\,\delta(\hat{s}+\hat{t}+\hat{u}) \qquad (1)$$

where $F_{a/A}$ is the distribution of quark a in hadron A ($x_a = p_a/p_A$ and k_a is a transverse momentum variable), $D_{C/c}$ is the distribution of hadron C in the jet initiated by quark c ($z_{C/c} = p_C/p_c$), and $d\sigma/d\hat{t}$ is the quark-quark scattering cross section (^ refers to quark-quark variables). That this naive extension to more complex processes is appropriate in the context of QCD has yet to be fully demonstrated but early indications[6] are that the naive model is, in fact, the correct starting point.

Hadronic Production of Heavy Hadrons

Having set the stage with the phenomenological applications of quarks, as illustrated in fig. 1, the phenomenological applications of gluons arise simply by replacing quarks with gluons in these

figures. Perhaps the first direct discussion of the possible role of gluons was in the hadronic production of hadrons containing charmed quarks[7,8]. The idea was to replace the $q\bar{q}$ pair in fig. 1c by gluons and the massive photon by the η_c, the pseudoscalar partner of the ψ/J particle, as shown in fig. 2a. To calculate one

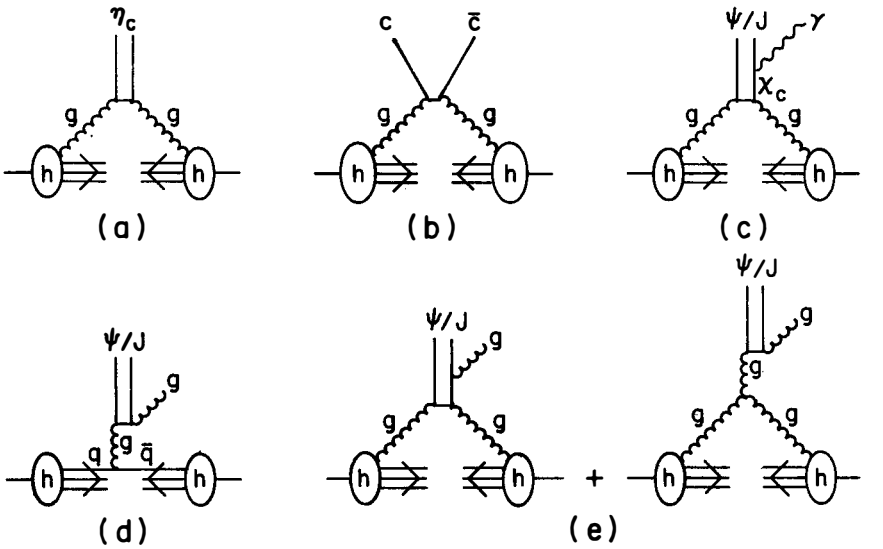

Fig. 2 Simple gluon processes: a) η_c production;
b) $c\bar{c}$ production;
c) $\psi/J + \gamma$ production;
d) and e) ψ/J + gluon production.

need only make an assumption as to the form of the gluon distribution in protons (the total momentum in glue is known to be about 50%), about which there are various theoretical biases (e.g., $f_g \sim (1 - x)^5$, $x = p_g/p_h$) and an assumption as to the $\eta_c \to gg$ coupling. One can also estimate in this model total hadronic production of charm via the gluonic production of an unconstrained $c\bar{c}$ pair as in the diagrams of fig. 2b. Such estimates can easily account for the 10-100μb charm production cross section suggested by the recent "beam dump" experiments discussed in this meeting[9]. The best measured cross section involving the production of the new heavy particles is for ψ/J production. It was suggested[7] that production might occur via the gluonic production of the χ_c states which would then electromagnetically decay to yield a ψ/J and a γ

as in fig. 2c. Recent data on ψ/J-γ coincidences suggest that this process may indeed account for part of the observed ψ/J signal[10]. Note that this mechanism allows a simple explanation of the suppression of ψ' production (but not T' production) since the χ_c' states are above the threshold for hadronic decays (while the corresponding states for the T' are presumably not).

More recent theoretical studies[8] have included consideration of the gluonic or $q\bar{q}$ production of color octet states which then decay into the ψ/J via gluon emission as in fig. 2d and 2e (we are explicitly ignoring the small 3 gluon coupling of ψ/J to $q\bar{q}$ and the role of charmed quarks in the hadronic sea). Analyses[8] involving a mix of these processes seem to allow a good explanation of the existing data including the sizeable ratio of $p\bar{p} \to \psi/J + X$ / $pp \to \psi/J + X$ which would be unity in a gluon dominated model. However, as $x = M_{\psi/J}/\sqrt{s}$ becomes small in larger s data one does expect gluon dominance for most model gluon distributions and it will be interesting to see if this ratio approaches one.

Another important test is to compare the excitation curves $(\sigma(s))$ for the ψ/J ($M^2 \sim 10$ GeV^2) with that for the T ($M^2 \sim 100$ GeV^2) to look for the predicted differences due to QCD scaling violation effects in the gluon distributions. Overall hadronic production of heavy particles appears to be a good place to test our phenomenological ideas about the role of gluons. At present the data are certainly consistent with expectations, including gluon distributions behaving essentially as $(1 - x)^5$.

Gluons in Large p_T Physics

The most promising arena for the observation of the characteristics of individual hadronic constituents in purely hadronic processes is the inclusive production of hadrons at large p_T[5]. As illustrated in fig. 1d this is conjectured to occur via the large angle scattering of two constituents[11]. In order to calculate this process within the context of QCD, even assuming the simple factorized form of fig. 1d and eq. (1), one must discuss not only the standard quark-quark scattering term (fig. 3a) but also include the possibility of gluon-quark scattering (fig. 3b), and the possibility of 2 gluons in (fig. 3c) or out (i.e., $q\bar{q} \to gg$, fig. 3d) or both[12,13] (fig. 3e). As in the previous section the

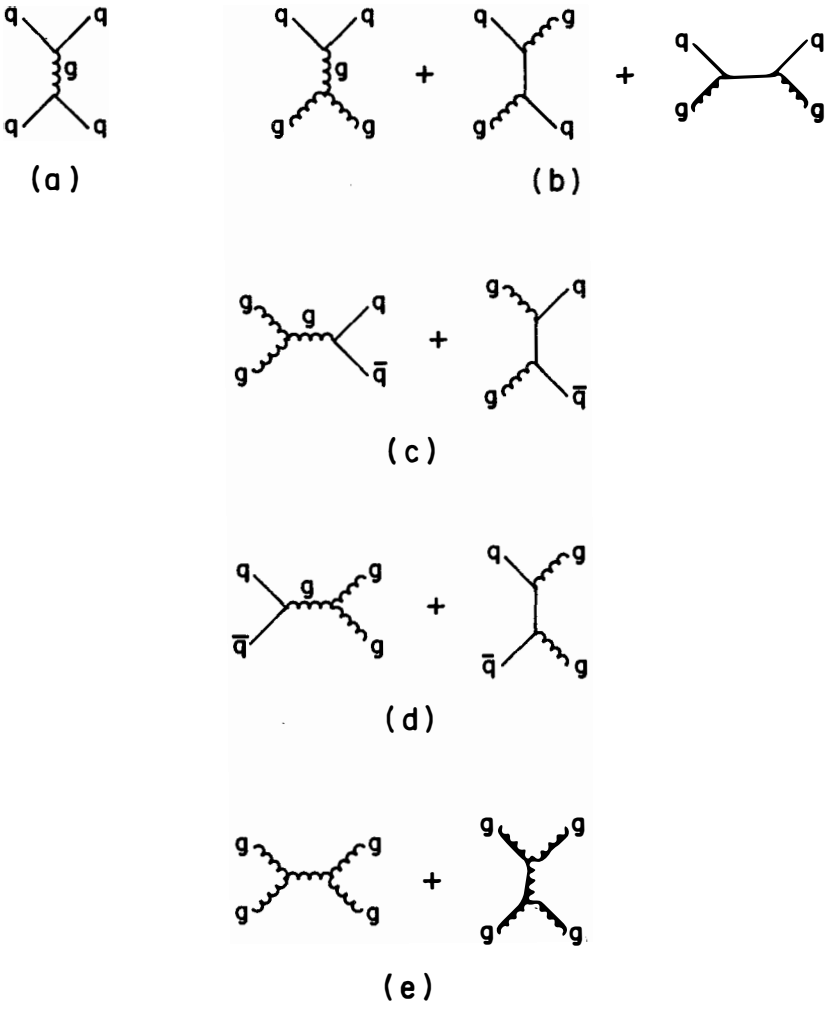

Fig. 3 Simple scattering: a) qq; b) qg; c) $gg \to q\bar{q}$; d) $q\bar{q} \to gg$; e) $gg \to gg$.

gluon distributions are presumed to be sharply peaked at small $x = p_g/p_h$. Furthermore, since a gluon must first fragment into quarks before it can start to produce hadrons, a jet initiated by a gluon is presumed to produce more hadrons with smaller average $z = p_h/p_g$ than a corresponding quark initiated jet. Thus the dominant effect of the inclusion of gluons in large p_T physics is to increase the cross section at small $x_T = 2p_T/\sqrt{s}$ which is particularly useful in fitting the higher s data from the ISR[12,13].

Of course one must also include the effects of gluons as they are realized in the nonscaling behavior of the quark, gluon and jet distributions. Several parameterizations of this momentum dependence are available[14,15] which are fairly similar for the experimentally relatively "well" determined quark distributions but differ considerably in the less well specified gluon distributions as noted below. These differences appear to arise from differing assumptions about the input shape of the gluon distribution [e.g., $(a + bx)(1 - x)^4$ instead of $(1 - x)^5$]. Finally, even for lowest order scattering, account must be taken of the feature of QCD that the effective coupling is a decreasing function of p_T^2. The result of the convolution of all these effects is to produce an inclusive cross section $Ed^3\sigma/d^3p$ which, at large p_T and fixed x_T, exhibits a behavior much more like the observed p_T^{-8} behavior than the naively expected p_T^{-4} form[12,13]. In fact, with the inclusion of some internal transverse momentum for the constituents within the initial hadrons, one can achieve a quite acceptable fit to the observed data over a wide energy range[12,13]. Unfortunately detailed fits within the presently accessible p_T range depend strongly on the assumed shape of the constituents' internal p_T distributions. At best one can only argue for the consistency of QCD and the simple factorizing picture with the data. To actually test the predictions of QCD will require data at considerably larger p_T's ($p_T \gg 4$ GeV/c) where the cross section should exhibit a slower fall off at fixed x_T. There is actually some evidence that this is the case[16].

Returning to the explicit role of gluons in large p_T physics, the results of ref. 13 (the reader is referred also to the talk of A. P. Contogouris elsewhere in these proceedings) suggest a sizable role indeed. For example in the process $pp \to \pi^o + X$ at 90° with $\sqrt{s} = 19.4$ GeV and at $p_T = 1.94$ GeV/c 46% of the triggers

are found to arise from glue jets while at p_T = 6 GeV/c the fraction is only 3%. At $\sqrt{s}$ = 53 GeV and p_T's of 2 and 9 the corresponding fractions are 43% and 7%. However the reader is warned that these results presumably are sensitive to using the gluon distributions of ref. 15 which have a larger density of intermediate x gluons than is generally assumed [i.e., an input shape like $(a + bx)(1 - x)^4$ rather than $(1 - x)^5$]. It would be informative to test this distribution in the hadronic production calculations of the previous section. As noted above the large gluon induced contribution at small x_T is very helpful in explaining the shape and magnitude of the existing data on single particle inclusive production.

A perhaps more striking result is the role of gluon induced jets for the particles produced opposite the large p_T trigger particle. Since gluon induced jets are assumed to be less efficient than quark jets at giving a large fraction of momentum to a single hadron, their role is relatively suppressed on the trigger side. However, in the calculations of ref. 13, the quark-gluon scattering term (fig. 3b) leads to a dominant contribution of gluon jets opposite the trigger. The fraction of opposite jets which are one gluon induced for the process $pp \to \pi^o + h^{\pm}_{opposite} + X$ are 76% and 43% at $p_{Trigger}$ = 1.94 GeV/c and 6 GeV/c at $\sqrt{s}$ = 19.4 GeV and 69% and 51% at $p_{Trigger}$ = 2 GeV/c and 9 GeV/c at $\sqrt{s}$ = 53 GeV. This large gluon jet contribution tends to reduce the number of large p_T (i.e.,large $x_E = p_h/p_{Trigger}$) hadrons opposite the trigger relative to a pure quark-quark model, an effect useful in order to understand the data[13]. Also the inclusion of even a small fraction of gluon induced jets on the trigger side will lead to a smaller average hadron momentum within an average jet. This means that for calorimeter (i.e., jet) triggers[17], the ratio prediction for the rate of jet versus single hadron triggers at a fixed p_T will increase as a result of the inclusion of gluons, an apparently desirable effect although the experimental situation is far from clear. In summary the gluons appear to play an essential role if one is to understand large p_T physics in terms of elementary constituent scattering[18]. At the same time the results of this area of study are not of sufficient rigor to actually be able to <u>test</u> QCD here.

Glue as a Source of Large p_T in the Drell-Yan Process

Since this question is discussed in detail elsewhere in these proceedings[19], the present discussion will be brief. The Drell-Yan process[4], fig. 1c, is viewed as the source of the large mass lepton pairs observed in pp collisions[20]. Since these pairs are seen to exhibit sizable average p_T ($\langle p_T \rangle \sim 800$ MeV/c) with respect to the beam direction, gluon emission, as illustrated in fig. 4a,

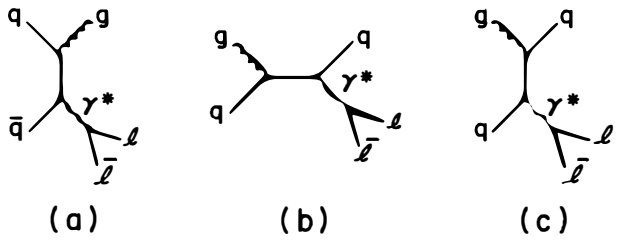

Fig. 4 Large p_T Drell-Yan: a) g emission;
b) and c) g incident and q emission.

has been discussed[21] as a possible source. Of course it was also noted[21] that gluons can participate as one of the incident constituents as illustrated in fig. 4b and 4c. The central difficulty in exploring the gluon emission contribution is that the diagram involved behaves as

$$d^2N/d^2p_T \sim 1/p_T^2 \qquad (2)$$

i.e., it exhibits an infrared divergence. Various methods have been proposed to handle this question including putting in an explicit quark mass or simply cutting off the distribution at small p_T. While it is likely that gluon physics plays an important role in the Drell-Yan process, it seems clear that simple gluon emission cannot explain all of the observed p_T of the lepton pair. Thus, at present energies, nonperturbative (i.e., noncalculable) sources of p_T are still important. Hence this is not the process to precisely

test out understanding of gluons and QCD. Thus while gluons are certainly an important part of the phenomenological understanding of various hadronic processes, this connection cannot yet be inverted to actually check whether QCD is the correct theory of Strong Interactions. One attempt to define processes which can provide precise tests is discussed in the next section.

Gluons in Precise Calculations

From the discussions of the previous sections it should be apparent that at least part of the difficulty of defining experimental tests of whether QCD is the correct theory arises from the presence of hadrons in the initial state with their attendant constituent distribution functions. Essentially the only reliable tool available for calculation is perturbation theory. Even when augmented by the simultaneous application of renormalization group techniques, one can, at present, only calculate the large momentum transfer behavior of these distribution functions, taking the low momentum behavior from the (presently rather incomplete) data. To attack the full hadron-hadron problem starting from first principles, i.e., the QCD Lagrangian, is at present impossible. A natural response to this situation is to study e^+e^- annihilation into hadrons which removes the problem of initial state hadronic wave functions. Furthermore, one must avoid introducing noncalculable quantities via the specification of the final state. For example, the single pion inclusive cross section is not calculable in perturbation theory alone. However, it does appear possible to calculate the total e^+e^- annihilation cross section in perturbation theory. The procedure is to calculate the cross section for the production of massless quarks and gluons in renormalized perturbation theory and then, using the renormalization group, replace the fixed renormalized coupling with the effective running coupling constant which behaves at large total energy W as

$$\bar{g}_W^2 \simeq \frac{8\pi^2}{(11-2/3N_f)\ln(W/\mu)} \tag{3}$$

where N_f is the number of quark "flavors" and μ defines the renormalization point. The parameter μ is generally chosen[22] to have a value around 500 MeV in order to minimize the $(\ln W/\mu)^{-2}$ corrections to the leading behavior of eq. (3). The result of this

perturbative calculation of σ_{tot} is in exact agreement with the results of the more rigorous scheme of studying the absorptive part of the photon propagator. The success of this asymptotically free perturbation calculation for σ_{tot} suggests[23] the possibility of the existence of an heriarchy of partial cross sections for the e^+e^- annihilation process which are both precisely calculable and accessible experimentally. Furthermore, since the validity of the perturbation calculation rests on the existence of a massless limit so that the renormalization group can be employed to put all non-trivial W dependence into the running coupling of eq. (3), one can interrogate the theory itself as to which quantities are appropriate to calculate in this fashion. In particular, within this scheme those quantities which exhibit explicit infrared singularities cannot be reliably calculated. For example, if a mass m is introduced for the gluon (or quark) to provide an infrared cutoff, some cross sections will be calculated as a power series in the quantity $(g^2 \ln W/m)$ which is not well behaved in the $W \to \infty$ or $m \to 0$ limit. This situation is interpreted as an indication that such cross sections cannot be reliably calculated in perturbation theory and therefore it is not possible to obtain intuition about these processes by considering simple perturbation diagrams. However, other quantities, like the total cross section, are free of such divergences and can be precisely calculated in perturbation theory[24] and should be directly comparable to experiment. This discussion is, of course, only relevant far from any explicit quark thresholds.

Cross sections of the nature discussed above are presently being studied[25] at the University of Washington. The basic idea is to consider inclusive processes which measure energy deposition in a fixed angular region. Such quantities should be insensitive to soft gluon emission or the branching of quarks into quarks and gluons, the usual sources of infrared divergences. Also it should be feasible to compare energy deposition calculated as if it occurs via quarks and gluons to experiment where it occurs in the form of hadrons. As demonstrated by low order calculations[25,26] these cross sections have a well defined perturbation expansion in the limit of zero quark and gluon mass. Thus the renormalization group can be used to replace g^2 by $\bar{g}_W^2$ where all the nontrivial W dependence is in $\bar{g}_W^2$. Hence for large enough W, the series

expansion is always rapidly convergent. The simplest such cross section is the "antenna pattern" $d\Sigma/d\Omega$ defined to be the hadronic power radiated into solid angle $d\Omega$ divided by the energy flux in the e^+e^- beams. Considering the case of e^+e^- beams polarized transverse to the beam direction and defining a polar angle ψ measured from the polarization direction, the order g^2 result is[25)]

$$\frac{d\Sigma}{d\Omega} = \frac{\alpha^2}{2W^2} \sum_f 3Q_f^2 \left[\sin^2\psi + \frac{\bar{g}_W^2}{2\pi^2} \cos^2\psi \right] \qquad (4)$$

where α is the fine structure constant ($\sim 1/137$) and Q_f are the electric charges of the various quark flavors in units of the electron charge. The relevant perturbation diagrams are displayed in fig. 5.

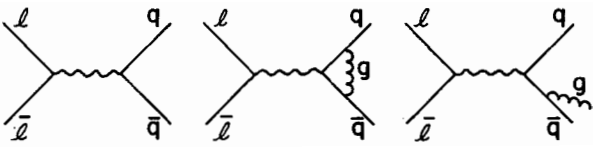

Fig. 5 $e^+e^- \to$ hadrons: a) $q\bar{q}g$;
b) virtual gluon;
c) gluon emission (+ crossed case).

This calculation does not include corrections due to the fragmentation of the quarks and gluons into hadrons which are of order m/W compared to the logarithmic terms calculated above. These power corrections can be estimated[25)] by assuming that the hadronic distribution within a jet is a function of the longitudinal momentum fraction times a rapidly cutoff transverse momentum distribution. This quark fragmentation effect modifies the basic order $(g^2)^0$ cross section to read

$$\frac{d\Sigma}{d\Omega}\,(\text{frag.}) = \frac{\alpha^2}{2W^2} \sum_f 3Q_f^2 \left[\sin^2\psi + \frac{1}{2} \langle \sin^2\eta \rangle (3\cos^2\psi - 1) \right] \cdot \qquad (5)$$

The quantity $\langle \sin^2\eta \rangle$ is essentially the energy weighted average (over the hadrons in the jet) opening angle of the jet induced by the fragmentation process (i.e., it is not a perturbative effect). With the above assumptions it has the form

$$\langle \sin^2\eta \rangle = \frac{\pi C \langle h_T \rangle}{2W} \tag{6}$$

where $\langle h_T \rangle$ is the average transverse momentum in a jet ($\langle h_T \rangle \sim 300$ MeV in the data) and C is the coefficient of the lnW dependence of the total multiplicity in e^+e^- annihilation ($\langle n \rangle \sim C \ln W$ + constant).

Comparison of eqs. (4) and (5) suggests the definition of a total jet opening angle

$$\langle \sin^2\eta \rangle_{TOTAL} \equiv \frac{\bar{g}_W^2}{2\pi^2} + \frac{\pi C \langle h_T \rangle}{2W} \tag{7}$$

where both the perturbative (precise) and nonperturbative (phenomenological-confinement) contributions are explicitly displayed. While this simple additive approach is certainly overly naive it probably does afford a reasonable estimate of the relative sizes of the two effects. With $N_f = 4$, $C = 2$, $\langle h_T \rangle = 300$ MeV, and μ (eq. 3) = 500 MeV, the perturbation contribution already dominates by a factor 3 at W = 30 GeV. The "full" cross section to order g^2 and additively corrected for quark fragmentation is

$$\frac{d\Sigma}{d\Omega} = \frac{\alpha^2}{2W^2} \sum_f 3Q_f^2 \left[1 + \frac{\bar{g}_W^2}{4\pi^2}\right] \left[\sin^2\psi + \frac{1}{2} \langle \sin^2\eta \rangle_{TOTAL} (3\cos^2\psi - 1)\right]. \tag{8}$$

The relative shape and size of this quantity with the parameter values given above is plotted for various energies in fig. 6.

While the prediction of eq. (8) is most directly tested with a calorimeter experiment (assuming that correction is made for heavy lepton production), making the assumption that the energy in neutral hadrons has the same angular distribution as that in charged hadrons and ignoring the caveat that one is to be far from thresholds, allows a comparison with existing charged hadron data. The resulting agreement is remarkably good[25].

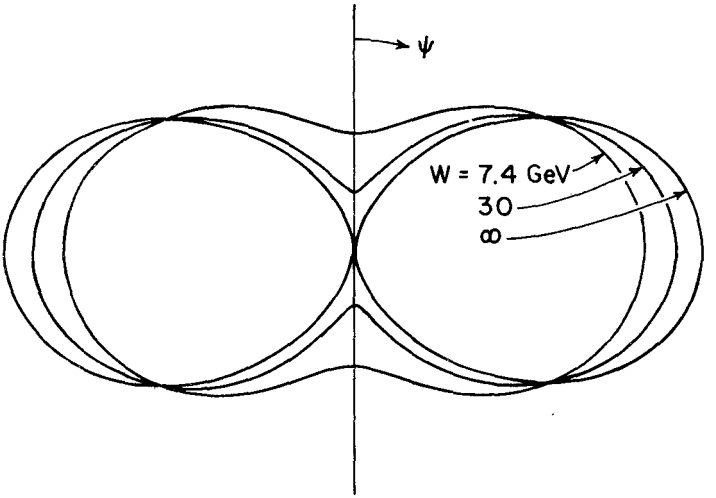

Fig. 6 Antenna pattern.

It is important to note that the individual contributions to eq. (4) arising from the energy in quarks and the energy in gluons separately exhibit infrared divergences. It is only the total energy cross section which is a meaningful quantity to study perturbatively. This point also applies to the question of looking at the energy and electric charge weighted cross section in order to see whether, on average, fractional charge resides near the edge of phase space as an indication of "quarkiness". Since the glue does not contribute to this cross section, it will exhibit infrared singularities and not be calculable perturbatively. Hence one should not anticipate that the expectations which arise from consideration of the simple perturbative diagrams of fig. 5 will be relevant. Also, while at order g^2 the quark production cross section (i.e., with no energy factor) is not divergent, it is found[26] to be divergent at order g^4 in keeping with the philosophy that the theory should not give sensible perturbative results for nonsensible quantities. Work is continuing[26] to study the form of higher order contributions to $d\Sigma/d\Omega$ and to illuminate the structure of

more complicated correlations in the heirarchy of perturbatively calculable cross sections.

Summary

Progress in the understanding of the role of glue in Strong Interactions is progressing on several fronts. Phenomenological studies of large p_T, Drell-Yan, and heavy particle production physics give strong, if somewhat peripheral, indications that gluons are indeed present in hadrons and with distributions consistent with naive expectations. At the same time more rigorous studies of the implications of gluons and QCD give every indication that confirmation that this is the correct theory is near at hand.

Acknowledgements

Helpful discussions with the author's many colleagues are gratefully acknowledged. Special thanks go to L. Brown, S. Brodsky, A. Contogouris, R. Field, R. Feynman, J. Gunion, P. Mockett, and C. Quigg. Also the efforts of Tran Thanh Van are acknowledged for making this talk possible.

Footnote and References

1) Recollections of a Caltech graduate student, S. D. Ellis, unpublishable.
2) For a discussion of other features of gluon physics not covered here see the other talks in these Proceedings. In particular see the contribution of G. Kane.
3) For a review of the fundamental properties of QCD, see W. Marciano and H. Pagels, Physics Reports 36, 137 (1978). See also H. Fritzsch, M. Gell-Mann and H. Leutwyler, Phys. Lett. 47B, 365 (1973); D. Gross and F. Wilczek, Phys. Rev. D8, 3497 (1973); S. Weinberg, Phys. Rev. Lett. 31, 494 (1973).
4) S. D. Drell and T. M. Yan, Phys. Rev. Lett. 25, 316 (1970).
5) See, e.g., A. P. Contogouris in these Proceedings. For a recent review see S. D. Ellis, "The Life and Times of Large p_T Physics: Diagnosis and Prognosis", to be published in the Proceedings of the Argonne APS Meeting, October, 1977; S. D. Ellis and R. Stroynowski, Rev. Mod. Phys. 49, 753 (1977).

6) C. T. Sachrajda in these Proceedings, Phys. Lett. 73B, 185 (1978) and CERN preprint TH.2459 (1978).
7) M. B. Einhorn and S. D. Ellis, Phys. Rev. Lett. 34, 1190 (1975), and Phys. Rev. D12, 2007 (1975); S. D. Ellis, M. B. Einhorn and C. Quigg, Phys. Rev. Lett. 36, 1236 (1976); C. E. Carlson and R. Suaya, Phys. Rev. D14, 3115 (1976) and Phys. Rev. D15, 1416 (1977).
8) For more recent studies see L. M. Jones and H. W. Wyld, Phys. Rev. D17, 1782 (1978); H. Fritzsch, Phys. Lett. 67B, 217 (1977); M. Glück, J. Owens and E. Reya, Florida State Univ. preprint FSU-HEP-770810 (1977) (to be published in Phys. Rev.); S. Nandi and H. R. Schneider, Bonn Univ. preprint BONN-HE-78-1 (1978).
9) See the various "beam dump" experiment talks in these Proceedings. See also P. Alebran et al., Phys. Lett. 74B, 134 (1978); T. Hansl et al., Phys. Lett. 74B, 139 (1978); P. C. Bosetti et al., Phys. Lett. 74B, 143 (1978).
10) J. H. Cobb et al., Phys. Lett. 72B, 497 (1978).
11) "Constituents" here refers to quarks and gluons. For a discussion of the possible role of $q\bar{q}$ "meson" constituents see the talk of J. Gunion in these Proceedings and, for earlier work, see, e.g., R. Blankenbecler, S. J. Brodsky and J. Gunion, Phys. Rev. D12, 3469 (1975) and, more recently, SLAC-PUB-2057 (1977).
12) See, e.g., R. Cutler and D. Sivers, Phys. Rev. D17, 196 (1978); B. Combridge, J. Kripfganz and J. Ranft, Phys. Lett. 70B, 234 (1977); J. Owens, E. Reya and M. Glück, Florida State Univ. preprint HEP-770907 (1977) (to be published in Phys. Rev.); A. P. Contogouris, R. Gaskell and S. Papadopoulos, Phys. Rev. D (in press); and A. P. Contogouris in these Proceedings.
13) R. D. Field, Phys. Rev. Lett. 40, 997 (1978); R. P. Feynman, R. D. Field and G. C. Fox, Caltech preprint CALT-68-651 (1978).
14) W.-K. Tung, Phys. Rev. D17, 738 (1978); A. Buras and K.J.F. Gaemers, Nucl. Phys. B132, 249 (1978).
15) G. C. Fox, Nucl. Phys. B131, 107 (1977).
16) A. G. Clark et al., "Inclusive π^0 Production from High Energy p-p Collisions at Very Large Transverse Momentum", CERN preprint (1978).
17) See, e.g., G. C. Fox, invited talk at the Argonne APS Meeting,

October, 1977, Caltech preprint CALT-68-630.
18) Again the reader is reminded of the alternative approach of the CIModel. See. ref. 11.
19) See the contributions of C. T. Sachrajda, R. Petronzio and G. Altarelli elsewhere in these Proceedings.
20) See the contribution of L. Lederman to these Proceedings and S. W. Herb et al., Phys. Rev. Lett. 40, 435 (1978).
21) A partial list of recent work in this field includes G. Altarelli, G. Parisi and R. Petronzio, CERN preprint TH.2450 (1978); C. S. Lam and T. M. Yan, Phys. Lett. 71B, 173 (1977); J. Kogut and J. Shigemitsu, Phys. Lett. 71B, 165 (1977); H. D. Politzer, Nucl. Phys. B129, 301 (1977); H. Fritzsch and P. Minkowski, Phys. Lett. 73B, 80 (1978); K. H. Craig and C. H. Llewellyn Smith, Phys. Lett. 72B, 349 (1978); F. Halzen and D. M. Scott, Phys. Rev. Lett. 40, 1117 (1978); K. Kajantie and R. Raito, Helsinki preprints HU-TFT-77-21 (1977) and HU-TFT-78-5 (1978); C. Michael and T. Weiler, Liverpool preprint LTH 42 (1978) (in these Proceedings); P. Kreiss and K. Schilcher, Johannes Gutenberg-Universität Mainz preprint (1978). See also the recent review by E. L. Berger, Argonne preprint ANL-HEP-PR-77-12 (1978) presented at the 3rd International Conference at Vanderbilt University, March, 1978.
22) See, e.g., A. DeRujula, H. Georgi and H. D. Politzer, Annals of Physics (N. Y.) 103, 315 (1977).
23) G. Sterman and W. Weinberg, Phys. Rev. Lett. 39, 1436 (1977).
24) For recent studies with this objective see ref. 25 and H. Georgi and M. Machacek, Phys. Rev. Lett. 39, 1237 (1977); E. Fahri, Phys. Rev. Lett. 39, 1587 (1977); A. DeRujula, J. Ellis, E. G. Floratos and M. K. Gaillard, CERN preprint TH.2455 (1978).
25) C. L. Basham, L. S. Brown, S. D. Ellis and S. T. Love, Phys. Rev. D17, 2298 (1978).
26) C. L. Basham, L. S. Brown, S. D. Ellis and S. T. Love, in preparation.

THE REALM OF GLUONS

J. F. Gunion[†+]
University of California, Department of Physics
Davis, CA 95616

Abstract

We discuss the role played by gluons in various phenomena of hadronic and deep inelastic physics, and how in hadronic physics one might hope to isolate a gluon jet.

† A. P. Sloan Foundation Fellow

+ Supported in part by the U.S. Department of Energy.

Introduction

It is generally recognized that gluons play an essential role in many aspects of high energy collisions. This talk will emphasize certain features of gluon physics which are crucial phenomenologically. We will concentrate on two distinct types of gluons:

a) Those which are an intrinsic virtual component of the Fock space of a color singlet hadron; and

b) Those which are radiated as a result of enforced color separation as in the $q - \bar{q}$ final state of e^+e^- annihilation.

In particular we shall focus on the distribution of soft gluons in phase space and how these distributions influence various phenomena. Our approach will be based on lowest order perturbation theory. In QED the lowest order photon emission graph combined with the knowledge that soft photon graphs exponentiate in a Poisson manner[1] is sufficient to calculate quantities of interest; in particular the number distribution $\frac{dN}{dy\, d^2q_\perp}$ (where y, the photon fractional (light-cone) momentum and $q_\perp$, the photon transverse momentum, are defined relative to the underlying photon source) is given directly by the lowest order real emission graph. We will presume that this applies also to gluons in QCD[2] -- calculations so far [3] indicate that if one thinks in terms of gluon bundles the appropriate exponentiation does occur. In any case the general features which we will discover from our low order calculations may have more general validity.

Virtual Gluons in a Color Singlet Bound State

We begin by investigating the gluon distribution predicted for a meson bound state of equal mass quarks by the lowest order graphs of Fig. 1.[4,5]

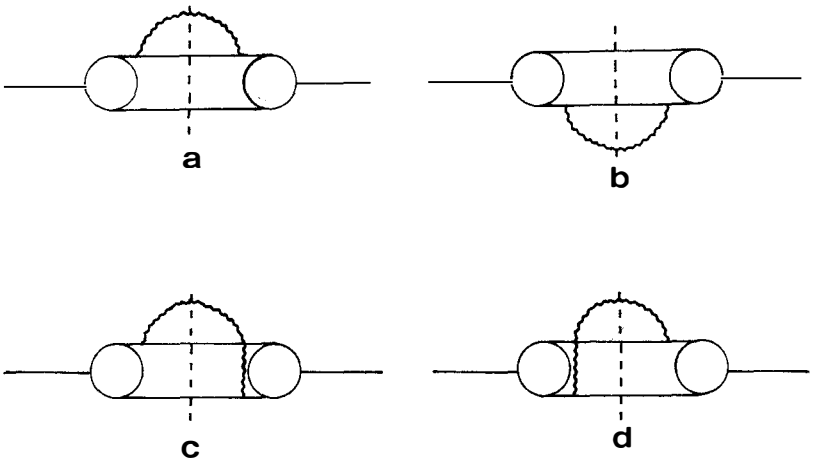

Fig. 1. Gluon emission graphs for a meson bound state.

Defining $y = (q_0 + q_3)/(p_0 + p_3)$ (p = hadron momentum, q = gluon momentum, $p_\perp = 0$) and $x = (k_0 + k_3)/(p_0 + p_3)$ (k is the quark momentum) we obtain

$$\frac{dN}{dy\, dq_\perp^2} \overset{y\to 0}{=} \frac{4}{3}\frac{\alpha_s}{\pi}\frac{1}{y}\frac{1}{q_\perp^2}\int_0^1 dx\, [2\, G_{q\bar{q}}(x,\vec{0}) - 2G_{q\bar{q}}(x,\vec{q}_\perp)] \qquad (1)$$

Here $G_{q\bar{q}}(x,\vec{q}_\perp)$ is simply related to the form factor of the meson

$$F(q_\perp^2) = (e_q + e_{\bar{q}})\int_0^1 dx\, G_{q\bar{q}}(x,(1-x)\vec{q}_\perp) \qquad (2)$$

with $F(0) = Q$ the total meson charge, so that $\int dx\, G(x,\vec{0}) = 1$. The transverse momenta of the quarks has been integrated over in the above. The 2 positive terms in Eq. (1) come from the (a) and (b) graphs diagonal in the quarks while the 2 negative terms arise from the cross-term graphs (c) and (d) in which the $q_\perp$ of the gluon is forced through the hadron wave function. In a dimensional counting framework[6] the $q\bar{q}$ form factor is monopole behaved at high momentum transfer, $q_\perp^2 \to \infty$; if we also assume that the most important x value is $\sim \frac{1}{2}$ for equal q and $\bar{q}$ masses we may introduce the parameterization

$$F(q_\perp^2) \simeq QG_{q\bar{q}}(\tfrac{1}{2}, \tfrac{1}{2}\, q_\perp) = \frac{Q}{1 + q_\perp^2/\Lambda_V^2} \qquad (3)$$

which is correctly normalized at $q_\perp^2 = 0$. Using these approximations in (1) we obtain

$$\frac{dN}{dy} \overset{y\to 0}{=} \frac{1}{y}\frac{4}{3}\frac{\alpha_s}{\pi} 2 \log\left(1 + \frac{4q_\perp^{2\ Max}}{\Lambda_V^2}\right) \qquad (4)$$

Here $q_\perp^{2\ Max}$ is determined by the kinematical limits in a particular situation; for example

$$q_\perp^{2\ Max} \approx f \begin{cases} s \text{ hadron scattering} \\ Q^2(\omega-1) \text{ deep inelastic scattering} \end{cases} \qquad (5)$$

The fraction f (< .5) corresponds to applying our results only to soft gluons.

We now wish to examine the general features of these simple results:

(1) $\frac{dN}{dy\, dq_\perp^2}$ [4] is intrinsically finite in the limit $q_\perp \to 0$ because of the color singlet cancellation. $\frac{dN}{dy}$ exhibits the logarithmic $q_\perp^2$ behavior typical of asymptotic freedom with a mass regulation determined by the hadron size.

(2) Quark counting applies[5]. The meson factor $2[G_{q\bar{q}}(x,0) - G_{q\bar{q}}(x,q_\perp)]$ is replaced by $3[G_{qq}(x,0) - G_{qq}(x,q_\perp)]$ (x is a fraction of a diquark momentum in this latter instance for a baryon 3 quark state). The functions G_{qq} and $G_{q\bar{q}}$ both of which describe a 2 quark "communication", are very similar in any simple theory obeying dimensional counting;[5] thus the number of virtual gluons in a hadron color singlet is proportional to the number of source quarks.

(3) There is a distinct possibility that the hadron size, $\frac{1}{\Lambda_V^2}$, is smaller for hadrons composed of heavier quark types, e.g. $\Lambda_\rho^2 < \Lambda_\phi^2 < \Lambda_\psi^2 < \Lambda_\Upsilon^2$.[5] This would in turn lead to progressively smaller numbers of gluons in these bound states. Whether or not the vector meson sizes really are proportional to the inverse vector meson masses themselves $\Lambda_V^2 \propto M_V^2$ (as might be guessed from monopole behavior combined with vector dominance) is a matter of speculation. Bag models exhibit little change in size with changing quark mass while linear potential models, with V = kr, have a size $\langle r^2 \rangle \propto (k\, m_q)^{-2/3}$ which also decreases relatively rapidly with increasing quark mass. Taking the vector dominance determination as an example we would obtain gluon densities in the ratio 6:5.3:3.1:1.1 for $\rho:\phi:\psi:\Upsilon$, at $q_\perp^{2\ Max} = 50\ GeV^2$. Possible consequences will be discussed shortly.

(4) The momentum carried by soft gluons in our approximation is[4]

$$P_g = \int^{\sim.5} dy\ y \frac{dN}{dy} \sim .5 \frac{4}{3} \frac{\alpha_s}{\pi} \left(2 \log \left(1 + \frac{4q_\perp^{2\ Max}}{\Lambda_V^2}\right)\right) \quad (6)$$

At $q_\perp^{2\ Max} = 50$, $\alpha_s \approx .4$ (for soft gluons), and $\Lambda_V^2 = M_\rho^2$, we obtain

$$P_g \approx .5 \quad (7)$$

consistent with most estimations of the gluon momentum fraction in light hadrons. This indicates that our QED based approach of using a lower order perturbative calculation plus presumed Poisson exponentiation is, at least, consistent.

Real Gluon Emission Through Enforced Color Separation[2,7)]

Once again we will use the lowest order calculation as a guide. Consider the case of e^+e^- annihilation in which the final state consists of a separating quark(3 of color) and anti-quark ($\bar{3}$ of color). As is well known these must radiate soft gluons (in a so called inside-outside cascade) which will eventually make $q\bar{q}$ pairs which in turn form into hadrons, see Fig. 2.

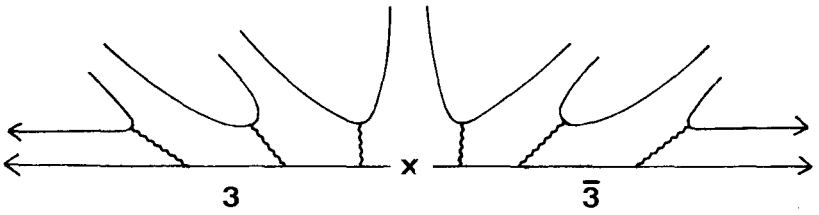

Fig. 2. Gluon emission in color separation followed by hadron production.

The observed number of hadrons will thus reflect the underlying number of soft gluons--perhaps being nearly identical as in the pair creation picture of Fig. 2. To calculate the number of soft gluons we consider the diagrams of Fig. 3.

Fig. 3. Lowest order gluon emission diagrams.

defining θ as the angle between the emitted gluon and the color triplet quark in the $q\text{-}\bar{q}$ center of mass. If q is the total gluon energy we find for q substantially less than the quark energy

$$\frac{dN}{dq\,dcos\theta} = \frac{2}{3}\frac{\alpha_s}{\pi}\frac{1}{q}\frac{(\beta_3 + \beta_{\bar{3}})^2(1-\cos^2\theta)}{(1-\beta_3\cos\theta)^2(1+\beta_{\bar{3}}\cos\theta)^2} \tag{8}$$

$$\frac{dN}{dq} = \frac{4}{3}\frac{\alpha_s}{\pi}\left\{\frac{1}{\beta_{3\bar{3}}}\log\frac{1+\beta_{3\bar{3}}}{1-\beta_{3\bar{3}}} - 2\right\} \tag{9}$$

Here $\beta_{3\bar{3}}$ is the relative velocity of the quark and antiquark. Integrating from some minimum value of q determined by the fact that gluons cannot be effective when their wavelength is longer than a typical (light) hadron size, we obtain in the limit $p_3\cdot p_{\bar{3}} \to \infty$

$$\langle n\rangle_{hadron} \sim \langle n\rangle_g \simeq \frac{4}{3}\frac{\alpha_s}{\pi}\left(\log\frac{2p_3\cdot p_{\bar{3}}}{m_3\, m_{\bar{3}}}\left(\log\frac{2p_3\cdot p_{\bar{3}}}{q^2_{min}} + C_1\right) + C_2\right). \tag{10}$$

Of course m_3 and $m_{\bar{3}}$ are presumably also replaced by hadron masses when confinement is taken into account. Let us now examine the general features of these results.

(1) There is a double logarithmic growth in multiplicity--it arises from a "collision" of the log which comes from the soft dq/q spectrum and one which arises from the light-cone angular singularity according to which the emitted gluon prefers to travel in the direction of one or the other of the source quarks.[8] The double logarithmic portion arises entirely from the region of integration in which the gluon momentum (in particular, transverse momentum) remains finite.

(2) The typical transverse momentum of the gluon may be obtained by examining the angular form which yields

$$\Delta\theta \sim 2\,\frac{m_3(\text{or } m_{\bar{3}})}{\sqrt{s}} \tag{11}$$

implying

$$\Delta q_T \simeq q\Delta\theta \simeq m_3\,\frac{2q}{\sqrt{s}} = m_3\,x_L \tag{12}$$

where x_L is the momentum fraction the gluon carries with respect to the quark source.

(3) The amount of gluon radiation (especially the $\ln^2 s$ term) is directly proportional to the effective charge squared of the 3 and $\bar{3}$, $\frac{4}{3}\alpha_s$. If one were to repeat the calculation for underlying octet sources (e.g. gluons) one would obtain radiation proportional to $3\alpha_s$[2]; the effective charge of a color 8 is 3/2 that of a color 3 or $\bar{3}$. One should note that only in a vector gluon theory is a gluon source expected to radiate gluons in a manner like that of a quark source; in particular a scalar gluon would tend to break into secondary gluons carrying equal momenta whereas a vector gluon will radiate, primarily, much softer secondary vector gluons due to the $\frac{dq}{q}$ type emission spectra typical of a vector gluon theory.

(4) The soft gluon radiation from a given quark type vanishes at the threshold for production of that quark. This is because $\beta_{3\bar{3}}$, the relative 3-$\bar{3}$ velocity, vanishes at threshold.[9]

Implications for Observable Phenomena

A. Enforced Color Separation

Let us first focus on enforced color separation. We have seen that in e^+e^- annihilation one may expect gluon radiation (followed by subsequent hadron formation) which is proportional to the 3 - $\bar{3}$ charge and a function of the invariant 3 - $\bar{3}$ energy, Color separation also occurs in a variety of other situations.

(a) In deep inelastic scattering the incident virtual photon strikes a quark (or antiquark) out of the target hadron leaving behind a $\bar{3}$ (or 3) system. In a strong coupling limit and for long wave length, soft, gluons it is reasonable to presume that this remaining $\bar{3}$ (or 3) system radiates as a single unit. Thus, as far as soft gluon radiation is concerned, the final state consists of a separating 3 and $\bar{3}$ with invariant energy $W^2 = Q^2(\omega-1)$. Because the physical situation is the same as in the e^+e^- final state we have

$$\langle n\rangle_{DI}(W^2) = \langle n\rangle_{e^+e^-}\ (s = W^2) \tag{13}$$

at least for the centrally produced slow hadrons.

(b) In $e^+e^- \to HX$ the hadron H is the fragment of a quark, $q \to Hq'$. Defining $z = p_H/p_q$ the left over color triplet quark, q', carries reduced momentum $(1-z)\sqrt{s}/2$ The antiquark $\bar{3}$ and this remaining 3 have invariant energy $(1-z)s$ and their enforced separation produces a hadronic multiplicity.

$$\langle n \rangle_{e^+e^- \to HX}(M_X^2 = (1-z)s) = \langle n \rangle_{e^+e^-} (s = M_X^2) \qquad (14)$$

(c) In $pp \to \mu^+\mu^- X$ a q from one proton and $\bar{q}$ from the other annihilate to form the μ-pair. Separating 3 and $\bar{3}$ systems are left behind with invariant energy M_X^2. Thus

$$\langle n \rangle_{pp \to \mu^+\mu^- X} (M_X^2) = \langle n \rangle_{e^+e^-} (s = M_X^2) \qquad (15)$$

Again we remind the reader that this "universality"applies only to the centrally produced multiplicity, i.e. the height of the (rising) central plateau, and that finite, energy independent, fragmentation multiplicity differences between processes can be expected.

(d) What about hadronic interactions?

Hadron-hadron collisions can proceed via either one of two simple QCD interaction mechanisms--wee(i.e. slow) quark exchange or annihiliation[2, 7] (closely analogous to $\mu^+\mu^-$pair production); or gluon exchange.[10] (See Figs. 4a and 4b.)

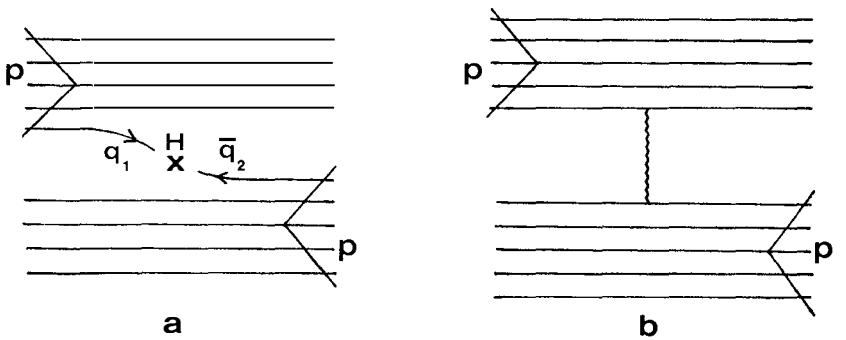

Fig. 4. Models for a hadron-hadron collision: a) "wee" $q\text{-}\bar{q}$ annihilation; (b) "wee" gluon exchange or annihilation.

(I) in the first case the annihilating q and $\bar{q}$ are very slow and essentially the entire energy of the incoming beams is retained by the separating 3 and $\bar{3}$ systems. Again, if these 3 and $\bar{3}$ systems radiate as coherent units, the multiplicity will be universally related to that in e^+e^- annihilation

$$\langle n\rangle_{pp\to X}(s) = \langle n\rangle_{e^+e^-}(s) \tag{16}$$

aside from finite fragmentation effects. Even these fragmentation pieces should be very similar to those seen in $\mu^+\mu^-$ pair production when $\tau = M^2_{\mu^+\mu^-}/s$ is small. In fact if this first, quark annihilation, mechanism does in fact dominate pp collisions, a close comparison to $\mu^+\mu^-$ pair production at small τ should yield many similarities.

(II) If gluon exchange dominates, the separating systems, in the final state, are color octets. One would then expect for the central multiplicity

$$\langle n\rangle_{pp\to X}(s) = \frac{9}{4}\langle n\rangle_{e^+e^-\to X}(s) \tag{17}$$

In both the models, I and II, the cross section is obtained by folding together two distribution functions e.g. for I

$$\sigma \propto \int dx_1 dx_2 G_1(x_1)\, G_2(x_2)\, \delta(x_1x_2s - M_H^2) \tag{18}$$

If both G(x)'s exhibit the Feynman $\frac{dx}{x}$ spectrum, corresponding to Pomeron behavior or to the creation of wee quark pairs from a dx/x gluon distribution, then the total cross section σ will ultimately grow as lns. If the G(x)'s contain the logarithms typical of slow particle emission in a vector gluon theory (Equation (4)), the cross section could grow as fast as $\ln^3 s$.

Whether or not universality of the central multiplicity does in fact obtain is still controversial. Albini et. al.[11] find their best fit to the pp multiplicity, over the entire energy range, requires both a lns and $\ln^2 s$ term. The $\ln^2 s$ form is consistent with our theoretical ideas and the coefficient of $\ln^2 s$ implies a value $\alpha_s \sim .4$ in Eq. (10). When they overlay this best fit on the multiplicity curves for the other reactions (a) - (c) and for e^+e^- annihilation (correcting for finite fragmentation effects by using an "available energy" variable), they obtain essentially perfect agreement--implying that multiplicity universality does hold and that mechanism (I) dominates in hadron collisions.

A single log, a + blns, fit to the different sets of data, pp vs. e^+e^-, does yield $b_{pp} > b_{e^+e^-}$ but largely because of the different energy ranges covered; in addition the fit to the overall pp multiplicity curve performed in this way has a very low χ^2. Another way of making the pp and e^+e^- universality apparent is by plotting e^+e^- and pp multiplicities vs. lns on the same graph.[12] The curves are seen to rise in parallel separated by a constant (fragmentation) multiplicity difference. A more direct comparison of central plateau heights has been attempted[13]; the e^+e^- plateau height, $\frac{dN}{d\eta}$ (charged) $\eta = 0$ (η = rapidity), is ≈ 1 at an energy for which the pp plateau height is ≈ 1.35. However a trigger requirement in the e^+e^- cross section and multiplicity (one particle with $x > .5$) makes direct comparison somewhat unreliable. In any case more data and additional independent tests are required.

We have suggested [7,14,15] that the power laws associated with the production of fast fragments in pp and other hadronic collisions provide a second independent test of which of the two mechanisms I or II dominates. For example consider $\frac{dN}{dx_\pi}$ ($pp \to \pi X$). Here x_π is (strictly) the light cone momentum fraction carried by the π relative to its underlying source jet, but it may be approximated by the radial scaling variable $E_\pi/E^\pi_{Max} = x^\pi_R$ which also vanishes at the phase space boundary. Of course at high energies (ISR is sufficient) $x_\pi \approx x^\pi_R \approx x^\pi_F$ where x^π_F is the usual Feynman longitudinal momentum fraction. In the annihilation model, I, the most favorable situation occurs when a 5-quark Fock state of the proton is considered. The π is then part of a 4-quark jet, see Fig. 5a, one

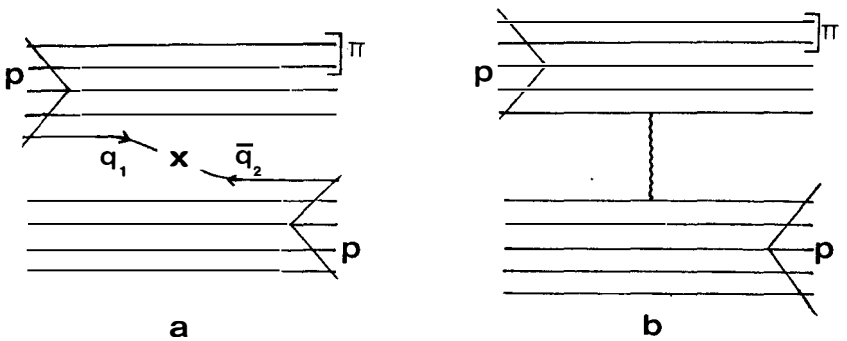

Fig. 5. Single particle fragmentation in pp collisions: a) $q\bar{q}$ annihilation model; b) gluon exchange model.

of the q's having participated in the annihilation. The 4-quark-jet fragments into the π leaving behind $n_s = 2$ spectators. Dimensional counting for fragmentation functions then predicts (See Ref. 14 and references therein.)

$$\frac{dN}{dx_\pi} \sim (1-x_\pi)^{2n_s-1} \sim (1-x_\pi)^3. \tag{19}$$

In the gluon exchange model, II, the 5th quark of the minimal 5 quark Fock state is not absorbed by the interaction (Fig. 5b); thus the π fragmentation leaves $n_s = 3$ spectator quarks behind implying

$$\frac{dN}{dx_\pi} \sim (1-x_\pi)^5. \tag{20}$$

Experimentally the best data is that of Sens et. al.[16] from ISR which shows $\frac{dN}{dx_\pi} \sim (1-x_\pi)^{3.5\pm3.1}$ over the $x_\pi = .3\div.8$ range. Related predictions for K^-, Λ and $\bar{\Lambda}$ are also possible. For instance fragmentation of a K^-, which has no quarks in common with the valence proton state, requires that one begin with a 7-quark proton Fock state ($uuds\bar{s}u\bar{u}$). The number of spectators to K^- fragmentation is then $n_s = 4$ and $n_s = 5$ for models I and II respectively. Thus the powers in (19) and (20) are each raised by 4 in going to $\frac{dN}{dx_{K^-}}$. Again experiment[16] prefers the annihilation power $\frac{dN}{dx_{K^-}} \sim (1-x_{K^-})^7$. Similar agreement is obtained for Λ and $\bar{\Lambda}$. For $x > .9$ the two oppositely directed jets of Fig. 5 become intermingled; the fragment absorbs so much momentum from the one forward (say) jet that the remaining spectators are slow moving and become confused with the oppositely directed jet. In this region one can expect Triple Regge phenomenology to become applicable. At low energies this intermingling occurs even at moderate x, making application of these ideas below FNAL energies unreliable. Other important checks are the π beam fragmentation reactions, particularly $\pi^+ p \to pX$. In the models of Ref. 15 the fragment, p, follows the valence quark distribution, $(1-x)^1$ for the π beam, while in the present approach $\pi^+ p \to pX$ and $pp \to \pi^+ X$ should exhibit the same power behavior. Available FNAL data[16] yields the expected similarity when examined in terms of x_F but the analysis should be redone in terms of x_R.

An especially critical test of model I vs. model II is the prediction[14] obtained in I for $pp \to \pi_1^+ \pi_2^+ X$ where the two pions travel in opposite directions along the center of mass beam direction. From Fig. 6 one obtains

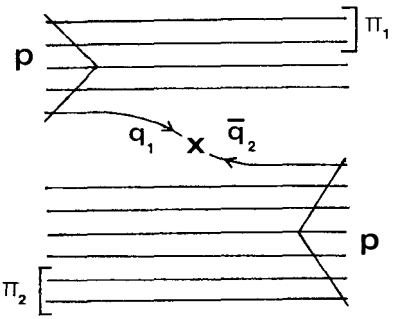

Fig. 6 Double π fragmentation, $pp \to \pi_1 + \pi_2 + X$, in the $q\bar{q}$ annihilation model - $(1-x_{\pi_1}) << (1-x_{\pi_2})$

$$\frac{dN}{dx_{\pi_1} dx_{\pi_2}} \sim (1-x_{\pi_1})^3 (1-x_{\pi_2})^7 \qquad (21)$$

for $(1-x_{\pi_1}) << (1-x_{\pi_2})$; a beam-target symmetric term with $1 \leftrightarrow 2$ makes experimental tests difficult without very high statistics data over substantial x_π ranges. The above form indicates a long range correlation between the two pions which is absent in the gluon exchange model and in the Triple Regge phenomenology.

Of course, one cannot exclude the possibility that both mechanisms--quark annihilation, I, and gluon exchange, II--contribute to the total hadron cross section--let us say with equal weight. The observation of a single fast fragment clearly favors the annihilation contribution (I) because of its lower fragmentation power. The double fragmentation situation is less clear; if $(1-x_{\pi_1})^3 (1-x_{\pi_2})^7$ is numerically smaller then $(1-x_{\pi_1})^5 (1-x_{\pi_2})^5$ then gluon exchange will again be a significant contribution. One would clearly require quite small $(1-x_{\pi_1})^2$ in order to achieve a clean separation, but in order to avoid the Triple Regge region $x_{\pi_1} < .9$ is required. Thus $.9 \geq x_{\pi_1} > .7$ high statistics data is necessary.

Indeed there is one type of observed long range correlation which favors the idea that contributions from both gluon exchange and quark exchange are present. Recalling that there is a higher multiplicity associated with the gluon exchange mechanism it is clear that if one looks for events with high multiplicity on one side of the rapidity axis, $\eta > 0$—

thus magnifying the gluon exchange contribution--one will also obtain above average multiplicity on the other side, $\eta < 0$. This effect seems to have been observed at both ISR[17] and FNAL[18] energies[19].

The observant reader will by this time have noticed that several other collision mechanisms are possible at a simple quark level. These include q(2q), quark-diquark, annihilation to a slow baryon; and two simultaneous $q\bar{q}$ annihilations. These intuitively seem less probable to us but we have not attempted to systematically normalize them relative to the simple choices I and II. Both, however, would lead to $\frac{dN}{dx_\pi} \sim (1-x_\pi)$ in the single fragmentation experiment.

We also remark that whatever the mechanism for hadronic collisions, even if it is gluon exchange, the final state jets have a primarily quark-like character. None of the above mechanisms succeed in isolating a lone gluon jet source.

Several of the other general features of hadron production through enforced color separation are also possibly observable. In e^+e^- annihilation one certainly passes the $c\text{-}\bar{c}$, charm threshold. At this point the centrally produced multiplicity should exhibit a dip. This is due to the fact that the additional cross section from this new contribution rises rapidly above threshold without as rapid a rise in the associated gluon (i.e. hadron) multiplicity--initially this new channel yields zero soft gluon multiplicity because of the low relative velocity of the separating c and $\bar{c}$. Unfortunately this dip is easily obscured by the higher finite fragmentation (or decay) multiplicity of D and $\bar{D}$, or D^* and $\bar{D}$ etc., which are produced at this threshold, compared to particles produced below charm threshold.[23]

The final general feature mentioned in the earlier section is that the $\langle q_T \rangle$ of gluons and, hence, of particles produced centrally can be expected to rise with the momentum fraction they carry

$$\langle p_T \rangle \sim \text{constant } x_L \qquad (22)$$

This effect is now thoroughly established in both deep inelastic and hadron collisions; it is termed the "sea gull" effect.[21]

B. Virtual gluon distributions

Turning now to the experimental implications of the virtual gluons associated with a color singlet bound state, there are only two easily observable consequences of the general features discussed. First we

note that for either of the hadronic collision mechanisms, quark or gluon exchange, total cross sections should exhibit quark counting relationships (when the type of quark involved is held fixed).[4,5] In the gluon exchange case this is a direct result[5] of the proportionality of the number of virtual gluons to the number of quarks. In the quark exchange case one imagines that the annihilating wee quark from each bound state has arisen from a soft virtual gluon. The number of wee quarks in a bound state is then directly proportional to the number of soft gluons and again quark counting obtains. One also sees that any extraction of quark momentum fractions for a pion bound state should indicate that a smaller fraction of the pion's total momentum should be carried by gluons than in the case of a proton state.

The second immediate observation is that total hadron cross sections (again for either the gluon or the quark exchange mechanism) should be sensitive to the effective sizes of the colliding hadrons[4,5]. For vector meson proton scattering, the larger Λ_V^2 (i.e. the smaller the size of the vector meson V) the fewer the number of gluons and hence the smaller the cross section. As discussed, at least two models yield increasing Λ_V^2 with vector meson mass ($\Lambda_\rho^2 < \Lambda_\phi^2 < \Lambda_\psi^2 < \Lambda_T^2$) resulting in decreasing cross sections

$$\sigma(\psi p) < \sigma(\phi p) < \sigma(\rho p) \qquad (23)$$

Experimentally[22] the cross sections appear to decrease somewhat more rapidly than any of the models predict. The logarithmic form of the functional dependence on Λ_V^2 suggests that the effect should be largest (in terms of a ratio or percentage) at low energy (low $q_\perp^{2\ Max}$) and should decrease continuously as the collision energy increases. This will be interesting to test.

This decrease of a gluon's coupling strength to a hadron as the hadron mass increases would also be reflected in a smaller probability for heavy quark hadron production as opposed to light hadron production from the soft--long wavelength--gluons produced in the final state of, for example, e^+e^- annihilation in response to $3\text{-}\bar{3}$ separation. This heavy-quark-hadron suppression would persist even after all threshold mass effects had become unimportant. Thus persistent dominance of light hadron production in final states at asymptotic energies may be observed experimentally.

How to isolate a gluon

So far we have seen no way to isolate a gluon jet on its own. How can we get rid of accompanying quarks? Various ways have been suggested in the literature such as trusting the picture that the ψ and T decay via emission of 3 gluons; gluon jet physics would then be apparent there.[23] Here I will concentrate on high transverse momentum approaches to isolating a gluon. As usual we imagine the production of a high transverse momentum particle in a hadron-hadron collision as proceeding via the scattering of two low transverse momentum secondary particles (e.g. q,g or q,M or g,g or ...) of the primary beams into oppositely directed high transverse momentum particles one of which is either directly observed or fragments into the observed particle. The scattering process of the secondaries is termed the fixed angle "subprocess". This separation is sketched in Fig. 7.

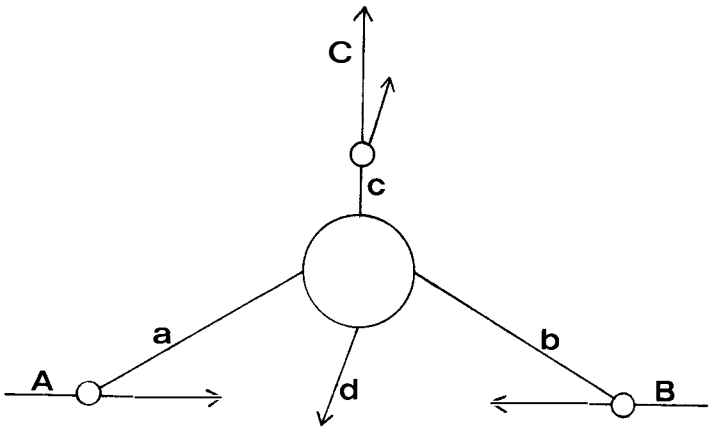

Fig. 7. A + B → C + X via subprocess a + b → c + d.

Basically one would like to achieve dominance of the gluon gluon → gluon gluon p_T^{-4} scaling subprocess over other contributions. In particular one must achieve a situation in which constituent interchange subprocesses (such as qM → qM) and other p_T^{-4} subprocesses (such as qq → qq) are unimportant. An excellent way to achieve this is by triggering on a $\bar{p}$ at high transverse momentum. First the constituent interchange (CIM) contributions to $\bar{p}$ production, deriving mainly from the $\bar{q}\,\bar{B} \to \bar{q}\,\bar{B}$ subprocess, are not large and are damped as $1/p_T^{12}$ at fixed $x_T = 2p_T/\sqrt{s}$. Estimates are [24] that at p_T's as low as 5 GeV/c, for the $\bar{p}$ trigger, CIM contributions

are small. For $p_T > 5$ GeV/c the production of $\bar{p}$'s in pp collisions is dominated by the p_T^{-4} subprocesses $gg \to gg \hookrightarrow \bar{p}$ and $gq \to gq, \hookrightarrow \bar{p}$ $q\bar{q} \to q\bar{q} \hookrightarrow \bar{p}$ being unimportant. (Here the $\hookrightarrow$ indicates which final particle of the subprocess fragments to the $\bar{p}$.) For $\varepsilon = 1 - x_T > .7$ the $gg \to gg \hookrightarrow \bar{p}$ contribution dominates the other; the jet opposing, or balancing, the observed $\bar{p}$ is then a gluon and the $\bar{p}$ itself is also the fragment of a gluon jet. Indeed, at ISR, the evidence of a larger than usual "same side" momentum in association with the highest p_T $\bar{p}$ triggers[25] (i.e. momentum carried by particles traveling in the same direction as the trigger $\bar{p}$ and hence part of the source jet) is suggestive of the higher gluon multiplicity.

One other possible production process for high transverse momentum gluon jets in hadron-hadron collisions involves the subprocess $qM \to gq$ analogous to the photon production process based on $qM \to \gamma q$. The observed high p_T photons at ISR probably arise from this latter[26,27]; it also certainly controls the exclusive reaction $\gamma N \to \pi N$, where it is combined with the nucleon form factor to predict the observed $1/s^7$ behavior of $\frac{d\sigma}{dt}(\gamma N \to \pi N)$. Using the normalization obtained[27] from $\gamma N \to \pi N$ for the $qM \to \gamma q$ cross section and making the replacement $\alpha \to \frac{4}{3}\alpha_s$ for $\gamma \to g$, one obtains astronomical gluon production cross sections in $pp \to gX$. Unfortunately (or fortunately for the sake of existing interpretations of high p_T phenomenology) there is[28] an extra "gauge invariance" induced cancellation, in going from the color singlet photon in $Mq \to \gamma q$ to the color octet gluon in $Mq \to gq$, which dramatically suppresses the gluon production from this source.

Conclusion

It is clear that the effects of gluons in hadron collisions are everywhere. They influence low transverse momentum phenemonology in a myriad of interesting ways but are hard to isolate on their own in that realm. Only at high momentum transfer do we see a distinct possibility for truly isolating a gluon jet and even there one must resort to specialized triggers and particular kinematic domains.

Acknowledgment

I would like to thank S. Ellis, S. J. Brodsky, R. Blankenbecler, S. Ono, D. Jones, A. Krzywicki, and A. Capella for helpful conversations.

Footnotes and References

1. D. Yennie, S. Frautschi and H. Suura, Ann. Phys. 13, 379 (1961) D. Yennie Brandeis Summer Institute 1963, p. 221.
2. S. J. Brodsky and J. F. Gunion, Phys. Rev. Letters, 37, 402 (1976).
3. J. Taylor, Oxford University preprint 1976.
4. S. J. Brodsky and J. F. Gunion in preparation.
5. For a closely related calculation see J. F. Gunion and D. E. Soper, Phys. Rev. D15, 2617 (1977).
6. S. J. Brodsky and G. R. Farrar, Phys. Rev. Letters, 3, 1153 (1973).
7. S. J. Brodsky and J. F. Gunion SLAC-PUB-1820. "Connection between lepton and hadron induced reactions" published in the proceedings of the VIIth International Colloquium on Multiparticle Reactions Tutzing, June (1976). See also G. Kane, Y-P. Yao, University of Michigan preprint, for an alternative view of octet gluon jets and multiplicity in hadronic collisions.
8. This source of the double log is implicit in the calculations of L. Bashan, L. Brown, S. Ellis, and S. Love, University of Washington, preprint 1978. I thank S. Ellis for a helpful conversation on this point.
9. A detailed phenomenological investigation of this effect is being carried out by S. J. Brodsky, J. F. Gunion and S. Ono.
10. F. E. Low, Phys. Rev. D12, 163 (1976); S. Nussinov, Phys. Lett. 34, 1286 (1975).
11. E. Albini, P. Capiluppi, G. Giacomelli, and A. M. Rossi, Bologna preprint (1975).
12. V. Lüth, SLAC Summer School 1977.
13. G. Hanson VIIth International Colloquium Multiparticle Reactions, Tutzing, (1976).
14. S. J. Brodsky and J. F. Gunion, "Hadronic Fragmentation as a Probe of the Underlying Dynamics of Hadron Collisions", Phys. Rev. D17, 848 (1978).
15. Related ideas have been discussed by R. Das and R. C. Hwa, Phys. Lett. 68B, 459 (1977). See also W. Ochs, Nucl. Phys. B118, 397 (1977).
16. J. C. Sens, et. al. CHLM collaboration and A. B. Clegg (private communication). The lower energy analysis of F. E. Taylor et. al. Phys. Rev. D14, 121 (1976), performed using x_R, is consistent with the high energy, high statistics Sens results, FNAL x_F analyses for $pp \to \pi^{\mp} X$ and $\pi^{\mp} p \to pX$ appear in R. L. Anderson et. al. Phys. Rev. Lett. 37, 1111 (1976). The $(1-x_F)$ powers are similar in these two but both differ somewhat from the $(1-x_R)$ powers of the Sens and Taylor analyses because of finite energy effects.
17. S. Uhlig et. al. Nucl. Phys. B132, 15 (1978).
18. T. Kafka et. al. Phys. Rev. Lett. 34,687 (1975).
19. A Reggeon approach to this effect is also possible. See A. Capella and A. Krzywicki, Orsay preprint 1978.
20. A detailed study of these competing effects is undertaken in Ref. 9.
21. See the related talks in these proceedings, especially that of G. Hanson, and the talk by C. Heusch in the VIIth International Colloquium on Multiparticle Reactions Tutzing (1976).
22. We use the value of $\sigma_T(\phi p)$ given by A. Silverman, in "Proceedings of the 1975 International Symposium on Lepton Photon Interactions at High Energies", Stanford (1976). For $\sigma_T(\psi p)$ see D. Hitlin, SLAC Summer School Proceedings (1976). These values give $\sigma_T(\rho p)$: $\sigma_T(\phi p)$: $\sigma_T(\psi p)$ = 8:4.5:1; however the extractions are

quite indirect and the energy dependence of the ratios is certainly not yet clear.
23. See for example S. J. Brodsky, D. G. Coyne, T. A. DeGrand, and R. R. Horgan, SLAC-PUB-2047.
24. J. F. Gunion and D. Jones, U.C. Davis preprint in preparation. For a summary of the results see J. F. Gunion "Interrelationship of the CIM and QCD" U.C. Davis preprint.
25. See, for example, the talk by R. Møller, XIIth Rencontre de Moriond, Flaine (1977).
26. R. Rückl, S. Brodsky, J. Gunion, in preparation.
27. R. Blankenbecler, S. Brodsky, J. Gunion SLAC-PUB-2057.
28. J. F. Gunion, S. J. Brodsky and R. Blankenbecler in preparation.

See the summary mentioned in Ref. 24.

STUDYING GLUON PROPERTIES EXPERIMENTALLY*,†

G.L. Kane
Physics Department
University of Michigan
Ann Arbor, MI 48109 USA

ABSTRACT

Ways are discussed in which gluons can be studied experimentlly, with emphasis on non-perturbative methods. Some possibilities are hadron multiplicities, central region particle ratios, σ_T, gluon resonances. It is argued that quark jets and gluon jets will behave qualitatively differently.

*Research supported in part by US Department of Energy

†This talk is based on work done in collaboration with Y.P. Yao

I. INTRODUCTION

It is believed today that Quantum Chromodynamics[1] (QCD) is a good candidate for a theory of strong interactions. QCD is a theory of colored quarks interacting with colored gluons. The major new features of the theory, and the ones which are crucial for the theory to have desirable properties such as asymptotic freedom and confinement, depend on the nature of the gluons and their interactions.

The gluons and their properties may be extremely difficult to study. They are thought not to interact with lepton or photon beams, so these probes will not help directly. Although an elegant theoretical edifice has been erected around QCD, additional experimental tests and experimental stimulation are desirable.

It is the purpose of this paper to argue that, under certain conditions, a large part of the data from ordinary hadron high energy interactions may be interpretable in terms of gluon interactions, and may provide extensive experimental tests of QCD. In addition, we argue that hard gluon jets may not occur; instead, a finite fraction of the energy may go into particle masses and increased multiplicity.

II. GLUON PROPERTIES

In this section we will summarize the relevant properties that gluons are expected to have, in two parts. The first includes standard, relatively well known ones, and the second set are more speculative, based partially on recent work[1] by Chang and Yao.

A. The most important single result is from the momentum sum rule: only about half of the momentum of a proton is carried by constituents which interact with weak and electromagnetic currents (in e^- and ν reactions), and the rest is interpreted as being carried by gluons. Thus we are assured that in all high energy collisions a sizeable fraction of the hadron consists of gluons which will interact strongly.

Another important property of gluons is that they are completely flavor-neutral. They do not distinguish charge, isospin, strangeness, etc. When gluons materialize into colorless mesons, apart from corrections for masses, the population of different mesons should be independent of all quantum numbers.

Since gluons do not recognize the existence of leptons, they can only be studied indirectly at machines with lepton beams, either through decays of charmonium or additional heavy quarkonium states[2], or through gluon bremsstrahlung from a struck quark[3].

The distribution of gluons in x (the fraction of the proton momentum that they carry) should be intermediate between that of the $q\bar{q}$ sea (which is concentrated at very small x) and that of the valence quarks (which extends to x = 1). This is because the gluons will couple strongly to the $q\bar{q}$ sea, but many of them will originate by bremsstrahlung from the valence quarks and carry a significant fraction of the valence quark's momentum. Two recent phenomenological analyses of the gluon distribution in x, G(x), are given in Ref. 4.

It is important to emphasize that the gluons are not the same as the $q\bar{q}$ sea, although clearly a sharp distinction between them is not possible. For example, the sea interacts with lepton probes while the gluons do not. At any instant, of order half of the proton momentum is carried by states which are neither valence nor sea quarks; the sea quarks carry only a few percent of the momentum. Indeed, since the gluons carry an order of magnitude more momentum than the sea, while the x distributions are not usually thought to be too different (the gluons having a larger tail at larger x), probably at every x the sea can be neglected for our present purpose of studying strong interactions and hadron production. We are assuming, of course, that production of final state hadrons can be interpreted as coming from gluons; this seems to be consistent with their role in strong interactions.

B. Now we turn to even more speculative properties of gluons and gluon interactions.

Consider gluon-gluon scattering. There will be resonances (often called glue balls). These are discussed in ref. 5-10, and reviewed in ref. 11. All authors expect resonances in the 1-2 GeV mass region, with a variety of quantum numbers.

These states must show up, if QCD is valid; or an explanation must be given as to why they do not. If they lie at higher mass an explanation must be given as to why the $q\bar{q}$ (and $q\bar{q}$ $q\bar{q}$ etc) states lie lower.

Some of the glue ball states have exotic quantum numbers relative to $q\bar{q}$, such as $J^{PC} = 1^{-+}$. This is one way to find them. All of them, of course, have $I^G = 0^+$. In general they give an extra multiplicity of states of each set of quantum numbers.

At least qualitatively, because of a "Zweig-rule" kind of argument, when states of glue go into $q\bar{q}$ mesons we expect a suppression, so there will not be wide states; large widths cannot be used as an excuse for not finding them. They will mix with $q\bar{q}$ states.

In general, attempts at QCD solutions will have predictions for the gluon-gluon cross section , σ_{gg}, at low and at high energies. These will be intrinsically non-perturbative. Perhaps, as discussed below, these can be related to observables such as multiplicities, central region clusters, particle ratios, σ_{tot}, etc.

For trying to decide how gluons will behave, probably the most important gluon property is the existence of strong three-gluon and four-gluon self-couplings. Because of these, one gluon rapidly multiplies into a cascade of several gluons. The probability of obtaining more gluons is enhanced when some have appeared; further, because of asymptotic freedom the coupling is expected to be stronger for softer gluons. Theoretically this "gluon splitting" may be fundamental for confinement.

Phenomenologically, gluon splitting suggests that gluon "jets" may be much different from quark jets. While the quark jets are expected to be hard, with much of the

momentum of the struck quark in the jet momentum, when a hard gluon is emitted there will be a cascade into a relatively large number of softer gluons, which eventually convert into hadrons. Consequently, we expect much more of the energy of a hard gluon to be converted into hadron mass than would happen for a quark jet.

This implies two important results:

(1) The multiplicity associated with gluons will be higher than for quarks.

(2) There may not be any hard "gluon jets" analogous to quark jets. Instead, gluon jets will be characterized by high multiplicity swarms of hadrons that are totally flavor-neutral.

Other workers who have studied gluon properties and discussed how to look for them have instead assumed that gluon jets would be similar to quark jets, although no compelling reasons have been given. An experimental choice between these approaches would be of great help in getting further insight into the theory. Note that for us the two results of high multiplicity and no hard gluon jets go together.

We should remark that the behavior of quark jets is what is normally expected. They remain hard for several reasons. The first is that quark masses keep intermediate states away from strong infrared singularities, and at the same time cause the running coupling constant to have an upper bound, with a scale set by the quark mass; this does not allow a quark to have much gluon bremsstrahlung compared to a gluon.

Another difference between quark and gluon interaction is that at a $\bar{q}qg$ vertex one can define a quark convection current, while at a ggg vertex the color doesn't know which way to go. So one can imagine differences arising in jet behavior. Chang and Yao (ref 1) have shown that the most probable dissociation for a scalar gluon in φ^3 theory in 6 dimensions is into two gluons each with half the mass, whereas a quark will tend to emit soft gluons. If this is relevant to QCD it gives another important difference. Yao (private communication) has shown in an SU(2), non-Abelian,

leading ℓn calculation that for quarks one will get exponentiation as in QED for the cross section for emission of soft gluons, but for gluons emitting soft gluons the combinatories are different and quite a different answer comes out. All this suggests as well that one should not use QED arguments for gluon properties.

III. REINTERPRETATIONS AND PREDICTIONS

Now we turn to discuss specific hadronic experimental quantities and how we might use them to learn about gluon properties and interactions. This list of possibilities includes the total cross section, the real part of the forward amplitude, the elastic differential cross section, central region clusters and their properties, multiplicities and particularly the growth in multiplicity at very high energies, particle ratios, double Pomeron exchange, and inclusive polarizations. Our most important result is probably the possibility that the behavior of particle ratios will permit a measurement of the gluon distribution function.

A. The Total Cross Section

Let us adopt the point of view[12] decribed in Section II that in a high energy collision the valence quarks are forward scattered and give rise to fragmentation region products, while the gluons interact. If the kinematical conditions are right, several pairs of gluons could be excited. Suppose the gluon-gluon cross section is large in the kinematical region

$$s_{gg} = s_o$$

where we guess $s_o \approx 4$ GeV^2. Assume the average momentum carried by a gluon is $\bar{x} = 0.15$ (e.g., with a distribution $xG \sim (1-x)^5$) and for simplicity let all gluons have the average $\bar{x}$.

Then for protons of momentum p the total energy squared is $s = 4p^2$, and the gluon pair subenergy is

$$s_{gg} = (\bar{x}p + \bar{x}p)^2 = \bar{x}^2 s.$$

Presumably the strong gluon-gluon interaction will cause the total cross section to rise; for our guesses it should begin to show this effect at

$$s \simeq s_{gg}/\bar{x}^2 = 180 \text{ GeV}^2$$

or at $p_L \simeq 90$ GeV, a reasonable estimate of where the rise actually begins.

This estimate is very crude, but illustrates the basic idea: perhaps the rise in σ_T can be interpreted as due to gluon interactions. Of course, we cannot prove this, but we can show that if it were correct it would be very fruitful, and that it is consistent with several other aspects of hadron interactions.

We also cannot show that pairwise gluon interactions will dominate, although it is reasonable that they should be important. However, if gluons interact strongly, when one hadron emits a pair they will self-interact, perhaps effectively forming a massive object, giving a shorter range and less important effect. Consequently, our approximation might be a good one.

A better calculation would begin by writing

$$\sigma_T^G = \int dx_1\, dx_2\, G(x_1)\, G(x_2)\, \sigma_{gg}(S_{gg}) \qquad (1)$$

where σ_T^G is the part of σ_T due to pairwise gluon interactions, $s_{gg} = x_1 x_2 s$, $G(x_1)$ is the gluon distribution function giving the probability of finding a gluon with momentum fraction x_1 (and similarly for x_2) and σ_{gg} is the gluon-gluon cross section. If we can determine the shape of $G(x)$ from particle ratio data (see below) and its normalization from the momentum sum rule, this would already give a useful constraint on σ_{gg}.

In particular, the way in which σ_{gg} changes with s_{gg} will be reflected in the s dependence of σ_T. Any theory or solution of QCD can test its distribution function and cross section here. The presence of a threshold or resonances in gluon-gluon scattering, the size of σ_{gg}, and the high energy behavior of σ_{gg} will all have an effect. One could even imagine relatively local variations in the energy dependence of σ_T.

There are of course too many unknowns to determine anything uniquely at present. But knowledge from other observables reflects back on these same quantities (see below) and theoretical knowledge will increasingly constrain them too.

If $G(x)$ behaves (as expected) as $1/x$, and if σ_{gg} has a threshold behavior $s_{gg}^{1+\epsilon}$ with $\epsilon \geq 0$ (again, as expected), then for $\sigma_{gg} \to$ constant as $s_{gg} \to \infty$ the asymptotic rise of σ_T is like $\ell n^2 s$, while if σ_{gg} falls as a power of s_{gg} the asymptotic rise of σ_T is $\ell n s$. Thus the QCD behavior can be tested.

If the rise is due to gluon interactions it would have to be the same for meson-baryon and baryon-baryon interactions, while if it were due to flavor carrying constituents it should differ for different reactions since the appropriate distributions would have different powers. While this cannot yet be tested clearly becasue there is no unique way to separate the Reggeon contributions, at higher energies it will be a useful check.

What about details? To be specific, we can take a model for σ_{gg} and calculate with the above formula for σ_T^G. If we use a gluon distribution $xG(x) = 3(1-x)^5$, and a single s-wave resonance of mass = 2 GeV, Γ = 200 MeV, which saturates its unitarity limit, we indeed find (absolutely normalized) reasonable numbers, with $\sigma_T^G \simeq 10$ mb at $s = 1000$ GeV^2, and rising as $\ell n s$ above about 1000 GeV^2. This indicates that more sophisticated calculations would be consistent with actual data for the rise.

In this section we have speculated that the physical origin of the rise in σ_T is the onset of gluon-gluon interactions. Perhaps by adopting this viewpoint it will be possible to say why and in precisely what way σ_T rises, and to test QCD calculations as well.

B. Central Region Clusters

Van Hove and Pokorski have suggested[12] that inelastic, central region, hadrons arise from gluons. They review the experimental evidence and propose that the clusters, in terms of which the data are interpreted, originate as gluons.

Ochs has observed[13] that particle ratios are not unity even at small x, implying that the Van Hove-Pokorski suggestion

cannot be the whole story at present energies. Nevertheless, we consider it a useful hypothesis and one which we expect will become more correct at higher energies. If it is basically correct, studying the clusters may lead to information about gluon properties.

We envisage a mechanism along the following lines. Valence quarks undergoing scattering will emit hard gluons. These will undergo splitting into a number of softer gluons which will convert into hadrons when they reach some minimum momentum and a sufficiencly strong coupling. As the energy increases, the number of clusters (hard gluons) will rise as more gluons are emitted, and individual clusters only to reflect each gluon having a larger amount of momentum. It is possible, in principle, to calculate the number of clusters, the cluster multiplicity, and the cluster mass distribution (threshold behavior, peak, resonances, high mass fall off) in QCD. Further complications will occur due to scattering of hard gluons. Although the situation will be very complicated, it seems fair to be optimistic that the main qualitative features of QCD in this area will be testable by studying cluster properties.

C. Particle Ratios and the Gluon Distribution Function

When gluons turn into hadrons we expect complete independence of flavor quantum numbers. In practice there will be corrections due to mass breaking, both in phase space and in effective coupling.

Particle ratios such as π^-/π^+, K^-/K^+, $\bar{p}/p$ will not need mass corrections. These should be unity at any x where gluons dominate. As discussed above, Ochs has observed that except at small x these ratios are not unity at present energies. Thus our strongest prediction is that as energy increases, particle ratios (π^-/π^+, K^-/K^+, $\bar{p}/p$) should approach one in any region of x where gluons dominate. As mentioned in the discussion of σ_T, at ISR energies the gluon contribution $\leq 1/4$ of the total so it is reasonable that the particle ratios are not one. But by high ISABELLE energies there should be a rapid approach of the particle ratios to one in the region $0 \leq x \leq 1/3$.

Present data go in this direction at $p_\perp = 0.4$ (where the data[14] is most favorable to our interpretation). For $\sqrt{s} \geq 23$ GeV and $x \leq 0.1$ the π^+/π^- ratio is consistent with unity. For K^+/K^- the ratio decreases from about 4 at $x=0.35$ to be consistent with 1 at $x \simeq 0.1$. For $p/\bar{p}$ the ratio is not 1 at any observed s,x but it appears to extrapolate to 1 at $x = 0$ at $\sqrt{s} \geq 23$ GeV. The energy dependence[15] at $x = 0$ is consistent with our expectations also. For π^+/π^- at $\sqrt{s} = 6.84$ GeV one has $\pi^+/\pi^- \simeq 1.5$, while for $\sqrt{s} \geq 19.6$ GeV $\pi^+/\pi^- = 1$. At $\sqrt{s} = 23$ GeV $K^+/K^- \simeq 1.3$, while for $\sqrt{s} = 63$ GeV, $K^+/K^- \approx 1$. For $p/\bar{p}$ even at $\sqrt{s} = 63$ GeV the ratio is 1.6.

If this approach to unity is observed to happen there is a considerable bonus, namely it automatically provides information about the shape of the gluon distribution function. Normally the gluon distribution function is not directly measureable since it cannot be probed with lepton or photon beams. It is deduced from the energy-momentum sum rule by assuming that whatever momentum is not carried by quarks at a given x is carried by gluons. The sum rule provides only one moment however, and there is considerable freedom in how the momentum is distributed between sea, valence quarks and gluons for $x \sim 1/3$.

Suppose the particle ratios at high energies go to unity in a certain x region, and then deviate increasingly from unity as x increases. For $x \geq 0.15$ we know from lepton-production that the $q\bar{q}$ sea is negligible, and we know approximately the valence quark distribution. Should the particle ratios go to unity in the region $x \geq 0.15$, we will know that the gluon distribution dominates the valence quarks, and where the particle ratios rise from unity, the gluon and valence quark distributions are comparable. Depending on the form the particle ratio data takes, it may be possible to determine several parameters in a functional form chosen for the gluon distribution. In particular, it should be possible to find out if the gluon distribution extends to larger x than is commonly thought (e.g., to $x \geq 0.5$).

D. Multiplicity at High Energies

One of the main implications of the importance of gluon splitting is that a hard gluon has a high probability of cascading into a number of soft gluons. These, being confined, will have to convert into hadrons. A large part of the energy of a hard gluon will end up in hadron masses, so the multiplicity of hadrons will be large.

If a non-vanishing fraction of the gluon energy always ends up in masses, then the multiplicity will grow as a power of the energy rather than as $\ell n E$. Possibly this is the physics underlying the increasingly rapid growth[16] of multiplicity at cosmic ray energies.

We can try to estimate how the multiplicity should grow at energies where gluons provide a significant part of the cross section.

Let us accept the premise that once a gluon is formed, it will continue to split in such a way that a finite fraction of the original energy goes into making mass for the daughters. (This fraction would have been unity, had there been no hadronization.)

Let r be the average number of daughters into which each parent can split, and let ε be the ratio of each daughter's mass to her parent's. From energy conservation

$$\varepsilon \leq \frac{1}{r} .$$

Let $\sqrt{s}$ be the mass of a cluster, then after successive splittings, each daughter has

$$m_o \equiv \sqrt{s}$$

$$m_1 = \varepsilon\, m_o,$$

$$m_2 = \varepsilon\, m_1,$$

$$\vdots$$

$$m_i = \varepsilon\, m_{i-1}, \text{ etc.}$$

This splitting terminates after n steps in m_n commeasures a hadronic mass, say m_π, i.e.,

$$m_n = \epsilon^n \sqrt{s} \cong m_\pi$$

or

$$n = \ell n(\sqrt{s}/m_\pi) \; / \; \ell n(1/\epsilon) \qquad (2)$$

Presumably after the n^{th} step there are only pions left, so the multiplicity is

$$n_\pi \cong c(r)^n \cong c(r)^{\ell n(\sqrt{s}/m_\pi)/\ell n(1/\epsilon)} = c(\sqrt{s}/m_\pi)^{\ell n r/\ell n\, 1/\epsilon} \qquad (3)$$

which shows that the multiplicity has power dependence on the cluster energy $\sqrt{s}$. Reasonable guesses might be c=1, r=2, ϵ=1/4, $\sqrt{s}$=2 GeV. These give p_π^{max}=0.9 GeV, $\langle n_\pi \rangle$=3.78, and a multiplicity growth of $s^{1/4}$. The main point is that eventually these quantities can be obtained as QCD prediction.

The main difference from models which give a power of ℓns for the multiplicity growth comes from the basic property of what fraction of the initial mass goes into particle masses. If the ratio of the daughter masses m_K to the original mass $m_o = \sqrt{s}$ stays non zero as $m_o \to \infty$, then the multiplicity grows as a power. If $m_K/m_o \to 0$ as $m_o \to \infty$, then the multiplicity grows as a power of ℓns.

E. Inclusive Polarization

Heller[17] has suggested the model shown in Fig. 1 as a way to generate large inclusive polarization. All conventional models predicted quite small polarizations, while what is observed[18] is large, of order 25%, for the Λ polarization perpendicular to the Λp plane. If such a mechanism can be shown to dominate in certain kinematical regions it would give useful checks on the gluon spin, the effective quark-gluon coupling, and effective quark and gluon masses in interactions.

The spin of the Λ will be the spin of the s-quark in a constituent quark approximation, since the (ud) pair are an isosinglet and a spin singlet. We have calculated the expected polarization using just the darker lines of Fig. 1 to see if we can find some criteria to test whether this

mechanism is reasonable.

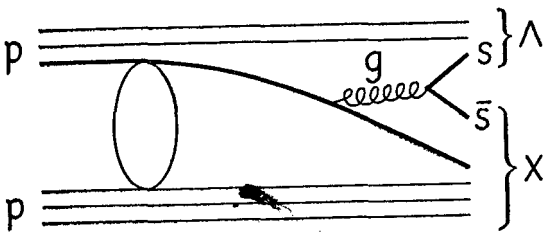

Figure 1

We find that polarization is indeed generated, and the effect could be large. How large depends on making a model for the unknown initial quark-quark scattering, which must give a complex, spin-dependent scattering. The only clear prediction we can make is that the result must have as a factor the mass of the polarized quark since for zero mass quarks their spin is in the direction of motion and cannot give polarization perpendicular to the scattering plane. This allows the prediction that the polarization in inclusive mucleon production and the Λ production are in the ratio of the nonstrange and strange constituent quark masses, $m_u/m_s \simeq 0.62$. Heller gives a correction factor of 17/19 for neutron and 2/3 for proton, due to the extent to which one quark carries the spin of the hadron in an SU(6) wave function. Combining these, we predict that

$$\frac{P(pp\to px)}{P(pp\to\Lambda x)} \approx 0.42$$

$$\frac{P(pp\to nx)}{P(pp\to\Lambda x)} \approx 0.55$$

(which is consistent with recent preliminary data from FNAL).

IV. CONCLUSIONS

We have argued for the point of view that much may be learned about gluon interactions from hadron data. While this is admittedly optimistic, some of the arguments are

strong enough to take seriously, and the increased knowledge available if our approach were correct seems more than sufficient to justify careful consideration of the ideas.

We have suggested that the physical origin of the rise of σ_T is gluon interactions, and that detailed properties of the rise can be related to basic aspects of QCD. Similar results hold for central region clusters. We believe that QCD predicts that particle multiplicities grow as a power of s at large s rather than as $\ln s$; this may explain effects in cosmic ray data. We predict an important feature of particle ratios at higher energies will be a rapid approach to unity over the region in x where the gluon distribution function dominates; if this is observed it may allow the experimental determination of the gluon distribution function. Since gluons do not interact directly with leptons or photons this may be the most direct way to measure the distribution function.

We also suggest that gluon jets will not be hard like quark jets, but will convert most of their energy into hadron masses, giving high multiplicity, flavor-neutral, slowly moving groups of hadrons.

Even if not all of our speculations are borne out, we hope that the possibility of additional experimental tests of QCD is sufficient justification for pursuing these questions.

REFERENCES

1. Shau-Jin Chang and York-Peng Yao, Michigan preprint UM HE 76-46; See also Shau-Jin Chang, York-Peng Yao, and Inga Karliner, Fermilab-Pub-77/50-THY.
2. T. Appelquist and D. Politzer, Phys. Rev. Lett. 34, 43 (1974); H. Fritzsch and P. Minkowski, Nuovo Cimento 30A, 393 (1975).
3. J. Ellis, M.K. Gaillard, and G.G. Ross, Nuc. Phys. B111, 253 (1976); E.G. Floratos, CERN preprint TH2261, Dec. 1976. H. Fritzsch and P. Minowski, CERN preprint.
4. R. Cutler and D. Sivers, ANL-HEP-PR-77-40; A.J. Buras and K.J.F. Gaemers, CERN TH2322, May 1977.
5. P.G.O. Freund and Y. Nambu, Phys. Rev. Lett. 34, 1645 (1975).
6. H. Fritzch and P. Minkowski, Nuovo Cimento 30A, 393 (1975).
7. R. Jaffe and K. Johnson, Phys. Lett. B60, 201 (1976).
8. R.L. Jaffe and J. Kiskis, Phys. Rev. D13, 1355 (1976).
9. W. Bardeen and R. Pearson, to be published.
10. J. Williamson, Phys. Rev. D13, 1327 (1976).
11. D. Robson, Nuc. Phys. B118, 212 (1977).
12. S. Pokorski and L. Van Hove, Acta. Phys. Pol. B5, 229 (1974); L. Van Hove and S. Polorski, Nucl. Phys. B86, 243 (1975); L. Van Hove, Acta, Phys. Pol. B7, 339 (1976).
13. W. Ochs, Nucl. Phys. B118, 397 (1977).
14. E. Albini et al., Summary of the Results of the Experiment on Charged Particle Production at Medium Angles Performed at the CERN ISR (R202), NP Internal Report 75-2.
15. K. Guettler et al., Nucl. Phys. B116, 77 (1976).
16. See, for example, the review by T.K. Gaisser, "Interactions of Cosmic Ray Hadrons from 10^4 to 10^6 GeV", Invited talk at the Conference on Prospects of Strong Interactions at ISABELLE, March 31-April 1, 1977. Gaisser remarks that one possibility for interpreting Extensive Air Shower data (although not a preferred one) is "transfer of much of the energy to production of many relatively slow particles".
17. K. Heller, "A Quark-Gluon Mechanism for Inclusive Polarization," Michigan preprint UM HE 77-38.
18. G. Bunce et al., Phys. Rev. Lett. 36, 1113 (1976).

GLUE BALLS, QUARKS, AND THE POMERON-f

Jan W. DASH
Centre de Physique Théorique, CNRS
31, Chemin Joseph Aiguier
F-13274 MARSEILLE CEDEX 2, FRANCE

ABSTRACT

I present three issues related to s-channel unitarity which argue in favor of the P-f identity model of diffraction of Chew, Rosenzweig, and Chan, and which argue against the traditional P+f model. These are (1) The violation of two component duality in modern P+f fits, (2) Threshold effects due to strangeness, charm, and baryon production (flavoring), and (3) Quark-loop renormalization of the QCD glueball, consistent with observed hadron multiplicities and dominant short range order. I also review P-f identity phenomenology.

Je vous présente des considérations ayant pour origine l'unitarité dans la voie s , qui favorisent le modèle de diffraction incorporant l'identité P-f et qui posent des problèmes aigus pour le modèle à deux composantes P+f. Seront traités (1) la dualité à deux composantes, (2) les problèmes liés aux seuils pour la production de parfums (flavoring), et (3) l'unitarisation de la glueball de QCD, d'une façon compatible avec les multiplicités de hadrons observées et avec l'ordre à courte portée. Je rappelle aussi la phénoménologie basée sur l'identité P-f.

I. INTRODUCTION

It has become habitual to associate the concept of diffraction with the two component Pomeron (P) + f model. The Harari-Freund [1] notion of two-component duality and the theoretical possibility of quarkless excitations (QCD glueball, dual closed string) is often cited as evidence for the separate existence of a Pomeron and f. The Pomeron, dual to the background, is supposed to be the glueball or closed string. The f, dual to resonances, is supposed to be nearly exchange degenerate, ideally mixed, and planar. More recently a different idea has developed, due to Chew, Rosenzweig [2], Chan [3], and others, called the "Pomeron-f identity". Here there is only one high-lying trajectory- the P-f. The P-f trajectory goes through the f-meson and is curved in t in a manner which involves the transition to a nearly planar amplitude at timelike t from a dominantly cylindrical amplitude at $t = 0$. These two schemes clearly differ in concept, and my purpose here will be to contrast them on a phenomenological level. The crucial aspect will be s-channel unitarity.

I will focus on three points which argue strongly in favor of the P-f identity and against the traditional P+f model [4].

(1). Two component duality, in contrast to the situation in 1969, is badly violated. Typically the f pole amplitude from P+f modern fits is dual to the resonances plus one-half the background.

(2). The P-f identity is quite successful in describing data. It not only has passed all important phenomenological tests (including several specific challenges directed against it), but it works better than the P+f model in one very important respect. The point can only be seen if one tries to build up the diffractive amplitude using s-channel unitarity. Called "flavoring" [5], the effect is due to the successive excitation of particles with different quantum numbers (flavors - strangeness, charm; and baryon number) in inelastic states. Within a dominant short range order picture, as exists at current energies, these threshold effects must "renormalize the Pomeron". This means that the bare Pomeron scaling law changes from $s^{\hat{\alpha}(t)}$ to $s^{\alpha(t)}$ with $\alpha > \hat{\alpha}$ in a well-defined way, both mathematically and phenomenologically.

Flavoring renormalization is analogous to the change in the scaling law on either side of a threshold for exciting a new quantum number in $e^+e^- \to$ hadrons. The details are different, but the effects are just as dramatic.

Actually, the "correct" theory of diffraction, built up as it is by unitarity, must be consistent with the observed multiplicities $\langle n_i \rangle$ ($i = K\bar{K}$, $B\bar{B}$, ...) of individual species of hadrons. That is, flavoring is not so much

a complication as a constraint on any model of diffraction that claims to be right.

The reason that I have so strongly emphasized this point here is that the P-f identity is in fact consistent with this important aspect of unitarity and short range order. Flavoring is a necessary ingredient in a successful P-f phenomenology [5]. In contrast, the traditional P+f model most probably fails this test.

(3). The last point involves the common idea of the association of a glueball at $\alpha^{*} = 1$ with the Pomeron separate from the f . I will argue that, on the contrary, the existence of an $\alpha^{*} = 1$ glueball in quarkless QCD does not imply the standard P+f scheme. Indeed, I shall argue that once quark-loop unitarization of such an object is included, the P-f identity is favored over the P+f model. The t-channel content of the Pomeron-f is made of $q\bar{q}$. Any possible t-channel glue content of the output Pomeron will be shown to be negligible.

II . THE FAILURE OF TWO COMPONENT DUALITY

The reason why the situation now is different from what it used to be is the discovery that total cross sections rise. Roughly, rising σ means that the P part σ_P rises, i.e. σ_P decreases as we go to lower energies. But then the f part $\sigma_f = \sigma - \sigma_P$ is bigger at lower energies that it would be if σ_P were constant. The bigger σ_f now tends to be too high to average the resonances.

In Fig. 1 I exhibit the experimental $I_t = 0$ πN amplitude $\mathrm{ImA'}^{+}(\nu, 0)$ corresponding to the resonances, and also to the resonances plus one-half the background. Here $\mathrm{ImA'}^{+}(\nu, 0) = \frac{1}{2}(\nu^2 - m_\pi^2)^{1/2}(\sigma_{\pi^+p} + \sigma_{\pi^-p})$ where $\nu = E_{lab}$. Also plotted are the $t = 0$ absorptive f pole amplitudes taken from several "conventional" P+f published fits [6] performed after 1974. By a "conventional" fit I mean that the P is basically a pole plus small cuts at $t = 0$, consistent with dominant short range order. Although the authors of these fits differ in their philosophy toward exchange degeneracy, the results are quite uniform. It is clear that, instead of averaging the resonances, the f actually averages the resonances plus one-half of the background, in contradiction to the idea of two component duality.

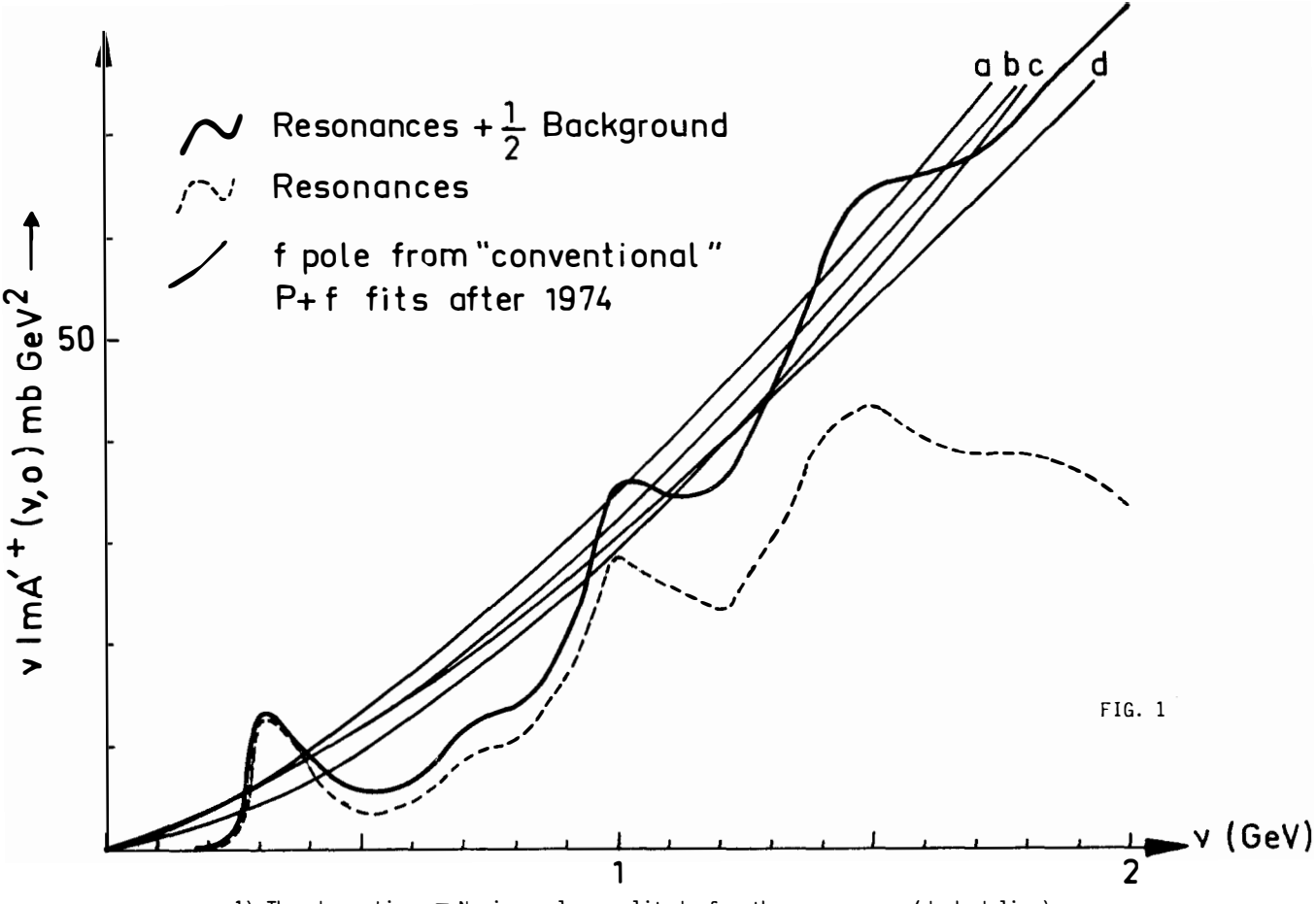

FIG. 1

1) The absorptive πN isoscalar amplitude for the resonances (dashed line), the resonances plus one-half the background (solid line), and the absorptive f-pole amplitudes from four recent conventional P+f fits. See ref.(6).

The failure of the P+f model to satisfy its own "postulate" is not shared by the P-f identity. A model dependent test of two-component duality within the P-f identity of the form Im T (planar) $\cong \langle$Im (resonances)$\rangle$, Im T (cylinder) $\cong \langle$Im (background)$\rangle$ has been performed. The reader is referred to Ref. (4) for a description of this as well as more details for the P+f case.

III. THE P-f IDENTITY

The P-f identity is based on a specific realization of Veneziano's topological expansion [7]. To the planar + cylinder level, the $I_t = 0$, $C = +$ amplitude T can be written as $T = T^{Pl} + T^{Cyl}$ as in the P+f model. In contrast, however, the partial wave amplitude T_j only has one high lying pole instead of two. (This statement will be refined in a moment when we discuss flavoring). The planar f, a pole in T_j^{Pl} at $j = \alpha_{Pl} \cong \frac{1}{2}$, is shifted upward by the cylinder amplitude according to the partial wave equation

$$T_j = T_j^{Pl} + T_j^{Pl}\, g\, C_j\, T_j \qquad (1)$$

The cylinder kernel C_j is taken as a nonsingular function of j near $j = 1$. This is quite sensible. In Regge models [3], the leading C_j singularity is a Regge-Regge cut at $j \lesssim 0$, as shown below :

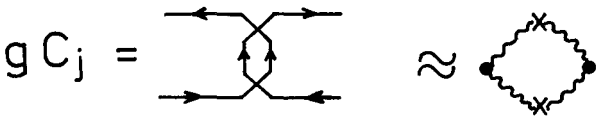

THE NONSINGULAR CYLINDER KERNEL C_j OF EQ. 1

Upon iterating eq.(1), the C_j kernel changes the direction of circulation of the quark loops between neighboring planar amplitudes. That is, the cylinder kernel produces transitions between the "back" and "front" of the cylinder on which quark loops circulate in opposite directions. Note that every t-channel cut (vertical line) on the cylinder cuts through quarks. Pictorially T_j is given by the iteration

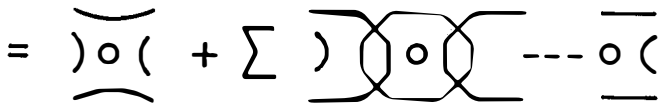

THE PARTIAL WAVE AMPLITUDE T_j OF THE P-f IDENTITY

The solution of eq.(1) is elementary,

$$T_j = T_j^{Pl}(1 - g\, C_j\, T_j^{Pl})^{-1} \qquad (2)$$

The fact that C_j is nonsingular near $j = 1$ means that there is only one high lying pole, the P-f. This is the P-f identity [2].

IV . FLAVORING

I next discuss flavoring, which as mentioned earlier, plays a most important role in distinguishing the P-f identity from the conventional P+f model. Here I can only mention the highlights ; the reader is referred to ref. 5 for a complete review.

The basic idea follows the old observation that the rise in σ seems correlated with the rise of $B\bar{B}$ production, which is an obvious threshold-like effect. This same sort of behavior is also observed for $K\bar{K}$ production, though at somewhat lower energies (the effective threshold is around $s = 30\ GeV^2$). Charm and possible other new flavors clearly will also exhibit such behavior at large s , though at present energies these effects are negligible. The experimental fact that the multiplicities $\langle n_i \rangle (i = K\bar{K}\ ,\ B\bar{B}\ ,\ldots)$ exhibit strong threshold-like behavior produces the flavoring effect on diffraction through s-channel unitarity.

In general unitarity constraints are very difficult to implement. Here we are fortunate. The existence of dominant short range order at present energies allows us to conclude that the dominant production amplitudes are multiperipheral, probably in clusters. Now any multiperipheral model with its kinematics properly treated contains t_{min} effects for production of $K\bar{K}$, $B\bar{B}$, ...

pairs. Independent of details, one always obtains partial wave amplitudes of the following (strong-coupling) form [5] :

$$T_j = \beta_j \left[j - \hat{\alpha} - g_K^2 e^{-b_K j} - g_B^2 e^{-b_B j} - \ldots \right]^{-1} \qquad (3)$$

The decaying $\exp(-bj)$ exponentials are just the kind that arise from the Froissart-Gribov formula due to thresholds in s-channel discontinuities at $\ln s = b$. These terms do two things. They produce smooth threshold modifications of cross section behavior (which, contrary to lore need not be oscillatory). They also renormalize the Pomeron (j-plane description). Denote

$\hat{\alpha}$ = unflavored pomeron $\hat{P}$ intercept. [$\hat{P}$ = pole in $\hat{T}_j$ where $\hat{T}_j = T_j(g_K = g_B = 0)$.]

α = flavored Pomeron P intercept (P = leading pole in T_j)

The unflavored $\hat{P}$ is built up from pion production alone. It is a pole in the "unflavored" partial wave amplitude $\hat{T}_j$. It is an auxiliary, though extremely useful object. The flavored Pomeron P is the leading pole in the full partial wave amplitude T_j. It is the bare Pomeron of the Reggeon Field Theory. The reader should note carefully that there are no "energy dependent trajectories". $\hat{\alpha}$ and α are numbers (or at $t \neq 0$ functions of t). Further the flavored intercept α is calculated from knowing the unflavored intercept $\hat{\alpha}$ and the threshold parameters which are fixed by data.

Now by (a) expanding T_j in a series in g_K, g_B ; or (b) by picking up the poles of T_j in the Sommerfeld-Watson transform, one is lead to two completely equivalent descriptions of σ.

$$\sigma = \begin{cases} \text{either} & \hat{\beta}\, s^{\hat{\alpha}-1} + \sum_{i=K,B,\ldots} g_i^2 f_I(s)\, \theta(\ln s - b_i) + \ldots \\ \text{or} & \beta\, s^{\alpha-1} + \sum_{i=1}^{\infty} \text{(complex pole terms)} \end{cases} \qquad (4)$$

Note that at low s, σ is given simply by the unflavored $\hat{P}$ scaling law $s^{\hat{\alpha}-1}$. At high s, σ is given simply by the flavored P scaling law $s^{\alpha-1}$. This is the flavoring renormalization of the (bare) Pomeron. This is shown pictorially below for the simple case of one $X\bar{X}$ flavoring threshold :

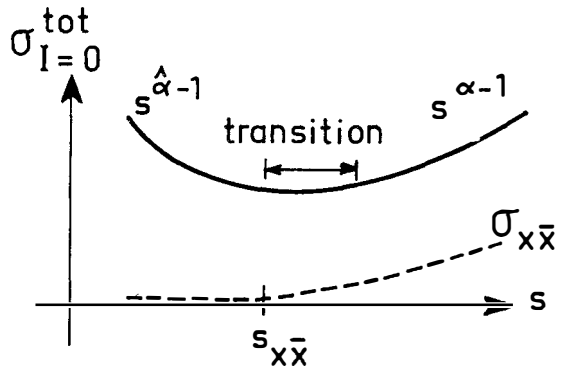

FLAVORING RENORMALIZATION EFFECT ON σ BY $X\bar{X}$ PRODUCTION

Here $s_{X\bar{X}}$ is around BNL (FNAL) energies for $K\bar{K}$ ($B\bar{B}$) production, and is determined by the experimental point at which $X\bar{X}$ production "takes off".

I stress again that the flavoring renormalization of the Pomeron is not model dependent. It occurs because (1) threshold-like behavior of $K\bar{K}$, $B\bar{B}$,... production exists, and (2) dominant short range order in rapidity exists.

The existence of flavoring in hadron scattering is rather like the now-familiar idea that the famous ratio R in e^+e^- annihilation approximately obeys one scaling law (ΣQ_i^2) below the threshold for exciting a new flavor and a different scaling law ($\Sigma' Q_i^2$) above that threshold, with a complicated transition region in between (e.g. the Ψ family at the charm threshold). Of course there are dynamical differences. In hadron physics the excitation thresholds are kinematically delayed. Moreover baryon number counts as a "flavor" because no $q^2 \to \infty$ argument is around to break up the qqq system. Pictorially $e^+e^- \to h$ flavoring due to a new $X\bar{X}$ flavor excitation looks like this :

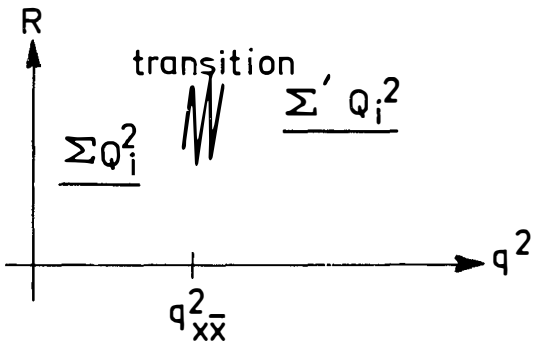

EFFECT ON $R(e^+e^- \longrightarrow h)$ DUE TO A NEW FLAVOR

The scaling law change from $\sum Q_i^2$ to $\sum' Q_i^2$ in R is analogous to the flavoring renormalization of the bare Pomeron scaling law from $s^{\hat{\alpha}}$ to s^{α} in hadron-hadron scattering.

Numerically, flavoring in hadron-hadron scattering is a very important effect. A detailed analysis yields [5]

$$\alpha - \hat{\alpha} \approx 0.2 \tag{5}$$

As we shall see in the next section this has quite important consequences.

V. P-f IDENTITY PHENOMENOLOGY

Here I shall list important phenomenological results within the P-f identity framework, concentrating only on $t \leq 0$ physics.

A. THE DUAL UNITARIZATION PROGRAM OF CHAN

The comprehensive dual unitarization program of Hong-Mo Chan and collaborators [3] has all been carried out within the context of the P-f identity. This was not, however, recognized at the outset.

B. TWO-BODY PHENOMENOLOGY

(1). The first major work incorporating the P-f identity was ref. 8 which contains one of the two existing global fits to all $0^- \frac{1}{2}^+ \to 0^- \frac{1}{2}^+$ data at and below BNL energies. This was done with what is now recognized to be the unflavored bare Pomeron $\hat{P}$, and the unflavored $\hat{P}$ intercept $\hat{\alpha}$ was taken at $\hat{\alpha} = 0.85$. The existence of a separate ideally mixed "f" was allowed for in the fit, but its intercept was consistent only with a value of around zero. The $\hat{P}$ intercept below one solves the enigmatic "phase problem" of absorption models, known to two-body phenomenologists, in an elegant way. Standard P+f treatments suffer from the problem that Regge-Regge cuts should vanish in an exchange-degenerate world, which gives incorrect phases if the P is a pole around 1 plus small cuts.

(2). Rising cross sections above BNL energies are quite consistent with the P-f identity and the above global fit. As mentioned several times, flavoring plays the key role. The flavored P has the calculated intercept $\alpha = 1.08$. Using the same flavoring in πN, KN, and NN scattering produces the correct shapes of all these cross sections through FNAL-ISR energies [5].

(3). Specific challenges to the P-f identity have all ignored the crucial aspect of flavoring. These include [6a] the observed increasing behavior of $2\sigma_{KN} - \sigma_{\pi N}$ and the ratio of forward real to imaginary amplitudes[9]. These data are well described within the P-f identity, as shown in ref. 5.

(4). Inelastic two body reactions have not been systematically analyzed, other than the $0^- \frac{1}{2}^+ \rightarrow 0^- \frac{1}{2}^+$ case. The assertion [10a] that K^* production poses a serious problem for the P-f identity has been reanalyzed by Tan, Tow, and Tran Than Van [10b] and shown to be false. However a complete analysis of vector meson production as well as reactions like $np \rightarrow pn$ where diffraction enters through absorption still needs to be performed.

C. MULTIPARTICLE PHENOMENOLOGY

(1). Mueller analysis is different in the P-f identity because at subenergies s_i which are below flavoring thresholds it is the unflavored $\hat{P}$ which controls the leading s_i dependence as $s_i^{\hat{\alpha}}$. In addition the $\hat{P} \times \hat{P}$ cut and unflavored $j \approx 0$ singularities can be present, as in the global fit [8]. Triple-Regge $pp \rightarrow pX$ and $\pi p \rightarrow Xp$ phenomenology using triple $\hat{P}\hat{P}\hat{P}$ and $\pi\pi\hat{P}$ terms was performed in ref. 11, where the $\hat{P}$ was first introduced. The existing data were indeed consistent with this description. However newer data exist that should be analyzed, with appropriate attention to flavoring renormalization in subenergies.

(2). The rising rapidity plateau has been analyzed by Jones [12], who concludes that flavoring may be a key issue here too. Flavoring can introduce new Mueller couplings which can make the rise of $d\sigma/dy$ occur at the same s as σ, instead of later. Further work along this line would be welcome.

(3). All flavoring phenomenology has been performed using the $pp \rightarrow K\bar{K}X$, $p\bar{p}X$ tabulation [13], assuming that the flavoring renormalization is universal for ap scattering ($a = p, \pi, K$) as it should be in a short range

order framework. This should be checked explicitly by tabulating $\pi p \to K\bar{K}X$, etc. data.

The overall conclusion is that the P-f identity, while not exhaustively tested, has passed all major phenomenological tests as well as a number of minor tests. The P-f identity moreover has the advantage of being consistent with flavoring.

On the other hand, the large flavoring effect is clearly inconsistent with the traditional P+f picture, at least within the conventional framework. For example, the flavoring renormalization of 0.2 required by the data for $K\bar{K}$ and $B\bar{B}$ production would renormalize an unflavored Pomeron $\hat{P}$ at one to a flavored P with intercept 1.2, which is much too high to fit total cross sections. Conversely, the complex poles in the flavoring-renormalized spectrum of T_j (eq.(3)) cannot approximate the f of the P+f model. This is because (1) the complex poles are complex, and anyway nowhere near $\frac{1}{2}$, and (2) they contain substantial strange $s\bar{s}$ and diquark $qq\,\bar{q}\bar{q}$ components, whereas the standard f is ideally mixed ; i.e. it supposedly contains only $u\bar{u}$ and $d\bar{d}$ components.

VI . WHY THE POSSIBLE EXISTENCE OF A GLUEBALL WITH INTERCEPT ONE DOES NOT IMPLY THE P+f MODEL

The major theoretical motivation for the P+f picture has been taken from the possibility of new quarkless effects ; a glueball in quarkless QCD [14, 15] or a closed string in dual models, which could produce a pole with intercept one. It is important first of all to remind the reader that this possibility suggestive as it may be, is unproven [14]. However, what I wish to point out is, even given the existence of such an object, the demonstration of the standard P+f picture is by no means guaranteed. The glueball concept, formulated as it is in a world without quarks, violates unitarity. The imposition of unitarity by adding quarks loops can substantially modify what one might naïvely believe to be the case. Specifically, I will show that

(1). The P-f identity is in fact consistent with the existence of a glueball in quarkless QCD, even with intercept one ;

(2). The P-f identity is not only a consistent result but the

preferred result over a possible P+f result. This will follow only from internal consistency, short range order and the total particle multiplicity $\langle n \rangle$ which increases roughly like $a \ln s$, where a is a big number ($a \gtrsim 3$). The P+f model results generally imply [16] particle multiplicities $\langle n \rangle$ which increase like $\epsilon \ln s$, where ϵ is a small number (e.g. $\epsilon \approx 1/6$).

I begin by considering the standard picture for the QCD glueball Pomeron, first introduced by Low and Nussinov [15]. There are no quarks at this stage, other than the external quarks. (Technically, the number of colors N_c has been taken to infinity) :

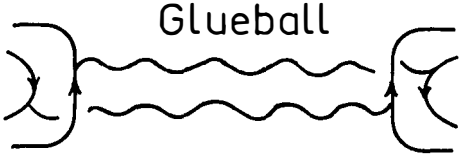

THE f-DOMINATED GLUEBALL POMERON IN QUARKLESS QCD

The two external quark loops fit on a cylinder topologically since they circulate in opposite directions. They produce a double planar f pole (f-dominated residues), and they exchange colored gluons to produce the glueball. The two gluons in the above drawing are only suggestive. Actually we expect the full content of quarkless QCD to enter and, in an as yet unknown way, perhaps lead to the j-plane result

$$C_j^{glue} = \frac{\beta_j^*}{j - \alpha^*} \qquad (6)$$

with $\alpha^* = 1$ or at least something close to one. The t-channel discontinuity away from the external quarks cuts through only glue.

Now the s-channel discontinuity of this amplitude is obtained by considering the two gluons in the figure as the s-channel discontinuity line. Clearly only two $q\bar{q}$ pairs are present, and in fact each has a "mass" on the order of $s^{1/2}$. This unphysical result is because the dynamics has not yet been regarded as including quark loops, which produce $q\bar{q}$ pairs in the s-channel unitarity sum. However, even at this stage, one sees a hint of what is to come. Any explicit glueball (associated with a t-channel discontinuity that does not cut through quarks) will produce a large rapidity gap and lead to a lack of $q\bar{q}$ pairs. This will ultimately produce problems with hadron multiplicities for the P+f model, though not for the P-f identity.

When quark loops are added, the cylinder topology will still dominate. This is because higher order topologies generate j-plane cuts, which are small effects. Because of short range order, there is a multiperipheral structure on the cylinder. Moving along the cylinder, a planar amplitude with quark loops circulating in one direction on the "back" of the cylinder undergoes a transition by means of a "cylinder kernel" to another planar amplitude with quark loops circulating in the other direction on the "front" of the cylinder (and conversely). Iterations of planar-cylinder-planar ... transitions along the cylinder generate the multiperipheral structure, consistent with a j-plane pole output. (Technically, nonsense zeros kill the cuts). So far I have done nothing unconventional, and in fact I am merely following Veneziano's suggestion that each of the original high "mass" $q\bar{q}$ pairs "decays" into a planar jet [17]. To go further I have to specify the "cylinder kernel".

Suppose that the cylinder kernel is chosen as C_j, the nonsingular function of eq. (1). Then the multiperipheral equation for the cylinder, with the planar amplitude added, is exactly eq.(1). Every t-channel cut goes through quarks. Since eq.(1) is the equation that generates the P-f identity, I have shown my first claim. THE POMERON-f IDENTITY IS CONSISTENT WITH THE EXISTENCE OF A GLUEBALL IN QUARKLESS QCD. What has happened is that the unitarization of this glueball has been chosen in such a way as to produce the P-f identity. Specifically, the unitarization of the cylinder turns the double planar f pole due to the f-dominated residues of the original glueball Pomeron into a planar f pole with a negative residue, which cancels the planar f in T_j^{Pl}. Technically, one should take note of the fact that it is the physical s-channel discontinuity which builds up the physical j-plane amplitude through the Froissart-Gribov formula. Because the non-unitarized and unitarized cylinder discontinuities are different (containing two $q\bar{q}$ pairs and many $q\bar{q}$ pairs, respectively), the non-unitarized glueball partial wave amplitude is different from the physical partial wave amplitude T_j. Thus there are important details which must depend on the quark loop dynamics, like the above negative residue planar pole in the cylinder. Another example is flavoring, which I have argued must occur and is clearly a quark-mass dependent effect. Those who would like to use color confinement to argue that the leading cylinder j-plane pole intercept shouldn't change much under unitarization have a built-in argument for saying that the P-f intercept should be around one. I do not believe that argument is a-priori reasonable, simply from the above observation regarding the Froissart-Gribov formula. Therefore I must rely on counting arguments like those of H. Lee and Veneziano or the more sophisticated computer calculations of Chan et al. [3] to say that the output P-f intercept should be around one,

the details being fixed by the necessity of being consistent with both low energy BNL data [8] and with flavoring [5] as described in the previous section on P-f phenomenology.

So far I have shown that one can have the QCD glueball in one limit, the nonunitarized quarkless limit, and the P-f identity in the real world once quarks are added. I will now argue that this is in fact the most reasonable solution. While it is formally possible to construct solutions that look rather like the P+f model, I will show that something always goes wrong - particle multiplicities are too small, the f does not have the properties that would be expected in the P+f model, short range order is violated, or double counting errors are committed.

To construct a solution that looks like the P+f model is at first glance easy. Instead of choosing the cylinder kernel as the nonsingular C_j kernel which generates the P-f identity, one chooses to have the possibility that some transitions between planar amplitudes on the cylinder take place through the intermediary of glueball transitions across the appropriate subenergies, leading to t-channel cuts through glue. To avoid confusion in terminology, I will call these transitions subglueball transitions. By consistency, the partial wave projection of each subglueball transition is just C_j^{glue} with its pole at $j = \alpha^x$. The relevant partial wave equation is now

$$T_j = T_j^{Pl} + T_j^{Pl}(g\, C_j + g_{glue}\, C_j^{glue})\, T_j \qquad (7)$$

Upon iteration T_j now looks like this :

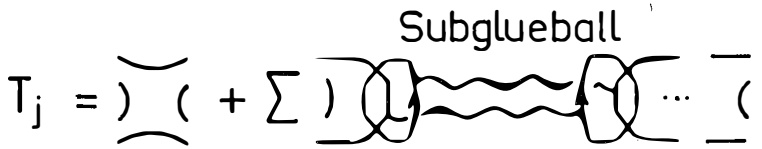

THE AMPLITUDE T_j OF THE SINGULAR EQUATION (7)

It is trivial to see that T_j indeed has two high lying poles. The glueball has been iterated through subglueball transitions interspersed between nonsingular C_j transitions, and the result is just a splitting of the two input glueball and planar poles to form two output poles that one may be tempted to call the P and f. This possibility, raised by a number

of authors, is formally similar to the old Schizophrenic Pomeron model of Chew and Snider [18]. We now point out the problems associated with this point of view.

P+f PROBLEM ONE : THE HADRON MULTIPLICITY IS TOO SMALL IF $\alpha^* = 1$.

Suppose that the glueball - and subglueball - intercept α^* is one (or around one). The problem, as hinted at before, is that each subglueball transition requires a lot of phase space. Given the total cross section $\sigma \approx \beta s^{\alpha-1}$, it is easy to see that the average number of subglueball transitions $\langle n_{sgb} \rangle$ satisfies

$$\langle n_{sgb} \rangle \approx (\alpha - \alpha^*) \ln s < 1/10 \ln s \qquad (8)$$

where I have used the experimental information that $\alpha < 1.1$. Thus at present energies, internal consistency and the total cross section requires there to be mostly only one (!) subglueball, which generates a large rapidity gap across the entire kinematic region. Thus, little phase space is available to produce $q\bar{q}$ pairs on either side of the subglueball transition. This means that the hadron multiplicity $\langle n \rangle$ is much too small, i.e. $\langle n \rangle \approx \epsilon \ln s$ where $\epsilon << 3$, the experimental value.

There are at least three examples of this of which I am aware. The first is the Schizophrenic Pomeron model [18], where the subglueball formally is a logarithmic cut near $j = 1$. Many calculations were done, typically producing $\langle n \rangle / \ln s \approx \frac{1}{2}$ [18,19]. A second example is the QED - based model of Cheng, Wu, and Walker [20]. Here the glueball is composed of two photons. Hence $\alpha^* = 1$, there are two hadrons between each subglueball, $\alpha = 1.08$, and so $\langle n \rangle / \ln s \approx 1/6$. A third example [16] is the phenomenology done by Pinsky and Snider [21], who fit σ using eq.(7) with $g = 0$. If we take one particle between subglueball transitions, then $\langle n \rangle / \ln s \approx 1/7$. In this last example the subglueball intercept was well below one ($\alpha^* = 0.85$), but even so the particle multiplicity is too small. Finally, Nussinov's "dressing-up of the Pomeron" [15] is also given by eq.(7), but as he did not bother to calculate multiplicities, he did not see the problem.

This $\langle n \rangle$ problem shows that the t-channel unitarity content of the Pomeron cannot contain any substantial pure-glue component if $\alpha^* \approx 1$, as is the case for the P+f model. Instead, the t-channel content of diffraction must be made up predominately of quarks, as is the case in the P-f identity. Calculations [3] show that no $\langle n \rangle$ difficulties are encountered in the P-f

identity.

P+f PROBLEM TWO : The f DOES NOT LOOK LIKE THE f OF THE P+f MODEL.

This problem arises under the following hypotheses. One imagines, that regardless of the possible value $\alpha^* = 1$ of the original glueball, the subglueball intercept is not 1 , but less than one. This may occur, because there may be additional renormalization effects of the quarkless QCD glueball due to quark loops which are not cut by the s-channel discontinuity [22], and so have not been explicitly included so far. How big this effect can be is a matter of conjecture in one sense, but we can be pretty sure from the above argument about multiplicities that if the subglueball really exists as a separate cylinder kernel its intercept must be $\alpha^* < \frac{1}{2}$. Still eq.(7) generates two poles. Now, however, the Pomeron is mostly the shifted planar f shifted using C_j as in the P-f identity and is mostly made up of quarks in the t-channel, while the putative output "f" will have a large glue component [17].

However, an "f" with a large glue component has all the wrong properties. The f of the P+f model is supposed to be planar and ideally mixed to a good approximation. However glue is inherently a cylindrical concept and a flavor singlet. It is also worth pointing out that an output "f" intercept near $\frac{1}{2}$ would, under the circumstances, be accidental. Actually it is quite unlikely since the input planar pole in T_j^{pl} at $\frac{1}{2}$ will repel any output pole in T_j well away from $\frac{1}{2}$.

In fact I believe that the only sensible result of this kind is an output glueball trajectory, after quark mixing, with intercept below zero. This is then quite consistent with the P-f identity.

P+F PROBLEM THREE : SHORT RANGE ORDER IS VIOLATED OR MULTIPLE COUNTING ERRORS ARE COMMITTED.

These errors are to be found in at least two papers [23, 24].

First, imagine that what I have called a "subglueball", composed only of glue (and perhaps uncut quark loops) is actually an intermediate quantity like a big "glueball resonance" which "later" decays into quark pairs which appear in the s-channel unitarity sum. Such a "decay" will of course have to be multiperipheral and cylindrical topologically in order to retain short range order. Hence, "subglueball decay" is indistinguishable in character

from the multiperipheral cylindrical structure which came from the original glueball and on which I have been basing the whole discussion. Thus one obtains nothing new by letting subglueballs "decay". If subglueballs "decay" into iterates of C_j then all final states are obtained by iterating C_j, and this simply produces eq.(1) and the P-f identity. If subglueball decays also include glue (as "sub-subglueballs"), one merely obtains eq.(7) as generating all final states. Hence there is really nothing to discuss ; the earlier treatment is complete.

However, ref.(23) imagines all $\alpha^* \approx 1$ subglueball decays to occur nonmultiperipherally, and so irreducibly with respect to C_j iterations. This is accomplished technically with the aid of a "minimum rapidity length" which stretches across the subglueball, and is introduced to avoid double counting. Double counting is indeed avoided. However, because each subglueball uses up so much phase space, the assumed nonmultiperipheral subglueball decay immediately results in all final states being dominated by non-multiperipheral configurations. But nonmultiperipheral final states are tantamount to dominant long range order, violating the data.

A second (and related) way that short range order can be violated is not to recognize that topologies of higher order than the cylinder generate j-plane cuts. These higher order topologies are also responsible for producing all the correct analyticity properties of multiparticle amplitudes, but dominant short range order (and the topological expansion) tells us that these are small effects at current energies. Clearly, if one is investigating the properties of the bare Pomeron pole before adding cuts (as we are), one should make sure not to include these higher topologies.

I close with a discussion of multiple counting errors. These occur under the following situation. Imagine starting with final states on the cylinder, all generated by C_j iteration. As I have said, this produces eq.(1) and the P-f identity. However, ref.(24) effectively tries to reorganize these final states as if they originated from $\alpha^* \approx 1$ subglueball decays, which makes eq.(7) and a P+f solution look relevant. The point is, this identification cannot be done uniquely, and multiple counting errors are thus committed. Technically, ref.(24) divides C_j into contributions from low and high rapidity gaps in its defining Froissart-Gribov integral, but this does not prevent the multiple counting errors. The point is simple. A nonsingular equation like eq.(1) cannot generate solutions to a singular equation like eq.(7) regardless of how one tries to rearrange things.

SUMMARY OF SECTION VI

There may indeed be a glueball in quarkless QCD with intercept one. However, because of unitarity the final result for the diffractive amplitude can be different from what one might expect. I have argued that after unitarization due to quark loops that a possible result -and the most plausible result- is the P-f identity, and not the traditional P+f model.

VII. CONCLUSIONS

QCD may or may not provide the fundamental theory of strong interactions. Unfortunately, present techniques preclude a realistic QCD calculation of diffraction scattering. Regardless, the ultimate character of diffraction must pass the test of unitarity. While this is notoriously difficult to incorporate, a major step forward has been taken with the topological expansion.

I have argued that the model of diffraction best consistent with unitarity is the Pomeron-f identity model. The quark loop unitarization of a QCD glueball is formally consistent with the P-f identity. Phenomenologically, the P-f identity is in good shape. An especially important point in this regard is the flavoring renormalization of the P-f , which arises from the requirement of consistency through unitarity with inelastic production of particles with different quantum numbers.

The P+f model, though steeped in tradition, suffers from three major flaws. These are (1) Modern P+f fits strongly violate two component duality, (2) The usual P+f model is incompatible with flavoring, and (3) Quark-loop unitarization of a QCD glueball probably cannot produce the P+f model (with the P containing glue in the t-channel) and be consistent with short range order and with observed hadron multiplicities.

I have concentrated in this paper on the short range order amplitude, whose j-plane projection is pole dominated. J-plane cut corrections, provided by the Reggeon Field Theory, are small effects at accessible accelerator energies. At superasymptotic energies where local scales, like the flavoring scales, become negligible the RFT scaling laws could become applicable. However, we should avoid complacency. Hints of big surprises at cosmic ray

energies exist. It may be that all present concepts of diffraction scattering are relevant only in a limited energy regime [25]

ACKNOWLEDGMENTS

Alex Martin participated in much of the work described here.

- REFERENCES -

1) H. HARARI, Phys.Rev.Lett. 20, 1395 (1968) ; P.G.O. FREUND, ibid p. 235 ; H. HARARI and Y. ZARMI, Phys. Rev. 187, 2230 (1969).

2) G.F. CHEW, C. ROSENZWEIG, Phys.Lett. 58B, 93 (1975) and Physics Reports (to appear).

3) H.M. CHAN and S.T. TSOU, Bielefeld Lectures, Rutherford preprint RL-76-080 (1976) and references therein.

4) J.W. DASH and A. MARTIN, Marseille preprint 77/P.964 (1977).

5) J.W. DASH, S.T. JONES, and E. MANESIS, Marseille preprint 77/P.912 (1977), to appear in Phys. Rev., and references therein.

6) The P+f fits in Fig. 1 are : (a) C. QUIGG and E. RABINOVICI, Phys. Rev. D13, 2525 (1976) ; (b) P. VOLKOVITSKII, A. LAPIDUS, V. LISIN, and K. TER-MARTIROSYAN, Sov.J.Nucl.Phys., 24, 648 (1976) ; (c) A. CAPELLA, J. KAPLAN, and J. TRAN THAN VAN, Nucl. Phys. B97, 493 (1975) ; (d) G. KANE and A. SEIDL, Rev. Mod. Phys., 48, 309 (1976). The data is from the phase shift analysis of E. Pietarinen, Budapest Conference (1977) (see R. Salmeron, Ecole Polytechnique preprint LPN HE/X/77).

7) G. VENEZIANO, Phys. Lett. 52B, 220 (1974) and Nucl. Phys. B74, 365 (1974).

8) N.F. BALI and J.W. DASH, Phys. Rev. D10, 2102 (1974). The philosophy toward all non-vacuum singularities is similar to that of the global fit of B.J. Hartley and G.L. Kane, Nucl. Phys. B57, 157 (1973).

9) J.C. RAMAO and P.G.O. FREUND, Univ. Chicago preprint 77.639 (1977).

10) (a) D. DUKE, Phys. Lett. 71B, 342 (1977).
(b) C.I. TAN, D. TOW, J.T.T. VAN, Phys.Lett. 74B, 115 (1978).

11) J.W. DASH, Phys.Rev. D9, 200 (1974).

12) S.T. JONES, LBL Berkeley preprint 6193 (1977).

13) M. ANTINUCCI et al., Nuovo Cimento Lett. 6, 121 (1973).

14) For the current status of Regge calculations in massive nonabelian gauge theories see J. BARTELS, Phys. Lett. 68B, 258 (1977). Regge QCD calculations for D = 4 do not exist.

15) F. LOW, Phys. Rev. D12, 163 (1975) ; S. NUSSINOV, Phys. Rev. D14, 246 (1976)

16) J.W. DASH, Phys. Lett. 61B, 199 (1976).

17) G. VENEZIANO, Nucl. Phys. B117, 519 (1976).

18) G.F. CHEW and D.R.SNIDER , Phys. Rev. D1, 3453 (1970), and D3, 420 (1971).

19) J.W. DASH, G. PARRY, and M. GRISARU, Nucl. Phys. B53, 91 (1973).

20) H. CHENG, J. WALKER, and T.T. WU, Phys. Lett. 44B, 97 (1973) and references therein.

21) S. PINSKY and D.R. SNIDER, Phys. Rev. D13, 1470 (1976).

22) G. VENEZIANO, private communication.

23) R. HONG TUAN, Orsay preprint 72/38 LPTHE (1977).

24) P. AURENCHE and L. GONZALES MESTRES, Ecole Polytechnique preprint A.270.0777 (1977).

25) J.D. BJORKEN, SLAC preprint 2041 (1977).

DIFFRACTIVE HADRON DISSOCIATION

K. Goulianos
The Rockefeller University
New York, N. Y. 10021

Abstract : Some simple general features of the diffractive hadron dissociation process are discussed with emphasis on its relation to elastic scattering and the total cross section of hadrons.

In the past few years, the diffraction dissociation process

$$h + A \to X + A \quad \text{at low} \quad t \tag{1}$$

has been studied for $h,A = p^{\pm}$, $\pi^{\pm}$, $K^{\pm}$ and also for $pd \to Xd$. The differential production cross section

$$d^2\sigma/dtdM_X^2 = f_{h,A}\,(s,t,M_X^2) \tag{2}$$

has been found to exhibit certain simple features. In this report, we review these features and examine some properties of hadron cross sections that can be derived from them. Specifically, we discuss:

(i) The s,t, and M_X^2 dependence of the diffractive cross sections,

(ii) the factorization of the diffractive vertex,

(iii) the first moment finite mass sum rule (FMSR) and the low mass enhancements of the diffractive cross section,

(iv) a comment on the s-dependence of the diffraction dissociation cross section,

(v) a relationship between the elastic and the total cross section of hadrons, and

(vi) the total cross section of the diffractive mass X with the nucleon -- and why the accepted method for extracting this cross section may be wrong!

With the exception of results from the Rockefeller experiment E-396 at Fermilab, all the experimental results referred to in this report are published. However, since this is not a summary of results but a review focusing on the elucidation of the points mentioned above, not all the published results on reaction (1) are quoted here.

High energies ($s \gtrsim 100$ GeV^2) are essential for observing a diffraction dissociation signal above the non-diffractive "background" from central collisions. This is illustrated in Fig. 1 for $pp \to Xp$. The cross section $d\sigma/dx$ ($x \equiv p_{\parallel}^*/p_{max}^* \simeq 1 - M_X^2/s$) which is approximately flat in the central x region increases dramatically with decreasing $1 - x$ in the region $1-x \lesssim 0.1$. This increase of the cross section is due to the diffraction dissociation of the proton which follows a $1/(1-x)$ law. For a given s, as $1-x \simeq M_X^2/s$ decreases, the value of M_X^2 enters the "resonance region" ($M_X^2 \lesssim 5$ GeV^2) and finally reaches the pion production threshold where the cross section must come down to zero. The higher the s, the lower the value of $1-x$ corresponding to a given mass M_X, and the higher the invariant $d\sigma/dx$ cross section for the diffractive production of this mass. Thus, large diffractive masses can be "seen" above background only at appropriately high values of s. This point is discussed quantitatively in Part I below.

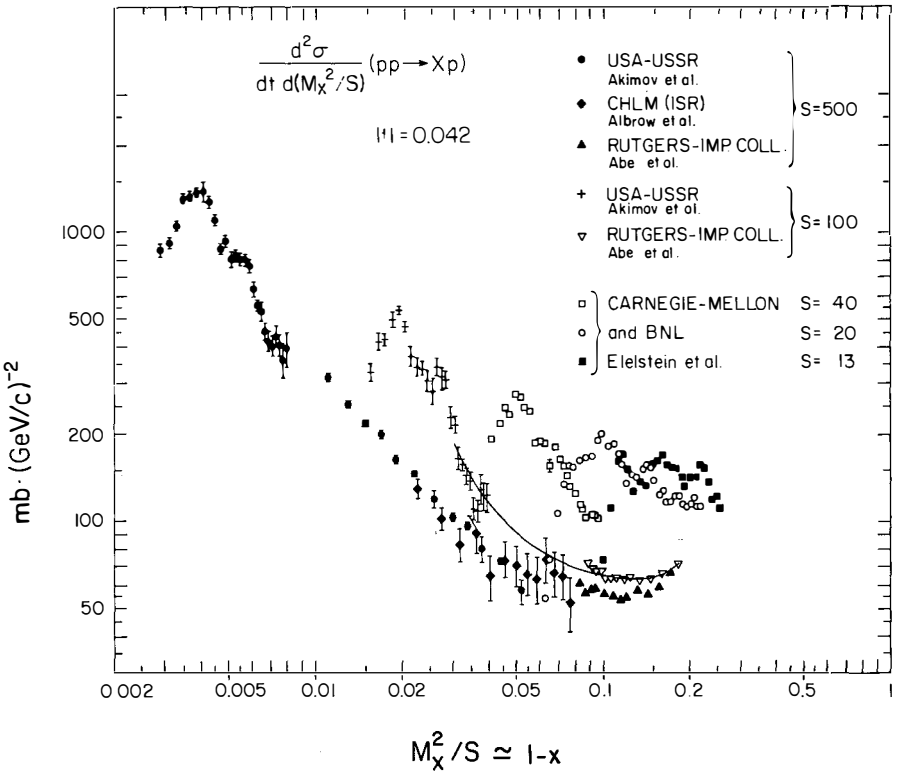

FIG. 1 - The invariant differential cross section $d^2\sigma/dtd(M_X^2/s)$ for pp → Xp at t = -0.042 $(GeV/c)^2$ and s from 13 to 500 Gev^2.

I. The s, t, and M_X^2 dependence of the diffractive cross section -

In the region $M_X^2 \gtrsim 5$ GeV^2, $|t| \lesssim 0.1$ $(GeV/c)^2$ and $1-x \lesssim 0.1$, the differential cross section for hA → XA is found experimentally to be described by the simple formula [5,6,7]

$$\frac{d^2\sigma}{dtdx} = \frac{A_1(1+B/s)}{1-x} e^{b_1 t} + A_2(1-x)\, e^{b_2 t} \qquad (3)$$

where the constants A_1, B, b_1, A_2 and b_2 depend on the particles h and A. The first term on the right hand side is identified with the diffractive cross section while the second term is presumably due to non-diffractive processes. This view is supported by the fact that the first term follows simple factorization rules as discussed in Part II below, while the second

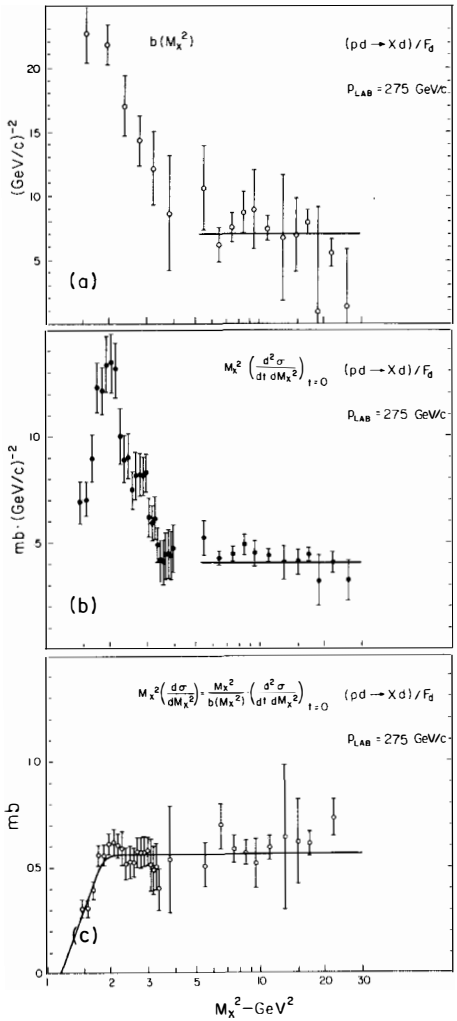

term does not follow these rules. The t-dependence is exponential as expected from a naive diffractive picture and the 1/1-x behavior is responsible for the increase of the cross section at small 1-x. For pp → Xp, the constants in Eq. (3) are approximately[5,6] $A_1 \simeq 4$ mb·(GeV/c)$^{-2}$, $B \simeq 65 \pm 25$ GeV^2 (including estimated systematic errors), $A_2/A_1 \simeq 100$, and $b_1 \simeq b_2 \simeq 7$ (GeV/c)$^{-2}$. Thus, at 1-x = 0.1 the diffractive and non-diffractive terms are approximately equal while at 1-x = 0.03 the diffractive term is responsible for about 90% of the inclusive cross section.

As M_X^2 decreases to values smaller than 5 GeV^2, the slope b increases thus causing a low mass enhancement at low t values. However, it is important to observe that the integral of the cross section over t behaves very smoothly over the entire mass region, as illustrated[4] in Fig. 2. This behavior is just what is necessary to satisfy the FMSR as discussed under Part III below.

FIG. 2 - Values for pp → Xp vs M_X^2, extracted from pd → Xd at 275 GeV/c. (a) The slope parameter, $b(M_X^2)$. (b) $d^2\sigma/dtdM_X^2$ multiplied by M_X^2 and extrapolated to t = 0 using $b(M_X^2)$. (c) Values of (b) above, divided by values of (a): $M_X^2(d\sigma/dM_X^2)$.

II. The factorization of the diffractive vertex -

It has been determined experimentally[5,7,9] that at low t and small M_X^2/s the diffractive vertex factorizes as follows:

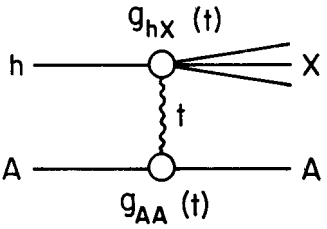

(4)

As a consequence of this factorization rule, the cross sections for a hadron dissociating on different targets scale as the corresponding elastic cross sections[5,7], while the cross sections for different hadrons dissociating on the same target scale as the corresponding total cross sections[9].

a) Proton dissociation on different targets A:

This has been studied for[7] A = $p^{\pm}$, $\pi^{\pm}$, $K^{\pm}$ (Single Arm Spectrometer) and for [5] A= d (USA-USSR Collaboration). The diagram for elastic scattering analogous to (4) is

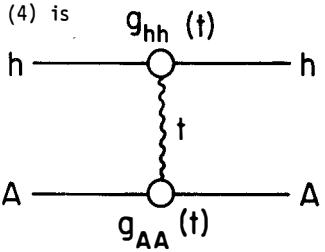

(5)

Comparing (5) with (4), factorization implies that

$$\frac{d^2\sigma/dtdx}{d\sigma^{el}/dt} = \frac{g_{hX}(t)\cdot g_{AA}(t)}{g_{hh}(t)\cdot g_{AA}(t)} = C_h(s,x,t) \qquad (6)$$

i.e., at given s, x and t, the ratio of the diffractive to the elastic cross section of a hadron h interacting with a target particle A is a constant independent of the target particle. As mentioned in Part I, it is the first term in Eq. (3) that factorizes in this manner while the second term (non-diffractive) does not factorize[5]. Fig. 3 illustrates a test of this factorization rule for proton dissociation on p and d targets[5]. It is important to notice that the test is performed at the same s-value and therefore at different incident proton momenta in the laboratory.

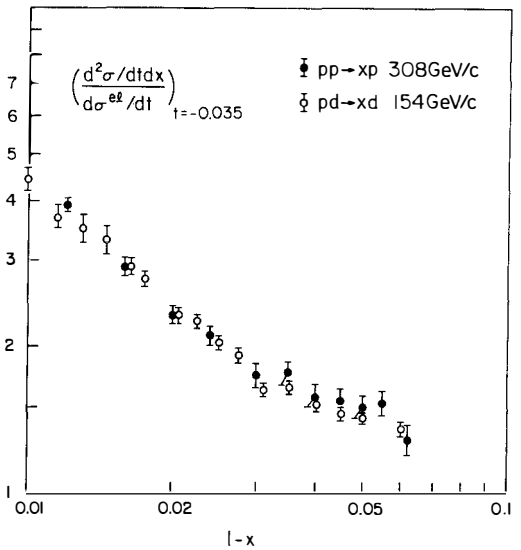

FIG. 3 -
The ratio $(d^2\sigma/dtdx)/(d\sigma^{el}/dt)$ versus 1-x at t = -0.035 $(GeV/c)^2$, for pp → Xp at 308 GeV/c and for pd → Xd at 154 GeV/c (same s value as for pp → Xp).

b) Different hadrons h dissociating on the same target particle A: This has been checked recently for[9] h = $p^{\pm}$, $\pi^{\pm}$, $K^{\pm}$ and A = p (Rockefeller experiment E-396 at Fermilab). From the diagrams below

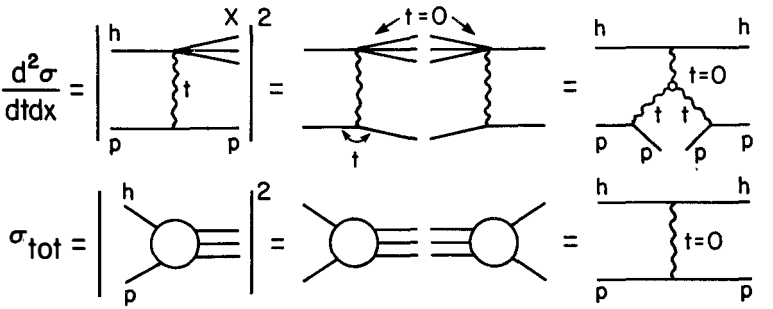

(7)

one concludes that

$$\frac{d^2\sigma}{dtdx} \Big/ \sigma_{tot} = C_p\,(s,x,t) \qquad (8)$$

i.e., the ratio of the diffractive to the total cross section of different hadrons dissociating on a proton is the same for all hadrons. Preliminary results of the Rockefeller experiment are given below:

Test of factorization

(h + p → X + p at 100 GeV/c)

h	R (arbitrary normalization)
p	1.00 ± 0.04
p^-	0.92 ± 0.11
π^+	1.10 ± 0.05
π^-	1.12 ± 0.03
K^+	0.86 ± 0.21
K^-	1.15 ± 0.14

$R \equiv (d^2\sigma/dtdx)/\sigma_{tot}$

$\left\langle \begin{array}{l} 0.02 < |t| < 0.1\ (GeV/c)^2 \\ 0.02 < 1-x < 0.05 \end{array} \right\rangle$

The agreement among the values of R for the various hadrons studied in this experiment is reasonably good.

Eq. (8) implies further that, for given s and x, the t distribution of all hadrons dissociating on a proton should be the same. This aspect of the factorization rule has not been checked yet.

III. The first moment finite mass sum rule (FMSR) and the low mass enhancements of the diffractive cross sections -

The FMSR is an extension of the finite energy sum rule for total cross sections. It derives from the hypothesis that the diffractive cross sections can be described either by s-channel resonance or by t-channel reggeon exchanges. Schematically,

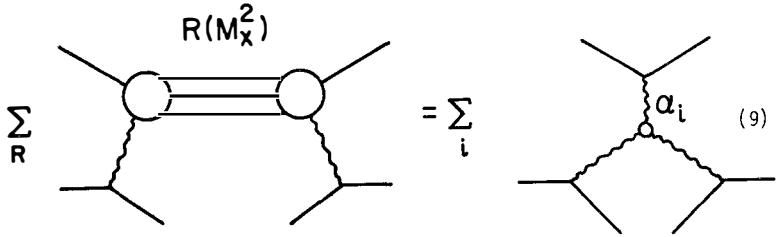

(9)

It is presumed that at high M_x^2 overlapping resonances result in a smooth behavior of the cross section described by diagrams on the right hand side of Eq. (9). This behavior, extrapolated to low M_x^2, should average over the non-smooth behavior caused by widely spaced resonances contributing to the left hand side of (9). Quantitatively, using analyticity and crossing symmetry, one derives[10] the first moment FMSR

$$|t| \frac{d\sigma^{e\ell}}{dt} + \int^{\nu_o} \nu \left(\frac{d^2\sigma}{dtd\nu}\right) d\nu = \int^{\nu_o} \nu \left[\frac{d^2\sigma}{dtd\nu}\right] d\nu \longleftarrow \left\{\begin{array}{l}\text{function obtained} \\ \text{from high } \nu\end{array}\right\} \qquad (10)$$

where $\nu = M_x^2 - M_h^2 = t$ is the cross-symmetric variable.

This rule has many far reaching consequences. Two of these consequences are described in Parts IV and V later on. Here we present the experimental tests of the rule and comment on its implications on the behavior of the low mass enhancements of the diffractive cross sections.

A very accurate test of the rule was first performed[4] on pd → Xd. Fig. 4 shows this test at $|t| = 0.035$ (GeV/c)^2.

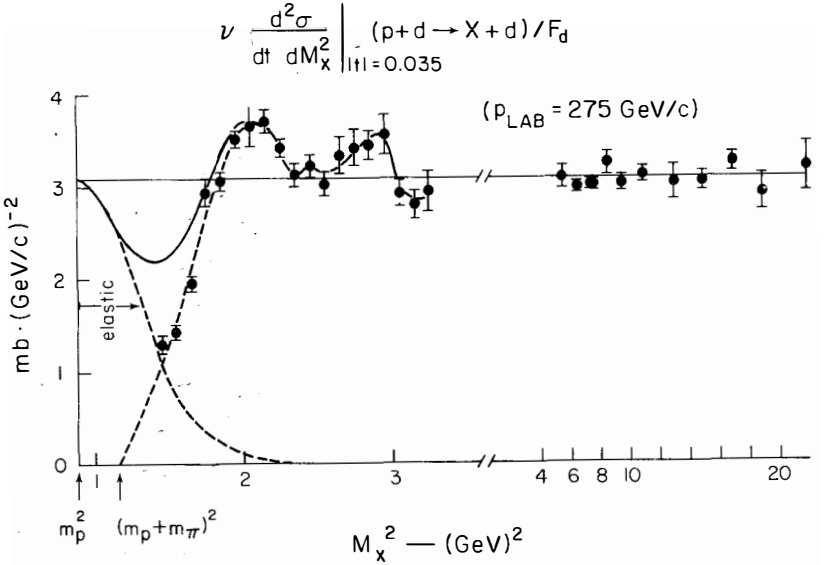

FIG. 4 - Test of the first-moment FMSR: Values of $\nu(d^2\sigma/dtdM_x^2)$ vs M_x^2 for $p_{lab} = 275$ GeV/c and $|t| = 0.035$ (GeV/c)^2.

The rule was tested for other t-values in the range $|t| < 0.1$ (GeV/c)^2 and was found to hold equally well (to a few % accuracy). As $t \to 0$, the term $|t|\ d\sigma^{el}/dt \to 0$ and therefore the low M_x^2 region must have a large b-slope in order for the rule to continue to hold at small t-values[11]. This is what is actually happening (see Fig. 2). In fact, as was mentioned before, the integral over t behaves approximately as $1/M_x^2$ even in the "resonance" region where it gradually drops with decreasing mass to become zero at the

pion production threshold. In this low mass region the b-slope increases with decreasing M_X^2 in such a manner as to satisfy the FMSR. This behavior of continuously increasing b-slope as one enters the low mass region has been observed also in pion and kaon dissociation[8]. In all cases, the slope of the low mass enhancement is about twice as large as the slope of the corresponding elastic scattering. These enhancements are the $N^*(1400)$ for $pp \to Xp$, the $A_1(1100)$ for $\pi p \to Xp$, and the $Q(1300)$ for $Kp \to Xp$. None is established as a resonance. Their behavior suggests that their production is of the same nature as the high mass diffractive dissociation and therefore it should have the same s-dependence and follow the same scaling rules discussed in Part II above.

Preliminary results from the Rockefeller experiment E-396 at Fermilab testing the FMSR are shown on the Table below:

Test of the 1st moment FMSR
(h + p → X + p at 100 GeV/c)

h	R
p	1.04 ± 0.05
$\bar{p}$	0.74 ± 0.14
π^+	1.05 ± 0.06
π^-	0.98 ± 0.03
K^+	1.62 ± 0.49
K^-	0.97 ± 0.15

$$R \equiv \frac{|t| \frac{d\sigma^{e\ell}}{dt} + \int_{4\ \mathrm{GeV}^2}^{} \nu \left(\frac{d^2\sigma}{dt\,d\nu}\right) d\nu}{\int_{4\ \mathrm{GeV}^2}^{} \nu \left[\frac{d^2\sigma}{dt\,d\nu}\right] d\nu} \leftarrow \left\{\begin{array}{l}\text{function extrapolated}\\ \text{from the region}\\ 4 < \nu < 10\ \mathrm{GeV}^2\end{array}\right\}$$

The values of R are compatible with unity as predicted by the FMSR.

IV. A comment on the s-dependence of the diffraction dissociation cross section -

The s-dependence of the high mass diffractive cross section has the form given in Eq. (3), $1 + B/s$, with $B \simeq 65 \pm 25\ \mathrm{GeV}^2$ for $pp \to Xp$. It was argued in Part III that the integral over t of the low mass diffractive production should have the same s-dependence as that of the high mass production if the result displayed in Fig. 3 i.e., the validity of the $1/M_X^2$ law all the way down into the "resonance region" were to hold at all s-values. From the FMSR, Eq. (10), one then obtains the result that the s-dependence of the diffractive cross section is the same as that of the integral $\int_0^\infty |t|\ (d\sigma^{e\ell}/dt)\ dt$. For $pp \to Xp$, $d\sigma^{e\ell}/dt \simeq (184/s)\ e^{2.8t} + 51\ e^{9.2t} + 23\ e^{19t}$ (ref.12), which multiplied by $|t|$ and integrated over t yields $0.67\ (1 + 35/s)$. This s-dependence is not statistically very different from the measured $1 + (65 \pm 25)/s$.

V. A relationship between the elastic and the total cross section of hadrons-

In Part IIb it was shown that the high mass diffractive cross section for $hp \to Xp$ scales as the total cross section, $hp \to$ anything. Furthermore, it was argued in Part III that the integral over t of the low mass diffractive production should scale as that of the high mass production if the $1/M_X^2$ law was to be true for every hadron h dissociating on a proton. It then follows that the integral over t of the high mass term minus that of the low mass term in the FMSR Eq. (10) should be proportional to the total cross section, σ_{tot}.

Thus, $\sigma_{tot} \sim \int |t| \, (d\sigma^{e\ell}/dt)dt = \sigma_{e\ell}/b_{e\ell}$, where in deriving the last step we assumed an $e^{b_{e\ell}t}$ form for $d\sigma^{e\ell}/dt$. Using the optical theorem at high energies where the ratio of the real to the imaginary part of the forward nuclear scattering amplitude (ρ-value) is close to zero, $d\sigma^{e\ell}/dt \simeq (\sigma_{tot}^2/16\pi)\, e^{b_{e\ell}t}$, one obtains further the result $\int |t| (d\sigma^{e\ell}/dt)\, dt \sim \sigma_{tot}^2/b_{e\ell}^2$. Thus, $\sigma_{tot} \sim \sigma_{e\ell}/b_{e\ell} \sim \sigma_{tot}^2/b_{e\ell}^2$, which yields the relationships

$$b_{e\ell}/\sqrt{\sigma_{tot}} = C\,(s) \qquad (11)$$

$$\sigma_{e\ell}/\sigma_{tot}^{3/2} = C'\,(s) \qquad (12)$$

where $C\,(s)$ and $C'\,(s)$ are universal functions of s which are the same for all hadrons interacting with a proton[13].

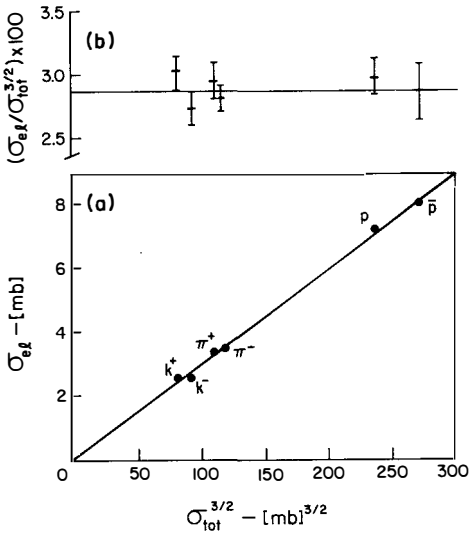

FIG. 5 - (a) The elastic cross section versus $\sigma_{tot}^{3/2}$ for various hadrons interacting with a proton at 100 GeV/c. (b) The ratio $\sigma_{e\ell}/\sigma_{tot}^{3/2}$ versus $\sigma_{tot}^{3/2}$ for the same data as in (a).

Fig. 5 shows $\sigma_{e\ell}$ as a function of $\sigma_{tot}^{3/2}$ for various hadrons interacting with a proton at 100 GeV/c. The ratio $\sigma_{e\ell}/\sigma_{tot}^{3/2}$ is remarkably constant for all hadrons in agreement with our result (12). Result (11) follows directly from (12) using the optical theorem. From Fig. 5, one now understands why the ψN elastic cross section is so small (about 30 μb for a 1 mb ψN total cross section).

VI. The total cross section of the diffractive mass X with the nucleon -

In proton dissociation on a deuterium target, the possibility exists for the dissociation to occur on one nucleon producing the particle X which then scatters elastically from the second nucleon, as follows:

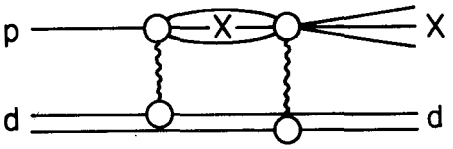

(13)

The forward elastic scattering of X is proportional to the X-nucleon total cross section, σ^{XN}. Using the Glauber theory, one then calculates the ratio of diffractive to elastic scattering for pp to that for pd to be

$$R \equiv \frac{\left(\frac{d^2\sigma/dtdx}{d\sigma^{e\ell}/dt}\right)_{pp}}{\left(\frac{d^2\sigma/dtdx}{d\sigma^{e\ell}/dt}\right)_{pd}} = 1 + 0.2\,\frac{\sigma^{XN}}{\sigma^{NN}} \qquad (14)$$

where the pp and pd cross sections are compared at the same incident proton momentum in the laboratory. Fig. 6 shows this ratio as a function of 1-x for two values of incident proton momentum[4]. In the coherence region (small 1-x), R tends to a constant corresponding to $\sigma^{XN} = 28 \pm 10$ mb.

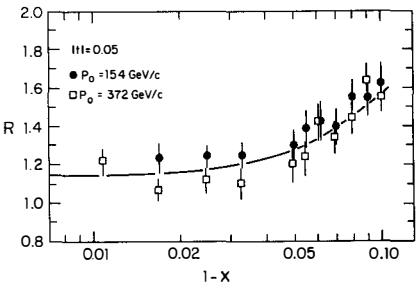

FIG. 6 -
The ratio $R = [(d^2\sigma/dtdx)/(d\sigma^{e\ell}/dt)]_{pp}/[(d^2\sigma/dtdx)/(d\sigma^{e\ell}/dt)]_{pd}$ versus 1-x for incident proton momenta of 154 and 372 GeV/c.

We would like to argue here that this long accepted method for determining the total cross section of an intermediate state X with the nucleon may not be valid. The argument goes as follows: We have shown that at the same $s \simeq 2m_{target} p_{lab}$ the ratio of the diffractive to the elastic cross section is the same for pp and pd, i.e., $R = 1$ (see Fig. 3). This is a consequence of the factorization rule discussed in Part IIa. If it were not for the s-dependence of the diffractive cross section (see Eq. 3), R would still be equal to unity when evaluated at the same incident proton momentum. But in Part IV we argued that the s-dependence of the diffractive cross section is tied up to that of elastic scattering through the FMSR. Thus, factorization of the diffractive vertex and the validity of the FMSR completely determine the value of R and consequently the value of σ^{XN}. At high energies, as the s-dependence of the diffractive cross section dies out (except for possible $\ell n s$ terms), σ^{XN} as calculated from (14) goes to zero. One sees already in Fig. 6 the trend of decreasing σ^{XN} as the energy increases. This behavior leads us to question the interpretation that R is related to σ^{XN} through Eq. (14).

ACKNOWLEDGEMENTS:

I would like to thank my colleagues from the Rockefeller Experiment E-396 at Fermilab[9] for allowing me to present the preliminary results of the experiment and for many useful discussions.

REFERENCES

Results from the USA-USSR Collaboration at the internal gas jet target at FERMILAB:

1) "Proton-Proton Diffraction Dissociation at Incident Energies from 175 to 400 GeV," V. Bartenev et al., Phys. Lett. 51B, 299 (1974).

2) "Excitation of High-Energy Protons into Low-Mass States in p-d Interactions," Y. Akimov et al., Phys. Rev. Lett. 35, 763 (1975).

3) "Diffraction Dissociation of High-Energy Protons in p-d Interactions," Y. Akimov et al., Phys. Rev. Lett. 35, 766 (1975).

4) "Analysis of Diffractive pd → Xd and pp → Xp Interactions and Test of the Finite-Mass Sum Rule," Y. Akimov, et al., Phys. Rev. D14, 3148, (1976).

5) "Diffraction Dissociation of High-Energy Protons on Hydrogen and Deuterium Targets," Y. Akimov et al., Phys. Rev. Lett. 39, 1432 (1977).

6) "Diffraction Dissociation of High-Energy Protons in pp and pd Interactions," D.F. Nitz, Ph.D. Thesis, University of Rochester, Department of Physics and Astronomy, Rochester, New York.

Results from the Single Arm Spectrometer at FERMILAB:

7) "Inclusive Hadron Scattering from 50 to 175 GeV/c," R.L. Anderson et al., Phys. Rev. Lett. 38, 880 (1977).

Results from Serpukov:

8) Y. Antipov et al., Nuclear Physics B63, 141-228 (1973).

Other References:

9) Rockefeller Experiment E-396 at FERMILAB: Cool, Goulianos, Segler, Snow, Sticker and White.

10) S.D. Ellis and A.I. Sanda, Phys. Lett. 41B, 87 (1972).

11) A. Capella, H. Hogaasen and V. Rittenberg, Phys. Rev. D8, 2040 (1973).

12) K. Goulianos, Phys. Rev. D14, 1445 (1976).

13) Result (11) was previously observed by Quigg and Rosner, Phys. Rev. D14, 160 (1976).

p-p SCATTERING POLARIZATION EXPERIMENTS AT HIGH ENERGY

Franco Bradamante
Istituto di Fisica dell'Università, Trieste,
and INFN, Sezione di Trieste

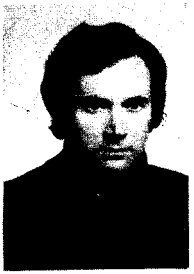

ABSTRACT

Recent data on the polarization of Λ's and p's inclusively produced in p-p collisions, and on the polarization parameter in elastic p-p scattering, are reviewed. New data at 150 GeV/c from the CERN-Padova-Trieste-Vienna experiment at the SPS are presented.

INTRODUCTION

In this talk I will review the most recent results obtained on spin effects in p-p scattering at high energy, and in particular I will report on the polarization experiment which is carried out at the CERN SPS.

I will first talk about some new data on the polarization of inclusive Λ and proton production. I will then mention some results coming form Argonne on the polarization and on the spin correlation parameters in elastic pp scattering at 11.75 GeV/c. Finally I will talk about the three experiments measuring the polarization parameter in pp elastic scattering at high energy, namely at the CERN SPS and at Fermilab.

As you will see, a few unexpected phenomena have been revealed, so that I hope to convince you that this field of research, on which at present just a few "amateurs" are active, might turn out to be quite interesting.

INCLUSIVE REACTIONS

About three years ago the neutral hyperon group[1] at FNAL discovered that 300 GeV protons produced polarized Λ's on berillium. The degree of polarization increased with the transverse momentum, and was as high as 30% at p_T = 1.5 GeV/c. The mechanism responsible for this unexpected phenomenon has not yet been understood, but it has been shown to be fairly independent of energy. An analysis[2] performed on the data from the Σ^0 lifetime experiment done at CERN in 1974 has given, at 24 GeV, essentially the same result found at FNAL, as can be seen in Fig. 1, where the two sets of data are compared.

It is interesting to note that preliminary data[3] on inclusive production of π^0 by 24 GeV/c protons on a polarized proton target at CERN also seem to indicate a large polarization, again at variance with the simple expectation of no polarization, due to the presence of a large number of contributing channels.

The polarization of inclusive protons produced in pp scattering is being measured at FNAL by a group from Indiana University[4]. They

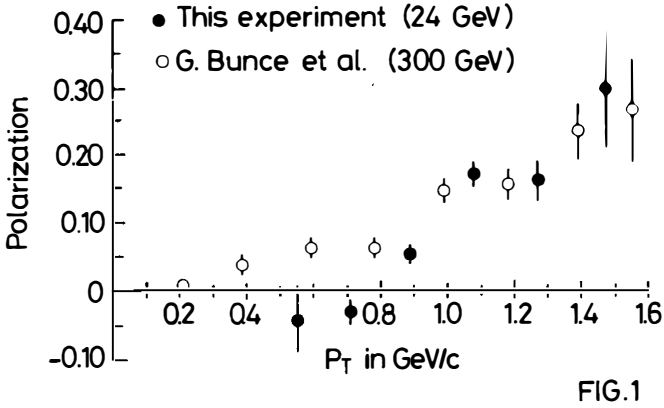

Fig. 1 : Polarization of Λ's inclusively produced on Be by 300 protons (Ref. 1) and on Pt by 24 GeV protons (Ref. 2).

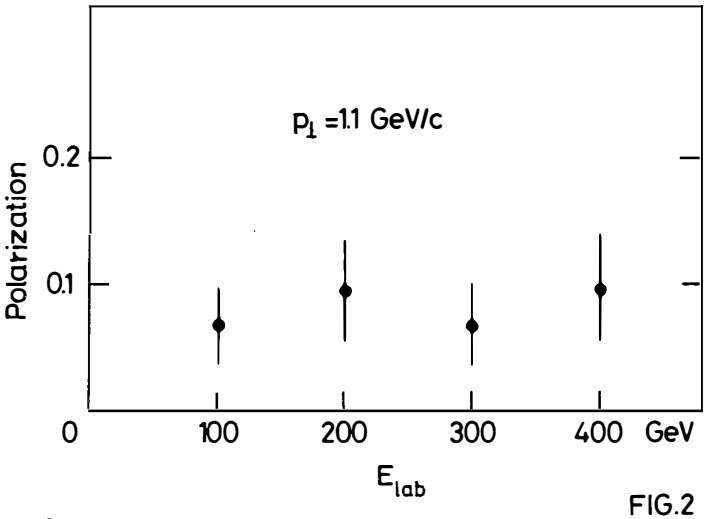

Fig. 2 : Preliminary polarization data for protons inclusively produced in P-C interactions (Ref. 5).

are using the same apparatus which is used to measure the polarization in elastic pp scattering, namely as target a hydorgen gas jet, pumped through the circulating FNAL beam, plus a superconducting spectrometer to detect the recoil proton, and a carbon polarimeter to measure the proton polarization. Preliminary data, at 1.1 GeV/c transverse momentum, and various energies, are quoted in the review article by H. Spinka[5], and are reproduced in Fig. 2. The polarization turns out to be large, of the order of 10%, and, as in the case of the Λ polarization, essentially independent of the incident proton energy. Again, it does not seem to be easy to find an explanation for these sizeable spin effects.

3. RESULTS FROM ARGONNE

The polarized beam at the Argonne ZGS gives this laboratory a unique facility to probe spin effects in the pp system. I will not talk about most of the results just because they are at "low energy" I will only list those which appeared over the past year, either as publications or in some preliminary form:

a) Data on total cross-section differences for longitudinally polarized beam and target, up to 6 GeV/c incident proton momentum[6,7].

b) More data on total cross-section differences for transversely polarized beam and target, in the range 1-3 GeV/c incident proton momentum[8].

c) Measurement of C_{LL}, the spin correlation parameter for longitudinally polarized beam and target at 6 GeV/c incident proton momentum, in the four-momentum transfer $|t|$ range from 0.1 to 0.8 $(GeV/c)^2$ [7].

d) Measurement of the polarization parameter in pp and pn scattering at 11.8 GeV/c, in the $|t|$ interval from 0.15 to 0.9 $(GeV/c)^2$ [9].

The only result I want to present from Argonne concerns the spin correlation parameter C_{nn} for elastic pp scattering at 11.75 GeV/c incident proton momentum. The experiment is a continuation of the one which A.D. Krisch described four years ago in Méribel[10]. The extracted polarized proton beam, about 10^{10} protons per 4.3 sec pulse,

was sent on a polarized proton target, and the elastically scattered events were detected by two spectrometers. Both the beam and the target polarizations P_B and P_T respectively were about 70%, and were oriented normal to the horizontal plane (the scattering plane). Data were taken in the four initial spin states ($\uparrow\uparrow$), ($\uparrow\downarrow$), ($\downarrow\uparrow$) and ($\downarrow\downarrow$), so that the spin-spin correlation parameter

$$C_{nn} = \frac{1}{P_B P_T} \frac{N_{\uparrow\uparrow} - N_{\uparrow\downarrow} - N_{\downarrow\uparrow} + N_{\downarrow\downarrow}}{\Sigma N_{ij}}$$

and the spin-orbit polarization parameter

$$A = \frac{2}{P_B + P_T} \frac{N_{\uparrow\uparrow} - N_{\downarrow\downarrow}}{\Sigma N_{ij}}$$

could be obtained from the four measured normalized elastic event rates N_{ij}. The results of this experiment[11] are shown in Fig. 3.

Where the data overlap with existing ones, the known trend of the polarization parameter A, namely the double-zero at $|t| \sim 0.6$ (GeV/c)^2 and the bump in the interference region, is confirmed. In the large transverse momentum region, however, there is just a smooth decrease to very low values, which means that the spin-orbit forces are small. In this large transverse momentum region C_{nn} data look quite interesting: while for lower p_T the behaviour of C_{nn} is similar to that of A, for $p_T^2 = 3.6$ (GeV/c)^2 C_{nn} suddenly increases and attains a value of 30% at $p_T^2 = 4$ (GeV/c)^2. This means that at this p_T the spin-parallel cross-section is a factor of two larger than the anti-parallel, as shown in Fig. 4, which gives the pure-spin cross-sections

$$\left(\frac{d\sigma}{dt}\right)_{\uparrow\uparrow} = \left\langle\frac{d\sigma}{dt}\right\rangle \left[1 + 2A + C_{nn}\right]$$

$$\left(\frac{d\sigma}{dt}\right)_{\downarrow\downarrow} = \left\langle\frac{d\sigma}{dt}\right\rangle \left[1 - 2A + C_{nn}\right]$$

$$\left(\frac{d\sigma}{dt}\right)_{\uparrow\downarrow} = \left(\frac{d\sigma}{dt}\right)_{\downarrow\uparrow} = \left\langle\frac{d\sigma}{dt}\right\rangle \left[1 - C_{nn}\right] .$$

As pointed out by the authors, the large-p_T cross-section already at this energy exhibits the (scaled) p_T dependence which is typical of

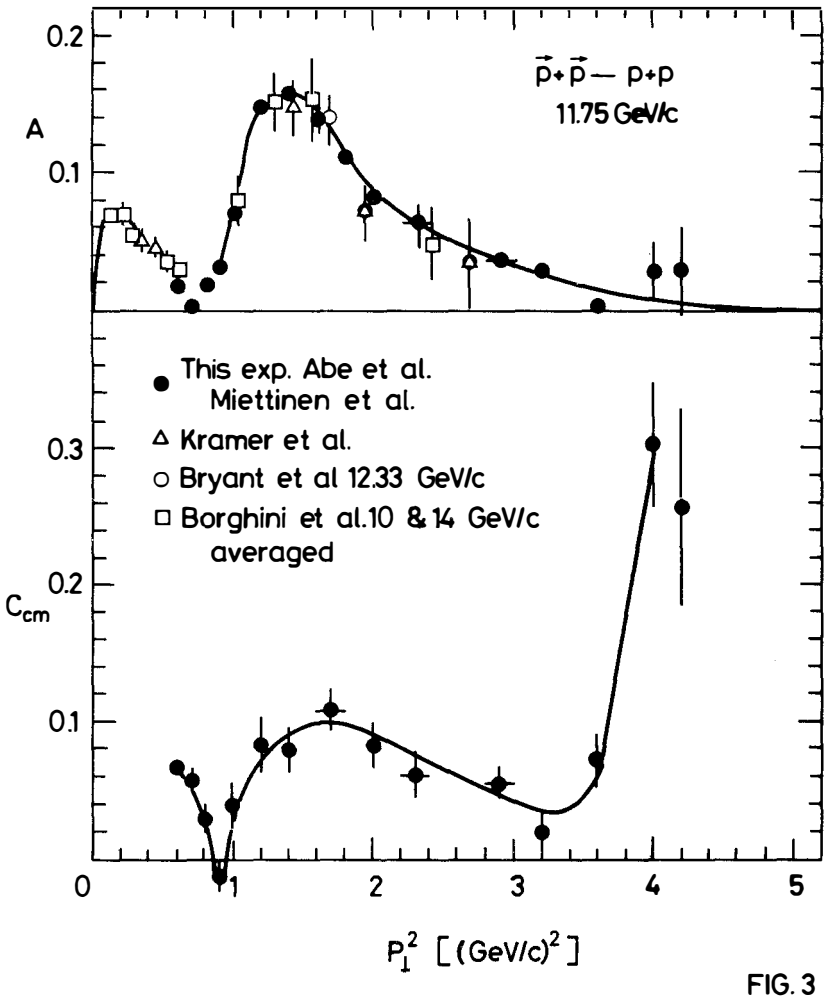

Fig. 3 : The polarization parameter A, and the spin correlation parameter C_{nn} from elastic p-p scattering at 11.75 GeV/c (Ref. 11). Earlier results from other experiments are also shown for completeness.

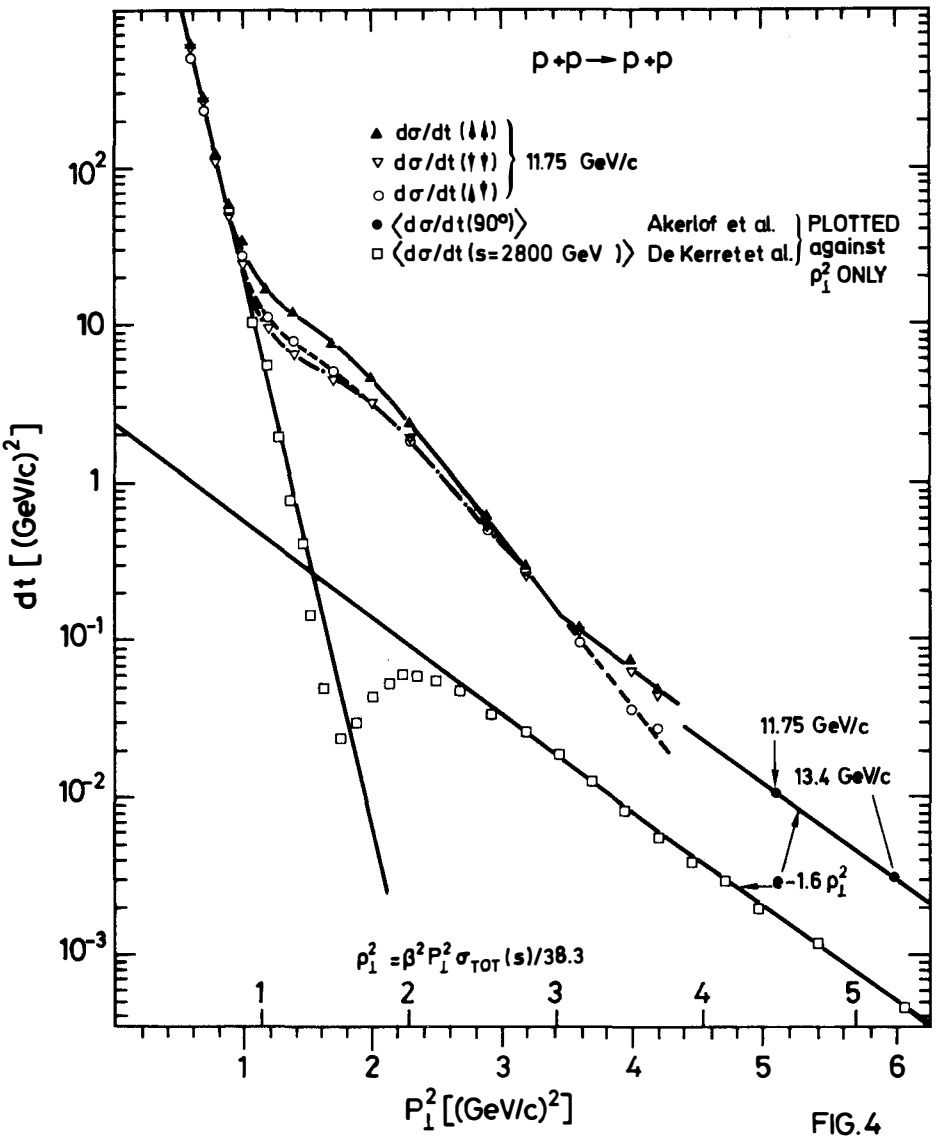

Fig. 4 : Elastic pp differential cross-sections at 11.75 GeV/c for the three pure spin states (↑↑), (↑↓), and (↓↓), normal to the scattering plane, as from Ref. 11. Also shown are the ISR data at s = 2800 GeV^2, plotted against the variable $\rho_T^2 = \beta^2 p_T^2 \sigma_{TOT}(s)/38.3$.

the ISR energy. The fact that this cross-section is dominated by the parallel-spin interaction might imply therefore that in general the hard scattering component is dominated by the parallel-spin interaction. Of course, it would be extremely interesting to know the p_T behaviour of the parallel and antiparallel components for higher values of p_T. New C_{nn} data for pp scattering at 90°C.M. exist, but extend only up to 5.5 GeV/c incident proton momentum, so there is no overlap with these data.

4. POLARIZATION IN HIGH-ENERGY ELASTIC pp SCATTERING

The activity which is going on in Argonne is unique because of the availability of a polarized proton beam. Although the situation might change in the future (there are proposals, both at CERN[13], and at FNAL[14], to construct high-energy polarized proton beams, or to use a polarized jet target[15] pumped through the CERN SPS circulating beam) at present the only available information on spin effects in high energy elastic pp scattering is provided by three experiments which measure the Polarization Parameter A.

The first is the Experiment 313, carried out at FNAL by the Indiana University team whom I already mentioned in Section 2, when reporting their result on the polarization of inclusively produced protons. Their aim is to measure the polarization parameter in elastic pp scattering from 20 to 200 GeV/c, at fixed t-values, in the region $0.3 < |t| < 1.$ $(GeV/c)^2$, using the hydrogen gas jet target technique I have already mentioned. Preliminary results[16] at $|t| = 0.3$ $(GeV/c)^2$ and at $|t| = 0.8$ $(GeV/c)^2$ are shown versus s, the squared C.M. energy, in Fig. 5. The same figure shows also some earlier data at lower energies, as well as some preliminary data from the second polarization experiment at Fermilab (E61), which I will describe next. The data at $|t| = 0.3$ $(GeV/c)^2$ exhibit a very fast decrease with s in the lower energy region, up to $s \simeq 20$ GeV^2. For higher energies, the polarization just remains very small, at the one per cent level. The data at $|t| = 0.8$ $(GeV/c)^2$, on the contrary, suggest that the $\sim$5% negative polarization observed at Serpukhov[17] might persist up to the highest energy investigated. Such a large polarization cannot easily be explained as interference between the Pomeron and a conventional Regge term[18]. A large polarization (solid lines in Fig. 5) is predicted

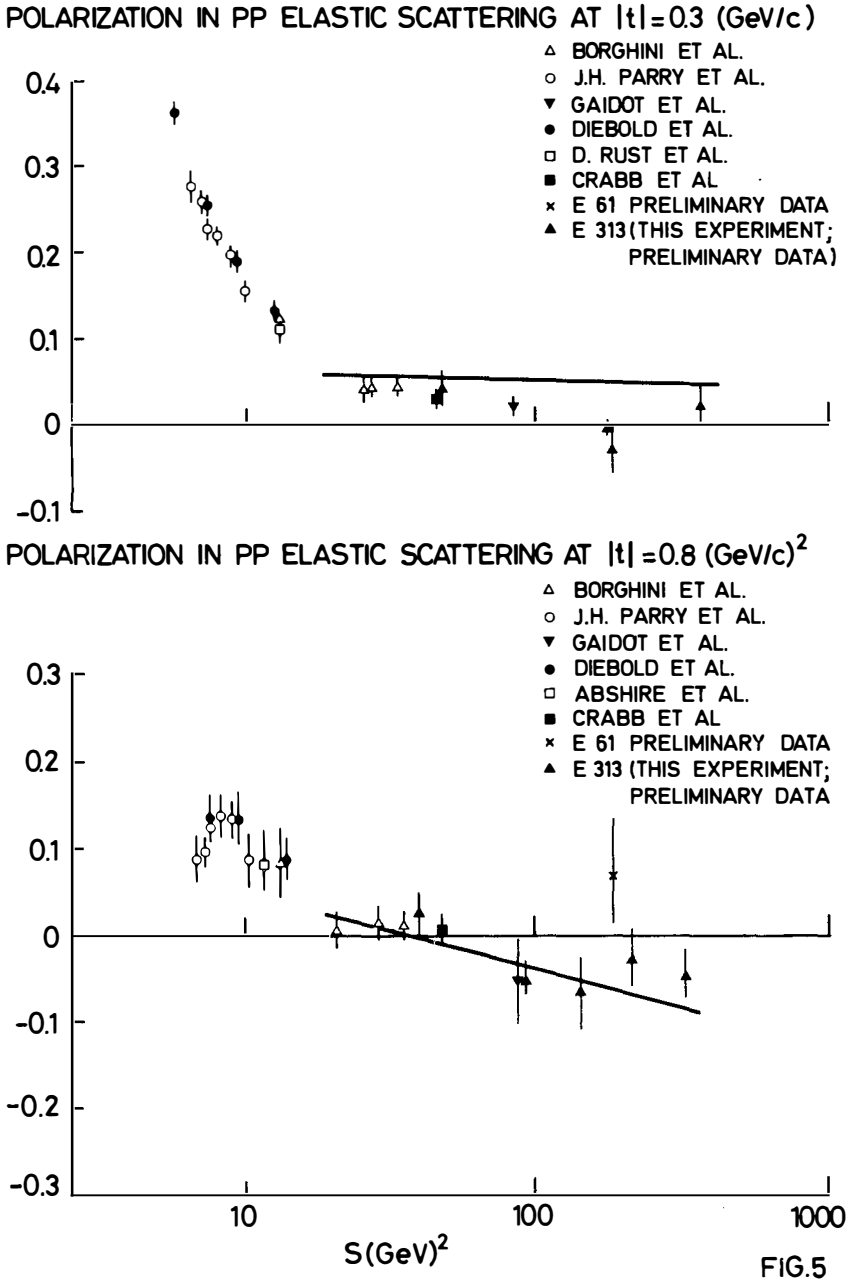

Fig. 5 : Preliminary polarization results for elastic p-p scattering at $|t|$ = 0.3 and 0.8 $(GeV/c)^2$ from the Experiment 313 at FNAL. The solid lines are the predictions of the model in Ref. 19.

for instance, by the unconventional model of Ref. 19, which gives up the assumption of the Pomeron having the quantum numbers identical to the vacuum, and computes a Pomeron exchange flip amplitude from the two-pion exchange cut in the t-channel. Although the preliminary data of this experiment do not suggest a s-dependence at large s, they are compatible, within the quoted errors, with the one suggested by the model.

The second polarization experiment running at FNAL is carried out by an Argonne-Berkeley-Fermilab-Harward-Suffolk and Yale collaboration. The incident beam, the M1 beam in the Meson Laboratory, scatters on an 8 cm long ethylene glycol polarized target, with a free proton polarization of ∿80%. Two spectrometer arms detect the scattered and the recoil particles, and two Čerenkov counters identify the scattered particle. Results for the polarization parameter in $\pi^+ p$ and $\pi^- p$ elastic scattering at 100 GeV/c have already been published[20]. Preliminary data at 100 and 300 GeV/c for pp scattering[5] are presented in Fig. 6, which shows for comparison some lower energy data (low-$|t|$[21]) and preliminary high-t[22]) data at 24 GeV/c, and the Serpukhov results at 45 GeV/c), and the preliminary results of the CENR experiment which had been communicated at Budapest last year[23]. All the data look similar for $|t| < 0.5$, showing polarization values decreasing somewhat with increasing $|t|$. For $|t|$ between 0.5 and 0.9 only the Serpukhov and the CERN data seem to suggest a negative-going polarization. For $|t|$ larger than 1 $(GeV/c)^2$ the statistical errors are such that it is difficult to identify a high energy trend in the data.

5. THE WA6 EXPERIMENT AT THE CERN SPS

I will now describe the experiment which a CERN-Padova-Trieste-Vienna collaboration is performing in the West Area of the CERN SPS (experiment WA6) and present some final results we have on pp scattering at 150 GeV/c[24].

The people participating in the experiment are G. Fidecaro, M. Fidecaro, S. Nurushev*), Ch. Poyer, V. Solovianov*) and A. Vascotto**) from CERN; F. Gasparini, M. Posocco and C. Voci from the Istituto di

*) Visitor from the Institute for High Energy Physics, Serpukhov, USSR
**) On leave from INFN, Trieste, Italy.

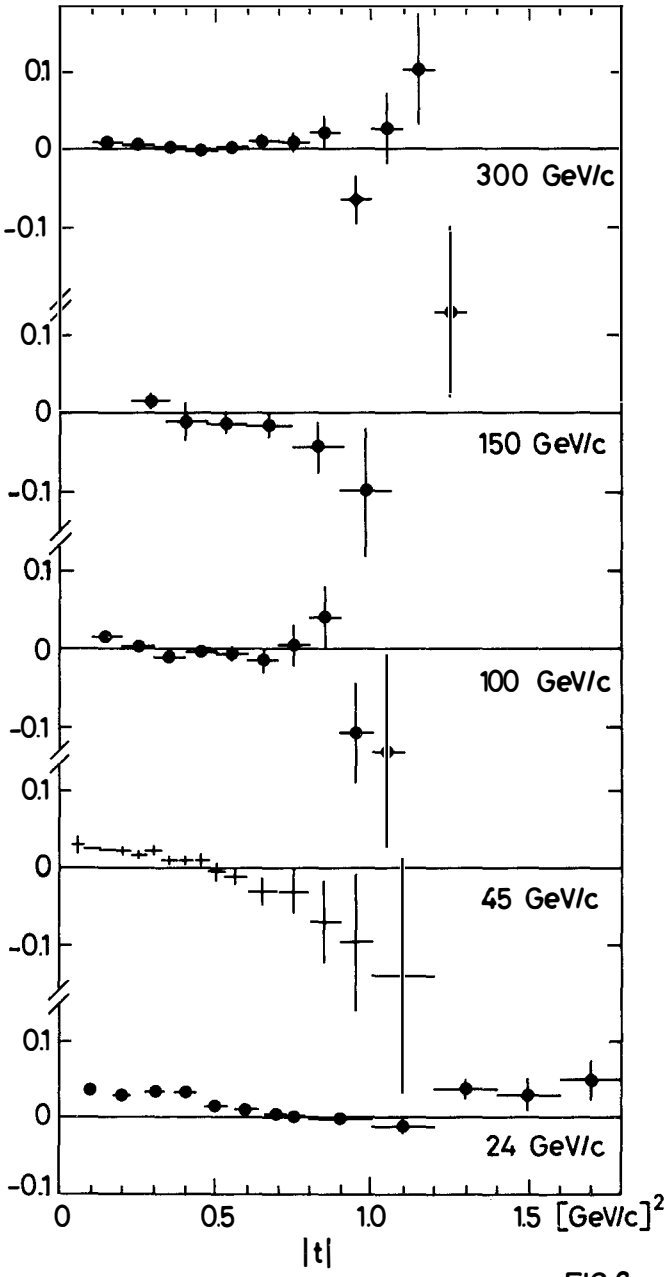

FIG.6

Fig. 6 : Polarization data in elastic p-p scattering at 24 GeV/c[21] (higher |t| data are preliminary[22]), 45 GeV/c[17], 100 GeV/c[5] (preliminary), 150 GeV/c[23] (preliminary) and 300 GeV/c[5] (preliminary).

Fisica dell'Università and INFN, Padova; R. Birsa, M. Giorgi, L. Lanceri, A. Penzo, L. Piemontese, P. Schiavon and A. Villari from the Istituto di Fisica dell'Università and INFN, Trieste; and W. Bartl, R. Frühwirth, Ch. Gottfried, G. Leder, W. Majerotto, G. Neuhofer, M. Pernicka, M. Regler, M. Steuer and H. Stradner from the Institut für Hochenergiephysik der Osterreichischen Akademie der Wissenschaften, Vienna, all of whom I want to thank for permission to show our data before they are published.

The apparatus, similar to the one of Experiment 61 at FNAL, is shown in Fig. 7. The H3 beam, 0.5 mrad production angle, 0.16 mrad horizontal divergence, 0.2 mrad vertical divergence, provided about 2.5×10^7 protons per burst (about 1 sec) on a 14 cm long propanediol polarized proton target (about 90% free protons polarization). Two spectrometers detected the scattered and the recoil protons with scintillation counter hodoscopes and M.W.P.C.'s, in the $|t|$ interval between 0.3 and 3. $(GeV/c)^2$. Data were taken simultaneously over the whole t-range, where the differential cross-section varied by more than five orders of magnitude. To write an event on tape we required:

a) at the counter level, an angular correlation between the forward and the backward hodoscope counters,

b) at the M.W.P.C. level, separate correlations between pairs of chambers in the forward and in the backward telescopes, so that only events with candidates with roughly the correct momentum and coming from the target were accepted in the two arms.

The overall triggering rate was finally reduced by suitably scaling down the low-$|t|$ triggers. In ten days of running we collected some two million events. The elastic p-p events were selected on the basis of the χ^2 given by a kinematical 4-C fit: the incident proton direction and momentum in the fit were just the corresponding beam parameters, averaged run per run. The quality of the signal and the level of the background at low χ^2 (events were finally accepted by a cut around 9, which corresponded to a 6% C.L.) can be estimated from the distributions shown for part of the data in Fig. 8, for two different $|t|$ values.

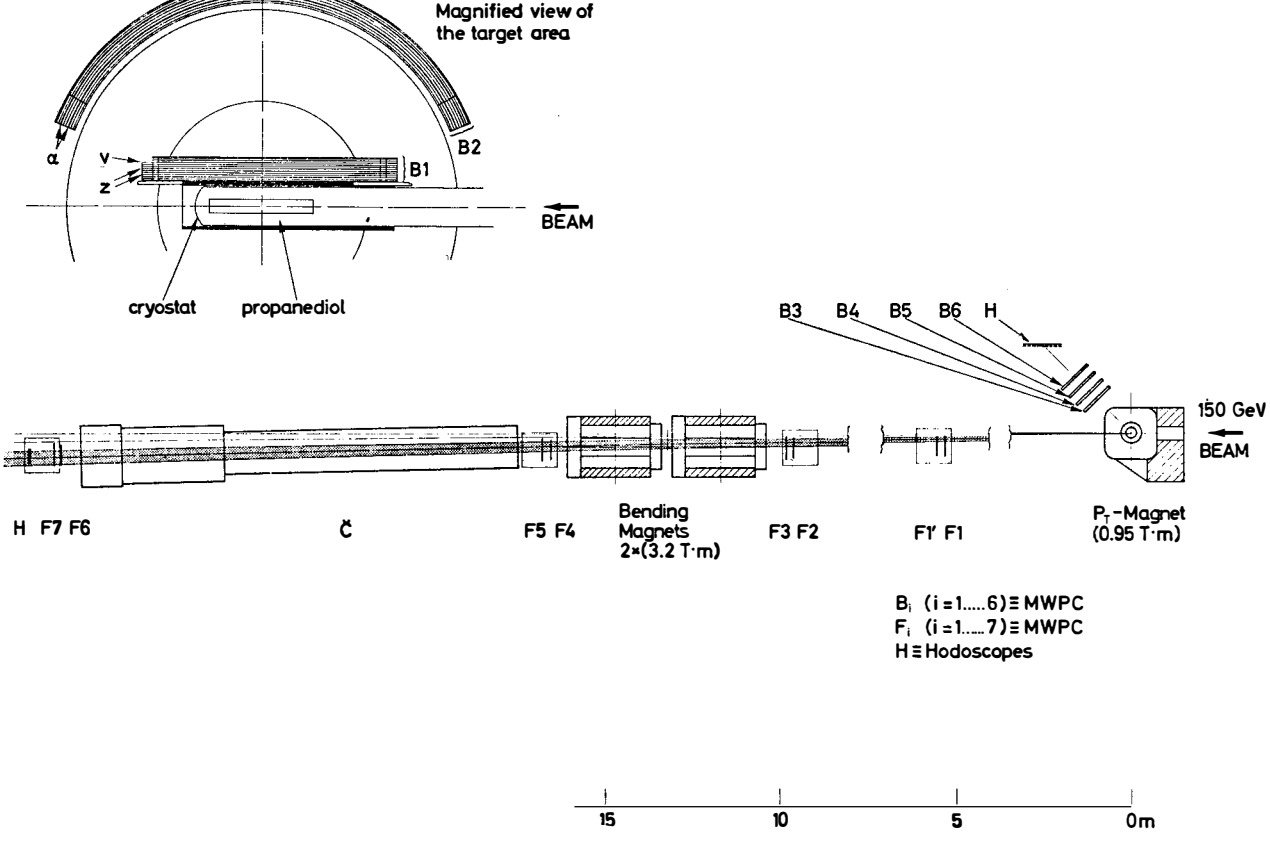

Experiment WA6: Polarization in pp and πp Elastic Scattering Fig. 7

Fig. 7 : Layout of the CERN-Padova-Trieste-Vienna experiment to measure the polarization parameter in elastic pp scattering at 150 GeV/c.

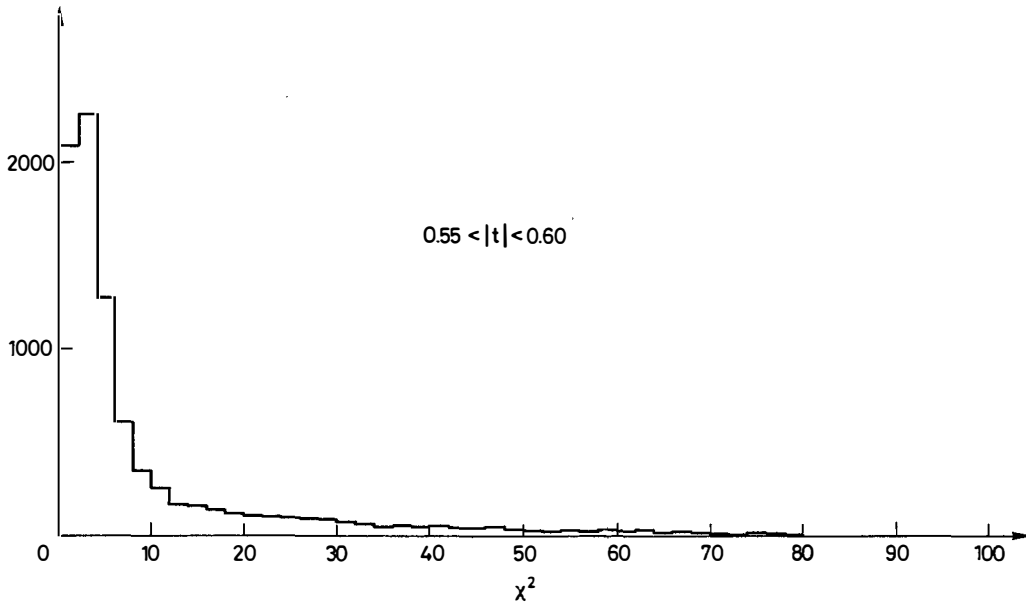

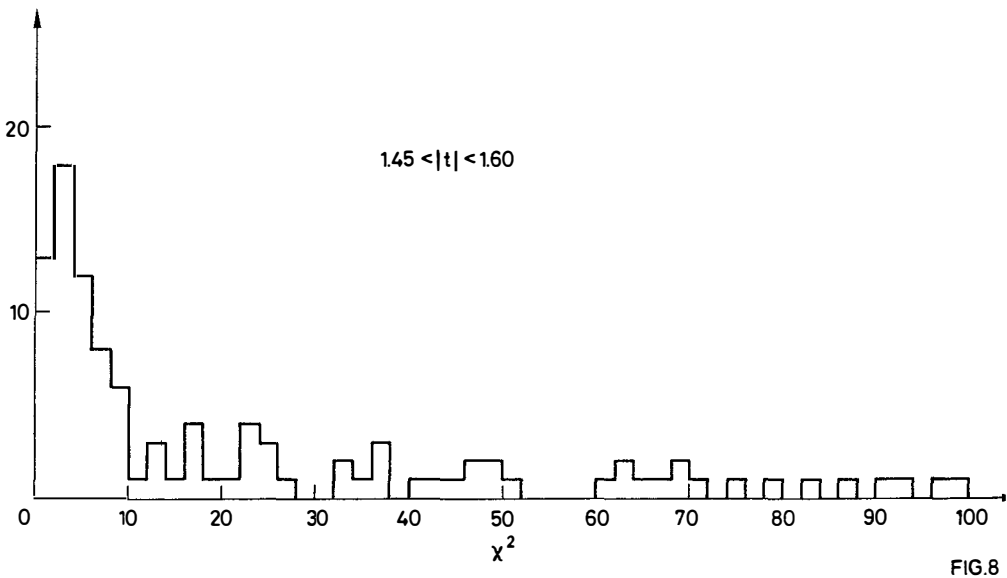

FIG.8

Fig. 8 : χ^2-distributions from the 4-C kinematical fit, for two values of $|t|$.

The polarization data are shown in Fig. 9. The position and negative target polarization runs have been normalized on the elastic events generated on a CH_2 dummy target, 1 cm thick, located in the beam, 4 cm after the polarized target, so the overall normalization error is rather small, about 1%. A large negative polarization, with the t-dependence suggested by the Serpukhov data, and by the preliminary data we have presented in Budapest last year, characterizes the data of Fig. 9. After the interference region, the polarization seems to become positive (to within one standard deviation).

The angular distribution of our elastic events, corrected by the appropriate efficiency factors, is shown in Fig. 10. No dip is yet visible in the interference region. Adding this result to the existing FNAL data[25], which show a deep dip at 200 GeV/c incident proton momentum, one concludes that the interference builds up very fast in energy. Clearly it is of great interest to spell out the energy dependence of the dip, and to monitor the behaviour of the polarization when the structure developes. We should run the experiment again in June, and our goal is an order of magnitude improvement in the statistics: but we have also plans further on, and we like to consider the results of Fig. 9 just a first glimpse into this high-energy domain.

6. CONCLUSIONS

I have shown you some data which point at large spin effects in pp scattering at high energy, effects which probably one could not have expected before the interference dip in the elastic channel was discovered at the ISR. There are also hints that high energy behaviour already characterizes the large p phenomena at energies much lower than the SPS, especially if one singles out the scattering in some definite spin states. Within one or two years many more data should come out from the experiments I have mentioned, and it will be quite a challenge for the existing constituents models to understand and reproduce those data.

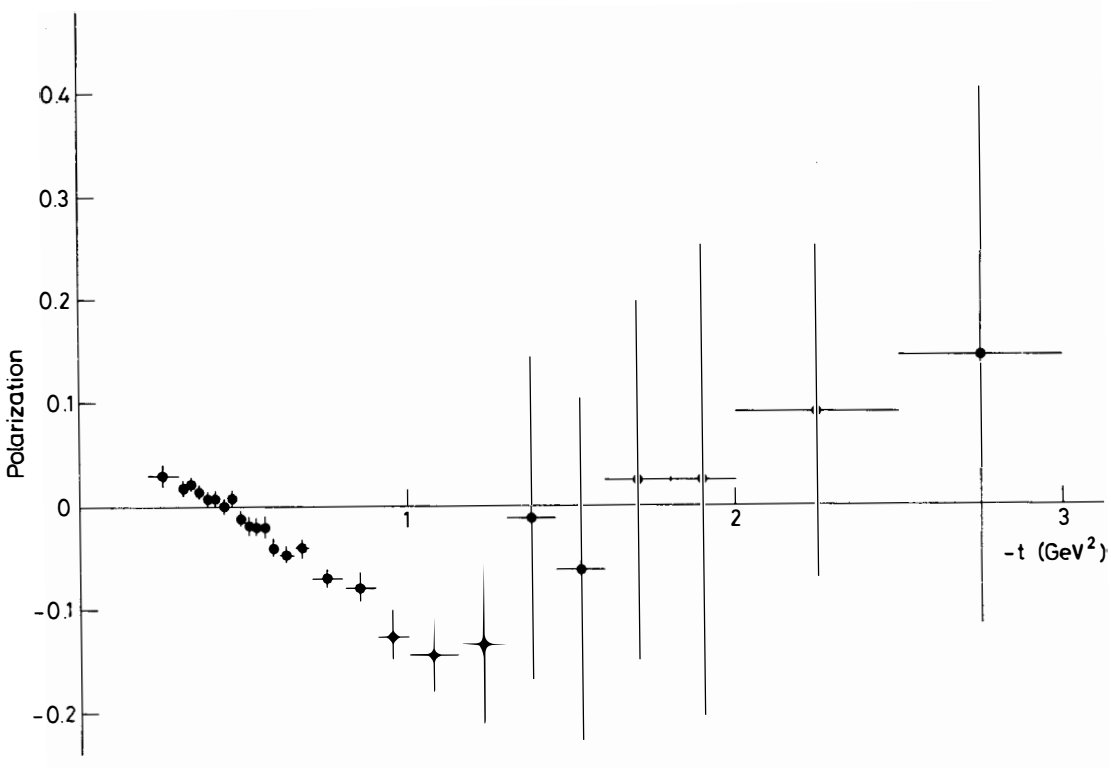

Fig. 9 : Results for the polarization parameter for elastic pp scattering at 150 GeV/c. Errors are statistical only: the overall normalization error is about 1%.

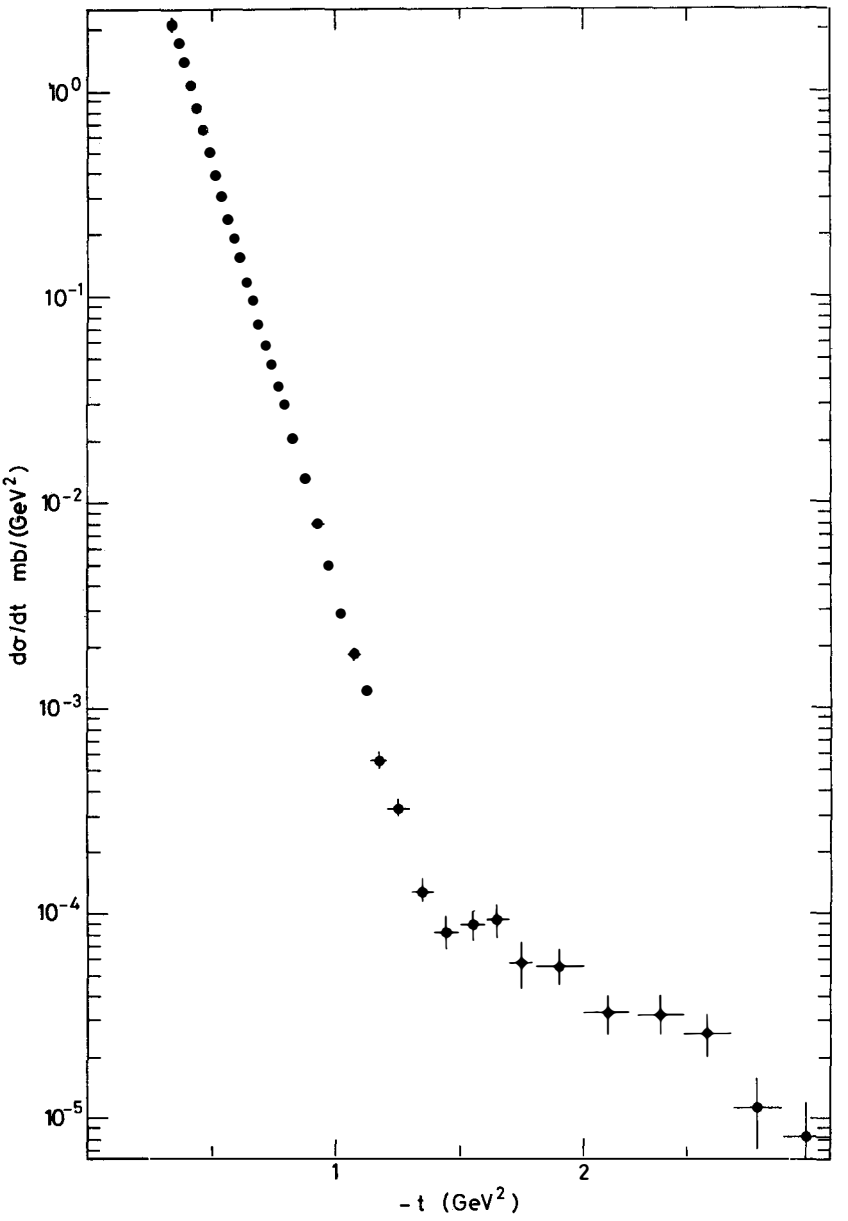

Fig.10 : Angular distribution for elastic pp scattering at 150 GeV/c.

REFERENCES

1) G. Bunce et al., Phys. Rev. Letters 36, 113 (1976).

2) K. Heller et al., Phys. Letters 68B, 480 (1977).

3) CERN-LAPP (Annecy)-Oxford Collaboration, Addendum, CERN/EEC-76/15 (1976).

4) M. Corcoran et al., Indiana University Preprint IUHEE 10.

5) H. Spinka, Argonne National Laboratory Preprint HEP-CP-77-80.

6) I.P. Auer et al., Phys. Letters 67B, 113 (1977).

7) I.P. Auer et al., Argonne National Laboratory Preprint HEP-PR-77-29.

8) E. Biegert, to be published.

9) S.L. Kramer et al., Argonne National Laboratory Preprint HEP-PR-77-74.

10) A.D. Krisch, Spin effects in proton proton scattering, Proceedings of the IX Rencontre de Moriond, 3-15 March, 1974, Vol. I, p. 103.

11) J.R. Fallon et al., University of Michigan Preprint HE 77-28.

12) A. Lin et al., University of Michigan Preprint HE 78-3.

13) A. Apokin et al., CERN Proposal SPSC/77-61/P87, July 1977.

14) I.P. Auer et al., Fermilab Proposal No. 581, January 1978.

15) J. Antille et al., CERN Proposal SPSC/77-71/P88, August 1977.

16) M.O. Corcoran et al., Indiana University Preprint IUHEE 9.

17) A. Gaidot et al. Phys. Letters 61B, 103 (1976).

18) See, for instance, W. Rarita et al., Phys. Rev. 165, 1615 (1968).

19) G.L. Kane and J. Pumplin, Phys. Rev. D 11, 1183 (1975).

20) I.P. Auer et al., Phys. Rev. Letters 39, 313 (1977).

21) D.G. Crabb et al., Nucl. Physics B121, 231 (1977).

22) Private communication from K. Kuroda.

23) G. Fidecaro et al., contribution to the European Conference on Partical Physics, Budapest, Hungary, 4-9 July, 1977.

24) G. Fidecaro et al., Evidence for spin effects in pp elastic scattering at 150 GeV/c, to be sent to Phys. Letters.

25) C.W. Akerlof et al., Phys. Letters 59B, 197 (1975).

A HIGH STATISTICS SPECTROMETER FOR THE STUDY OF ENERGY DEPENDENCE OF RESONANCE PRODUCTION

M.N. Kienzle-Focacci
University of Geneva, Switzerland

Abstract: The Geneva spectrometer is running at the CERN SPS to obtain information on the channels

$$\pi^{\pm}p \to K^0K^{\pm}p, \quad K^{\pm}p \to K^0\pi^{\pm}p, \quad p^{\pm}p \to \Lambda K^{\pm}p,$$
$$\pi^{\pm}p \to \pi K\bar{K}p, \quad K^{\pm}p \to KKKp, \quad p^{\pm}p \to pKKp,$$
$$\pi^{\pm}p \to \pi p\bar{p}p, \quad K^{\pm}p \to \Lambda pp,$$

at 50 GeV incident energy, with momentum transfer to the proton $0.05 < |t| < 1$ $(GeV/c)^2$.

Preliminary results on the positive 50 GeV data are presented.

1. INTRODUCTION

The energy dependence of exclusive two-body reactions is an important feature for understanding the dynamics of strong interactions. In the framework of a Regge-pole model, all the reactions dominated by the exchange of a Regge trajectory connecting particles and resonances must decrease rapidly with energy ($\sigma \propto p^{-n}$, n = 1-2). At high energies only the Pomeron exchange, whenever possible, will contribute. A study of exclusive channels at high energies will then give information primarily on the structure of the Pomeron.

The present group*) performed a high statistics experiment for the reactions $\pi^- p \to K^0_S K^- p$, $K^\pm p \to K^0_S \pi^\pm p$, and $pp \to \Lambda K^+ p$ at 10 GeV/c incident momentum[1-6] at the CERN PS. The study of the same reactions at higher energies, with comparable statistics, will allow us to define the effective Regge trajectory of the process and to separate the different exchange contributions by amplitude analysis. Preliminary results obtained at 50 GeV/c at the CERN SPS are presented here.

2. EXPERIMENTAL SET-UP AND DATA SELECTION

The system design (Fig. 1) is essentially the same as at the PS experiment[1]: a beam spectrometer to identify the incident particle and to analyse its direction and momentum, a recoil proton arm to measure direction and momentum of the recoil proton, and a forward spectrometer to measure the direction of the forward decay particles. No forward spectrometer magnet is used, so the momenta of the forward particles must be calculated by momentum conservation. We then have two kinematical constraints for events with a V^0 ($V^0 = K^0_S$ or Λ^0) configuration. We choose them as the total energy balance and the V^0 mass (Fig. 2).

The data acquisition system was improved with respect to the PS experiment by seven miniprocessors, which allow a maximum acquisition rate of 800 events/1 sec burst and perform the full geometrical analysis of the events during the 8 sec interburst. This allows us also to collect data on channels with three forward particles coming from the proton vertex (no V^0). For these events the energy balance is the only kinematical constraint (Fig. 3), and we separate π from K and p with a 16 cell threshold Čerenkov counter in the forward system.

The complete set of channels we may analyse is listed in Table 1, where the 50 and 10 GeV/c statistics are compared.

---

*) The SPS experiment is being performed by a Collaboration from Geneva and Lausanne Universities: B. Cleland, A. Delfosse, P.A. Dorsaz, P. Extermann, J.L. Gloor, O. Guisan, M.N. Kienzle-Focacci, G. Mancarella, M. Martin, R. Mermod, P. Muhlemann, C. Nef, T. Pal, P. Rosselet, A. Vriens, R. Weill, H. Zeidler.

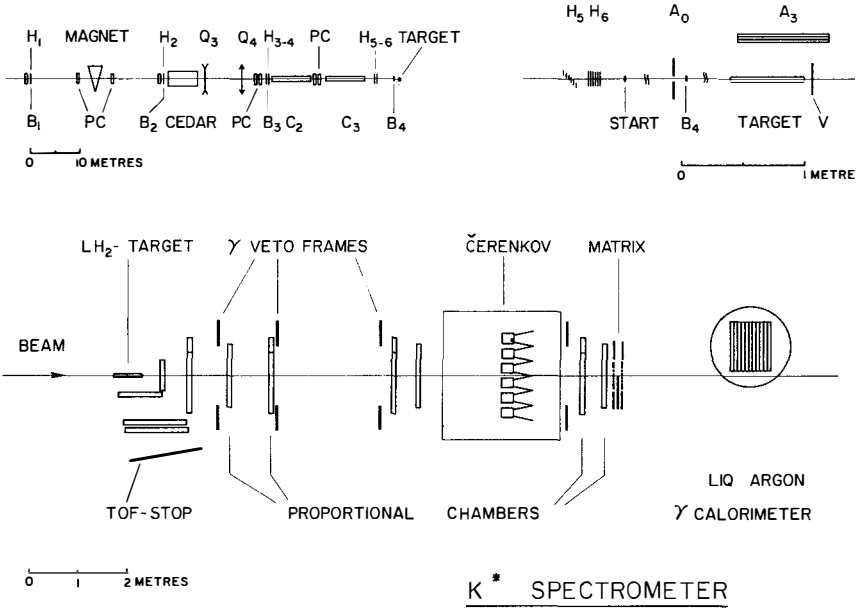

Fig. 1 Experimental layout

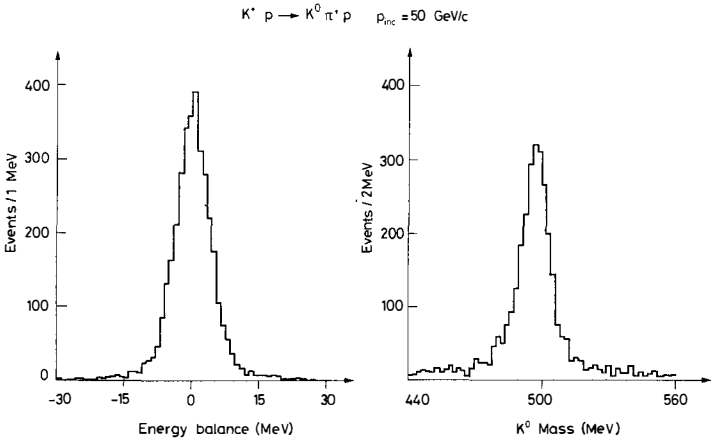

Fig. 2 Distribution of the kinematical constraints: ΔE (energy balance) and K^0 mass for the reaction $K^+p \to K^0_S\pi^+p$ ($K^0_S \to \pi^+\pi^-$) at incident momentum p_{inc} = 50 GeV/c

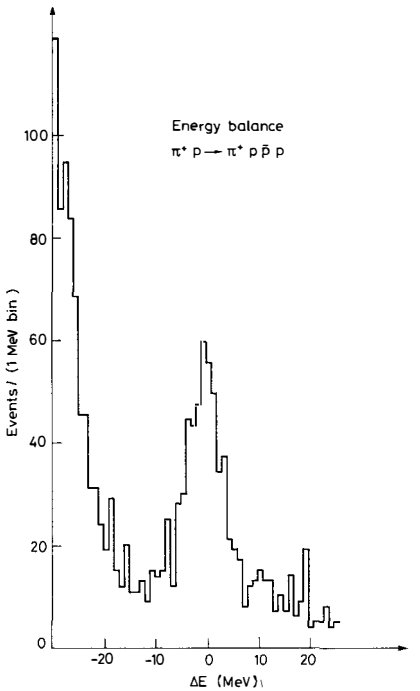

Fig. 3 Distribution of the kinematical constraint ΔE for the reaction $\pi^+p \to \pi^+p\bar{p}p$

Table 1

Statistics of the reactions $X\,p \to M\,p$
$[0.07 \leq |t| \leq 1\ (GeV/c)^2$, elastic $\leq M \leq M_{max}$
$(M_{max} = 2.3, 4.5$ for $p_{inc} = 10, 50$ GeV/c)]

Events with two kinematical constraints				Events with one kinematical constraint		
X	M	p_{inc} = 10 GeV/c	p_{inc} = 50 GeV/c	M	p_{inc} = 10 GeV/c	p_{inc} = 50 GeV/c
π	K^0K^+	-	24 000	$(\pi KK)^+$	-	200 000
				$(\pi p\bar{p})^+$	-	20 000
	K^0K^-	40 000	(40 000)	$(\pi KK)^-$	80 000	(200 000)
				$(\pi p\bar{p})^-$	-	(20 000)
K	$K^0\pi^+$	46 000	10 000	$(KKK)^+$	10 000	5 000
	$\bar{\Lambda}p$		1 000			
	$K^0\pi^-$	18 000	(10 000)	$(KKK)^-$	4 000	(5 000)
	$\Lambda\bar{p}$		(1 000)			
p	ΛK^+	12 000	15 000	pKK	9 000	20 000
	$\bar{\Lambda}K^-$	-	(7 000)	$\bar{p}KK$	-	(10 000)

Note: 10 GeV/c data have already been published[1-6]. 50 GeV/c positive data are under analysis. We are at present running on a 50 GeV/c negative beam. The numbers in parentheses are an estimate of the final sample we will have.

3. DATA ANALYSIS

The small background contamination ($\sim$ 5%) and good mass resolution ($\sigma \sim$ 10 MeV) give clean mass spectra (Fig. 4a). The forward system does not deform appreciably the angular acceptance, as one can see from the raw data angular distributions in $K^*(890)$ and $K^*(1420)$ regions (Figs. 4b and 4c).

The analysis of the positive data is in progress: Fig. 5 shows the moments of the K^+ angular distribution in the Gottfried-Jackson system for the channel $\pi^+p \to K^0K^+p$ (about 1/3 of the full sample). The moments have been corrected for acceptance with the method described in Ref. 1. The ratio between M = 2 and M = 0 even moments (J = 4 and J = 2) in the A_2 region show that the data may well be described by D^+ only. At higher masses only the signal of the 4^+ wave[5] (mass $\sim$ 1950 MeV) is still present.

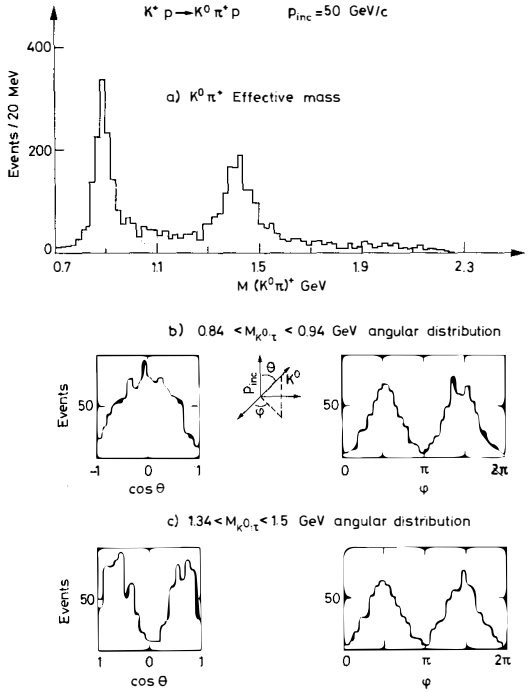

Fig. 4 (a) Effective mass of the $(K^0\pi)^+$ system after a kinematical fit has been applied to the data; (b) Decay angular distribution (cos θ and φ) of the events in the K*(890) region; (c) Decay angular distribution of the events in the K*(1420) region.

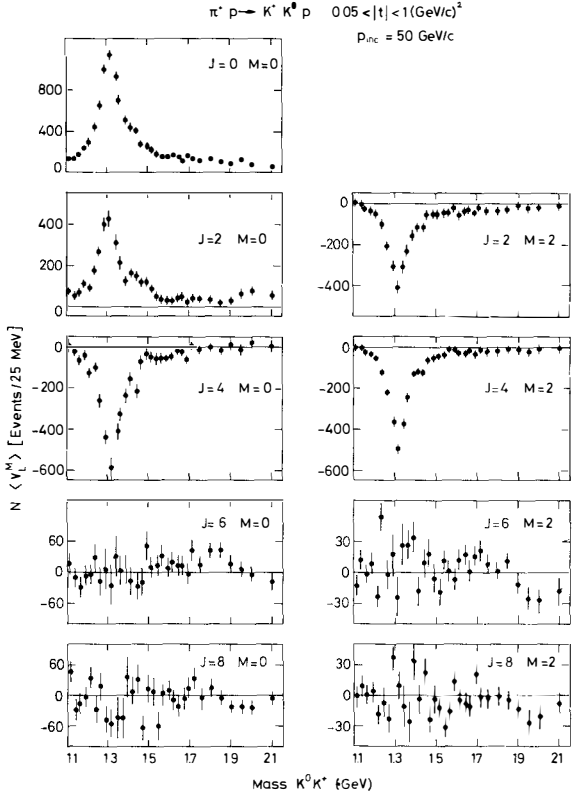

Fig. 5 The moments $N\langle Y_J^M\rangle$ of the $K_S^0K^+$ decay angular distribution as a function of K^0K^+ mass, in the t interval $0.05 < |t| < 1\ (GeV/c)^2$

REFERENCES

1) R. Baldi et al., Systematic study of $K\pi$ production in the reaction $K^{\pm}p \to K^0_S\pi^{\pm}p$: technique and measurements at 10 GeV/c, submitted to Nuclear Phys. B.

2) A.D. Martin et al., A study of A_2- and g-resonance production in $\pi^-p \to K^-K^0p$, submitted to Nuclear Phys. B.

3) A.D. Martin et al., Amplitude and natural parity exchange analysis of $K^{\pm}p \to (K\pi)^{\pm}p$ data at 10 GeV/c, submitted to Nuclear Phys. B.

4) T. Böhringer, Thesis, Dissociation diffractive dans la réaction $pp \to p\Lambda K^+$ à 10 GeV/c, CERN EP Internal Report 77-15 (1977).

5) R. Baldi et al., Observation of a spin 4, isospin 1, meson resonance, submitted to Phys. Letters B.

6) R. Baldi et al, Phys. Letters 68B, 381 (1977).

PROBING PARTON STRUCTURES WITH REAL PHOTONS*

Clemens A. Heusch
University of California
Santa Cruz, Calif.

Abstract

We discuss the information that is likely to become available from a measurement of high-$p_\perp$ single-photon production in deeply inelastic photon-hadron collisions, and its implication for the parton picture of hadronic interactions.

In this lecture, I will present some ideas on the information that is about to be obtained in a program of scattering of energy-tagged photons up to E_γ = 200 GeV, at the Fermi National Accelerator Laboratory.[1] In particular, I will stress the questions these experiments may answer with respect to the parton model of the hadrons.

Much attention in this Conference is being focused on the Drell-Yan mechanism[2] for the production of charged lepton pairs in hadron-hadron collisions. While some of the observed features of e^+e^- and $\mu^+\mu^-$ production agree well with the basic tenets of this model[3]—in particular, the difference between pp and πp-initiated reactions and certain scaling properties—it is certain that a study of the presently available dilepton data is far removed from providing a stringent test of the parton hypothesis via the Drell-Yan process. The hadron-hadronic interaction clearly appears to have too many complicating features to serve as a basic test case, and you have heard of many attempts at this meeting to make the exchange and emission of gluons describe some of them.

Recall, however, that the original postulate of the parton structure of hadrons was motivated by the scaling behavior observed in the scattering of photons, albeit virtual ones, off hadrons. The locality of the photon coupling provides the decisive ingredient of the usefulness of the graph

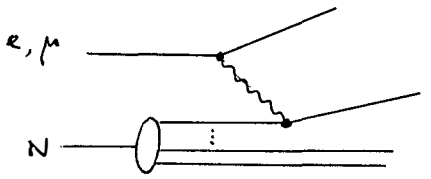

but enters only in the final state in the Drell-Yan graph. The salient difference is that in lepton scattering, the measured structure functions sum over all hadronic (final-state) channels, whereas the Drell-Yan graph picks individual hadronic two-body channels as in-states. Bjorken and Paschos[4] have early on pointed out the possibility of a more stringent test of the quark-parton model if we introduce photons not

only in the initial, but also in the final state of the reaction. They suggested the study of the process

$$\gamma N \to \gamma + \text{hadrons},$$

where the final-state photon should carry a large transverse momentum. For large $p_\perp$, the final-state photon can then tentatively be identified as being produced in a process of the type

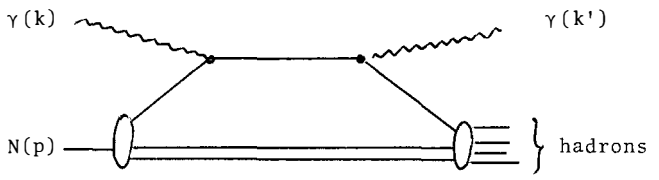

This graph, if it can be experimentally separated, is capable of yielding important information on the basic tenets of the parton model, invented for the interpretation of the scaling of the W_1, νW_2 functions of electro-production: the latter can be expressed as

$$\nu W_2^{ep,en}(\nu,Q^2) = \sum_N P(N) \times f_N(x) \left\langle \sum_i Q_i^2 \right\rangle_{p,n}$$

with the P(N) the likelihood of finding an N-parton configuration inside the target particle, p or n, $f_N(x)$ their distribution in $x \equiv \frac{Q^2}{2m\nu}$ and Q_i the quark charges (= photon couplings to the point constituents), ν is the laboratory energy loss of lepton or photon, respectively; Q^2 is the negative mass squared of the virtual photon. In complete analogy, the inelastic Compton graph leads to a structure function that incorporates the parton charges twice, and can therefore be written as

$$\nu W_2^{\gamma p,\gamma n} = \sum_N P(N) \times f_N(x) \left\langle \sum_i Q_i^4 \right\rangle_{p,n} .$$

The immediate application, suggested by Bjorken and Paschos, is a measurement of the ratio $R \equiv \frac{\left\langle \sum_i Q_i^4 \right\rangle_{p,n}}{\left\langle \sum_i Q_i^2 \right\rangle_{p,n}}$ through the

observables $\left.\frac{d^2\sigma}{d\Omega' dk'}\right|_{\nu W} = \frac{\nu^2}{kk'} \left.\frac{d^2\sigma}{d\Omega' dE'}\right|_{\ell N}$. It will clearly give an indication of the parton charges. The ratio R obviously equals one for integrally charged partons. For fractionally charged Gell-Mann -- Zweig quarks, the exact ratio is obviously dependent upon the number of sea quark-antiquark pairs that contribute to νW_2. In the absence of a color degree of freedom, Bjorken and Paschos estimated the existence of bounds $\frac{1}{3} < \frac{\sigma_{\gamma p}}{\sigma_{ep}} < \frac{5}{9}$ for identical kinematic regions. In a fairly detailed analysis of electroproduction data, Goswami and Majumdar[5] derived a number of inequalities, bounds and sum rules for γp and γn collisions; they test not only the parton concept per se, but also contain implications for the number of sea quarks/partons as well as the parton distribution function. Subsequently, Chanowitz[6] analyzed the implications of identifying the partons with the colored quarks of either the Han-Nambu variety or the Gell-Mann-Fritzsch scheme. With the introduction of the color degree of freedom, the electromagnetic current acquires a color octet piece that can change the color label of quarks:

$$J_{e.m.} = J_{1,8} + J_{8,1}$$

(where the first index refers to flavor, the second to color). For a single-photon process this can be of importance only above color threshold. The 2-photon process $\gamma N \to \gamma + x$, however, contains a singlet projection of $J_{1,8} \cdot J_{1,8}$, and may therefore show color effects even below color threshold.

Chanowitz demonstrated that, to the extent that the scaling properties of the structure functions prove correct, integrally charged colored Han-Nambu quarks will still yield a ratio R=1, with certain gauge models yielding even larger values. For fractionally charged colored quarks, the predicted bounds remain unchanged from the colorless case.

What, then, is the inherent importance of a measurement of this inelastic Compton graph, if it can be experimentally

isolated? It does several rather unique things:

1) It tests the point-parton hypothesis critically: initial and final-state particles are connected by one parton line; the parton propagator enters the cross-section explicitly.[7]
2) It provides a test of the parton model that can give information on such parameters as momentum distributions of partons and their mean number inside the nucleon.[5]
3) If scaling is observed to hold for $\nu W_2^{\gamma N}$, it allows a new determination of average parton charge parameters, and thereby of the parton-quark identification.[8]

Of these points, the first has the most fundamental importance: it gives a calculable level at which a physical process must be observed minimally. Failing that, the quark-parton model as we know it today is in serious jeopardy.

Given the importance of the information that can thus be obtained, I will now discuss the likelihood that the inelastic Compton graph can in fact be isolated and observed. Let us discuss this question from two angles: First, assuming the identifiability of single photons as opposed to photons stemming from 2γ, 3γ,... decays of mesons, what confidence can we have in their coming from the inelastic Compton graph?

It was noticed early on that, in order to make the calculations of Bjorken and Paschos applicable, the origin of the final-state photon must be certain to be the parton originally struck,

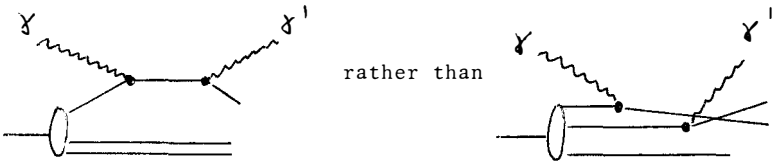

Clearly, the struck parton must propagate for a time short w.r.t. the parton-parton interaction time. This condition

comes more easily true, the larger Q^2. In the limit we have the "swallow-tail diagram", which gives no contribution from spin-½ partons. However, let us note that the momentum transfer needed to have the final-state photon emitted by a parton other than the one that absorbed the incoming photon, tends to disperse the available $p_\perp$ among the proton's constituents, so that the Bjorken-Paschos graph should predominate at the higher $p_\perp$ values.

To gain a fuller picture of single photon inclusive yields, we recall the general scheme worked out by Blankenbecker, Brodsky, and collaborators[9] for hadronic interactions, which adds quark-meson and quark-baryon interactions to the basic quark-quark process. In this context, the $p_\perp$ characteristics are dictated by the number of elementary fields involved in the interaction. They showed that, under the assumption that general Bjorken scaling hold, the graphs of the "Constituent Interchange Model" (CIM) are characterized by a transverse momentum dependence:

$$\frac{d\sigma}{dp_\perp^2} \propto \varepsilon^n p_\perp^{-m}$$

Here, $\varepsilon^n \equiv (1-x)^n$ stands for the scaling function ($\sim \nu W_2$), and m is given by the number of basic fields. In this picture, the inelastic Compton graph will be characterized by

$$\frac{d\sigma}{dp_\perp^2} \propto \varepsilon^3 p_\perp^{-4}$$

which is $\approx (1-x)^3 p_\perp^{-4}$ in the regime where νW_2 decreases. Inclusive photon production, on the other hand, can be due to a multitude of graphs where one or several quarks/partons as well as gluons are being interchanged. In sharp contrast to the above behavior, a "vector-dominance-type" graph like

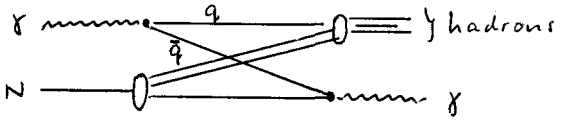

etc.

leads to a behavior

$$\frac{d\sigma}{dp_\perp^2} \propto \varepsilon^{0 \text{ or } 1}\, p_\perp^{-12} ,$$

whereas many other graphs involving various exchanges of hadronic constituents lead to intermediate $p_\perp$ behavior. We note here that

a the more complicated the exchange, the more the available $p_\perp$ will be diluted among final-state particles. Only the inelastic Compton graph leads to as 'gentle' a $p_\perp$ fall-off as $p_\perp^{-4}$;

b as we get closer to the edge of phase space, $x \to 1$, ε becomes small and may well dominate the observed cross-section.

The only published investigation of inclusive photon production from γp collisions[10] indicates that a sizable yield may be found at SLAC energies. Within the large errors of the results, the likeliest interpretation is that of a CIM conglomerate. We should, however, note that, for this experiment, the ε^N term tends to suppress the inelastic Compton graph severely. Higher energies are clearly needed to establish its existence and properties.

Consequently, in an upcoming experiment at Fermilab,[1] the Santa Cruz group will attempt to isolate the inelastic Compton graph by measuring $\gamma p \to$ single photons plus anything over a large solid angle, at $p_\perp$ values of 1 to 3 GeV. The implication for the separability of a behavior according to the transverse momentum dependence is, for the parameters

$$\left.\begin{aligned} t &\approx p_\perp^2 = 1 \text{ to } 9 \text{ (GeV/c)}^2 \\ \nu &\equiv E_\gamma - E'_\gamma = 10 \text{ to } 60 \text{ GeV} \end{aligned}\right\}$$

$$x = \frac{t}{2m\nu} = 0.01 \text{ to } .2 .$$

In this x range, however, the scaling function $\nu W_2(x)$ is essentially constant.[8] If a measurement of the $p_\perp$ dependence can be performed with sufficient accuracy to tell the power behavior cleanly apart, the ε^n dependence will thus not falsify or hide it. Even with modest statistics, the difference between the two extreme terms mentioned, $p_\perp^{-4}$ vs. $p_\perp^{-12}$, should be easily distinguished over this available

$p_\perp$ range!

Second, we ask: is a credible separation of single-photon yields from the totality of final-state particles containing π^o, η^o, ω^o,... and their decay photons possible? Present indications are that this can indeed be achieved if we limit ourselves to k'/k values > 0.3.

To understand this point, let us take a brief glimpse at the experimental setup currently in the tune-up stages at Fermilab:

Fig. 1 shows the basic setup: tagged photons with well-defined energies up to ∿200 GeV impinge on a 80 cm long liquid hydrogen target at a rate of $\sim 10^5$-10^6 per machine burst. The detection apparatus consists of two basic units: a forward detector, surrounding the beam axis with an aperture defined by its 1.50 m transverse dimension and its position that can be varied between ∿8 m and ∿30 m (it moves on a set of rails); and a recoil detector that surrounds the target at laboratory angles between 45^o and 90^o.

In order to keep all electromagnetic backgrounds at a minimum, there is no magnet in the system. The forward detector measures the energy and trajectory of all showering particles with an accuracy that can be gleaned from Fig. 2: 2a shows a pulse-height distribution for a 135 GeV electron beam incident on the forward detector: the energy is seen

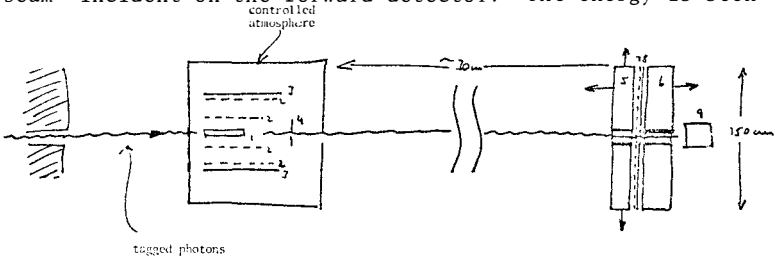

1. 80 cm liquid hydrogen target
2. drift chambers ($\Delta\phi \sim 2\pi$)
3. ToF counters
4. multiplicity counter
5. $7x^o$ 1st shower segment ($+1x^o$)
6. $11x^o$ 2nd shower segment
7. vertical hodoscope
8. horizontal hodoscope
9. central "plug" counter, $20x^o$

Figure 1: Layout for E-152 at Fermilab.

to be measured to an accuracy defined by σ = 1.6%. The shower location is measured by a fine-grain low-grade scintillator hodoscope; Fig. 2b gives transverse pulseheight distributions, binned by the width of the hodoscope elements. The gist of this information is that (1) high-energy showers due to photons or electrons can be located to an accuracy of $\lesssim$ 0.5 cm; and that (2) single-photon events can be separated from their worst "contaminants", symmetrically decaying π^o of, say, 100 GeV, at the percent level. (The two showers from 100 GeV π^o decay are separated by 8.4 cm at 30 m distance.) The loss due to very asymmetrically decaying π^o or η^o is not serious.

While the forward detector consists of total absorption counters interspersed with a hodoscope, the recoil detector is a multi-drift-chamber device that sees large-angle tracks and is not vital for these measurements.

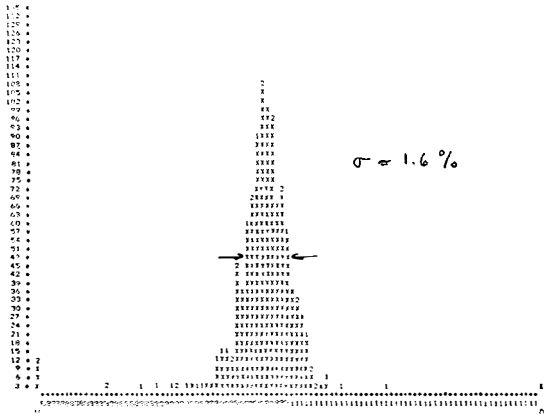

Figure 2A: Blown-up pulseheight spectrum for 135 GeV electron in shower bank of forward detector.

In an experimental run extending through spring and summer, several thousand events at $p_\perp$ values > 1 are due to be collected. I feel confident that our knowledge of basic facts on the parton structure of the hadrons will be considerably deepened by the level of their observation.

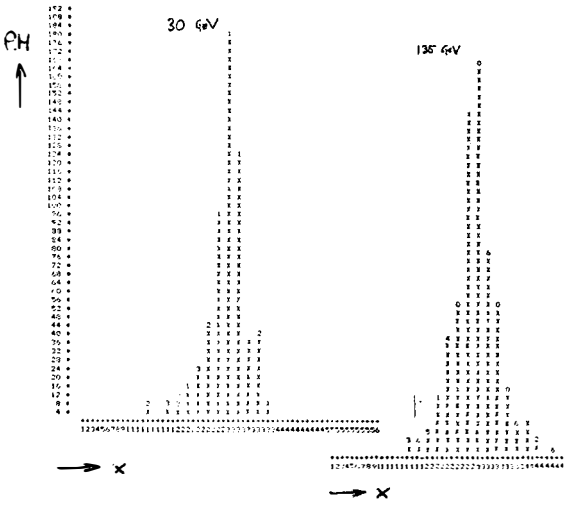

Figure 2B: Transverse size of showers in hodoscope location: bins are 3 cm. each. Electron energies: 30 GeV, 135 GeV.

Conclusion:

A clean test of the quark-parton picture of the hadronic interaction appears to be imminently available from the Santa Cruz Experiment 152 at Fermilab. While for the small momentum-transfer process $\gamma p \to \gamma p$ (elastic Compton scattering), the hadronic structure of the photon is tested as in the vector dominance picture, high-$p_\perp$ photon scattering, $\gamma p \to \gamma$ + hadrons, has a unique way of providing information on the structure of the target hadron. This two-photon process is thus expected to complement the somewhat confusing present evidence on the parton picture gleaned from recent experiments on lepton pair production in hadron-hadron collisions.

1) Fermilab Experiment 152. Experimenters: A. Breakstone, D. Dorfan, S. Flatté, A. Grillo, C. Heusch, V. Palladino, T. Schalk, A. Seiden, D. Smith.

2) S. D. Drell, T. M. Yan, P.R.L. 25, 316 (1970); Ann.Phys. (N.Y.) 66, 578 (1971).

3) J. Pilcher, these proceedings. L. Lederman, these proceedings.

4) J. D. Bjorken, E. A. Paschos, PR 185, 1975 (1969).

5) D. N. Goswami, D. P. Majumdar, PR. D4, 2090 (1971).

6) M. S. Chanowitz, LBL preprint 5312 (1976).

7) S. J. Brodsky and P. Roy, P.R. D3, 2914 (1971) pointed out limitations of field-theoretical justifications of the Bjorken-Paschos mechanism.

8) J. K. Kim (these proceedings) demonstrates that more complicated gauge models such as the broken unified color gauge theory of Pati and Salam can yield higher photon rates due to contributions from colored gluons.

9) See, e.g., R. Blankenbecler, S. J. Brodsky, P.R. D10, 2973 (1974).

10) D. O. Caldwell et al., P.R.L. 33, 868 (1974).

TESTS OF COLOR EFFECTS IN PATI-SALAM MODEL

Jae Kwan Kim and Hyun Kyu Lee
Department of Basic Science
Korea Advanced Institute of Science
Seoul, Korea

Abstract: In the unified color gauge theory of Pati and Salam, we show that the color effects are dominant in deep inelastic compton scattering and the calculations from this theory fit the experimental data very well.

Color[1] gauge theory is widely used in calculating the processes involving strong interaction at present time. However, there are two different types of models according to whether the color symmetry is broken or exact. It is an interesting and important problem for high energy physisists to test these two different points of view with experimental data. In this article, deep inelastic compton scattering data is compared with the predictions from these models and it is shown that the model with broken color symmetry by Pati and Salam[2] is definitely preferred.

The general property of the spontaneously broken unified color gauge theory, as proved by Pati and Salam[3] and by Rajasekaran and Roy[4], is that the color cannot be brightened with its whole strength in lepton-hadron processes. In this theory electron(or muon)--hadron interaction proceeds through the exchange of color photon and its orthogonal color gauge partner with the same strength. However, because of the opposite sign in amplitudes between them, the color brightening is suppressed by a factor $\Delta^2=(|q^2|/M^2+1)^{-2}$ which vanishes effectively for high momentum transfer $|q^2|>4M^2$. Thus the integer charged quarks in the unified color gauge theory would behave as if they are fractionaly charged in electron(muon)--hadron interactions asymptotically. Therefore, treating the quarks and color gluons as partons, the color contributions appear as small scaling violations (10 to 20% of flavor contributions)[3,4,5] which are not inconsistent with the present experimental data of deep inelastic electron(muon) --hadron scattering. According to the same cancelling mechanism, the color contributions from the spontaneously broken color gauge theory in all lepton hadron interactions are not so differ-

ent from the small corrections due to the asymptotically free theory[6] of exact color symmetry that one cannot find any distinctive differences between them at present energy range.

Hence, it is very important to choose appropriate physical processes in which the color suppression of the unified color gauge theory doesn't appear for the present energy range of experiments. Deep inelastic Compton scattering is the typical one, where the probing photon see the colors with its whole strength (integer charged color quarks and color gluons). Recent experiment[7] on deep inelastic Compton scattering, using 21 GeV bremsstrahlung photon beam, shows that the predictions from the conventional non gauge quark model (even for the integer charged quark model) are too low to fit the experimental data and the discrepancies are too large to be explained by the small corrections from the exact color symmetry theory. Thus it has been argued that the parton model does not have much to do with the deep inelastic compton scattering processes.[8] However, because of the large color effects of the unified color gauge theory, the situation is quite different from the conventional models; and the purpose of this article is to explain the experimental data by using the unified color gauge theory[2] combined with parton model.

In the unified color gauge theory, there are two types of partons in the hadrons: color quarks and color gluons with integer charges. The contributions of the quarks to the deep inelastic Ccmpton scattering are well known as[9]

$$\frac{d^2\sigma^{\text{quark}}}{d\Omega\, dE} = \frac{\alpha^2}{4E_0^{\,2}\sin^2(\frac{1}{2}\theta)}\left[\frac{E}{E_0}+\frac{E_0}{E}\right]\sum_{i,\alpha} Q_{i,\alpha}{}^4 f_{i,\alpha}(x), \tag{1}$$

and the contributions of the color gluons with mass M are calcu-

lated[10] as

$$\frac{d^2\sigma^{\text{gluon}}}{d\Omega\, dE} = \frac{\alpha^2}{4E_0^2 \sin^2(\frac{1}{2}\theta)} \left[4 - 2\left(\frac{E}{E_0} + \frac{E_0}{E}\right) + \frac{4}{3}\left\{\left(\frac{E}{E_0}\right)^2 + \left(\frac{E_0}{E}\right)^2\right\} + \frac{4}{3M^2}(E_0 - E)^2 \sin^2\theta\right] \sum_j Q_j^4 g_j(x). \quad (2)$$

Here E_0 and E are the energy of the incident and the scattered photon respectively; and i, α, and j refer respectively to the types of flavor (u, d, and s), three quark colors, and color gluon octets. The distribution functions of the quarks and the color gluons are represented as $f_{i,\alpha}(x)$ and $g_j(x)$ with their respective quantum numbers. The total double differential cross section is given by

$$d^2\sigma/d\Omega\, dE = d^2\sigma^{\text{quark}}/d\Omega\, dE + d^2\sigma^{\text{gluon}}/d\Omega\, dE. \quad (3)$$

For convenience, the color independent distribution functions are defined as

$$f_i(x) = \tfrac{1}{3}\sum_\alpha f_{i,\alpha}(x), \quad F_i(x) = (\sum_\alpha Q_{i,\alpha}^4) f_{i,\alpha}(x), \quad g(x) = \tfrac{1}{8}\sum_j g_j(x), \quad G(x) = (\sum_j Q_j^4) g(x), \quad (4)$$

because the known hadrons are color singlets. It can be easily seen that the quark contributions in the unified color gauge theory are larger than the other conventional models where $G(x)=0$ because

$$F_u(x) = \tfrac{5}{2} F_u^{\text{IC}}(x) = (\tfrac{2}{3})^3 F_u^{\text{FC}}(x), \quad F_{d,s}(x) = 3F_{d,s}^{\text{IC}}(x) = 27F_{d,s}^{\text{FC}}(x), \quad (5)$$

where IC and FC refer to the integer charged and to the fractional charged quark model, respectively. With Eq.(4), Eq.(3) becomes

$$\frac{d^2\sigma}{d\Omega\, dE} = \frac{\alpha^2}{4E_0^2 \sin^2(\frac{1}{2}\theta)} \times \left([\sum_i F_i(x)] \left(\frac{E}{E_0} + \frac{E_0}{E}\right) + G(x) \left\{ 4 - 2\left(\frac{E}{E_0} + \frac{E_0}{E}\right) + \frac{4}{3}\left[\left(\frac{E}{E_0}\right)^2 + \left(\frac{E_0}{E}\right)^2\right] + \frac{4}{3M^2}(E_0 - E)^2 \sin^2\theta \right\} \right). \quad (6)$$

Before integrating Eq.(6) over the bremsstrahlung spectrum

to get the experimental cross sections, one must specify the mass of the color gluon and parametrize the parton distribution function $f_i(x)$ and $g(x)$. The most probable range of the color gluon mass was recently found to be about 1 to 2 GeV by Pati, Sucher, and Woo.[11] For the quark distribution functions $f_i(x)$, the parametrization obtained from the analysis of leptonic deep-inelastic scattering[12] is used. But there is little information on the gluon distribution functions. We assume the color gluon distribution function to be a form of sea-quark-like distribution. With this assumption the gluon distribution function is parametrized by the conventional sealike functions as

$$g(x) = A(1-x)^p/x. \tag{7}$$

The normalization constant A can be obtained from the deep-inelastic electron- or muon-nucleon scattering experiments in which there must be neutral partons carrying about 50% of the nucleon momentum.[13] The color gluons are identified as neutral partons and the normalization constant is calculated in this analysis as

$$8\int_0^1 x g(x) = 0.5. \tag{8}$$

Among the various values of p, the calculation with $p = 8$ fits the experimental data better than the other values of p and is shown in Fig.1 as solid lines. This value of p is consistent with the values used in various analyses done previously on the basis of the quark-parton model.[13,14] The predictions from Eq. (6) are found to be insensitive to the mass of the color gluon, provided $M \gtrsim 1$ GeV. Thus the deep-inelastic Compton-scattering data are consistent with the constraint on M given by Pati, Sucher, and Woo.[11] The conventional quark-model calculations are shown in the same figure. The predictions from the frac-

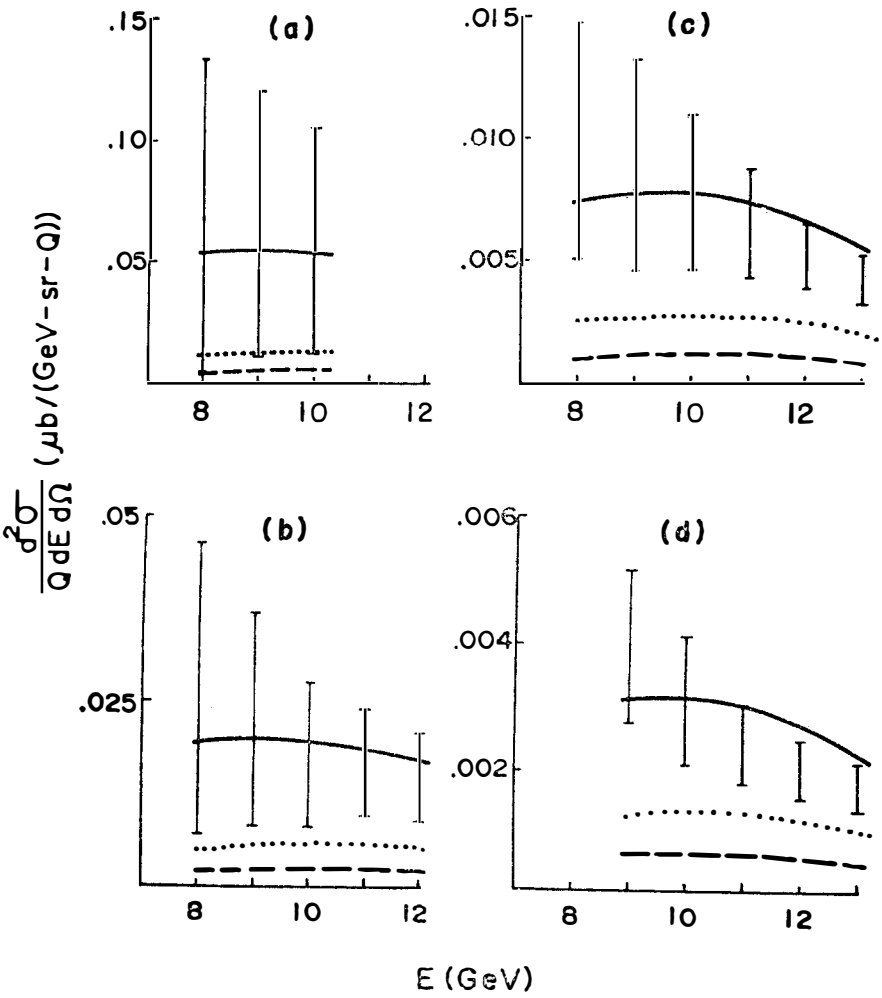

Fig. 1. Double-differential cross sections of the deep-inelastic Compton scattering per equivalent quantum (Q) for four values of p_T: (a) 1.1 GeV/c, (b) 1.3 GeV/c, (c) 1.5 GeV/c, and (d) 1.7 GeV/c, from Caldwell et al. (Fef. 7). Solid lines are the predictions by the unified color gauge theory using Eq.(6) in the text. Dashed curves are predictions from the conventional fractionally charged quark model. Dotted curves are predictions by the integer-charged model (Ref. 7).

tionally charged quark model, shown as dashed lines, are far below the experimental data and the discrepancies are too large to be explained by the small corrections from the exact color symmetry theory. The calculations from the integer-charged quark model are also shown in the same figure as dotted lines. The results are somewhat larger than the fractionally charged quark-model calculations but the values are too low to fit the experimental data.

We have presented the evidence of the color brightening of the unified color gauge theory in the deep-inelastic Compton-scattering experiment. The main point to be stressed in this article is that the charged color gluons are necessary to fit the experimental data of the deep-inelastic Compton scattering. Therefore, we need a model in which the color effects can be shown to be small corrections in the lepton-hadron interactions but the color effects are dominant contributions in the photon-hadron interactions. We would like to conclude that the spontaneously broken unified color gauge theory of Pati and Salam[2] satisfies both of the requirements very well.

This research was supported by Euisok Research Foundation.

REFERENCES

1. M.Y. Han and Y. Nambu, Phys. Rev. 139, B1006 (1965), for recent reviews see O.W. Greenberg and C.A. Nelson, Phys. Reports 320, 69 (1977)

2. J.C. Pati and A. Salam, Phys. Rev. D8, 1240 (1973); D10, 275 (1974)

3. J.C. Pati, in "Gauge Theories and Modern Field Theory", eds., R. Arnowitt and P. Nath (M.I.T., Cambridge, 1976); J.C. Pati and A. Salam, Phys. Rev. Lett. 36, 11 (1976)

4. G. Rajasekaran and P. Roy, Pramana 5, 303 (1975); Phy. Rev. Lett. 36, 355 (1976)

5. J.C. Pati and A. Salam, ICTP preprints IC/76/76.

6. H.D. Politzer, Phys. Rev. Lett. 30, 1346 (1973); D. Gross and F.W. Wilzeck, Phys. Rev. Lett. 30, 1343 (1973)

7. D.O. Caldwell et al., Phys. Rev. Lett. 33, 868 (1974)

8. F.J. Gilman, in "Proceedings of the 17th International Conference on High Energy Physics, London, England, 1974", ed. by J. Smith (Rutherford High Energy Laboratory, Didcot, Berkshire, England, 1975)

9. J.D. Bjorken and E.A. Paschos, Phys. Rev. 185, 1975 (1969)

10. H.K. Lee and J.K. Kim, Phys. Rev. Lett. 40, 485 (1978) ; Phys. Rev. D, (1978, to be published)

11. J.C. Pati and J. Sucher and C.H. Woo, Phys. Rev. D15, 147 (1977)

12. R. McElhaney and S.F. Tuan, Phys. Rev. D8, 2267 (1973); Nucl. Phys. B72, 487 (1974)

13. R.D. Field and R.P. Feynman, Phys. Rev. D15, 2590 (1977)

14. D.W. Duke and F.E. Taylor, FERMILAB-Pub-77/95-THY (unpublished)

RFT AND OTHER THINGS

P. Grassberger
University of Wuppertal,
Germany

Abstract: Reggeon field theory is shown to be mathematically equivalent to a simple chemical process where a radical can undergo diffusion, absorption, autocatalytic production, and recombination. Physically, these "radicals" are wee partons. The mathematical apparatus of RFT can thus be replaced by a very intuive and physically simple picture of interacting partons.

Résumé: On montre que la theorie des reggeons est mathématiquement équivalent à un processus chimique simple, où un radical peut subir la diffusion, l'absorption, la reproduction autocatalytique, et la récombinaison. Physiquement, ces "radicaux" sont des partons mous. L'appareil mathématique de la RFT est donc remplacé par une image intuive et physiquement simple des partons interagissants.

The aim of this talk, based on work by K. Sundermeyer and myself [1], is to show that the highly non-trivial mathematical apparatus of reggeon field theory (RFT) corresponds indeed to a very simple physical model. Thus, while the mathematical treatment will stay accessible only to experts, non-experts can replace it by their physical intuition.

To start with, let me recall some facts of

1. Reggeon Field Theory

The basic objects we shall study are the k-pomeron amplitudes of a given state $|\Phi(y)>$,

$$\phi_k(\vec{b}_1,\ldots\vec{b}_k;y) = \frac{1}{\sqrt{k!}} <o|\psi(\vec{b}_1)\ldots\psi(\vec{b}_k)|\Phi(y)>. \qquad (1)$$

Here, $\psi(\vec{b})$ is the pomeron field, and we work evidently in the Schrödinger picture where

$$\frac{d}{dy}|\Phi(y)> = -H|\Phi(y)> . \qquad (2)$$

In practice, $|\Phi(y)>$ will be produced by an external particle with rapidity y, whence ϕ_k corresponds graphically to the vertex:

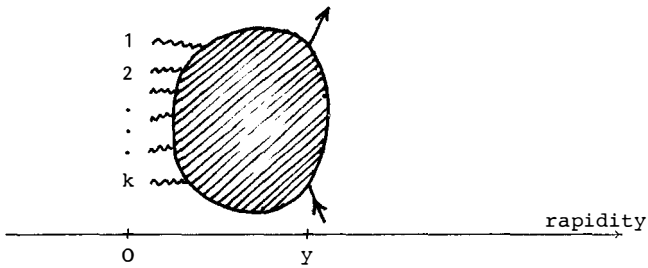

For simplicity, we shall in the following work only in zero transverse dimensions (D = 0), although the results are true in any number of dimensions. In D = 0, we replace $\psi(\vec{b})$ and $\psi^\dagger(\vec{b})$ by annihilation and creation operators a and $a^\dagger$, and the theory is defined by the hamiltonian

$$H = (1-\alpha_p)a^\dagger a + \frac{ir}{2}a^\dagger(a^\dagger+a)a + \frac{\lambda}{4}a^{\dagger 2}a^2 . \qquad (3)$$

Here, α_p, r, and λ are bare parameters, and the quartic coupling has been included for reasons which will become evident below.

Alternatively, the physical content of the theory is completely contained in the equations of motion of the amplitudes

$$\frac{d}{dy}\phi_k = (\alpha_P - 1)k\phi_k - \frac{ir}{2}(k-1)\sqrt{k}\,\phi_{k-1} - \frac{ir}{2}k\sqrt{k+1}\,\phi_{k+1} - \frac{\lambda}{4}k(k-1)\phi_k . \qquad (4)$$

The theory defined by Eqs.(3) or (4) and their generalizations to $D \neq 0$ has a number of well-known features which greatly complicate its mathematical analysis:

- H is not hermitean;
- in $D > 1$ there occurs a critical phenomenon at $\alpha_P = \alpha_c$ similar to a second order phase transition;
- for $\alpha_P > \alpha_c$, one cannot as in other theories with second order transitions build the Hilbert space around a new shifted vacuum: both the unperturbed ground state and the shifted vacuum seem to be stable;
- as there is no unanimity among experts about the latter point, there exist claims both that σ_{tot} decreases with energy for $\alpha_P > \alpha_c$ [2], and that σ_{tot} increases $\sim \ell n^2 s$ [3].

At this point, I shall leave the further discussion to the experts, and pass on to my next subject which is

2. Chemical Reactions

Instead of justifying my interest in this field, I simply ask you for some patience: in order not to get lost in discussions about the underlying physical picture, I shall first present some mathematical facts, and give my physical interpretation later.

We consider radicals called R which are contained in a vessel together with other molecules N and M. The number of the latter is kept fixed. We assume that we stir well so that the only relevant observable is the number of radicals R which can change due to the following reactions:

$$R + N \underset{\mu}{\overset{\kappa}{\rightleftarrows}} 2\,R \qquad \text{(autocatalysis)} \qquad (5a)$$

$$R + M \xrightarrow[\kappa']{} A \qquad \text{(absorption)} \qquad (5b)$$

$$R + R \xrightarrow[\nu]{} B \qquad \text{(recombination)}. \qquad (5c)$$

The molecules A and B are inert.

If one neglects all fluctuations, one can easily convince oneself of the "rate equation"

$$\frac{d}{dt}\langle n\rangle = \kappa n_N \langle n\rangle - \kappa' n_M \langle n\rangle - (\tfrac{\mu}{2}+\nu)\langle n\rangle^2 \ . \qquad (6)$$

Here, n is the number of R, while n_N and n_M are the (fixed) numbers of N and M. Using generating function techniques[1], one can also set up the analog equations where all fluctuations are exactly taken into account. For the binominal moments

$$n_k = \langle n(n-1)\ldots(n-k+1)\rangle \qquad ; \ k = 1,2,3,\ldots \qquad (7)$$

one finds, with $\sigma = \kappa n_N$ and $\rho = \kappa' n_M$,

$$\frac{d}{dt}n_k = (\sigma-\rho)kn_k + \sigma(k-1)kn_{k-1} - (\tfrac{\mu}{2}+\nu)kn_{k+1} - \tfrac{\mu+\nu}{2}k(k-1)n_k \ . \qquad (8)$$

The crucial observation now is that Eq.(8) has exactly the same structure as Eq.(4). More precisely, Eqs.(8) and (4) become identical if we identify

- time with rapidity (not with i×rapidity!)
- reggeon parameters in a suitable way with rate parameters, and
- $\sqrt{k!}\,\phi_k/\phi_o$ with $(i\sqrt{(\mu/2+\nu)/\sigma})^k \cdot n_k$, i.e. the k-pomeron amplitude with the k-th binomial moment.

Notice that the equivalence exists only when the quartic coupling is non-zero. Indeed, the usefulness of such a coupling has been pointed out also in the standard formulation[4),5)] for purely mathematical reasons.

In order to arrive at RFT with $D \neq 0$, one has to replace the vessel by the full space of D dimensions. Also, one replaces stirring by diffusion, and one assumes that interactions are local. In this way one finds in a rigorous way that the k-pomeron amplitudes correspond to the inclusive k-radical densities.

As a first application of this analogy, let me discuss the nature of the phase transition. The 1-pomeron Green's function

$G(\vec{b}',\vec{b};y) = \langle o|\ \psi(\vec{b}')\, e^{-Hy}\, \psi^+(\vec{b})\,|o\rangle$ corresponds in our model to the density at point $\vec{b}'$ and time $t = y$, provided a single radical was implanted at $t = o$ at the point $\vec{b}$. Now $\alpha_P << 1$ corresponds to the case of weak autocatalytic production but large absorption ($\sigma >> \rho$; see Eqs. (8),(4)), and thus the density will decrease exponentially with time. If we increase α_P (i.e. enhance production and/or suppress absorption), the decrease of the density will be slower and slower until, for $\alpha_P = \alpha_c$, the total number of radicals increases, and for $\alpha_P > \alpha_c$ even the asymptotic density is non-zero. The occurence of this "non-equilibrium phase transition" has first been observed by Schlögl[6], who used the rate equation Eq.(6). The order parameter is thus the asymptotic density which is proportional to the asymptotic opacity at finite impact parameter.

We are thus immediately led to the conclusion that the Froissart bound is saturated for $\alpha_P > \alpha_c$, in agreement with Ref.[3]. This conclusion is based not so much on a sophisticated mathematical analysis (the mathematical methods applied so far to the above kind of chemical reactions are rather crude [7-9]), but on our physical intuition: the solution suggested by White[2] would mean that, when enhancing the production rate through the critical value, the density at large (fixed) time first increases but then decreases again. (Notice also that our formulation is non-perturbative, and thus no ambiguity arises as how the theory is to be defined for $\alpha_P > \alpha_c$).

3. Physical interpretation

Up to now, our findings might merely represent a mathematical curiosity, without any deep physical meaning. But it is not: the underlying physics is the parton model, and the radicals R are nothing but wee partons.

As stressed by Feynman[10], the parton density inside a hadron of rapidity y reaches from zero to y:

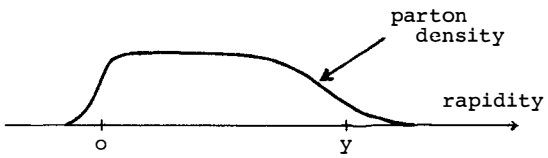

If partons were non-interacting during a boost of the hadron from y to y'>y, their density after the boost would reach down only to y'-y, in contrast to the above assumption. For consistency, we must thus assume that wee partons are created during the boost:

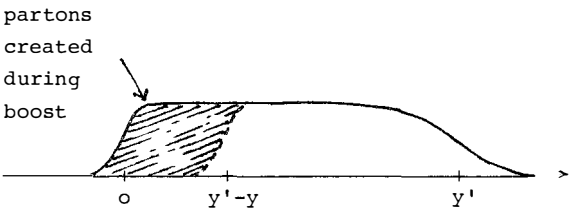

Feynman's hypothesis was now that hard partons do not interact, and thus only wees can have created new wees by splitting. Including possible recombinations, the following can happen to wee partons during a boost:

* wee $\rightleftharpoons$ wee + wee
* wee $\longrightarrow$ hard
* wee + wee $\longrightarrow$ hard

These are exactly the same reactions as in Eq.(5), and thus wees behave during a boost exactly as the above radicals behave during time evolution.

4. Discussion and outlook

Several applications and extensions of the above ideas are immediate[1,11]. I have no time to discuss them here. Instead, I would like to stress the importance of having a physical interpretation of RFT for improving the extremely crude underlying model. What I think of in particular are energy conservation[12], hard scattering effects, and a more realistic description of parton splitting as e.g. provided by the Altarelli-Parisi equations in QCD[13]. More fundamentally, our approach shows clearly that the parton model (and RFT in particular) is a stochastic approximation to the underlying basic field theory (QCD?) and a basic question is how to justify such an approximation.

References

1) P.Grassberger and K.Sundermeyer, Wuppertal preprint WU B 78-1 (1978).

2) A.R.White, CERN preprints TH 2259 (1977), 2449 (1978).

3) D.Amati et al., Nucl.Phys. B112, 107; B114, 483 (1976).

4) J.B.Bronzan and R.L.Sugar, Phys.Rev. D16, 466 (1977).

5) M.Ciafaloni, M.Le Bellac, and G.Rossi, Nucl.Phys. B130, 388 (1977).

6) F.Schlögl, Z.Physik 253, 147 (1972).

7) C.W.Gardiner, K.J.McNeil, D.F.Walls, and I.S.Matheson, J.Stat.Phys. 14, 307 (1976).

8) A.Nitzan, P.Ortoleva, J.Deutch, and J.Ross, J.Chem.Phys. 61, 1056 (1974).

9) C.Y.Mou, G.Nicolis, and R.M.Mazo, Oregon preprint (1977).

10) R.P.Feynman, 5th Hawaii Topical Conf. on Particles; P.N.Dobson et al., Eds. (1973).

11) P.Grassberger, Nucl.Phys. B125, 83 (1977); P.Grassberger and F.Guerin, Nucl.Phys. B13 (1978); P.Grassberger and K.Sundermeyer, preprint WU B 78-3 (1978).

12) A.Capella, these proceedings.

13) G.Altarelli and G.Parisi, Nucl.Phys. B126, 298 (1977).

FORWARD-BACKWARD MULTIPLICITY CORRELATIONS

A. Capella
Laboratoire de Physique Théorique et Particules Elémentaires,

Orsay(France)

Abstract : The correlation function between the multiplicities in the forward and backward center of mass hemispheres measured at CERN-ISR are quantitatively reproduced in the framework of the reggeon theory in the eikonal approximation, with standard parameters determined from elastic scattering data only.

Résumé : Les fonctions de correlation entre les multiplicités dans les hémisphères avant et arrière mesurées au CERN-ISR sont reproduites de façon quantitative dans le cadre de la théorie de reggeons, dans l'approximation eikonal, avec des paramètres standard déterminés à partir des seules données élastiques.

The purpose of this talk is to present a brief survey of some results obtained in collaboration with A. Krzywicki. For details consult ref. [1].

The effective hadronic forces have a short range in rapidity space and are soft. Thus one expects no dynamical long-range rapidity correlations in multiparticle final states : short range order (SRO). The useful concept of SRO is related to the idea of representing diffractive scattering by the exchange of the Pomeron Regge pole - the latter resulting from the contribution of final states obeying short range order in the unitarity equation. However, a Regge pole cannot satisfy by itself unitarity and one has to consider its successive iterations in the s-channel. It is easy to show that the latter violate SRO and introduce long-range rapidity correlations.

Recently, an ISR collaboration has measured the correlation between the multiplicities in the forward and backward center of mass hemispheres. A sizeable correlation is found which does not decrease through the ISR energy range. If such a long-range rapidity correlation is due to the multi-Pomeron-exchange amplitudes, its numerical value puts strong constraints on these amplitudes. It turns out that the eikonal model, with the proton-proton-pomeron coupling determined from elastic scattering data, yields the measured value of the forward-backward correlation.

First, we are going to obtain the expression of the forward-backward correlation in a very general frame work, without any dynamical assumptions regarding the relative strength of the various multi-pomeron amplitudes.

Let N(y) denote the rapidity density of secondary (charged) particles. For definiteness we work in the c.m.s ; the total energy in this frame is denoted by W. We assume that N(y) is the sum of a fluctuating number of "elementary" densities

$$N(y) = \sum_{j=1}^{n} N_o^{(j)}(y) \ , \qquad (1)$$

with the following properties :

(a) Distinct "elementary" densities are statistically independent :

$$< N_o^{(j)}(y) N_o^{(k)}(y') > = < N_o^{(j)}(y) >< N_o^{(k)}(y) > \text{ for } j \neq k.$$

(b) All "elementary" densities have identical average properties

and thus the superscript (j) is usually superfluous.
(c) The moment functions $\langle N_o(y_1)...N_o(y_k)\rangle$ exhibit short range rapidity correlations only.

From eq.(1) and properties (a) and (b) one finds :

$$\langle N(y) \rangle = \langle n \rangle \langle N_o(y) \rangle \tag{2}$$

$$\langle N(y)N(y') \rangle = \langle n \rangle \langle N_o(y)N_o(y') \rangle + n(n-1) \langle N_o(y) \rangle \langle N_o(y') \rangle \tag{3}$$

The standard inclusive correlation function is defined as

$$C(y,y') = \langle N(y)N(y') \rangle - \langle N(y) \rangle \langle N(y') \rangle - \langle N(y) \rangle \delta(y-y') \tag{4}$$

Using relations (2) and (3) one gets

$$C(y,y') = C_{SR}(y,y') + x(0) \langle N(y) \rangle \langle N(y') \rangle \tag{5}$$

where we have introduced the specific symbol

$$x(\alpha) = \langle n^{2(1-\alpha)} \rangle / \langle n^{1-\alpha} \rangle^2 - 1 \tag{6}$$

and(*)

$$C_{SR}(y,y') = \langle n \rangle [\langle N_o(y)N_o(y') \rangle - \langle N_o(y) \rangle \langle N_o(y') \rangle - N_o(y)\delta(y-y')]$$

is just $\langle n \rangle$ times the standard correlation function for an "elementary" density - which, according to condition (c) is a short-range one. Thus, a long-range correlation is present if and only if $\langle n^2 \rangle \neq \langle n \rangle^2$, i.e. if n fluctuates.

Let us introduce the forward-backward correlation. In the following $N_F(N_B)$ denotes the number of (charged) secondaries with positive (negative) center of mass rapidities :

$$N_F = \int_{y>0} dy\, N(y) \quad , \quad N_B = \int_{y<0} dy\, N(y). \tag{7}$$

[Obviously $\langle N_F \rangle = \langle N_B \rangle = \langle N \rangle / 2$].

(*) The above formula for C_{SR} does not take into account possible Bose-Einstein symmetrization effects which are not relevant for our discussion.

We are interested in the correlation between N_B and N_F. More precisely, we consider the regression of N_B versus N_F, i.e. the dependence of the average backward multiplicity, $\langle N_B(N_F)\rangle$ on the forward multiplicity N_F[3]. As is well known, $\langle N_B(N_F)\rangle$ would be a linear function of N_F if $N_{B,F}$ were normally distributed. This linearity is actually expected and is borne out by the data. The linear regression is a standard problem in probability theory. We set $\langle N_B(N_F)\rangle = a + b\, N_F$ and we determine the coeficients a and b by requiring that $\langle [N_B - (a+b\, N_F)]^2\rangle$ is as small as possible. The result for the slope b is

$$b = \{ \langle N_F\, N_B\rangle - \langle N_F\rangle \langle N_B\rangle \} / \{ \langle N_F{}^2\rangle - \langle N_F\rangle^2 \}$$

or, using eqs.(4) and (7)

$$b = \int_{y>0} dy \int_{y'<0} dy' C(y,y') / \{ \int_{y>0} dy \int_{y'>0} dy' C(y,y') + \langle N_F\rangle \} \qquad (8)$$

Eq.(8) is exact and independent of any model. With exact SRO, $b \to 0$ when $\langle N\rangle \to \infty$. This is obvious from eq.(8): the numerator is of order 0(1), while the denominator increases indefinitely. The situation changes radically in the presence of long-range correlations ($x(0) \neq 0$). It can be seen from eqs. (5) and (8) that in this case one expects $b \to 1$. This limit should be approached from below if the short-range correlation is positive (this is the case experimentally).

In order to perform the integrals in eq.(8) one has to know $C_{SR}(y,y')$. The short range rapidity correlations have been extensively studied. People often fit the shape of $C_{SR}(y,y')$ with a Gaussian

$$C_{SR}(y,y') \sim \exp\{ - (y-y')^2/4\delta^2 \}, \qquad (9)$$

and find $\delta \simeq 0.6$[4]. The normalization for $y \simeq y' \simeq 0$ can be obtained from eq.(5) :

$$C_{SR}(0,0) = \{ R(0) - x(0) \} \langle N(0)\rangle^2, \qquad (10)$$

where R is the normalized inclusive correlation function

$R(0) = \langle N(0)^2\rangle / \langle N(0)\rangle^2 - 1,$

which is almost constant through the ISR energy range ($R(0) = 0.6$)[5]

It is now trivial to compute the numerator of eq.(8) - for which eqs.(9) and (10) can be used. In order to compute the denominator we use :

$$\int_{y>0} dy \int_{y'>0} dy'\, C(y,y') = f_2/2 - \int_{y>0} dy \int_{y'<0} dy'\, C(y,y'), \qquad (11)$$

where f_2 is Mueller's correlation parameter $f_2 = D^2 - \langle N \rangle$ which is of course, known from experiment. The final result is

$$b = Q/\{(D/N)^2 - Q\} \qquad (12a)$$

$$Q = x(0)/2 + 4 \langle N(0) \rangle^2 \delta^2 \{R(0) - x(0)\} \langle N \rangle^2 \qquad (12b)$$

Setting $x(0) = 0$, one can use eq.(12) to compute the contribution to b expected when there are only short-range rapidity correlations. At the highest ISR energies, one finds $b \simeq 0.1$ whereas the experimental value is $b \simeq 0.3$. It is therefore excluded that the forward-backward multiplicity correlation results from the short-range correlation. Obviously, in order to compute the contribution to b of the long-range correlation one needs a dynamical theory of the multi-pomeron amplitudes which, in turn, allow one to compute $x(0)$. Before turning to this calculation, we have to emphasize that eq. (12) is not realistic at present energies. Indeed, the total c.m. energy, W, has to be partitioned among the n "elementary" densities. Thus, the energy relevant for one "elementary" density is, in average, roughly equal to W/n. This introduces some modifications in the derivation of eqs.(12) given above. These modifications are straightforward if one parametrizes $\langle N \rangle$ and $\langle N(0) \rangle$ by a power of W in the ISR energy range. It turns out that $\langle N \rangle = 2.10\, W^{0.435}$ and $\langle N(0) \rangle = 0.777 W^{0.256}$ describe the data reasonably well in this energy range. One then obtains instead of eq.(12b)

$$Q = x(0.435)/2 + 4 \langle N(0) \rangle^2 \delta^2 \{R(0) - x(0.256)\}/\langle N \rangle^2 \qquad (12b')$$

Let us turn next to the calculation of $x(\alpha)$. The averaging with respect to n involved in this calculation is defined as

$$\langle n^\alpha \rangle = \sum_{n=1}^{\infty} \sigma_n n^\alpha / \sum_{n=1}^{\infty} \sigma_n,$$

where σ_n is the cross-section for the production of n "elementary" densities (n cut pomerons in a regge language). Obviously, σ_n, can only be obtained in a dynamical framework. We have used perturbative reggeon calculus in the eikonal approximation. It turns out that the contribution to x(0) of the reggeon graphs proportional to the first power of the triple pomeron coupling is smaller than 15 %. (This is due to a partial cancellation between those graphs). Thus, the effect of inelastic diffraction in the forward-backward correlation is very small and we restricted ourselves to the purely eikonal graphs. The only parameter is the proton-proton-pomeron coupling which was parametrized as g(t) = a exp(bt) ; the parameters a and b were determined from the experimental values of σ_{tot}^{pp} and σ_{el}^{pp} (the ratio of the two-pomeron cut over the one pomeron exchange is then of the order of 0.3). Thus one can compute σ_n with no free parameter, using the AKG cutting rules[6]. From eqs.(12a) and (12b') we obtained then b ≃ 0.3 at the highest ISR energies - in excellent agreement with the experimental result. It should be pointed out that eqs.(12a) and (12b'), together with the experimental value of b, put a very strong constraint on any model for the multipomeron amplitudes. It is remarkable that the standard eikonal model passes the test (many other models will not).

Before concluding, I would like to mention that the above mechanism for long-range rapidity correlations predicts a very specific violation of the local compensation of charge in multiparticle events : the violation should appear in the 4th order zone correlation function, and is absent from the 2nd order correlation function - the only one measured until now.

REFERENCES

[1] A. Capella and A. Krzywicki, Orsay preprint LPTPE 78/5, to be published in Phys. Rev.

[2] S. Uhlig et al. Nucl. Phys. B132, 15 (1978).

[3] A discussion of this problem can be found in J. Benecke and J. Kühn, Munich preprint MPI-PAE/Pth 36/77 and J. Benecke et al. Nucl. Phys. B110, 488(1976). Comments on the same problem, based on identical physical premises as those of our paper can be found in A. Capella and A. Krzywicki, Proc. of the XIIth Rencontre de Moriond 1977 (ed. J. Tran Thanh Van) and M. Le Bellac, Proc. European Conf. on High Energy Physics Budapest 1977.

[4] T. Kafka et al. Phys. Rev. D16, 1261(1977),
K. Eggert et al. Nucl. Phys. B86, 201(1975),
S.R. Amendolia et al. Nuovo Cim. 31A, 17(1976).

[5] See the reviews by L. Foà, Physics Reports 22C, 1(1975) and J. Whitmore, Physics Reports 27C, 187(1976) which contain references to the original works.

[6] V.A. Abramovskii, O.V. Kancheli and V.N. Gribov, Proc. XVIth Int. Conf. on High Energy Physics, Chicago-Batavia 1972.

SUMMARY TALK - HADRONIC INTERACTION SESSION

Steven Frautschi *
Laboratoire de Physique Théorique et Particules Elémentaires,**
Orsay(France)

Abstract: We review the recent work on calculating jets and large p_T events by perturbative QCD. Special emphasis is placed on the QED origins of the ideas. We also discuss prompt lepton pairs and baryonium.

Résumé: Nous rendons compte des calculs récents concernant les jets et les évènements à grand p_T dans le cadre du chromodynamique quantique (QCD) perturbatif. Les origines (électrodynamique quantique: QED) de ces idées sont mises en évidence. Nous discutons aussi de la physique des paires de leptons à grands moments transverses et de la physique du baryonium.

* On sabbatical leave from California Institute of Technology Pasadena, California 91125 U.S.A.

** Laboratoire associé au C.N.R.S. Postal address: LPTPE. Bât.211 Université de Paris-Sud 91405 Orsay France.

Introduction

In the summary I shall focus on three subjects: calculating with QCD in perturbation theory, prompt lepton pairs, and baryonium. QCD perturbation theory will be treated in greatest detail because I feel it has been the key new theoretical development at the conference.

I. Calculating Jets and Large p_T Events by Perturbative QCD.

In spite of its beauty, QCD has been frustrating inasmuch as so disappointingly little can be derived about the observed hadrons - for example, one cannot prove that quarks and gluons bind to form p's and π's. The trouble is that while we hope eventually to use non-perturbative techniques, for example solitons or instantons, the only reliable calculational technique available at present is perturbation theory -the expansion in powers of the quark-gluon coupling strength g^2.

Calculations of the vacuum polarization indicate that $\alpha_k \equiv g_k^2/4\pi$, the "effective" or "running" coupling constant, varies with momentum transfer k in the manner depicted in Fig.1. At $k << 1$ GeV, one finds $\alpha_k \gtrsim 1$: perturbation theory clearly fails. At $k > 1$ GeV, the logarithmic falloff of α_k raises the hope that perturbation theory can be applied. But unfortunately,as in QED, the actual expansion parameter in most practical calculations turns out to be $\alpha_k \ell n\, k/m > 1$, where m is either the quark or the gluon mass, so the hope that perturbation theory will converge is frustrated.

Why does α_k commonly appear multiplied by $\ell nk/m$? A very general insight into the phenomenon, based on elementary quantum mechanics, was offered by Lee and Nauenberg[1] in 1964. Consider the Hamiltonian

$$H = H_o + \alpha H_I \tag{1}$$

with

$$H_o \psi_n = E_n \psi_n . \tag{2}$$

In second order perturbation theory we have

$$\psi'_i = \psi_i + \alpha \sum_{n \neq i} \frac{(H_I)_{ni} \psi_n}{E_i - E_n} . \tag{3}$$

The key point is that large changes occur, even for small α, if the states are nearly degenerate.

Suppose, for example, that ψ_i represents the electron state and the ψ_n represent the continuum of $e+\gamma$ states. We let γ have

Nevertheless, factors such as $\alpha_k \ln E/m_q \ln E/m_H$, of order $\gtrsim 1$, remain. The phenomena of bremsstrahlung in QCD and QED seem so closely related that it is natural to try to use the very general Lee-Nauenberg analysis to locate experimental quantities which are free of these logarithms.

I shall discuss several cases which illustrate the main points of the recent work.

Case A is the reaction

$$e^+e^- \to \gamma \to \text{hadrons} . \qquad (13)$$

Old application: In $e^+e^- \to$ hadrons the γ is colorless and all hadronic final states, degenerate and nondegenerate, are summed over. Thus all $\ln p/m_q$ and $\ln p/m_{gluon}$ terms should cancel and the rate should be expansible in powers of α_k. And indeed, one finds by explicit calculation

$$R \equiv \frac{\sigma(e^+e^- \to \gamma \to \text{hadrons})}{\sigma(e^+e^- \to \gamma \to \mu^+\mu^-)} = \sum_i Q_i^2 \left(1 + \frac{\alpha_k}{\pi}\right) . \qquad (14)$$

The fact that the second term does not contain a logarithm, and is thus only a correction of order 20 %, is of course crucial to the phenomenological use of R as an indicator of fundamental charges.

New application: While R is very important, the information on quark jets contained in perturbation theory has been lost by summing over final states. Sterman and Weinberg[3] sought to retain the information on jets while obtaining a convergent expansion in α_k at the same time. For this purpose they considered the cross-section

$$(e^+e^- \to \gamma \to q\bar{q} + q\bar{q}\,\text{gluons} + \ldots)$$

for events with all but a fraction ε of the energy lying inside a pair of opposing cones of half-angle δ (Fig.3). As discussed in the photon case, the gluon bremsstrahlung is strongest when k and θ (the angle between the gluon line and the emitting q or $\bar{q}$ line) are small. These are the configurations where the $q\bar{q}$ gluon state is nearly degenerate with the $q\bar{q}$ state. To sum over all approximately degenerate states one must integrate not only over small k (the upper limit being characterized by ε rather than ΔE in the Sterman-Weinberg formalism) but also over $\theta \leq \delta$ (ie. over hard collinear gluons). The dominant correction term is thereby softened

a small fictitous mass m_γ ; thus the continuum E_n begins at $E_o + m_\gamma$. In this example the sum in (3) becomes an integral of type $\int dE_n/(E_i - E_n)$ with lower limit $E_i + m_\gamma$ and some high energy cutoff M, and the change in state is

$$\psi'_i - \psi_i \sim \alpha \ell n M/m_\gamma . \qquad (4)$$

The diagnosis that the logarithm is caused by nearly degenerate states immediately suggests the cure:

To obtain physical quantities expansible in α_k rather than $\alpha_k \ell n k/m$ one must sum over the nearly degenerate states.

The logs resulting from mixing among the nearly degenerate states then cancel out. This is a reflection of what happens in the degenerate limit where $\ell n\, m_\gamma$ becomes singular. The standard prescription for eliminating the singularity is to diagonalize H_I in the subspace of degenerate states, which of course can only be done if we include all the degenerate states together.

A famous example is the behavior of QED as $m_\gamma \to 0$. The rate for each of the individual processes

$$\begin{aligned} ep &\to ep \\ ep &\to ep\gamma \\ &\cdots\cdots\cdots \end{aligned} \qquad (5)$$

has logarithmic infrared divergences as $m_\gamma \to 0$. But when these degenerate final states are summed over, one finds that

$$\sum_n \sigma(ep \to ep + n\gamma)$$

with

$$\sum_{i=0}^{n} E_i \leq \Delta E \qquad (6)$$

is finite.

Another example is the logarithmic divergence of QED as $m_e \to 0$. Of course, this example is less famous because m_e is not really zero, and the effective expansion parameter $\alpha\, \ell n\, k/m_e$ which occurs remains substantially less than one for the physical value of m_e. But in QCD we shall be interested in the analogous expansion parameter $\alpha_k \ell n k/m_q$, which can exceed unity. The $\ell n\, m_e$ divergence arises from the familiar property that bremsstrahlung from a fast-moving charge is emitted preferentially at small angles. For example in $ep \to ep\gamma$, the amplitude for radiation off the final charge line (Fig.2) is proportional to

$$A = \frac{2\,\varepsilon \cdot p_2}{(k + p_2)^2 - m_e^2} \qquad (7)$$

where ε_μ is the photon polarization, and we treat the electron as spinless for simplicity. Using the on-shell kinematics $k^2=0$, $p_2^2=m_e^2$ we find

$$A = \frac{\varepsilon \cdot P_2}{k \cdot p_2} \quad \cdots\cdots\cdots$$

$$= \frac{\varepsilon \cdot p}{k(E_2 - p_2 \cos\theta)} \quad \cdots\cdots\cdots \qquad (8)$$

where θ is the angle between $\vec{p}_2$ and $\vec{k}$. At $p_2 >> m_e$, we have $E_2 \simeq p_2$ and (8) becomes

$$A \simeq \frac{\varepsilon \cdot p_2}{k p_2 \left(1 - \cos\theta + \frac{m_e^2}{2p_2^2}\right)} \quad \cdots\cdots\cdots \qquad (9)$$

which exhibits clearly the preferential emission at small angles and the role of m_e in cutting it off. When the energy dominator becomes small the e and e γ states become nearly degenerate; this happens in (9) not only at $k \to 0$ but also at $\theta \to 0$. When $m_e=0$ the small angle behavior $(1-\cos\theta)^{-1} \sim \theta^2/2$ of the denominator is only partially compensated by the effect of transverse γ polarization in the numerator $[\varepsilon . p_2 = -\vec{\varepsilon} \cdot \vec{p}_2 = -p_2 \sin\theta \sim -p_2\theta]$; overall the amplitude is of order $1/k\theta$. Squaring the amplitude and integrating over phase space, we find that the key factors at small k and θ are

$$\int \frac{d^3k}{k_o} \int d\cos\theta \left| \frac{1}{k\theta} \right|^2 \sim \int \frac{dk}{k} \int \frac{d\theta}{\theta} \qquad (10)$$

The integral over k, cut off by a fictitious photon mass, leads to $\ell n\, p_2/m_\gamma$; the integral over θ , cut off by m_e/p_2 as we have seen in Eq.(9), leads to $\ell n\, p_2/m_e$.

In a familiar case such as the calculation of $\sigma(ep \to ep)$ at high energy and large angle, the $O(\alpha)$ radiative corrections reduce the elastic rate by (approximately) a factor

$$[\ 1 - \alpha c\ \ell n\ \frac{p}{m_e}\ \ell n\ \frac{p}{m_\gamma}\ ] \qquad (11)$$

where c is of order 1. When we add $\sigma(ep \to ep\gamma)$ with $k \leq \Delta E$ as dictated by the experimental conditions, the overall reduction factor is softened to the finite value

$$[\ 1 - \alpha c \ell n\ \frac{p}{m_e}\ \ell n\ \frac{p}{\Delta E}\ ]\ , \qquad (12)$$

still a substantial reduction because the numerous nearly-degenerate final states involving hard $(k > \Delta E)$ photons with small θ are not counted by the experiment.

In 1959 Kinoshita and Sirlin[2] noted a case where the experimental conditions imply a sum over all the nearly-degenerate states- hard, nearly-collinear photons as well as soft photons -with the corresponding disappearance of $\ell n\ m_e$ as well as $\ell n\ m_\gamma$ factors. Specifically they calculated the order α radiative corrections to $\mu \to e\ \nu\bar{\nu}$. As usual the virtual-photon correction reduced the rate for $\mu \to e\ \nu\bar{\nu}$ by a factor of the form (11). Adding the rate for $\mu \to e\ \nu\bar{\nu}\gamma$ with $k \leq \Delta E$ removed the $\ell n\ m_\gamma$ singularity, leaving the standard correction of the form (12). Finally, when the <u>total</u> rate was calculated including all hard as well as soft photons (i.e. by raising ΔE to its kinematics limit) the remaining $\ell n\ m_e$ singularity cancelled leaving a small correction of order α . To summarize : one finds a divergent $[O(\alpha \ell n\ p/m_e\ \ell n\ p/m_\gamma)]$ change in the final state ($e\ \nu\bar{\nu}$ replaced by $e\ \nu\bar{\nu}\gamma$ and, eventually, multi-photon states), a substantial but finite $[\ O(\alpha\ \ell n\ p/m_e)\ ]$ change in electron energy (depletion of large p_e increase in small p_e events as the hard collinear photons borrow energy) and a small $[O(\alpha)]$ change in overall rate.

With these classic results for QED in mind, it is quite easy to understand the recent proposals for QCD. Of course, QCD differs in certain respects, for example:

i) Both gluons and quarks are colored so both can radiate bremsstrahlung.

ii) In confined QCD, hadrons have no overall color, so there are no true infrared divergences -all integrals representing color radiation are cut off at a long -wavelength or low- frequency scale set by the hadron binding energy m_H.

from $\alpha_k \ln \sqrt{s}/m_q \ln \sqrt{s}/m_{gluon}$ to $\alpha_k \ln \delta \ln \varepsilon$. For sufficiently large δ and ε (eg. $\delta = 15°$ and $\varepsilon = 0.2$) the corrections are of order α_k with no large logarithms. Thus Sterman and Weinberg obtain calculable jets characterized by a cone with

$$p_T \sim p_L \delta \sim \frac{\sqrt{s}}{2} \delta \qquad (15)$$

rather than by the usual cylinder characterized by a constant p_{T_o}. If they had included in their jets only $p_T < p_{T_o}$, gluons would have been emitted copiously at larger p_T, ie. cylindrical jets would not contain most of the events and would be subject to large corrections of order $\alpha_k \ln \sqrt{s}/p_{T_o}$.

In summary: the perturbative QCD corrections reduce the $q\bar{q}$ final state by a factor of form $1 - \alpha_k \ln \sqrt{s}/m_q \ln \sqrt{s}/m_H$, ie. by close to 100 %, largely replacing it by a $q\bar{q}$ gluon state, but when the two nearly degenerate states are added the overall rate is changed by only $O(\alpha_k)$. The original back-to-back momenta of the q and $\bar{q}$ get spread over a distribution that peaks within opposing cones of order 15° (2-jet events) with a tail at larger angles (3-jet events).

In attempting to verify the Sterman-Weinberg proposal one encounters a complication: the non-perturbative conversion of quarks and gluons into hadrons. One assumes (without good theoretical justification) that this introduces a further contribution of order 350 Mev to the transverse momentum within a jet. At present energies ($\sqrt{s} \lesssim 8$ GeV) the perturbative contribution $p_T \alpha \sqrt{s}$ is not sufficiently greater than the non perturbative contribution 350 Mev to verify that p_T is rising -especially since jets are not visible below about $\sqrt{s} = 4$ GeV. However, when $\sqrt{s}$ is increased to the 20-30 GeV range in the next generation of colliding beams, a clean test should be possible. The outcome will be crucial for the theory.

Case B is typified by the reaction

$$p + p \rightarrow p + p \qquad (16)$$

at large angles such as 90 °. A typical subprocess is $qq \rightarrow qq$ with gluon exchange. Evidently pp scattering is an exclusive process, with nearly-degenerate states not summed in either the initial or final state. Therefore, the Lee-Nauenberg type argument cannot be employed to justify the use of perturbation theory in this case.

Case C is typified by the reaction

$$e + p \rightarrow e + X. \qquad (17)$$

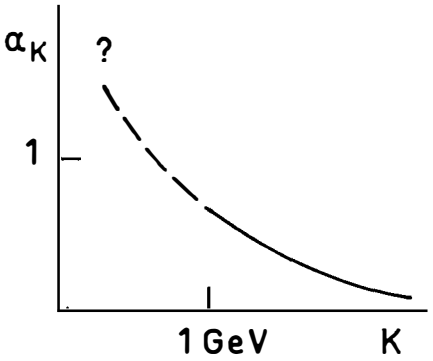

Fig. 1 : The dependence of $\alpha_k = g_k^2/4\pi$ on k in QCD.

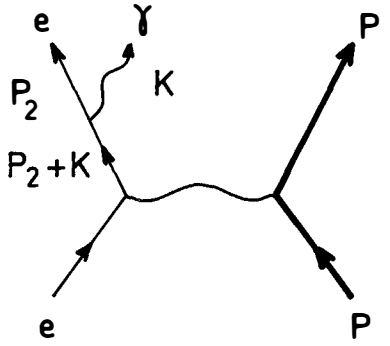

Fig. 2 : The lowest order Feynman diagram for radiation off the final electron line in ep → epγ.

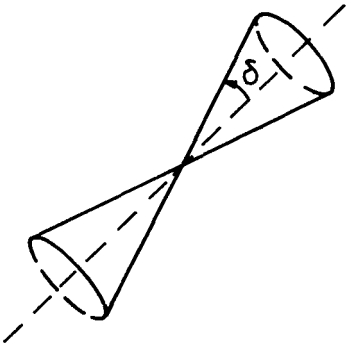

Fig. 3 : Two opposing cones of half-angle δ.

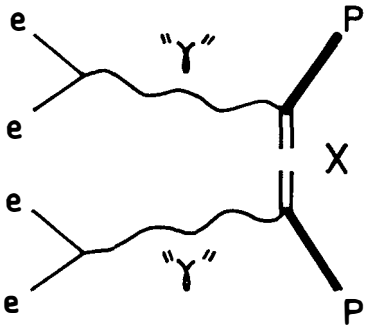

Fig. 4 : Diagramatic representation of the squared matrix element for ep → eX.

Old application: It is well known that the cross-section factors into the known ee"γ" vertex times the absorptive part of the forward Compton amplitude for a virtual photon (Fig.4).

$$\sigma(ep \to eX) \propto \text{Im Amp } (\text{"}\gamma\text{"}p \to \text{"}\gamma\text{"}p;\ 0^\circ) \qquad (18)$$

This forward Compton amplitude is normally studied by means of the operator product expansion, but it is interesting to look at it from the present perspective. The forward amplitude represents an important case intermediate between examples A and B. From one point of view, although all final states are summed over, states nearly degenerate with the initial state are not summed; therefore we expect that the radiative corrections give large logarithms and a non-convergent perturbation series.

On the other hand, we are dealing with forward elastic scattering, and from QED we expect that if no acceleration of charge (color) occurs, there should be no radiation. So we have essentially a case of ∞ times zero, and closer investigation is required.

For QED the investigation was made by Kinoshita in a classic 1962 paper[4]. For QCD, while not everyone is convinced yet, analogous results have been found in low-order perturbation theory and, in leading log approximation, to all orders[5] The Kinoshita result, for forward elastic amplitudes, is that large logarithms do occur, but only in the form of multiplicative factors associated with the charged (colored) external lines. These large, factoring logarithms refer to the dissociation of e into e+ γ , q into q + + gluon, etc.... In our case this implies

i) Everything about "γ"p $\to$ "γ"p can be calculated in perturbation theory except the state

$$|p> = C_1\ |qq\bar{q}> + C_2\ |qqq\ \text{gluon}> + C_3\ |qqqq\bar{q}> \ \ldots \qquad (19)$$

which must be treated by phenomenological "structure functions".

ii) Because of the factorization property, the structure function for $|p>$ is independent of the process; thus once determined in "γ"p $\to$ "γ"p it can be applied to any process one desires.

iii) If one attempts to estimate the proton structure functions in perturbation theory via diagrams such as Fig.(5), one obtains contributions of order $\alpha_k \ln(Q^2/m_q^2)$. These are the "scaling violations".

iv) The qualitative trend of the scaling violations can be seen as follows: radiation of photons (gluons) occurs in response to acceleration of the charge (color) and grows with acceleration. Thus the gluon emission grows with the momentum transfer Q^2 received from

"γ". But the gluon takes energy from the original parton. Thus, with growing Q^2, the distribution of Feynman x in the proton structure function will shift to lower values -quarks with large x will be depleted and quarks with low x will be enhanced. This is the same trend found in work based on renormalization group calculations on "moments" of the distribution function[6].

New application: recently Politzer[7], Hinchliffe and Llewellyn-Smith[7], Sachrajda[8], and others have extended the method of Case C to a class of inclusive reactions which, unlike $e^- p \to e^- X$, could not be treated by previous QCD analyses. An example is the large p_T behavior of $pp \to \pi X$. To reduce this to the previous case I use the Mueller relation

$$\sigma(pp \to \pi X) \propto \text{Im Amp}\,[\,\bar{\pi}\, pp \to X \to \bar{\pi}\, pp;\ 0^\circ\,] \ . \tag{20}$$

Once again the initial state is unsummed and unaccelerated, so the Kinoshita analysis implies a factorization, with all $\alpha_k \ell n E/m_q$ terms absorbed into $|p>$ structure functions and the $|\pi>$ fragmentation function. The remaining effects involve only powers of α_k and are thus calculable.

Example I (Contogouris, Gaskell and Papadopoulos[9]; Field[10]). The behavior

$$d\sigma/dp_T(pp \to \pi X) \sim p_T^{-n} \tag{21}$$

expected at fixed $x_T = 2p_T/\sqrt{s}$ has posed a famous problem for QCD. Experimentally one has

$$n_{exp} \sim \begin{cases} 8.3, & p_T = 2\text{-}6 \text{ GeV} \\ 6.6, & p_T = 5\text{-}16 \text{ GeV}^{11)} \end{cases} \tag{22}$$

Theoretically, estimates in the lowest order [$O(g^4)$] using the scattering of valence quarks [Fig.(6)] yield

$$n_{th} = 4 \ . \tag{23}$$

In addition to Fig.(6) there are also $O(g^4)$ diagrams involving gluon constituents. These have recently been included[12]; they increase the magnitude at low x_T without changing the prediction $n_{th}=4$.

The new work[9,10] modifies the effective value of n_{th} by including the following effects:

i) The logarithmic variation in the "running" coupling constant g_k^2 (this occurs in the $O(g^6)$ and higher corrections to the rate).
ii) $\ell n\ p_T/m_q$ corrections in the structure and fragmentation functions (again these occur in the $O(g^6)$ and higher corrections to the rate).
iii) "Intrinsic p_T".
The result is a qualitative success; each of the new effects increases the effective value of n_{th}, and each increases n_{th} more at intermediate than at high p_T, so all effects act to reduce the discrepancy between theory and experiment.

For example, the logarithmic variation of the running coupling constant is essentially

$$g^2(p_T) \sim \frac{g^2(p_{T_o})}{1 + \frac{25}{24\pi^2} g^2(p_{T_o})\ \ell n\ p_T/p_{T_o}} \qquad (24)$$

The factor $g^4(p_T)$ in the rate therefore falls with increasing p_T. In the present p_T range, a $\ell n\ p_T$ variation is approximately equivalent to $p_T^{1/4}$; thus $g^4(p_T) \sim p_T^{-1/2}$ and effect (i) contributes a shift $\Delta n_{th} \simeq 1/2$ in the power. Evidently this shift falls with p_T. The logarithmic scaling violations in each structure and fragmentation function contribute a similar shift in the effective power behavior. Finally, the assumption that the incoming parton distribution has an "intrinsic p_T spread" makes it easier to achieve total p_T on the order of 2 or 3 GeV, but of course has little effect on reactions with really large p_T.

Quantitatively these effects can add up to change the effective n_{th} from 4 to 8 at intermediate p_T, but the numerical result is sensitive to parameters. The contribution (i) from the running coupling constant is reliable but small. The contribution (ii) from the scaling violations is large but somewhat less reliable: since the corrections are large one should go beyond $O(g^6)$; this can be done by means of renormalization group analysis on the moments of the distribution but the coefficient of each moment is a parameter to be fit (from deep inelastic scattering in the case of the proton structure function). Finally the "intrinsic p_T" (iii) is the largest contribution of all, but is completely phenomenological. Thus it cannot be said that n=8 is <u>predicted</u> by the theory; rather the new theoretical developments appear to have converted a major

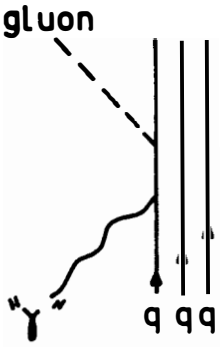

Fig. 5 : Diagram for a typical matrix element contributing to the scaling violation in the proton structure function.

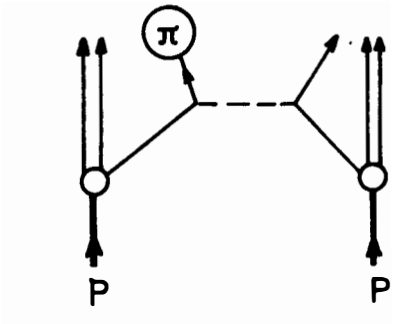

Fig. 6 : Diagram representing lowest order valence quark contribution to $pp \to \pi X$.

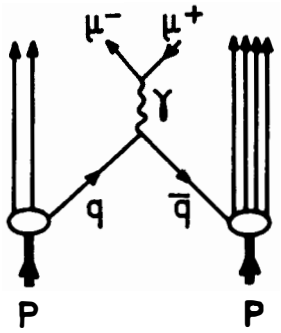

Fig. 7 : Drell-Yan diagram for $pp \to \mu^+\mu^- X$.

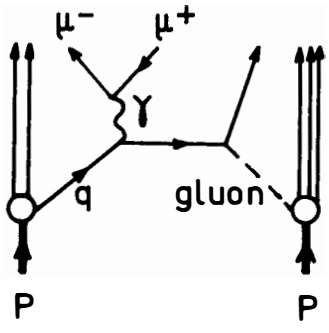

Fig. 8 : Order g^2 contribution to $pp \to \mu^+\mu^- X$ involving a gluon constituent of the proton.

discrepancy between theory and experiment into a more minor problem of understanding details.

Example II (work reported at this meeting by Petronzio[13] and Michael[14]) . The cross-section

$$d\sigma/dp_T(pp \to "\gamma" + X) \quad \text{with} \quad "\gamma" \to \mu^+\mu^-$$

can be treated in the same way as $pp \to \pi X$[7,8]. The order g^0 contribution is given by the Drell-Yan diagram (Fig.7). Even if the quark constituents are given a reasonable amount of intrinsic p_T, it is too small to explain the several per cent of events which have p_T= 2 to 5 GeV. The $O(g^2)$ corrections, for example Fig.(8), introduce gluon constituents and are capable of fitting the p_T=2 to 5GeV events. That brings us to the second major topic of the meeting.

II. Prompt Lepton Pairs.

When "prompt" leptons were first studied at large p_T, their origin was quite unclear. By now a fairly detailed picture has emerged. If we plot $d\sigma(pp \to \mu^+\mu^- X)/dM_{\mu\mu}$ versus $M_{\mu\mu}$ (Fig.9) we find three regions where different production mechanisms, each interesting in its own right, are at work:

Region I consists of the peaks at $M_{\mu\mu} \simeq$ 3 and 9 GeV. These peaks arise from basically new physics (charmonium and upsilon production).

Region II is the straight part of the curve at $M_{\mu\mu} >$ 3 GeV. It is interpreted in terms of hard constituent-constituent collisions such as the Drell-Yan mechanism (Fig.7). We note that the original reaction

$$p + p \to \mu^+\mu^- + X \tag{25}$$

does not, by itself, provide a very incisive test of the $q\bar{q} \to \gamma \to \mu^+\mu^-$ subcollision of Drell-Yan; while the distribution of valence quarks in the proton is rather well known from $e^-p \to e^-X$, the distribution of "sea" $\bar{q}$'s in the proton is less well determined.

The more recently studied reaction

$$\pi + p \to \mu^+\mu^- + X \tag{26}$$

reported on by Pilcher[15] and Romana[16] has the advantage that it can proceed by collision of a valence $\bar{q}$ from the pion with a valence q from the proton. Even without knowing the detailed distribution of partons within the pion one can say that

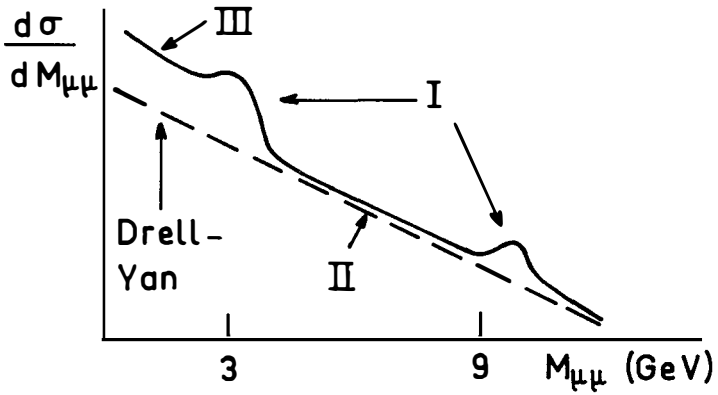

Fig. 9 : $d\sigma\ (pp \to \mu^+\mu^-\ X)/dM_{\mu\mu}$ experimental (solid line) and Drell-Yan (dotted line).

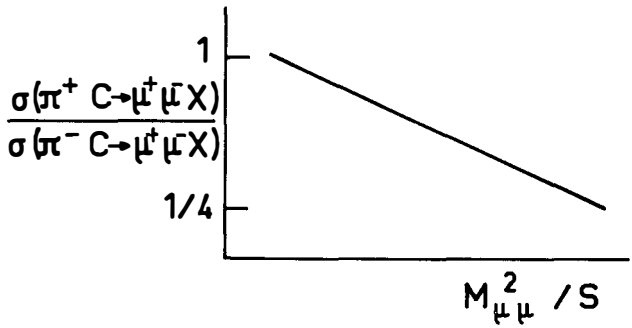

Fig. 10 :Schematic representation of the data for $\sigma(\pi^+C \to \mu^+\mu^-\ X)/\sigma(\pi^-C \to \mu^+\mu^-\ X)$.

$$\frac{\sigma(\pi^+ C \to \mu^+\mu^- X)}{\sigma(\pi^- C \to \mu^+\mu^- X)} \longrightarrow \frac{1}{4} \qquad (27)$$

at large Feynman x (where valence constituents dominate), because the valence $\bar{q}$ in π^+ is $\bar{d}(Q^2_d = 1/9)$ whereas the valence $\bar{q}$ in π^- is $\bar{u}$ $(Q^2_u = 4/9)$. This prediction is nicely satisfied by the data (Fig.10). That the presence of a valence $\bar{q}$ in the pion truly favors $\sigma(\pi p \to \mu^+\mu^- X)$ over $\sigma(pp \to \mu^+\mu^- X)$ at large Feynman x is now strikingly verified by the data[16] (Fig.11) which shows the ratio of these two processes reaching 300 at large $M^2_{\mu\mu}/s$. In the near future it should be possible to extract the parton distribution within the pion from $\pi p \to \mu^+\mu^- X$ data.

When it becomes experimentally feasible, study of the reaction

$$\bar{p} + p \to \mu^+ + \mu^- + X \qquad (28)$$

will also be interesting as emphasized by Lederman[17]. Here the $\bar{p}$ is the source of valence $\bar{q}$'s, with the same (relatively well-known) x-distribution as the valence q's in p. Thus, knowledge of the absolute rate for this reaction would provide one of our few clean tests of the color factor of 3.

The successful fits to the Drell-Yan model achieved in $pp \to \mu^+\mu^- X$ involve the rates integrated over p_T. The model fails to describe the small fraction of events in which the pair has large p_T. Here other processes must be at work, and we have described earlier in the talk how gluon constituents and QCD corrections can be used to explain the data. In the particular case of $pp \to \mu^+\mu^- X$ with its absence of valence $\bar{q}$'s it is believed that these corrections may be significant even at small p_T.

Region III refers to $M_{\mu\mu} < 3$ GeV. The $\mu^+\mu^-$ pairs are most numerous here, and most of the early events which called attention to the puzzle of large p_T leptons came from this region. Nevertheless, this region has been less productive of insights into the fundamental mechanisms involved. The Drell-Yan prediction is typically a factor of 10 below the data at $M_{\mu\mu} < 3$ GeV, and no simple quark picture or other comprehensive explanation has worked. It appears that here one is in the relatively low-momentum region where perturbative QCD breaks down and the quark dynamics becomes more complicated.

For example, M. Duong-Van[18] reported on a model which makes no mention of quarks,but is based on the subprocess $\pi\pi \to \gamma \to \mu^+\mu^-$

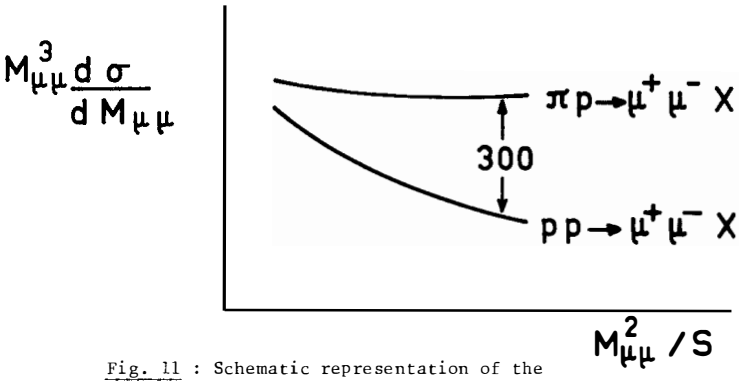

Fig. 11 : Schematic representation of the data for $M^3_{\mu\mu}\ d\sigma/dM_{\mu\mu}$ in $\pi p \to \mu^+\mu^- X$ and $pp \to \mu^+\mu^- X$.

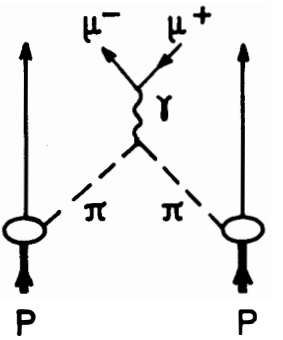

Fig. 12 : Diagram contribution of the subprocess $\pi\pi \to \gamma \to \mu^+\mu^-$ to $pp \to \mu^+\mu^- X$.

(Fig.12). Taking account of the pion form factor in the time-like region, this SLAC model fits the data well at the ρ peak and below, while falling too low at $M_{\mu\mu} > 1$ GeV (Fig.13). Expressed in quark language, this model would involve soft $q\bar{q}$ pairs and gluons in a complicated way.

An alternative explanation of pair production at $M_{\mu\mu} < 3$ GeV, based on quark bremsstrahlung, had been proposed by Farrar and Frautschi[19] and others.

In addition to the Dalitz μ-pair conversions of virtual photons it required real γ's in copious amounts [$\gamma/\pi > 10\%$ at large s, p_T]. The experiment of the Willis group, reported to us by Rehak[20], attacked this question by studying μ pairs down to $M_{\mu\mu}$ = a couple of hundred MeV. They were able to account for essentially all μ pairs without quark bremsstrahlung, and thus [using the tight connection between low-$M_{\mu\mu}$ Dalitz pairs and real γ's in a bremsstrahlung mechanism] estimate a limit

$$\gamma_{\text{direct}} / \pi^0 < 1\ \%$$

on real γ's in a range p_T=2 to 3 GeV, $\sqrt{s}$=52 GeV where a substantially higher value was expected in the quark bremsstrahlung model.

III. Baryonium, etc.

A third major theme of the meeting was baryonium. Strictly speaking the name "baryonium" refers to B=0 levels with small Γ_{meson}. Sometimes, but not always, they also have small Γ_{total}. Recently this subject has flowered forth experimentally[21] to the point where there are now on the order of 10 levels at $M > 2M_N$ and 5 levels at $M < 2M_N$ that are candidates for baryonium.

Baryonium states have long been expected on the basis of NN potentials suitably crossed to the $N\bar{N}$ channel[22]. They are required by the quark duality diagrams for $N\bar{N} \to N\bar{N}$[23]. More recently, they have been extensively treated by Johnson and Thorn, Jaffe, Chan and Høgaasen and others[24] in the MIT bag model, where the original baryonium states appear as just one example of a whole class of multiquark resonances.

I propose to call the Johnson-Thorn-Jaffe-Chan-Høgaasen theory of these multiquark resonances the "baguette model" in honor of the long thin French bread, which resembles the highly streched bags

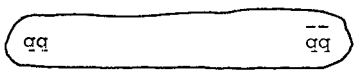

used in the model. The length $r \sim \sqrt{s}$ of the baguette ensures that

$$\ell = |\vec{r} \times \vec{p}| \sim \sqrt{s} \times \sqrt{s} \sim s \qquad (29)$$

lies as high as possible, near the leading Regge trajectory. The high orbital angular momentum plays the essential role of inhibiting the decay into mesons via recombination of the q's and $\bar{q}$'s at the ends of the baguette.

A crucial test of the bag model for multiquark configurations such as $qq\bar{q}\bar{q}$ is that exotic resonances are also predicted. Why complicate in this manner the highly successful $q\bar{q}$ model of mesons when it has predicted exactly the observed states up to now, and when no exotic state has ever been well authenticated ? Jaffe[24] and Høgaasen[24] have given us the answer: the quarks and gluons of QCD provide degrees of freedom that should express themselves in a richer spectrum of mesons than is provided by $q\bar{q}$ alone, and the semiphenomenological bag Lagrangian predicts a greatly expanded spectrum.

Let us review from another standpoint some of the reasons why multiquark levels are both expected and hard to see. I begin by reminding you of the dual-resonance model plot of J versus M^2 (Fig.14) where the degeneracy at a given M^2 increases rapidly as one proceeds from the leading to the daughter trajectories. The degeneracies of lower trajectories are so great that the overall level density $\rho(M)$ in this model increases as

$$\rho(M) \sim e^{bM} \qquad (30)$$

with b of order m_π^{-1}.

Next consider the J versus M^2 plot from the point of view of the bag model (Fig.15). This model also predicts $\rho(M) \sim e^{bM}$. On the other hand, taking nonexotic mesons as an example, the density of $q\bar{q}$ states only rises as a power, $\rho(M) \sim M^p$. Such states are dominant only at low M or on the leading trajectory. As the mass is increased (or as we proceed down from the leading trajectory) successively more complicated states such as $qq\bar{q}\bar{q}$, $q\bar{q}$ gluon etc... are found, and it is the sum over all of these states which grows exponentially.

If we fix our attention on a particular set of quantum numbers J, J_z, B,S,I,Q..., the level density still grows as e^{bM}. The typical level width is $\Gamma \gtrsim m_\pi$ for most hadron resonances. Thus the spacing between levels rapidly becomes less than Γ, ie the levels overlap above a mass which is on the order of 2 GeV for low J,

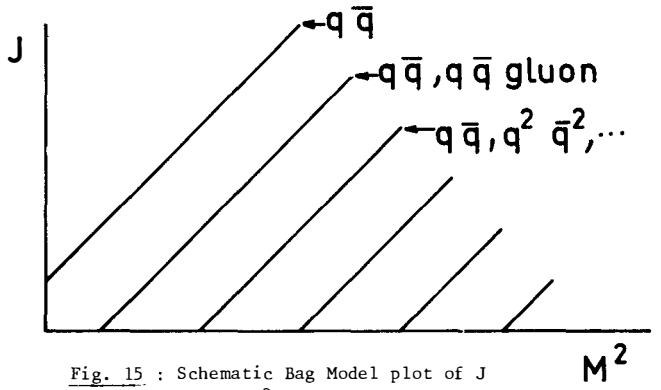

Fig. 15 : Schematic Bag Model plot of J versus M^2.

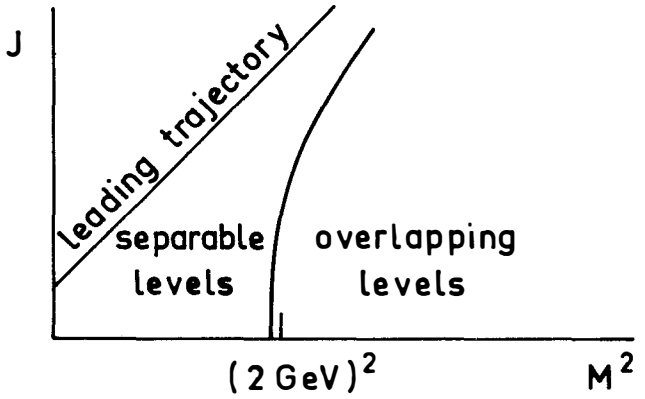

Fig. 16 : Schematic plot indicating where Γ_p (M,J) is large enough to make individual levels (of a given J^P, B, S, I,...) overlap.

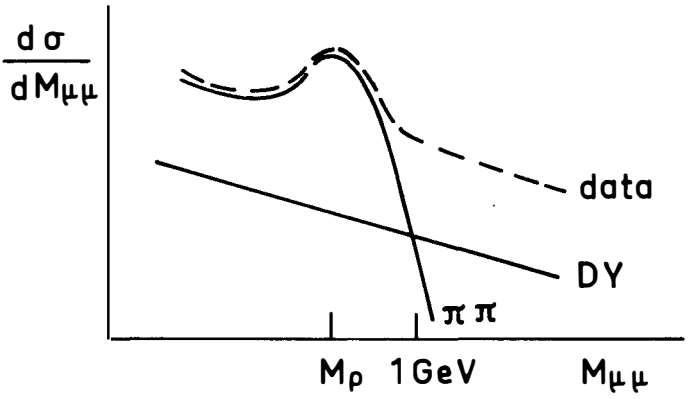

Fig. 13 : Schematic comparison of the data, Drell-Yan (DY) prediction, and $\pi\pi \to \gamma \to \mu^+\mu^-$ subprocess prediction for $pp \to \mu^+\mu^- X$.

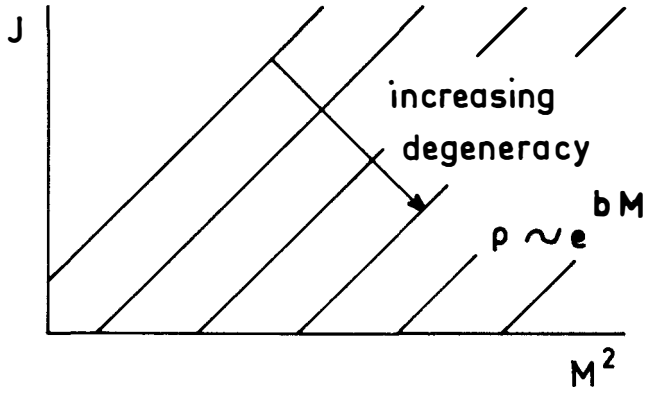

Fig. 14 : Dual Resonance Model plot of J versus M^2.

somewhat higher for higher J[25] (Fig.16). In the overlap region, ordinary levels do not stand out as individual resonance peaks and cannot be isolated even by phase shift analysis on a given reaction. Thus they are hard to see ; one is reduced to looking for statistical effects such as Ericson fluctuations[26]. The relevance for the bag model is that most multiquark levels are in the overlap region.

It follows that only rather special multiquark states have a good chance to stand out experimentally:

i) "Baguette" states near the top trajectory may have $\Gamma_{tot} \ll m_\pi$, or at least have small Γ_{meson}, as discussed earlier.

ii) In an exotic channel, the first couple of exotic resonances should not overlap even if they have rather high masses (as predicted by Jaffe[24]) and normal widths of order m_π .

But even in these favorable cases, the multiquark states usually couple rather weakly to "normal" states. Thus theorists should furnish not only lists of states, but also suggestions for favorable production and formation reactions.

Conclusion

If there was a common thread running through this meeting, it was a process of taking more seriously the gluons and associated quark pairs suggested by the full QCD dynamics, even though the solution of QCD remains as elusive as ever.

In conclusion I wish to thank the founder and organizer of the Moriond Conferences, Tran Thanh Van, for his efforts towards making this meeting so fruitful and pleasant.

REFERENCES

1. T.D.Lee and M.Nauenberg, Phys.Rev.133,B1549(1964).
2. T.Kinoshita and A.Sirlin, Phys.Rev.113,1652(1959).
3. G.Sterman and S.Weinberg, Phys.Rev.Lett.39,1436(1977).
4. T.Kinoshita, J.Math.Phys.3, 650(1962).
5. D.Amati, R.Petronzio and G.Veneziano; report to this conference by R.Petronzio.
6. A.de Rujula, H.Georgi and H.D.Politzer, Phys.Rev.D.10, 2141 (1974).
7. H.D.Politzer, Nucl.Phys.B129, 301(1977); I.Hinchliffe and C.H.Llewellyn-Smith, Phys.Lett.66B,281(1977).
8. C.T.Sachrajda, Phys.Lett.B73,185(1978); report to this conference.
9. A.P.Contogouris, R.Gaskell and S.Papadopoulis, Phys.Rev.D1 (in press); A.P.Contogouris, report to this conference.
10. R.D.Field, Phys.Rev.Lett.40,997(1978).

11. A.Clark et al., Phys.Lett.74B,267(1978); reported to this conference by J.Teiger.
12. B.Combridge, J.Kripfganz, and J.Ranft, Phys.Lett.B70,234(1977); J.Owens, E.Reya and M.Gluck, FSU preprint HEP 77-09-07 and Erratum; R.Cutler and D.Sivers, Phys.Rev. D17 ,196(1978).
13. G.Altarelli, G.Parisi and Petronzio, CERN preprints TH-2450, reported to this conference by R.Petronzio. See also H.Fritzsch and P.Minkowski,Phys.Lett.73B, 80(1978); C.S.Lam and T.M.Yan, Phys.Lett.71B, 773(1977); K.Kajantie, J.Lindfors and R.Raito Helsinki preprint HU/TFT/78-5.
14. C.Michael, report to this conference.
15. J.E.Pilcher, report to this conference.
16. A.Romana, report to this conference.
17. L.Lederman, report to this conference.
18. M.Duong-van and R.Blankenbecler, reported to this conference by M.Duong-van.
19. G.R.Farrar and S.Frautschi, Phys.Rev.Lett.36,1017(1976).
20. P.Rehak, report to this conference.
21. T.Carter, B.R.French, L.Montanet, and J.Six, reports to this conference.
22. R.Vinh Mau, report to this conference.
23. J.L Rosner, Phys.Rev.Lett.21,950(1968); Phys.Lett 33B,493(1970).
24. K.Johnson and C.B.Thorn, Phys.Rev.D13, 1934(1976); R.Jaffe Phys.Rev.D15,267,281(1977); Chan Hong-Mo and H.Høgaasen, Phys. Lett.72B,121,400(1977); Chan Hong-Mo, M.Fukujita, H.Høgaasen, and R.Jaffe,reports to this conference.
25. S.Frautschi, Nucl.Phys.B91,125(1975).
26. T.E.O.Ericson and T.Mayer-Kuckuk, Ann.Rev.Nucl.Sci.16,183(1966); S.Frautschi, Nuovo Cimento 12A, 162(1972); K.A.Jenkins et al., Phys.Rev.Lett. 40, 429(1978).

MORIOND PROCEEDINGS

N° 1	First Rencontre de Moriond	: 2 vol (1966)
N° 2	Second Rencontre de Moriond	: 2 vol (1967)
N° 3	Third Rencontre de Moriond	: 2 vol (1968)
N° 4	Fourth Rencontre de Moriond	: 1 vol (1969)
N° 5	Fifth Rencontre de Moriond	: 1 vol (1970)
N° 6	Electromagnetic and Weak Interactions	: (1971)
N° 7	High-Energy Phenomenology	: (1971)
N° 8	Two Body Collisions	: (1972)
N° 9	Multiparticle phenomene and inclusive reactions	: (1972)
N° 10	Electromagnetic and Weak Interactions	: (1973)
N° 11	The Pomeron	: (1973)
N° 12	High energy hadronic interactions	: (1974)
N° 13	High energy leptonic interactions	: (1974)
N° 14	Phenomenology of hadronic Structure	: (1975)
N° 15	Charm, Color and the J	: (1975)
N° 16	New fields in hadronic physics	: (1976)
N° 17	Weak Interactions and neutrino physics	: (1976)
N° 18	Storage Ring Physics	: (1976)
N° 19	Leptons and Multileptons	(1977)
N° 20	Deep Scattering and Hadronic Structure	(1977)
N° 21	Color Symmetry and Quark Confinement	(1977)
N° 22	**Phenomenology of Quantum Chromodynamics**	**(1978)**
N° 23	**Gauge Theories and Leptons**	**(1978)**

18 STORAGE RING PHYSICS

CONTENTS

19 LEPTONS AND MULTILEPTONS

CONTENTS

— STORAGE RING PHYSICS

F. Laplanche, « Evidence for resonant structure near 1780 MeV in e^+e^-annihilation observed at DCI (Orsay) » ; F. M. Renard, « Theoretical comments on the ψ' (1.78) vector meson » ; V. Luth, « K$\bar{\text{K}}$ production in e^+e^-annihilation » ;H. K. Nguyen, « Direct evidence for charmed particles in e^+e^-annihilation at Spear » ;M. L. Perl, « Evidence for, and properties of, the new charged heavy lepton » ; V. Blobel, « Recent results on e^+e^-annihilationfrom Pluto at Doris » ; W. Wallraff, « New results on e^+e^-annihilation at energies around the charm threshold obtained with the Dasp detector at the Desy Storage Ring Doris » ; W. Bartel, « Neutral and radiative decays of the J/ψ particle » ; M. Greco, « Radiative decays of old and new mesons » ; S. Matsuda, « Pair production of charm in e^+e^-annihilation » ; M. Davier, « Expected physics at Petra-Pep Energies ».

II — DEEP INELASTIC SCATTERING

H. Spitzer, « New electroproduction results from Desy » ; C.A. Heusch, « Some topics concerning vector meson in charged lepton-nucleon scattering » ; J. J. Aubert, « Actual limitations in the deep inelastic experiment and how the European muon collaboration can improve it » ; F. Hayot, « Description of inclusive hadron production in deep inelastic lepton-nucleon scattering ».

III — NEUTRINO PHYSICS

C. Baltay, « Dilepton production by neutrinos in neon » ; P. Mine, « Dimuons and trimuons produced by neutrinos and antineutrinos » ; C. T. Murphy, « Search for neutrino induced dimuon events in the 15 foot neon bubble chamber with a two plane EMI » ; A. Benvenuti, « Properties of neutrino induced trimuon events » ;C. Matteuzzi, « *ve* interactions in Gargamelle » ; G. Bertrand, « Observation of a likely example of the decay of a charmed particle » ; A. B. Entenberg, « Elastic neutrino proton and antineutrino proton scattering » ; J. C. Vander Velde, « Neutrino interactions in the 15-foot hydrogen bubble chamber search for charmed particles » ; L. R. Sulak, « Experimental studies of the acoustic detection of particle showers and neutrino physics beyond 10 TeV

IV — THEORETICAL LECTURES

M. Gourdin, « Currents quarks and high energy experiments » ; J. Kaplan, « Some aspects of weak interactions in models with 4 quarks or more » ; H. Fritzsch, « Flavourdynamics of leptons » ; M. K. Gaillard, « Asymptotic freedom and deep inelastic scattering » ; C. Quigg, « Issues in charmed particle spectroscopy » ; L. L. Wang, « Anticipating the intermediate boson » . K. Kang, « Flavour-changing neutral currents in elastic and deep-inelastic neutrino scattering ».

V — SUMMARY

K. Goulianos, « The finish (summary and conclusion) ».

20 DEEP SCATTERING AND HADRONIC STRUCTURE

CONTENTS

21 COLOR SYMMETRY AND QUARK CONFINEMENT

This is a book with chapters based on talks given at the XIIth Annual Rencontre de Moriond (April 1977) plus an added pedagogical introduction. The book is intended to be useful for learning about Color Symmetry, how to work with it, and how it can be tested experimentally.

CONTENTS

22 PHENOMENOLOGY OF QUANTUM CHROMODYNAMICS

CONTENTS

23 GAUGE THEORIES AND LEPTONS

CONTENTS